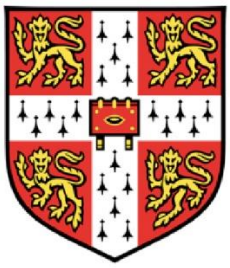

UNIVERSITY OF CAMBRIDGE

Asymmetric Catalysis with Brønsted Acids: Experiments and Calculations

This thesis is submitted for the degree of Doctor of Philosophy at the University of Cambridge

by

Guillermo Caballero García

of

Pembroke College

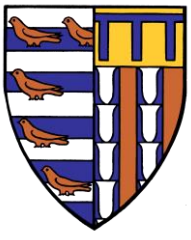

September 2020

Declaration

This thesis is the result of my own work and includes nothing which is the outcome of work done in collaboration except as specified in the text. It is not substantially the same as any work that has already been submitted, or, is being concurrently submitted for a degree, diploma or other qualification at the University of Cambridge or any other University or similar institution. It does not exceed the prescribed limit of 60,000 words.

Guillermo Caballero García

2020

Abstract

Asymmetric Catalysis with Brønsted Acids: Experiments and Calculations

The research described herein focuses on enantioselective catalysis using BINOL-based Brønsted acids. The initial part of this work comprises the development of chiral phosphoric acids and *N*-triflylphosphoramides having alternative groups at the 3,3'- positions, different from the widely common aryl scaffolds. These motifs include heavily hindered silyl groups and aryl sulfones. Such catalysts were used to design enantioselective ring-closing reactions to furnish nitrogen-based heterocycles *via* iminium ions as reactive intermediates. Two of the transformations presented in this work include imino-Diels-Alder and Pictet-Spengler reactions. Moreover, a *S*,*O*-thioacetalization reaction to furnish 1,3-oxathiolanes enantioselectively is presented. In the latter project, after thorough and systematic screenings, it was noteworthy that the catalyst loading of *N*-triflylphosphoramides could be lowered down to 0.5 mol%, showcasing these catalysts as an efficient diversion from phosphoric acids in asymmetric synthesis.

In addition to the experimental work, computational investigations were conducted. Molecular modelling focused on accounting for the stereochemical output of an enantioselective aza-Darzens reaction that uses a bulky chiral BINOL-based phosphoric acid. For such, hybrid Quantum Mechanics / Molecular Mechanics methods—mostly the ONIOM approach to calculate such large systems with the whole catalyst structure—were used in order to find diastereomeric transition states and to understand how the catalyst induces chirality during the enantiodetermining step. Furthermore, through these DFT calculations, an alternative mode of activation for the imine substrate was envisaged, different from the usual N-H hydrogen bonding with the catalyst. Therein, the imine is protonated by the acid; however, the resulting iminium ion interacts with the catalyst through non-classical C-H hydrogen bonds. The calculated transition states for this quite unusual mode of activation showed to be the lowest in energy. Moreover, with such model, the predicted sense and amount of enantioinduction was in accordance with the values reported experimentally.

Acknowledgements

First of all, I want to thank my supervisor, Jonathan Goodman, for the opportunity to join his research group to carry out my PhD. I appreciate his endless optimism and his particular way to look at chemical reactions—in which a lot can be learnt out of every single experiment. Moreover, I want to thank him for providing me with funding for the last two terms of my PhD.

I also want to thank Ian Paterson—not only for his helpful feedback in group meetings—but mostly for encouraging me to supervise the part III M5 course. Thanks to that, I discovered how enjoyable stereochemistry is.

Special thanks are given to CONACYT, Mexico and the Cambridge Trust for providing me with funding throughout my PhD with a CONACYT Cambridge Scholarship (reference: 600435/438243).

Lab work would not have been smooth without the impressive support of the technical staff. In particular, I want to thank Naomi Hobbs, Nic Davies, Carlos Davies and Nick Foot for keeping the lab running. I also thank the NMR service, Andrew Mason and Duncan Howe for running some of my NMR samples. In addition, the mass spec team for recording HRMS for my samples. Furthermore, I want to thank Susan Begg for her support keeping the CMI office running. The Phipps group is also acknowledged for allowing me to use the chiral SFC equipment.

I want to thank Joaquin Barroso-Flores, UAEM-UNAM, and Jacinto Sandoval-Liras, UNAM, for proof-reading my thesis at a short notice and for providing useful feedback.

Special thanks to my fellow Mexican friends in Cambridge. For cheering me up with a nice beer when chemistry was not working or when I was feeling under the weather—also for tolerating my taste of music. You guys made me feel like at home.

Finally yet importantly, I greatly appreciate my undergraduate supervisors, Joaquin Barroso-Flores and Moises Romero-Ortega for encouraging me to do a PhD and for their endless support when I was applying.

Table of Contents

Abbreviations

Å	Angstrom
Ac	acetyl
Ad	adamantadyl
aq.	aqueous
Ar	aryl group
BA	Brønsted acid
BINOL	1,1'-binaphthol
Bn	benzyl
Boc	*tert*-butyloxycarbonyl
^{t}Bu	*tert*-butyl
conc.	concentrated
CSA	camphorsulfonic acid
Cy	cyclohexyl
DCE	dichloroethane
DCM	dichloromethane
DFT	Density Functional Theory
DIPEA	di*iso*-propylethyl amine
DMAP	dimethylaminopyridine
DMF	*N*,*N*-dimethyl formamide
DMS	dimethylsulfide
DMSO	dimethylsulfoxide
dr	diastereomeric ratio
ee	enantiomeric excess
ent	enantiomer
eq.	equation
equiv.	equivalent
ES	electrospray
Et	ethyl
EWG	electron-withdrawing group
[H_8]-BINOL	5,5',6,6',7,7',8,8'-octahydro-1,1'-binaphthol

HOMO	highest occupied molecular orbital
IDPA	imidodiphosphoric acid
IPA	*iso*-propanol
IRC	intrinsic reaction coordinate
LCMS	liquid chromatography coupled with a mass spectrometer
LDA	lithium di*iso*-propyl amide
LUMO	lowest unoccupied molecular orbital
mCPBA	meta-chloroperbenzoic acid
MDPS	methyldiphenylsilyl
Me	methyl
MM	molecular mechanics
MOM	methoxymethylene
MS	molecular sieves
MTBE	methyl *tert*-butyl ether
NTPA	*N*-triflylphosphoramide
ONIOM	our own n-layered integrated molecular orbital and molecular mechanics
OPLS3	optimised potentials for liquid simulations
PA	phosphoric acid
PE	petroleum ether
PES	potential energy surface
PG	protecting group
Ph	phenyl
PMB	*para*-methoxybenzyl
PMP	*para*-methoxyphenyl
^{i}Pr	*iso*-propyl
py	pyridine
rac	racemic
rt	room temperature
sc	*s-cis*
SP	single-point (energy)
SPINOL	1,1'-spirobiindane-7,7'-diol
st	*s-trans*
T	temperature
TADDOL	tetraaryl-2,2'-disubstituted 1,3-dioxolane-4,5-dimethanol

TBS	*tert*-butyldimethylsilyl
TES	triethylsilyl
Tf	triflyl, trifluoromethanesulfonyl
TFA	trifluoroacetic acid
TFAA	trifluoroacetic anhydride
THF	tetrahydrofuran
TIPS	tri*iso*-propylsilyl
TLC	think layer chromatography
TMEDA	*N*,*N*,*N*,*N*-tetramethylethylenediamine
TMS	trimethylsilyl
TS	Transition State
Ts	tosyl, 4-toluenesulfonyl
UFF	Universal Force Field
VAPOL	2,2'-diphenyl-(4-biphenanthrol)

Chapter 1

Introduction

1.1. Asymmetric organocatalysis: Chiral Brønsted acids

Making molecules with high levels of stereoselectivity has always been an outstanding challenge in organic chemistry. The field of asymmetric synthesis has attracted the attention and effort of many research groups trying to imitate nature in synthesising a wide variety of compounds with high levels of stereocontrol and using mild reaction conditions.[1] Such a task can be addressed by asymmetric organocatalysis.[2–5] The application of organocatalysis is widely appreciated in the medicinal chemistry area because of the high enantiomeric ratios that organocatalysts can achieve in order to supply a specific enantiomer for clinical trials.[6,7] In addition, pharmaceutical compounds that cannot tolerate contamination by metal impurities may benefit from these methodologies.[8]

Nowadays, there is a huge repertoire of organocatalysts, with an impressive variety of molecular shapes and functionalities, designed for either general substrates or specific transformations. These catalysts can be classified into four broad categories according to their catalytic cycle and mechanism for activating substrates: Lewis bases, Lewis acids, Brønsted bases and Brønsted acids.

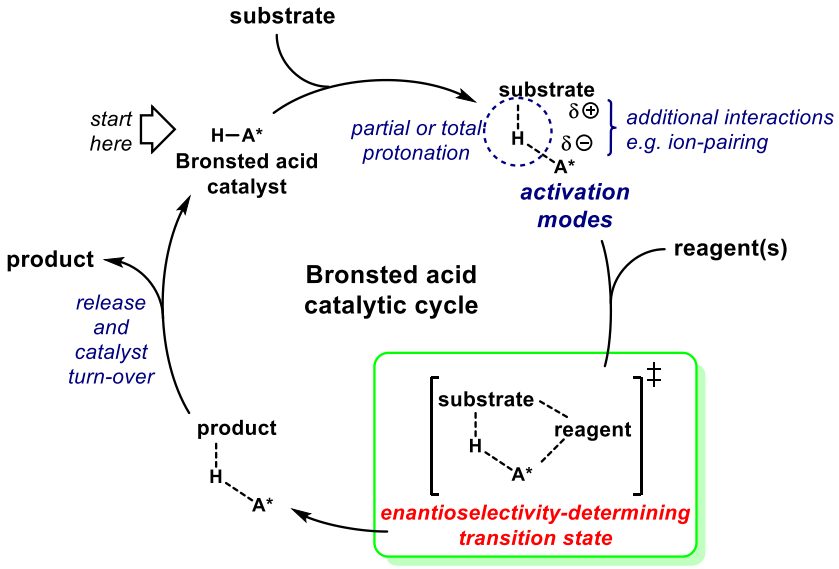

Scheme 1.1: A general catalytic cycle for Brønsted acid-catalysed asymmetric transformations.

Brønsted acids initiate their catalytic cycle by partial or complete protonation of a potentially electrophilic substrate (Scheme 1.1). During the initial step in the mechanism, the electrophile is activated by lowering its LUMO energy. In addition, secondary interactions are likely to occur in order to stabilise an intermediate or transition state as well. These, are mainly studied in a computational perspective.[9] Amongst these secondary interactions, ion pairing or π–π stacking of aromatic groups are frequently

observed. Within the catalytic cycle, the most important stage is the enantioselectivity-determining step. There, the chiral information in the catalyst is transferred to favour one diastereomeric transition state over the other. This chirality-based bias is promoted by the catalyst's architecture.

Hydrogen bonding has proved to catalyse a large number of reactions in a similar way in which enzymes exploit this interaction in order to achieve high levels of selectivity.[10] Most of the recently developed Brønsted acids lock the substrates through hydrogen bonding in the transition state.[11] If highly acidic catalysts are used, complete protonation and ion pairing is likely to occur.

One of the most popular chiral Brønsted acids are phosphoric acids (PAs). Since the first reports from Akiyama and Terada,[12–15] these catalysts have been widely utilised in asymmetric synthesis.[16–18] Several reviews are devoted to chiral PAs and the chemical transformations they catalyse. Amongst these numerous reactions, but not necessarily limited to, include asymmetric Mannich reactions,[19] Diels-Alder reactions,[20] cycloadditions,[21] multicomponent reactions,[22] addition reactions to carbonyls,[23] addition to imines[24,25] and asymmetric C-C bond forming reactions.[18] Apart from experimental reports, several computational studies have been conducted trying to explain the origins of enantioselectivity in PA-catalysed reactions.[26,27]

1.2. BINOL-based Phosphoric Acids

BINOL, **1.1**, is one of the most popular chiral templates for asymmetric transformations (Figure 1.1).[28] Its C_2 axial symmetry provides a chiral pocket that makes it suitable to be utilised as a chiral ligand. However, one of the most important features of the BINOL backbone are the 3,3'- positions. Therein, substituents can be easily installed to modify the shape of the chiral pocket in order to enhance enantiocontrol in asymmetric transformations. These groups are responsible to promote enantioselectivity. In addition, the 6,6'- positions of the BINOL framework offer alternative sites for modification. These latter positions are mainly used to install hydrophobic chains to improve solubility or electron-withdrawing groups to increase acidity. Amongst the most common 3,3'- substituents in **1.2** are aryl scaffolds. Moreover, silicon-based and heteroaryl groups are often found, yet, in fewer cases. The synthesis of 3,3'- disubstituted BINOLs **1.2** will be discussed in Chapter 2.

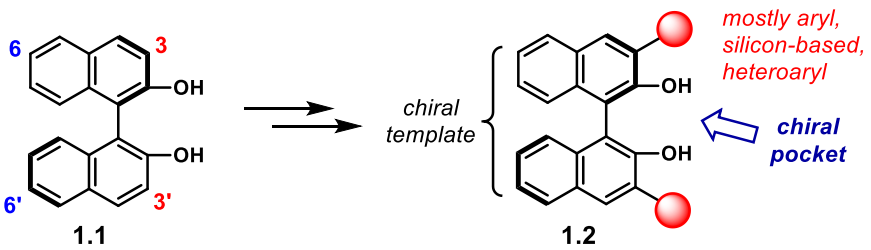

Figure 1.1: *(R)*-BINOL as a versatile chiral template for organocatalysts.

BINOLs **1.2** have been utilised in enantioselective organocatalysis due to their hydrogen bond donor character.[29] In addition, BINOL-derived Brønsted acids have been used for the same purpose. BINOL-

based PAs **1.3** are one of such molecules and one of the key catalysts in the present work (Figure 1.2). Not only BINOL has been used as a versatile chiral template for PAs. Other frameworks have shown to be suitable as well. The partially hydrogenated BINOL backbone, as in **1.4**, has been widely used as a framework for Brønsted acids as it offers alternative conformations in comparison to the standard BINOL. Rotation-restricted biphenyls, as in **1.5** are also found in PAs. The related scaffold, VAPOL, **1.6**, has also been used as a template in asymmetric transformations; yet, it does not offer much accessible modification as in the case of BINOL. Amongst recent chiral PAs with an alternative framework are SPINOL-based PAs **1.7**.[30] The group of Lin is pioneer in using this template in asymmetric Brønsted acid catalysis.[31]

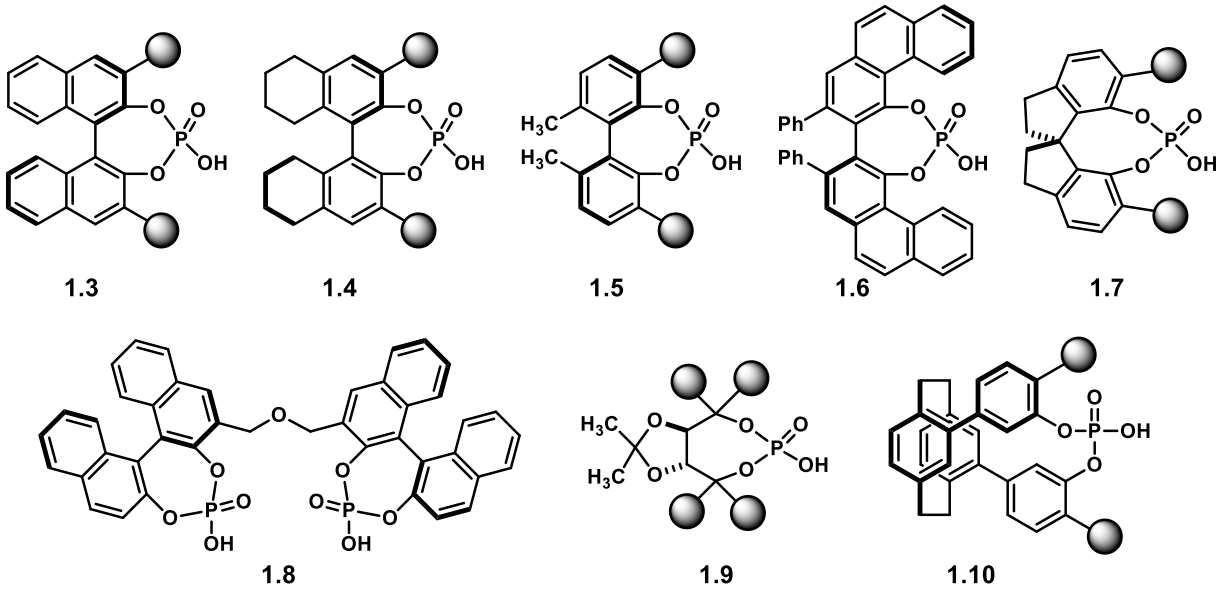

Figure 1.2: Variety in chiral templates for PAs.

Amongst exotic chiral templates, dimeric BINOL frameworks **1.8** feature as another type of *bis*-PA for asymmetric catalysis.[32,33] Yet, these type of chiral Brønsted acids have not been studied in detail. PAs with a TADDOL backbone, **1.9** have also been developed.[34] The parent diol, however, was found to be a suitable catalyst to activate carbonyl groups *via* hydrogen bonding.[35] Finally, one of the latest reported PAs were inspired by a [2.2]-paracyclophanyl template.[36] The group of Lin developed a methodology for the synthesis of catalysts **1.10**, which afforded outstanding enantiocontrol in an asymmetric aza-Friedel-Crafts reaction.[37]

The chiral templates presented previously are not the only ones in which a Brønsted acid active site or acidic motif can be installed. Further development has been made in designing new chiral frameworks. For instance, since the development of SPINOL,[38] **1.11** (Figure 1.3), several groups have been inspired by this scaffold and made different chiral analogues. These SPINOL-inspired structures include, but are not limited to, a cyclohexyl-fused SPINOL **1.12**,[39] oxo-SPINOL **1.13**[40] and aza-SPINOL **1.14**.[41] However, apart from **1.11**, the other compounds have not been utilised as frameworks for PAs or other Brønsted acids. This is partly because the synthesis of such templates comprises several steps to arrive to the corresponding diol in a racemic fashion. Resolution of the racemic mixture is thus required. Moreover,

further steps are needed to install additional substituents in order to modify the shape of the catalyst's chiral pocket. In contrast, for the case of BINOL-derived PAs, both the *(R)* and *(S)*-BINOL enantiomers are commercially available.

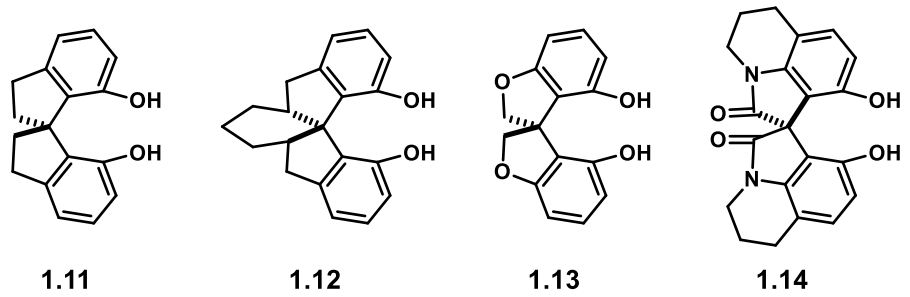

1.11 **1.12** **1.13** **1.14**

Figure 1.3: SPINOL-inspired chiral templates recently developed.

1.3. Enhancing Reactivity

Chiral PAs have been mostly employed for the activation of rather basic electrophilic substrates. One such example are imines. The highly basic nitrogen atom can be readily protonated by the PA or engage into strong hydrogen bonding. This depends on the reaction media and on the catalyst's acidity. Therefore, less basic substrates are more challenging to activate with PAs. A solution to accomplish this task is to use a more acidic catalyst, as most of the time, acidity correlates with catalytic activity. In that context, the groups of Rueping and Leito concluded that the ability to induce chirality in a reaction is up to the catalyst structure; however, reactivity—that is, the reaction rate—depends on the acidity of the active site.[42]

Several approaches have been made in order to increase the acidity of BINOL-based PAs **1.15** (Scheme 1.2). One of them is the introduction of a strong electron-withdrawing motif in the catalyst's active site—accounting that a more delocalised negative charge in the conjugate base increases the strength of the acid. In this context, N-H Brønsted acids have become popular.

The group of Yamamoto developed a series of BINOL-based *N*-triflylphosphoramides (NTPAs) **1.16**.[43] There, the triflyl motif increases the acidity of the Brønsted acid both by inductive effects from the trifluoromethyl group and by resonance.[44] Since then, NTPAs have been used as stronger chiral Brønsted acids for enantioselective transformations.[45] In particular, for carbonyl group activation. The group of Rueping has been pioneer in these type of stronger Brønsted acids in asymmetric catalysis.[46]

In addition, *bis*(sulfonyl)imides **1.17** and *bis*(sulfuryl)imides **1.18** were developed as even stronger Brønsted acids as an alternative to NTPAs.[47–49] They have also shown excellent catalytic activity in enantioselective reactions. However, they have not been studied as extensively as PAs or NTPAs. Despite the excellent results reported by these two types of catalysts, they are out of the scope of this thesis and will not be discussed exhaustively. The primary sphere of the present work focuses mostly on BINOL-based PAs and NTPAs.

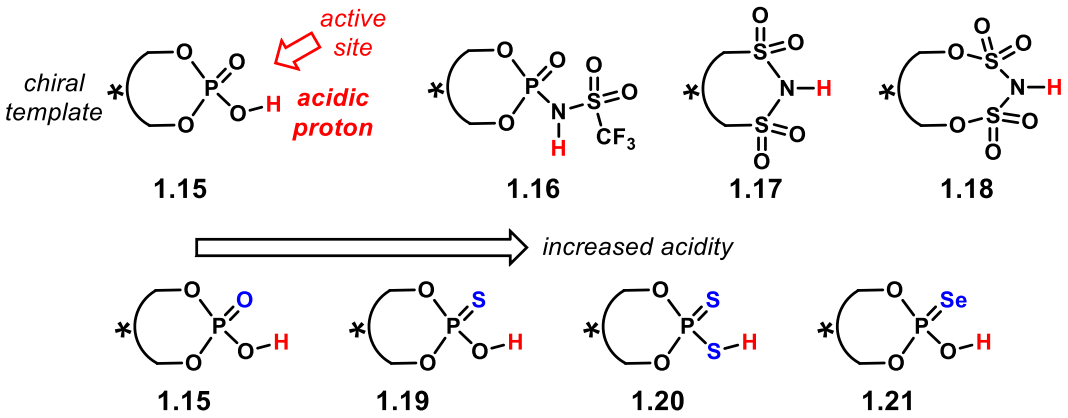

Scheme 1.2: Approaches in which to increase the acidity of the catalyst. Top row: by adding electron-withdrawing groups to the catalyst's active site. Bottom row: by adding heteroatoms to further stabilise the counter anion.

In addition to the introduction of electron-withdrawing groups to increase the catalyst acidity, a second approach consists of changing oxygen atoms in **1.15** for softer elements: sulfur and selenium. This increases the acidity of the active site by stabilising the counter anion. Thiophosphoric acids **1.19**, dithiophosphoric acids **1.20** and selenophosphoric acids **1.21** have been synthesised as stronger alternatives to 'standard' PAs. Although they achieve impressive levels of enantiocontrol, they are rather limited to a small number of reactions. Moreover, analogous catalysts for NTPAs have been made—*i.e.* thio and seleno NTPAs. One of the main reasons why these thio and seleno Brønsted acids are not as popular as the most common PAs and NTPAs is a result from the fact that, in some cases, they follow a reaction mechanism different from Brønsted acid catalysis. That is, the softer sulfur and selenium atoms prefer to act as Lewis bases.

A great deal of research in this field comprises the study of the Brønsted acidity of these catalysts, whether BINOL-derived or not. As mentioned before, catalytic activity is intimately related to the acidity of the catalyst's active site. In this context, several research groups have developed acidity scales in order to explain reactivity. Two such scales correspond to experimental p*K*a values (Scheme 1.3).

The groups of Berkessel and O'Donoghue determined the p*K*a values in DMSO for a series of Brønsted acids (Scheme 1.3*a*).[50] Their work shows that, indeed, NTPAs are more acidic than PAs. In turn, *bis*(sulfuryl) and *bis*(sulfonyl)imides are more acidic than NTPAs—the former two catalysts BA-**1.1** and BA-**1.2**, however, were found to have very similar p*K*a values. This trend can be observed in the p*K*a values for Brønsted acids BA-**1.1** (1.74) < BA-**1.2** (1.77) < NTPA-**1.1** (3.34) < PA-**1.1** (3.37). Herein, it is clear how the resonance effect of the electron withdrawing groups directly attached to the active site lowers the p*K*a. In addition, the chiral framework can affect the acidity of the catalyst. This is shown with PA-**1.1** and [H_8]-PA-**1.1** where the hydrogenated backbone decreases the acidity by 0.75 p*K*a units. As expected, the substituents at the 3,3'- positions of the BINOL core influence acidity as well. In general, the more electron withdrawing the substituents, the lower the p*K*a values, as exemplified by PA-**1.2** and PA-**1.3**. However, for electron neutral aromatic rings or with electron donating groups the acidity does not seem to vary that much, keeping the p*K*a values within 0.73 units for PA-**1.4**, PA-**1.5**, PA-**1.6**, PA-**1.7** and PA-**1.8**. For these catalysts, the authors claim that because the aryl groups are not conjugated to the

active site, similar p*K*a values are obtained; thus, the differences ought to be caused by the steric environment. Yet, it is not entirely clear how the remote trifluoromethyl groups in PA-**1.2** strongly influence the acidity. Despite the useful trends observed in this acidity scale, it is rather limited to a few PAs. Only one example was reported in the publication for NTPAs as well as for *bis*(sulfonyl) and *bis*(sulfuryl)imides.

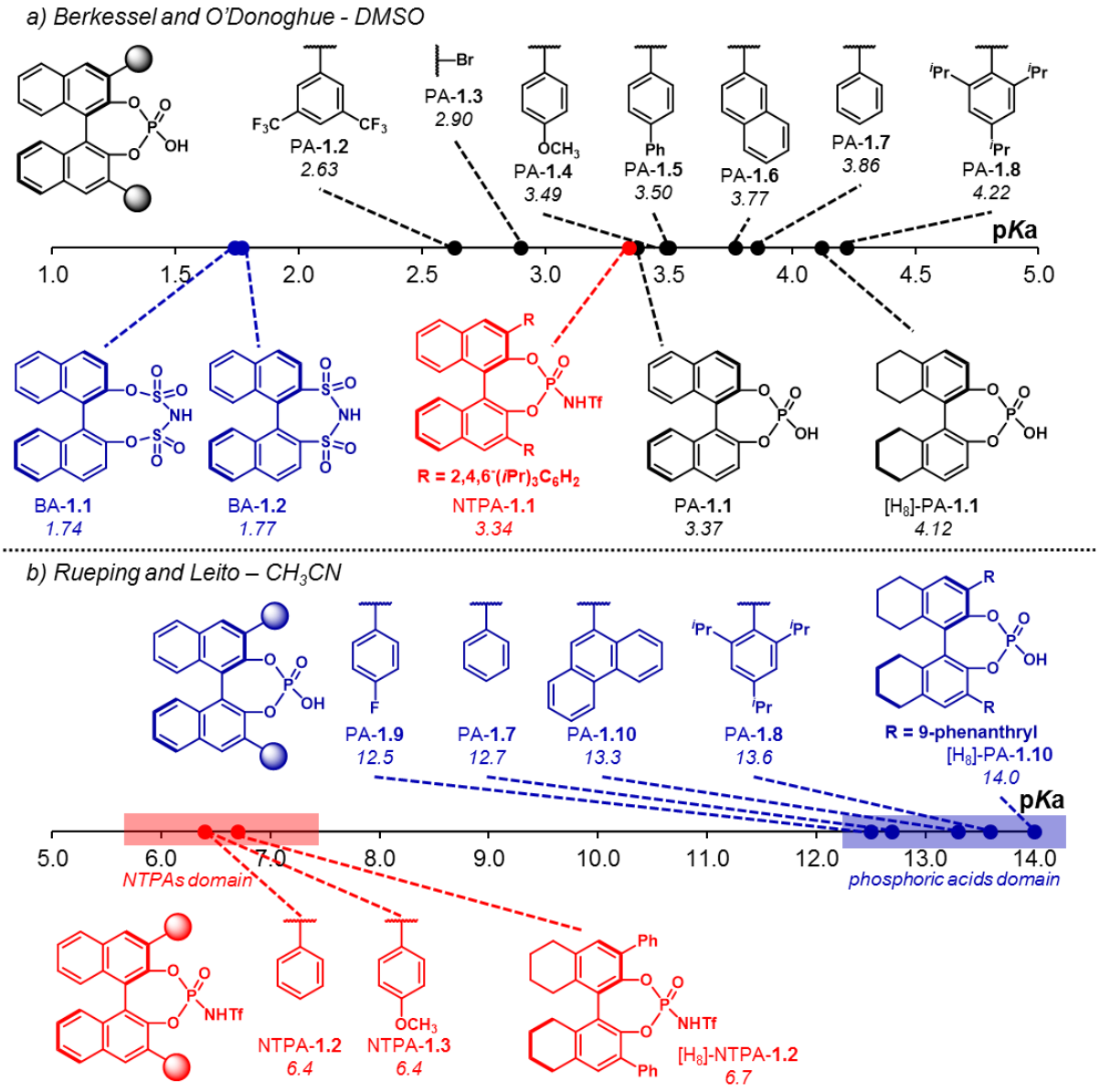

Scheme 1.3: Experimentally determined acidity scales for Brønsted acids. a) Berkessel and O'Donoghue acidity scale determined in DMSO. b) Rueping and Leito acidity scale determined in acetonitrile.

The groups of Rueping and Leito built up another acidity scale, determined experimentally in acetonitrile (Scheme 1.3*b*).[42] In their experiments, they found that, in acetonitrile, PAs cover a range of p*K*a values from 12.5 to 14.0, whereas, the more acidic NTPAs comprise a 6.3 to 6.9 region of the scale. This shows, again, the higher acidity of NTPAs against PAs. For the p*K*a values of PAs, a similar trend to that found by Berkessel and O'Donoghue was observed. The more electron poor catalyst PA-**1.9** has a lower p*K*a, 12.5, than electron neutral PA-**1.7** and PA-**1.10** (12.7 and 13.3, respectively). The more sterically

demanding PA-**1.8** is slightly less acidic (p*K*a = 13.6). In addition, this study is in agreement with the fact that a hydrogenated BINOL-backbone decreases the acidity of the catalyst, in this case by 0.7 p*K*a units, as shown by PA-**1.10** and [H_8]-PA-**1.10**. This is also the case for NTPA-**1.3** and [H_8]-NTPA-**1.3**, yet, the decrease in acidity is only about 0.3 p*K*a units, suggesting that, perhaps, the resonance effect is stronger in NTPAs than in PAs. Moreover, for NTPAs, the electronic nature of the 3,3' substituents seems to have little or no effect in the catalyst's acidity, as shown for NTPA-**1.2** and NTPA-**1.3**, which both have a p*K*a=6.4.

In the latter acidity scale, the authors also determined the rate constants for a Nazarov cyclisation using the catalysts under study. They found a linear correlation between the catalyst's p*K*a and –log(*k*) for the reaction. This implies that a more acidic catalyst gave a faster reaction rate. Thus, activation of the substrates is more efficient with lower p*K*a Brønsted acids—enantioselectivity, on the other hand, depends on the catalyst architecture.

In contrast to an acidity/reactivity scale defined by p*K*a values, the group of Franz proposed an alternative hydrogen-bonding scale based on ^{31}P-NMR shifts.[51] In their work, the authors showed that 3,3'-substituents with electron withdrawing motifs increase the hydrogen bond donor character of PAs. In addition, their NMR shifts measurements, relative to triethylphosphine oxide as H-bond acceptor, showed a better correlation of H-bond ability with catalytic activity than p*K*a values. Despite their report comprises a set of 66 H-bond donors, it only considers three PAs and no NTPAs.

Taking a hydrogenation reaction of imines as a model reaction and substrate, the group of Gschwind developed an internal acidity scale.[52] They found that the internal acidity in PA-imine complexes correlates closely with reactivity, which also depends on the *(E)*/*(Z)* geometry of the imine. Using ^{1}H and ^{15}N NMR and $^{1}J_{NH}$ coupling constants they established that the interactions in the catalyst-substrate complex are essential to describe acidity. However, this seems not to be applicable for catalysts with a heavily congested active site.

Apart from experiments, computational methods have become increasingly popular for the calculation of p*K*a values, as they offer a good alternative when experimental data is not available. The groups of Lin and Chen developed such an acidity scale for PAs using calculated p*K*a values, derived from a thermodynamic cycle, at the SMD(DMSO)/M06-2X/6-311++G(*2df*,*2p*) // B3LYP/6-31+G(*d*) level of theory (Scheme 1.4).[53] With their calculated p*K*a values, they showed how acidity varies when changing heteroatoms in the active site of the catalyst, that is, replacing the P=O moiety in PA-**1.1** for P=S or P=Se. As expected, it was found that the p*K*a decreases when going from PA-**1.1** (3.37) to thioPA-**1.1** (1.08) to selenoPA-**1.1** (-1.21). The same trend was found for NTPA-**1.4** (-3.40), thioNTPA-**1.4** (-3.83) and selenoNTPA-**1.4** (-4.58) in a different study.[54] In addition, changing the –OH moiety in PA-**1.1** for –SH leads to a dramatic decrease of 6.21 p*K*a units (thioPA-**1.1'** p*K*a=-2.84). Substituting both oxygen atoms in the active site for sulfur increases acidity even more (dithioPA-**1.1** p*K*a=-4.21). That places these last two catalysts within an acidity range similar to NTPAs.

Further, this computational method was used to calculate p*K*a values of PAs and NTPAs with other chiral frameworks, different from BINOL. In the case of PAs, it was found that the SPINOL backbone in SPA-

1.1 increased the p*K*a to 4.20 (PA-**1.1** p*K*a=3.37). Moreover, the partially hydrogenated BINOL backbone further increased the p*K*a of [H_8]-PA-**1.1** to 4.61. Such observation is in accordance with the experimentally determined p*K*a values in DMSO. For the case of NTPAs, a partially hydrogenated BINOL also increases the p*K*a by 0.7, again in agreement with experimental values. Conversely, a SPINOL framework enhances the acidity of the catalyst in comparison with the parent BINOL-NTPA (SNTPA-**1.4** p*K*a=-3.76 against NTPA-**1.4** p*K*a=-3.40), albeit in a small amount.

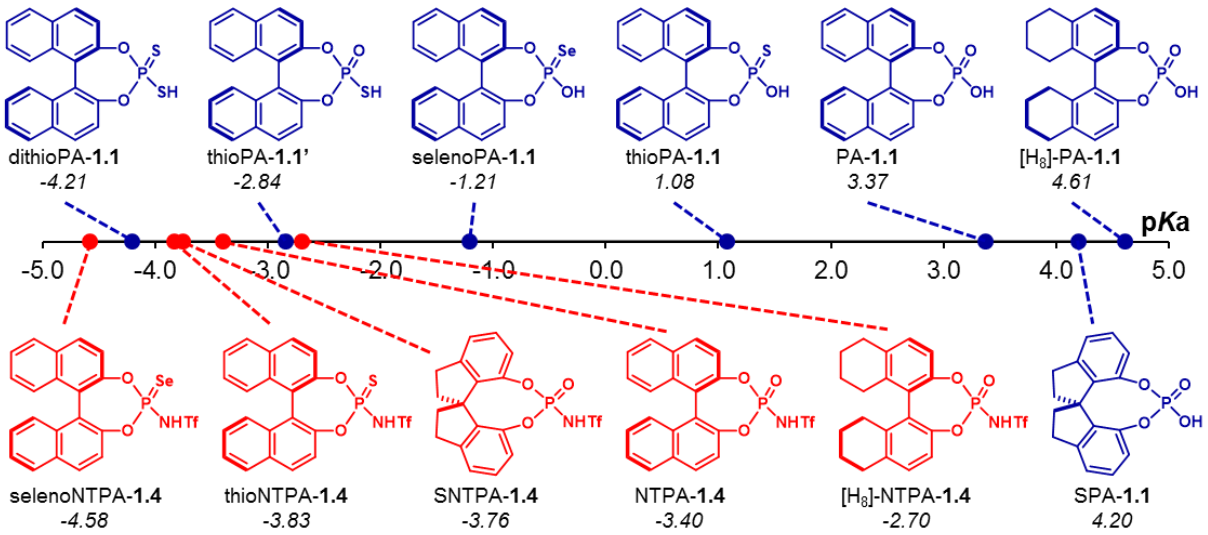

Scheme 1.4: Acidity scale calculated by the groups of Li and Chen at the SMD(DMSO)/M06-2X/6-311++G(*2df*,*2p*) // B3LYP/6-31+G(*d*) level of theory.

In addition, the authors calculated the p*K*a values for three 3,3' disubstituted NTPAs (Figure 1.4). As expected, the p*K*a values did not vary too much, staying in a -3.88 to -3.08 range. However, it was found that electron-withdrawing substituents enhance the acidity of the catalyst, in comparison to electron donating ones.

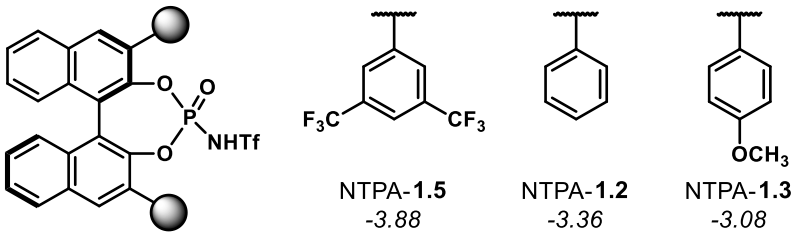

Figure 1.4: Calculated p*K*a values for 3,3'- disubstituted NTPAs.

This last acidity scale shows the power of computational chemistry while accounting for catalytic activity. From a different perspective, the group of Barroso-Flores calculated the surface maximum electrostatic potential at the acidic hydrogen atom for a series of carboxylic acids and used it as an alternative physical chemical descriptor for acidity.[55] Such calculations require only a small fraction of time in comparison to a full thermodynamic cycle, thus, offering a time-efficient method for Brønsted acids. In addition, this methodology proved to be robust, when used to calculate minimum surface electrostatic potentials in

order to determine p*K*b values and isoelectric points in aminoacids.[56] Such approach has not been applied to PAs or NTPAs yet, and it could offer an alternative acidity descriptor for catalyst activity.

The aforementioned acidity scales highlight the correlation of p*K*a with catalyst activity. Yet, as previously discussed, enantioselectivity still remains up to the catalyst architecture; in the case of BINOL-based Brønsted acids, to the substituents in the 3,3'- positions.

1.4. Activation modes and enantioinduction

As discussed in the last section, the acidity of the catalyst is a suitable parameter to evaluate its activity. The more acidic the catalyst, the faster a reaction would go. Therefore, such a knowledge of acidity scales is important in order to study the mechanisms in which the catalyst activates the substrates. On the other hand, enantioinduction depends on the shape of the chiral pocket created by the 3,3' substituents. Most of the time, explaining how enantioselectivity arises is complex. Much computational effort has been devoted to understand that.

The catalyst—active site and chiral framework—can be drawn in one of the ways presented in Figure 1.5. The right projection simplifies the naphthyl groups as well as the 3,3' substituents. This projection can be used to explain both how the substrates are activated and, in a qualitative picture, how the chiral pocket controls enantioselectivity. The group of Goodman has used this representation extensively to illustrate enantioselectivity in several reactions, including asymmetric allylboration of ketones,[57] addition reactions of imines,[58,59] enantioselective Friedel-Crafts reactions of indole with imines,[60] asymmetric allylboration of aldehydes,[61] asymmetric propargylation of aldehydes and ketones,[62,63] asymmetric boronate additions,[64] and Pictet-Spengler reactions.[65]

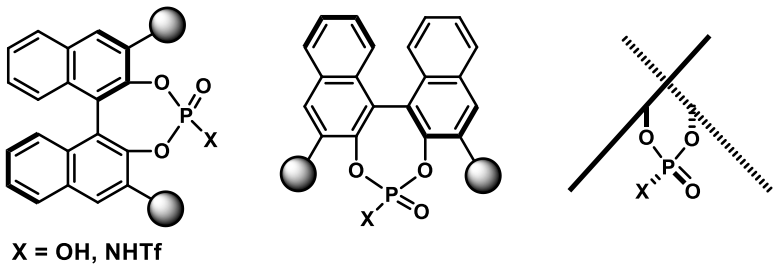

Figure 1.5: Different representations of BINOL-based PAs and NTPAs. The left representation is the most commonly used, as it shows the axial chirality in the catalyst, unambiguously. The representation in the centre, highlights the active site. This one is less used. The right projection places the viewpoint across the C_2 axis of the catalyst and allows sketching the active site and the chiral pocket in a way to be used to qualitatively account for enantioinduction without the need of sophisticated calculations.

Different activation modes have been proposed and studied. The most common ones are summarised in Figure 1.6. Given that imines are the most widely used substrates in PA or NTPA-catalysed reactions, these activation modes are clearly exemplified with imines as substrates.

The first of these activation modes arises when the catalyst forms one or two hydrogen bonds to one of the substrates (Figure 1.6*a*). For example, in **1.22**, the imine forms a hydrogen bond with the N-H moiety to one of the oxygen atoms in the phosphate group. Herein, due to the *(E)*-geometry of the iminium, one hydrogen bond is formed. However, in the case of **1.23**, the *(Z)*-imine can form two interactions with the catalyst active site. Apart from the N-H···O-P hydrogen bond, a second non-classical hydrogen bond is formed between the phosphate group and the C-H formyl-like hydrogen atom in the imine—due to the double bond geometry, such an interaction is not possible with an *(E)*-iminium ion. When using NTPAs as catalysts, this activation mode is preferred for aldehydes. In **1.24**, it is likely that the more acidic NTPA protonates the aldehyde. Therefore, two hydrogen bonds are formed: an OH···NTf and a non-classic one with the formyl C-H hydrogen atom.

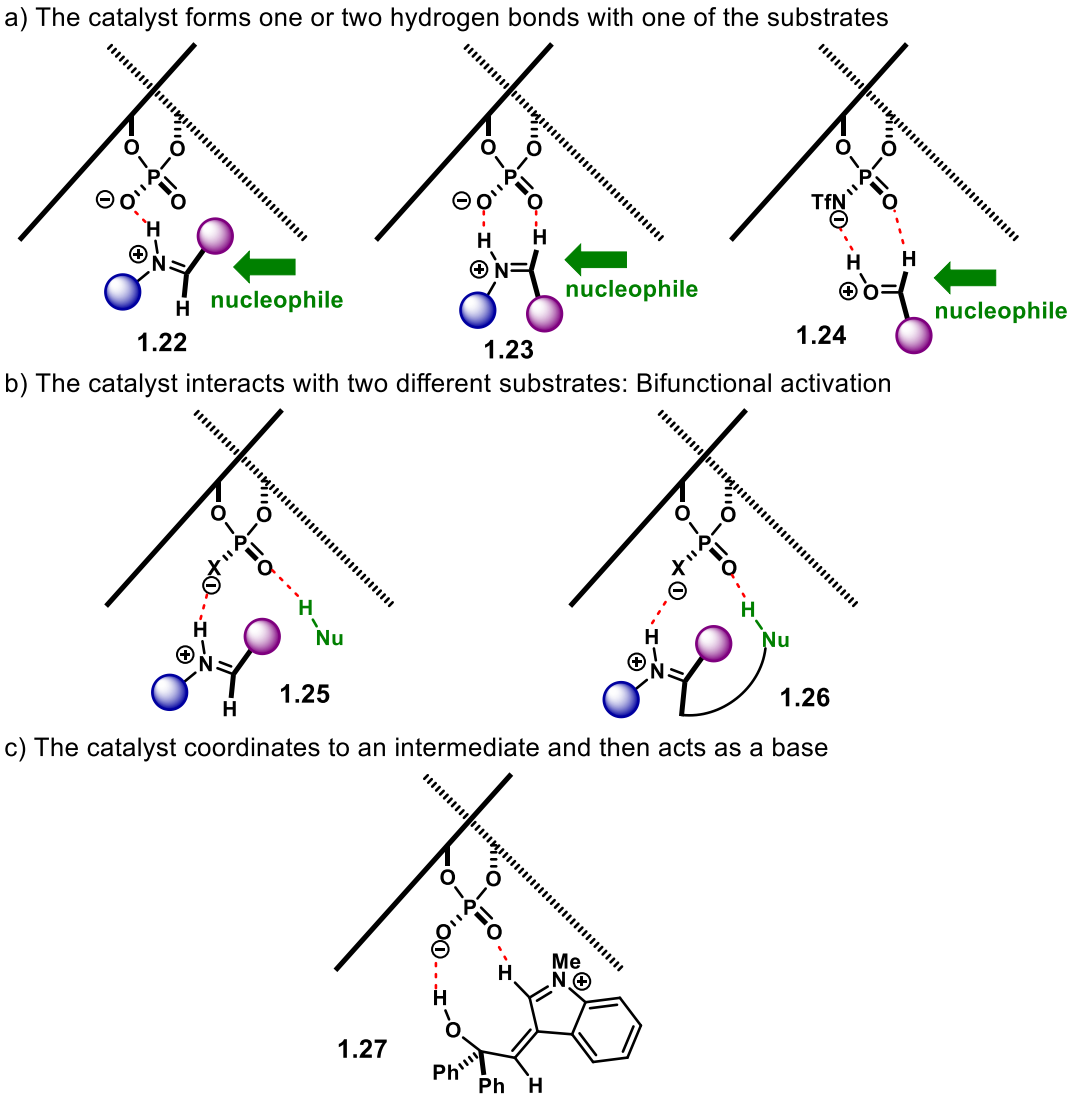

Figure 1.6: Activation modes for Brønsted acid-catalysed reactions. a) The catalyst forms one or two hydrogen bonds with one of the substrates; this is generally called a mono-activation mode. b) The catalyst interacts with two different substrates; this is a bifunctional activation mode. In this case, the nucleophile can be tethered to the electrophile to promote an intramolecular reaction. c) The catalyst coordinates to an intermediate and then acts as a base. This activation mode generally comprises rearomatisation or rearrangement steps.

Accounting for enantioinduction in a qualitative way can be clear with the projections presented. For a mono-activation mode, the substrate is locked into the catalyst's chiral cavity. Then, one of the 3,3' substituents blocks one of the reactive enantiotopic faces of the iminium or carbonyl; thus leaving the other face available for an incoming nucleophile. In the case of imines, the *(E)/(Z)* geometry would depend on a number of factors, including the relative size of the imine's substituents, the energy gap between the conformations of the *(E)* and *(Z)* geometries and the size of the catalyst's 3,3' scaffolds.[52,66]

In the second type of activation mode, the catalyst interacts with two different substrates (Figure 1.6*b*). Herein, two hydrogen bonds are formed. Such a bifunctional activation mode **1.25** has been used in order to account for high levels of enantioinduction in several reactions. This is because when the two substrates are attached to the catalyst's active site a rigid transition state would be favoured, thus allowing for efficient enantio-differentiation. In addition, the nucleophile can be tethered to the electrophile in an intramolecular reaction, **1.26**. This provides extra rigidity to the transition state in asymmetric ring-closing reactions.

Another activation mode arises when the catalyst coordinates to an intermediate and then acts as a base. This activation mode, as in **1.27**, is generally found in rearomatisation steps, desymmetrisations and rearrangements. Recently, the group of Grayson reported a computational study of a semi-pinacol rearrangement that features this activation mode.[67]

As mentioned in section 1.1, asymmetric transformations catalysed by PAs have been widely studied and reviewed. However, less attention has been devoted to NTPA-catalysed reactions. In this context, the following section comprises a review of NTPA-catalysed addition reaction to imines. Given that up to date, the number of NTPA-catalysed reactions is increasing exponentially, the focus of the next section will be on imines, highlighting the activation modes and, where possible, an explanation for enantioselectivity would be provided using the projections presented in Figure 1.6.[a]

1.5. Addition reactions to Imines catalysed by *N*-triflylphosphoramides

Nucleophilic additions to imines are, perhaps, the most widely exploited and studied reactions using PAs as Brønsted acid catalysts. The high basicity of the nitrogen atom in aldimines or ketimines makes them suitable substrates to be activated by PAs or NTPAs. Herein, for the case of NTPAs, the acidity of the catalyst plays a key role in activation. Due to their higher acidity, in comparison with PAs, full protonation is more likely to occur when NTPAs are used as catalysts. This section focuses on enantioselective addition reactions to imines using NTPAs as chiral Brønsted acids. Despite most of these class of transformations can be successfully achieved using PAs, for some substrates and reactions a more acidic catalyst was required, whether to enhance reactivity or to provide higher levels of stereocontrol.

[a] In addition to this thesis, a full review of NTPA-catalysed reactions was prepared, and is expected to be published in due course. Therein, the asymmetric transformations involving NTPAs from 2011 onwards are presented and discussed in full detail.

1.5.1. Aza-Darzens reactions

Aziridines are an important family of chiral building blocks, mostly used in the synthesis of enantioenriched amines. Therefore, asymmetric methodologies to obtain these three membered heterocycles are highly desirable. In this context, the aza-Darzens reaction utilises imines as starting materials to build up the aziridine core. The group of Maruoka reported a versatile enantioselective aza-Darzens reaction (Scheme 1.5).[68] Starting from *N*-Boc protected aldimines **1.28**, the reaction with α-diazo compounds **1.29** yields chiral trisubstituted aziridines **1.30** as single *trans*-diastereoisomers with excellent enantiocontrol. The 3,3'-diphenyl NTPA was selected as catalyst for this transformation. The high levels of diastereo- and enantiocontrol are remarkable for a catalyst that does not bear heavily bulky substituents in the 3,3'-positions. The reaction works well for *N*-Boc aryl aldimines bearing *meta* and *para* substituents. The oxazolidinone motif in the α-diazo compound was found to serve as an important template to improve reactivity.

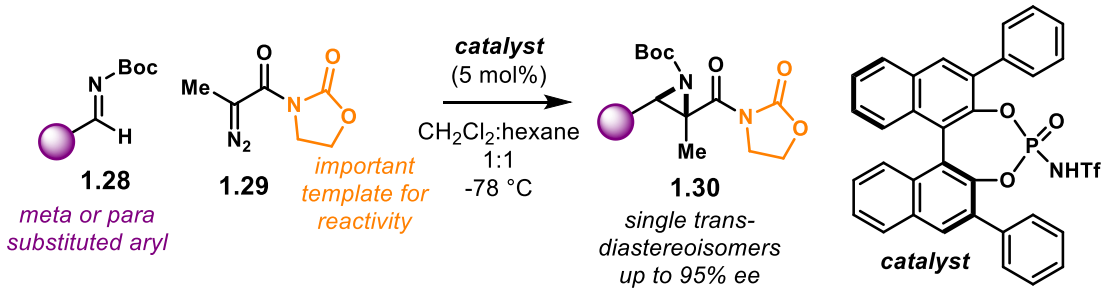

Scheme 1.5: Enantioselective synthesis of aziridines from *N*-Boc protected aldimines and α-diazo compounds, developed by the group of Maruoka.

PAs did not work for this transformation, which plausibly points out to the need of the fully protonated iminium ion **1.31** for the reaction to occur (Scheme 1.6). Given that the α-diazo compound cannot engage in hydrogen bonding with the anion of the NTPA, monoactivation of iminium is very likely to be happening. In addition, the use of low polarity reaction media strongly suggest a tight ion-pair as the reactive species. An alternative model like **1.32**, using a *(Z)*-iminium might be helpful to account for enantiocontrol.

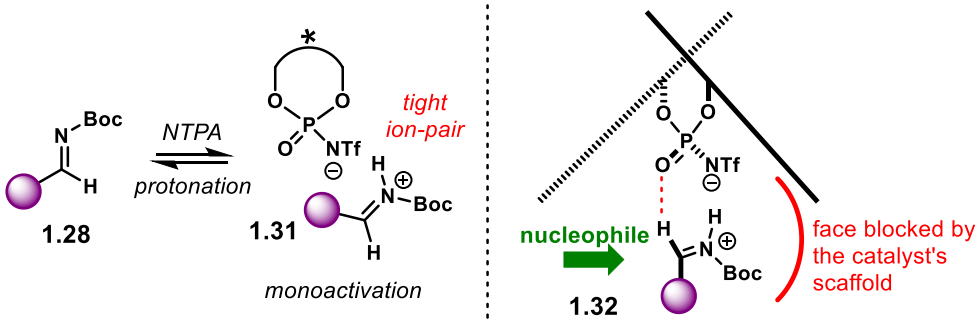

Scheme 1.6: Iminium activation mode and projection to explain enantioselectivity in a qualitative way.

In addition, a complementary route to tertiary substituted aziridines was also included in the same publication (Scheme 1.7). Using highly reactive ketimino esters **1.33** and α-unsubstituted diazo

compound **1.34**, aziridines **1.35** are obtained with excellent diastereo- and enantiocontrol. Exhaustive tuning of the substrate's structures had to be done to achieve the best reaction conditions. For instance, the *N*-Boc, *tert*-butyl ester and oxazolidinones motifs were found to be crucial. However, no detailed explanation is given.

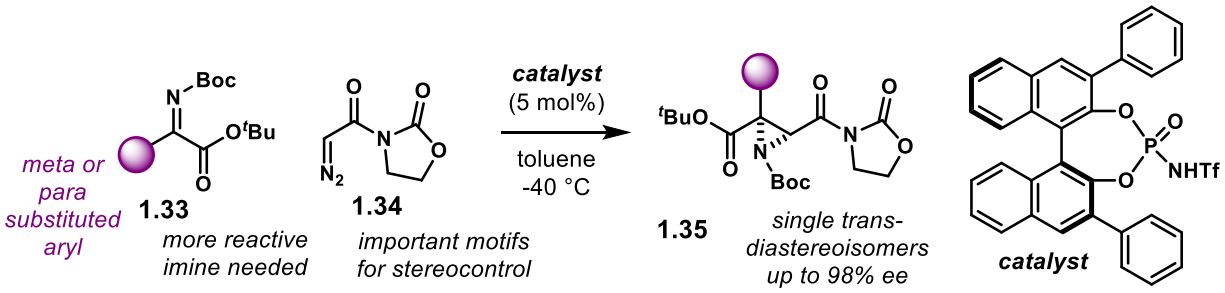

Scheme 1.7: Enantioselective synthesis of aziridines from ketimino esters and α-unsubstituted diazo compounds, developed by the group of Maruoka.

The group of Bew developed another enantioselective aza-Darzens reaction (Scheme 1.8).[69] As in the previously discussed one, PAs did not promote the addition at all. The more acidic 3,3'-*bis*(anthracenyl) NTPA was found to be the best catalyst in terms of reactivity and enantiocontrol. Therein, imines **1.36** react with α-diazo ester **1.37** to furnish *cis*-aziridines **1.38** as single diastereoisomers with excellent enantiocontrol. The reaction tolerates a wide variety of aryl and heteroaryl aldimines. The bulky 2-*tert*-butoxyphenyl *N*-protecting group was necessary to achieve outstanding enantioselectivities. In addition, the low catalyst loading, 1 mol%, is remarkable.

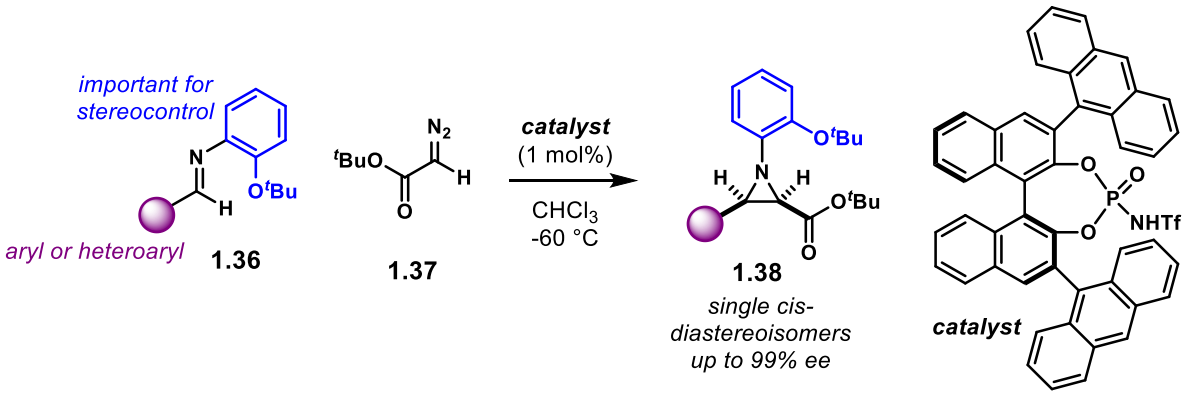

Scheme 1.8: Enantioselective synthesis of aziridines from aldimines and α-diazo compounds, developed by the group of Bew.

Mechanistically, imine **1.36** is protonated by the catalyst (Scheme 1.9). A tight ion-pair between iminium **1.39** and the NTPA anion is likely to be formed. Moreover, an intramolecular hydrogen bond is formed with the *tert*-butoxy motif in the *N*-protecting group. This hydrogen bond might also lock the conformation of the iminium ion and block one of the enantiotopic faces. This is important as the 1,2- addition step is both diastereo- and enantiodetermining, which has to occur through a monoactivation mode. With intermediate **1.40** formed, nitrogen extrusion, also possibly assisted by the NTPA anion, delivers product **1.38**. The two bulky *tert*-butyl groups in **1.40** have to be as far away from each other to avoid steric clash

in the addition step. This, as suggested by the authors, accounts for the high diastereoselectivity observed. It is, however, not entirely clear, how enantioinduction arises.

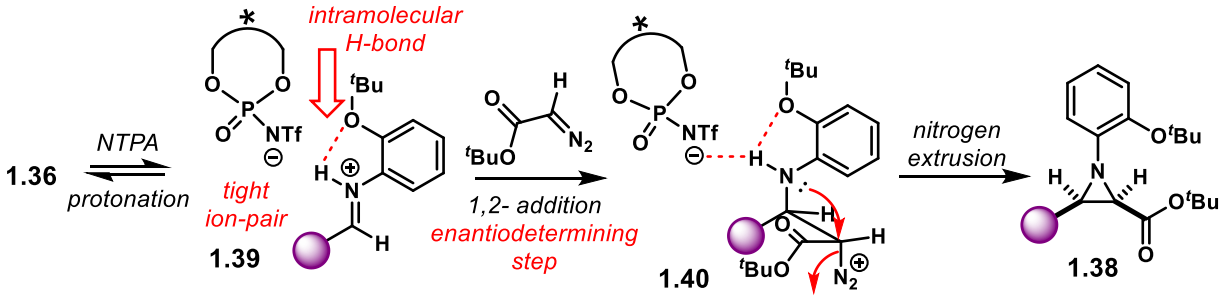

Scheme 1.9: Mechanism and activation mode for the aza-Darzens reaction reported by the group of Bew.

This methodology can be performed either with preformed imines or in a one-pot, two-step sequence. This is highlighted in the same publication with a short enantioselective synthesis of (+)-Chloramphenicol **1.44** (Scheme 1.10). The synthesis uses this new methodology as the key step to set up both of the stereocentres in the molecule. Starting with *p*-nitrobenzaldehyde **1.41** and aniline **1.42**, the corresponding imine is generated *in-situ*. Then, addition of **1.37** affords *N*-protected aziridine **1.43** in 99% yield and 96% *ee* as key intermediate. Further steps furnish (+)-Chloramphenicol **1.44**.

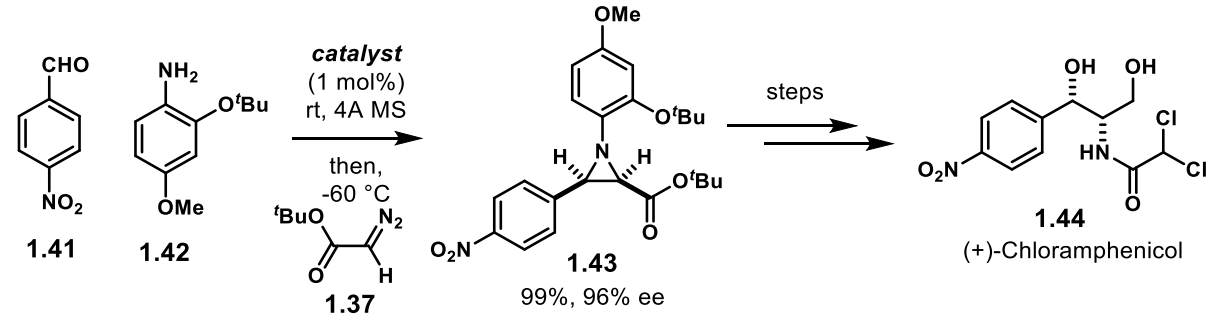

Scheme 1.10: A short, enantioselective synthesis of (+)-Chloramphenicol.

1.5.2. Reduction reactions

The field of asymmetric reductions of imines is mainly dominated by PAs. Such catalysts are acidic enough to activate the substrates and achieve remarkable levels of enantiocontrol. Therefore, limited examples of catalytic reductions using NTPAs have been reported to date.

The group of Enders reported one example of an NTPA-catalysed reduction (Scheme 1.11*a*).[70] In the reaction, methyl ketimines **1.45** react with catecholborane to afford secondary amines **1.46** in modest enantioselectivities. Several parameters of this reaction were studied in detail. The benzyl *N*-protecting group in the imine was found to get the best reactivity/enantiocontrol balance. The substrate scope is, however, limited to aryl methyl imines. Catalyst *(R)-NTPA*-**1.1** achieved the highest enantioselectivities. PAs did catalyse the reaction affording comparable yields but with diminished enantiocontrol. This fact suggests that an activation mode different from protonation might be operating. The authors propose that

the actual active catalyst is an NTPA-borane complex (**1.47**, Scheme 1.11*b*). Such complex might then serve as a Lewis acid to activate the imine. Bifunctional activation of both the imine and the reducing agent triggers the reaction. The authors also suggest that the *(E)/(Z)* ratio of the imine might affect the observed enantioselectivity, yet, this was not clarified.

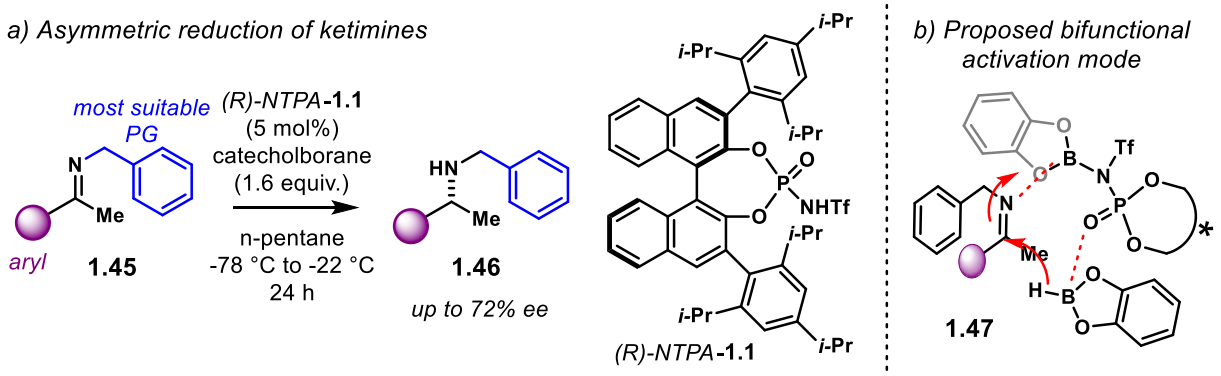

Scheme 1.11: a) Asymmetric reduction of ketimines using catecholborane, reported by the group of Enders. b) Proposed bifunctional activation mode. Herein, the NTPA-borane complex serves as the catalytic species.

1.5.3. Mannich-Mukaiyama reactions

The Mannich reaction is an outstanding method to make C-C bonds while installing an amine motif.[19] The use of iminium ions in this transformation makes it suitable for an asymmetric NTPA-catalysed version. The groups of Kano and Maruoka reported an enantioselective Mannich-Mukaiyama reaction (Scheme 1.12*a*).[71] This transformation also features an *(E)*-selective double bond isomerisation. The reaction presents *(Z)*-substrates **1.48** as key Mannich precursors and Mukaiyama reagents **1.49** to afford products **1.50** with excellent enantiocontrol and up to 1:20 *(Z)*/*(E)* ratios. A partially hydrogenated BINOL-backbone NTPA was used as catalyst. In the reaction mechanism, precursor **1.48** is protonated by the NTPA (Scheme 1.12*b*). Elimination of a $BocNH_2$ motif in **1.51** might be assisted by hydrogen bonding to deliver iminium ion **1.52**. Isomerisation of the double bond is likely to occur at this stage of the reaction. Enantioselective 1,2- addition to the iminium ion with subsequent loss of the TMS group gets the desired product.

Zhou and Yamamoto developed a series of highly acidic catalysts for Mannich-Mukaiyama reactions (Scheme 1.13).[72] Using an NTPA with *bis*(nitrated) 3,3' groups, they design an enantioselective Mannich-Mukaiyama reaction of *N*-phenyl imines **1.53** and ketene silyl ether **1.54** to furnish anilines **1.55** in good yields and up to 95% *ee*. This transformation features a carefully designed catalyst. The nitro groups in the 3,3' aryl scaffolds provide a higher acidity to the catalyst's active site. Moreover, the *para*- methyl group serves as a steric deadlock to keep the nitro moieties orthogonal to the aryl ring. This forces the oxygen atoms in the nitro groups to point towards the active site, increasing the acidity through an intramolecular hydrogen bonding. Furthermore, such oxygen atoms may serve as extra coordinating groups to stabilise any key intermediate.

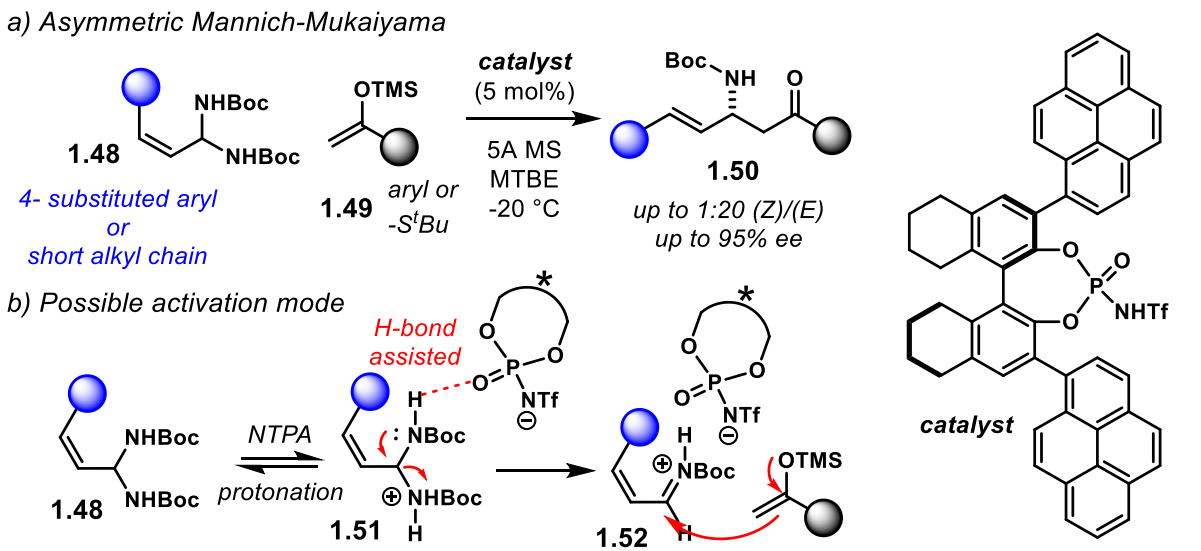

Scheme 1.12: a) Asymmetric Mannich-Mukaiyama reaction, developed by the groups of Kano and Maruoka. b) Possible mechanism and activation mode. Isomerisation of the double bond is likely to occur in the iminium ion prior to the nucleophile addition.

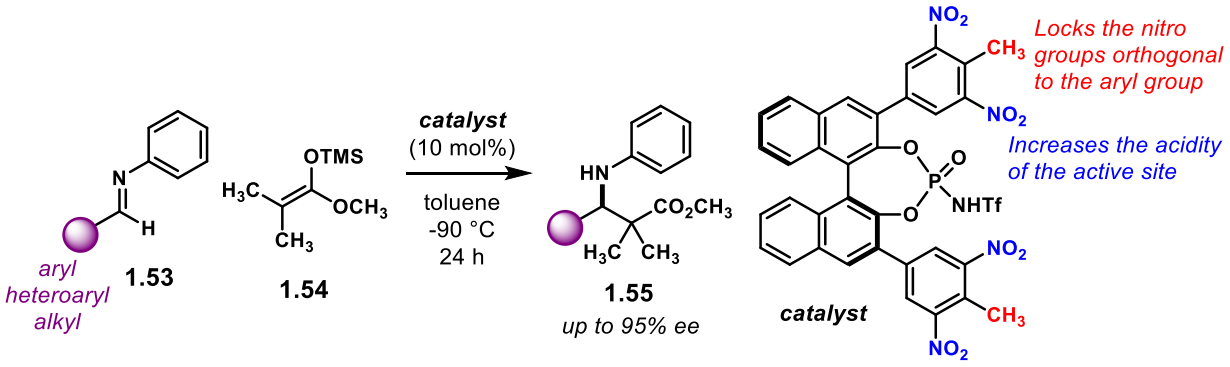

Scheme 1.13: Asymmetric Mannich-Mukaiyama reaction using highly acidic NTPAs developed by Zhou and Yamamoto.

1.5.4. Other Mannich-like reactions

The group of Jiang developed an exquisite asymmetric *aza*-Piancatelli/Friedel-Crafts cascade cyclisation (Scheme 1.14).[73] Nonetheless, the enantiodetermining step features a Mannich-like addition. The reaction uses furans **1.56** and anilines **1.57** to furnish seven-member heterocycles **1.58** with excellent diastereo- and enantioselectivity (>20:1 *dr* and up to 97% *ee*). Furthermore, the final product features three contiguous stereocentres. A wide variety of substituted furans reacted to achieve excellent stereocontrol. Substitution in the aniline component is also tolerated. An NTPA with a partially

hydrogenated BINOL backbone was the best catalyst for this transformation. PAs did not promote the reaction at all.

Mechanistically, this is a very interesting transformation. The authors did not account for the observed diastereocontrol. However, I propose a mechanism as well as a plausible activation mode of the reacting species (Scheme 1.15). Initially, protonation and subsequent dehydration of **1.56** yields cationic intermediate **1.59**, possibly stabilised by ion pairing. Addition of aniline **1.57** furnishes hemi-aminal **1.60**. Ring opening, presumably facilitated by protonation, leads to enol-iminium ion **1.61**. Double hydrogen bonding to the catalyst active site would sit the substituents in the reacting faces *anti-* to each other. In this case, the chiral pocket must be tight enough to lock this conformation, accounting for the remarkable enantiocontrol and the *anti-* relationship. After this Mannich-like ring closure, the catalyst might still be locking intermediate **1.62**, which resembles an activated α,β- unsaturated carbonyl compound. Moreover, from such conformation, it can be accounted for the other observed *syn-* relationship. Subsequent attack of the pyrrole motif triggers the Friedel-Crafts stage of the cascade in a highly diastereoselective fashion, further leading to product **1.58**.

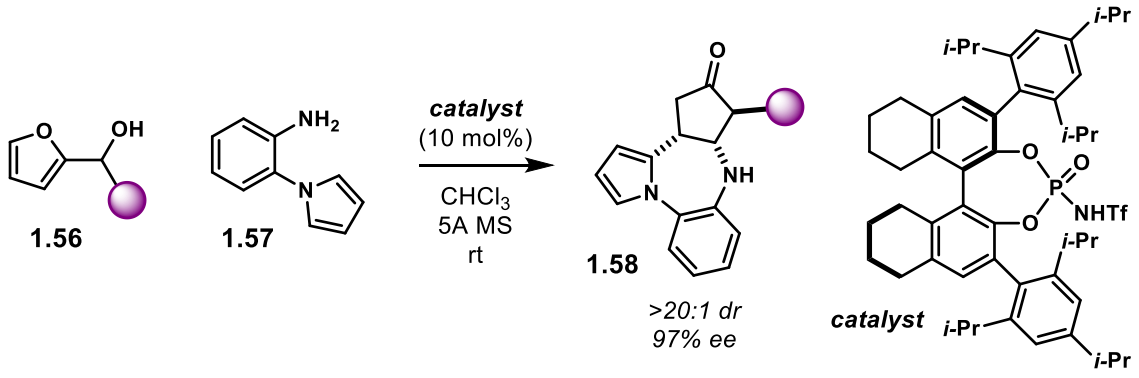

Scheme 1.14: Asymmetric *aza*-Piancatelli/Friedel-Crafts cascade cyclisation developed by the group of Jiang.

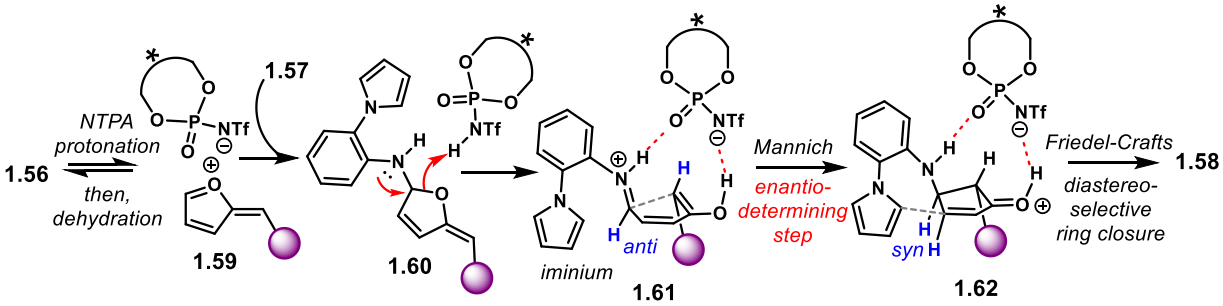

Scheme 1.15: Proposed reaction mechanism and activation mode for the reaction reported by the group of Jiang.

To finalise this section on addition reactions to imines, a metal NTPA-catalysed Mannich reaction was reported by the group of Smith (Scheme 1.16).[74] This transformation uses starting material **1.63** and aldehydes **1.64** to furnish enantioenriched quinolones **1.65** as single diastereoisomers. PAs were tried as catalysts, however, low reactivity was observed. On the other hand, the reaction gave higher yields, albeit with modest enantiocontrol, when the copper(II) salt of *(R)-NTPA*-**1.1** was used. The dimethylamido motif on **1.63** was found to be essential for reactivity and stereocontrol, presumably, due to its

coordination ability to the copper(II) centre. The reaction worked reasonably well for several aldehydes. Aryl aldehydes gave low enantioselectivity, regardless the substitution on the phenyl ring. Conversely, alkyl aldehydes were shown to improve enantiocontrol. Bulky substrates like cyclohexancarbaldehyde or pivaldehyde were beneficial. In addition, the low catalyst loading, 1 mol%, is remarkable.

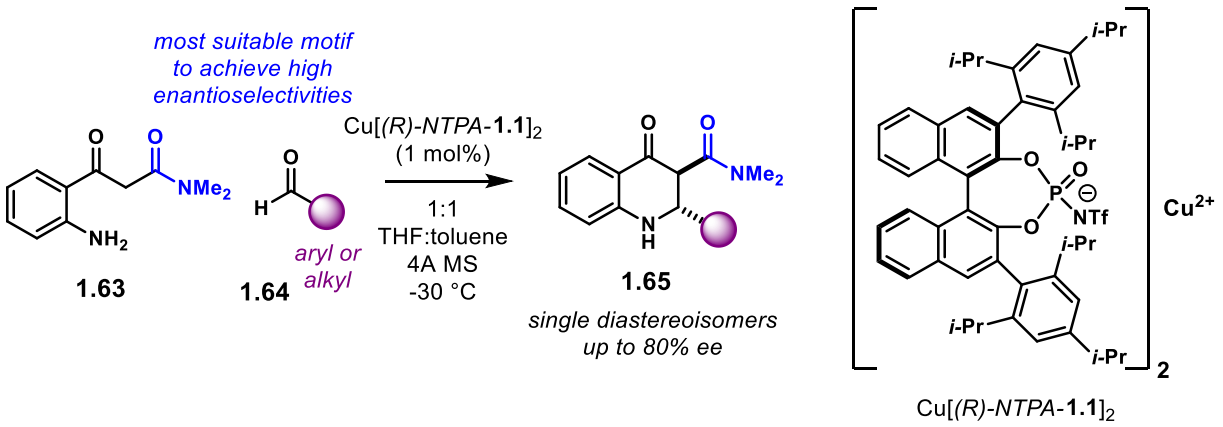

Scheme 1.16: Enantioselective copper(II)-NTPA Mannich reaction, developed by the group of Smith.

This reaction uses the actual copper(II) *N*-triflylphosphorimidate, therefore, the reaction mechanism is expected to be different from that of NTPAs in the free acid form. Initially, imine **1.66** is formed out of the corresponding starting materials (Scheme 1.17). A Knoevenagel condensation was shown not to be operational. Then, as suggested by the authors, deprotonation of **1.66** generates copper(II) enolate **1.67**. One of the NTPA anions serves as chiral ligand for the copper centre. At the same time, the other anion activates the imine through iminium-tight ion pairing in a Brønsted acid-like fashion. Subsequent cyclisation and epimerisation of **1.68** yields product **1.65**.

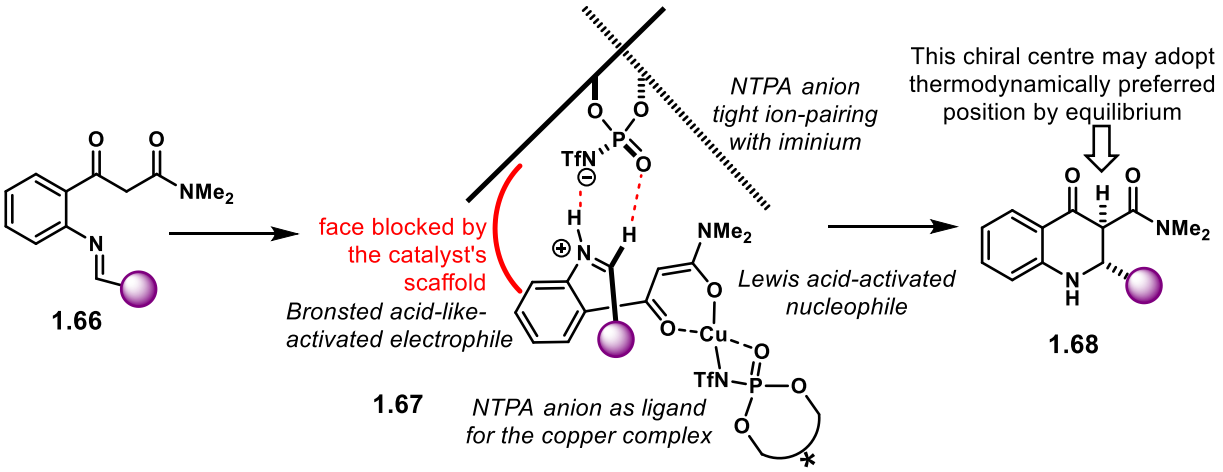

Scheme 1.17: Suggested mechanism for the Mannich reaction reported by the group of Smith. The enantiodetermining step is controlled by the two NTPA anions, each of them serving distinct modes of activation. However, a projection like in **1.67** accounts for the stereochemical output in **1.68**. Therein, it seems plausible that the iminium adopts a *(Z)* geometry to engage with the catalyst *via* two hydrogen bonds.

1.6. Thesis scope and overview

The following chapters comprise a detailed account of the work done throughout my PhD. I tried to write the chapters in such a way that they can be read as independently as possible from each other, yet, trying to unify them through the main research topic: chiral Brønsted acid-catalysed reactions. Several projects were conducted throughout my PhD, I tried to devote one chapter for each of the projects.

Chapter 2 comprises the synthesis of BINOL-based Brønsted acids, both PAs and NTPAs. The highlights of this chapter include the synthesis of heavily hindered PAs with silicon-based scaffolds in the 3,3'-positions. The featured scaffolds were proposed from molecular mechanics conformation searches and from DFT calculations—the latter, in collaboration with JP Reid in the Goodman group. Therein, a synthetic methodology to install such groups was developed. In addition, a new type of 3,3'- substituents, based on aryl sulfones, was designed. In this case, a new route for the synthesis is covered.

In chapter 3, an asymmetric synthesis of 1,3-oxathiolanes is discussed. The chapter starts with an introduction about sulfur-containing heterocycles with one or more stereocentres. The medicinal applications of such compounds are briefly described, as well as recent catalytic asymmetric reactions using Brønsted acids to afford sulfur-containing compounds. The main body of this section comprises the optimisation of a reaction to make 1,3-oxathiolanes in an enantioselective fashion. However, the study focuses on the Brønsted acids themselves. For instance, on how the catalyst loading and the acidity of the catalyst have a tremendous influence in the reaction output.

Moving on with PAs and NTPA-catalysed reactions, chapter 4 is devoted to the synthesis of nitrogen-containing heterocycles using iminium ions as key intermediates—this is the largest chapter of my thesis. It also contains several brief introductory sections to present to the reader the relevance of the compounds that were attempted to synthesise. The chapter begins with the design of an asymmetric imino-Diels-Alder reaction. This one was inspired by previous publications and computational modelling that I conducted myself. Throughout this reaction, several modifications to the substrate had to be made, as the reaction was proved to be challenging. One of such modified substrates led to the discovery of a process to synthesise complex polyheterocycles with five chiral centres as single diastereoisomers—herein I want to thank A Howarth in the Goodman group for his help and assistance with the DP4-AI computations to elucidate the relative stereochemistry of the product. The enantioselective version of that reaction, using PAs and NTPAs, proved to be feasible. Based on the observed reactivity patterns from the previous reaction, a Brønsted acid-catalysed Pictet-Spengler reaction was designed. Several parameters were evaluated to make the molecules presented therein. Such include catalysts' acidity and loading, electronic and steric structure of the substrates, reaction time, temperature and additives employed. After several attempts, an asymmetric synthesis of seven-membered nitrogen and oxygen-containing heterocycles is presented—10,11-dihydrodibenzo[*b,f*]-[1,4].oxazepine as the core structure.

The final chapter, chapter 5, comprises a detailed computational study of an enantioselective aza-Darzens reaction reported by the group of Akiyama. State-of-the-art computational techniques were used to model and study the reaction—amongst them, the ONIOM method was used to model the transition

states of the reaction. This transformation features a heavily hindered PA as the catalyst, which bears silicon-based scaffolds at the 3,3'-positions. Thus, modelling this reaction would be complementary to the experimental design of that type of catalysts. A good agreement between the calculated and experimental enantiomeric ratios and sense of enantioinduction was obtained. In addition, after thorough conformation searches and transition state modelling with simplified substrates and catalyst, an alternative activation mode was envisaged. Such activation mode involves a non-classical hydrogen bond from the catalyst's anion to the intermediate iminium ion and was found to be lower in energy than the initially proposed activation modes for imines (*cf.* Figure 1.6).

This series of projects show how versatile Brønsted acids are. However, it is also highlighted one of the inherent difficulties in enantioselective organocatalytic reactions. The main bottleneck in enantioselective reaction discovery is the catalyst choice, as several PAs or NTPAs must be screened in order to achieve high levels of enantiocontrol. This is far from trivial. Not only the catalyst itself but also the structure and electronic properties of the substrates play a crucial role.

Finally, computational methods are a powerful tool that helps to explain the output of enantioselective reactions. Despite the current computational power available, most of chiral Brønsted acids have a complex and large molecular structure, making transition state modelling challenging and time-consuming. Nevertheless, experiment and computation is a valuable dyad to understand chemical reactions.

Chapter 2

Synthesis of BINOL-backbone Brønsted Acids

2.1. The General Picture

The common precursors leading to both PAs and NTPAs are 3,3' disubstituted BINOLs **2.1** (Scheme 2.1). Several catalysts with an impressive variety of 3,3' scaffolds have been reported in the literature. However, the most popular ones are those where the aforementioned substituents are aryl motifs. An exhaustive list of aryl-based PAs can be found in the reviews published by the groups of Rueping[16] and Lin.[31] In addition, silicon-based scaffolds have been introduced; however, not too many catalysts bear these class of substituents. Later in this chapter, in section 2.4, such type catalysts are discussed. In addition, an improved methodology to install these relatively larger scaffolds is presented. Moreover, sulfone-based substituents have not been reported for PAs or NTPAs. In section 2.5, *bis*-sulfonylated catalysts are added to the list of BINOL-based Brønsted acids.

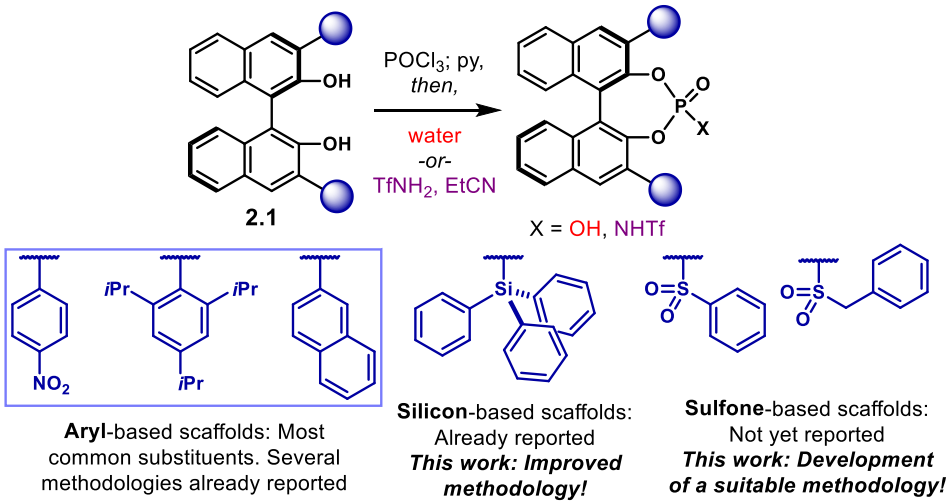

Scheme 2.1: BINOL-based Brønsted acids. Aryl-based scaffolds are the most widely used, followed by silicon-based substituents. Sulfone-based Brønsted acids have not yet been reported, in this work a simple methodology to install the sulfone motifs in the 3,3' positions is envisaged.

Syntheses of aryl-based Brønsted acids are widely reported. Several methods can be utilised in order to install such groups in the BINOL framework. A general procedure is shown in Scheme 2.2. The most common route to BINOL-based Brønsted acids starts with a MOM-protection of *(S)*- or *(R)*-BINOL **2.2** to deliver *bis*-protected BINOL **2.3**. After that, an *ortho* lithiation-iodination sequence installs iodine functionality at the 3,3' positions. Protected precursor **2.4** can then undergo a Suzuki cross-coupling reaction with an aryl boronic acid in order to install the aryl scaffolds, thus affording **2.6**. However, a Kumada cross-coupling reaction, which uses the corresponding Grignard reagent made out of the aryl bromide, is required for heavily hindered scaffolds. Alternatively, the *ortho* lithiation sequence can be used to install a boronic acid functionality in the BINOL framework and undergo a Suzuki cross coupling

of **2.5** with an aryl bromide or iodide. With the 3,3' substituents in place, MOM- deprotection of compound **2.6**—generally reported using aqueous HCl—affords the common 3,3' disubstituted BINOL precursor **2.1**. This, now can be transformed whether into PA **2.7** or NTPA **2.8**.

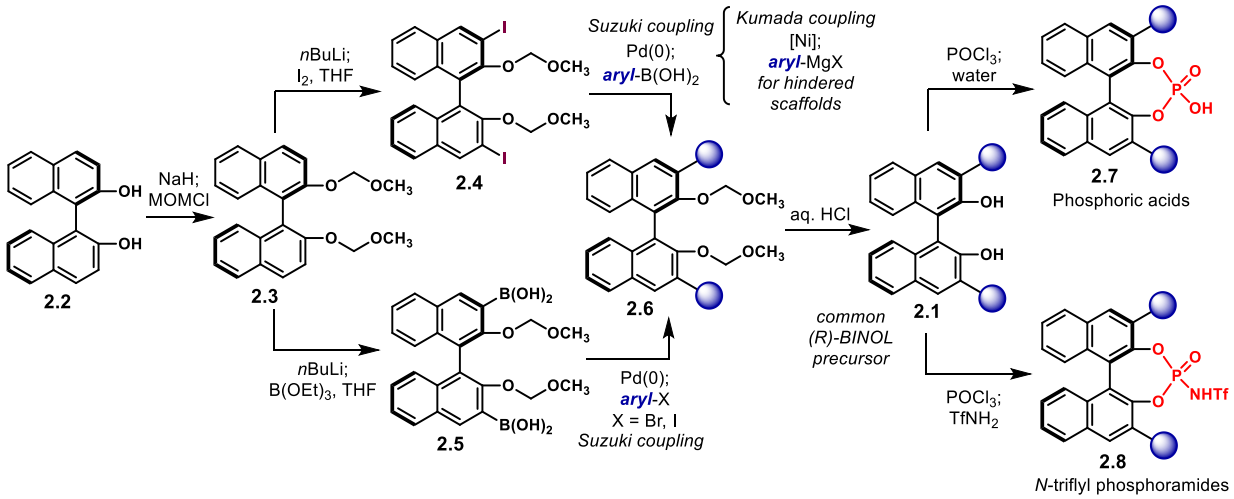

Scheme 2.2: Most popular procedure to synthesise BINOL-Brønsted acids.

2.2. The Catalyst's Active Site

Installing the active site in PAs has few variations amongst the reported methodologies (Scheme 2.3). Most reported syntheses of PAs from BINOLs **2.1** utilise phosphorus (V) oxychloride as the phosphorylating reagent. Pyridine is used both as a base and as a solvent for the reaction. Occasionally, chlorinated solvents, like CH_2Cl_2 are also suitable. For those cases, an *N*-base is needed to promote the reaction. Amongst such bases, triethylamine, DIPEA or DMAP are often used. DMAP is a convenient base—used in conjunction with pyridine—when heavily bulky scaffolds are present. Reaction temperature depends mostly on the size of the 3,3' substituents. Small groups may react even at room temperature. On the other hand, harsher conditions, like refluxing pyridine at 115 °C, are needed to achieve full consumption of the starting material.

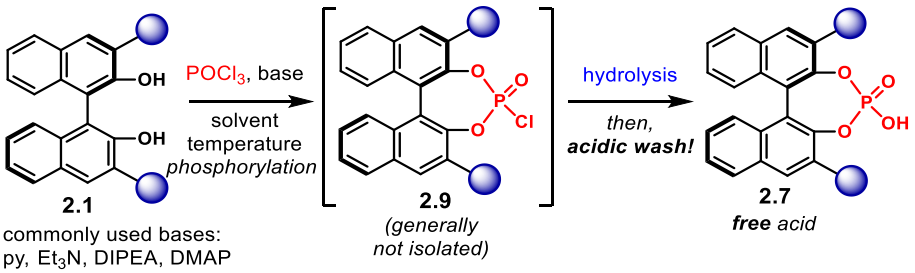

Scheme 2.3: Installing the active site in PAs.

This initial step delivers phosphoryl chloride **2.9**, which in most of the cases is not isolated. After that, hydrolysis affords PAs **2.7**. For this last step, high temperatures are often required. In most of the cases,

water alone would hydrolyse the chloride. However, it is also common to use refluxing aqueous HCl for the same purpose.

During the work-up stage, it is important to remove all pyridine if used as solvent. A thorough reverse extraction with aqueous HCl gives good results. This delivers the PA in its free, fully protonated form. However, further purification is usually required. PAs can be readily purified through column chromatography. The main drawback of this method is that the resulting PA comes out contaminated with metal impurities from the silica gel, and the isolated product is generally a metal phosphate instead of the free acid.[75] This can have dramatic effects in reactivity and enantiocontrol.[76–78] In addition, Simón and Paton have conducted computational studies regarding the different stereochemical outputs when metal phosphates and PAs are used as catalysts.[79] Therefore, recovering the PA as its free form is paramount. An efficient way to do so after purification by column chromatography is through washing with aqueous HCl.[a] Recrystallisation is preferred if chromatography can be avoided.

The synthesis of NTPAs is not that different from that of PAs. Once the 3,3'- disubstituted BINOL **2.1** is prepared, the next step is to place the highly acidic *N*-triflylphosphoramide motif, *i.e.* the active site. Three main protocols are reported in the literature (Scheme 2.4).

Method A: Phosphorylation – triflamide addition

In the first methodology (Scheme 2.4*a*), phosphoryl chloride **2.9** is obtained in a similar fashion in which it is made for PAs. This chlorinated precursor is not isolated but reacted in the same pot with $TfNH_2$ using propionitrile as a high boiling point solvent. After work-up and purification, NTPAs **2.8** are obtained.[b] The main advantage of this protocol is its fast phosphorylation, as well as it avoids the use of pyridine. Moreover, as it is the most popular method to synthesise NTPAs, it is relatively well established.[74,80–83] On the other hand, large excess of organic bases are required in the first step (DMAP, 2.0 equiv. and Et_3N, 7.0 equiv.). In addition, the high temperatures and prolonged reaction times constitute the major drawbacks of this method.

Method B: Phosphoramidation – hydrolysis

This protocol (Scheme 2.4*b*), developed by the group of List,[84–86] uses *N*-triflylphosphorimidoyl trichloride ($Cl_3P{=}NTf$)[87,88] as phosphorylating agent to afford intermediate **2.10**. Subsequent hydrolysis yields NTPAs **2.8**. The much shorter reaction times, room temperature and high yields makes this protocol an incredibly appealing alternative. In addition, this method is not limited to triflylamide, other perfluorinated sulfonamides are also suitable substrates.[89,90] The use of strict anhydrous conditions and the synthesis of $Cl_3P{=}NTf$ may be the main disadvantage.

Method C: Phosphobromination – triflamide addition – oxidation

[a] There is not an exact procedure to do this. Some authors report that washing several times–four times at least–with 6N HCl recovers the acid in its free form. However, other publications suggest that washing only twice with 1N HCl might be sufficient.

[b] If column chromatography is used to purify the catalyst, the same aqueous HCl washing used for PAs must be done to afford the NTPA as the free acid.

Recently developed by the group of Terada,[91,92] this methodology comes as an appealing alternative to those ones previously discussed (Scheme 2.4*c*). Treatment of **2.1** with PBr_3 in pyridine affords intermediate **2.11**. Addition of triflamide readily displaces bromide to deliver compound **2.12** that is subsequently oxidised to NTPAs **2.8**. This one-pot procedure has the main advantage to be completed in a short reaction time—compared to method A, for instance. Yet, due to the last oxidation step, groups in the 3,3'- positions prone to oxidation are incompatible.

Furthermore, PAs **2.7** can be easily converted into the corresponding NTPAs **2.8** (Scheme 2.5). Reaction of **2.7** with either $POCl_3$ or oxalyl chloride furnishes phosphoryl chloride **2.9** which can be transformed into **2.8** with $TfNH_2$ in refluxing propionitrile.[93,94]

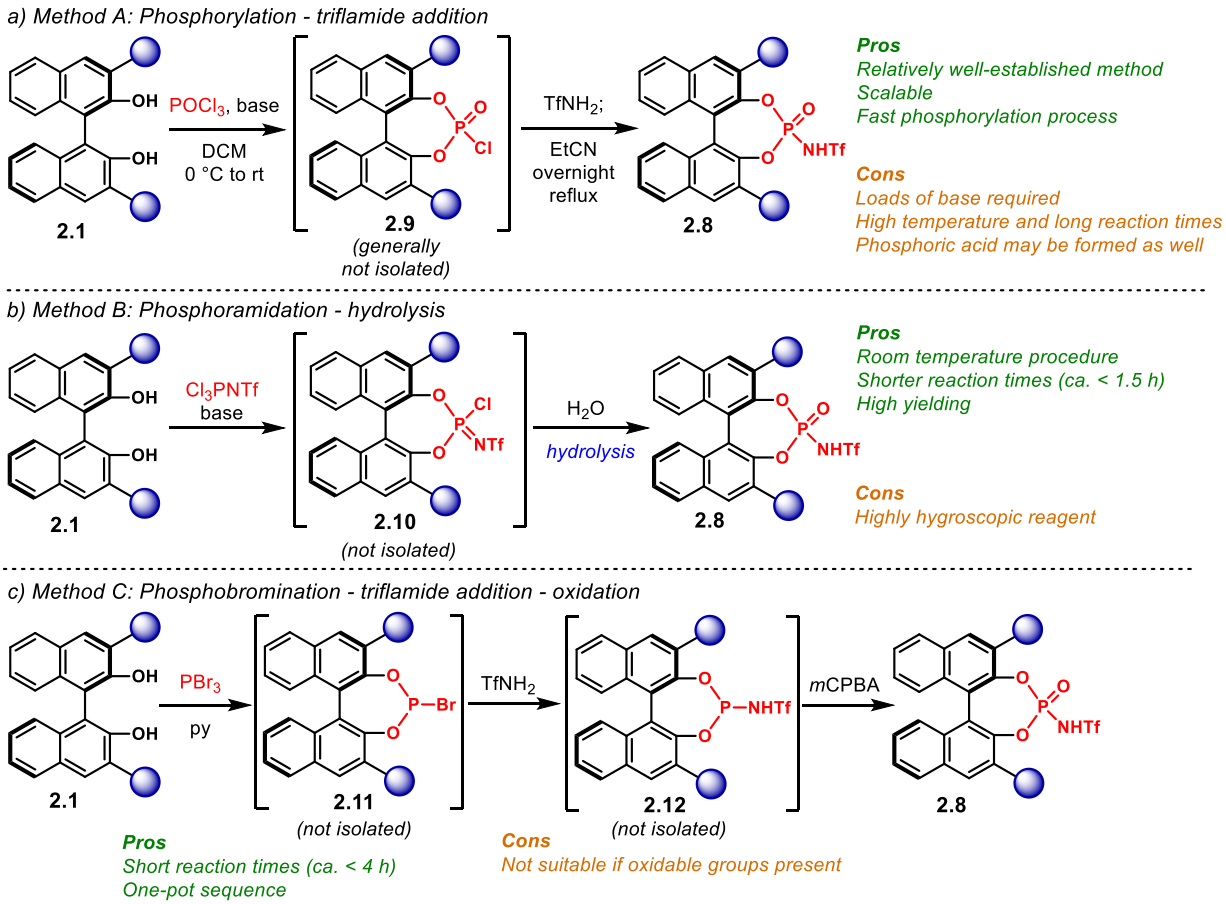

Scheme 2.4: Installing the active site in NTPAs.

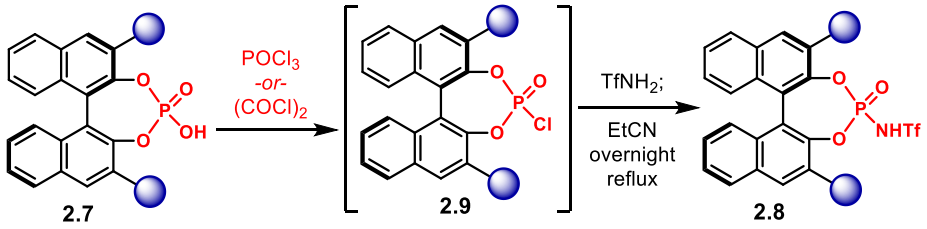

Scheme 2.5: Conversion of PAs to NTPAs.

2.3. Conventional Scaffolds in BINOL-Brønsted Acids

In order to have an initial stock of Brønsted acids, a small library of PAs and NTPAs was synthesised. Starting with three phosphoric acids (Scheme 2.6). *(R)-PA*-**1**, the simplest BINOL-based PA, was obtained in 72% yield following the procedure reported by Jacques and Fouquey, starting from enantiomerically pure *(R)*-BINOL **2.2**.[95] This procedure was used to make most of the PAs that are reported herein. However, as it will be discussed later in this chapter, some modifications had to be made to optimise the reaction with other substrates.

(R)-PA-**2** was also synthesised. Starting form *(R)*-BINOL, protection of the hydroxyl groups with methoxymethylene chloride[96] afforded MOM-protected BINOL **2.3** in 81% yield, which is one of the key precursors for more Brønsted acids discussed throughout this chapter. The reaction is clean and straightforward; if done carefully, there is no need to purify the product by column chromatography; however, recrystallisation from methanol gives better results. In the next step, ortho lithiation and iodination furnishes **2.4** in 90% yield. Subsequent MOM-deprotection in methanolic HCl[97] delivers 3,3'-diiodo-BINOL **2.13** in 75% yield. With this precursor in hand, following an adapted protocol from the group of Berthiol,[98] the corresponding *(R)-PA*-**2** was obtained in 72% yield.

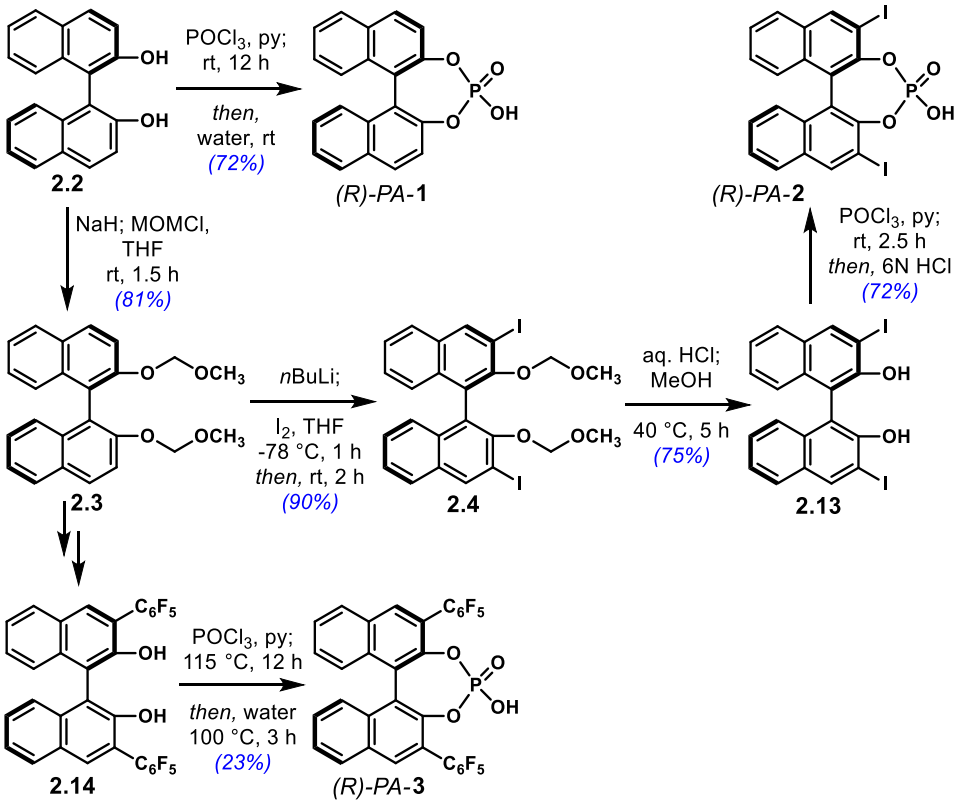

Scheme 2.6: Synthesised phosphoric acids.

In addition, *(R)-PA*-**3**, bearing perfluorinated phenyl scaffolds, was synthesised from BINOL **2.14**, which was already available in our group. However, this precursor can be synthesised from **2.3** following literature methods.[99,100] The procedure reported by the group of List[75] afforded the free acid in 23% yield.

To have a small library of NTPAs, *(R)-NTPA*-**3** was synthesised following the methods reported in the literature (Scheme 2.7). Commencing from **2.4**, Suzuki cross-coupling reaction with 3,5-*bis*-(trifluoromethyl) boronic acid afforded compound **2.15** in 92% yield. The procedure reported by the group of Rueping was used.[80] After acidic hydrolysis, BINOL **2.16** was obtained quantitatively. Then, in order to install the *N*-triflylphosphoramide moiety, the protocol reported by Tius was used.[101] *(R)-NTPA*-**3** was obtained as the free acid in 83% yield.[a]

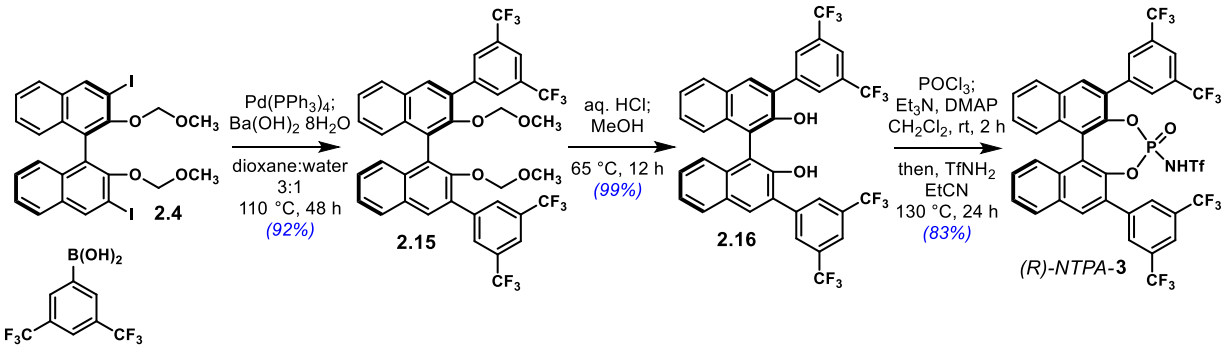

Scheme 2.7: Synthesis of *(R)-NTPA*-**3**.

To try a different methodology to install the acidic functionality in the NTPAs, catalysts *(R)-NTPA*-**4** and *(R)-NTPA*-**2** were synthesised following the protocol from the group of Terada (Scheme 2.8).[91] Starting material **2.17** was already available in our group. Treatment with PBr_3, $TfNH_2$ and *m*CPBA afforded the corresponding catalyst in 67% yield.[b] Likewise, *(R)-NTPA*-**2** was obtained in 80% yield. The group of Phipps kindly donated BINOL precursor **2.18**.

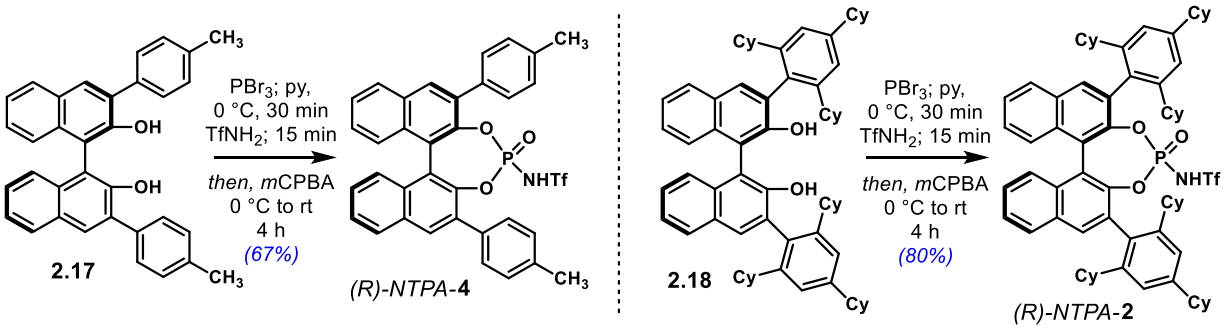

Scheme 2.8: Synthesis of *(R)-NTPA*-**4** and *(R)-NTPA*-**2** using the methodology reported by the group of Terada.

[a] During initial attempts to synthesise NTPAs, I noticed that, for methodologies that use propionitrile (EtCN) as solvent, the best results were obtained with the solvent freshly distilled from CaH_2. A CaH_2 propionitrile solvent still is ideal. Drying over 4Å molecular sieves proved to be inefficient.

[b] In the reported methodology, addition of $TfNH_2$ is done in one portion at -78 °C, however, the solvent freezes at this temperature. Portionwise addition of $TfNH_2$ at 0 °C was done instead.

2.4. Silicon-based Scaffolds in BINOL-Brønsted acids

Since 2012, the group of List have been developing a new class of chiral Brønsted acids: imidodiphosphoric acids (IDPAs, Scheme 2.9*a*).[102,103] These catalysts have presented themselves as a powerful and complementary alternative to accomplish 'difficult' transformations in which typical BINOL-based PAs fail to promote a reaction or to achieve high enantiomeric ratios (Scheme 2.9*b*).[104–109]

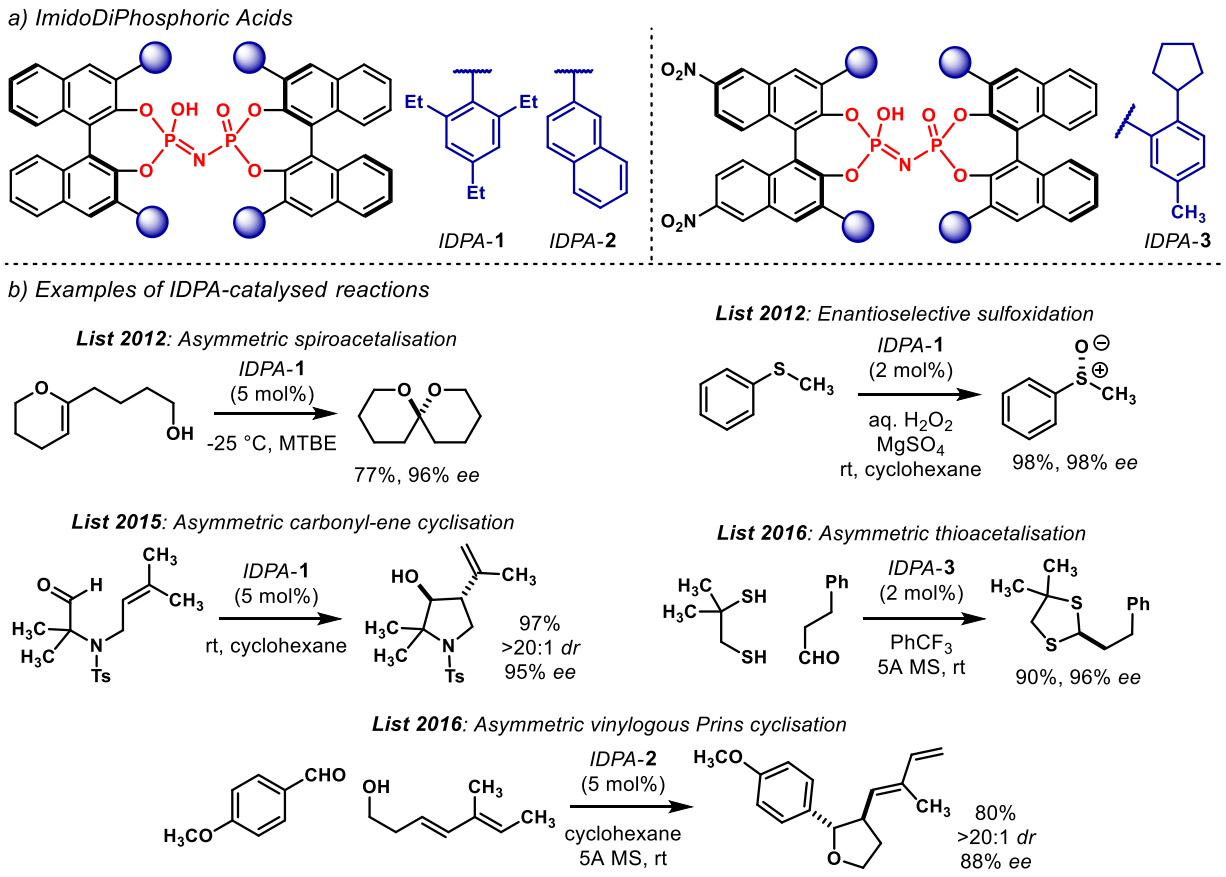

Scheme 2.9: a) Imidodiphosphoric acids developed by the group of List. b) Selected examples of IDPA-catalysed reactions.

The success of IDPAs is attributed to their confined active site, which is deeply encumbered inside the catalyst's chiral pocket (Figure 2.1*a*). The limited space available within the active site of IDPAs tightly accommodates the substrates to achieve higher stereocontrol. In sharp contrast, the active site in BINOL-based PAs is still accessible (Figure 2.1*b*), therefore, allowing high conformational flexibility for the incoming substrates. Such a lack of confinement diminishes enantio-differentiation and thus, delivers low enantiocontrol when small substrates are used. The groups of Paton[110] and Sunoj[111] have studied IDPA-catalysed reactions computationally. Through DFT calculations, both groups have rationalised that the large number of non-covalent interactions between the substrates and the substituents of the catalyst are responsible, in a large extent, to control the stereochemical output.[112,113] This is also true for BINOL-based catalysts and have been studied computationally by the group of Goodman.[66,114–116] Therefore, the remote aryl substituents in BINOL-based catalysts might limit the number of favourable non-covalent interactions between the catalyst chiral cavity and the reacting species.

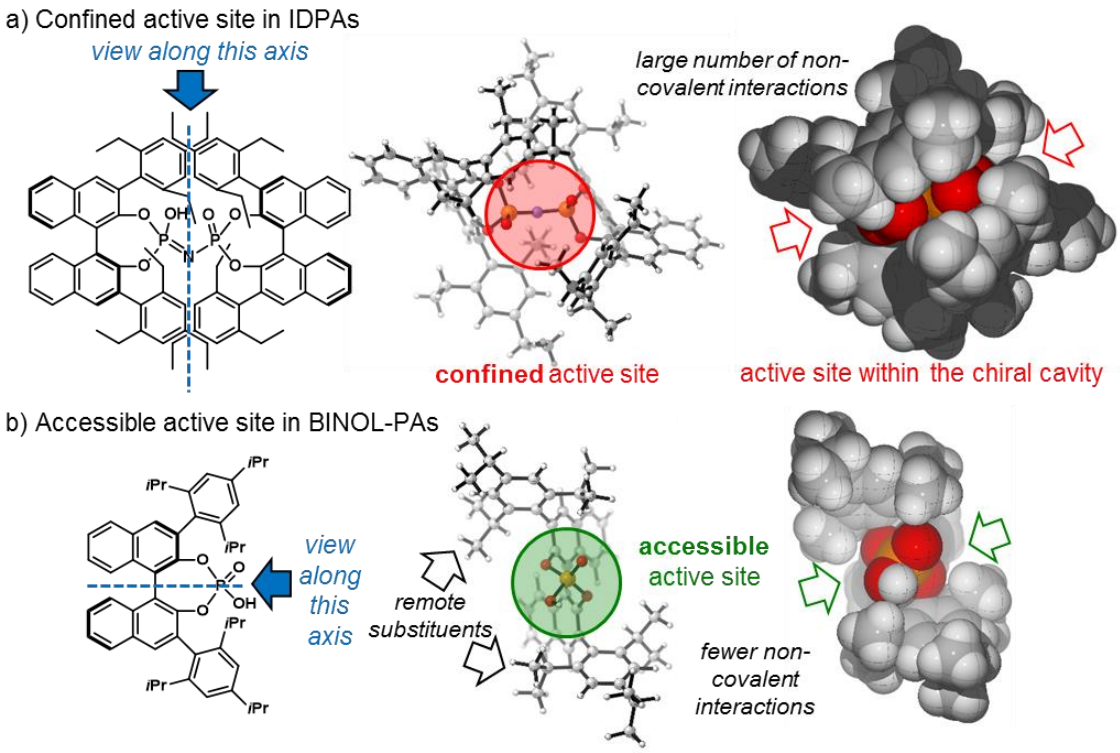

Figure 2.1: a) Confined active site in IDPAs. The close substituents provide a larger number of non-covalent interactions to allow better enantio-differentiation. Stick and space-filling models for *IDPA*-**1** were created from the Cartesian coordinates available in the Cambridge Crystallographic Data Centre database CCDC 864762 (http://www.ccdc.cam.ac.uk) b) Accessible active site in PAs. The relatively remote substituents might provide fewer non-covalent interactions with the substrates. Stick and space-filling models for *(R)-PA*-**4** correspond to the lowest-energy conformer found with the MMFF force field.[117]

In this context, and in collaboration with another member in the group of Goodman, we rationalised that a similarly confined active site could be generated with bulkier 3,3' scaffolds in the BINOL-backbone. For this purpose, silicon-based scaffolds were chosen as suitable candidates (Figure 2.2). The sp^3 hybridised silicon atom, which is directly attached to the 3,3' carbon atoms in the BINOL framework, creates a chiral pocket different from that in aryl-based substituents. As an initial step, a series of conformation searches of those three catalysts were run—*(R)-PA*-**5**, *(R)-PA*-**7** and *(R)-PA*-**8**—using the OPLS3[118] force field.[a] The idea behind that was to have a qualitative picture of how encumbered the active site will be and how could it be modified.

As shown in Figure 2.2*a*, the sp^3 silicon molecular propeller sits the phenyl motifs closer to each other. This encloses the active site. Thus, it would be expected that these scaffolds interact more favourably with the incoming substrates as the active site is tightened. However, as shown in the space-filling model, *(R)-PA*-**5** might not be bulky enough in order to provide a confined active site.

[a] Conformation searches were performed with the MacroModel programme using the OPLS3 force field. A mixed torsional/ low-frequency mode method without constraints was used. An energy window of 10 kcal mol^{-1} was set with 10000 steps to exhaust the conformation space. For *(R)-PA*-**5**, 18 unique conformers were found within 5 kcal mol^{-1}. For *(R)-PA*-**7**, 22 unique conformers were found within 5 kcal mol^{-1}. For *(R)-PA*-**8**, 619 unique conformers were found within 2 kcal mol^{-1}.

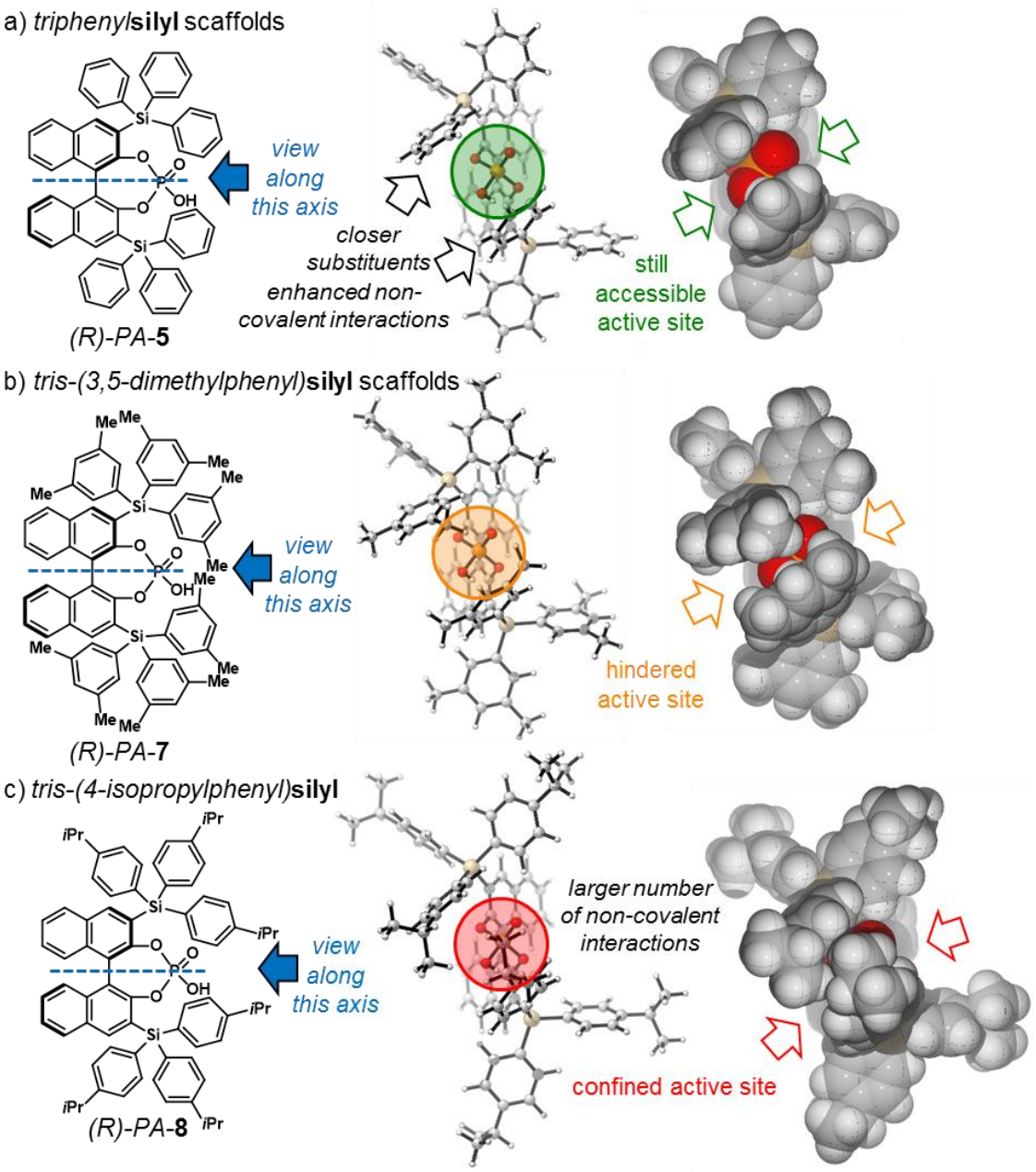

Figure 2.2: a) Triphenylsilyl scaffolds in the BINOL-framework may increase the number of non-covalent interactions. b) tris-(3,5-dimethylphenyl)silyl scaffolds. c) tris-(4-isopropylphenyl)silyl scaffolds. Stick and space-filling models for the catalysts correspond to the lowest-energy conformers found with the OPLS3 force field.

It was hypothesised that using *tris*-(3,5-dimethylphenyl)silyl scaffolds would tighten the chiral pocket of the catalyst (Figure 2.2*b*). As seen in *(R)-PA*-**7**, the extra methyl groups in the *meta* positions of the phenyl rings might not have a dramatic effect. Nevertheless, the phosphoryl group is more hindered than in *(R)-PA*-**4** (*cf.* Figure 2.1*b*) or in *(R)-PA*-**5**.

Finally, a good degree of confinement can be appreciated in *(R)-PA*-**8** (Figure 2.2*c*), which bears *tris*-(4-*iso*propylphenyl)silyl substituents. The space-filling model shows—at least in a qualitative but promising way—that the active site of the catalyst is now properly confined. This one resembles that of *IDPA*-**1** (*cf.*

Figure 2.1*a*). Therefore, *(R)-PA*-**8** would be a catalyst that mimics IDPAs the closest; thus, aiming for high enantiocontrol in asymmetric catalysis.

In order to test this hypothesis and prove if catalyst *(R)-PA*-**8** can achieve high levels of enantiocontrol through multiple non-covalent interactions, the asymmetric sulfoxidation reaction reported by the group of List was taken as a model reaction (Scheme 2.10).[104] In the publication, methylphenylsulfide **2.19** is readily oxidised to sulfoxide **2.20** with aqueous hydrogen peroxide. Using imidodiphosphoric acid *IDPA*-**1**, the reaction achieves full conversion with an impressive 98% *ee*. However, all aryl-based catalysts afforded modest conversions and low enantioselectivities (16% to 56% *ee*). It is noteworthy that regardless the steric bulk in the 3,3'- diaryl substituents, the enantioselectivities were low. In addition, using *(R)-PA*-**5**, which bears the triphenylsilyl scaffolds, provided the opposite sense of enantioinduction, yet in a low enantiomeric ratio (-12% *ee*).

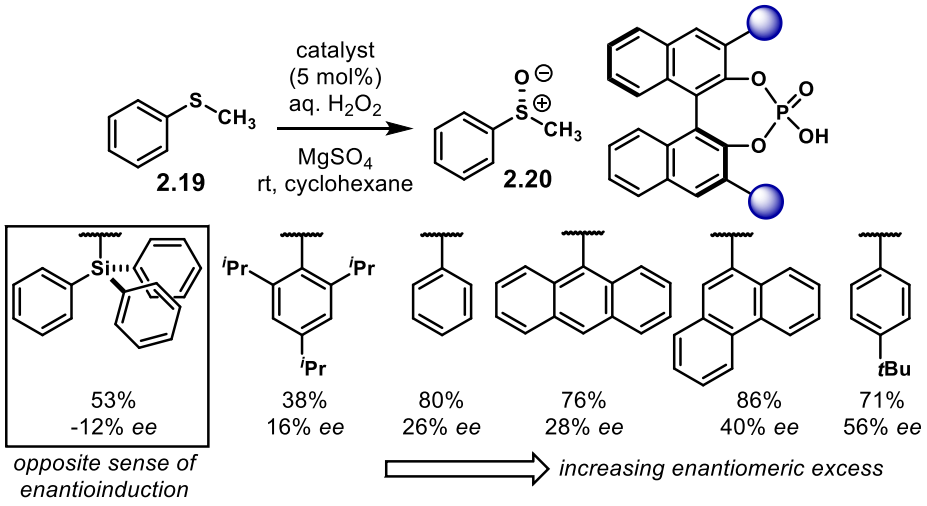

Scheme 2.10: Asymmetric sulfoxidation reported by the group of List.

The computational study on this reaction, conducted by the group of Sunoj,[111] revealed that the H_2O_2 molecule is activated deep inside the chiral cavity of *IDPA*-**1**, thus limiting the conformations of the attacking sulfide. In addition, multiple non-covalent interactions between the catalyst's scaffolds and the incoming nucleophile orient the substrates in a specific way to properly fit inside the chiral pocket. This, however, is not the case for *(R)-PA*-**4**, which due to the more open active site, is not able to lock the reagents in a rigid transition state. Additionally, due to the relatively remote 3,3'- diaryl scaffolds (*cf.* Figure 2.1*b*), less non-covalent interactions can help to stabilise a particular diastereomeric transition state.

With this in mind, Jolene Reid, my collaborator in the Goodman group, ran a couple of preliminary DFT calculations of the sulfoxidation reaction with catalyst *(R)-PA*-**8** (Figure 2.3). **TS1** was found to be favoured over **TS2** by 3.8 kcal mol^{-1}. This corresponds to a calculated >99% *ee* in favour of the *(S)*-enantiomer—without Boltzmann averaging. As the calculations suggest, and shown in **TS1**, *(R)-PA*-**8** would provide a tight chiral pocket for the substrates. This is also reflected in the calculated enantiomeric ratio.

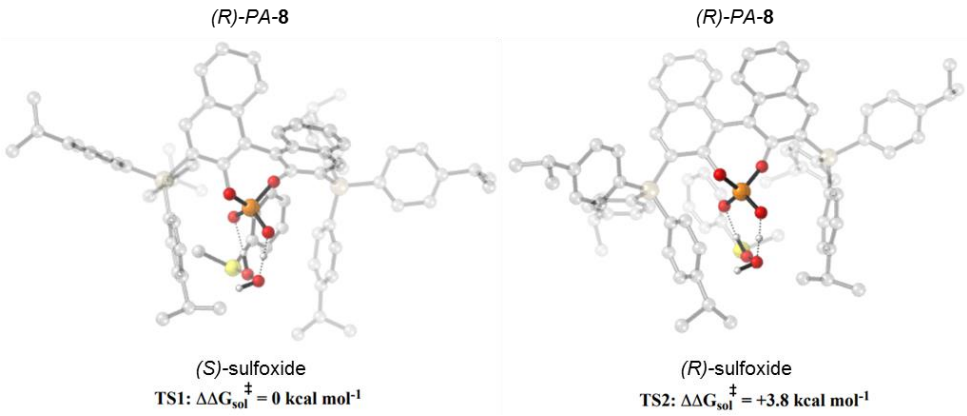

Figure 2.3: Competing transition states for the sulfoxidation reaction of methylphenyl sulfide with catalyst *(R)-PA*-**8**. Geometry optimisations were done at the ONIOM(B3LYP/6-31G(*d*,*p*):UFF) level of theory.[119,120] Grayed-out regions were taken in the MM layer and full colour regions in the QM layer.[a] Single-point energies were then calculated on the optimised geometries at the M06-2x/6-31+G(*d*,*p*) level of theory.[121] Non-critical *H*-atoms are omitted for clarity.[b]

With these promising computational results and the qualitative reasoning out of the force field conformation searches, a synthetic campaign towards silicon-based scaffolds in BINOL-Brønsted acids started.

It is well documented that silicon-based PAs have been used successfully in many enantioselective transformations—*(R)-PA*-**5**, which bears triphenylsilyl motifs, is particularly effective. Amongst them are Friedel-Crafts reactions of iminium ions,[122–124] asymmetric reduction of imines,[125,126] Mannich additions,[127] aza-Darzens aziridinations[128] and multicomponent reactions.[129] In addition, reactions involving *(R)-PA*-**5** have been studied computationally in the group of Goodman.[114]

There are two main protocols reported in the literature to install silicon-based scaffolds in the 3,3'-positions of the BINOL framework (Scheme 2.11). The first method uses a retro-Brook rearrangement as the key step (Scheme 2.11*a*). Starting from *(R)*-3,3'-dibromo BINOL **2.21**, which is easily synthesised from (R)-BINOL in three steps, the hydroxyl groups are silylated in a protecting group-fashion strategy. The corresponding chloro or bromo silanes are used for this purpose. Then, compound **2.22** is treated with *t*BuLi to promote a retro-Brook rearrangement in order to afford BINOL **2.23**. The group of Yamamoto developed such strategy.[130] Several improvements have been implemented to this methodology.[131,132] One of those, was reported by the group of Rueping to install the silyl motifs in a hydrogenated [H_8]-BINOL backbone.[80]

The second pathway to *bis*-silylated BINOL **2.23** uses the ortho lithiation approach (Scheme 2.11*b*). Starting from MOM-protected BINOL **2.3**, the silyl scaffolds are installed directly in the ortho lithiation step to afford compound **2.24**.[125,128,133] After that, hydrolysis of the protecting groups with aqueous HCl delivers BINOL **2.23**. With this BINOL precursor, obtained using either methodology, the usual steps towards PAs or NTPAs can be performed.

[a] Full computational details for ONIOM calculations are provided in Appendix 1.
[b] Credits for these two calculated transition states and energies correspond to JP Reid in the Goodman group.

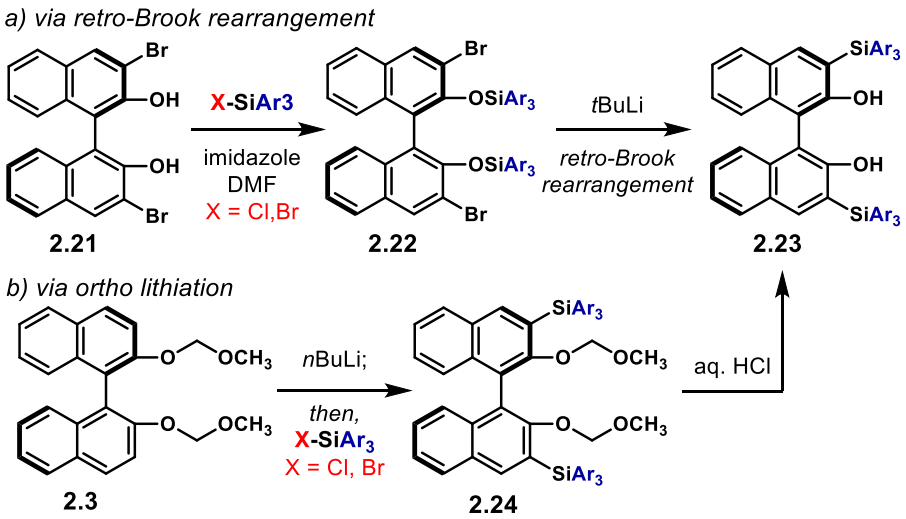

Scheme 2.11: Synthesis of silylated BINOLs *via* a) a retro-Brook rearrangement or b) an ortho lithiation- addition strategy.

The silylation saga commenced with the synthesis of **2.21** (Scheme 2.12). MOM-protected BINOL **2.3** was treated with *n*BuLi followed by bromine in pentane to afford compound **2.25** in 86% yield. Then, following the protocol reported by the group of List, aqueous HCl hydrolysis in methanol afforded the desired BINOL **2.21** in 99% yield.[97] Other hydrolysis protocols, in which the reaction is conducted either in 1,4-dioxane[134] or THF[135], gave similar results; however, methanol was the best solvent to avoid column chromatography afterwards.

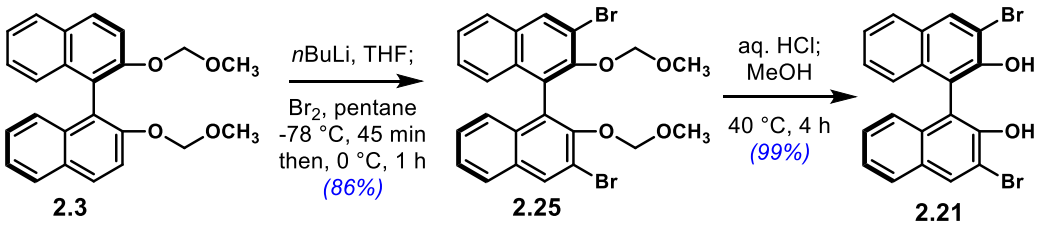

Scheme 2.12: Synthesis of 3,3'-dibromo-BINOL.

With key precursor **2.21** in hand, *(R)-PA*-**5** was synthesised (Scheme 2.13). Silyl protection of **2.21** with chloro triphenylsilane in DMF and imidazole afforded **2.26** in 86% yield after 12 hours at room temperature.[a] Then, the retro-Brook rearrangement with *tert*-butyl lithium at -78 °C afforded BINOL **2.27** in 99% yield.[b] For this reaction, a modified protocol reported by Terada worked best.[136]

Then, it was proceeded to synthesise the corresponding phosphoric acid. Different methods were tried in order to optimise the reaction (Table 1). Initially, the reaction conditions reported by the Group of Gong were attempted (entry 1).[137] With 2.25 equiv. of $POCl_3$ at 60 °C no product was observed after 18 h. This suggests that a higher temperature may be required to phosphorylate the quite hindered BINOL. In order to improve the reaction, 3.0 equiv. of $POCl_3$ were used, a higher temperature and longer reaction time

[a] The reaction can also be performed in CH_2Cl_2 with triethylamine or DMAP. This protocol gives similar results.
[b] Reaction at 0 °C afforded the desired BINOL **2.27** in 26% yield.

(entry 2). This method afforded the desired PA in 31% yield. Increasing the load of $POCl_3$ up to 5.0 equiv. and with DMAP as an additive, the product was obtained in 82% yield (entry 3). Finally, 6.0 equiv. of $POCl_3$ with 2.5 equiv. of DMAP in refluxing pyridine for 36 h were the best reaction conditions for this transformation (entry 4). Catalyst *(R)-PA*-**5** was obtained in 84% yield.

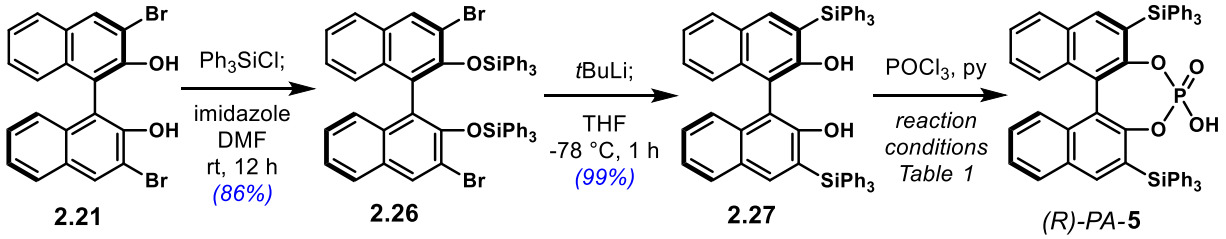

Scheme 2.13: Synthesis of *(R)-PA*-**5**.

Table 1: Optimisation of the phosphorylation reaction for *(R)-PA*-**5**

entry	**$POCl_3$ equiv.**	**additive (equiv.)**	**T /°C**	**time /h**	**yield %**
1	2.25	-	60	18	-
2	3.0	-	115	36	31
3	5.0	DMAP (2.0)	115	36	82
4	6.0	DMAP (2.5)	115	36	**84**

In order to expand the library of NTPAs, catalyst *(R)-NTPA*-**5** was also synthesised (Scheme 2.14). Following the protocol reported by Yamamoto,[43] *(R)-NTPA*-**5** was obtained in 71% yield form BINOL **2.27**.

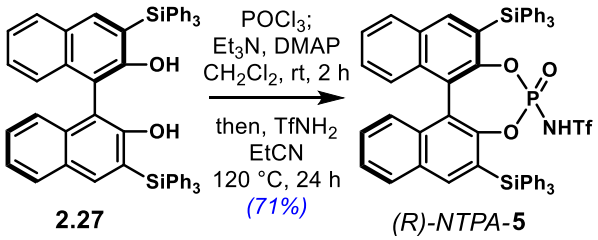

Scheme 2.13: Synthesis of *(R)-NTPA*-**5**.

To further expand the library of silicon-based Brønsted acids, *(R)-PA*-**6** and *(R)-NTPA*-**6**, each bearing *tert*-butyldimethylsilyl (TBS) substituents in the 3,3' positions were prepared (Scheme 2.14). Starting from BINOL **2.21**, TBS protection with chloro *tert*-butyldimethylsilane in triethylamine and CH_2Cl_2 afforded **2.28** in 89% yield. The alternative method with imidazole and DMF yielded the desired product only in 14% yield. Then, upon treatment with *tert*-butyl lithium, BINOL **2.29** was obtained in 99% yield. Phosphoric acid *(R)-PA*-**6** was obtained in 72% yield and *(R)-NTPA*-**6** in 72% yield.

In addition, *(R)-NTPA*-**7**, which bears methyldiphenylsilyl substituents in the 3,3' positions was synthesised (Scheme 2.15). This catalyst was included as a less hindered reference in comparison with *(R)-NTPA*-**5**. Protection of **2.21** with chloro methyldiphenyl silane to obtain **2.30** was accomplished in 88%

yield. Then, the retro-Brook rearrangement with *tert*-butyl lithium afforded BINOL **2.31** in 99% yield. After that, using the methodology reported by Terada,[91] *(R)-NTPA*-**7** was obtained in 75% yield.

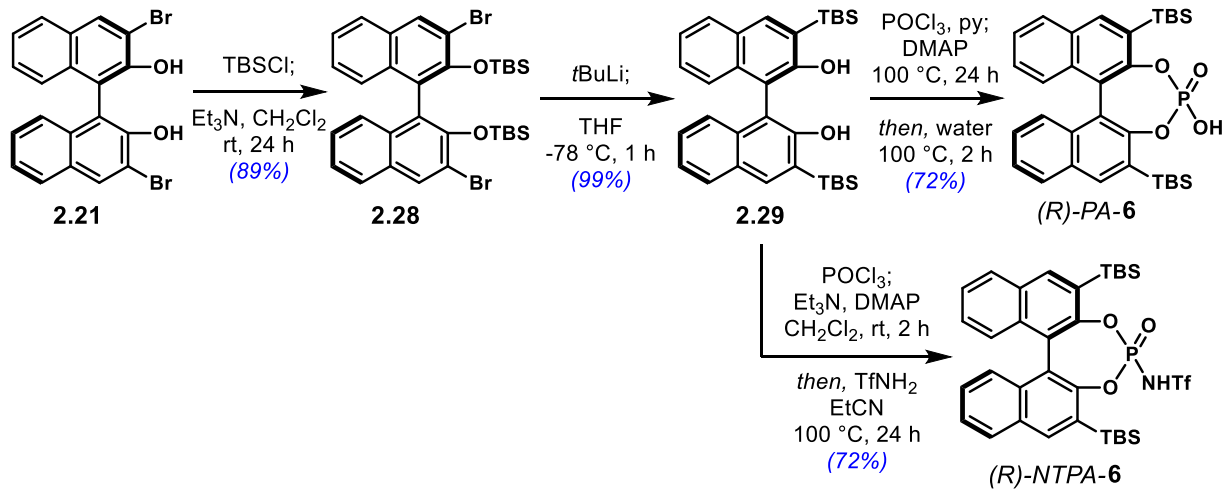

Scheme 2.14: Synthesis of *(R)-PA*-**5** and *(R)-NTPA*-**5**. TBS = *tert*-butyldimethylsilyl.

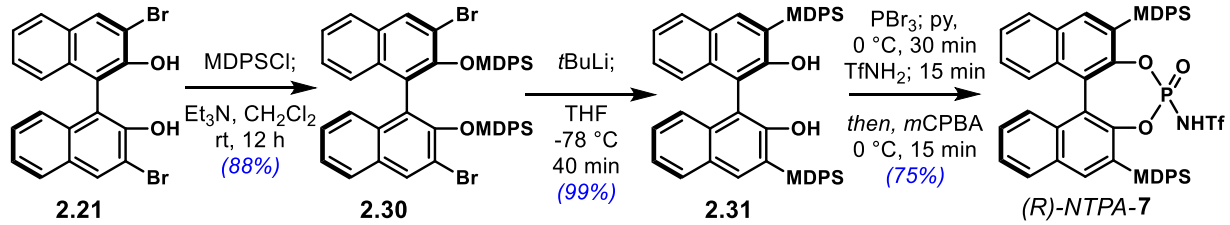

Scheme 2.15: Synthesis of *(R)-NTPA*-**7**. MDPS = methyldiphenylsilyl.

With these catalysts in hand, the journey to synthesise the more hindered *(R)-PA*-**7** and *(R)-PA*-**8** started (*cf.* Figure 2.2*b* and 2.2*c*, respectively). As it was already discussed at the beginning, the introduction of the silyl motifs requires either the silyl chloride or bromide (*cf.* Scheme 2.11). Therefore, this was the starting point of the synthesis.

4-*iso*propylphenyl bromide **2.32** was the starting point to make the corresponding silyl chloride and bromide (Scheme 2.16). 4-*iso*propylphenylsilyl chloride **2.33** was obtained in 64% yield from the aryl bromide upon treatment with *n*BuLi and $SiCl_4$.[138] To make the silyl bromide there are two protocols reported in the literature. The first one, published by the group of Akiyama,[128] uses *t*BuLi and $SiCl_4$ to make *tetrakis*(aryl)silane **2.34**. This was obtained in 37% yield. Then, reaction with bromine delivers **2.35**, which was used as the crude reagent. The other method, on the other hand, turned to be more reliable and easier to operate. From bromide **2.32**, *tris*-(4-*iso*propylphenyl)silane **2.36** was obtained in 65% yield.[139] Then, reaction with bromine in CH_2Cl_2 at 0 °C affords silyl bromide **2.35** after 10 min.[131] This reagent was used in the silylation optimisation without further purification.

Tris-(3,5-dimethylphenyl)silyl halides were synthesised in a similar fashion (Scheme 2.17). From aryl bromide **2.37**, reaction with *n*BuLi and $SiCl_4$ afforded silyl chloride **2.38**,[138] which was also used as a crude to optimise the reaction. In order to make the silyl bromide, **2.37** was treated with *n*BuLi followed

by addition of $SiHCl_3$.[139] The reaction afforded silane **2.39** in 66% yield. Hydrogen-bromine exchange delivered silyl bromide **2.40**,[131] which was used as a crude.

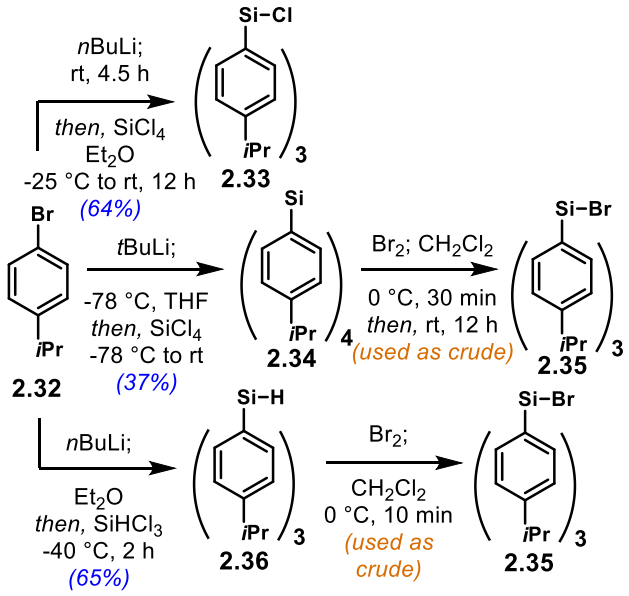

Scheme 2.16: Synthesis of 4-*iso*propylphenylsilyl halides.

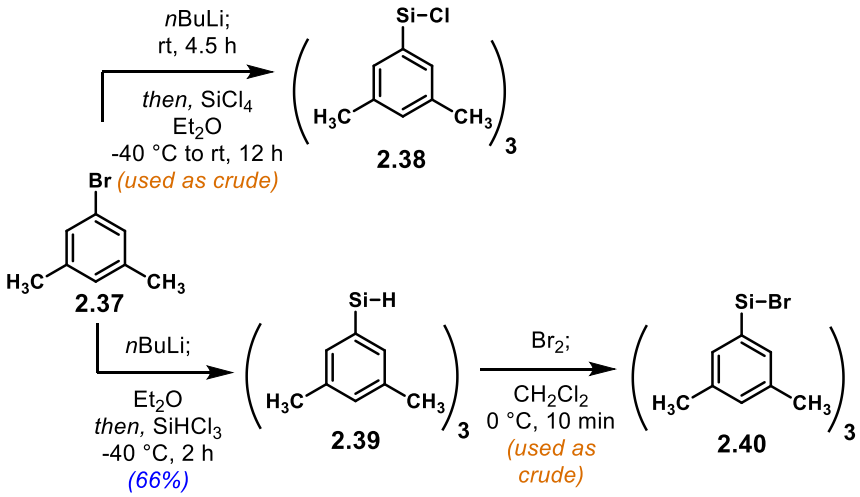

Scheme 2.17: Synthesis of 3,5-dimethylphenylsilyl halides.

With the corresponding silyl chloride and bromide, the following step was the optimisation of the silyl protection reaction towards *(R)-PA*-**7**, from BINOL **2.21** to obtain the *bis*-silylated BINOL precursor **2.41** (Table 2). The first attempts were done using silyl chloride **2.38**. The first reaction conditions tried were the same as for compound **2.26**—imidazole in DMF at rt (entry 1). After 7 days, no product was observed. Then, the same input was tried at a higher temperature (entry 2). No successful results, again. Therefore, the conditions that worked for compounds **2.28** and **2.30** were tested—triethylamine in CH_2Cl_2 at rt (entry 3). Unfortunately, no product was observed. After that, a procedure reported by the group of Stawinski was attempted—which uses iodine and DMAP in THF to silylate alcohols (entry 4).[140] The reaction was not successful. As an alternative, a modified version of the protocol reported by Chong was tried (entry 5).[141] The idea behind these reaction conditions was to silylate BINOL **2.21** in a similar fashion in which

(R)-BINOL, **2.2**, is protected with MOMCl to obtain **2.3**. Interestingly, after 48 h, the reaction afforded the mono- silylated product **2.42** in 46% yield. A variation of the method reported by Corey[142]—2,6-lutidine in CH_2Cl_2 (entry 6)—did not work either.[a]

Table 2: Optimisation of the silylation reaction towards *(R)-PA*-**7**.

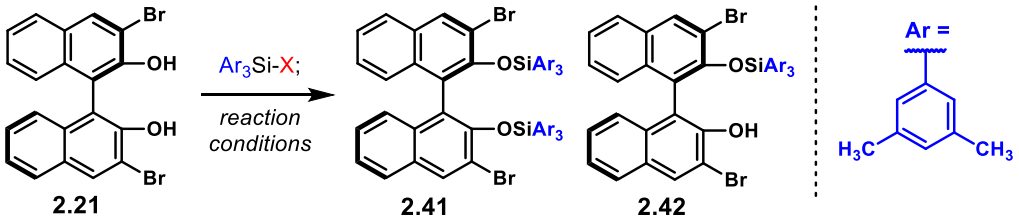

entry	X	base (equiv.)	solvent	T /°C	time /days	2.41 yield %	2.42 yield %
1	Cl	imidazole (3.0)	DMF	rt	7	-	-
2	Cl	imidazole (3.0)	DMF	60	4	-	-
3	Cl	Et_3N (2.5)	CH_2Cl_2	rt	3	-	-
4	Cl	I_2 (5.0), DMAP (6.0)	THF	rt	4	-	-
5	Cl	NaH (3.0)	THF	0 °C to rt	2	-	46
6	Cl	2,6-lutidine (3.0)	CH_2Cl_2	0 °C to rt	7	-	-
7	Br	Et_3N (3.0)	CH_2Cl_2	rt	1	-	10
8	Br	2,6-lutidine (3.0)	CH_2Cl_2	0 °C to rt	6	-	58
9	Br	DMAP (3.0)	CH_2Cl_2	rt	1	**93**	-

[a] At this point, I started to think whether the *bis*-silylation reaction was 'thermodynamically possible' or not, in terms of steric hindrance. Therefore, I pictured a qualitative way to figure it out using simple force field conformation searches. Using species in Scheme 2.18, I proposed a 'thermodynamic feasibility'.

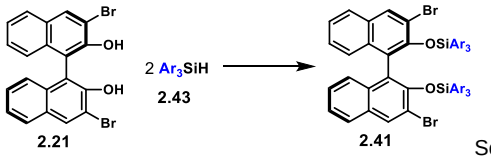

Scheme 2.18

$$\Delta E_{Silylation} = E_{2.41} - 2E_{2.43} - E_{2.21} \quad \text{(eq. 1)}$$

For this approach, I described the silylation thermodynamic feasibility ($\Delta E_{silylation}$) as defined by the OPLS3 force field energy by equation 1. Therein, $E_{2.41}$ is the energy of bis-silylated BINOL; $E_{2.43}$, can be accounted as the energy of *one* silyl motif, which comes out of species **2.43**; and $E_{2.21}$ corresponds to the energy of BINOL **2.21**. The results for some selected motifs are shown in Figure 2.4. Therefore, as I define the thermodynamic feasibility scale relative to triphenylsilyl (-5.7 kcal mol^{-1}) and triethylsilyl (TES, -20.4 kcal mol^{-1})—both of which were obtained experimentally in good yields—all the silylated BINOLs laying in between should be thermodynamically feasible. For example, the TBS BINOL (-18.1 kcal mol^{-1}) lays between the scale extreme values, and was obtained experimentally. Thus, it has to be the case that BINOLs *bis*-protected with *tris*-(3,5-dimethylphenyl) silyl and *tris*-(4-*iso*propylphenyl) silyl motifs are thermodynamically feasible to obtain.

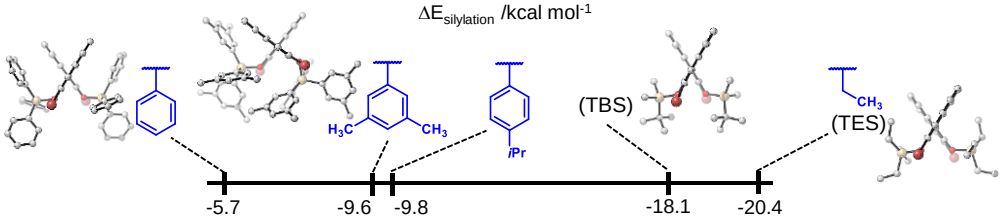

Figure 2.4: Qualitative thermodynamic feasibility scale. Energies are given in kcal mol^{-1}, are relative to the OPLS3 force field, and are not Boltzmann-averaged. Models shown correspond to the lowest-energy conformers.

Then, attention was turned to silyl bromide **2.40** as a more reactive electrophile. Reaction with triethylamine in CH_2Cl_2 (entry 7) afforded mono- silylated BINOL **2.42** in 10% yield. Using 2,6-lutidine as a base improved the yield of **2.42** to 58%, however, the *bis*- silylated BINOL **2.41** was not observed (entry 8). Finally, with DMAP as a base in CH_2Cl_2 at rt (entry 9) the desired product **2.41** was obtained after 24 h in 93%. The mono- silylated product **2.42** was not observed in this case.

After the exhausting silylation saga, compound **2.41** was treated with the retro-Brook rearrangement conditions to yield BINOL **2.44** in 85% yield (Scheme 2.19). Then, after phosphorylation and hydrolysis, *(R)-PA*-**7** was obtained in 79% yield.

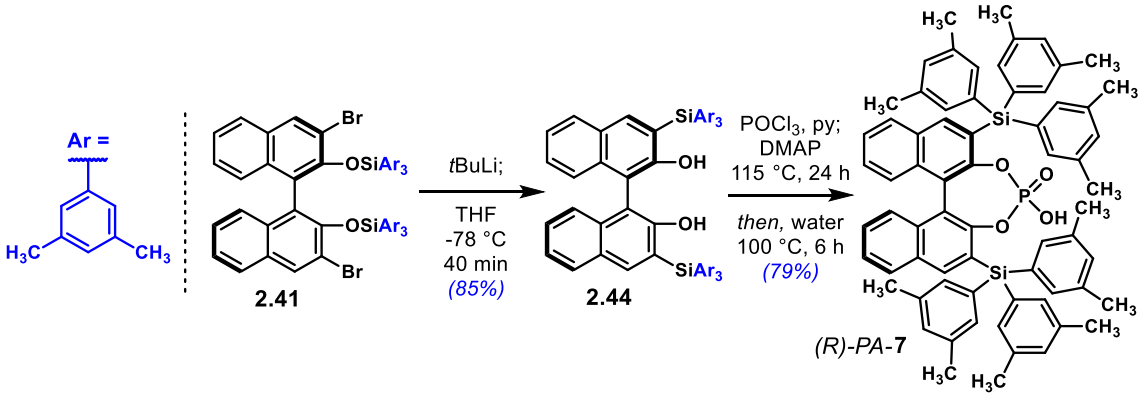

Scheme 2.19: Synthesis of *(R)-PA*-**7**.

En route to *(R)-PA*-**8**, the optimisation to obtain *bis*-silylated BINOL **2.45** was done simultaneously with that of **2.41**. Initially, direct installation of the silyl motifs with the ortho lithiation method was tried (*cf.* Scheme 2.11*b*), however, unsuccessfully. Therefore, a short screening of conditions was conducted to obtain **2.45** (Table 3).

Table 3: Optimisation of the silylation reaction towards *(R)-PA*-**8**.

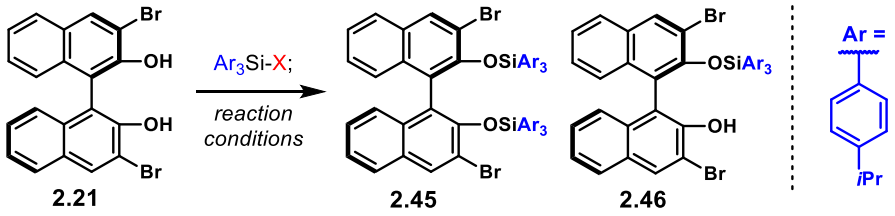

entry	X	base (equiv.)	solvent	T /°C	time /days	2.45 yield %	2.46 yield %
1	Cl	imidazole (3.0)	DMF	60	4	-	-
2	Cl	Et_3N (2.5)	CH_2Cl_2	rt	1	-	-
3	Br	DMAP (3.0)	CH_2Cl_2	rt	1	**89**	-

Reaction of **2.21** with silyl chloride **2.33** in DMF and imidazole (entry 1) did not work. The same was true for the reaction conducted in CH_2Cl_2 with triethylamine (entry 2). Fortunately, using DMAP as the base in

CH_2Cl_2 at rt (entry 3) afforded the desired *bis*-silylated BINOL **2.45** in 89% yield after 24 h. The mono-silylated BINOL **2.46** was not observed.

Compound **2.45** was treated with *t*BuLi to afford BINOL **2.46** in 88% yield (Scheme 2.20). Then, using the optimised phosphorylation-hydrolysis reaction conditions, catalyst *(R)-PA*-**8** was obtained in 66% yield.

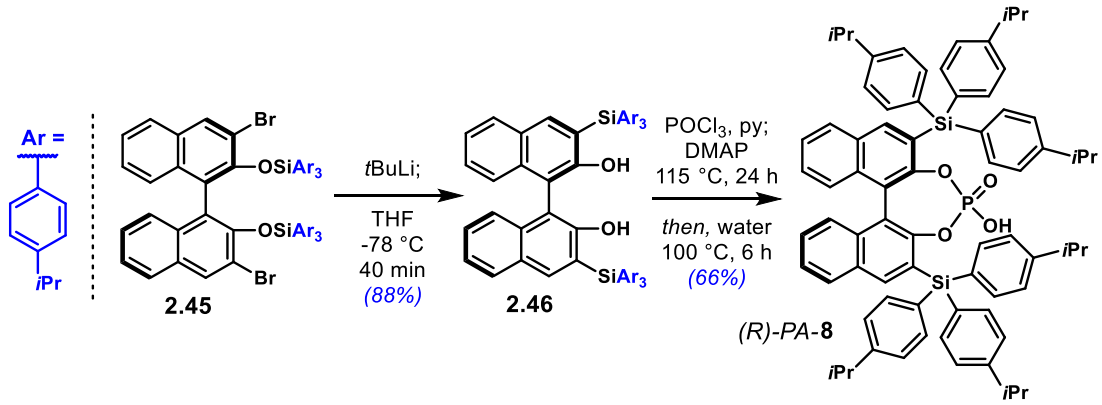

Scheme 2.20: Synthesis of *(R)-PA*-**8**.

With catalysts *(R)-PA*-**5**, *(R)-PA*-**7** and *(R)-PA*-**8**, it was proceeded to test if the confined, hindered active site could yield remarkable enantiocontrol as obtained for IDPAs (*cf.* Scheme 2.9). The catalysts were tried in the asymmetric sulfoxidation reaction, which was reported by the group of List.[104] The reactions were performed using the same conditions as described in the publication (solvent, temperature and reaction time). The results are summarised in Table 4.

Table 4: Asymmetric sulfoxidation reaction using silicon-based PAs.

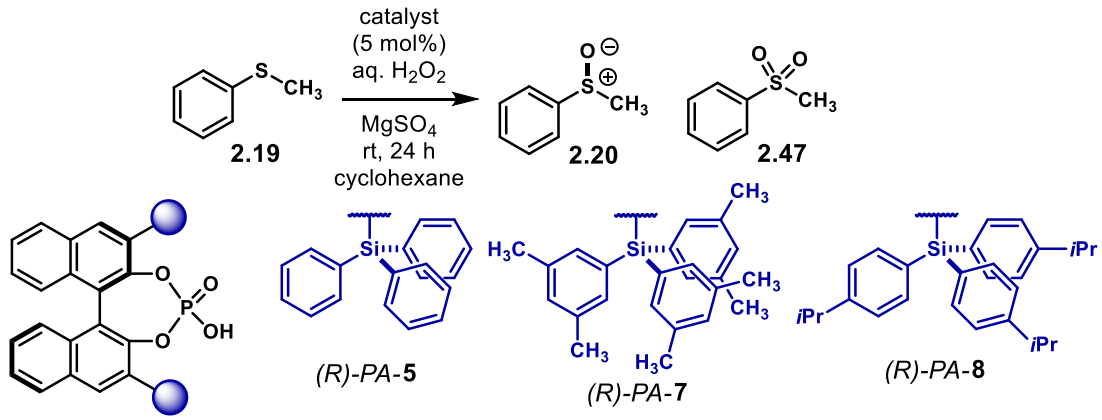

entry	**catalyst**	**% conversion**[a]	**2.20 : 2.47 ratio**[a]	**2.20 *ee***[b]
1	none	full	10 : 1.3	NA
2	*(R)-PA*-**5**	full	10 : 2.7	2%
3	*(R)-PA*-**7**	full	10 : 0.8	0
4	*(R)-PA*-**8**	full	10 : 0.6	-11%

Reaction conditions: Thioanisole **2.19** (0.10 mmol), H_2O_2 (11 µL, 0.105 mmol, 30% aq.), $MgSO_4$ (50 mg), cyclohexane (0.1 M). [a] Determined out of the crude NMR spectra. [b] Determined in chiral reverse phase HPLC.

The control reaction without catalyst (entry 1) achieved full conversion of the starting material **2.19**. Sulfoxide **2.20** was obtained along with sulfone **2.47** in a 10:1.3 ratio. With catalyst *(R)-PA*-**5** (entry 2), full conversion of the starting sulfide was also observed, yet with low enantiocontrol (2% *ee*). In addition, a higher sulfoxide:sulfone ratio was observed (10:2.7). This might suggest that the PA is indeed catalysing the reaction; yet, the active site is open enough for the sulfoxide to keep reacting with the activated H_2O_2. *(R)-PA*-**7** (entry 3) achieved full conversion and a lower sulfoxide:sulfone ratio (10:0.8). This may be indicative that the active site is now too hindered for sulfoxide **2.20** to undergo further oxidation—*i.e.* considering that **2.20** is sterically more demanding than **2.19**. However, no enantiocontrol was observed. The much more hindered catalyst *(R)-PA*-**8** (entry 4), also achieved full conversion. For this case, the sulfide:sulfone ratio was even lower (10:0.6), suggesting, therefore a more encumbered active site. To our disappointment, enantioselectivity was low (-12% *ee*); however, the opposite sense of enantioinduction was observed.

The preliminary calculations done with *(R)-PA*-**8** (*cf.* Figure 2.3) predicted a higher enantiomeric ratio to be obtained (>99% *ee*). This was not the case. One reason for the calculations to have failed might be due to the MM (UFF force field) part of the ONIOM optimisation. However, according to computational studies by Simón, Goodman and Paton, that is unlikely.[79,110,143] Thus, an incomplete conformation search or, more likely, the B3LYP functional in the optimisation step might be the proximal cause for the incorrect prediction.[144]

In this context, I independently performed ONIOM calculations to get insights on why the initial prediction of enantioselectivity did not work. As shown in **2.48** (Scheme 2.21), the catalyst's backbone and 3,3'-substituents were modelled using the UFF force field. The active site of the catalyst and the reacting substrates were modelled at the DFT level. As a qualitative description of the system was intended, single-point energy corrections at a higher full-DFT level were not performed.

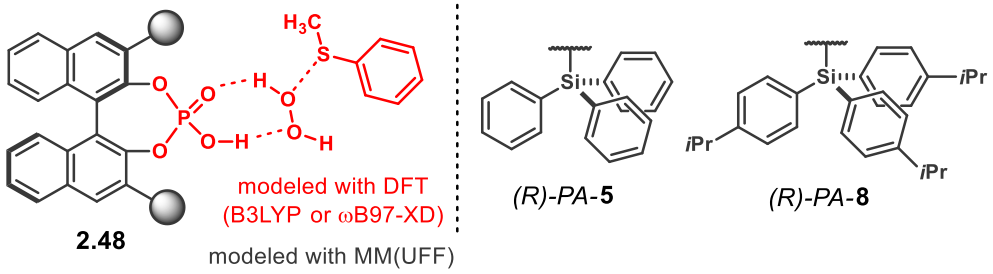

Scheme 2.21: ONIOM approach to model the transition states for the asymmetric sulfoxidation reaction. The catalyst's backbone and 3,3'- substituents were taken into the MM layer using the UFF force field (shown in gray). The active site of the catalyst and the reacting substrates were taken into the QM-DFT layer (shown in red).

As a starting point, the transition states for the sulfoxidation reaction using catalyst *(R)-PA*-**5** were calculated (Figure 2.5*a*). These calculations were done at the ONIOM(B3LYP/6-31G(*d*,*p*):UFF) level of theory and were intended to serve as a 'control experiment'. **TS 2.1-R** was found to be the lowest energy transition state, favouring the *(R)*-enantiomer of the product by 0.75 kcal mol^{-1} over **TS 2.1-S**, which yields the *(S)*-enantiomer. This energy difference corresponds to a calculated 56% *ee*, which is much higher than the actual value obtained experimentally (2% *ee*, *cf.* Table 4). The energy difference might be

overestimated due to the B3LYP component in the optimisation.[145] In addition, a more exhaustive conformation search has to be done to found all possible transition structures as lower-energy structures might have been missed. After that, TS calculations for the asymmetric sulfoxidation using catalyst *(R)-PA*-**8** were done at the same level of theory (Figure 2.5*b*). **TS 2.2-S** was found to be the lowest-energy transition state, yielding the *(S)*-enantiomer of the product which is opposite for what was obtained using *(R)-PA*-**5**. Therefore, my qualitative calculations are predicting an opposite sense of enantioinduction, which was observed experimentally. The TS yielding the *(R)*-enantiomer, **TS 2.2-R**, was found to be 1.03 kcal mol^{-1} higher than **TS 2.2-S**. This energy difference corresponds to a calculated 70% *ee*. This value is, again, higher than the experimentally obtained. However, I predicted a lower enantioselectivity than the one calculated before (*cf.* Figure 2.3). For this case, the overestimated energies might also be due to the B3LYP component of the optimisation or an incomplete conformation search.

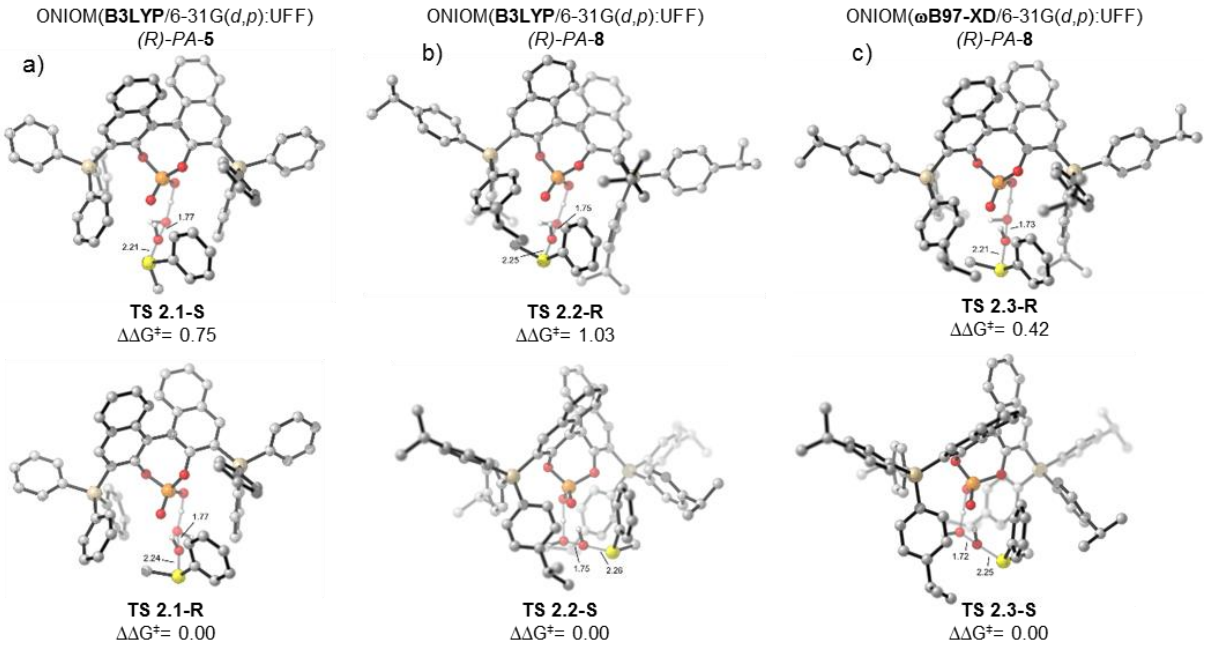

Figure 2.5: Lowest-energy transition states for the asymmetric sulfoxidation reaction of thioanisole. a) With catalyst *(R)-PA*-**5** at the ONIOM(B3LYP/6-31G(*d*,*p*):UFF) level of theory. b) With catalyst *(R)-PA*-**8** at the ONIOM(B3LYP/6-31G(*d*,*p*):UFF) level of theory and c) with catalyst *(R)-PA*-**8** at the ONIOM(ωB97-XD/6-31G(*d*,*p*):UFF) level of theory. Energies are given in kcal mol^{-1} and are not Boltzmann-averaged. None of the calculations were single-point energy corrected at a higher, full-DFT level of theory.

In order to verify if the B3LYP functional could be the cause for the overestimated energies, the ONIOM optimisations for the reaction with catalyst *(R)-PA*-**8** were done using a different DFT functional. For this case, the ONIOM(ωB97-XD/6-31G(*d*,*p*):UFF) level of theory was used. **TS 2.3-S** was found to be the lowest-energy transition state for these other set of calculations (Figure 2.5*c*). The *(S)*-enantiomer of the product was also favoured—the same as for the B3LYP functional. In sharp contrast with the B3LYP calculations, **TS 2.3-R** was calculated to be 0.42 kcal mol^{-1} higher than **TS 2.3-S**. This energy difference corresponds to a calculated 34% *ee*. Such value is still overestimated, yet closer to the actual

experimental 11% *ee*. Therefore, the ωB97X-D functional provides a better description of this system in the optimisation stage.

In summary, the overestimated initial predictions with *(R)-PA*-**8** might have been due to the B3LYP functional during the ONIOM optimisation. In addition, a more complete conformation search has to be done in order to exhaust all possible transition state geometries.

2.5. Sulfone-based Scaffolds in BINOL-Brønsted Acids

To the best of our knowledge, PAs bearing sulfone-based motifs in the 3,3'- positions have not been used in asymmetric synthesis (*cf.* Scheme 2.1). The closest related structures reported to date include BINOLs with sulfide-based scaffolds, albeit limited. Such compounds have been used as ligands in asymmetric reactions using transition metals,[146–149] precursors for phosphine ligands[150] or directly as organocatalysts.[151,152]

In an attempt to design new PAs, it was hypothesised that including sulfone scaffolds into the catalyst architecture could be useful. As shown in Scheme 2.22*a*, the sulfone motifs could increase the acidity of the catalyst, **2.49-A**. This could be promoted by an intramolecular hydrogen bond from the acidic proton to the sulfonyl moiety. It has been reported that such intramolecular hydrogen bonds increase the acidity of the phosphoric acid's active site.[136] In addition, the oxygen atoms in the sulfone are prone to provide additional Lewis basic sites. The Lewis basic oxygen atoms in the sulfone can contribute with additional interactions between the catalyst and the substrates. Moreover, the tetrahedral shape in the sulfone motif might create a different chiral pocket (Scheme 2.22*b*), in comparison to the well-established aryl scaffolds. In that case, I hypothesise that—in the suitable dielectric medium—the sulfone motifs might align themselves in opposing dipoles, **2.49-B**. That alignment could furnish a tighter chiral pocket as the aryl substituents would be pointing towards the active site.

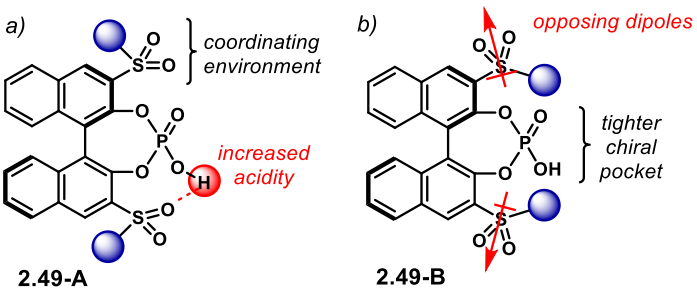

Scheme 2.22: Two plausible conformations for sulfone-based PAs. a) An intramolecular hydrogen bond can increase the acidity of the catalyst. b) In an opposing dipoles model the aryl motifs would be pointing toward the active site, thus, tightening the chiral pocket.

The journey towards these new type of catalysts started by designing a suitable route in which to install the 3,3' substituents. In the reports by the groups of Cook and Lloyd Jones,[146,153] which use 3,3'-*bis*(triflyl)-BINOL **2.51**, the substituents are installed *via* a thia-Fries rearrangement (Scheme 2.23*a*). Starting from

bis-(triflyl)-protected BINOL **2.50**, addition of LDA triggers the rearrangement to afford BINOL **2.51**. The procedure, although it looks simple, is mainly limited to fluorinated sulfones (*e.g*. -Tf). In this context, it was considered a generalised thia-Fries rearrangement inspired by the retro-Brook reaction that was utilised to install the silicone scaffolds (section 2.4). If a similar process could work in a thia-Fries way, it would be useful to functionalise BINOLs with larger variety of sulfone-based scaffolds. Starting from *(R)*-3,3'-dibromo-BINOL **2.21** (Scheme 2.23*b*), triflated product **2.52** was obtained in 87% yield. However, the next step towards **2.51** using *tert*-butyl lithium was unsuccessful.

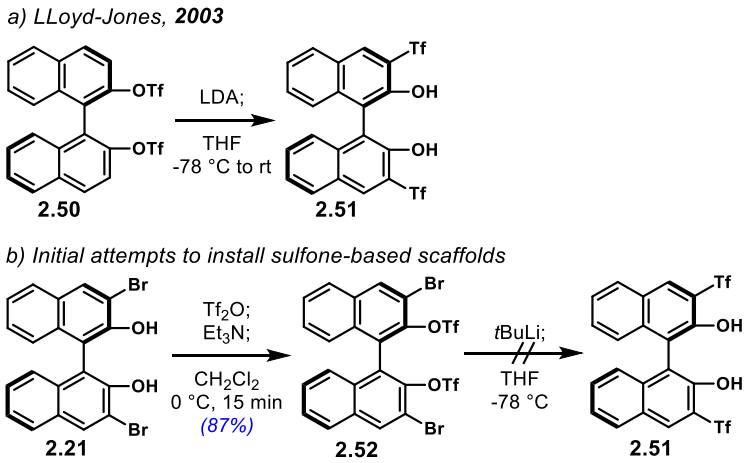

Scheme 2.23: a) Thia-Fries rearrangement reported by the group of Lloyd-Jones. b) Initial attempt to install the sulfone motifs in the 3,3' positions.

After the unsuccessful initial attempt, attention was turned to alternative ways in which to install the sulfone scaffolds (Scheme 2.24). 3,3'-*bis*(sulfone)-BINOL **2.53** can be obtained from cleavage of the MOM protecting groups in **2.54**. The latter compound can be furnished *via* an mCPBA oxidation of the corresponding sulfide **2.55**, which can be obtained from MOM-protected BINOL **2.3**. In addition, this strategy seems suitable to use *bis*-sulfide scaffolds as well. Alternatively, another pathway to directly deliver the sulfone motifs in the *ortho* lithiation step was envisaged. This can be achieved utilising a sulfonyl chloride, or another suitable leaving group **2.56**. With a subsequent deprotection BINOL **2.53** can be obtained.

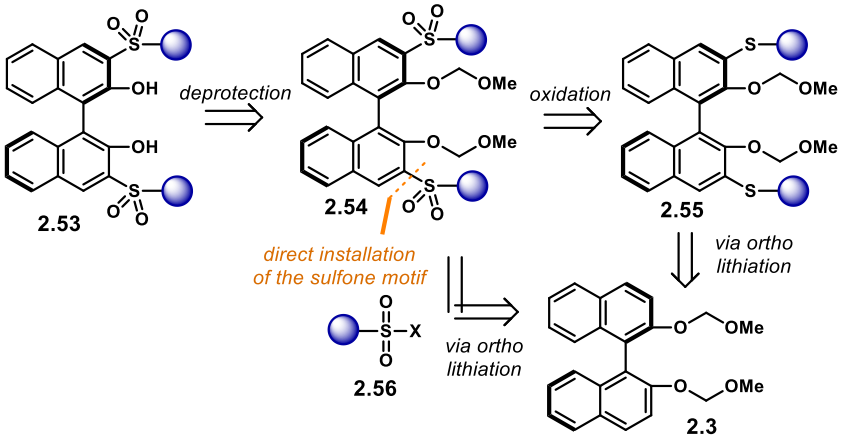

Scheme 2.24: Proposed retrosynthetic analysis to obtained sulfone-based BINOLs.

The forward synthesis of sulfone-based Brønsted acids is presented in Scheme 2.25. Starting from MOM-protected BINOL **2.3**, *ortho* lithiation followed by addition of phenylsulfenyl bromide—freshly prepared from thiophenol and bromine—afforded compound **2.57** in 64% yield. Then, oxidation with *m*CPBA delivered *bis*-sulfone **2.58** in 92% yield. Initially, a similar procedure for the oxidation step, reported by the group of Kamimura, was tried;[154] however, it did not work for this substrate. Removal of the protecting groups with aqueous HCl in methanol[97] afforded BINOL **2.59** in 96% yield.

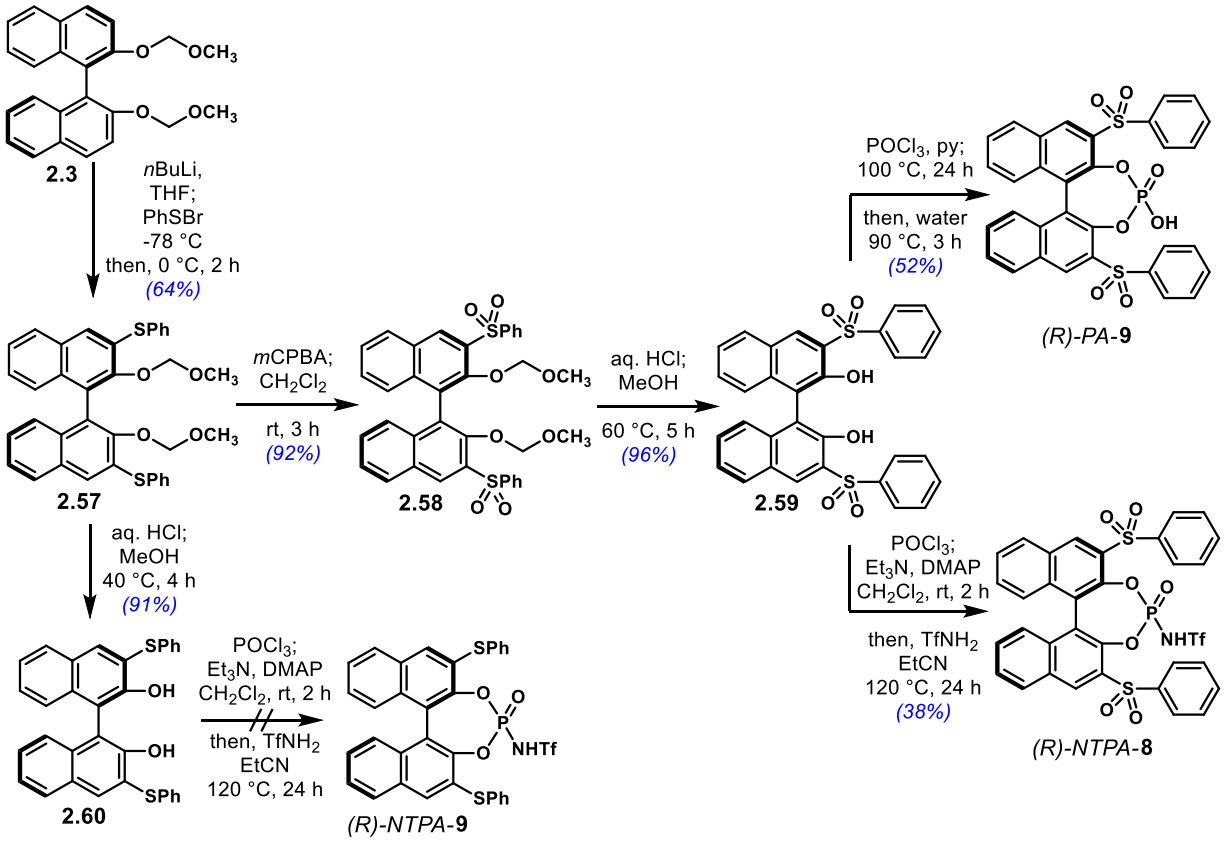

Scheme 2.25: Synthesis of sulfone-based Brønsted acids.

With *bis*-sulfone BINOL **2.59** in hand, *(R)-PA*-**9** was obtained in 52% yield. The standard procedure for making PAs—phosphorus (V) oxychloride in pyridine followed by hydrolysis—worked well. Moreover, *(R)-NTPA*-**8** was also synthesised. The methodology reported by the group of Tius[101] afforded the desired catalyst in 38% yield. Presumably, most of the yield is lost during the acidic wash step to recover the catalyst in the free acid form. The compound seems to be polar enough to be dissolved in a substantial amount in the aqueous phase.

In addition, attempting to make a catalyst with different electronic properties but still having a sulfur atom attached to the 3,3'- positions, *(R)-NTPA*-**9** was synthesised. Removal of the MOM protecting groups in **2.57**, afforded BINOL **2.60** in 91% yield—this compound has been previously reported and used as a chiral ligand in copper catalysed reactions.[155] The same procedure to synthesise *(R)-NTPA*-**8** failed to prepare catalyst *(R)-NTPA*-**9**. Possibly, the very different electronic properties of the catalyst's scaffolds are incompatible with this methodology.

It was thought about what conformations a catalyst with an additional rotatable bond would have. In this context, and following a similar methodology for the catalysts discussed above, *(R)-PA*-**10** was targeted (Scheme 2.26). Similar to *(R)-PA*-**9** but with an additional methylene group, it might offer different non-covalent interactions or provide a different chiral pocket for the substrates to react.

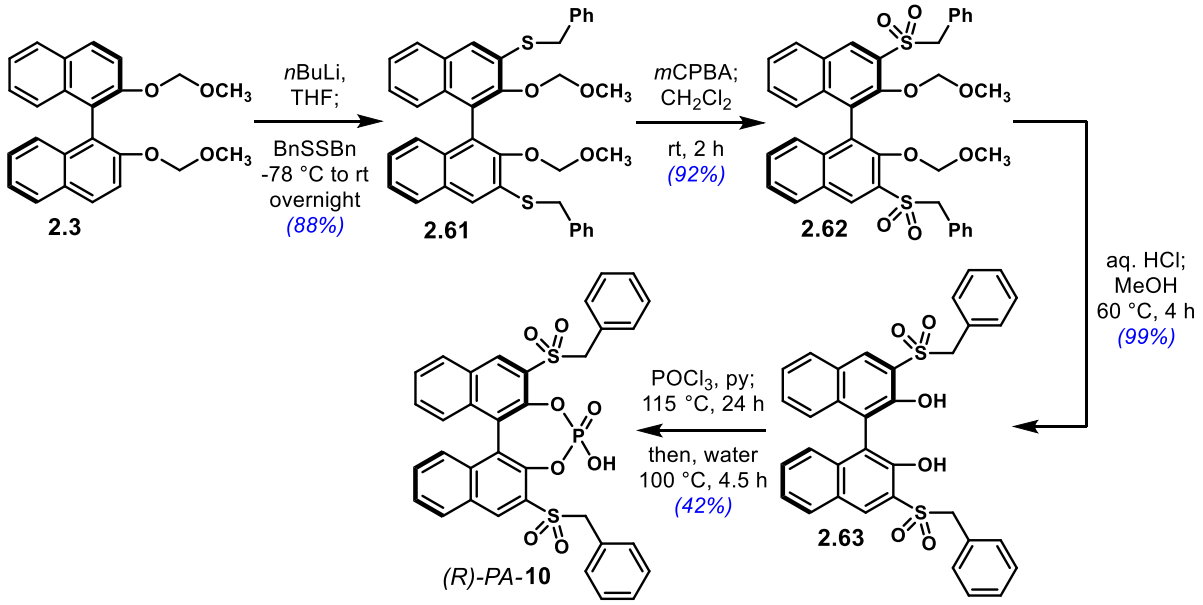

Scheme 2.26: Synthesis of *(R)-PA*-**10**.

MOM-protected BINOL **2.3** was treated with the usual otrho lithiation process. Addition of dibenzyl disulfide afforded compound **2.61** in 88% yield.[a] *m*CPBA-oxidation delivered **2.62** in 92% yield. After removal of the protecting groups, BINOL **2.63** was obtained in 99% yield. Then, using a similar procedure as the one reported by the group of List,[75] *(R)-PA*-**10** was obtained as the free phosphoric acid in 42% yield.

With the aforementioned methodology successful, synthetic efforts turned to the alternative way to install the sulfone motifs directly. Such a process would save the oxidation step. The results of the initial experiments are summarised in Table 5.

Starting from MOM-protected BINOL **2.3**, the standard *ortho* lithiation conditions delivers the *bis*-lithiated species, ready for the electrophile to be added. Initially, tosyl chloride (4-methylphenylsulfonyl chloride) was tried as the sulfonylating reagent (entry 1). Unfortunately, no reaction was observed. The original idea of using sulfonyl chlorides came from their wide availability; in addition, they can be readily accessed from sulfonic acids. The lack of reactivity might have been due to low electrophilicity of the sulfur atom in tosyl chloride. Therefore, an electron-poorer sulfonyl chloride would deliver *bis*-sulfonylated product **2.54**. As a more reactive species, 4-nitrophenyl sulfonyl chloride was tried (entry 2). Reaction occurred; however, dichlorinated product **2.65** was obtained in 20% yield—the mono chlorinated product, not

[a] One of the main disadvantages of this methodology is the use of the disulfide, which delivers one equivalent of the corresponding thiol during the work-up step—I tried to make the corresponding benzylsulfenyl bromide in a similar fashion I made phenylsulfenyl bromide. However, the reaction did not work and the methodology with the disulfide was used instead.

shown, was also obtained, in 25% yield. In such an electron-deficient sulfonyl chloride, nucleophilic attack on the chlorine atom was preferred. Although similar reactions with electrophilic chlorine atoms are known, it showed that sulfonyl chlorides might not be the most suitable reagents for this sulfonylation reaction.

Table 5. Initial attempts to install the sulfone motifs in the ortho lithiation step.

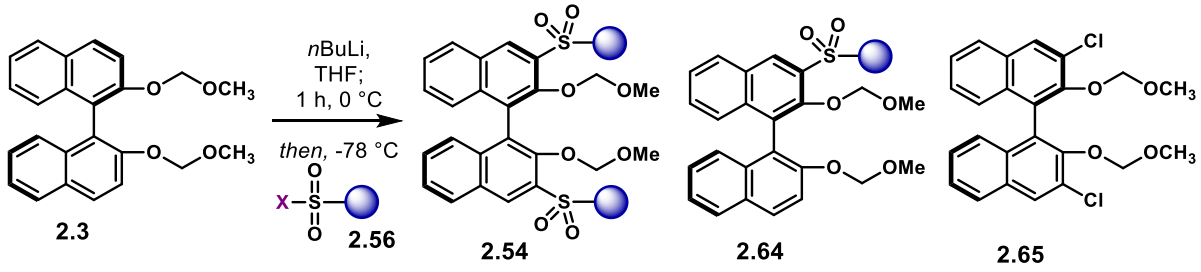

entry	X	*aryl*	**result** (yield)
1[a]	Cl	4-methyl phenyl	*no reaction*
2	Cl	4-nitro phenyl	**2.65** (20%)
3	F	4-methyl phenyl	**2.54** (21%), **2.64** (45%)

Reaction conditions: arylsulfonyl halide added as a solution in THF at -78 °C; then, the reaction is stirred overnight with the cooling bath to allow temperature to reach rt slowly. [a] Tosyl chloride was recrystallized from $CHCl_3$-PE, dried overnight in high vacuum and was free from tosic acid.

Looking for similar sulfonylation reactions, two methodologies reported by the groups of Snieckus[156] and Kozlowski[157] suggested that sulfonyl fluorides are suitable electrophiles for *ortho* lithiation-addition reactions. With this in mind, tosyl fluoride was synthesised following the protocol reported by the groups of Lin and Lo.[158] As shown in entry 3, reaction took place to afford the *bis*-sulfonylated product **2.54** in 21% yield along with the mono-sulfonylated product **2.64** in 45% yield.

With these encouraging results, attention was turned to synthesise the more complex phosphoric acid *(R)-PA*-**11**, as shown in Scheme 2.27 in the following page. As a starting point, 2,4,6-tri*iso*propylphenyl-sulfonyl fluoride **2.67** was prepared.[158,159] Reaction of the corresponding sulfonyl chloride **2.66** with potassium fluoride in acetonitrile afforded **2.67** in 99% yield. Then, *otho* lithiation of **2.3** followed by addition of the freshly prepared fluoride afforded *bis*-sulfonylated precursor **2.68** in 72% yield. MOM-deprotection in refluxing HCl solution in methanol delivered BINOL **2.69** in 44% yield. The latter reaction required an overnight reaction time to fully consume the starting material. After that, treatment with $POCl_3$ and DMAP in pyridine with subsequent hydrolysis afforded the desired phosphoric acid in 75% yield as the free acid after HCl wash—DMAP was used in the phosphorylation step as the hydroxyl moieties might be heavily hindered by the 3,3'- substituents.

In summary, a synthetic route to afford sulfone-based chiral phosphoric acids was developed. In addition, an NTPA—featuring such 3,3' groups—was also prepared. Shown in Scheme 2.28, in the next page, are the aryl sulfone-based Brønsted acids synthesised in this work.

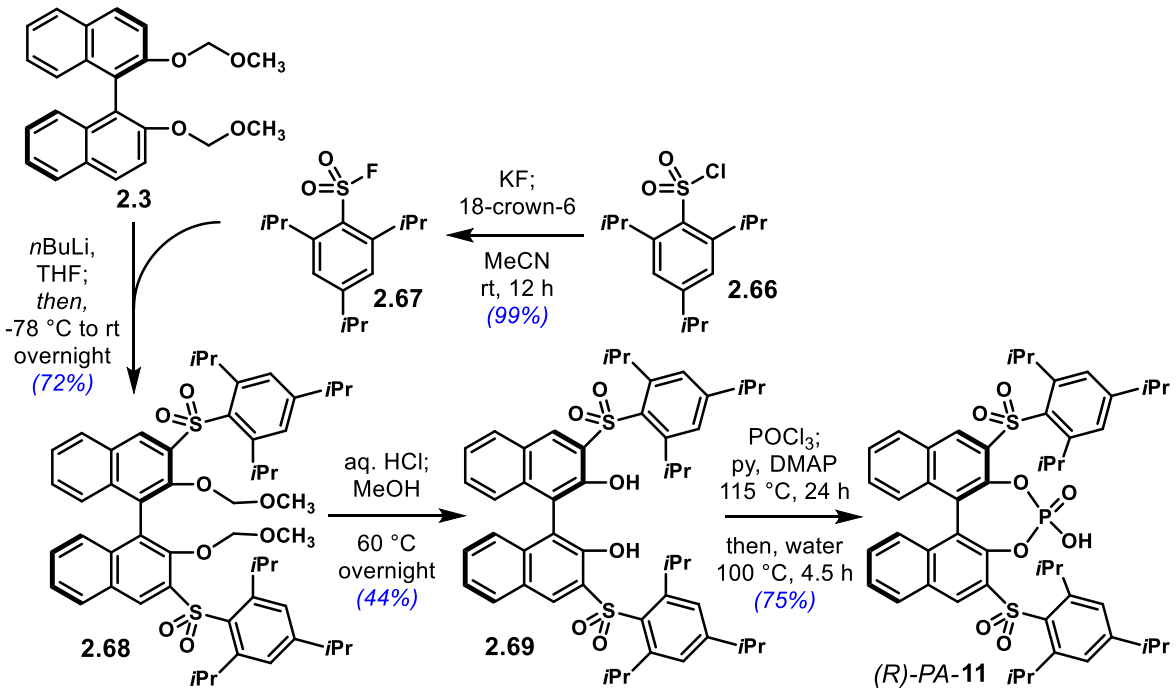

Scheme 2.27: Synthesis of *(R)-PA*-**11**.

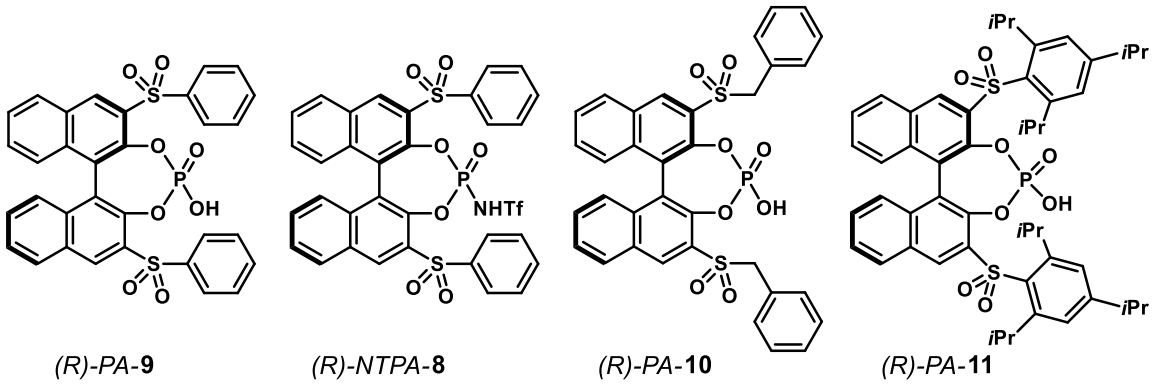

Scheme 2.28: BINOL-aryl sulfone-based Brønsted acids synthesised in this work.

On the next page, there is a list of the BINOL-based Brønsted acids used throughout this work. To avoid confusion or ambiguity, the labels on such a list are used consistently throughout this thesis.

List of PAs and NTPAs used in this work

a) BINOL-based phosphoric acids

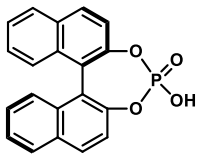

(R)-PA-**1**

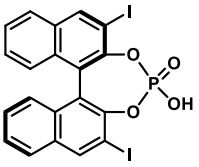

(R)-PA-**2**

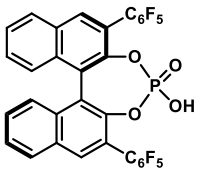

(R)-PA-**3**

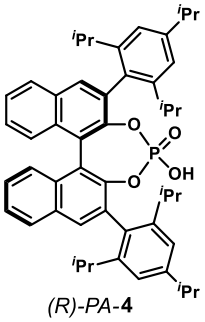

(R)-PA-**4**

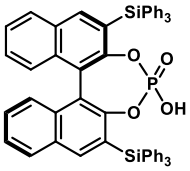

(R)-PA-**5**

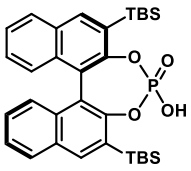

(R)-PA-**6**

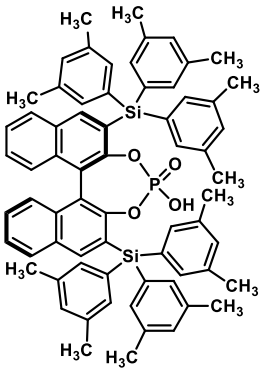

(R)-PA-**7**

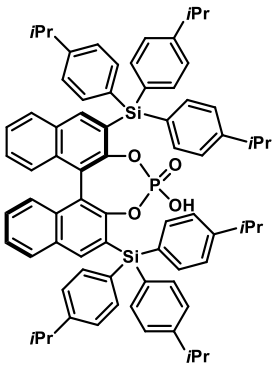

(R)-PA-**8**

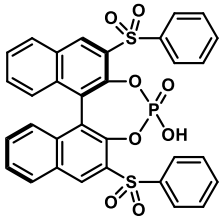

(R)-PA-**9**

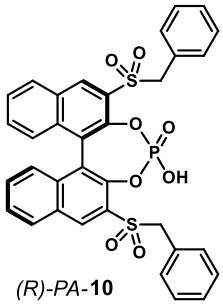

(R)-PA-**10**

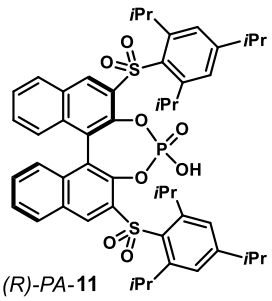

(R)-PA-**11**

b) BINOL-based N-triflylphosphoramides

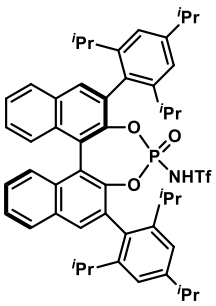

(R)-NTPA-**1**

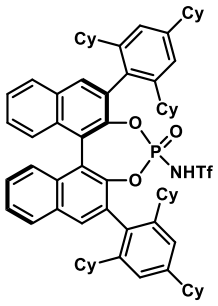

(R)-NTPA-**2**

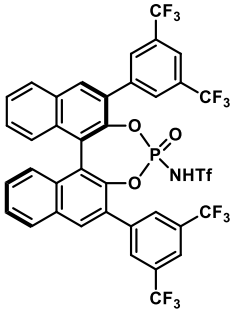

(R)-NTPA-**3**

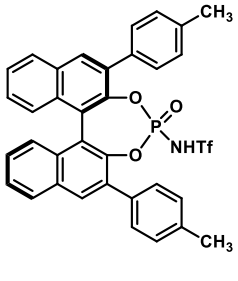

(R)-NTPA-**4**

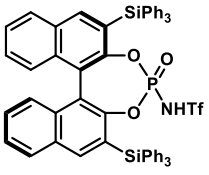

(R)-NTPA-**5**

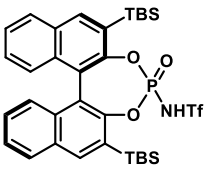

(R)-NTPA-**6**

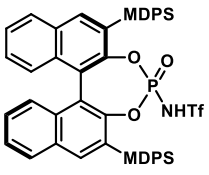

(R)-NTPA-**7**

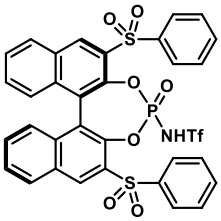

(R)-NTPA-**8**

Chapter 3

Asymmetric Synthesis of *S*-containing Heterocycles

3.1. Organocatalysis and sulfur-containing compounds

Sulfur-containing compounds are ubiquitous in nature.[160–163] In addition, molecules with a chiral centre adjacent to a sulfur atom have important biological activity.[164,165] Some examples of such compounds are presented in Figure 3.1. Indole sulfides like **3.1** have shown to be inhibitors of HIV replication.[166] Saturated *S*-containing heterocycles **3.2** are important molecules in agricultural and medicinal chemistry.[167] Chiral (*S*,*N*)-ketal **3.3** have shown to be an inhibitor for human tumour cells,[168] as well as the family of spirocyclic compounds **3.4**.[169] Compound **3.5** showed to be a potent and selective inhibitor of the *Mycobacterium tuberculosis* protein tyrosine phosphatase B.[170] For this latter example, the *(R)*-enantiomer was ten times more potent than the *(S)*. In such cases were a specific enantiomer is more potent, asymmetric and catalytic syntheses are highly desirable.

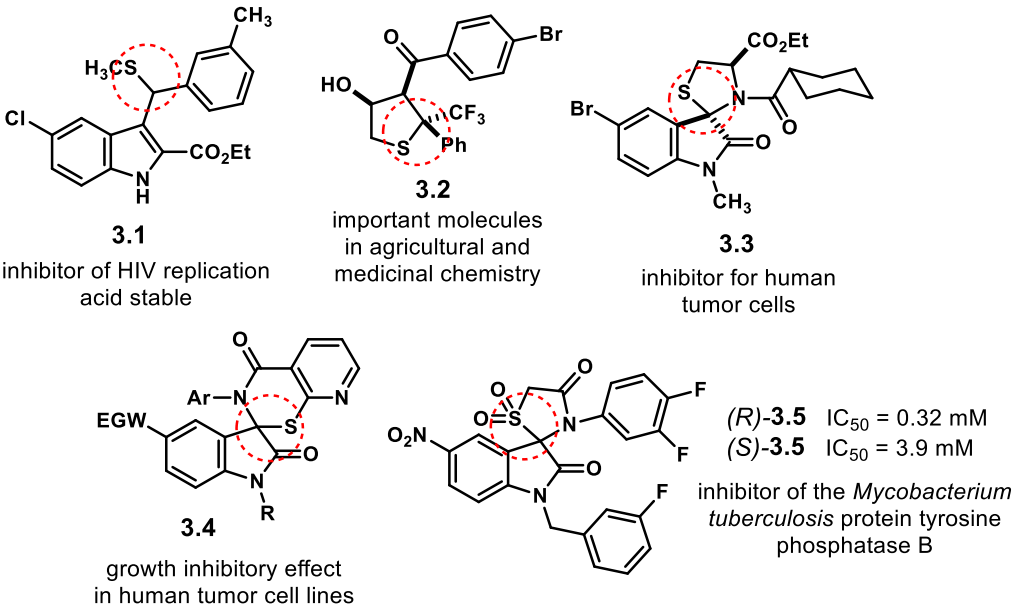

Figure 3.1: Bioactive chiral compounds containing a sulfur motif.

Several catalytic and enantioselective methodologies for the construction of sulfur-containing compounds have been reported.[171] Amongst recently developed organocatalysts for such purpose are Lewis bases like proline derivatives,[172] chiral amines,[173] selenophosphoramides,[174] cinchona alkaloids,[175] cinchona alkaloid-phosphoramides[176] and cinchona alkaloid-squaramides.[167] However, the number of Brønsted acid catalysts for these transformations is less. Recent examples that use chiral Brønsted acids are shown in Scheme 3.1. In these transformations, a chiral centre is installed as well as a sulfur motif.

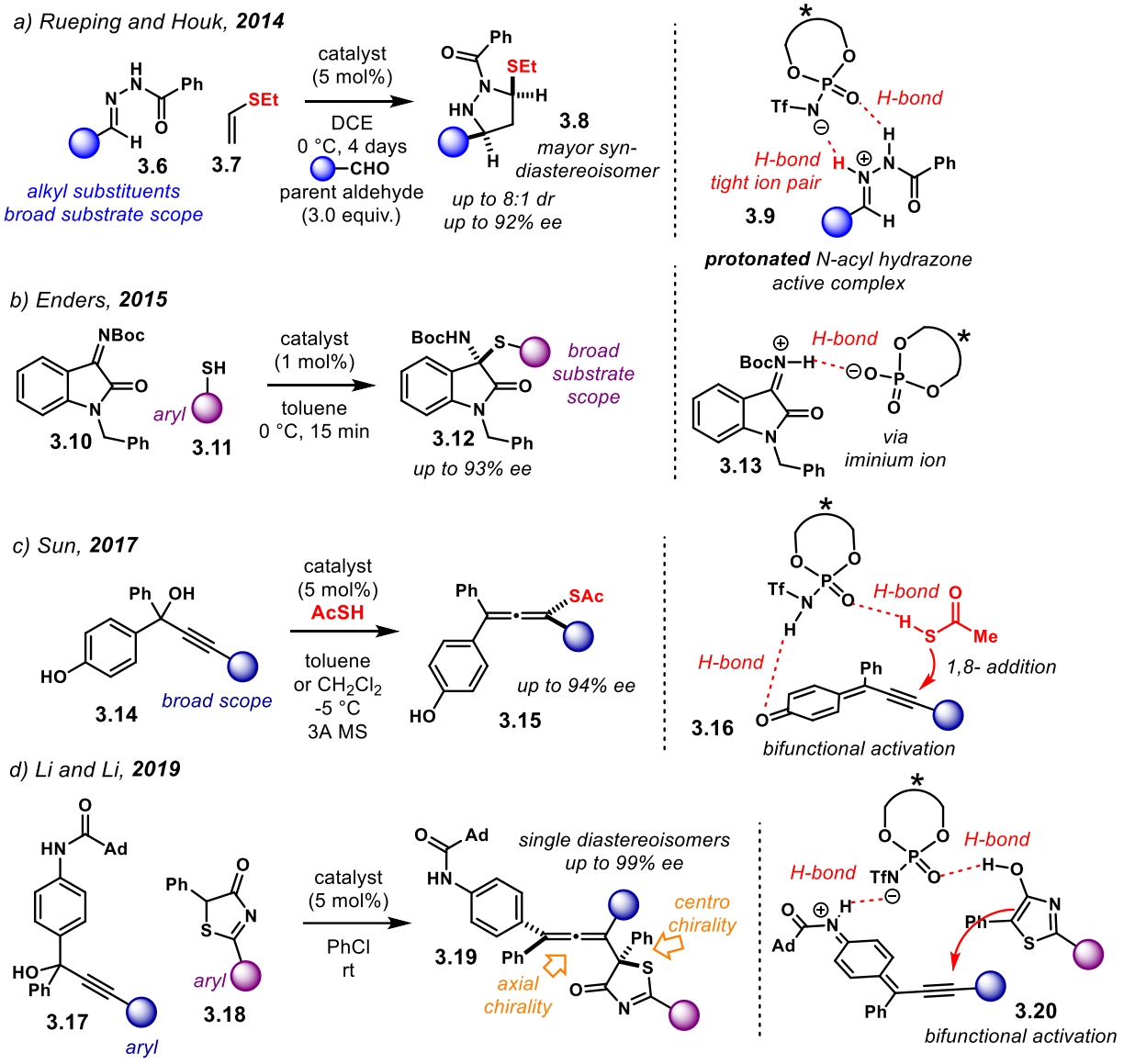

Scheme 3.1: Enantioselective Brønsted-acid catalysed reactions. a) Asymmetric (3+2)-cycloaddition reported by the groups of Rueping and Houk. b) Asymmetric *N*,*S*-acetalisation reported by the group of Enders. c) Enantioselective synthesis of tetrasubstituted allenes reported by the group of Sun. d) Enantioselective synthesis of tetrasubstituted allenes reported by the groups of Li and Li.

In 2014, the groups of Rueping and Houk reported an asymmetric (3+2) cycloaddition reaction of *N*-acyl hydrazones **3.6** with ethyl vinyl thioether **3.7** using an NTPA as Brønsted acid catalysis (Scheme 3.1*a*).[177] The reaction affords heterocycles **3.8** in excellent yields and with good stereocontrol (up to 8:1 *dr* and up to 92% *ee*). Using DFT calculations, it was determined that the reaction goes through a protonated *N*-acyl hydrazone complex **3.9**.

Later, in 2015, the group of Enders published an enantioselective synthesis of *N*,*S*-acetals **3.12** using a PA as catalyst (Scheme 3.1*b*).[178] Isatin-derived imines **3.10** are activated by PA protonation in order to allow addition of thiophenols **3.11**. It is believed that the reactive intermediate is iminium ion **3.13**. The reaction features a wide substrate scope in the thiophenol counterpart and excellent enantiocontrol (up to 93% *ee*).

In another example, the group of Sun reported a creative asymmetric synthesis of tetrasubstituted allenes **3.15** (Scheme 3.1*c*).[179] This reaction does not deliver a centrochirality element but installs a sulfur moiety within an axially chiral product. The reaction uses propargylic alcohols **3.14** and an NTPA as Brønsted acid catalyst. Through a protonation-dehydration sequence, the starting material generates intermediate **3.16**. Therein, the catalyst acts in a bifunctional activation mode to deliver the incoming sulfur nucleophile.

The groups of Li and Li published a similar reaction in which starting materials **3.17** react with **3.18** in an asymmetric fashion to afford allenes **3.19** (Scheme 3.1*d*).[180] In this case, both an axial and a centrochiral unit are formed, the latter bearing a tetrasubstituted chiral centre with a sulfur motif on it. The authors propose that an aza-quinone methide intermediate **3.20** is the reactive species. Such intermediate, as well as the incoming nucleophile, are activated bifunctionally by the counter anion of the NTPA catalyst. The reaction affords tetrasubstituted allenes **3.19** as single diastereoisomers with outstanding enantiocontrol (up to 99% *ee*).

As we have seen, most of the reported chiral Brønsted acid-catalysed reactions make use of nitrogen-based electrophiles—*activated imines*—relying on protonation and hydrogen bonding to activate the substrates (Scheme 3.2*a*). Imines **3.21** are readily available compounds. Their high basicity due to the nitrogen atom lone pair makes them good substrates for Brønsted acid activation. If the catalyst is highly acidic, as in the case of NTPAs, the substrate is likely to be fully protonated forming an iminium ion, **3.22**. Otherwise, a hydrogen-bonded imine-catalyst complex like **3.23** is more likely. In both cases, as hydrogen bonds are formed, the catalyst's counter anion is responsible for controlling stereoselectivity.

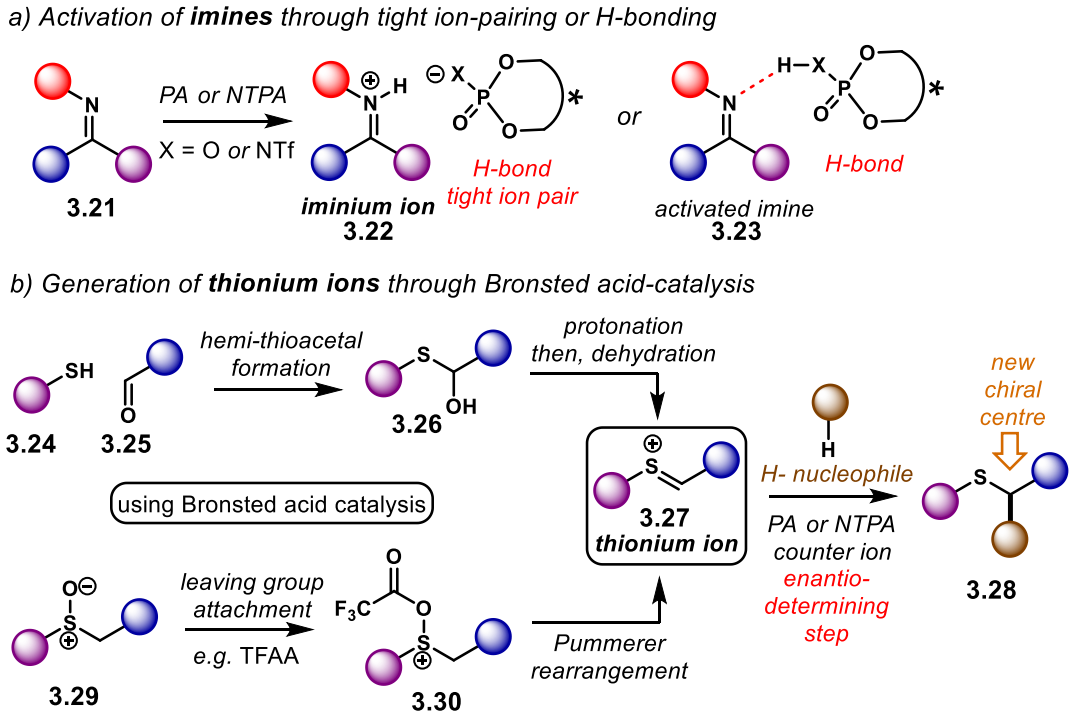

Scheme 3.2: a) Activation of imines through Brønsted acid catalysis. Such activation can be achieved whether through protonation and tight ion-pairing or through a strong hydrogen bond. b) Generation of thionium ions via Brønsted acid catalysis.

In the cases discussed above (*cf.* Scheme 3.1) the sulfur-containing motif comes in the nucleophilic partner. In this context, less attention has been given to thionium ions **3.27** (Scheme 3.2*b*) as sulfur-based electrophilic species within the field of enantioselective Brønsted acid catalysis. There are two plausible ways in which thionium ions can be generated and be used as suitable electrophiles for enantioselective addition reactions. One of these methods commences with thiols **3.24** and aldehydes **3.25**. Both starting materials react, in a Brønsted acid-catalysed reaction, to form hemithioacetals **3.26**. Then, either a PA or an NTPA, protonates the intermediate. Subsequent dehydration furnishes thionium ion **3.27**. After that, addition of an H-nucleophile, driven by the counter anion of the catalyst, would afford product **3.28**, enantioselectively. In the second approach to thionium ions, a leaving group can be attached to a sulfoxide **3.29**. After losing such a group in **3.30** *via* a Pummerer rearrangement fashion, **3.27** would be ready for the enantioselective nucleophilic addition. Several reactions going through intermediate thionium ions have been reported by the group of Procter, in an approach they call the connective Pummerer reaction.[181–187] However, such transformations use stoichiometric amounts of Lewis or Brønsted acids and are not reported to be enantioselective.

The first approach to thionium ions from a thiol and an aldehyde would be very useful, as it will provide easy access to chiral sulfur compounds. In addition, ketones could afford quaternary stereocentres next to the sulfur motif. Such a methodology, using thionium ions as key intermediates in the enantiodetermining step, could even be applicable to make some of the molecules presented at the beginning of the chapter. This is exemplified in Scheme 3.3.

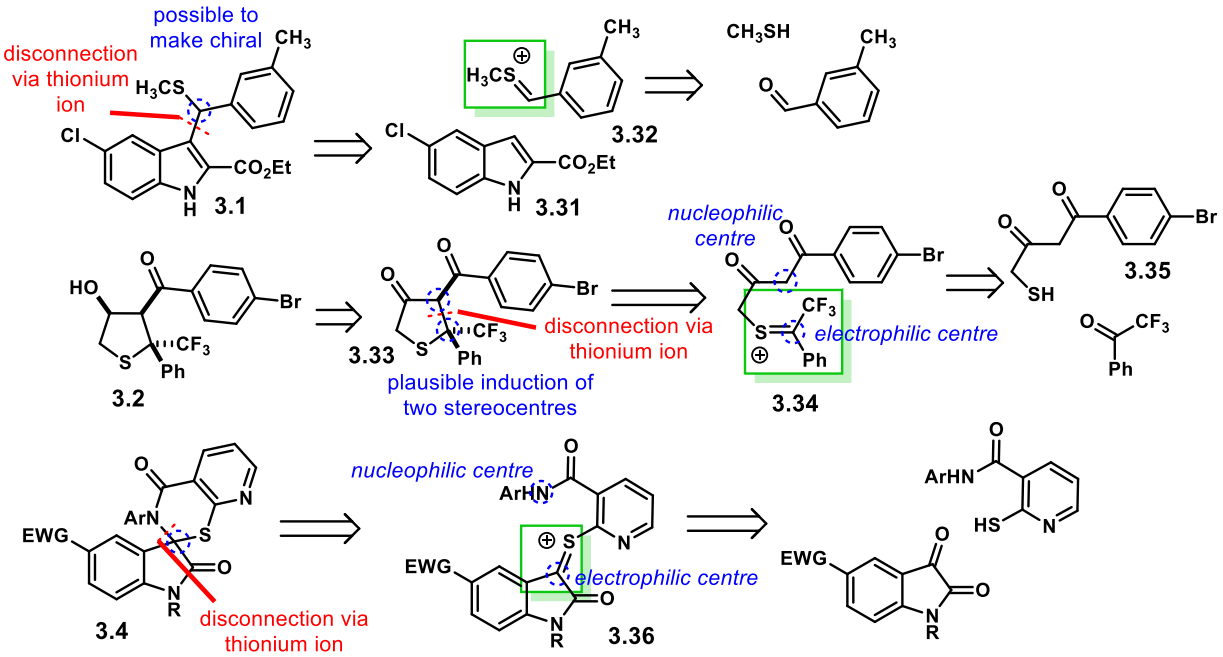

Scheme 3.3: Plausible ways in which bioactive molecule can be synthesised using a thionium ion disconnection.

In order to emphasise how desirable would be an asymmetric reaction going through thionium ions as key intermediates, molecules **3.1**, **3.2** and **3.4** might be synthesised using such an approach. Compound **3.1** can be disconnected back to indole **3.31** and thionium ion **3.32**. The latter species could be generated from the corresponding aldehyde and methylmercaptan. For molecule **3.2** a diastereoselective reduction

can trace back to intermediate **3.33**. A thionium disconnection would deliver **3.34**, which has the possibility of generating two stereocentres in the addition step. This thionium ion could then be generated from trifluoroacetophenone and thiol **3.35**. Finally, compound **3.4** can be disconnected back to thionium ion **3.36**, which in turn can be obtained from the corresponding isatin and thiopyridine. Although these retrosynthetic approaches might look speculative, they actually display how convenient a thionium ion intermediate can be.

3.2. Towards an enantioselective synthesis of 1,3-oxathiolanes

A recent example with Brønsted acid catalysis, reported by the group of List, uses a thionium ion in the enantiodetermining step (Scheme 3.4).[188] The group developed an asymmetric thioacetalisation using IDPAs as catalyst. PAs did not promote the transformation at all. Reaction of **3.37** with aldehydes **3.25** affords heterocycles **3.38** with excellent enantiocontrol (up to 98% *ee*). The reaction starts with the formation of hemi-thioacetal **3.39**. After that, it undergoes a protonation-dehydration sequence to get thionium intermediate **3.40**. Then, enantioselective cyclisation delivers product **3.38**.

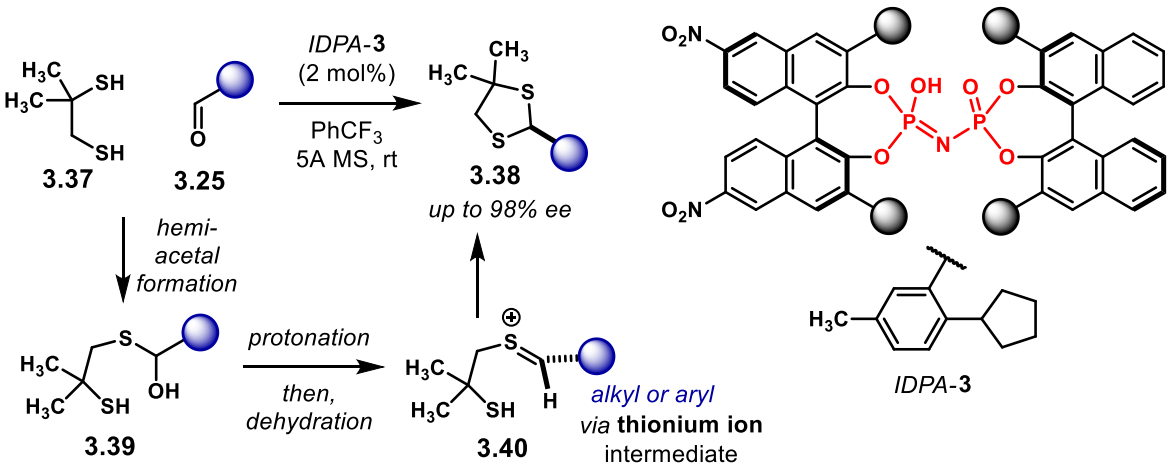

Scheme 3.4: Catalytic asymmetric thioacetalisation reported by the group of List.

With this precedent in mind, a catalytic, enantioselective synthesis of 1,3-oxathiolanes, **3.44**, was envisaged (Scheme 3.5). Starting from an aldehyde **3.25** and 2-mercapto ethanol **3.41**, addition of a Brønsted acid, whether a PA or an NTPA, would form hemi-thioacetal **3.42**. Then, considering the catalyst is acidic enough, a protonation-dehydration sequence would afford intermediate **3.43**. After that, an enantioselective ring closure would afford the desired product **3.44**. In addition, apart from aldehydes, ketones could be suitable substrates too, which in turn could furnish enantioenriched products with a quaternary chiral centre. Although several methodologies to synthesise these *S*,*O*-heterocycles have been reported,[189–198] none of them makes them in an enantioselective fashion.

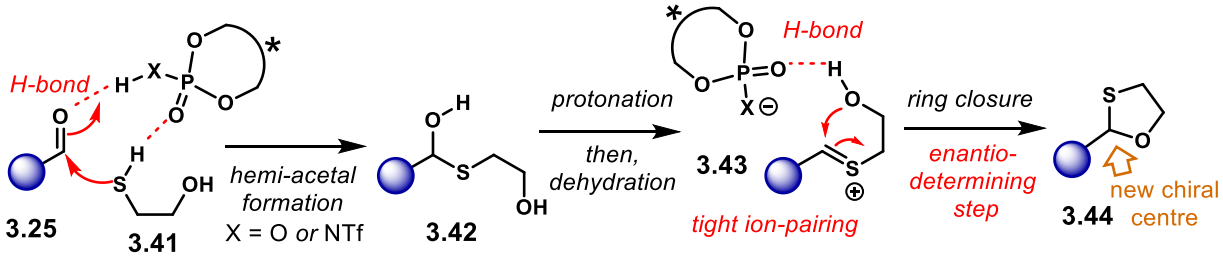

Scheme 3.5: Design of a catalytic and enantioselective synthesis of 1,3-oxathiolanes.

There were several things to take into account when designing this reaction. Firstly, how acidic the catalyst should be in order to activate the aldehyde in the hemi-thioacetal formation step—in the reaction reported by the group of List (*cf.* Scheme 3.4) PAs did not work, presumably due to their low acidity compared to that of IDPAs. In this case, how feasible would it be that a PA could catalyse the reaction? However, if acidity was the main drawback, the more acidic NTPAs would then be able to activate aldehyde **3.25**. Carbonyl activation has shown to be feasible with NTPAs.[23] The protonation-dehydration step, however, should not be unfavourable. Secondly, the thionium ion intermediate **3.43** has to be tightly bound to the catalyst active site in order to achieve high enantiocontrol. In addition, the free –OH moiety in **3.43** can hydrogen-bond to the catalyst. This interaction would be favourable as it can provide more rigidity to the transition state. Finally, this simple reaction can be a good starting point to test the catalysts synthesised in Chapter 2.

As an initial approach, different Brønsted acids were tested in order to evaluate their catalytic activity. Benzaldehyde **3.45** and 2-mercaptoethanol **3.41** were chosen as model substrates to screen the reaction conditions. Chloroform, rt and a 5 mol% catalyst loading were fixed. The starting hypothesis was that the stronger the acid, the higher the catalytic activity will be. Therefore, the yield of the reaction would provide useful insights. The results for seven Brønsted acids in an initial screening are presented in Table 3.1, in the following page. Chloroform was chosen as reaction media.

Acetic acid (**i**, entry 1) did not give a promising result, affording product **3.46** in only 2% yield. On the other hand, trifluoroacetic acid (**ii**, entry 2) performed slightly better, yielding 27% of the product within the same reaction time, 24 h. Therefore, it is clear that a more acidic catalyst—lower p*K*a—promotes the reaction. *rac*-BINOL **iii**, bearing two hydrogen-bond donor sites did not catalyse the reaction (entry 3). Again, the lower the p*K*a, the higher the yield. Acetic acid and BINOL, with p*K*as of 12.3 and 12.98, respectively, are not suitable catalysts for this reaction. However, trifluoroacetic acid, p*K*a = 3.45, does catalyse the reaction.

Then, stronger Brønsted acids were tried. Tosic acid (**iv**, p*K*a = 1.6) and camphorsulfonic acid (**v**, p*K*a = 1.2) gave better results, affording product **3.46** in 86% and 85% yield, respectively (entries 4 and 5). These results point out that catalytic activity is closely related to the catalyst's acidity. For instance, acetic acid seems to be acting merely as a hydrogen-bond donor, in the same way BINOL does. The same argument might be true for trifluoroacetic acid. The acidity of the catalysts, as well as the yields obtained so far, suggest that protonation of the carbonyl group, or a strong hydrogen bond with the catalyst, is essential for the reaction to proceed.

Table 3.1: Initial screening of Brønsted acids.

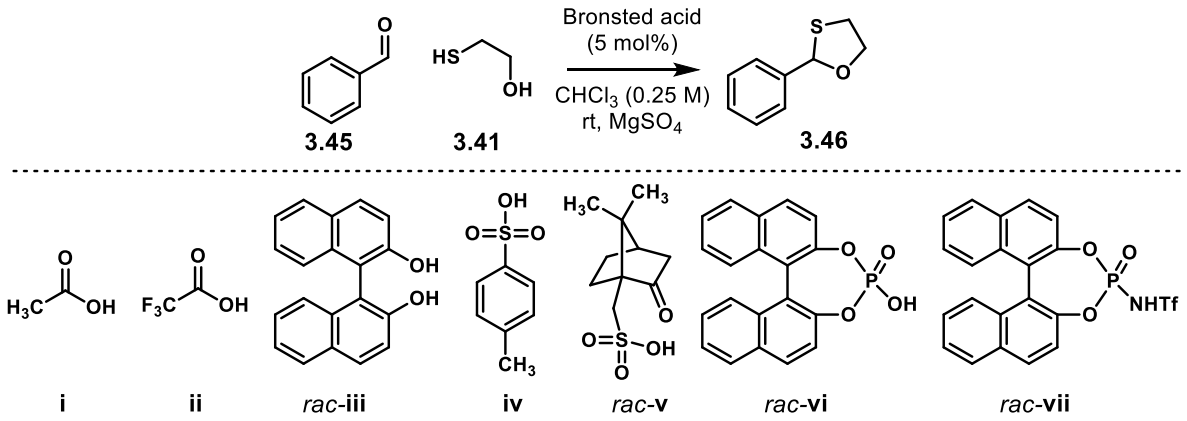

entry	**Brønsted acid**	**time**	**yield**[a]	**p*K*a** (DMSO)
1	**i**	24 h	2%	12.3
2	**ii**	24 h	27%	3.45
3	*rac*-**iii**	48 h	1%	12.98
4	**iv**	24 h	86%	1.6
5	*rac*-**v**	24 h	85%	1.2
6	*rac*-**vi**	24 h	89%	3.37
7	*rac*-**vii**	24 h	84%	2.49

Reaction conditions: Benzaldehyde (0.15 mmol, 1.0 equiv.), 2-mercaptoethanol (0.18 mmol, 1.2 equiv.), $MgSO_4$ (50 mg). [a] Yields correspond to the isolated product. p*K*as in DMSO are shown for comparison purposes.

In order to evaluate if chiral BINOL-based Brønsted acids might be suitable catalysts, racemic BINOL-PA **vi** and racemic BINOL-NTPA **vii** were tested in the reaction. Both catalysts performed similar to the strongest acids used so far. Product **3.46** was obtained in 89% and 84% yields (entries 6 and 7, respectively). Therefore, both PAs and NTPAs can be good catalysts for this transformation.

With these encouraging results, some relatively unhindered PAs were tried for the same model reaction—as well as two highly electron-deficient BINOLs. The results are summarised in Table 3.2 in the following page.

As a 'control' catalyst, *(R)-PA*-**1**, with a 5 mol% catalyst loading, was tried (entry 1). Reaction of **3.45** and **3.41** in chloroform at rt afforded the desired product **3.46** in 74% yield after 24 h. As expected, no significant enantioinduction was observed (3% *ee*). The slightly more hindered catalyst *(R)-PA*-**2** was tried next (entry 2). The same reaction conditions as before afforded the product in good yield but with no significant enantiocontrol (77%, 3% *ee*). Then, changing the solvent for benzene, which has a lower dielectric constant, afforded the product in 80% yield after 72 h. The longer reaction time might suggest a stronger hydrogen bond between the catalyst and the aldehyde is formed in a more polar medium. Enantiocontrol was also negligible (2% *ee*). Then, PA **3.47** was tried at a higher catalyst loading (10 mol%) but diluting the reaction. Reaction in toluene gave a modest yield with but no enantiocontrol after

6 days (entry 4, 46% yield). Reactivity diminished when cyclohexane was used as solvent (entry 5). Compound **3.46** was obtained in 13% yield after 7 days with no enantioselectivity.

Table 3.2: Screening of unhindered PAs.

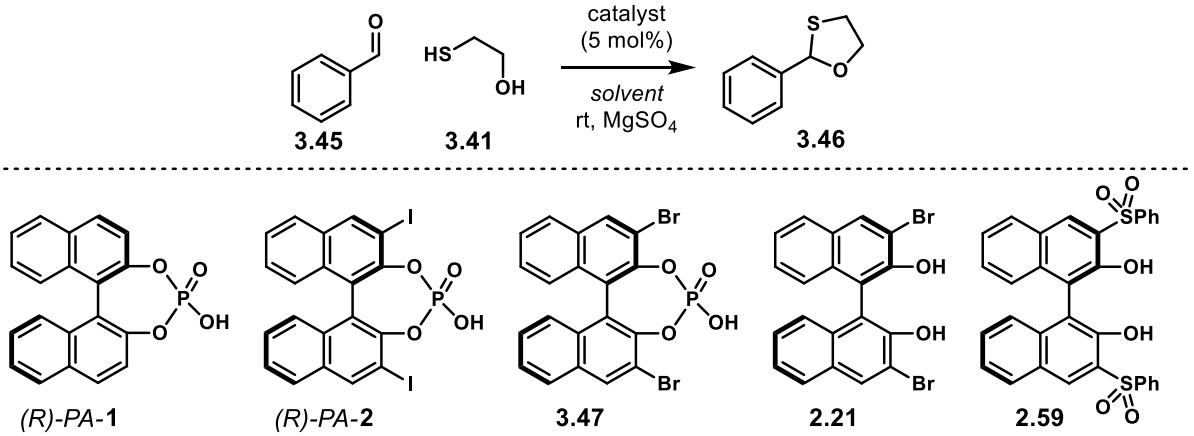

entry	**catalyst**	**solvent**	**time**	**yield**[a]	***ee***
1	*(R)-PA*-**1**	$CHCl_3$ (0.25 M)	24 h	74%	3%
2	*(R)-PA*-**2**	$CHCl_3$ (0.25 M)	24 h	77%	3%
3	*(R)-PA*-**2**	C_6H_6 (0.25 M)	72 h	80%	2%
4	**3.47** (10 mol%)	toluene (0.1 M)	144 h	46%	0
5	**3.47** (10 mol%)	cyclohexane (0.1 M)	168 h	13%	0
6	**2.21**	$CHCl_3$ (0.25 M)	48 h	2%	0
7	**2.59**	$CHCl_3$ (0.25 M)	48 h	6%	1%

Reaction conditions: Benzaldehyde (0.10 mmol, 1.0 equiv.), 2-mercaptoethanol (0.12 mmol, 1.2 equiv.), $MgSO_4$ (50 mg), catalyst (5 mol%) unless something else specified. [a] Yields correspond to the isolated product.

In addition, BINOLs **2.21** and **2.59** were tried in the reaction (entries 6 and 7). The idea was that due to the electron-withdrawing groups in the 3,3'- positions acidity could improve. However, that was not the case. Both BINOLs slightly promoted the reaction after 48 h.

As it was expected, the unhindered BINOL-based PAs did not provide good enantiocontrol in the reaction. Therefore, a series of catalysts with bulkier 3,3'- substituents were tried. The results are presented in Table 3.3 on the next page. As starting point, catalyst *(R)-PA*-**4** was tried. Reaction in chloroform (entry 1) afforded the desired product in 39% yield and 12% *ee* after 24 h. Doubling the reaction time (entry 2) slightly improved both the yield and the enantioselectivity (46%, 19% *ee*). Both the yield and enantiocontrol further improved when the reaction was done in benzene (entry 3). After 48 h a 56% yield and 33% *ee* were obtained. Next, the catalyst loading and dilution was evaluated, along as with other non-polar solvents. Toluene and a 10 mol% catalyst loading made the reaction sluggish but with modest results (entry 4). 43% yield and 33% *ee* was obtained, albeit after 6 days. Changing the solvent to cyclohexane showed to be detrimental for both reactivity and enantiocontrol (entry 5). 16% yield and 23% *ee* was achieved after 6 days of reaction. Therefore, it seems that dilution—going from 0.25 M to 0.1 M—

decreases the reaction rate considerably, yet similar results could be obtained at expense of higher catalyst loading (comparing entries 3 and 4).

Table 3.3: PAs screening

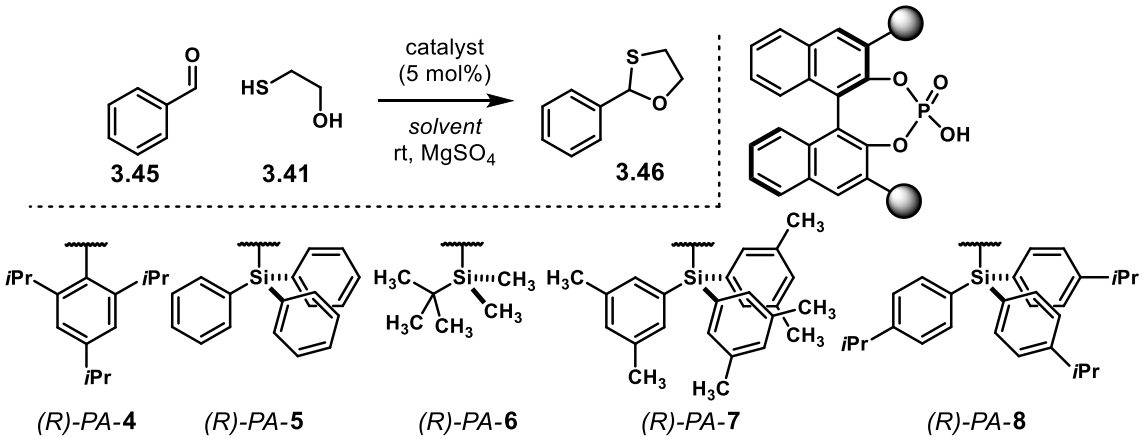

entry	**catalyst**	**solvent**	**time**	**yield**[a]	***ee***
1	*(R)-PA*-**4**	$CHCl_3$ (0.25 M)	24 h	39%	12%
2	*(R)-PA*-**4**	$CHCl_3$ (0.25 M)	48 h	46%	19%
3	*(R)-PA*-**4**	C_6H_6 (0.25 M)	48 h	56%	33%
4	*(R)-PA*-**4** (10 mol%)	toluene (0.1 M)	144 h	43%	33%
5	*(R)-PA*-**4** (10 mol%)	cyclohexane (0.1 M)	144 h	16%	23%
6	*(R)-PA*-**5**	$CHCl_3$ (0.25 M)	48 h	33%	3%
7	*(R)-PA*-**5**	C_6H_6 (0.25 M)	48 h	40%	13%
8	*(R)-PA*-**5**	C_6H_6 (0.25 M)	72 h	47%	12%
9	*(R)-PA*-**5** (10 mol%)	cyclohexane (0.1 M)	96 h	18%	15%
10	*(R)-PA*-**6**	$CHCl_3$ (0.25 M)	48 h	31%	15%
11	*(R)-PA*-**6**	C_6H_6 (0.25 M)	48 h	41%	19%
12	*(R)-PA*-**6**	C_6H_6 (0.25 M)	72 h	51%	15%
13	*(R)-PA*-**7**	$CHCl_3$ (0.25 M)	48 h	6%	-5%
14	*(R)-PA*-**7**	C_6H_6 (0.25 M)	72 h	19%	-8%
15	*(R)-PA*-**8**	$CHCl_3$ (0.25 M)	48 h	17%	-5%
16	*(R)-PA*-**8**	C_6H_6 (0.25 M)	72 h	38%	6%

Reaction conditions: Benzaldehyde (0.10 mmol, 1.0 equiv.), 2-mercaptoethanol (0.12 mmol, 1.2 equiv.), $MgSO_4$ (50 mg), catalyst (5 mol%) unless something else specified. [a] Yields correspond to the isolated product.

Next, the family of catalysts with silicon-based scaffolds were tested in this reaction. Catalyst *(R)-PA*-**5**, which has triphenylsilyl 3,3'- substituents, afforded the product in 33% yield when the reaction was done in chloroform for 48 h (entry 6). However, the enantiocontrol, 3% *ee*, was not significant. On the other hand, if benzene is used as reaction media (entry 7), both the yield and, noticeably, enantioselectivity improve (40%, 13% *ee*). Leaving the reaction longer, for 72 h, with the same conditions slightly rises the yield to 47% (entry 8) without further enantioinduction (12% *ee*). Dilution and double the catalyst loading

in cyclohexane made the reaction slower (entry 9), as seen before. After 4 days, the product is obtained in 18% yield and a slightly increased 15% *ee*.

The less hindered catalyst *(R)-PA*-**6** turned out to give better results. Reaction in chloroform for 48 h afforded the product in 31% yield and 15% *ee* (entry 10). Changing the solvent to benzene improved both reactivity and enantiocontrol (41%, 19% *ee*, entry 11). Longer reaction time, 72 h (entry 12), increased the yield to 51%. However, the enantioselectivity was slightly diminished to 15% *ee*. This might suggest that a racemisation process starts to take place if the reaction is left for a long time.

Finally, the bulkiest silicon-based catalysts were tried. As expected, the active site of these catalysts seems to be too hindered for the reagents to fit in the chiral cavity. Reaction in chloroform for 48 h with catalyst *(R)-PA*-**7** only gave a 6% yield with a low -5% *ee* (entry13). Despite those discouraging results, it is noticeable that the opposite sense of enantioinduction is obtained with catalyst *(R)-PA*-**7**. When the reaction was done in benzene for 72 h (entry 14), the yield improved to 19%. In addition, the enantioselectivity showed a minor increase to -8% *ee*, again, with the opposite sense of enantioinduction.

Catalyst *(R)-PA*-**8**, which has a confined active site, made the reaction slow (entry 15). After 48 h in chloroform, the product was obtained in 17% yield and -5% *ee*. With a longer, 72 h, reaction time in benzene, the yield improved to 38% (entry16). This was not the case for enantiocontrol (6% *ee*). Interestingly, with the same catalyst *(R)-PA*-**8**, the opposite senses of enantioinduction, yet low, were observed when solvent with different polarities were tried (compare entries 15 and 16).

The results from table 3.3 show that chiral PAs indeed catalyse the *O*,*S*-acetal formation. In addition, the reaction can be done enantioselectively. However, the low and modest yields might be indicative that the catalyst is not acidic enough to push the reaction to higher yields. Moreover, the catalyst's scaffolds have to be further improved to achieve better enantiocontrol. So far, *(R)-PA*-**4**, was shown to be the best PA for this transformation (56% yield, 33% *ee*, entry 3).

In this context, the next set of catalysts screened were the more acidic NTPAs. Initially, the reaction was tried using four different catalysts, in chloroform at rt. Also, to be consistent with the reaction time, all reactions were run for 24 h. Table 3.4 in the next page summarises the initial screening with NTPAs towards chiral 1,3-oxathiolanes.

Catalyst *(R)-NTPA*-**1** gave product **3.46** in 81% yield (entry 1). However, no enantiocontrol was observed. *(R)-NTPA*-**5**, which has silicon-based scaffolds, also afforded the product in good yield (79%, entry 2). Again, no enantiocontrol was observed. Then, the less hindered silicon-based catalyst *(R)-NTPA*-**6** was tried (entry 3). The desired product was obtained in 75% yield but without enantioselectivity. Finally, catalyst *(R)-NTPA*-**8** was tried (entry 4). A good 78% yield was obtained, yet with no enantiocontrol. Possibly, for NTPAs, chloroform was such a polar solvent that did not allow a tight ion-pair (*cf.* **3.43**, Scheme 3.5). Therefore, a non-polar solvent could have been able to stabilise such an intermediate and provide good enantiocontrol. Unfortunately, this was not the case. Reaction in benzene with *(R)-NTPA*-**5** afforded the product in 71% yield with no enantiocontrol (entry 5). The same was true for catalyst *(R)-NTPA*-**6** under the same reaction conditions (entry 6).

Table 3.4: Initial screening of NTPAs.

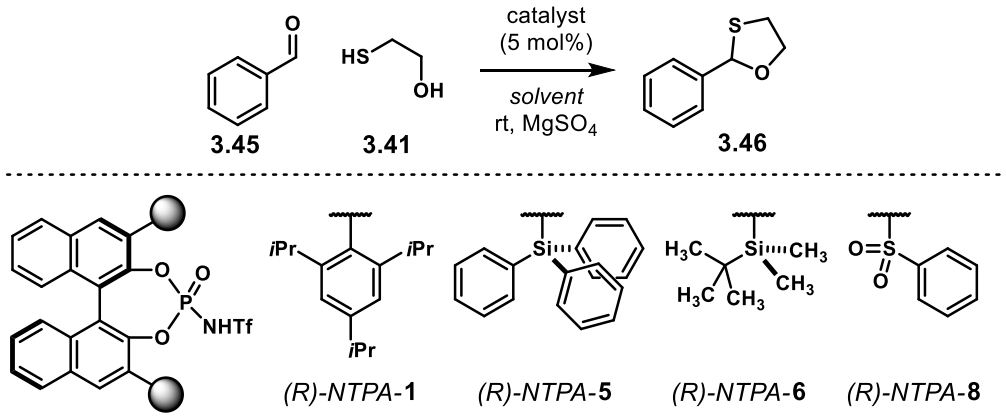

entry	catalyst	solvent	time	yield[a]	*ee*
1	*(R)-NTPA*-**1**	$CHCl_3$ (0.25 M)	24 h	81%	0
2	*(R)-NTPA*-**5**	$CHCl_3$ (0.25 M)	24 h	79%	0
3	*(R)-NTPA*-**6**	$CHCl_3$ (0.25 M)	24 h	75%	0
4	*(R)-NTPA*-**8**	$CHCl_3$ (0.25 M)	24 h	78%	0
5	*(R)-NTPA*-**5**	C_6H_6 (0.25 M)	24 h	71%	0
6	*(R)-NTPA*-**6**	C_6H_6 (0.25 M)	24 h	71%	0

Reaction conditions: Benzaldehyde (0.10 mmol, 1.0 equiv.), 2-mercaptoethanol (0.12 mmol, 1.2 equiv.), $MgSO_4$ (50 mg), catalyst (5 mol%). [a] Yields correspond to the isolated product.

Given that no enantiocontrol was observed at all for NTPAs, it might be that a racemisation process takes over after a certain time. In order to get insight into how the enantioselectivity varies a series of experiments following the reaction through time were conducted. Using a 5 mol% catalyst loading, the reaction was followed in benzene at rt. Catalysts *(R)-PA*-**5** and *(R)-NTPA*-**5** were used and the results are presented in Figure 3.2.

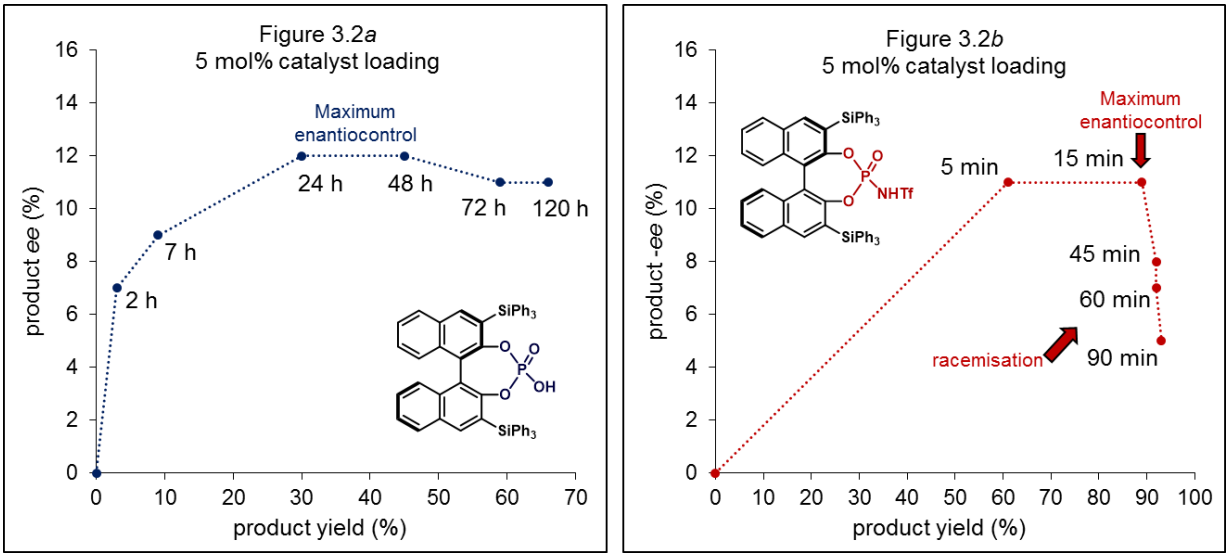

Figure 3.2: a) Reaction following with *(R)-PA*-**5**. b) Reaction following with *(R)-NTPA*-**5**. Reactions conducted in benzene at room temperature.

To start with, the reaction of benzaldehyde with 2-mercapto ethanol was followed through time with catalyst *(R)-PA*-**5** (Figure 3.2*a*). In the graph is presented the product yield against the product enantiomeric excess. Plotting the data in that way shows how both the yield and *ee* vary through time. Each point, therefore, corresponds to a different time. In 2 h, the product is obtained in 3% yield and 7% *ee*. Leaving the reaction for a longer time improves both. At 7 h, the product has reached 9% yield and 9% *ee*. It is clear that the PA is catalysing the reaction, albeit slowly. After 24 h, the product is afforded in 30% yield and with an increased 12% *ee*. With additional 24 h—48 h in total—the product is obtained in 45% yield and 12% *ee*. So far, for the first 48 h of reaction, the yield increases and enantiocontrol reaches a maximum. At 72 h, the yield is further improved to 59%. However, the enantioselectivity diminishes slightly (11% *ee*). Leaving the reaction for a longer time, 120 h, 5 days, the yield does not seem to increase more than 66%. The same is true for enantioinduction (11% *ee*).

On the other hand, when *(R)-NTPA*-**5** was used (Figure 3.2*b*), both yield and enantiomeric excess boost up to 61% and -11% *ee*, respectively. This, just during the first *five minutes* of reaction. At 15 minutes, the yield builds up to 89%. However, this is not the case for the enantiomeric excess, which 'stays' in -11% *ee*. Interestingly, at 45 minutes, the enantioselectivity sharply drops to -8% *ee*. The improvement of yield is minimal (92%). Hence, at this point—or even before—a racemisation side reaction takes over the process. At 60 minutes, the yield remains practically invariant as the enantioselectivity drops to -7% *ee*. At 90 minutes, the situation is similar. The yield remains unchanged and the enantiomeric excess drops further down to -5% *ee*. Therefore, if the reaction was left for 24 h, full racemisation would be expected, as it was shown previously on Table 3.4. This suggests that, at a 'high' catalyst loading, NTPAs start to behave in a general catalysis fashion and start to promote the reverse reaction, thus, racemising the enantioenriched product. If that is the case, a lower catalyst loading should avoid or diminish the racemisation reaction but still promote the enantioselective formation of the product.

With this in mind, the reaction was followed in benzene at rt using a catalyst loading of 0.5 mol% for *(R)-NTPA*-**5** (Figure 3.3*a*). Even for such a low catalyst loading, the reaction with *(R)-NTPA*-**5** proceeds more efficiently than the one with the corresponding PA. After just five minutes, the enantioselectivity boosts up to -13% *ee*, albeit with a low 12% yield. At 15 minutes, the yield doubles, 26%; however, the enantiomeric excess slightly diminishes to -12% *ee*. After 30 minutes, the product is obtained in 46% yield without modification in the enantioselectivity value. Further, 52% yield is achieved at 60 minutes, keeping a constant enantiomeric excess (-12% *ee*). Herein, a plateau of constant enantioinduction is reached, while the product yield is still increasing. At 3 h, with an 80% yield, the product can still be obtained with -12% *ee*. At 6 h, the yield increments up to 86% at the expense of enantiocontrol, which drops down to -11% *ee* at this point. Here, the racemisation process starts to take over. Pushing the reaction time to 9 h does not enhance the yield, yet the enantioselectivity drops to -10% *ee*. Finally, when the reaction is left for 24 h, enantiocontrol diminishes to -5% *ee*. The yield remains at 86%. Therefore, if the reaction is stopped between 3 and 6 h, a good yield can be obtained without jeopardising enantioselectivity.

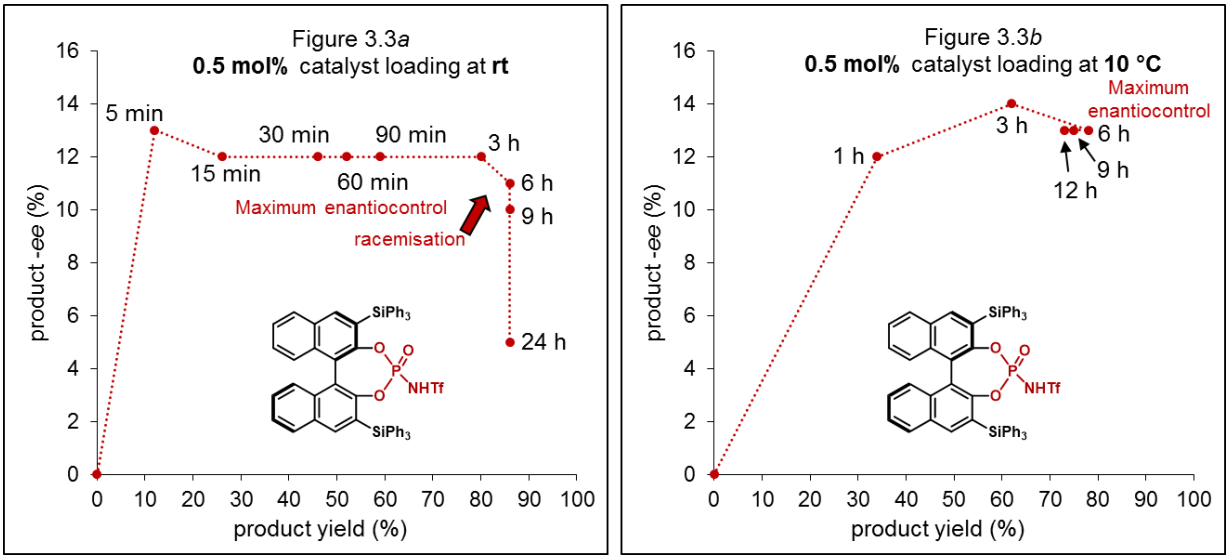

Figure 3.3: Reaction following with *(R)-NTPA*-**5** (0.5 mol%) at a) room temperature. b) 10 °C. Reactions conducted in benzene.

A similar trend was observed when the reaction was followed with the same conditions but at 10 °C. At a lower temperature, the reaction becomes sluggish. 30% yield and -12% *ee* were obtained after 1 h. At 3 h, the product was afforded in 62% yield and a maximum -14% *ee* was achieved. Doubling the reaction time, to 6 h, increases the yield to 78%. Here, it seems that the racemisation process starts to take over, as the enantiocontrol slightly drops to -13% *ee*. However, at longer reaction times, the enantiocontrol remains constant while the product yield diminishes marginally, down to 75% at 9 h and 73% after 12 h.

As these results suggest, a slightly higher *ee* could be obtained if the temperature is lowered. Hence, a temperature screening was conducted. In order to reach lower temperatures than the freezing point of benzene (5 °C), the screening was done in toluene using *(R)-NTPA*-**5** with a 0.5 mol% catalyst loading. In addition, to achieve a reasonable yield/enantioselectivity balance, the reactions were run for 5 h. The results are presented in Table 3.5 on the next page.

As might have been expected, at a high temperature, 40 °C (entry 1), the reaction proceeds in excellent yield, albeit with low enantiocontrol (87% and -6% *ee*). At room temperature, product **3.46** is obtained in 86% yield and -11% *ee* (entry 2). Lowering the temperature to 12 °C has no effect on enantioselectivity and the product is obtained still with an acceptable 73% yield (entry 3). Further decrease of temperature to 0 °C diminishes the product yield to 68% (entry 4). Enantioselectivity seems not to be affected. Reaction at -15 °C dramatically reduces the yield down to 20% (entry 5). Interestingly, this was not detrimental nor favourable for enantiocontrol. At a lower temperature, -40 °C (entry 6), the reaction still proceeds, yet with a low 18% yield. Enantiocontrol remains at -11% *ee*. It is surprising how enantiocontrol is not improved at lower temperatures but remains consistent. Thus, for a reasonable yield/enantioselectivity balance, reaction at room temperature for 5 h is optimal.

Table 3.5: Temperature screening

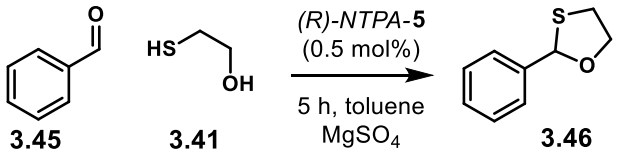

entry	**temperature**[a]	**yield**[b]	***ee***
1	40 °C	87%	-6%
2	26 °C (rt)	86%	-11%
3	12 °C	73%	-11%
4	0 °C	68%	-11%
5	-15 °C	20%	-11%
6	-40 °C	18%	-11%

Reaction conditions: Benzaldehyde (0.15 mmol, 1.0 equiv.), 2-mercaptoethanol (0.18 mmol, 1.2 equiv.), $MgSO_4$ (50 mg), toluene (0.25 M), catalyst (0.75 mg, 0.5 mol%). [a] Temperatures below rt were kept with cooling baths: dry ice/1,4-dioxane, 12 °C; ice water, 0 °C; dry ice/benzylic alcohol, -15 °C; dry ice/acetonitrile, -40 °C. [b] Yields correspond to the isolated product.

Next, the catalyst loading was revisited. While following the reaction through time (*cf.* Figure 3.3*a*), 0.5 mol% was chosen arbitrarily. Therefore, a quick check on the catalyst loading was done. The experiments were performed in toluene and at room temperature. The results are summarised in Table 3.6.

Table 3.6: A quick screening of catalyst loading.

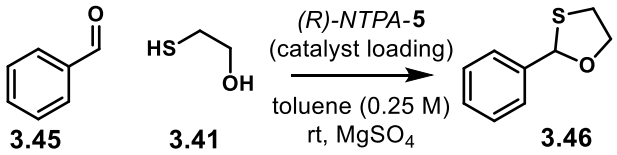

entry	**catalyst loading**	**time**	**yield**[a]	***ee***
1	1.0 mol%	15 min	46%	-10%
2	1.0 mol%	1 h	71%	-10%
3	1.0 mol%	3 h	76%	-7%
4	0.5 mol%	6 h	86%	-11%
5	0.1 mol%	6 h	30%	-11%
6	0.1 mol%	24 h	37%	-11%

Reaction conditions: Benzaldehyde (0.15 mmol, 1.0 equiv.), 2-mercaptoethanol (0.18 mmol, 1.2 equiv.), $MgSO_4$ (50 mg), toluene (0.25 M). [a] Yields correspond to the isolated product.

When catalyst *(R)-NTPA*-**5** was used at a 1 mol% load (entry 1), product **3.46** is obtained in 46% yield and -10% *ee* after 15 minutes. If the reaction is left longer, for 1 h, still with a 1 mol% of catalyst, the product is obtained in 71% and -10% *ee* (entry 2). In that case, the yield improves while the enantioselectivity remains constant. Presumably, an enantiocontrol plateau is reached at this point. At 3 h, still with 1 mol% of catalyst loading, the yield improves slightly (76%, entry 3); however, the

enantiomeric excess starts to go down (-7% *ee*). Entry 4 was included as a control reference. With 0.5 mol% loading the desired product is afforded in 86% yield and -11% *ee* after 6 h. Lowering the catalyst loading to 0.1 mol% did not have a dramatic effect on enantiocontrol, albeit, it was detrimental for reactivity. After 6 h, the product is obtained in 30% yield and -11% *ee* (entry 5). Longer reaction time, 24 h, did not improve the yield significantly (37%, entry 6).

The equivalents of 2-mercapto ethanol were also taken into account during the screenings. No change in enantioselectivity was observed when 1.0, 1.5, 2.0 or 2.5 equivalents were used. The other parameters were kept at 0.5 mol% loading, toluene (0.25 M) and rt. Yields remained within a 73-84% range.

After all the parameters screened so far, the best results were achieved with a 0.5 mol% catalyst loading at rt for 4-6 h. A low polarity solvent like benzene or toluene performs well, the latter being preferred due to its low toxicity.

With that set of optimal conditions, four NTPAs were tested in the reaction. The results are shown in Table 3.6. In contrast to the results presented previously with 5 mol% catalyst loading (*cf.* Table 3.4), enantioselectivities could be recorded with 0.5 mol%, quenching the reaction after 4.5 h. Catalyst *(R)-NTPA*-**1** afforded product **3.46** in 65% yield and -28% *ee*. In sharp contrast, the corresponding *(R)-PA*-**4**, afforded the same product in 56% yield and 33% *ee* (*cf.* Table 3.3, entry 3): similar yield but with the opposite sense of enantioinduction.

Table 3.6: Screening of NTPAs with optimised reaction parameters.

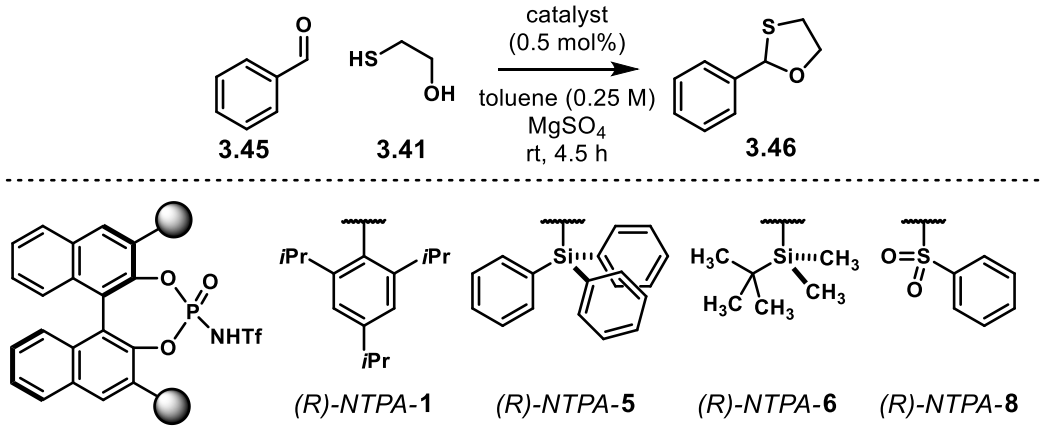

entry	**catalyst**	**yield**[a]	***ee***
1	*(R)-NTPA*-**1**	65%	-28%
2	*(R)-NTPA*-**5**	77%	-9%
3	*(R)-NTPA*-**6**	64%	1%
4	*(R)-NTPA*-**8**	63%	-4%

Reaction conditions: Benzaldehyde (0.15 mmol, 1.0 equiv.), 2-mercaptoethanol (0.18 mmol, 1.2 equiv.), $MgSO_4$ (50 mg), toluene (0.25 M), catalyst (0.5 mol%). [a] Yields correspond to the isolated product.

(R)-NTPA-**5** gave the desired product in 77% yield and -9% *ee* (entry 2). This result also withstands with the analogous PA, *(R)-PA*-**5**, which afforded the opposite enantiomer in 47% yield and 12% *ee* (*cf.* Table 3.3, entry 8). The less hindered silicon-based catalyst *(R)-NTPA*-**6** furnished the product in 64% yield,

albeit with only 1% *ee* (entry 3). A similar output was obtained with *(R)-NTPA*-**8**, which bears sulfone-based scaffolds (entry 4); the product was obtained in 63% yield with -4% *ee*.

Considering everything, several trends emerge. For most of the cases, an opposite sense of enantioinduction is achieved when changing the active site of the catalyst from PA to NTPA whilst keeping the same 3,3' substituents. In general, higher enantioselectivities are obtained with PAs, albeit a higher 5 mol% catalyst loading and longer reaction times (up to 48 h) are needed. On the other hand, with NTPAs, higher yields are afforded at a tenth of the catalyst loading, 0.5 mol%, and in shorter reaction times (4-6 h). Yet, the enantioselectivities are low but can be improved.

The next step was to evaluate if a larger ring size in the product could improve enantiocontrol. Thus, the reaction of benzaldehyde **3.45** and 3-mercapto propanol **3.48** to yield heterocycle **3.49** was tried. The catalyst screening is presented inTable 3.7 on the next page. Both PAs and NTPAs were tested using catalyst loadings of 5 mol% and 0.5 mol%, respectively. The reactions were conducted in toluene at rt.

Catalyst *(R)-PA*-**4** afforded the desired product in 31% yield and 9% *ee* after 48 h (entry 1). The analogous catalyst *(R)-NTPA*-**1** gave the product in 57% yield and -13% *ee* after 5 h (entry 2). Herein, an opposite sense of enantioinduction is also observed when changing from the PA to the NTPA whilst keeping the same 3,3' substituents.

Then, silicon-based catalysts were tried. *(R)-PA*-**5** afforded the desired product in 12% yield and 14% *ee* (entry 3). The corresponding *(R)-NTPA*-**5** gave a higher 68% yield but with lower enantiocontrol, -8% *ee* (entry 4). Enantioreversal is also observed. Catalyst *(R)-PA*-**6** furnished the product in 56% yield and -2% *ee* (entry 5). The analogous *(R)-NTPA*-**6** gave the heterocycle in 76% yield and 4% *ee* (entry 6). For these two catalysts, enantioselectivity was low. Possibly due to the larger substrate, as more conformations might be available for the transition state. In addition, the small chiral cavity created by the TBS substituents might not provide the transition state with enough rigidity to allow good enantio-differentiation.

Finally, two of the sulfone-based catalysts were tried. *(R)-PA*-**9** gave the product in 49% yield and 2% *ee* after 5 h (entry 7). Because of the higher acidity of sulfone-based PAs, which arises from intramolecular hydrogen bonding with the sulfonyl moiety, the reaction time for these types of PAs is within the same magnitude as for NTPAs. *(R)-NTPA*-**8** furnished the product in 78% yield after 5 h, albeit with no enantiocontrol (entry 8).

In conclusion, although the enantioselectivities were low, it is possible to make *S*,*O*-heterocycles in an asymmetric fashion using chiral Brønsted acids. In general, but not in all cases, opposite senses of enantioinduction were observed when the active site of the catalyst is varied from a PA to the NTPA, whilst keeping the same 3,3' substituents in the catalyst framework. In order to achieve higher levels of enantiocontrol, further catalyst screening ought to be done. It is well-known that catalyst screening stage is the main bottle-neck when attempting to discover enantioselective transformations.

Finally, one of the key elements in this chapter is the high acidity of NTPAs, in comparison with PAs. Such is the acidity of NTPAs that it makes them very active catalysts. For the thioacetalisation reactions

studied in this chapter a catalyst loading as low as 0.5 mol% was found to deliver this transformation in an efficient way.

Table 3.7: Catalyst screening for 6-membered rings.

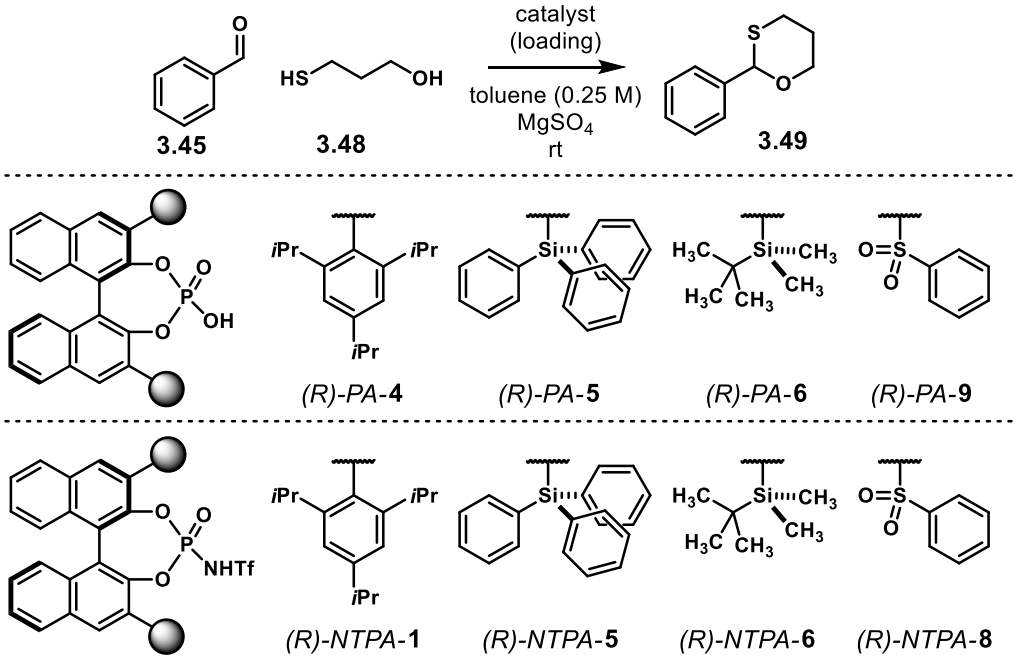

entry	**catalyst**	**time**	**yield**[a]	***ee***
1	*(R)-PA*-**4** (5 mol%)	48 h	31%	9%
2	*(R)-NTPA*-**1** (0.5 mol%)	5 h	57%	-13%
3	*(R)-PA*-**5** (5 mol%)	48 h	12%	14%
4	*(R)-NTPA*-**5** (0.5 mol%)	5 h	68%	-8%
5	*(R)-PA*-**6** (5 mol%)	48 h	56%	-2%
6	*(R)-NTPA*-**6** (0.5 mol%)	5 h	76%	4%
7	*(R)-PA*-**9** (5 mol%)	5 h	49%	2%
8	*(R)-NTPA*-**8** (0.5 mol%)	5 h	78%	0

Reaction conditions: Benzaldehyde (0.15 mmol, 1.0 equiv.), 3-mercaptopropanol (0.18 mmol, 1.2 equiv.), $MgSO_4$ (50 mg), toluene (0.25 M). [a] Yields correspond to the isolated product.

Chapter 4

Asymmetric Synthesis of *N*-containing Heterocycles

4.1. Designing ring-closing reactions

Many natural products and bioactive compounds feature nitrogen-heterocycles in their molecular structure.[199–204] Therefore, catalytic and enantioselective approaches to build up these molecules are highly desirable.[205] In this context, the aza-Diels-Alder reaction is a powerful synthetic tool to furnish high molecular complexity.[206] Thus, it has received a lot of attention in the synthesis of natural products.[207] Particularly, imines, are suitable electrophiles for this transformation.[208] Several catalytic methods are reported to date—although the majority focus on the piperidine scaffold and use enamine catalysis.[209–213] Amongst them, chiral Brønsted acids have been shown to be useful catalysts for the construction of structurally diverse *N*-heterocycles.[214] Chiral PAs were shown to be effective catalysts for enantioselective aza-Diels-Alder reactions (Scheme 4.1).

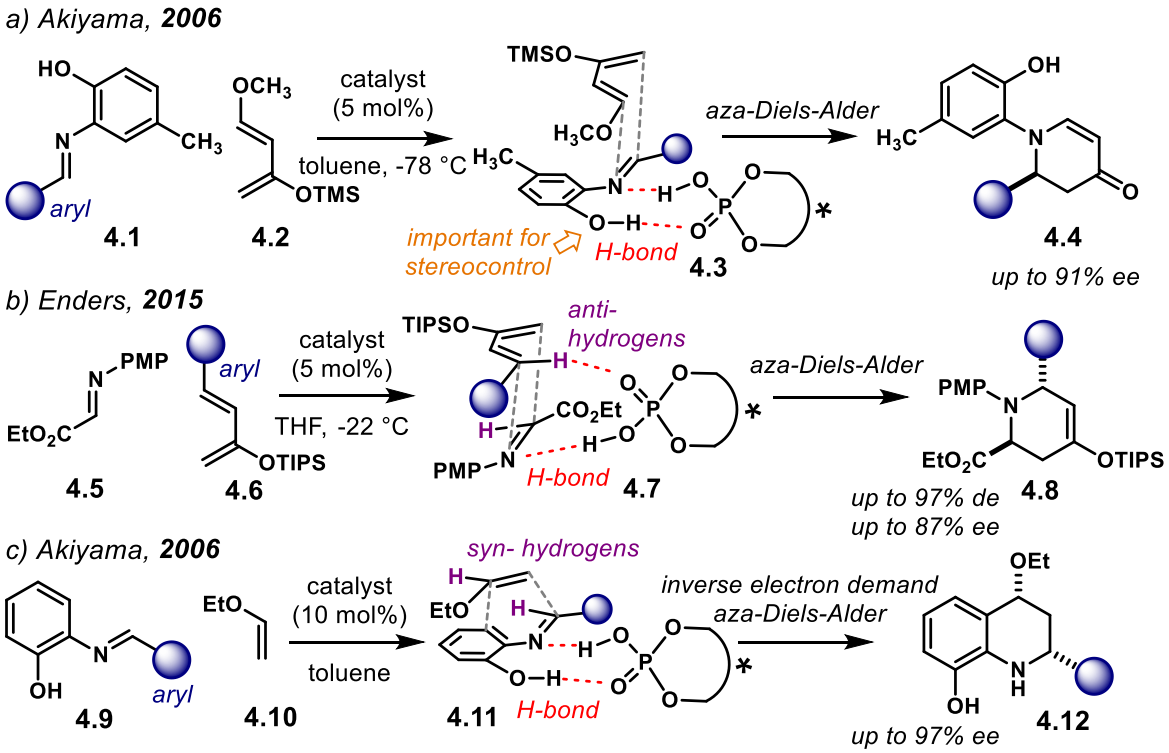

Scheme 4.1: Chiral phosphoric acid-catalysed aza-Diels-Alder reactions.

The group of Akiyama reported the first asymmetric PA-catalysed aza-Diels-Alder reaction (Scheme 4.1*a*).[215] Therein, aryl imines **4.1** react with Danishefsky diene **4.2**. The catalyst activates the imine through a dual activation mode, **4.3**. For such, two hydrogen bonds are formed between the catalyst's active site and the substrate. The second hydrogen bond, which is formed between the hydroxyl moiety in the imine and the phosphoryl oxygen in the catalyst, was needed for both reactivity and stereocontrol.

Then, the enantioselective aza-Diels-Alder step affords heterocycles **4.4** in good yields and up to 91% *ee*. Moreover, the same year, the same group reported a similar reaction using the pyridinium salt of a PA.[216]

The group of Enders reported a related aza-Diels-Alder reaction (Scheme 4.1b).[217] The more reactive imine **4.5** reacts with dienes **4.6** in the presence of a chiral PA. Despite that an activation mode was not proposed, it is likely that the imine engages to the catalyst through hydrogen bonding, as shown in **4.7**. Once the imine is locked in the chiral cavity, the aza-Diels-Alder reaction takes place. Possibly, the diene might be interacting with the catalyst through a non-classical hydrogen bond. Such interaction would provide extra rigidity to the transition state in order to account for the impressive stereocontrol. Subsequently, heterocycles **4.8** are obtained with excellent *anti*- diastereoselectivity and with up to 87% *ee*.

In addition, the group of Akiyama envisaged an inverse electron demand aza-Diels-Alder reaction (Scheme 4.1*c*).[218] Aryl imines **4.9** react with ethyl vinyl ether **4.10**—in what can also be regarded as a Povarov reaction. The catalyst locks the imine to its active site through a dual activation mode, **4.11**. Then, the dienophile approaches the activated substrate while sitting both hydrogen atoms in a *syn*-relationship. Thus, this affords *syn*-**4.12** with excellent stereocontrol (up to 97% *ee*). Similar inverse electron demand reactions have also been reported by the groups of Masson[219,220] and the group of Sun.[221]

NTPAs have also been successful catalysts for cycloaddition reactions that furnish *N*-heterocycles (Scheme 4.2). The group of Shi reported a reaction between amino benzylic alcohol **4.13** and hydroxy-styrenes **4.14** (Scheme 4.2*a*).[222] With a highly acidic NTPA, substrate **4.13** is protonated. After dehydration, a reactive aza-*o*-quinone methide is generated. The, the catalyst locks both substrates through multiple hydrogen bonds to promote the aza-Diels-Alder reaction in an asymmetric fashion, **4.15**. It was found that the free hydroxyl moiety in the styrene component was important to achieve good levels of enantiocontrol. Heterocycles **4.16** were obtained as single diastereoisomers with good enantioselectivities. The aza-*o*-quinone methide approach has also been successfully applied in asymmetric Friedel-Crafts reactions.[223]

The same year, the group of Rueping envisaged a similar reaction. Therein, benzylic alcohols **4.17** react with non-hydroxylated styrenes **4.18** (Scheme 4.2*b*).[224] A reactive aza-*o*-quinone methide is also a key intermediate in this methodology. As no hydrogen bond donors are present in **4.18**, a catalyst-intermediate complex has to provide a rigid chiral environment. Transition state **4.19** shows a plausible way in which the catalyst activates the diene component of the aza-Diels-Alder reaction. An endo approach of the styrene defines the *syn*- relative stereochemistry in product **4.20**. The reaction yields single diastereoisomers with remarkable enantioselectivity. In order to account for the excellent stereocontrol, the authors propose that the aza-*o*-quinone methide intermediate is locked inside the catalyst's chiral pocket through multiple hydrogen bonds, including several non-classical CH interactions as shown in **4.21**.

Later on, the group of Schneider reported an intramolecular variant of this aza-*o*-quinone methide approach, also using a chiral NTPA as catalyst (Scheme 4.2*c*).[225] Their procedure allows the construction of a bicyclic *bis*-benzo-fused system bearing up to two chiral centres with an impressive control of enantioselectivity. The benzylic alcohol precursor **4.22** undergoes a protonation-dehydration sequence to furnish the aza-*o*-quinone methide intermediate, which is locked in the catalyst's chiral cavity, **4.23**. Then, endo cycloaddition sits the *syn*- relationship in the final product **4.24**. These bicyclic structures were obtained as single diastereoisomers in up to 82% *ee*.

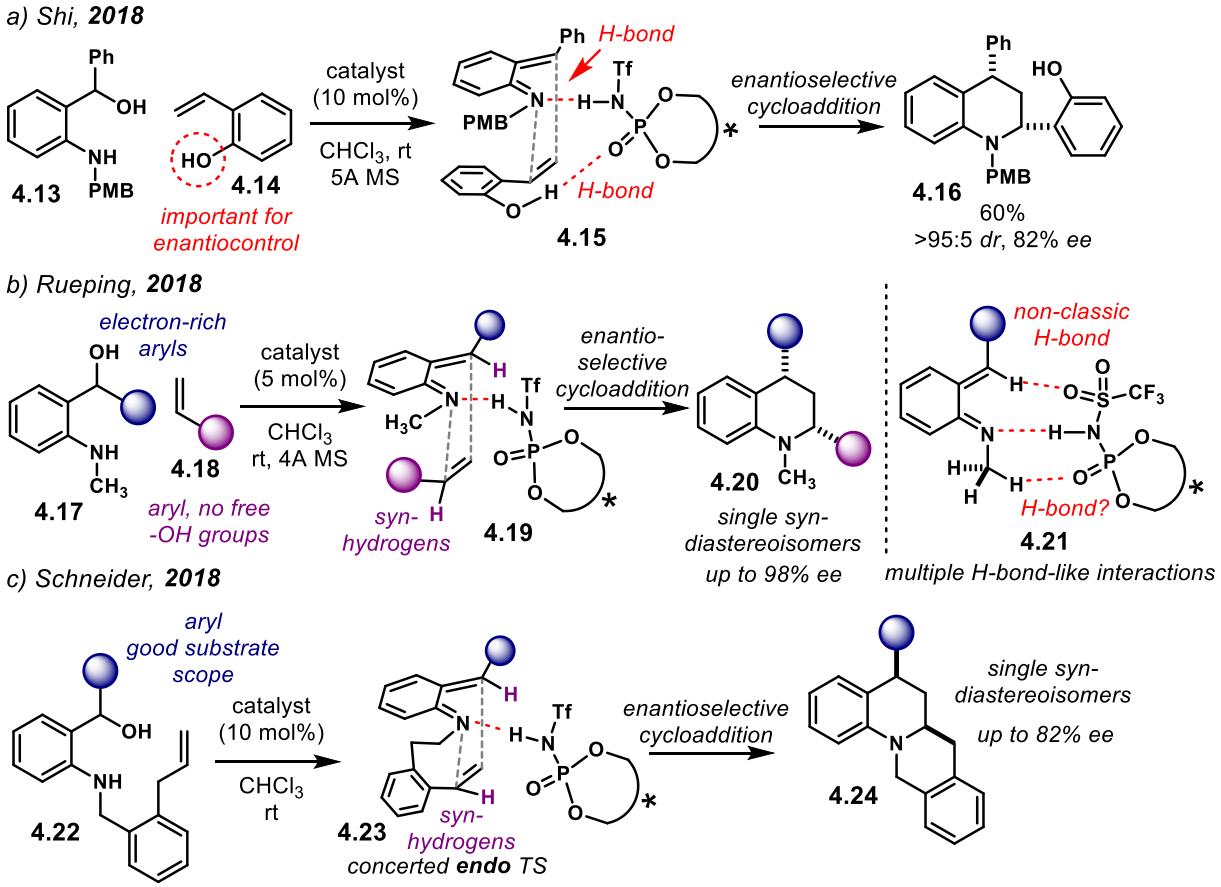

Scheme 4.2: NTPA-catalysed cycloaddition reactions.

The latter strategy has the advantage of constructing multiple cycles in a single step due to the tethered alkene. A general retrosynthetic approach for such a methodology using aza-*o*-quinone methides as key reactive intermediates is pictured in Scheme 4.3*a* on the next page. Therein, heterocycles **4.25** can be disconnected back to the quinone methide intermediate **4.26**. This, in turn can be generated from the corresponding benzylic alcohol **4.27** through a protonation-dehydration sequence promoted by the catalyst.

Inspired by such a versatile disconnection, an alternative procedure to construct complex heterocyclic systems was proposed, as shown in Scheme 4.2*b*, also in both a catalytic and enantioselective fashion. Heterocycles **4.28** can be disconnected back to iminium ion **4.29** as key intermediate. The tethered diene motif would render an intramolecular imino-Diels-Alder reaction. Through Brønsted acid catalysis, the iminium can be formed from the corresponding aldehyde **4.30**—or ketone as well, both readily available—

and non-protected amines **4.31**. This methodology would have three main advantages: 1) The installation of at least two chiral centres in an enantio-controlled way, 2) the use of readily available starting materials and 3) the use of an unprotected amine in a one-pot procedure that would not require the isolation of the intermediate imine or iminium. In addition, the length of the alkyl chain of the amine could, in principle, be extended to afford different ring sizes in the final product.

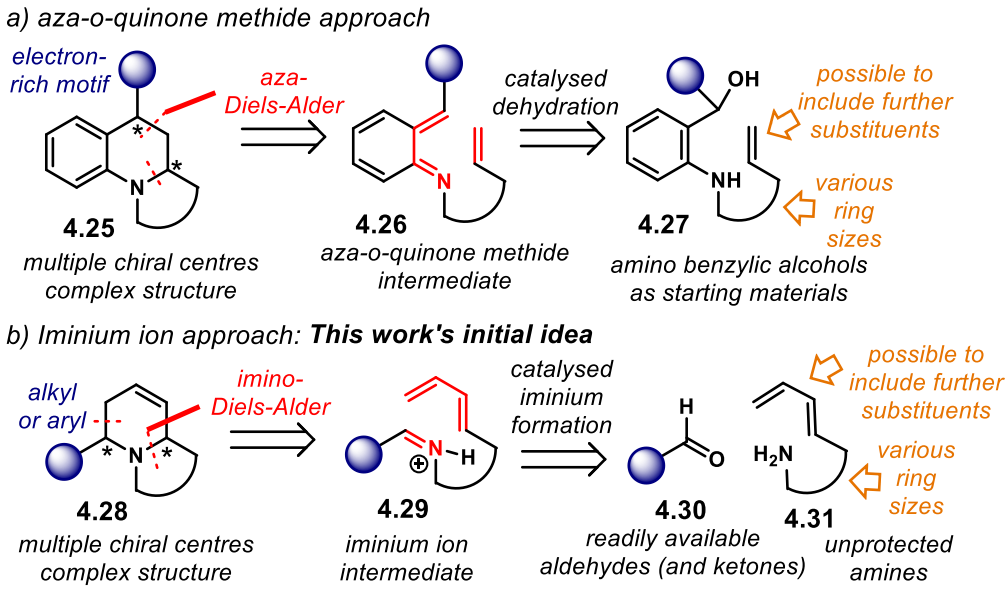

Scheme 4.3: a) aza-*o*-quinone methide approach for the construction of complex heterocyclic systems. b) The initial idea towards complex heterocycles *via* an iminium-Diels-Alder reaction.

The imino-Diels-Alder reaction has been extensively studied.[226] However, the asymmetric version of such reaction mostly relies on Lewis acids with chiral ligands, yet not many reports exist using chiral Brønsted acids.[227] In addition, the imino-Diels-Alder reaction has been successfully used as the key step in the synthesis of natural products, two of which are presented on Scheme 4.4.

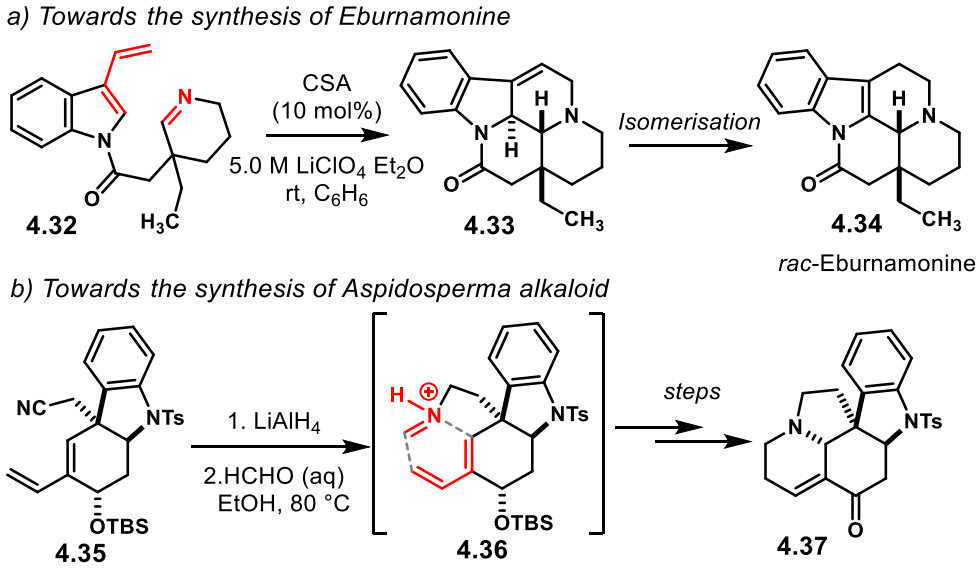

Scheme 4.4: Applications of the imino-Diels-Alder reaction in the synthesis of natural products.

The group of Grieco reported a total synthesis of Eburnamonine **4.34** (Scheme 4.4*a*).[228] In that publication, key precursor **4.32** was prepared. Then, reaction with 10 mol% CSA delivered the complex polycyclic system **4.33**. The high polarity media using $LiClO_4$ was needed for reactivity.[229] Despite the cycloaddition proceeds with a catalytic amount of CSA as a Brønsted acid, the synthesis is racemic, yet, excellent diastereocontrol was observed. A subsequent double bond isomerisation step delivered *rac*-Eburnamonine **4.34**.

In another report, the group of Cho envisaged an imino-Diels-Alder reaction as a key step towards the synthesis of the Aspidosperma alkaloid (Scheme 4.4*b*).[230] Therein, the nitrile precursor **4.35** was reduced to the corresponding amine, which upon treatment with formaldehyde, affords iminium ion **4.36** to undergo the cycloaddition step. Further manipulations delivered the key Aspidosperma alkaloid structure **4.37**. As in the previously discussed reaction, the aza-Diels-Alder step is not enantioselective. The newly formed chiral centres are control by the stereochemistry of the substrate.

In the context of imino-Diels-Alder reactions, the group of Grieco reported the first examples of such reactions in an intramolecular fashion (Scheme 4.5).[231] Using amine hydrochloride **4.38** (Scheme 4.5*a*), iminium ion **4.39** was formed upon treatment with aqueous formaldehyde. Then, upon heating, the hydroindolizine hydrochloride skeleton **4.40** is formed *via* an imino-Diels-Alder reaction. The process was reported to work in excellent yield, yet, racemic.

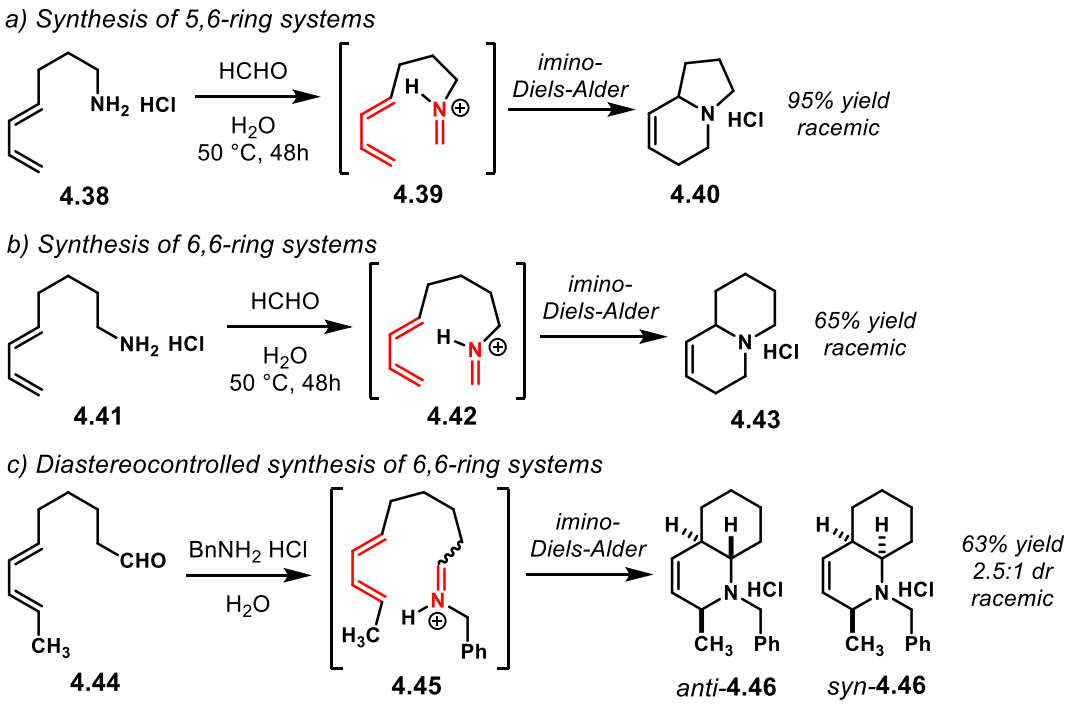

Scheme 4.5: Intramolecular imino-Diels-Alder reactions reported by the group of Grieco.

Furthermore, within the same publication, the construction of the analogous 6,6-ring system was reported (Scheme 4.5*b*). Using hydrochloride **4.41** and aqueous formaldehyde, iminium ion **4.42** is obtained. Subsequent cycloaddition delivers the quinolizine framework in its hydrochloride form **4.43**, in modest yield and in a racemic fashion. In addition, a related imino-Diels-Alder reaction was also taken into

account (Scheme 4.5*c*). Treatment of aldehyde **4.44** in benzyl amine and hydrochloric acid forms iminium ion **4.45**. Then, diastereoselective cycloaddition affords compounds **4.46**. The reaction works in a modest yield and with modest diastereocontrol in favour of *anti*-**4.46**. Herein, the products are obtained as the corresponding hydrochlorides and in a racemic fashion.

Since then, several imino-Diels-Alder reactions have been reported, yet, in a racemic fashion, diastereoselectively through substrate control or using Lewis acids with chiral ligands.[232] In this context, a catalytic and enantioselective imino-Diels-Alder reaction would be desirable. Thus, inspired by this rather old reaction, a Brønsted acid-catalysed enantioselective version of Grieco's reaction was designed (Scheme 4.6). With the free amine **4.47**, it was hypothesised that, upon treatment with a synthetic equivalent of formaldehyde (*e.g.* formalin), an equilibrium could be established if a Brønsted acid is present, whether a PA or a NTPA. This would furnish iminium ion **4.48**. Then, such intermediate would be locked inside the catalyst's chiral pocket. Hydrogen bonding or ion-pairing might stabilise the iminium ion and provide extra rigidity in the transition state, **4.49**. Additional interactions, like non-classical CH hydrogen bonds might also favour the reaction and help to enantio-differentiation. After that, enantiodetermining intramolecular imino-Diels-Alder cyclisation would afford product **4.50**. Therefore, this reaction would be a model example to start with.

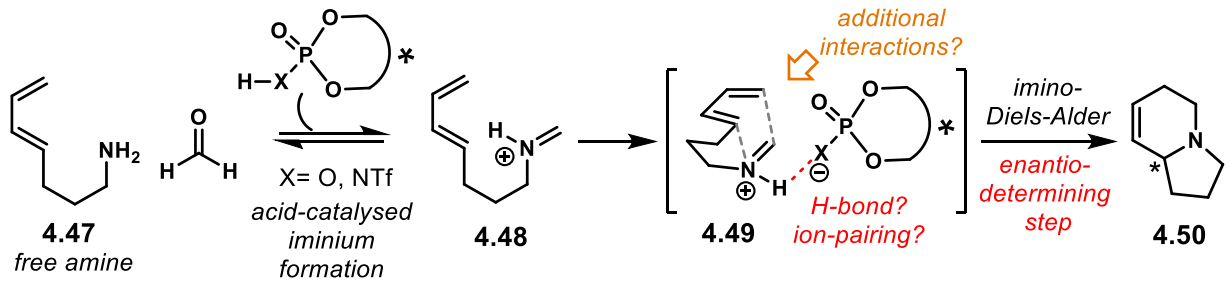

Scheme 4.6: Designing a catalytic enantioselective Grieco's reaction.

Apart from experimental studies, the imino-Diels-Alder has also caught the attention of computational chemists. Several studies are reported in this area.[233,234] Amongst the computational studies, the group of Whiting calculated a series of imino-Diels-Alder reactions.[235] Their results indicate that imines bearing electron-withdrawing motifs are more reactive than alkyl or aryl imines with electron neutral substituents. In this case, therefore, an iminium ion, with a positive charge on the nitrogen atom should be far more reactive. In other words, an acid-catalysed imino-Diels-Alder reaction ought to be faster than its thermal non-catalysed version.

With this on mind, and to have a theoretical support, the transition state for the cycloaddition of **4.48** was calculated, as well as for the free imine—these initial calculations did not take into account the catalyst, PA or NTPA, only the protonated imine for the acid-catalysed reaction.[a] The lowest-energy transition

[a] Transition state structures were optimised at the B3LYP/6-31G(*d*,*p*) level of theory and the Gibbs free energies were corrected through single-point energy calculation at the M06-2X/def2-TZVPP level of theory.

states for the thermal and the acid-catalysed reactions are presented in Figures 4.1*a* and 4.1*b*, respectively.

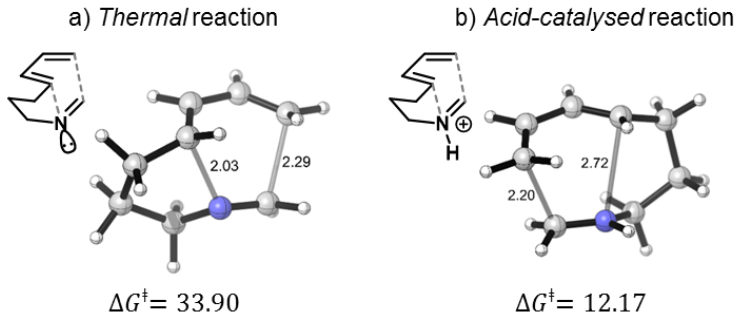

Figure 4.1: Lowest-energy transition states for the a) thermal and b) acid-catalysed imino-Diels-Alder reaction. Gibbs free energies were calculated at the M06-2X/def2-TZVPP//B3LYP/6-31G(*d*,*p*) level of theory and are presented in kcal mol^{-1} and are relative to the corresponding imine and iminium. Labelled distances are presented in Angstroms.

As shown in the transition states, the thermal imino-Diels-Alder reaction proceeds with a barrier height of 33.90 kcal mol^{-1}. On the other hand, when the imine is protonated, the corresponding iminium ion has a much lower barrier height of 12.17 kcal mol^{-1}, less than half of the value for its thermal version. Thus, the cyclisation of iminium **4.48** should be favoured at room temperature and the chiral anion of the catalyst should control the stereochemical output. In addition, the group of Houk calculated the transition states for the 6,6-ring systems (*cf.* Scheme 4.5*b* and *c*).[236] Their study also suggests that the acid-catalysed reaction should go considerably faster than the thermal cycloaddition.[a]

With these precedents on the imino-Diels-Alder reaction, and the calculations suggesting a favourable acid-catalysed reaction, the first experiments towards an enantioselective synthesis of **4.50** started. In addition, the quite small size of the substrates could be advantageous to test the silicon-based PAs synthesised in Chapter 2, which should provide good enantiocontrol due to their confined active site.

4.2. Initial attempts

As a starting point, amine **4.47** was synthesised (Scheme 4.7). Following a modified procedure reported by the group of Danishefsky,[237] divinyl carbinol **4.51** reacted with triethyl orthoacetate and a catalytic amount of propionic acid to afford ester **4.52** in 66% yield. A similar procedure reported by the group of Overkleeft, which uses toluene as solvent,[238] was also tried and provided similar results. Then, aminolysis of the ester was performed using aminochloromethyl aluminium, as described by the group of Weinreb.[239] Amide **4.53** was obtained in 80% yield.[b] Next, reduction to the corresponding amine **4.47** with $LiAlH_4$ was tried. Several reaction conditions, including the scale of the reaction and purification methods were tried.

[a] That study was conducted on the corresponding transition states for iminium ions **4.42** and **4.45** (*cf.* Scheme 4.5). However, that was not the case for the 5,6-ring system, **4.39**. In addition, I also performed the calculations for **4.42** at the M06-2X/def2-TZVPP//B3LYP/6-31G(*d*,*p*) level of theory. These results were in accordance with those reported by the group of Houk.

[b] The procedure needs the fresh preparation of the aluminium reagent, which is made out of ammonium chloride and a solution of trimethylaluminium in toluene. The also commercially available solution in hexane provides similar results.

The reaction, as well as the purification of the product were shown to be challenging. The procedures reported by the group of Marks served as a basis to optimise the reaction.[240,241] Table 4.1 summarises the attempts made to reduce amide **4.53** to amine **4.47**.

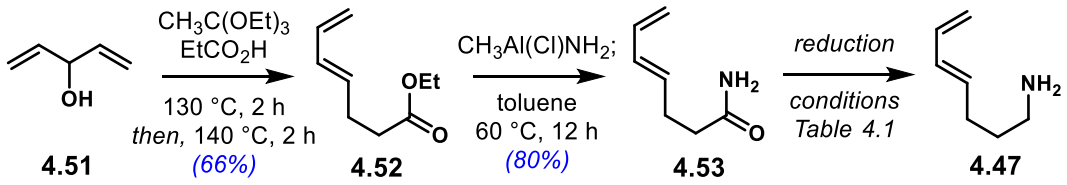

Scheme 4.7: Synthesis of diene-amine **4.47**.

Table 4.1: Reaction conditions for the synthesis of amine **4.47**.

entry	**scale**[a]	**$LiAlH_4$ equiv.**	**solvent**	**temperature**	**time**	**purification**	**yield %**
1	63 mg	1.4	THF (0.17 M)	rt	4 h	-	-
2	330 mg	1.4	THF (0.07 M)	rt	5 h	vacuum distillation	-
3	187 mg	1.4	THF (0.08 M)	rt	3 h	column with Et_3N	**53**
4	1.5 g	1.4	THF (0.08 M)	rt	6 h	Kugelrohr	10
5	0.5 g	1.4	THF (0.1 M)	rt	12 h	Kugelrohr	35
6	190 mg	2.0	Et_2O (0.08 M)	rt	5 h	column with Et_3N	36
7	300 mg	3.0	THF (0.1 M)	50 °C	12 h	Kugelrohr	35
8	160 mg	3.0[b]	THF (0.1 M)	rt	24 h	column with Et_3N	25
9	250 mg	6.0[b]	THF (0.1 M)	60 °C	12 h	column with Et_3N	32
10	0.68 g	10.0	THF (0.1 M)	60 °C	24 h	column with Et_3N	**50**

[a] Relative to the amount of starting material. [b] A commercially available 1.0 M solution of LiAlH4 in THF was used.

The first attempt to reduce amide **4.53** to amine **4.47** was conducted in a 63 mg scale using 1.4 equiv. of $LiAlH_4$ (entry 1). After 4 h at rt, no product was observed. Then, a larger scale was attempted while diluting the reaction (entry 2). After 5 h at rt, product **4.47** was observed in TLC, however, it was presumably lost during vacuum distillation, which might be attributed to the relatively small scale at which the reaction was performed. Nevertheless, similar reaction conditions but purification done on silica gel with 2.5% triethylamine in the eluent afforded the desired product in 53% yield (entry 3). Under similar reaction conditions, but with a longer reaction time, a large-scale preparation was attempted (entry 4). Kugelrohr distillation provided amine **4.47** in only 10% yield. Doubling the reaction time and using Kugelrohr distillation improved the yield slightly (35%, entry 5). Varying the solvent (entry 6) or increasing the temperature to 50 °C (entry 7) afforded the product in 36% and 35% yield, respectively. Using a commercially available 1.0 M solution of $LiAlH_4$ in THF (entry 8) afforded the product in 25% yield when the reaction was done at rt. So far, purification by column chromatography using Et_3N in the mobile phase was shown to give good results. Doubling the equivalents of the reducing agent in solution and heating up to 60 °C provided amine **4.47** in 32% yield (entry 9). Finally, reduction with 10.0 equiv. of $LiAlH_4$ and 60 °C reflux for 24 h (entry 10), afforded the desired product in 50% yield.

With amine **4.47** in hand, several attempts to synthesise indolizine-like heterocycle **4.50** were done. The results are summarised in Table 4.2 on the next page. As a starting point, similar reaction conditions to those reported by the group of Grieco were tried.[231] For the initial attempts, stoichiometric amounts of Brønsted acids were tried. Using HCl as acid catalyst with 2.0 equiv. of formaldehyde (37% aq. solution) did not furnish any product at 50 °C after 48 h (entry 1). In this case, the fact of using HCl instead of the amine hydrochloride might have been a reason why the reaction did not work. Then, 6N HCl was tried as a 'diluted' Brønsted acid, however unsuccessfully (entry 2). In addition, reaction with TFA at rt for 12 h was tried, yet no product was observed (entry 3). The next attempts were done using organic solvents as reaction media. This could favour the formation of the imine for subsequent cyclisation. In addition, $MgSO_4$ was used as a drying agent to remove water from the formaldehyde solution and allow the starting materials to react in the solvent. Conducting the reaction in $CDCl_3$ with TFA at rt for 48 h did not afford the product (entry 4). Then, trifluoroethanol was used as a solvent (entry 5). It has been reported that aza-Diels-Alder reactions using TFA are accelerated in high polarity media like trifluoroethanol.[242] However, reaction at rt for 24 h proved unsuccessful.

Given that the reactions did not furnish product **4.50** neither at rt or 50 °C, the next variable considered was increasing the temperature. Therefore, the reaction was tried using TFA and $MgSO_4$ as drying agent in *m*-xylene at 100 °C (entry 6). After 24 h full consumption of the starting material was observed. However, the product was shown difficult to isolate. Purification was done in silica gel with 5% Et_3N. Traces of, presumably, **4.50** were detected by NMR (Figure 4.2). As shown in Figures 4.2*a* and 4.2*b*, the doublets arising from the diene motif in **4.47** do not appear in the ^{1}H-NMR spectrum in Figure 4.2*b*, shown in the yellow box. Instead, two signals, possibly from the double bond in the heterocycle are shown at 5.96 and 5.66 ppm, shown in the blue box. In addition, another multiplet at 4.35 ppm might correspond to the CH moiety α to the nitrogen atom, shown in the purple box. Even though the starting material reacted, it was difficult to pin down whether the observed product was indeed heterocycle **4.50** or not.

It could have been the case that $MgSO_4$ acted as a Lewis acid. To verify this, the reaction was carried out using the same reaction conditions in the absence of the drying agent (entry 7). Surprisingly, the same product as in entry 6 was obtained (Figure 4.2*c*). The NMR signals in the blue and purple boxes match those on Figure 4.2*b*. In addition, LCMS ES+ TIC analysis suggested that the heterocycle is obtained as its protonated form. A 124.32 (m/z) value was observed, for a calculated 124.11 (m/z) corresponding to protonated **4.50**. Moreover, LCMS ES- TIC showed a peak with 112.96 (m/z), which is very close to a calculated 112.99 (m/z) for the trifluoroacetate anion. Thus, it is possible that **4.50** was obtained as its trifluoroacetate salt—the anion coming from TFA used as Brønsted acid. This indicates that the basicity of the product could inhibit the reaction if it is tried with a catalytic amount of a Brønsted acid. In addition, this might be the reason why it was difficult to isolate the product by silica gel chromatography. Lowering the temperature to 70 °C had a negative impact (entry 8). No product was observed in this case.

Table 4.2: Initial attempts to synthesise **4.50** in a racemic fashion

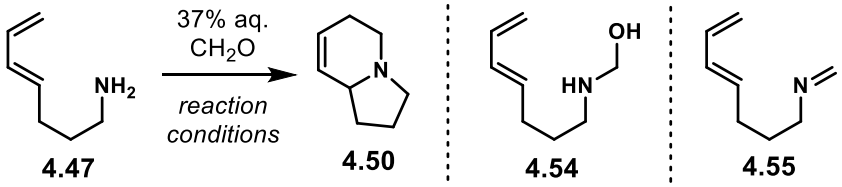

4.47 **4.50** **4.54** **4.55**

entry	**Brønsted acid**[a]	**CH_2O equiv.**	**solvent**[b]	**additive**	**temperature**	**time**	**yield %**
1	conc. HCl (1.0)	2.0	neat	-	50 °C	48 h	-
2	6N HCl (1.0)	2.0	neat	-	50 °C	48 h	-
3	TFA (1.0)	2.0	neat	-	rt	12 h	-
4	TFA (1.0)	0.8	$CDCl_3$ (0.5 M)	$MgSO_4$	rt	48 h	-
5	TFA (1.0)	2.0	TFE (0.37 M)	$MgSO_4$	rt	24 h	-
6	TFA (1.0)	0.8	*m*-xylene (0.5 M)	$MgSO_4$	100 °C	24 h	trace
7	TFA (1.0)	2.0	*m*-xylene (0.5 M)	-	100 °C	24 h	70
8	TFA (1.0)	2.0	toluene (0.5 M)	-	70 °C	24 h	-
9	TsOH (1.0)	2.0	*m*-xylene (0.5 M)	-	100 °C	24 h	-
10	TsOH (1.0)	2.0	*m*-xylene (0.5 M)	$MgSO_4$	100 °C	24 h	-
11	TFA (10 mol%)	2.0	neat	-	50 °C	48 h	-
12	TFA (10 mol%)	2.0	$CHCl_3$ (1.1 M)	-	40 °C	48 h	-
13	-	0.8	neat	-	rt	3 h	
14	-	2.0	neat	-	60 °C	6 h	-
15	-	2.0	*m*-xylene (0.5 M)	$MgSO_4$	100 °C	24 h	-

Reaction conditions: amine **4.47** (0.15 mmol, 1.0 equiv.). [a] Equivalents of Brønsted acid shown in brackets. [b] Concentration relative to the amine starting material.

Tosic acid was also tested as a Brønsted acid for this racemic reaction (entry 9). However, heating at 100 °C in *m*-xylene did not afford the product. Adding $MgSO_4$ as a drying agent did not furnish the product either (entry 10). Thus, so far the most suitable conditions have been heating at 100 °C using a stoichiometric amount of TFA. Consequently, the neat reaction with 10 mol% TFA at 50 °C did not work even after 48 h (entry 11). Furthermore, conducting the reaction in chloroform with 10 mol% TFA at 40 °C was unsuccessful (entry 12).

A series of control experiments were also performed. For these, no catalyst was added to the reaction. Reaction without solvent at rt for 3 h afforded a product which could possibly be hemiaminal **4.54** (entry 13). As shown in Figure 4.2*d*, the diene motif it is present, highlighted in the yellow box. Moreover, the aliphatic signals in the 3.0-1.0 ppm region move to lower shifts, suggesting the presence of a slightly electron donating moiety. Furthermore, in Figure 4.3, the ^{13}C-NMR spectra for **4.47** and the isolated product (entry 13) are compared. It is also evident that the diene moiety is present in the isolated product and has barely changed. However, the extra peak at 74.5 ppm suggest a quite shifted carbon, which can be attributed to the hemiaminal carbon atom, highlighted in the orange box. In that case, it can be the case that hemiaminal **4.54** is obtained at rt during the first hours of reaction.

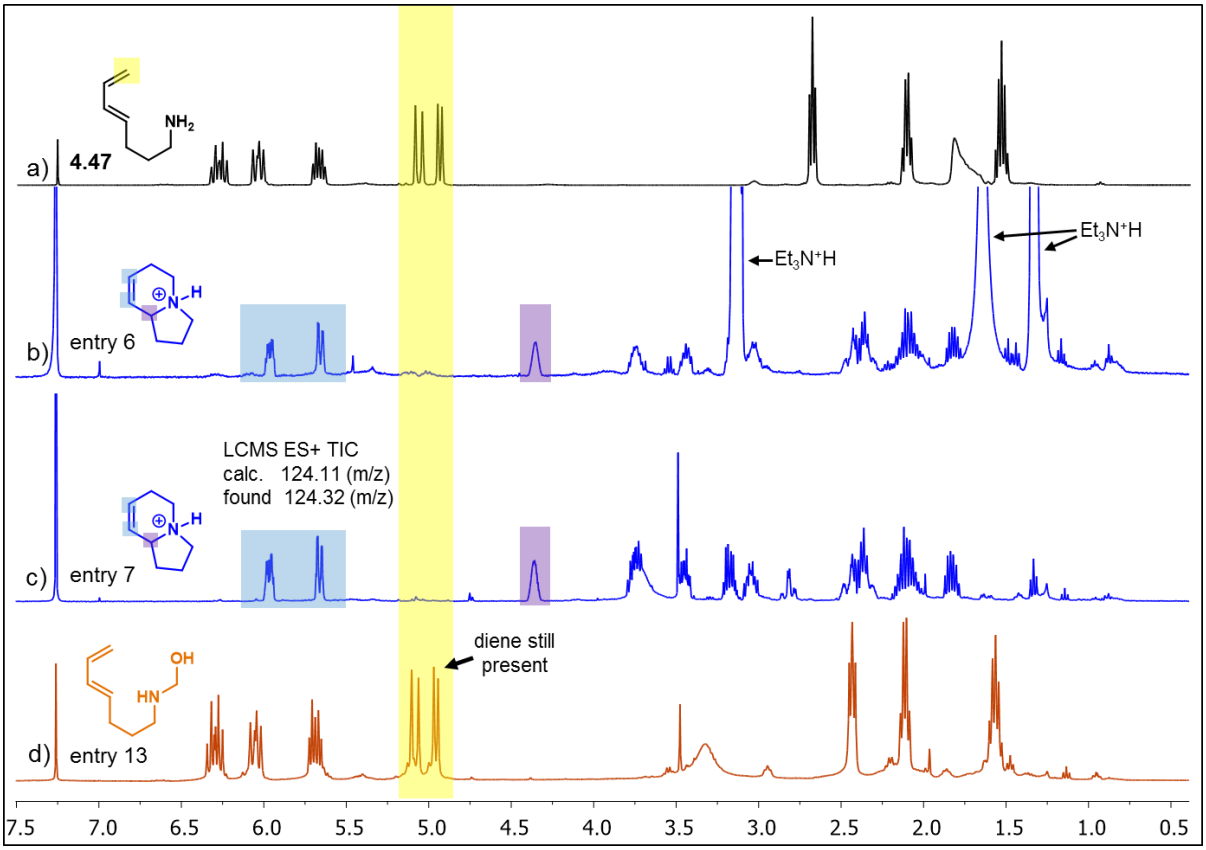

Figure 4.2: ^{1}H-NMR (400 MHz, $CDCl_3$) spectra for a) starting material **4.47**, b) entry 6, c) entry 7 and entry 13. Entries correspond to experiments presented in Table 4.2.

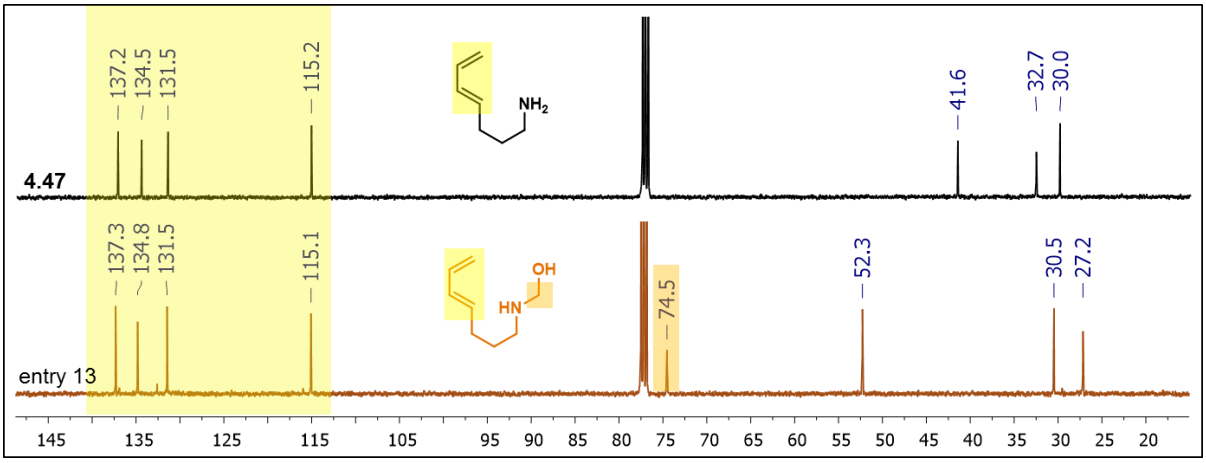

Figure 4.3: ^{13}C-NMR (100 MHz, $CDCl_3$) spectra for starting material **4.47**, and hemiaminal **4.54**. Entry 13 corresponds to experiments presented in Table 4.2.

Two more experiment were conducted in the absence of an acid catalyst, but at higher temperatures. Heating both starting materials without solvent at 60 °C did not afford any product after 6 h (entry 14). This suggests that hemiaminal **4.54** is formed at low temperatures at the beginning of the reaction. Then, it is consumed as the reaction proceeds or at higher temperatures. Reaction in *m*-xylene at 100 °C did not furnish any product after 24 h (entry 15). This strongly indicates that a Brønsted acid is needed to form heterocycle **5.50**, at a high temperature though. In none of the reactions, imine **4.55** was detected.

This might be because alkyl imines are relatively unstable and prone to polymerisation in acidic media,[243,244] which arise whether from the catalyst itself or during silica gel purification.

This series of experiments indicated that, even when forming heterocycle **4.50** was possible, the need of a stoichiometric amount of a Brønsted acid might be disadvantageous for an enantioselective methodology. Thus, attention was turned to substrate modification. As starting point, it was envisaged that an aromatic ring in the product structure could be helpful, both for reaction monitoring through TLC and for isolation. In this context, the next step was trying the reaction of amine **4.47** with benzaldehyde **4.56**. Those results are presented in Table 4.3. With Brønsted acid catalysis, imine **4.57** would be expected to be formed, protonated and undergo an imino-Diels-Alder reaction to afford substituted heterocycle **4.58**.

Table 4.3: Attempts to synthesise heterocycle **4.58**

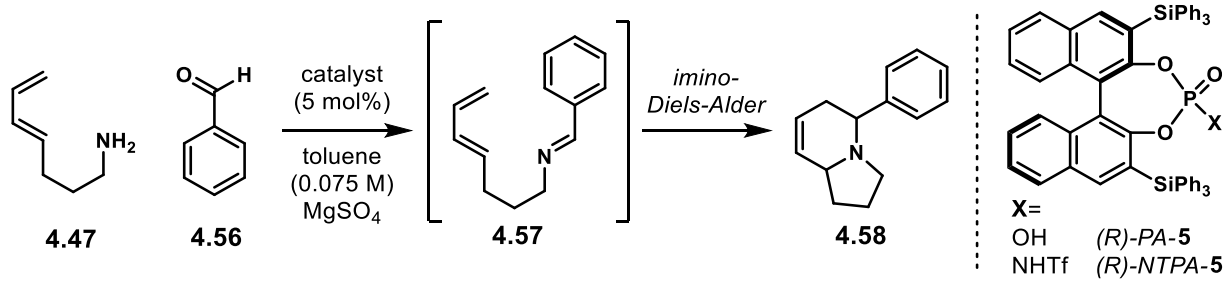

4.47 **4.56** **4.57** **4.58**

entry	**catalyst**	**temperature**	**time**	**4.57 yield %**	**4.58 yield %**
1	TFA	rt	24 h	49	-
2	*(R)-PA*-**5**	rt	24 h	57	-
3	*(R)-NTPA*-**5**	rt	24 h	43	-
4	*(R)-NTPA*-**5**	50 °C	72 h	52	-
5[a]	*(R)-PA*-**5**	80 °C	72 h	NA	-
6[a]	*(R)-NTPA*-**5**	80 °C	72 h	NA	-

Reaction conditions: benzaldehyde (0.15 mmol, 1.0 equiv.), amine **4.47** (0.18 mmol, 1.2 equiv.), toluene (2 mL, 0.075 M), $MgSO_4$ (25 mg). Yields correspond to isolated compounds. [a] These two reactions were conducted with imine **4.57** as starting material in a 0.08 mmol scale in toluene (0.8 mL, 0.1 mL), no $MgSO_4$ was added.

To start with, reaction of amine **4.47** and benzaldehyde **4.56** was conducted in toluene using TFA as catalyst (entry 1)—$MgSO_4$ was kept as a drying agent to remove water from the imine formation step and push the equilibrium towards the imine. After 24 h at rt, imine **4.57** was isolated in 49% yield. However, the expected product **4.58** was not observed. It was hypothesised that, in a non-polar medium like toluene, the conjugate base of the Brønsted acid might be ion-paired with the protonated imine. In such a scenario, if a mildly confined phosphoric acid locks imine **4.57** in its chiral pocket, it could be possible that the 3,3' substituents could 'compress' the transition state and grant access to heterocycle **4.58**. With this idea, *(R)-PA*-**5** was tried. It was expected that the non-planar triphenylsilyl groups could perform the aforementioned transition state compression. Unfortunately, this was not the case (entry 2). At rt, imine **4.57** was obtained in 57% yield after 24 h.

Apart from the idea of 'compressing the transition state', it was thought that a PA might not be acidic enough to fully protonate the imine and trigger the cycloaddition step. Thus, the more acidic—and mildly hindered—*(R)-NTPA*-**5** was used as catalyst (entry 3). After 24 h at rt, imine **4.57** was isolated in 43% yield. Yet, no product was observed—again. Therefore, the next step was to increase the reaction temperature. Heating at 50 °C afforded imine **4.57** in 52% yield (entry 4). Even after 72 h—3 days—product **4.58** was not detected.

In a further attempt to make heterocycle **4.58**, the isolated imine **4.57** was submitted. Reaction with *(R)-PA*-**5** in toluene at higher concentration and temperature, 80 °C, was unsuccessful after 72 h (entry 5). Next, the more acidic *(R)-NTPA*-**5** was tried (entry 6). In a similar way, product **4.58** was not observed after heating at 80 °C for 3 days.

These experiments can be accounted in the following manner. It might be possible that, once iminium ion **4.59** is formed, the transition state leading to the cyclisation product is too hindered (Figure 4.4). The aromatic ring might be large enough to clash whether with the NH moiety or with the approaching diene. In addition, even though iminium ions are electrophilic, the LUMO in **4.59** could be quite too high in energy to undergo the aza-Diels-Alder reaction. However, if an iminium ion like **4.60** is used instead, there would be several advantages. Firstly, due to the carbonyl group attached to the electrophilic iminium carbon, the energy of the corresponding LUMO would be considerably lower. Secondly, the protonated iminium could possibly be locked in an *s-cis* conformation, this, will sit the substituents away from the approaching diene motif, thus, avoiding steric clash. Finally, the extra carbonyl group in the dienophile component can grant access to secondary orbital interactions that would favour the cycloaddition reaction.

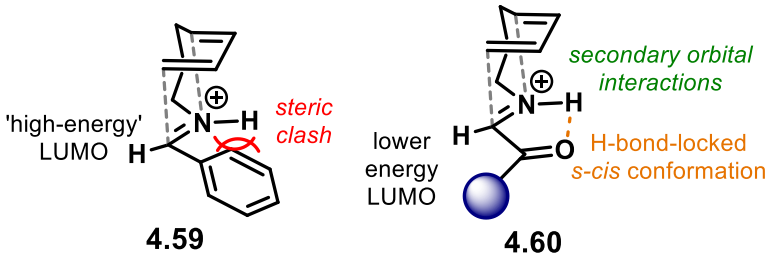

Figure 4.4: Proposed transition state structures for the imino-Diels-Alder cycloaddition of iminium ions **4.59** and **4.60**.

Following this reasoning, the reaction of amine **4.47** with more electron deficient aldehydes **4.61** was tried. The results using ethyl glyoxylate and phenyl glyoxal are summarised on the next page on Table 4.4. To start with, the reaction with ethyl glyoxylate in chloroform was tried (entry 1). In this case, no Brønsted acid was used. After 24 h at rt, product **4.62** was not observed—which was expected due to the missing acid to protonate the imine. Instead, imine **4.63** was isolated in 30% yield. However, using 10 mol% tosic acid as catalyst and the same reaction conditions neither **4.62** nor **4.63** were observed (entry 2).

Next, phenyl glyoxal was used instead, as it would provide a slightly more electrophilic imine. Thus, reaction of **4.47** and phenyl glyoxal was tried in CH_2Cl_2 without an acid catalyst (entry 3). After 1h at rt, imine **4.64** was isolated in 41% yield. The corresponding cyclisation product was not observed. Then, the

same reaction was done at 40 °C for a longer time, 12 h (entry 4). Imine **4.64** was isolated in 47% yield. This suggests that the imine is readily obtained during the first hours of reaction, even without heating.

Table 4.4: Attempts to make heterocycles **4.62** using more reactive iminium ions

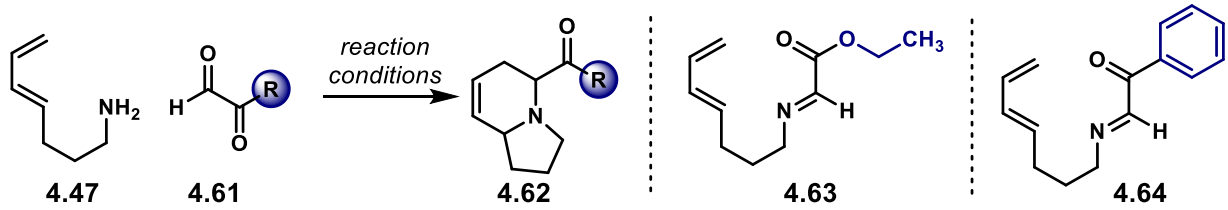

4.47 **4.61** **4.62** **4.63** **4.64**

entry	R	Brønsted acid	solvent	additive	temperature	time	yield %
1	OEt	-	$CHCl_3$ (0.5 M)	$MgSO_4$	rt	24 h	30[a]
2	OEt	TsOH (10 mol%)	$CHCl_3$ (0.5 M)	$MgSO_4$	rt	24 h	-
3	Ph	-	CH_2Cl_2 (0.2 M)	$MgSO_4$	rt	1 h	41[b]
4	Ph	-	$CHCl_3$ (0.5 M)	-	40 °C	12 h	47[b]
5	Ph	TsOH (1.0 equiv.)	CH_2Cl_2 (0.2 M)	$MgSO_4$	rt	24 h	-
6	Ph	TFA (1.0 equiv.)	CH_2Cl_2 (0.2 M)	$MgSO_4$	rt	24 h	-

Reaction conditions: amine **4.47** (0.15 mmol, 1.0 equiv.), aldehyde **4.61** (0.18 mmol, 1.2 equiv.) [a] Isolated yield of imine **4.63**. [b] Isolated yield of imine **4.64**.

In order to push the reaction to completion, the next experiments were done using a stoichiometric amount of Brønsted acids. Reaction with tosic acid in CH_2Cl_2 at rt for 24 h did not afford product **4.62**, nor imine **4.64** was observed (entry 5)—$MgSO_4$ was also used in these reactions as a water catching agent. Similar results were obtained when 1.0 equiv. of TFA was used (entry 6). None of the products were detected after 24 h.

So far, using different aldehydes to improve the reactivity of the intermediate iminium ion did not proof successful. Thus, the next stage was to look at the other substrate: the amine.

4.3. An unexpected discovery

So far, the proposed substrate modifications—targeted to the aldehyde component—did not help to improve the reaction towards heterocycles **4.65** (Scheme 4.8). In addition, it might have been the case that **4.65**—a very basic bicyclic tertiary amine—was caught in the silica gel during purification, thus, showing no product (*c.f.* Table 4.4, entries 2, 5 and 6). In this case, introduction of an extra phenyl ring to the product, as in **4.66**, would avoid those drawbacks. In such a structure, the nitrogen atom would have an aniline-like character—whose basicity would be lessened. In addition, *N*-aryl imine **4.67** would also be a more stable intermediate. The latter precursor, obtained from aniline **4.68** and aldehydes **4.30**.

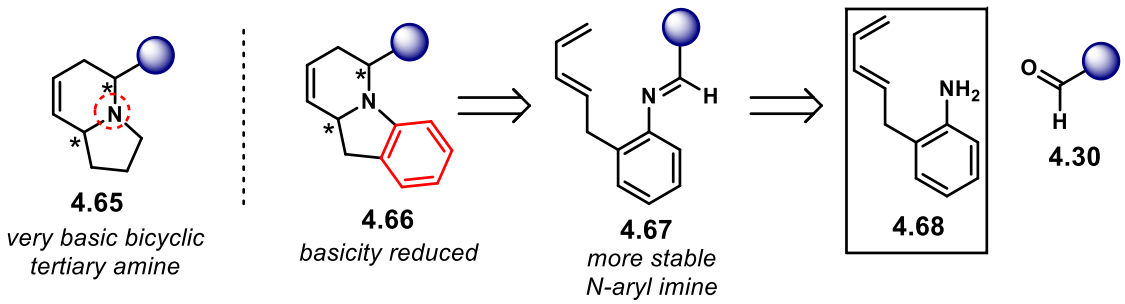

Scheme 4.8: An alternative approach to 5,6-ring systems. Introduction of the aromatic moiety would reduce the basicity of the nitrogen atom, thus, providing a more stable intermediate.

The journey now commenced with the synthesis of aniline **4.68** (Scheme 4.9). Starting from divinyl carbinol **4.51**, treatment with phosphorus (III) tribromide afforded 5-bromopenta-1,3-diene **4.69** in 63% yield.[245] Then, lithium-bromine exchange in *o*-bromonitrobenzene **4.70** followed by addition of **4.69** afforded compound **4.71**—*vide infra* for the reaction optimisation. Finally, following the protocol reported by Wolfe,[246] reduction of the nitro group in **4.71** with zinc furnished aniline **4.68** in 73% yield.[a]

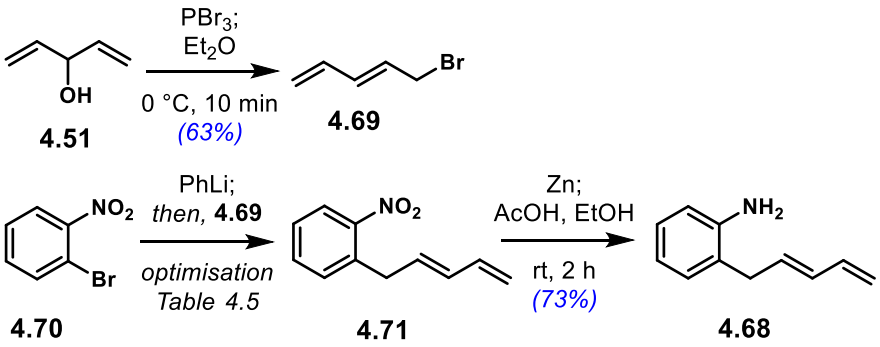

Scheme 4.9: Synthesis of starting material **4.68**.

During the synthesis of aniline **4.68**, the reaction conditions to get nitro compound **4.71** were optimised. The results are presented on Table 4.5 on the next page. The initial set of reaction conditions that were tried were those reported by the group of Pirrung.[247] Lithium-bromine exchange in **4.70** was performed by phenyl lithium, then, bromide **4.69** was added followed by TMEDA (entry1). This protocol did not provide compound **4.71**. Next, another methodology reported by the same group was tried.[248] Similar reaction conditions as before but without TMEDA afforded the desired product in 41% yield (entry 2). Leaving the reaction overnight provided little improvement (entry 3), suggesting that the allylation takes place within 2-3 h. Using bromide **4.69** as the limiting reagent was shown to be beneficial (entry 4). Product **4.71** was obtained in 53% yield. Addition of TMEDA, however, was shown to be detrimental (entry 5).

[a] The reaction afforded the desired aniline **4.68** when the reaction was done in a 65 mg scale. The same reaction conditions afforded the product in 62% yield on a 0.6 g scale. In addition, when doing the reaction at a larger scale, heating up to 30 °C was shown to be beneficial for the reaction.

Table 4.5: Optimisation of the allylation reaction.

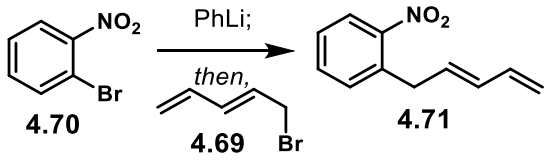

entry	PhLi equiv.	4.69 equiv.	solvent	additive	time	yield %
1	1.0	1.6	THF (0.09 M)	TMEDA (1.0 equiv.)	1.5 h	-
2	1.2	1.6	THF (0.1 M)	-	2 h	41
3	1.2	1.5	THF (0.1 M)	-	12 h	42
4	1.2	0.5	THF (0.1 M)	-	3 h	**53**
5	1.2	0.5	THF (0.1 M)	TMEDA (1.0 equiv.)	3 h	40

With aniline **4.68** the imino-Diels-Alder reaction was tried using aryl aldehydes (Scheme 4.10). Reaction of **4.68** with benzaldehyde **4.56** was tried using 10 mol% of TsOH as catalyst. Reaction in CH_2Cl_2 for 48 h at rt afforded imine **4.72** in 23%. Heterocycle **4.73** was not observed. Next, 4-chlorobenzaldehyde **4.74** was used thinking that a more electron deficient imine would favour the cyclisation step. However, after 5 days of reaction with 10 mol% of TFA in chloroform at 50 °C imine **4.75** was obtained in 33% yield—for this reaction, powdered 4Å molecular sieves were used as an alternative water-catching agent. Again, the cyclisation step seemed not to be favoured, as the expected product **4.76** was not observed.

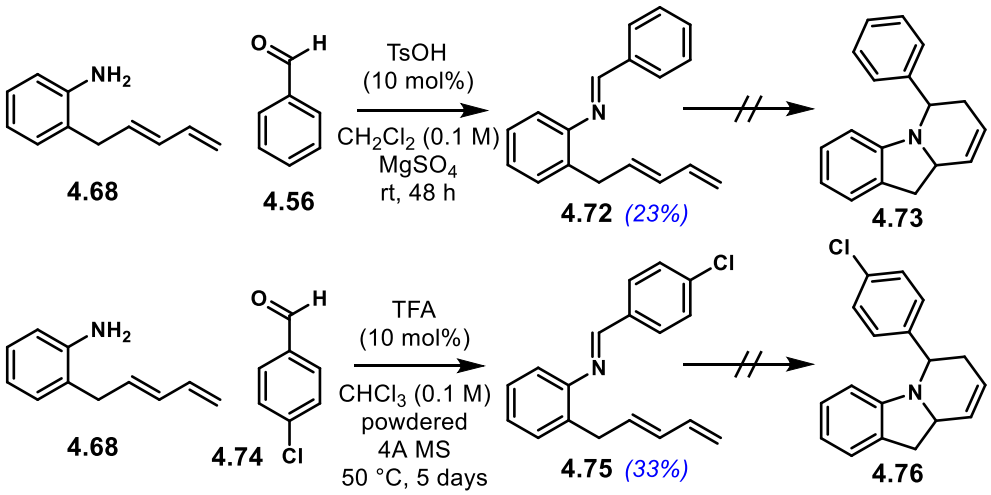

Scheme 4.10: Initial attempts for the imino-Diels-Alder with substrate **4.68**.

It is possible for these reactions, that a hindered transition state similar to **4.59** (*cf.* Figure 4.4) is the reason why the cyclisation step is not favoured. In that case using an α-keto aldehyde might overcome that problem (*cf.* Figure 4.4). Therefore, the reaction of aniline **4.68** and phenyl glyoxal **4.77** was tried. The results for such reactions are reported in Table 4.6.

Table 4.6: An unexpected reaction

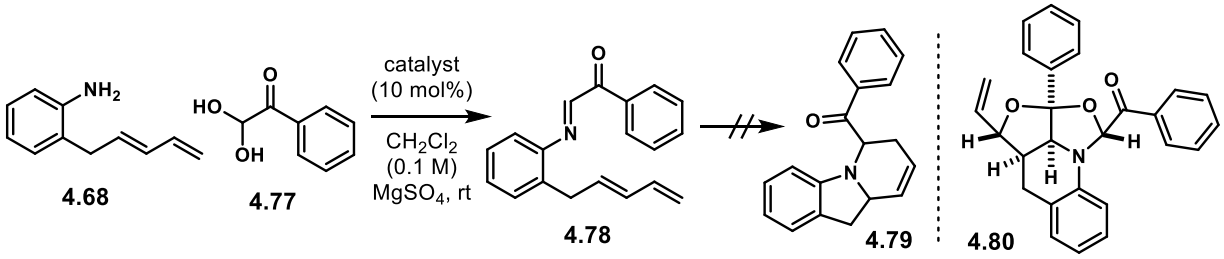

entry	**catalyst**	**4.77 equiv.**	**time**	**4.78 yield %**	**4.80 yield %**
1	-	1.1	12 h	79	-
2	AcOH (10 mol%)	1.1	48 h	80	-
3	TsOH (10 mol%)	1.5	9 h	-	13
4	TsOH (10 mol%)	2.5	18 h	-	29

Reaction conditions: aniline **4.68** (0.1 mmol, 1.0 equiv.), CH_2Cl_2 (1 mL, 0.1 M), $MgSO_4$ (70mg), rt. Yields correspond to isolated products. Only relative stereochemistry shown in **4.80**.

Without a Brønsted acid, **4.68** reacted with **4.77** to form imine **4.78** in 79% yield after 12 h (entry 1). Without a catalyst, it was expected that heterocycle **4.79** would not be formed. Then, the reaction was done using a weak Brønsted acid. Reaction with 10 mol% of AcOH afforded imine **4.78** in 80% yield (entry 2). Even though this reaction was left for 48 h, product **4.79** was not observed, presumably, AcOH might not be acidic enough to protonate the imine and trigger the cycloaddition step.

Surprisingly, when tosic acid was used in 10 mol%, neither imine **4.78** nor heterocycle **4.79** was observed. Instead, product **4.80** was isolated in 13% yield after 9 h (entry 3). Increasing the equivalents of phenyl glyoxal to 2.5 and the reaction time to 9 h improved the yield of **4.80** to 29% (entry 4). This was, certainly, an unexpected reaction outcome. In both cases (entries 3 and 4), product **4.80** was isolated as a single diastereoisomer, which is quite impressive given that the product has five stereocentres—for such a case, a total of 32 diastereoisomers is possible.

In order to determine the relative stereochemistry—which already was presented in **4.80**—a colleague in the Goodman group ran a DP4-AI analysis to find out which diastereoisomer was obtained.[249,250] This method has been used extensively to determine relative stereochemistry in organic molecules.[251–253] With this approach, the relative stereochemistry shown in **4.80** was determined with a 99% probability using both ^{1}H and ^{13}C NMR data. In addition, compound **4.80** was found to be the lowest-energy diastereoisomer.

A mechanism to account for relative stereochemistry in compound **4.80** is presented in Scheme 4.11. Initially, imine **4.78** is formed out of the corresponding starting materials. Then, it is protonated to furnish iminium ion **4.81**. Given that the imino-Diels-Alder product was not observed, the diene motif has to behave as a C-nucleophile instead of a 'typical' diene that undergoes a cycloaddition. In this context, the first step in this cascade would be the attack of a double bond to the iminium ion—as this step sets the first two stereocentres, it would also be the enantiodetermining step if the reaction was done with a chiral Brønsted acid. From the DP4-AI analysis, the hydrogen atoms from the nucleophile and electrophile

(highlighted in purple in structures **4.82**) have to be *syn*- to each other. Therefore, this stereochemical relationship can be established in two possible transition states. ***Z*-4.82** sits both hydrogen atoms *syn*- to each other; however, this ring closure needs the iminium to be in a *(Z)*-configuration, which is higher in energy that the corresponding *(E)*-iminium. In addition, **Z-4.82** sits the iminium *C*-substituent in a pseudo-axial position, thus, such a conformation might be disfavoured. On the other hand, if the iminium ion has an *(E)*-configuration, the addition step can go *via* ***E*-4.82**. In this conformation, both hydrogen atoms are still *syn*- to each other. The alkene nucleophile, however, will adopt an axial position, yet the stable *(E)*-iminium might be overcoming such an energy penalty. In addition, the iminium ion would be locked in an *s-cis* conformation assisted by an intramolecular hydrogen bond with the carbonyl group. Such a hydrogen bond is absent in the *(Z)*-iminium. Also, if the alkene motif were to be equatorial, ***anti*-4.82**, which would sit the hydrogen atoms in an *anti*- relationship, would give the wrong diastereoisomer. This transition state would be disfavoured due to steric clash between the relatively large equatorial substituents. Hence, cyclisation *via* ***E*-4.82** furnishes allylic carbocation **4.83**.

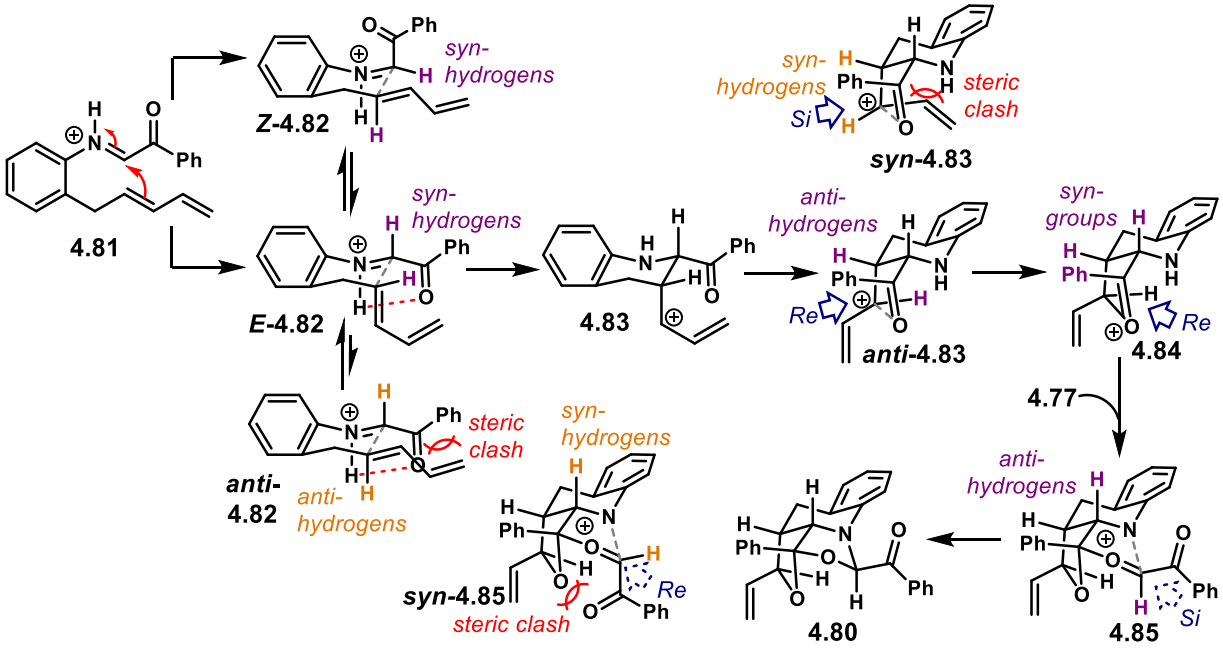

Scheme 4.11: Proposed reaction mechanism for the formation of product **4.80** from iminium ion **4.81**. This mechanism also accounts for the relative stereochemistry suggested by the DP4-AI calculation.

Then, the next ring closure comes from the attack of the carbonyl group in the ketone to the freshly formed carbocation—quite similar to a Prins reaction. In order to account for the relative stereochemistry, attack of the carbonyl to the *Re* face of the cation would sit the highlighted hydrogen atoms in an *anti*-relationship, shown in ***anti*-4.83**. Further, in this conformation, the vinyl moiety is pushed far away from the cage structure to avoid steric clash. Attack to the carbocation's *Si* face, as in ***syn*-4.83**, will place the vinyl motif clashing with the cage structure. In addition, that transition state would give the wrong diastereoisomer.

After ring closure, intermediate **4.84** is obtained. In that structure, the groups highlighted in purple are *syn*- to each other, which is in agreement with the results obtained form DP4-AI. Then, another equivalent

of phenyl glyoxal is required. This, will attack oxy-carbenium ion **4.84** on the *Re* face, as this is the less hindered one, affording **4.85**. The final ring closure would undergo *via* **4.85**. Attack to the *Si* face of the alkylated aldehyde sits the ketone pseudo-equatorial, far from the encumbered cage structure. Such a conformation, places the highlighted hydrogen atoms in an *anti-* relationship, in accordance with the relative stereochemistry. Ring closure furnishes final product **4.80**. The alternative ring closure *via* ***syn-*4.85** attacks the *Re* face of the electrophile. This places the ketone in a pseudo-axial position, clashing with the cage structure and providing the wrong diastereoisomer.

For clarity purposes, Figure 4.5 shows both the flat and 3D-like structure of compound **4.80**. The relative stereochemistry shown, derived from the DP4-AI analysis and the proposed reaction mechanism.

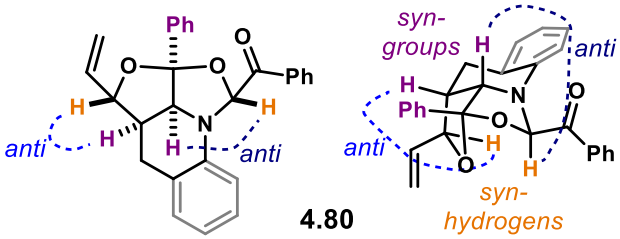

Figure 4.5: Flat and 3D-like structures for compound **4.80**.

This unexpected reaction delivers compound **4.80** as a single diastereoisomer. Thus, the next question was whether it can be obtained enantioselectively. The results for an initial screening using both PAs and NTPAs is presented on Table 4.7 on the next page. The reaction was conducted at rt for 24 using $MgSO_4$ as a water-catching agent. Instead of doing the reaction in CH_2Cl_2 as for the racemic version, toluene was used as a low polarity medium. The idea behind it was that in a solvent with a low dielectric constant, a tight ion pair between the iminium ion and the catalyst counter anion would be favoured, thus achieving better enantiocontrol.

As starting point, catalyst *(R)-PA*-**2** was tried (entry 1). Compound **4.80** was obtained in 9% without enantiocontrol. This might be due to the quite small substituents at the 3,3' positions. In addition, a 9% yield against a 10 mol% catalyst loading might be indicative that the reaction was not catalytic, but stoichiometric. Next, two of the sulfone-derived PAs were tried, also in a 10 mol% loading. *(R)-PA*-**10** afforded the desired product in 18% yield, albeit in a poor 3% *ee* (entry 2). Next, *(R)-PA*-**9** was tried, obtaining **4.80** in 18% yield and 11% *ee* (entry 3). The slightly better enantioselectivity might be due to the missing extra rotatable bond in *(R)-PA*-**9**. Then, *(R)-PA*-**4** was tried (entry 4). The product was afforded in 33% yield and with slightly improved enantiocontrol (16% *ee*).

It was thought that PAs were not acidic enough to fully protonate the imine. Hence, NTPAs were tried. In such a case, it was expected that the imine would be completely protonated and a proper ion pair formed, so, enhancing enantiocontrol. In addition, regarding the results presented in Chapter 3, the catalyst loading for NTPAs was lowered to 2.5 mol%. *(R)-NTPA*-**1** was tried first (entry 5). Product **4.80** was obtained in a rather disappointing 4% yield. However, with quite good enantioselectivity (-43% *ee*). The opposite sense of enantioinduction was achieved with that catalyst.

Table 4.7: Attempts to synthesise **4.80** enantioselectively.

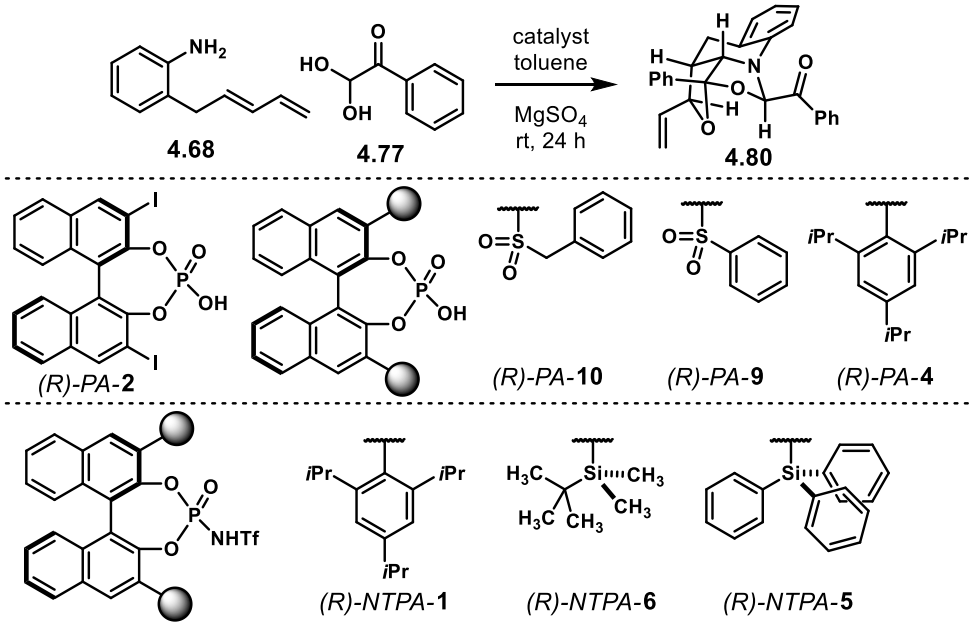

entry	**catalyst (loading)**	**concentration**	**yield**[a]	***ee***
1	*(R)-PA*-**2** (10 mol%)	0.1 M	9%	0
2	*(R)-PA*-**10** (10 mol%)	0.1 M	18%	3%
3	*(R)-PA*-**9** (10 mol%)	0.1 M	18%	11%
4	*(R)-PA*-**4** (5 mol%)	0.1 M	33%	16%
5	*(R)-NTPA*-**1** (2.5 mol%)	0.1 M	4%	-43%
6	*(R)-NTPA*-**6** (2.5 mol%)	0.1 M	13%	34%
7	*(R)-NTPA*-**5** (2.5 mol%)	0.1 M	12%	32%
8[b]	*(R)-NTPA*-**5** (2.5 mol%)	0.05 M	19%	31%

Reaction conditions: aniline **4.68** (0.1 mmol, 1.0 equiv.), phenyl glyoxal (0.25 mmol, 2.5 equiv.), $MgSO_4$ (72 mg, 0.6 mmol, 6 equiv.), toluene (1 mL, 0.1 M), rt, 24 h. [a] yields correspond to isolated product. Only the relative stereochemistry is shown. [b] For this reaction the imine was pre-formed at rt for 8 h, then, the reaction diluted to 0.05 M and the catalyst added.

Next, two of the silicon-based NTPAs were tested. *(R)-NTPA*-**6** afforded the desired product in 13% yield and 34% *ee* (entry 6). Herein, it is clear that the reaction was catalytic. Despite the low yield, enantioselectivity was far better than those obtained with PAs. Next, the mildly hindered *(R)-NTPA*-**5** was used (entry 7). Product **4.80** was obtained in 12% yield and modest enantioselectivity (32% *ee*). In this case, a slightly more confined active site did not make quite of a difference. In an attempt to improve both yield and enantiocontrol, the reaction was set up without a catalyst in order to allow the imine to be formed first (entry 8). Then, the reaction was diluted and catalyst *(R)-NTPA*-**5** added afterwards. After stirring at rt for 24 h, the desired product was isolated in a slightly improved 19% yield and comparable 31% *ee*. This experiment suggests that concentration has a small effect on the yield. However, it is possible that the product starts degrading at some point due to the strong acids used.

In general, NTPAs afforded better enantiocontrol than PAs. On the other hand, yields seemed improved by PAs. In that case, PAs' low acidity may not degrade the imine or the product as fast as NTPAs do,

thus showing higher yields. In addition, it was surprising that *(R)-NTPA*-**1** furnished the product with the opposite sense of enantiocontrol. At this point, there is no obvious explanation. A detailed computational study would be helpful in this case.

After such an unexpected reaction discovered, further modification of the substrate was investigated. This changed the reaction under study from an aza-Diels-Alder to other types of ring closing reactions, to be carried out enantioselectively.

4.4. Towards an enantioselective Pictet-Spengler reaction

The last modification in the substrate attempting to make heterocycles *via* an aza-Diels-Alder reaction turned into an unexpected transformation. Mechanistically, as discussed in the last section, the diene moiety in **4.81** attacks the iminium ion in a nucleophilic fashion, rather than going through a cycloaddition. Therefore, taking advantage of this discovery, another way to build up complex molecular structures might arise if a *C*-nucleophile is installed instead of the diene, as shown in **4.86** (Scheme 4.12). The next question, then, was to find out a suitable nucleophile. For instance, an aromatic ring can be used as a nucleophilic partner, **4.87**; however, an unsubstituted aryl might not be nucleophilic enough to attack the iminium ion. Thus, adding an electron-donating moiety would increase the reactivity of the aromatic ring, like in compound **4.88**. Yet, the nucleophile might not be reactive enough and regioselectivity issues may arise. Thus, adding an extra methoxy group, **4.89** would make the aryl group more reactive and there would not be problems with regioselectivity.

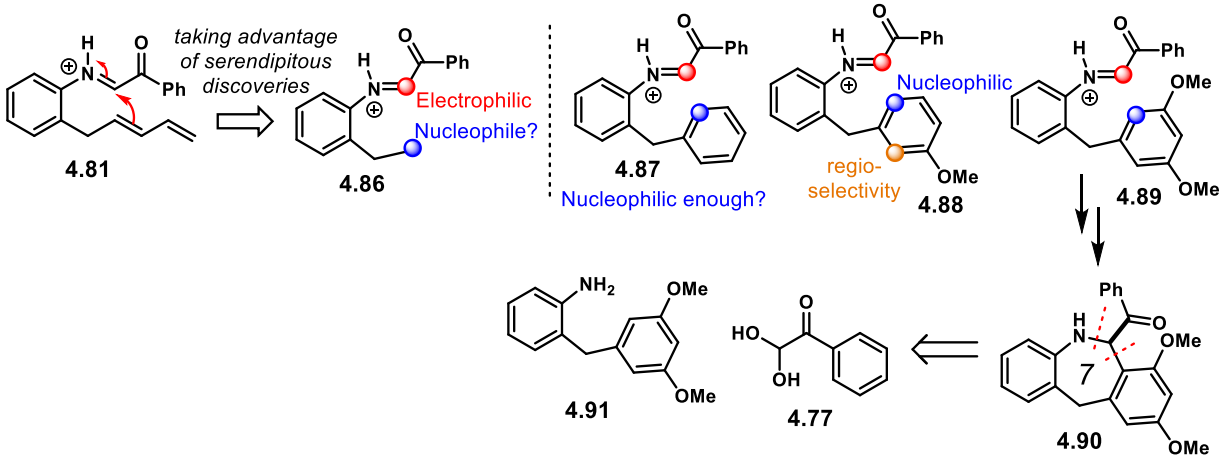

Scheme 4.12: Design of an enantioselective Pictet-Spengler reaction.

In this scenario, iminium ion **4.89** would undergo a ring closing reaction *via* a Mannich-Friedel-Crafts sequence, also known as the Pictet-Spengler reaction.[254] This procedure will yield the seven-member heterocycle **4.90** with the possibility to install a chiral centre. Thus, a chiral Brønsted acid could make this reaction enantioselectively. In a disconnection approach, compound **4.90** can be made out of aniline **4.91** and phenyl glyoxal **4.77**.

The Pictet-Spengler reaction has been widely studied and revised.[255] The asymmetric version of this transformation has been extensively applied to the total synthesis of natural products and bioactive molecules.[256] This reaction offers a direct and straightforward approach to the synthesis of six-member heterocyclic systems.[257] Yet, reports highlighting the construction of seven-membered heterocycles are scarce.

In the field of organocatalysis, the group of Jacobsen has developed several enantioselective strategies for the construction of *N*-heterocycles using the Pictet-Spengler reaction and chiral thioureas as catalysts.[258–261] In addition, they have applied their methodologies in the synthesis of natural products.[259] These thiourea-catalysed reactions have been subject of computational studies as well.[262] Moreover, the construction of six-membered rings in an enantioselective Pictet-Spengler fashion has also attracted the attention of chiral Brønsted acids, achieving excellent levels of enantiocontrol.[263–266] However, catalytic enantioselective reactions to make seven-membered rings are rather limited,[267,268] even though such medium-size ring systems are ubiquitous in natural products.[269]

An enantioselective and organocatalytic methodology to construct seven-membered *N*-heterocycles would be desirable. Recent examples in which Brønsted acid-catalysis and seven-membered rings are featured are presented in Scheme 4.13 on the following page.

The group of Kundu developed a racemic methodology to construct seven-membered rings (Scheme 4.13*a*).[270] Such a protocol uses a Pictet-Spengler reaction in the ring-closing step. In this reaction, anilines **4.92**—, which bear a tethered indole as the nucleophilic partner—react with aldehydes or methyl ketones to furnish iminium ions **4.93** under the acidic reaction conditions. Then, such an intermediate undergoes the 7-*endo-trig* cyclisation step to afford heterocycles **4.94** after a rearomatisation step. In a complementary fashion, using TFA as a catalyst, aniline **4.95** forms iminium ions **4.96**. Subsequent Pictet-Spengler sequence affords **4.97**. Both regioisomeric heterocycles, **4.94** and **4.97** are obtained in excellent yields, albeit racemic.

The group of Lin later developed a similar reaction, performed in an enantioselective fashion (Scheme 4.13*b*).[271] Therein, aniline **4.95** reacts with trifluoromethyl aryl ketones **4.98** in the presence of a chiral SPINOL-derived PA. The reaction furnishes *N*-heterocycles **4.99** in good yields and up to 99% *ee*. The authors propose that the reaction mechanism goes *via* iminium ion **4.100**. The catalyst activates this intermediate in a bifunctional manner. Both N-H motifs—from the iminium ion and from the nucleophilic indole—engage in hydrogen bonding with the oxygen atoms in the catalyst. Such a tight and ordered transition state accounts for the impressive levels of enantiocontrol achieved in this reaction.

In a related reaction, also reported by the group of Lin, seven-membered imines **4.101** react with pyrroles and indoles in the presence of another chiral SPIRO-PA (Scheme 4.13*c*).[272] This nucleophilic addition affords *N*-heterocycles **4.102** with up to 93% *ee*. An activation mode similar to **4.100** is proposed. This reaction grants access to a quaternary chiral centre, yet, the enantiodetermining step does not involve the actual construction of the seven-membered ring scaffold.

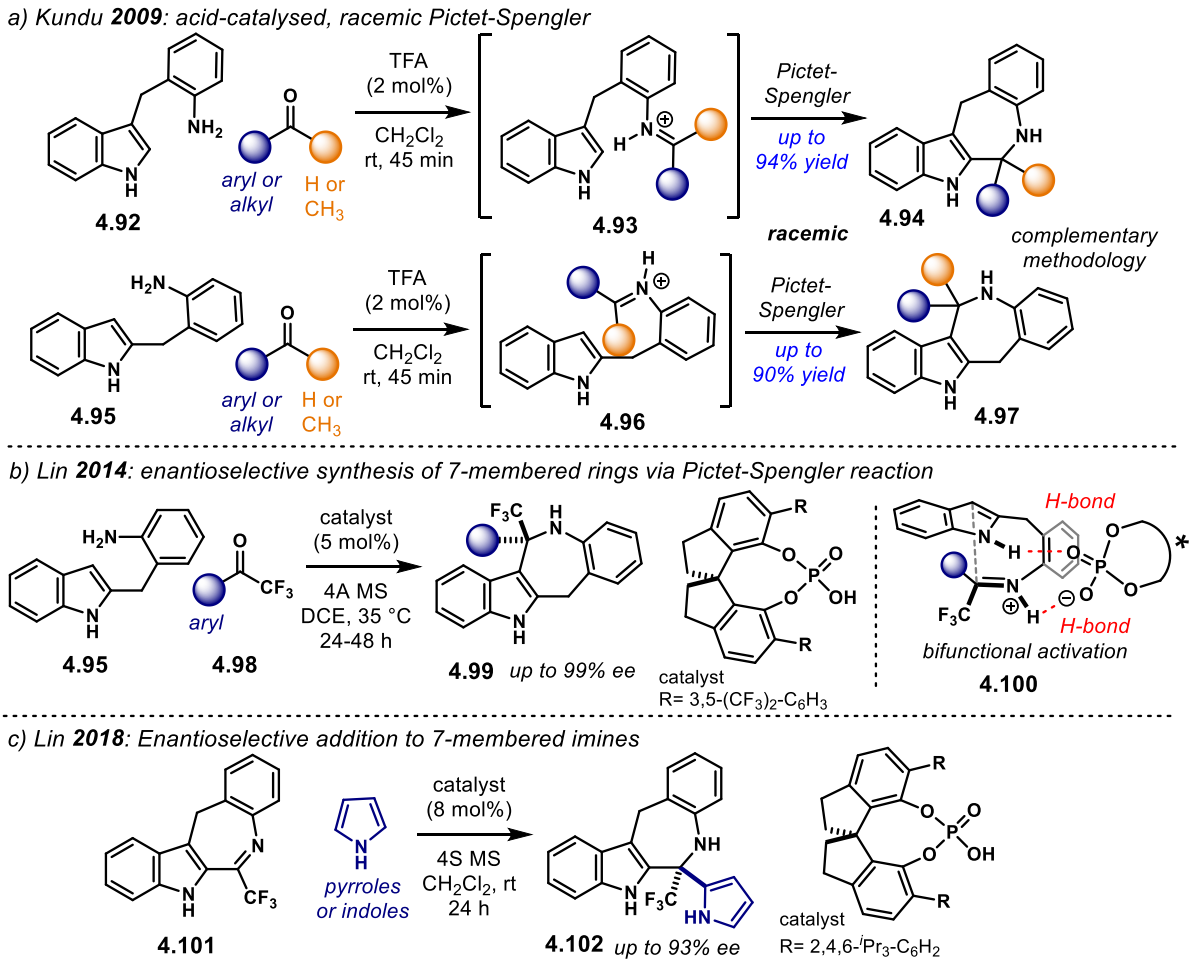

Scheme 4.13: a) racemic TFA-catalysed Pictet-Spengler reaction reported by the group of Kundu. b) Enantioselective Pictet-Spengler reaction with trifluoromethyl aryl ketones, reported by the group of Lin. c) Enantioselective addition to 7-membered imines, reported by the group of Lin.

In the aforementioned reactions, the nucleophilic partners were highly nucleophilic indole or pyrrole motifs. In this context, a question here was, whether or not imines **4.89** would undergo a Pictet-Spengler cyclisation. Reports in which aryl motifs are used as nucleophiles are scarce. Two such reports use iminium ions as reactive species and the highly acidic NTPAs as organocatalysts (Scheme 4.14).

The group of You developed a double Friedel-Crafts strategy for the asymmetric synthesis of fluorenes using an iminium ion in the enantiodetermining step (Scheme 4.14*a*).[273] In the first (not enantioselective) Friedel-Crafts reaction, indole **4.103** reacts with aldehyde **4.104**, which presumably is activated by hydrogen bonding through the carbonyl group, to give secondary alcohol **4.105**. Then, this alcohol is protonated by the NTPA and dehydrates to yield a vinylogous iminium ion **4.106**. Such iminium is likely to be locked to the catalyst active site through hydrogen bonding and ion pairing. In the subsequent step, the dimethoxy phenyl ring attacks the electrophile in a 1,4- addition fashion. Both the free N-H moiety and the 2-methyl group in the iminium ion were found to be essential for enantiocontrol. Moreover, an electron-rich, nucleophilic aryl is crucial for reactivity. After the addition step, rearomatisation of **4.107** delivers enantioenriched fluorenes **4.108** and regenerates the catalyst.

The group of Lette developed an elegant method for the construction of fused *N*-heterocycles (Scheme 4.14*b*).[274] In this two-step methodology, imide **4.109** reacts with organolithium reagents—methyl lithium or *n*-butyl lithium shown in the scheme—to furnish hydroxy amides **4.110**. Upon treatment with a chiral NTPA, the hydroxyl moiety is protonated. Subsequent dehydration furnishes reactive *N*-acyl iminium ion **4.111**. *N*-acyl iminium ions have proven to be suitable substrates in Brønsted acid-catalysed enantioselective transformations. Intramolecular 1,2- addition of the aryl substituent in the enantiodetermining step yields intermediate **4.112**. After that, rearomatisation delivers enantioenriched heterocycles **4.113** in acceptable yields, albeit with modest enantioselectivities (up to 67% *ee*).

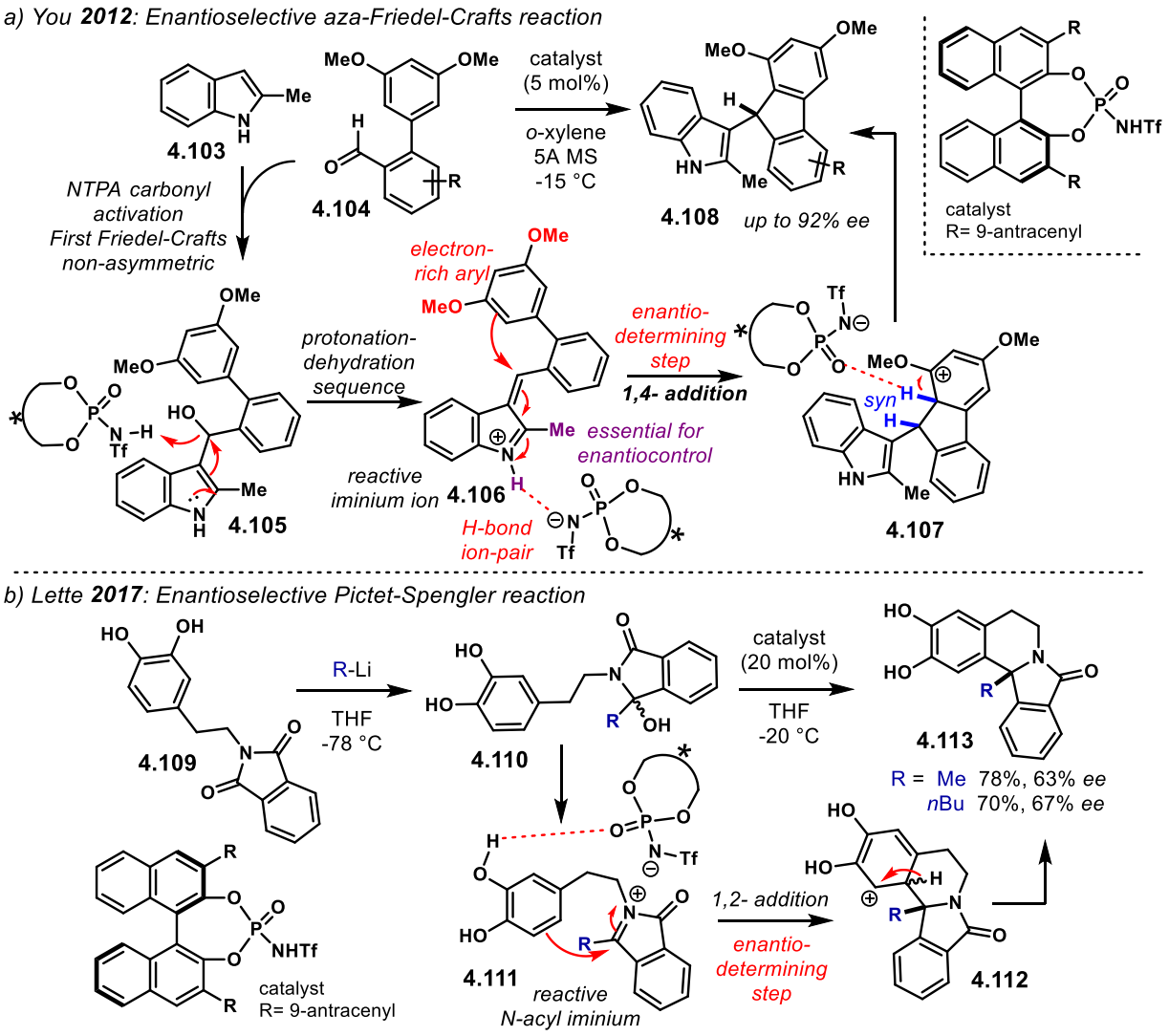

Scheme 4.14: a) Enantioselective aza-Friedel-Crafts reaction, developed by the group of You. b) Enantioselective Pictet-Spengler reaction using *N*-acyl iminium ions, reported by the group of Lette. In these two examples, the nucleophilic partner is an electron-rich aryl group.

With these precedents, a Pictet-Spengler reaction in which an aryl group serves as a nucleophile seems feasible. The initial idea is further developed on Scheme 4.15. Starting from aniline **4.91** and phenyl glyoxal **4.77**, iminium ion **4.89** can be formed in the presence of a catalytic amount of a Brønsted acid, whether a PA or an NTPA. Such an iminium ion would be very reactive due to the extra carbonyl group.

A plausible mode of activation is presented in **4.114**. The iminium ion is likely to be locked in an *s-cis* conformation due to an intramolecular hydrogen bond. This would engage with the catalyst's active site through hydrogen bonding or tight ion pairing. In addition, it is possible that π-π stacking interactions would provide extra rigidity to the transition state, thus, enhancing enantiocontrol. Stereoselective 1,2-addition—in a Friedel-Crafts fashion—would deliver intermediate **4.115**, which, after rearomatisation, affords seven-membered heterocycle **4.90**, enantioselectively. One of the main challenges for enantiocontrol in this reaction arises from the proposed mono-activation mode. Generally, in Brønsted acid-catalysed reactions, high enantiomeric excesses are attributed to a bifunctional activation mode where the catalyst engages both with the electrophilic and with the nucleophilic partners.

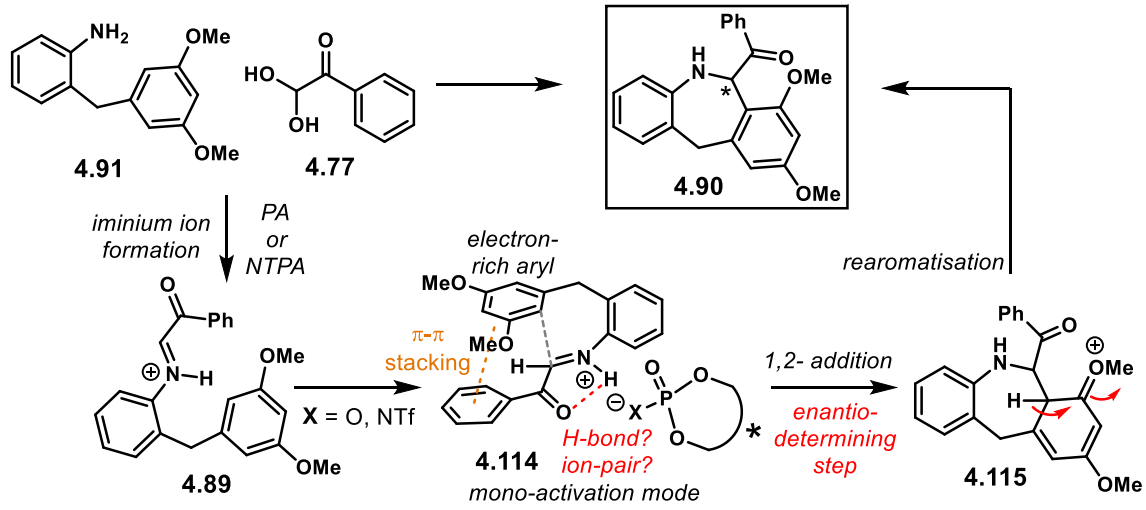

Scheme 4.15: Approach for an enantioselective Brønsted acid-catalysed Pictet-Spengler reaction.

Therefore, the new adventure towards an enantioselective Pictet-Spengler reaction started with the synthesis of aniline **4.91** (Scheme 4.16). Nitro compound **4.117** was prepared following the lithium-bromine exchange methodology as before, using phenyl lithium.[247,248] 2-bromonitrobenzene **4.70** and different 3,5-dimethoxybenzyl halides **4.116** were tried, with or without additives. Table 4.8 on the following page summarises the optimisation of this reaction.

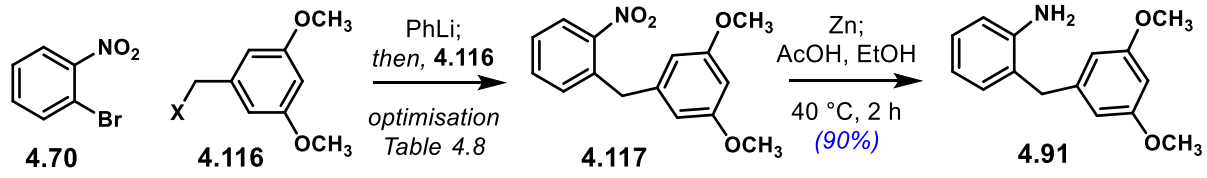

Scheme 4.16: Synthesis of starting material **4.91**.

Following the reaction conditions reported by the group of Pirrung,[248] compound **4.117** was obtained in 33% yield (entry 1). Shortening the reaction time to 3.5 h under the same conditions improved the yield to 44% (entry 2). This shows that it might not be necessary to leave the reaction overnight. The yield of **4.117** was slightly enhanced when the reaction was left for 5 h (53%, entry 3). Such conditions afforded a 44% yield when the reaction was performed in a 1.8 g scale (entry 4). In order to boost the yield, some additives were tried as well. In such an attempt, copper (I) bromide-dimethyl sulfide complex was added

so as to form the corresponding organocuprate (entry 5). However, the reaction did not work. In another attempt to form the organocuprate, copper (I) iodide was used (entry 6), yet, unsuccessfully. Using TMEDA as an additive to stabilise the organolithium reagent afforded product **4.117** in 52% yield (entry 7). Despite this was a good yield, it seems that using TMEDA did not improve the reaction, as similar results are obtained when it is not used (entries 3 and 4).

Table 4.8: Optimisation of reaction conditions for nitro compound **4.117**

entry	**scale**[a]	**X**	**additive**	**time**	**yield %**
1	300 mg	Br	-	12 h	33
2	0.6 g	Br	-	3.5 h	44
3	300 mg	Br	-	5 h	**53**
4	1.8 g	Br	-	5 h	**44**
5	300 mg	Br	CuBr-DMS (0.5 equiv.)	12 h	0
6	300 mg	Br	CuI (0.5 equiv.)	12 h	0
7	300 mg	Br	TMEDA (1.2 equiv.)	12 h	**52**
8	300 mg	I	-	5 h	30
9	300 mg	I	TMEDA (1.2 equiv.)	12 h	35
10	300 mg	OTs	-	5 h	6

Reaction conditions: 2-bromonitrobenzene (1.0 equiv.), THF (0.1 M), PhLi (1.2 equiv. 1.9 M solution in Bu_2O), -78 °C, 5-10 min. Then, 3,5-dimethoxybenzyl halide (1.5 equiv.), -78 °C to rt. [a] scale relative to 2-bromonitrobenzene.

In order to improve the reaction, 3,5-dimethoxybenzyl iodide was used as a more reactive electrophile.[275] The reaction without additives afforded the desired product in 30% yield after 5 h (entry 8). So far, the corresponding bromide performs better. Addition of TMEDA showed a slightly increase in yields (35%, entry 9). As a final experiment, the presumably more reactive 3,5-dimethoxybenzyl tosylate was made and tested (entry 10).[276] However, product **4.117** was isolated in only 6% yield. Thus, the best reaction conditions for this transformation seem to be those presented on entries 3 and 4.

With compound **4.117**, reduction of the nitro group with zinc and acetic acid in ethanol afforded aniline **4.91** in 90% yield.[246] During the optimisation of this reaction, it was noticed that the reduction worked best at 40 °C. Room temperature afforded the aniline in 62% yield.

The reaction of aniline **4.91** with phenyl glyoxal **4.77** was next studied, aiming to synthesise seven-membered heterocycle **4.90**. Initially, several PAs were tested. The results for the PAs screening are presented on Table 4.9 on the next page. As starting point, a control reaction without a catalyst was done (entry 1). After 72 h, the intermediate imine **4.118** was isolated in 43% yield. Compound **4.90** was not observed. This points out that, without a catalyst, the racemic background reaction is not an issue. Therefore, as a second control reaction, tosic acid was used as a Brønsted acid (entry 2). After 24 h, the desired product **4.90** was isolated in 51% yield. In this case, imine **4.118** was not observed, suggesting full consumption of both the imine and the starting material.

The next step, was conducting the reaction with chiral Brønsted acids. In this case, PAs in a 10 mol% catalyst loading. *(R)-PA*-**3** afforded heterocycle **4.90** in 62% yield and -9% *ee* (entry 3). *(R)-PA*-**4**, on the

other hand, gave the product in 37% yield and 16% *ee* after 36 h (entry 4). In addition, the latter reaction also afforded imine **4.118** in 15% yield. These two experiments indicate that the acidity of the catalyst is important to fully consume the imine—this was observed with the more acidic *(R)-PA*-**3** due to the perfluorinated 3,3' substituents. The reaction took longer with a less acidic catalyst. Moreover, *(R)-PA*-**4** achieved better enantiocontrol, suggesting that the size of the 3,3'- groups might play an important role in enantioselection. In addition, despite the fact that both of these PAs bear aryl-type scaffolds, opposite senses of enantioinduction were observed, albeit low.

Table 4.9: Screening of PAs for the enantioselective synthesis of **4.90**

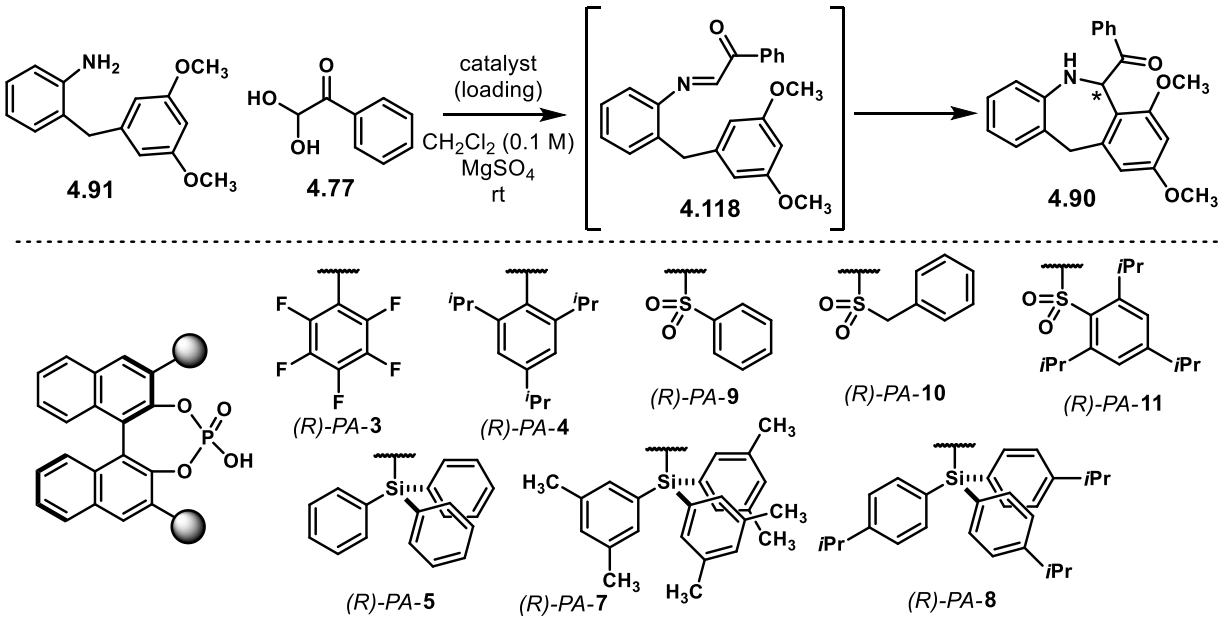

entry	**catalyst**	**time**	**4.118 yield %**[a]	**4.90 yield %**[a]	***ee***[b]
1	-	72 h	43	-	NA
2	TsOH (20 mol%)	24 h	-	51	NA
3	*(R)-PA*-**3** (10 mol%)	24 h	-	62	-9%
4	*(R)-PA*-**4** (10 mol%)	36 h	15	37	16%
5	*(R)-PA*-**9** (10 mol%)	24 h	-	55	7%
6	*(R)-PA*-**10** (10 mol%)	24 h	-	49	-3%
7	*(R)-PA*-**11** (10 mol%)	24 h	-	51	-3%
8	*(R)-PA*-**5** (10 mol%)	36 h	13	44	0
9	*(R)-PA*-**7** (10 mol%)	100 h	34	42	-8%
10	*(R)-PA*-**8** (10 mol%)	100 h	30	48	3%

Reaction conditions: aniline **4.91** (0.11 mmol, 1.0 equiv.), phenyl glyoxal **4.77** (0.12 mmol, 1.1 equiv.), CH_2Cl_2 (1.1 mL, 0.1 M), $MgSO_4$ (40 mg), rt. [a] yields correspond to isolated products. [b] enantiomeric excess determined by chiral SFC.

Given that acidity played an important role to push the imine towards **4.90**, two more acidic PAs were tried: those bearing sulfone-based scaffolds. Catalyst *(R)-PA*-**9** afforded the desired product in 55% yield after 24 h (entry 5). In this case, full consumption of the imine was observed, however, enantiocontrol

was low (7% *ee*). The related catalyst, *(R)-PA*-**10**, which is equally acidic but has an extra rotatable bond, afforded compound **4.90** after 24 h in 49% yield and -3% *ee* (entry 6). Herein, imine **4.118** was also fully consumed. Even though these two catalysts have a similar molecular architecture, it is yet not clear how opposite senses of enantioinduction are obtained. Furthermore, the more hindered *(R)-PA*-**11** was also tried (entry 7). Compound **4.90** was obtained in 51% yield after 24 h with poor enantiocontrol (-3% *ee*).

Next, steric confinement around the catalyst's active site was evaluated. For such, the silicon-based scaffolds are appropriate PAs. The mildly hindered *(R)-PA*-**5** gave the desired product in 44% yield without enantioselection (entry 8). In addition, 36 h were needed, which was three-fold the time it took the more acidic catalysts. Moreover, imine **4.118** was isolated in 13% yield. The more hindered silicon-based PAs seemed not to be suitable for the reaction under study. *(R)-PA*-**7** afforded **4.90** in 42% yield and -8% *ee* after 100 h (entry 9). In addition, imine **4.118** was isolated in 34% yield. This points out that a hindered catalyst may not always be the best choice for a given transformation. Further, *(R)-PA*-**8** required a 100 h reaction to get imine **4.118** in 30% yield and heterocycle **4.90** in 48% yield and 3% *ee* (entry 10).

After evaluating the PAs presented on Table 4.9, it is shown that for this reaction, more acidic Brønsted acids are needed to enhance the yield. In this context, a series of NTPAs were tried. In general, the yields were higher than those obtained with PAs. The results for such a screening are presented on Table 4.10 on the following page.

As the reaction gave better yields with more acidic catalysts, for the NTPA screening, the steric hindrance was evaluated first. *(R)-NTPA*-**5**, in a 10 mol% loading, afforded the desired product in 59% yield after 16 h, yet with only 3% *ee* (entry 1). Imine **4.118** was not observed. Then, the same catalyst, *(R)-NTPA*-**5**, was tried in a 2.5 mol% loading (entry 2). Product **4.90** was obtained in 58% yield and low 4% *ee* after 24 h. Imine **4.118** was isolated in 4% yield. Thus, for the case of NTPAs, a catalyst loading as low as 2.5 mol% is as effective as 10 mol%. It was also thought that, using a low polarity solvent could improve enantioselectivity. In principle, a tighter ion-pair between the reactive iminium ion and the catalyst counter anion might be favoured, thus allowing better enantiocontrol (*cf.* **4.114**). However, this was not the case. When the reaction was done with 2.5 mol% *(R)-NTPA*-**5** in toluene, imine **4.118** and heterocycle **4.90** were isolated, both in 23% yield (entry 3). In addition, such reaction took 48 h and yielded the product in a racemic fashion.

Diminishing the steric demand of the catalyst's scaffolds seemed to have a beneficial effect. *(R)-NTPA*-**6**—which bears methyldiphenyl silyl scaffolds—afforded **4.90** in 58% yield and slightly improved -12% *ee* (entry 4). Then, the less hindered *(R)-NTPA*-**6** was tried (entry 5). Product **4.90** was isolated in 64% yield and -6% *ee*. The low enantiocontrol might be attributed to the relatively small catalyst's scaffolds.

Next, a series of aryl-based scaffolds were tried. Catalyst *(R)-NTPA*-**1** gave product **4.90** in 43% yield and -12% *ee* after 24 h (entry 6). Imine **4.118** could be isolated in 2% yield. The related catalyst, *(R)-NTPA*-**2** (entry 7), showed to be less active. After the same reaction time, 24 h, **4.90** was obtained in 42% yield, yet, imine **4.118** was isolated in 21% yield. This suggests a slower reaction, possibly, due to the more sterically demanding catalyst. However, enantioselectivity was highly improved, up to -32% *ee*. So

far, this was the best enantiocontrol observed for this reaction. Catalyst *(R)-NTPA*-**3** afforded the desired product in 48% yield, albeit with low enantiocontrol, 6% *ee* (entry 8). To conclude the screening, the more acidic *(R)-NTPA*-**8** afforded only product **4.90** after 24 h, in 61% yield but racemic (entry 9).

Table 4.10: Screening of NTPAs for the enantioselective synthesis of **4.90**

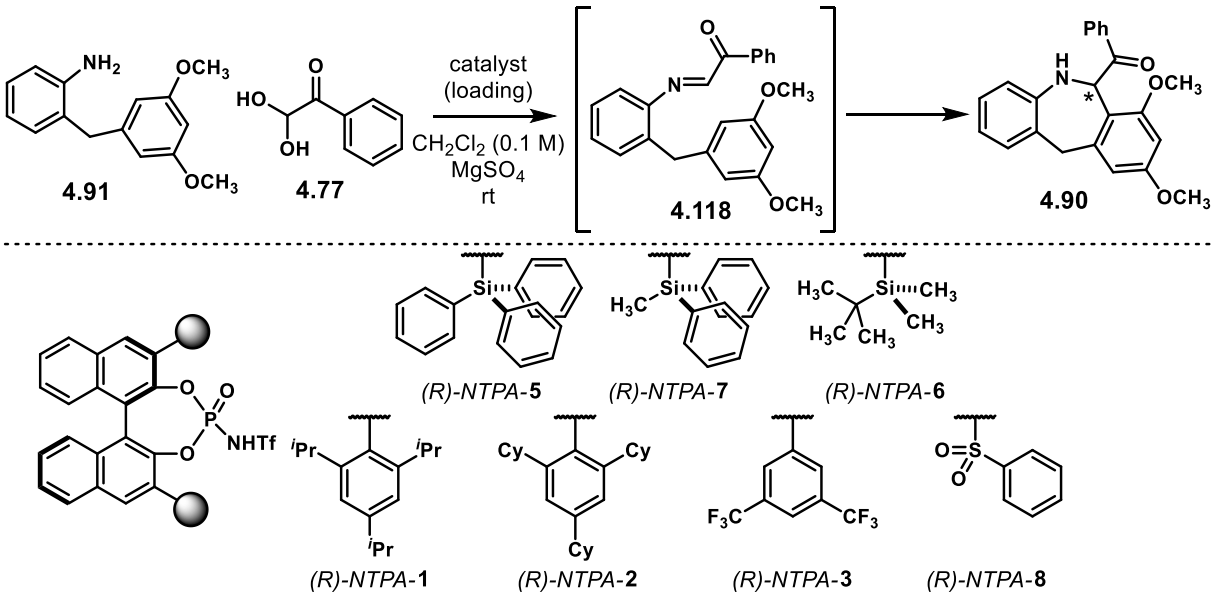

entry	**catalyst**	**time**	**4.118 yield %**[b]	**4.90 yield %**[b]	***ee***[c]
1	*(R)-NTPA*-**5** (10 mol%)	16 h	-	59	3%
2	*(R)-NTPA*-**5** (2.5 mol%)	24 h	4	58	4%
3[a]	*(R)-NTPA*-**5** (2.5 mol%)	48 h	23	23	0
4	*(R)-NTPA*-**7** (2.5 mol%)	24 h	-	58	-12%
5	*(R)-NTPA*-**6** (2.5 mol%)	24 h	-	64	-6%
6	*(R)-NTPA*-**1** (2.5 mol%)	24 h	2	43	-12%
7	*(R)-NTPA*-**2** (2.5 mol%)	24 h	21	42	-32%
8	*(R)-NTPA*-**3** (2.5 mol%)	24 h	-	48	6%
9	*(R)-NTPA*-**8** (2.5 mol%)	24 h	-	61	0

Reaction conditions: aniline **4.91** (0.11 mmol, 1.0 equiv.), phenyl glyoxal **4.77** (0.12 mmol, 1.1 equiv.), CH_2Cl_2 (1.1 mL, 0.1 M), $MgSO_4$ (40 mg), rt. [a] Reaction conducted in toluene (1.1 mL, 0.1 M). [b] yields correspond to isolated products. [c] enantiomeric excess determined by chiral SFC.

With a highly acidic catalyst and a carbonyl group α to the chiral centre, it is plausible that racemisation might occur in **4.90** (Scheme 4.17). A concerted protonation-deprotonation between product **4.90** and the catalyst could take place in order to get enol **4.119** which could be protonated again to furnish ***ent*-4.90**.

In this context, 4-chlorobenzaldehyde **4.74** was tried as an alternative substrate for the reaction. The reaction, as well as the results of a preliminary screening are presented on Table 4.11 on the following page, using a 20 mol% TsOH as Brønsted acid. For this reaction, it was expected aniline **4.91** to react with **4.74** to furnish imine **4.120**. Then, this one would undergo an acid-catalysed Pictet-Spengler reaction

to afford heterocycle **4.121**. In this case, the iminium ion that would trigger the cyclisation might not be that reactive due to the lack of the carbonyl group.

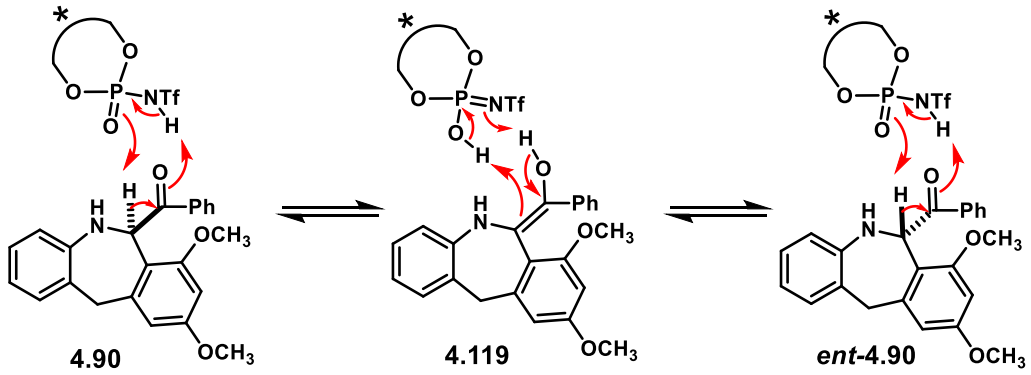

Scheme 4.17: Plausible mechanism for the racemisation of product **4.90**.

Table 4.11: Attempts to synthesise compound **4.121** in a racemic fashion.

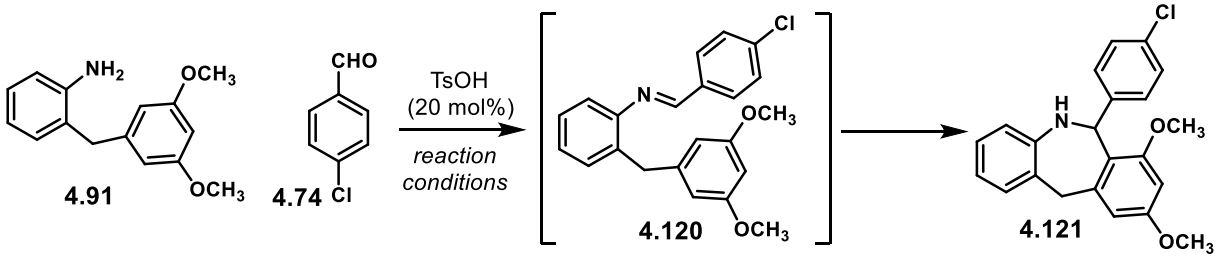

entry	solvent	temperature	time	4.120 yield %[a]	4.121 yield %[a]
1	CH_2Cl_2 (0.1 M)	rt	48 h	NI	-
2	toluene (0.1 M)	60 °C	48 h	NI	-
3	toluene (0.1 M)	90 °C	48 h	16	18
4	*m*-xylene (0.1 M)	120 °C	24 h	-	15

Reaction conditions: aniline **4.91** (0.11 mmol, 1.0 equiv.), 4-chlorobenzaldehyde **4.74** (0.12 mmol, 1.1 equiv.), solvent (1.1 mL, 0.1 M), TsOH (0.022 mmol, 20 mol%), $MgSO_4$ (40 mg). [a] yields correspond to isolated products. NI=imine was observed but Not Isolated.

As a starting point, the reaction was done in CH_2Cl_2 at rt (entry 1). After 48 h, only imine **4.120** was observed on TLC, however it was not isolated. Instead, CH_2Cl_2 was evaporated and the residue dissolved in toluene. Then, the reaction was heated up to 60 °C and stirred for 48 h (entry 2). Imine **4.120** was still present on TLC but compound **4.121** was not observed. Thus, the temperature was increased to 90 °C (entry 3). After 48 h, the desired product **4.121** was isolated in 18% yield, along with unreacted imine (16%). Another attempt was tried on *m*-xylene at 120 °C (entry 4). After 24 h, heterocycle **4.121** was afforded in 15% yield. Imine **4.120** was no longer observed in this case.

From these experiments, it is clear that the iminium ion derived from **4.120** is not as reactive as **4.114** (*cf.* Scheme 4.15). It took 24 h at 120 °C to afford a low yield of **4.121**. Therefore, **4.74** might not be a suitable

substrate to try with chiral Brønsted acids. Instead, it was hypothesised that a different substrate with a carbonyl group that could enhance the reactivity of the imine would work. Further, it would be desirable not to have potentially enolisable hydrogen atoms in the final product. In this context, two reactions were tried, in a racemic fashion to start with (Scheme 4.18). Reaction of **4.91** with **4.122** proceeded sluggishly to afford imine **4.123** in 35% yield after heating at 120 °C for 72 h. Imine **4.123** was isolated in a 3:1 *E/Z* ratio. Heterocycle **4.124** was not observed. In a similar fashion, reaction of **4.91** with **4.125** afforded imine **4.126** in 38 % yield. In that case, the reaction took 96 h at 120 °C. Moreover, heterocycle **4.127** was not observed. In these reactions, ketimines **4.123** and **4.126** did not provide iminium ions electrophilic enough to undergo the subsequent Pictet-Spengler reaction. Thus, it was decided to revisit the nucleophilic counterpart.

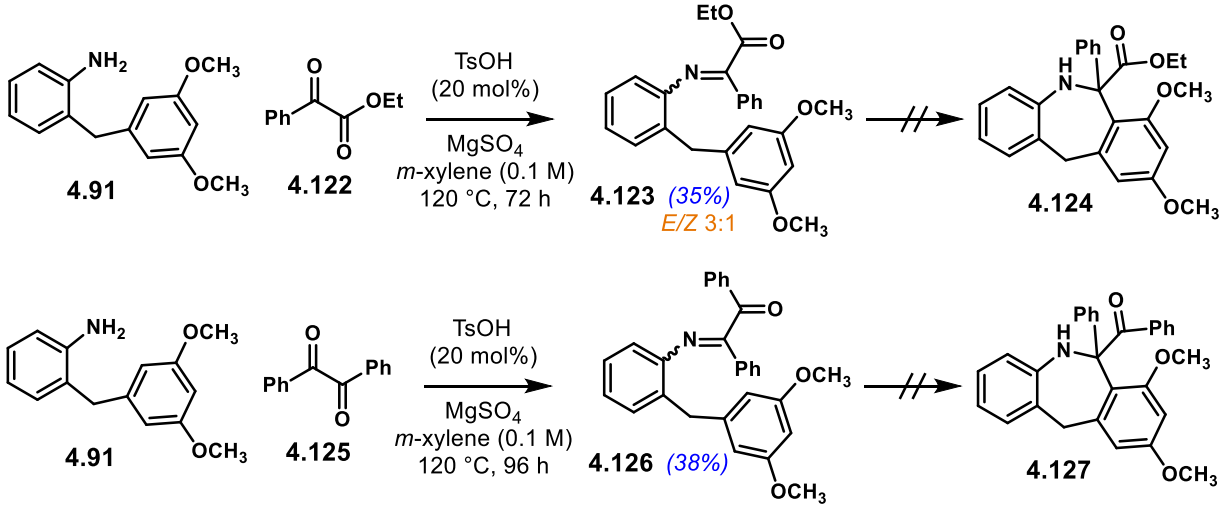

Scheme 4.18: Attempts to synthesise 7-membered heterocycles bearing a quaternary stereocentre.

Looking for a more nucleophilic substrate it was thought that aniline **4.131** would be a suitable option (Scheme 4.19). The extra oxygen atom would raise the HOMO energy of the aryl motif, making it more reactive. Thus, the synthesis of **4.131** started with 2-fluoronitrobenzene **4.128** and 3,5-dimethoxyphenol **4.129**. Heating at 95 °C in DMF with K_2CO_3 afforded nitro compound **4.130** in 94% yield.[277] Then, reduction with zinc provided aniline **4.131** in 85% yield.[246]

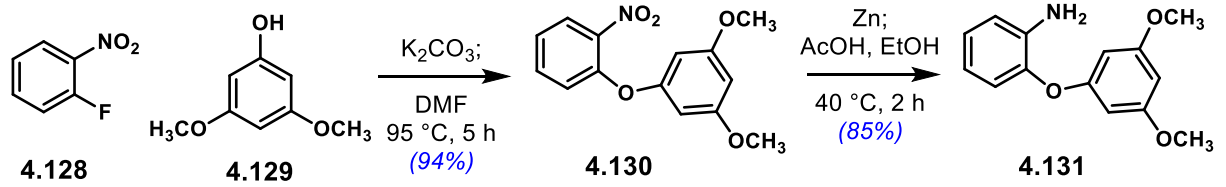

Scheme 4.19: Synthesis of aniline **4.131**.

With aniline **4.131**, aldehydes **4.77**, **4.74** and **4.132** were evaluated as suitable substrates for the Pictet-Spengler reaction (Scheme 4.20). For such screening, 10 mol% TFA was used as Brønsted acid. In this case, powdered 4Å molecular sieves were used as a water-catching additive. The reactions were conducted in chloroform at rt for 24 h.

Phenyl glyoxal **4.77** reacted smoothly to afford heterocycle **4.134** in 40% yield. However, if a chiral Brønsted acid were tried, this product may also have the disadvantage of having a potentially enolisable hydrogen atom at the chiral centre. Intermediate imine **4.133** was not observed. Secondly, 4-chloro benzaldehyde **4.74** was used. Imine **4.135** was not observed, presumably, it all was converted to product **4.136**, which was obtained in 86% yield. On the other hand, 2-hydroxybenzaldehyde **4.132** gave imine **4.137** in 84% yield. Heterocycle **4.138** was not observed. For the latter reaction, it might be possible that an intramolecular H-bond would be established between the imine N-atom and the H-atom from the hydroxyl moiety. This would further decrease the basicity of **4.137**, thus making protonation by the Brønsted acid less feasible.

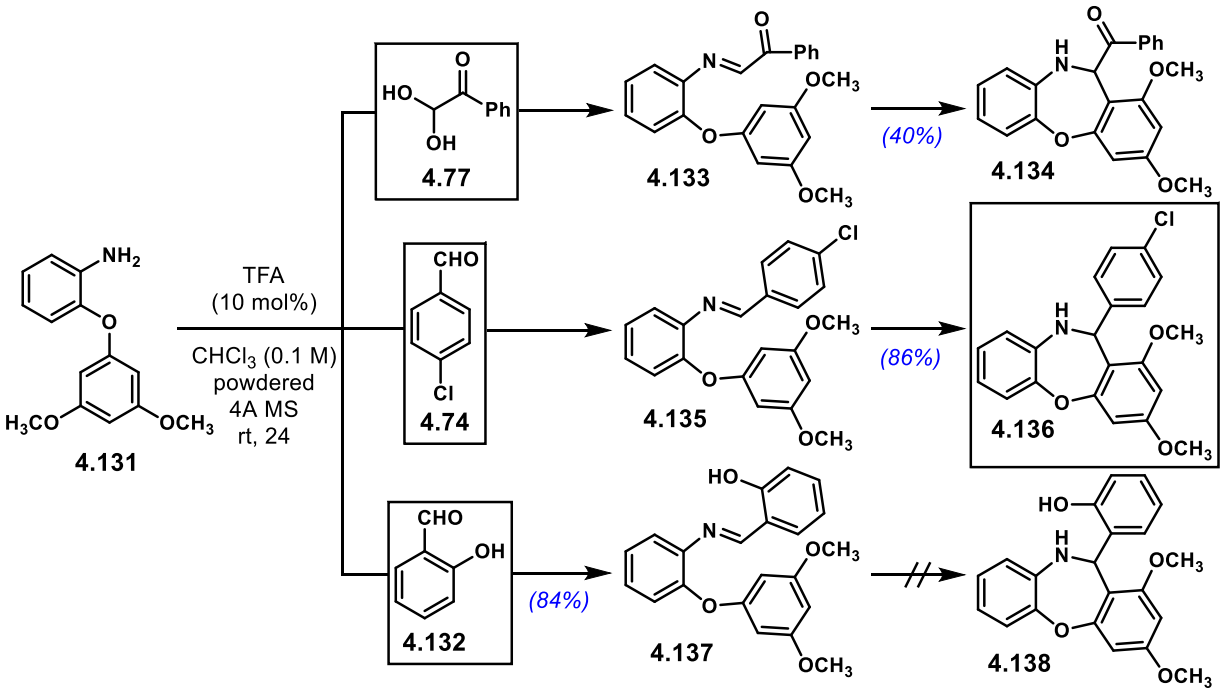

Scheme 4.20: Small screening of aldehydes. The reactions were conducted in a 0.1 mmol scale with 1.1 equivalents of the corresponding aldehyde.

Therefore, 4-chlorobenzaldehyde **4.74** was chosen as a model substrate to investigate the Pictet-Spengler reaction in an enantioselective fashion. Several chiral PAs and NTPAs were evaluated. The results are presented on Table 4.12 on the following page.

Catalyst *(R)-PA*-**2** afforded compound **4.136** in 5% yield after 96 h at rt (entry 1). It was rather unexpected that this quite acidic and unhindered catalyst gave such a low yield. No enantiocontrol was observed in this case. The slightly more acidic *(R)-PA*-**3** gave the desired product in 60% yield, yet without enantiocontrol (entry 2). The more hindered catalyst *(R)-PA*-**4** enhanced the reactivity. Product **4.136** was obtained in 82% yield but no enantiocontrol was achieved (entry 3). Similar results were obtained with catalyst *(R)-PA*-**5**—albeit it was expected that the more hindered triphenylsilyl scaffolds would improve enantioselectivity. **4.136** was afforded in 80% yield, again, with no enantiocontrol (entry 4).

The next step was trying the reaction with the same catalysts but at a higher temperature, 40 °C. In general, reactivity was improved. *(R)-PA*-**2** provided **4.136** after 96 h in a higher 32% yield, albeit racemic

(entry 5). *(R)-PA*-**3** gave an 87% yield in 48 h, no enantiocontrol was observed (entry 6). A similar result was obtained with catalyst *(R)-PA*-**4**, 94% yield after 48 h, no enantiocontrol (entry 7). It was thought that changing the solvent to one with a low dielectric constant could favour a tight ion-pair between the iminium ion and the catalyst. Thus, the reaction was done in benzene. However, product **4.136** was obtained in 46% yield after 120 h; again, in a racemic fashion (entry 8). Catalyst *(R)-PA*-**5** gave similar results as before; the product was isolated after 48 h in 92% yield with no enantiocontrol (entry 9).

Table 4.12: Screening of chiral Brønsted acids for the enantioselective synthesis of **4.136**

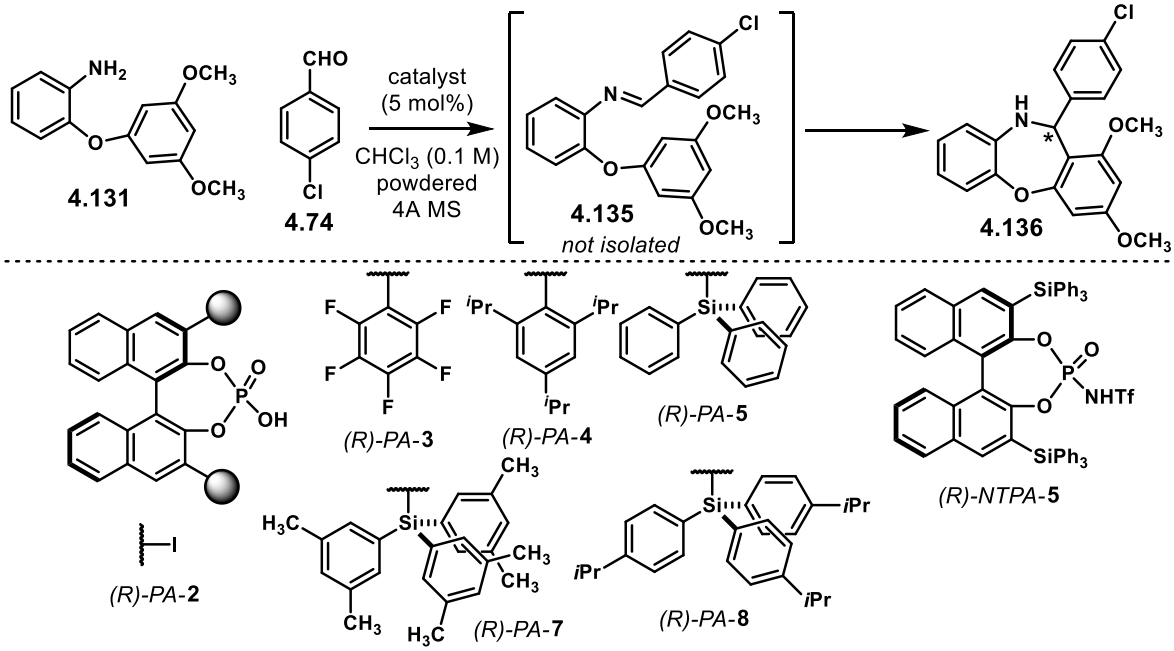

entry	**catalyst**	**temperature**	**time**	**yield %**[c]	***ee***
1	*(R)-PA*-**2**	rt	96 h	5	0
2	*(R)-PA*-**3**	rt	96 h	60	0
3	*(R)-PA*-**4**	rt	96 h	82	0
4	*(R)-PA*-**5**	rt	96 h	80	0
5	*(R)-PA*-**2**	40 °C	96 h	32	0
6	*(R)-PA*-**3**	40 °C	48 h	87	0
7	*(R)-PA*-**4**	40 °C	48 h	94	0
8[a]	*(R)-PA*-**4**	40 °C	120 h	46	0
9	*(R)-PA*-**5**	40 °C	48 h	92	0
10	*(R)-PA*-**7**	40 °C	120 h	76	0
11	*(R)-PA*-**8**	40 °C	48 h	86	0
12	*(R)-NTPA*-**5**	40 °C	24 h	91	0
13[b]	*(R)-NTPA*-**5**	40 °C	24 h	87	0
14[a],[b]	*(R)-NTPA*-**5**	40 °C	72 h	89	0

Reaction conditions: aniline **4.131** (0.1 mmol, 1.0 equiv.), 4-chlorobenzaldehyde **4.74** (0.11 mmol, 1.1 equiv.), $CHCl_3$ (1 mL, 0.1 M), powdered 4Å molecular sieves (100 mg). [a] reaction done in benzene (1 mL, 0.1 M). [b] using 1 mol% of catalyst loading [c] yields correspond to isolated products.

So far, no enantiocontrol has been observed after trying these catalysts. Therefore, it was hypothesised that the more heavily hindered silicon-based scaffold PAs would provide a better, tighter chiral cavity to achieve good enantio-differentiation. Unfortunately, this was not the case. *(R)-PA*-**7** gave the desired product after 120 h in 76% yield; no enantiocontrol was observed (entry 10). The more hindered catalyst, *(R)-PA*-**8**, gave **4.136** after 48 h in 86% yield; no enantiocontrol was observed (entry 11).

A final attempt was made changing the catalyst to the more acidic *(R)-NTPA*-**5**. Reaction with 5 mol% of catalyst loading gave **4.136** in 91% after 24 h; in a racemic fashion (entry 12). Lowering the catalyst loading to 1 mol% had a negligible effect. The reaction was completed in 24 h, the product isolated in 87% yield and no enantiocontrol was observed (entry 13). The last attempt was changing the reaction media to benzene while keeping the 1 mol% catalyst loading. However, product **4.136** was obtained in 89% yield after 72 h and in a racemic fashion (entry 14).

So far, none of the reaction conditions or catalysts tried could afford heterocycle **4.136** in an enantioselective fashion, even when catalysts with different electronic and steric properties were tried. Therefore, a new series of control experiments were conducted.

Four control experiments were conducted in order to evaluate the racemic background reaction, paying special attention to the additives used. This was because the common denominator in the reactions presented on Table 4.12 was the use of powdered molecular sieves as water-catching agent. The results from these control experiments are presented on Table 4.13. The temperature and reaction time were fixed to room temperature and 24 h, respectively. In addition, a qualitative TLC picture is presented in Figure 4.6.

Table 4.13: Control experiments. Background racemic reaction.

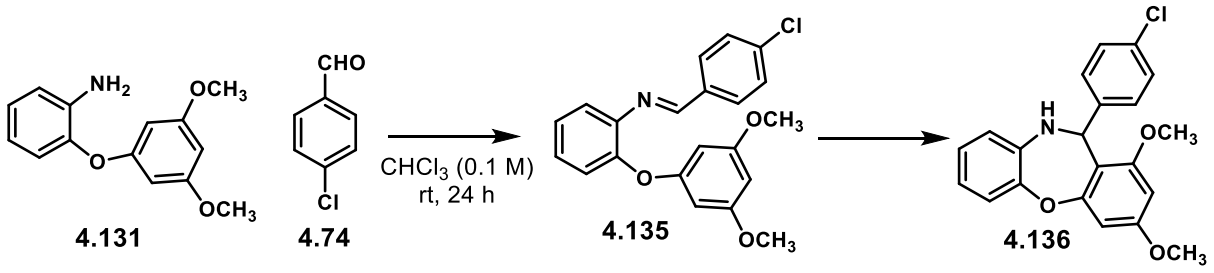

entry	**catalyst**	**additive**	**4.131 : 4.135 : 4.136**[b]
1	-	-	1 : 1.5 : 0
2	-	powdered 4Å MS[a]	1 : 0.5 : 7
3	-	$MgSO_4$ (5.0 equiv.)	1 : 1.5 : 0
4	TFA (10 mol%)	$MgSO_4$ (5.0 equiv.)	0 : 1 : 1.8

Reaction conditions: aniline **4.131** (0.1 mmol, 1.0 equiv.), 4-chlorobenzaldehyde **4.74** (0.11 mmol, 1.1 equiv.), $CHCl_3$ (1 mL, 0.1 M), rt, 24 h. [a] 4Å molecular sieves 8-12 mesh CAS:70955-01-0. [b] relative ratios for each entry were determined from the NMR integrals.

Conducting the reaction in the absence of a catalyst and additive provides imine **4.135** (entry 1). From the NMR integrals, it is estimated that a 1:1.5 ratio of unreacted started material and imine is present after 24 h. In sharp contrast, when using powdered 4Å molecular sieves, most of the starting material has

reacted and heterocycle **4.136** is formed (entry 2). In this experiment, no catalyst was used, showing that molecular sieves are, indeed, catalysing the reaction. A 1:7 ratio of unreacted starting material and product was observed.

The control experiment using $MgSO_4$ as water-catching agent but no catalyst gave a very similar output to the experiment without additives (entry 3). A 1:1.5 ratio of **4.131** and imine **4.135** was observed. This suggests that $MgSO_4$ does not affect the imine formation. However, it may play an important role if the reaction is done enantioselectively with a chiral Brønsted acid. On the other hand, if TFA is added to the reaction, product **4.136** is now formed (entry 4); pointing out that a Brønsted acid is needed for the Pictet-Spengler reaction.

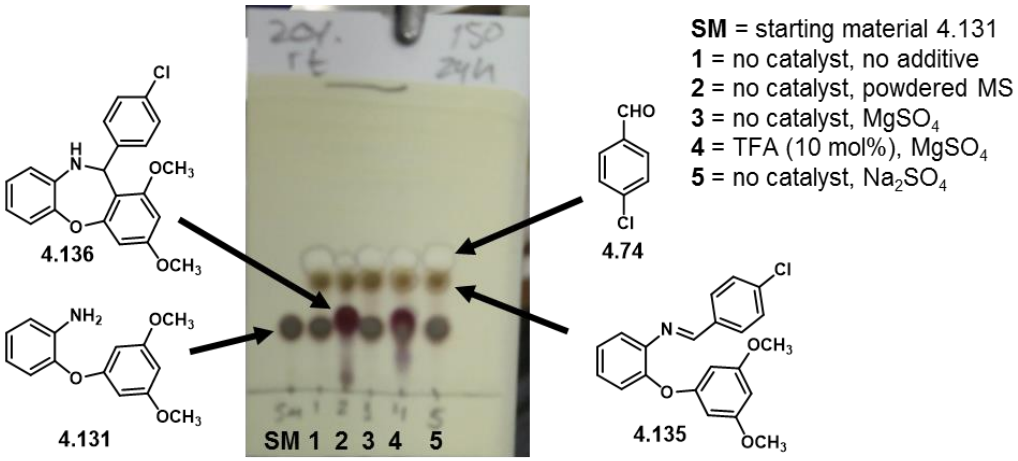

Figure 4.6: TLC of the control reaction after 24 h at rt. TLC was run in 20% EtOAc in hexane. Experiment 5 is not presented in the table of results.

From the TLC picture (Figure 4.6), it is clear that heterocycle **4.136** is formed whether when a catalytic amount of TFA is present or when molecular sieves are used on their own. In addition, the reaction with molecular sieves seems to go faster than the Brønsted acid-catalysed one. Therefore, yields presented on Table 4.12 were boosted due to the water-catching agent. Furthermore, as the background reaction was, presumably, considerably faster that the PA or NTPA-catalysed one, no enantioselectivity was observed.

As it is known that molecular sieves contain metals—mostly aluminium, calcium and magnesium—it is possible that they are acting as Lewis acids to catalyse the reaction. It has been reported that several reactions can be carried out using metals as Lewis acids and PAs as chiral ligands.[80,278,279] This has also been studied computationally.[280] In addition, metal phosphates have also been used to catalyse enantioselective reactions.[281] Amongst these metal-PA catalysed reactions, ytterbium and indium have shown to promote good levels of enantiocontrol when combined with chiral phosphoric acids.[282,283]

With these precedents—but also mostly out of curiosity—two reactions were set up using two different Lewis acids and *(R)-PA*-**4** as chiral ligand. The catalyst loading of the Lewis acid was kept at 2.5 mol% and that of the PA to 5 mol%. Such a 1:2 Lewis:Brønsted acids ratio was suggested by the group of Luo

and was shown to be the optimal.[283] The results attempting to make heterocycle **4.136** in an enantioselective fashion are presented on Table 4.14.

For an initial attempt, indium (III) bromide was tried as Lewis acid (entry 1). The reaction proceeded smoothly in CH_2Cl_2 at rt to afford product **4.136** in excellent 93% yield after 24 h. However, the enantiocontrol was not good, achieving only -5% *ee*. Despite the fact that enantioselectivity was not as high as expected, this dual catalytic system proved to deliver the product in high yield under mild reaction conditions. Furthermore, it is possible to induce chirality in the product, yet a thorough study evaluating more Lewis and Brønsted acids is needed. In another attempt, ytterbium (III) triflate was evaluated as Lewis acid (entry 2). Product **4.136** was obtained in 86% yield, albeit racemic.

Table 4.14: Lewis acid-Brønsted acid catalysed Pictet-Spengler reaction.

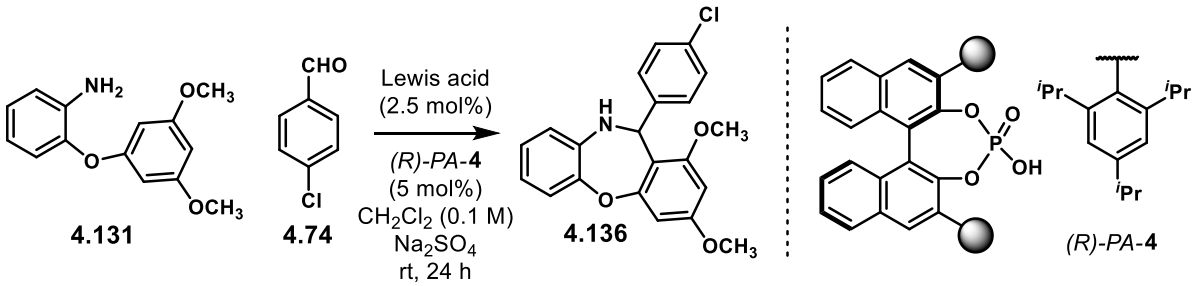

entry	**Lewis acid**	**yield %**[a]	***ee***
1	$InBr_3$	93	-5%
2	$Yb(OTf)_3$	86	0

Reaction conditions: aniline **4.131** (0.1 mmol, 1.0 equiv.), 4-chlorobenzaldehyde **4.74** (0.11 mmol, 1.1 equiv.), Na_2SO_4 (71 mg, 5.0 equiv.), CH_2Cl_2 (1 mL, 0.1 M), rt, 24 h. [a] yields correspond to isolated products.

These experiments show that these dual catalytic systems are worth to be working on them. However, this is out of the scope of this work. Nevertheless, it is hoped that it serves as an initial basis for future projects regarding Lewis acid-Brønsted acid catalysed transformations.

Now knowing that molecular sieves were catalysing the reaction, the obvious step was to use a different water-catching agent. Thus, a new catalyst screening was set up using $MgSO_4$. The results are presented on Table 4.15 on the next page. Both PAs and NTPAs were evaluated in this Pictet-Spengler reaction.

As starting point, the reaction was conducted in chloroform as solvent at 50 °C. In general, yields were considerably lower when molecular sieves were no longer used. Yet, enantioselectivity was observed. Catalyst *(R)-PA*-**2** was shown not to be the most suitable one. Product **4.136** was obtained in 26% yield and -6% *ee* after 192 h—8 days (entry 1). *(R)-PA*-**3** was sluggish when catalysing the reaction; **4.136** was afforded in 9% yield but with slightly improved enantiocontrol (-16% *ee*, entry 2). Catalyst *(R)-PA*-**4** was neither the most effective one in terms of reactivity, as it gave the product in only 5% yield (entry 3). However, a promising 38% *ee* was observed. Conducting the reaction in IPA as solvent were shown to be detrimental for both reactivity and enantiocontrol (5% yield and 7% *ee*, entry 4). It might be the case that the protic solvent binds to the catalyst or isolates the cationic intermediate, thus, preventing the formation of a tight ion pair that could enhance enantiocontrol.

Table 4.15: Screening of chiral Brønsted acids and reaction conditions for the enantioselective synthesis of **4.136**. *Molecular sieves were not used.*

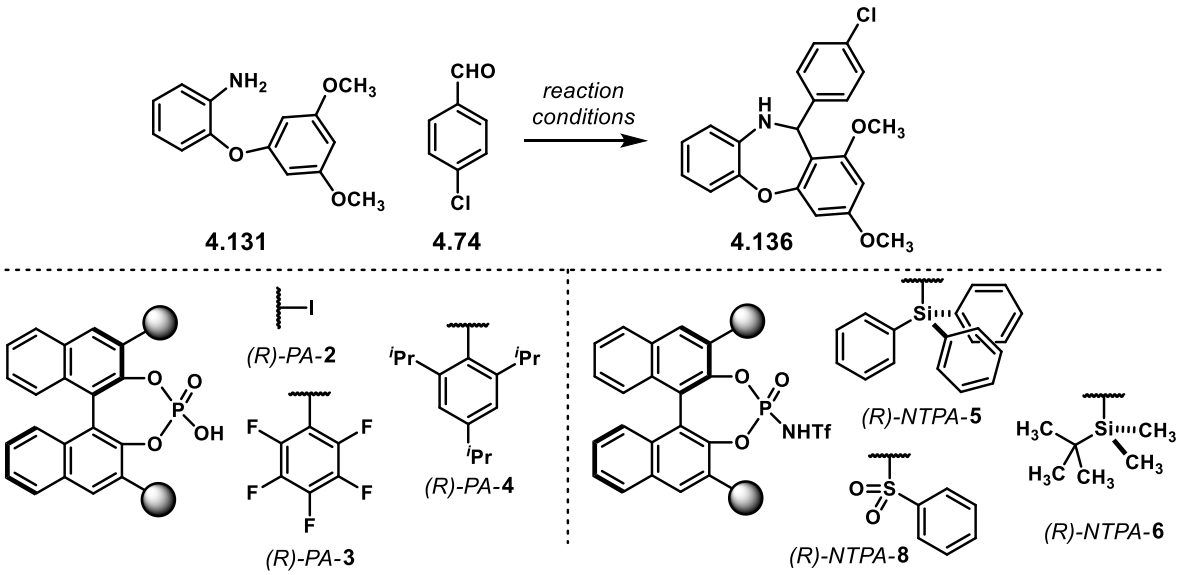

entry	catalyst	solvent	temperature	time	yield %[a]	*ee*
1	*(R)-PA*-**2** (5 mol%)	$CHCl_3$ (0.1 M)	50 °C	192 h	26	-6%
2	*(R)-PA*-**3** (5 mol%)	$CHCl_3$ (0.1 M)	50 °C	192 h	9	-16%
3	*(R)-PA*-**4** (5 mol%)	$CHCl_3$ (0.1 M)	50 °C	192 h	5	38%
4	*(R)-PA*-**4** (5 mol%)	IPA (0.1 M)	50 °C	192 h	5	7%
5	*(R)-PA*-**4** (5 mol%)	*m*-xylene (0.1 M)	100 °C	72 h	17	**48%**
6	*(R)-NTPA*-**5** (5 mol%)	$CHCl_3$ (0.1 M)	50 °C	192 h	traces	NA
7	*(R)-NTPA*-**5** (1 mol%)	$CHCl_3$ (0.1 M)	50 °C	192 h	-	NA
8	*(R)-NTPA*-**5** (5 mol%)	*m*-xylene (0.1 M)	50 °C	96 h	3	25%
9	*(R)-NTPA*-**5** (5 mol%)	*m*-xylene (0.1 M)	130 °C	24 h	**70**	27%
10	*(R)-NTPA*-**6** (5 mol%)	*m*-xylene (0.1 M)	50 °C	96 h	50	0
11	*(R)-NTPA*-**8** (3.5 mol%)	*m*-xylene (0.1 M)	50 °C	96 h	17	-5

Reaction conditions: aniline **4.131** (0.1 mmol, 1.0 equiv.), 4-chlorobenzaldehyde **4.74** (0.11 mmol, 1.1 equiv.), $MgSO_4$ (60 mg, 5.0 equiv.), solvent (1 mL, 0.1 M). [a] yields correspond to isolated products.

Next, higher temperatures were tried in order to improve the yields. In addition, *m*-xylene was used as a low dielectric constant solvent to favour a thigh ion pair between the catalyst and the reactive species. Using *(R)-PA*-**4**, the reaction was conducted at 100 °C for 72 h (entry 5). In this case, the yield was slightly improved to 17%. Moreover, enantioselectivity was boosted to 48% *ee*. This suggests that, indeed, a non-polar solvent is a favouring factor for enantiocontrol, as well as a higher temperature to push the reaction to completion.

An initial screening was also performed with NTPAs. *(R)-NTPA*-**5** did not show to promote the reaction effectively, despite its higher acidity in comparison with PAs. Only trace amounts of **4.136** were detected after 192 h at 50 °C (entry 6). At a lower catalyst loading no product at all was observed (entry 7). Changing to a non-polar reaction medium, *m*-xylene, afforded 3% yield of **4.316** after 96 h (entry 8).

Despite the poor yield, the reaction was shown to be enantioselective (25% *ee*). Heating up to 130 °C enhanced reactivity (entry 9). Heterocycle **4.136** was obtained in 70% yield after 24 h. Yet, enantioselectivity just improved slightly to 27% *ee*. Catalyst *(R)-NTPA*-**6** improved reactivity. Heterocycle **4.316** was afforded in 50% yield, yet, in a racemic fashion (entry 10). This might emphasise the need of a more hindered chiral pocket for this type of transformation. Finally, *(R)-NTPA*-**8** was tried, however, it could only afford **4.316** in a low 17% yield and -5 *ee* (entry 11).

These results show that a set of reaction conditions for further optimisation would be conducting the reaction in *m*-xylene at 100 °C. Despite the fact that some yields were low at this temperature, enantioselectivity was improved. Therefore, the full set of synthesised PAs were evaluated, in *m*-xylene at 100 °C, with a 5 mol% catalyst loading and using $MgSO_4$ as water-catching agent. The results are presented on Table 4.16 on the next page.

As an initial control experiment, the reaction was left with no catalyst (entry 1). After 48 h, product **4.136** was observed in only 2% yield—the corresponding imine **4.135**, however, was formed in 83% yield. This suggests that the racemic background reaction might not be an issue. The simplest catalyst, *(R)-PA*-**1**, afforded compound **4.136** in 40% yield and 5% *ee* after 96 h (entry 1). A slightly increase in the steric demand of the 3,3'- substituents, as in *(R)-PA*-**2**, improved the yield to 59%, yet, this was not the case for enantioselectivity (entry 2).

The slightly more acidic *(R)-PA*-**3** afforded compound **4.136** in 81% yield and -14% *ee* after 48 h (entry 4). Herein, it seems that the higher acidity of this catalyst boosted the yield, yet with low enantiocontrol. The more sterically demanding *(R)-PA*-**4** showed sluggish reactivity, even after 96 h (entry 5). Compound **4.316** was obtained in a low 18% yield and 38% *ee*. This last result sharply contrasts with the previously obtained 17% yield and 48% *ee* using the same catalyst at the same temperature, however, the reaction time in that case was shorter (72 h, *cf.* Table 4.15, entry 5). This might suggest that an enantioerosion process starts to take over after certain time.

The next set of catalysts evaluated were those with silicon-based scaffolds. *(R)-PA*-**5** gave both a low yield and poor enantiocontrol (14% yield, 9% *ee*, entry 6), possibly due to the sterically demanding chiral pocket. Further increasing the hindrance of the active site inhibited the reaction. When catalysts *(R)-PA*-**7** and *(R)-PA*-**8** were used, only trace amount of product was detected on TLC (entries 7 and 8). In these cases, the active site of the catalyst seems to be too hindered for the intermediate imine to fit into it.

Next, the more acidic sulfone-based catalysts were evaluated. Surprisingly, the yields were not as high as expected. *(R)-PA*-**9** afforded product **4.136** in 15% yield and racemic (entry 9). The similar catalyst *(R)-PA*-**10** gave similar results, 18% yield and -6% *ee* (entry 10). Finally, the more hindered *(R)-PA*-**11**, afforded the desired product in 39% yield and only 1% *ee*; the yield was modestly improved as the reaction was left for 70 h (entry 11).

So far, for this reaction using PAs as Brønsted acids, the best enantioselectivity was obtained with catalyst *(R)-PA*-**4** after 48 h (48% *ee*, *cf.* Table 4.15, entry 5). Yet, the yield is not optimal (17% yield). In order to improve the yield and the enantioselectivity of this reaction, more PAs are need to be tested. PAs with electron-withdrawing groups on the 3,3' substituents might increase the acidity and, in turn, boost the

yield. On the other hand, a more subtle evaluation of the steric size of such scaffolds is needed to get higher enantiocontrol.

Table 4.16: Screening of PAs for the enantioselective synthesis of **4.136**.

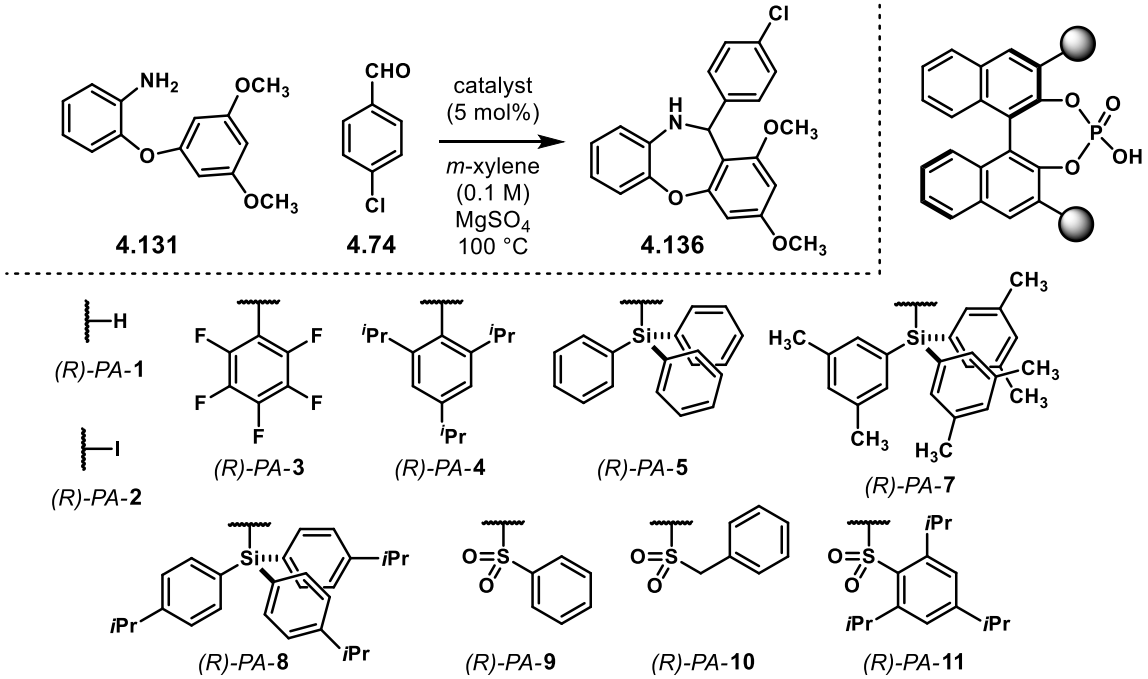

entry	**catalyst**	**time**	**yield %**[a]	***ee***
1	none	48 h	2[b]	NA
2	*(R)-PA*-**1**	96 h	40	5%
3	*(R)-PA*-**2**	48 h	59	0
4	*(R)-PA*-**3**	48 h	81	-14%
5	*(R)-PA*-**4**	96 h	18	38%
6	*(R)-PA*-**5**	96 h	14	9%
7	*(R)-PA*-**7**	96 h	traces	NA
8	*(R)-PA*-**8**	96 h	traces	NA
9	*(R)-PA*-**9**	48 h	15	0
10	*(R)-PA*-**10**	48 h	18	-6%
11	*(R)-PA*-**11**	70 h	39	1%

Reaction conditions: aniline **4.131** (0.1 mmol, 1.0 equiv.), 4-chlorobenzaldehyde **4.74** (0.11 mmol, 1.1 equiv.), catalyst (0.005 mmol, 0.05 equiv.), $MgSO_4$ (60 mg, 5.0 equiv.), *m*-xylene (1 mL, 0.1 M), 100 °C. [a] yields correspond to isolated products unless otherwise stated. [b] NMR yield determined using 1,3,5-trimethoxybenzene as internal standard.

In order to address the reactivity problem, the more acidic NTPAs were evaluated in the reaction. In general, the reaction times were shorter and the yields higher than the reactions done with PAs. The results for such screening are presented on Table 4.17.

Table 4.17: Screening of NTPAs for the enantioselective synthesis of **4.136**.

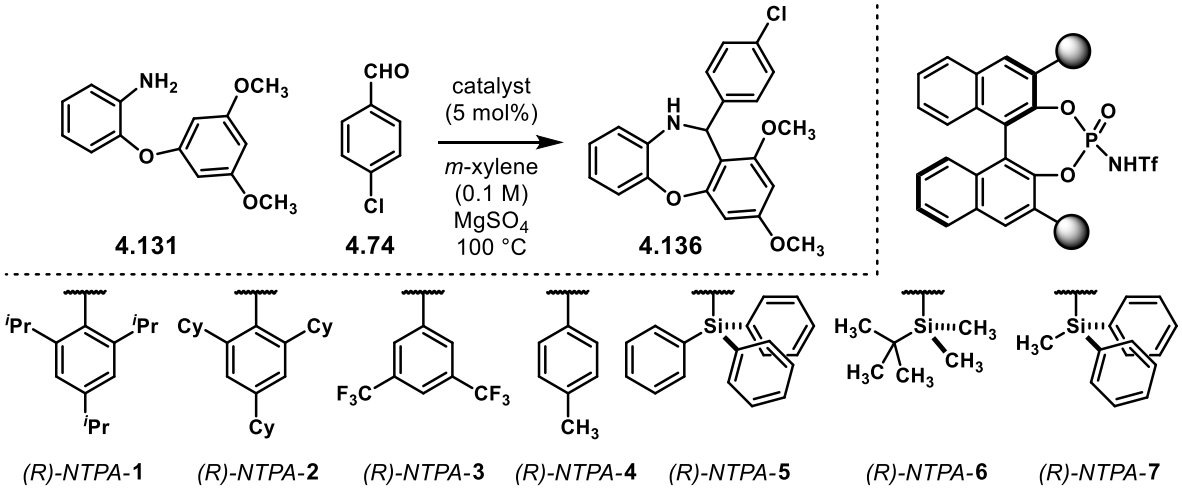

entry	**catalyst**	**time**	**yield %**[b]	***ee***
1	*(R)-NTPA*-**1**	30 h	**87**	**-38%**
2	*(R)-NTPA*-**2**	48 h	82	21%
3	*(R)-NTPA*-**3**	30 h	70	-5%
4	*(R)-NTPA*-**4**	30 h	78	4%
5	*(R)-NTPA*-**5**	48 h	**75**	**50%**
6[a]	*(R)-NTPA*-**5**	48 h	70	30%
7	*(R)-NTPA*-**6**	7 h	81	-8%
8	*(R)-NTPA*-**7**	48 h	87	4%

Reaction conditions: aniline **4.131** (0.1 mmol, 1.0 equiv.), 4-chlorobenzaldehyde **4.74** (0.11 mmol, 1.1 equiv.), catalyst (0.005 mmol, 0.05 equiv.), $MgSO_4$ (60 mg, 5.0 equiv.), *m*-xylene (1 mL, 0.1 M), 100 °C. [a] reaction done using Na_2SO_4 as water-catching agent (71 mg, 5.0 equiv.). [b] yields correspond to isolated products

(R)-NTPA-**1** afforded compound **4.136** in 87% yield and -38% *ee* after 30 h (entry 1). The similar but more hindered *(R)-NTPA*-**2** gave a good 82% yield after 48 h (entry 2). However, enantiocontrol was not as good as for the other catalyst; the product was obtained in 21% *ee*. For these two catalysts, it is intriguing how similar 3,3'- scaffolds and the same active site provide opposite senses of enantioinduction. It is not clear how this happens. Thus, computational chemistry could provide useful insights in this case, not only to understand the distal causes of enantiocontrol, but also to modify the scaffolds to enhance enantioselectivity.

Other aryl-based catalysts gave good yields albeit poor enantiocontrol. *(R)-NTPA*-**3** afforded the desired product in 70% yield and -5% *ee* (entry 3). In a similar fashion, *(R)-NTPA*-**4** furnished **4.136** in 78% yield but only with 4% *ee* (entry 4). These two catalysts might suggest that—in the case of catalysts with aryl-based scaffolds—the *meta* and *para* substituents may not be as important as the *ortho* motifs. This trend can be visualised in Figure 4.7. Yet, in order to prove this hypothesis, a larger library of aryl-based NTPAs has to be synthesised—possibly as a starting point, different groups in the *ortho* positions of the scaffolds might help to enhance steric interactions and boost enantiocontrol.

Then, the silicon-based NTPAs were evaluated possibly, due to their more confined active site, enantiocontrol could be improved. For *(R)-NTPA*-**5**, this was the case. After 48 h, heterocycle **4.136** was obtained in a good 75% yield and with improved 50% *ee* (entry 5). For this catalyst, it seems that a more encumbered active site had a positive effect in enantiocontrol. In addition, this catalyst provided the opposite sense of enantioinduction than the one obtained with *(R)-NTPA*-**1**. As a matter of control experiment, the same reaction with catalyst *(R)-NTPA*-**5** was conducted using Na_2SO_4 instead of $MgSO_4$ as water-catching agent (entry 6). The yield was similar, although the enantioselectivity dropped considerably to 30% *ee*. This suggests that the amount of water present in the reaction—coming from the formation of the imine—has a deep impact on enantiocontrol and that $MgSO_4$ is more effective to catch it.

Next, the less hindered *(R)-NTPA*-**6** was tried. The reaction was completed in 7 h, much faster than the other catalysts (entry 7). This could be due to the more accessible active site of this catalyst. Compound **4.136** was obtained in 81% yield and with -8% *ee*.[a] This possibly attributed to the lack of steric demand. Thus, the more hindered *(R)-NTPA*-**7** was tried (entry 8). Product **4.136** was obtained in a good 87% yield after 48 h. However, this was not the case for enantiocontrol, as only 4% *ee* was observed. This is in sharp contrast with catalyst *(R)-NTPA*-**5**, as changing one phenyl group for a methyl dramatically drops the enantioselectivity from 50% *ee* to 4% *ee*.

So far, using NTPAs, the best result was obtained with catalyst *(R)-NTPA*-**5** (75% yield, 50% *ee*, entry 5). Still, enantiocontrol is modest, yet, it could be improved. In this case, the next step would be synthesising a new series of silicon-based NTPAs taking the triphenylsilyl scaffolds as starting point and introducing different substituents in different positions (Figure 4.7).

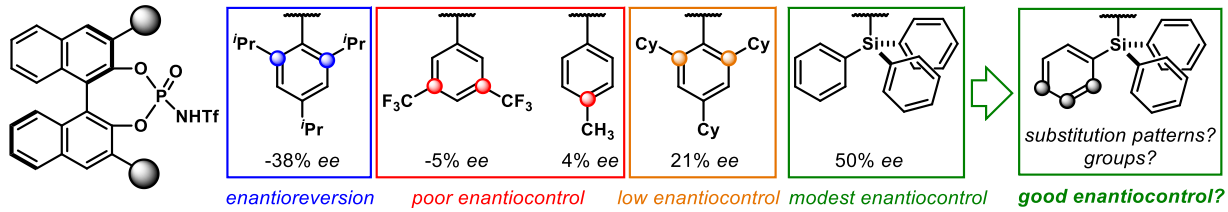

Figure 4.7: The effect of NTPAs' substituents on enantioselectivity.

[a] The reaction was also tried using 0.5 mol% of this catalyst. After 48 h, the desired product was isolated in 32% yield and -3% *ee*.

Chapter 5

Understanding enantioselectivity in an aza-Darzens reaction

5.1. A brief introduction

The aza-Darzens reaction is one of the best methods to synthesise aziridine building blocks.[284] Several asymmetric methodologies have been developed to make these molecules,[285] paying special attention to catalytic methods.[286,287] In this context, chiral Brønsted acids—both PAs and NTPAs—were shown to achieve outstanding levels of stereocontrol.[69,288–290] One of such catalytic and enantioselective transformations was developed by the group of Akiyama (Scheme 5.1).[288] In their report, phenyl glyoxal-derived aldimine **5.1** reacts with ethyl diazo acetate **5.2** in the presence of a chiral PA to afford *cis*-aziridine **5.3** as a single diastereoisomer and with good enantioselectivities. For this reaction, the 3,3' substituents of the catalyst had a tremendous impact on enantiocontrol. Catalysts *(R)-PA*-**5** and *(R)-PA*-**5.5** provided low enantiocontrol, followed by *(R)-PA*-**5.4** which gave a modest -64% *ee*. On the other hand, catalysts *(R)-PA*-**5.6** and *(R)-PA*-**4** afforded the desired product with excellent enantioselectivities (90% *ee* and -88% *ee*, respectively).

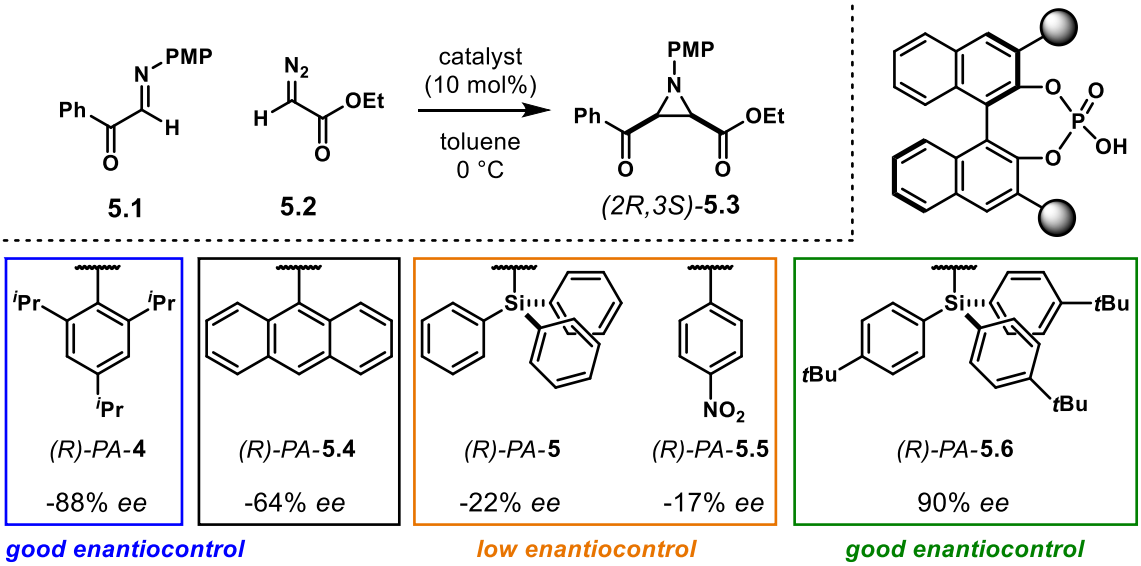

Scheme 5.1: Enantioselective aza-Darzens reaction developed by the group of Akiyama

One of the rare and unique features of this reaction is that opposite senses of enantioinduction are obtained with *(R)-PA*-**5.6** and *(R)-PA*-**4**, despite the fact that both catalysts share the same *(R)*-BINOL backbone. It has been shown that structurally similar catalysts, with small or subtle variations in the 3,3' substituents can lead to different results.[66] Such outputs range from increasing the yield and enantioselectivity of a reaction, up to achieving opposite senses of enantioinduction. Computational studies in Jonathan Goodman's group have been done in order to rationalise the role of the 3,3' substituents in chirality transfer.[66,115,291] Silicon-based-scaffolds catalysts are a noticeable example in

which quite simple structural variations in these motifs can lead to different outputs.[292,293] One of these cases, the asymmetric aza-Darzens reaction is the topic of the present chapter.

There are several points to address in this reaction. For instance, there are not too many chiral PAs with silicon-based substituents in the 3,3' positions—in comparison with the most common aryl scaffolds. As was discussed in chapter 2, silicon-based scaffolds can be easily installed; starting from commercially available *(R)*-BINOL. In addition, computational studies regarding the transfer of chirality using these catalysts can lead to a better understanding of the role of silicon-based scaffolds in chirality transfer. The group of Goodman reported one such example addressing a Pictet-Spengler reaction.[114]

Having a closer look at the catalysts' chiral pockets, there are similar structural features between *(R)-PA*-**4** and *(R)-PA*-**5** (Figures 5.1a and 5.1b, respectively). Such similarity could explain the same sense of enantioinduction when these catalysts are used in the reaction (-88% *ee* and -22% *ee*). However, there is a somewhat different chiral pocket in the case of *(R)-PA*-**5.6** (Figure 5.1c). In this case, the phosphate active site is heavily hindered by the 3,3' substituents. Moreover, steric clash between the *tert*-butyl groups—or possibly dispersion forces—encumbers one of the oxygen atoms, leaving it less available to interact with any potential substrates. This different, tighter chiral pocket created by the silyl substituents may be the reason for which opposite senses of enantioinduction are observed. Therefore, the focus of this chapter comprises transition state (TS) calculations in order to understand how diastereo and enantioselectivity is achieved in the enantioselective aza-Darzens reaction under study.

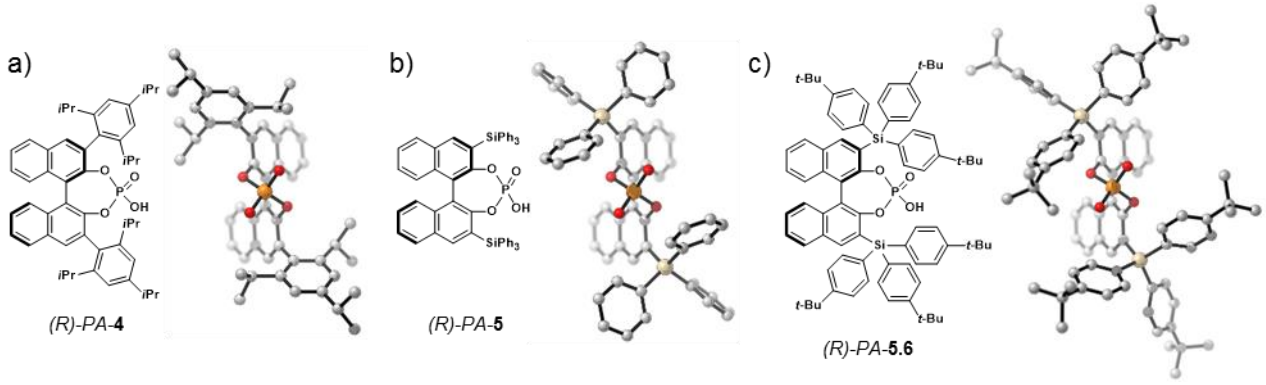

Figure 5.1: a) *(R)-PA*-**4**, b) *(R)-PA*-**5**, c) *(R)-PA*-**5.6**. Lowest energy conformers found using the OPLS3 force field. The phosphates, instead of the actual phosphoric acids are shown for clarity and to emphasise the C_2 symmetry of the chiral pockets.

In this chapter, a detailed computational study of this aza-Darzens reaction is presented. Full computational details are provided in Appendix 1. The main aim herein is to understand how chirality is transferred from catalyst *(R)-PA*-**5.6** to the final major enantiomer.

5.2. Proposing a mechanistic picture

A feasible mechanistic picture for the aza-Darzens reaction under study is presented on Scheme 5.2. In the first step of the mechanism, the chiral PA activates substrates **5.1** and **5.2**. Activation of imine **5.1** can be achieved either by hydrogen bonding, or by ion pairing. The latter activation mode would need full protonation of the imine's *N*-atom. In addition, the corresponding iminium ion might be a more reactive substrate than a hydrogen-bonded imine. Then, a 1,2- addition takes place. The nucleophilic carbon atom in the diazoester attacks the π bond in the imine/iminium leading to intermediate **5.7**. Therein, both chiral centres at C2 and C3 would be defined; therefore, this step is both diastereo and enantiodetermining. From an enantioselective view point, it has been established that the 1,2- addition step is irreversible.[294] To avoid ambiguity, throughout the rest of the chapter, the labels for C2 and C3 are those presented on Scheme 5.2—these labels apply for both intermediate **5.7** and product **5.3** to keep track of these two carbon atoms throughout the mechanistic analysis.

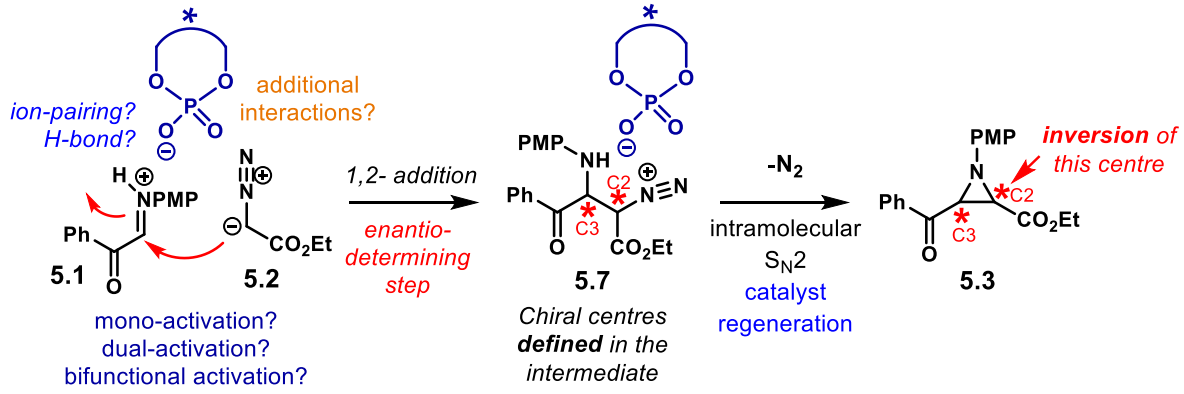

Scheme 5.2: Proposed reaction mechanism for the enantioselective aza-Darzens reaction.

After intermediate **5.7** is formed, ring closure and nitrogen elimination *via* an intramolecular S_N2 reaction yields aziridine **5.3**. This last step inverts the chiral centre at C2 formed in the addition step. Given that nitrogen extrusion could happen so fast and is entropically favoured, it is very likely that the 1,2- addition step might also be rate-determining in the reaction.

Regarding intermediate **5.7**, there are four possible diastereoisomers to be formed in the 1,2- addition step: two *anti*-**5.7** and two *syn*-**5.7** (Scheme 5.3). Intermediate *(2S,3S)*-**5.7** yields the major enantiomer of the product—*(2R,3S)*-**5.3**—after ring closure with inversion at C2. Diastereoisomers *syn*-**5.7**, which lead to *trans*-**5.3**, are assumed to have higher energy transition states in the Brønsted acid-catalysed reaction, given that only the *cis* aziridines are observed experimentally. Therefore, in order to understand enantioselectivity, attention was paid to structures *(2S,3S)*-**5.7** and *(2R,3R)*-**5.7** in the 1,2- addition step.

Because the 1,2- addition step is intermolecular, several ways in which the substrates approach to each other must be considered in order to account for the formation of the new C-C bond. Several conformations and configurations of the starting materials could also influence the stereochemical output: both for the uncatalysed and the catalysed reaction. Moreover, the lack of symmetry and the large number of rotatable bonds in the reagents would make the conformation analysis even more challenging.

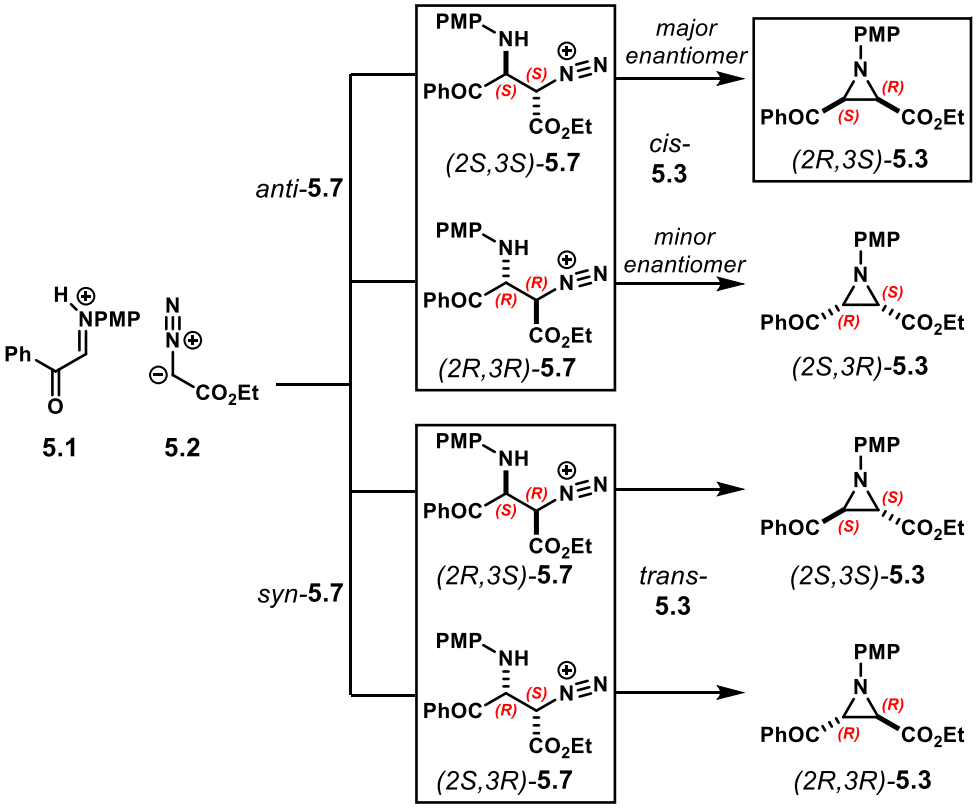

Scheme 5.3: Possible diastereoisomers to be formed in the uncatalysed reaction. For the chiral Brønsted acid-catalysed reaction, *(2R,3S)*-**5.3** is the major enantiomer, which, in turn, comes from *anti*-diastereoisomer *(2S,3S)*-**5.7**.

5.3. Starting materials: The uncatalysed reaction

The imine. Imine **5.1**, or its corresponding iminium ion, can react either in an *(E)* or *(Z)* configuration (Figure 5.2). This would depend on which isomer, *(E)* or *(Z)*, is favoured during the imine double bond formation. Also, it has been shown that imines can undergo *E*/*Z* isomerisation in acidic media, which seems feasible under the reaction conditions.[295,296] Furthermore, it has been shown that the *E*/*Z* ratios in aldimines can also vary depending on the polarity of the solvent.[297] Thus, *E*/*Z* isomerism in the imine or iminium ion leads to different enantiotopic faces being attacked by the incoming nucleophile.

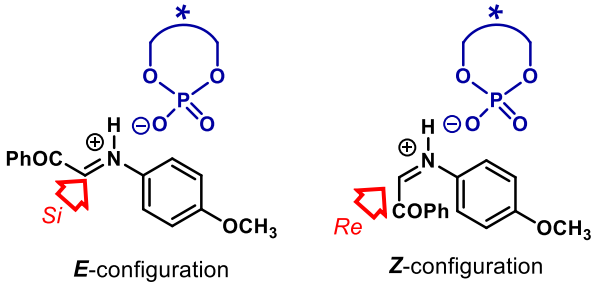

Figure 5.2: Different configurations of the iminium ion can lead to opposite chiral centres depending on which enantiotopic face is attacked.

In addition, due to the α-keto group, the imine or iminium ion can present itself in an *s-cis* or *s-trans* conformation (Figure 5.3). Although the keto moiety does not participate directly in the formation of the chiral centre, different conformations might enhance steric or hydrogen bond interactions when the reagents approach to each other. Furthermore, the *s-cis/s-trans* conformers could modify the energy difference between the *(E)* and *(Z)* configurations.

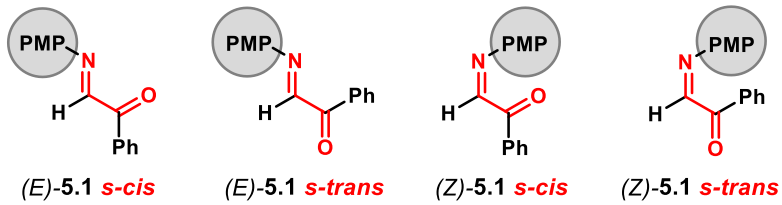

Figure 5.3: Possible configurations and conformations of imine **5.1**.

In order to assess which imine or iminium configuration would be the most plausible one in the transition state, their relative ground state energies were compared. These, for imine **5.1** and its corresponding iminium ion, including the four possible arrangements shown in Figure 5.3. These, taking into account both *(E)* and *(Z)* isomers as well as *s-cis* and *s-trans* conformations. Gas-phase energies were calculated at the ωB97X-D/def2-TZVPP // ωB97X-D/6-31G(*d*) level of theory. The results for such analysis are presented on Figure 5.4.

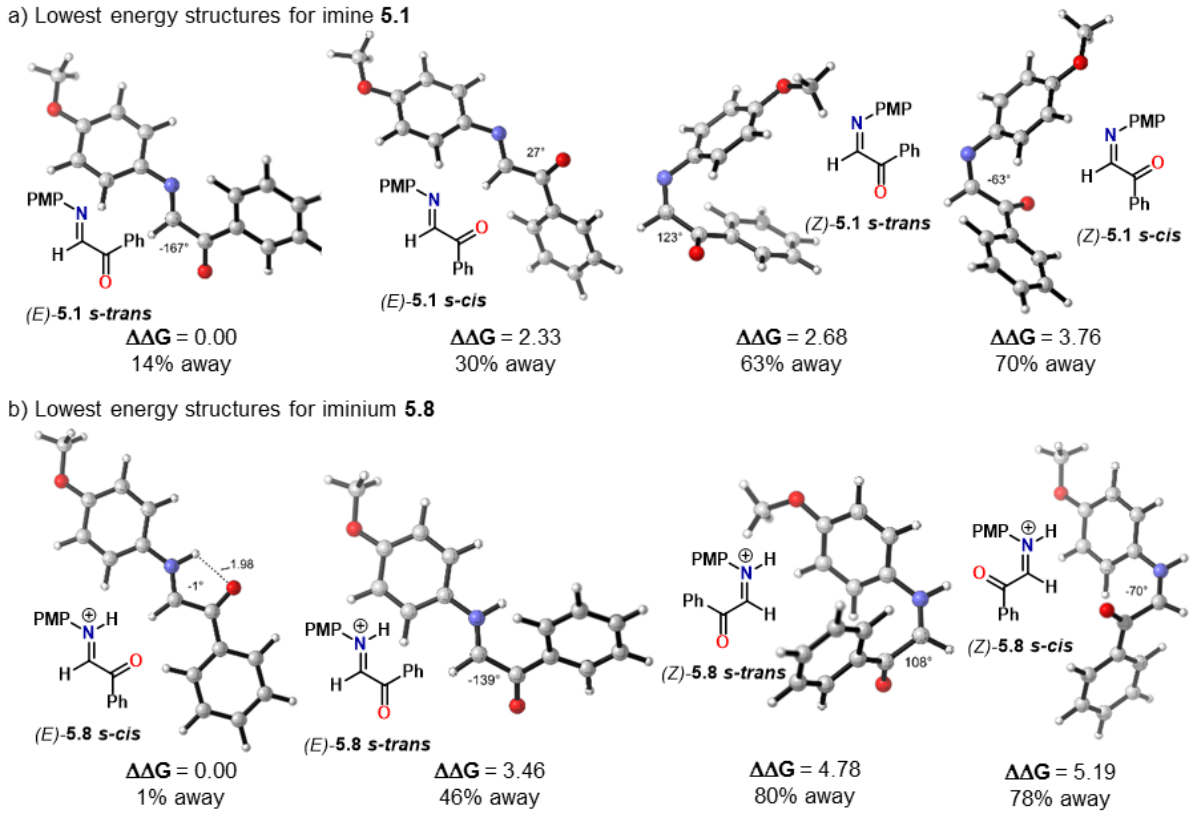

Figure 5.4: a) Lowest energy conformers for imine **5.1**. b) Lowest energy conformers for iminium ion **5.8**. Energy differences are presented in kcal mol^{-1}. Angles correspond to the N=C-C-O dihedrals and the percentages to how much the conformer deviates from a full *s-cis* or *s-trans* geometry.

For imine **5.1**, the *(E)*- configurations are favored over the corresponding *(Z)* ones (Figure 5.4a). *(E)*-**5.1**-*s-trans* turned to be the lowest in energy, followed by *(E)*-**5.1**-*s-cis* by 2.33 kcal mol^{-1}. The *(Z)* configurations, *(Z)*-**5.1**-*s-trans* and *(Z)*-**5.1**-*s-cis* resulted in 2.68 and 3.76 kcal mol^{-1} higher in energy than the lowest one, respectively. In the case of the free imine **5.1**, a 2.68 kcal mol^{-1} energy preference was calculated for the *(E)* configuration over the *(Z)* one.[a]

An interesting trend appears between the energies of the imine conformers and the dihedral angles defined by the N=C-C-O atoms. The further away the dihedral deviates from the ideal *s-cis* 0°, or *s-trans* 180° angles, the higher the energy of the corresponding conformation of the imine.[b] This can be seen in the cases of *(E)*-**5.1**-*s-trans* and *(Z)*-**5.1**-*s-cis*. In the former conformer, which is the lowest one in energy, the deviation from the ideal *s-cis* angle is 14%. On the other hand, the latter conformer, whose energy is 3.76 kcal mol^{-1} higher that the lowest one, deviates 70% away from the ideal 0° angle in an *s-cis* conformation.

In the case of iminium ion **5.8**, the energy differences are more pronounced (Figure 5.4b). Both of the *(E)* conformers are lower in energy than the corresponding *(Z)* isomers. *(E)*-**5.8**-*s-cis* was found to be the lowest in energy, whereas, *(E)*-**5.8**-*s-trans* was calculated 3.46 kcal mol^{-1} higher. The larger energy gap and swap from the *s-trans* to the *s-cis* conformation, in comparison with **5.1**, seems to be due to a strong 1.98 Å intramolecular hydrogen bond, formed between the protonated imine and the adjacent keto group.[298] Such interaction locks the iminium ion in the *s-cis* conformation, which is practically in an ideal 0° *s-cis* angle. In sharp contrast, *(E)*-**5.8**-*s-trans* deviates 46% away from an ideal 180° angle. The *(Z)* configurations turned to be much higher in energy than the non-protonated imines. *(Z)*-**5.8**-*s-trans* and *(Z)*-**5.8**-*s-cis* were found to be 4.78 and 5.19 kcal mol^{-1} higher in energy, respectively, relative to the lowest-energy structure.

According to the model for chiral PA-catalysed reactions on imines, as proposed by Simón and Goodman, if the mean of $\Delta\Delta_{E/Z}G_{imine}$ and $\Delta\Delta_{E/Z}G_{iminium}$ is preferred by more than 3 kcal mol^{-1} in favour of the *(E)* configuration in the ground state structures, the most favoured transition state imine geometry will be *(E)*.[143,291] This is found to be the case for **5.1** and **5.8**. This mean was calculated to be 3.73 kcal mol^{-1} for species on Figure 5.4. Hence, it is highly probable that an imine or iminium ion with an *(E)* configuration would be preferred in the lowest energy transition state.

---

[a] More than one conformer was found for each of the cases (*ie. s-cis, s-trans, (E), (Z)*), yet, they were within only 1.0 kcal mol^{-1}.

[b] In the case of *s-cis* imines—or iminium ions as well—the percentage in which the N=C-C-O dihedral angle deviates from an ideal 0° can be calculated with equation 5.1

$$deviation\% = \frac{|\emptyset|}{90°}100 \quad (eq.5.1)$$

where *deviation%* is the percentage in which the dihedral angle deviates from an ideal 0°, and ϕ is the dihedral angle, defined as above. Taking the absolute value of ϕ avoids ambiguity regarding how the dihedral is defined. The 90° in the denominator ensures that this equation applies for *s-cis* conformations.

In the case of *s-trans* imines—or iminium ions as well—the deviation percentage from an ideal 180° can be calculated with equation 5.2

$$deviation\% = \frac{180° - |\emptyset|}{90°}100 \quad (eq.5.2)$$

where *deviation%* is the percentage in which the dihedral angle deviates from an ideal 180°, and ϕ is the dihedral angle, defined as above. The 90° in the denominator and the 180° in the numerator ensure that this equation applies for *s-trans* conformations.

The nucleophile. The orientation of the nucleophile, **5.2**, relative to imine **5.1** is also crucial. This defines the other chiral centre. With the imine fixed, the diazoester can attack with its *Re* or *Si* face (Figure 5.5a). Furthermore, two conformers, *s-cis* and *s-trans*, are possible (Figure 5.5b). The energy difference between these conformers was calculated to be 0.45 kcal mol^{-1} in favour of **5.2**-*s-cis*. Such small value implies that both conformers are feasible to appear in the 1,2- addition transition states. Similar to imine **5.1**, the different orientations—conformations—of the diazo moiety may enhance steric or non-covalent interactions within the transition states and, most importantly, within the catalyst chiral cavity. In order to simplify the conformation searching and the TS calculations, methyl diazoacetate **5.9** was used instead.

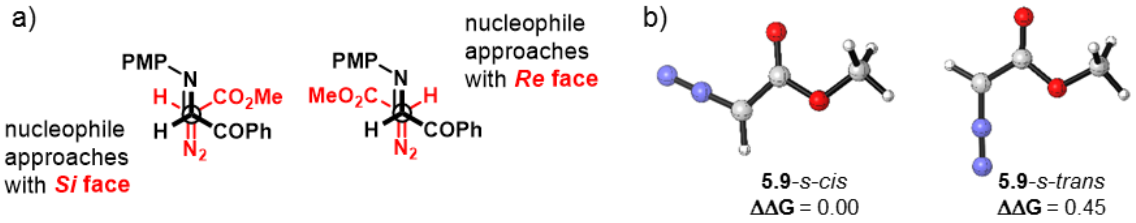

Figure 5.5: a) Newman projections showing two approaches of the diazoester to the *Si* face of the imine. This yields the *syn* and *anti* diastereisomers when the nucleophile attacks with its *Si* face or *Re* face, respectively. b) *s-cis* and *s-trans* conformations of methyl diazoacetate. Energies are presented in kcal mol^{-1}.

As a starting point, the energy difference between the diastereoisomeric intermediates, *anti*-**5.10** and *syn*-**5.10**, was calculated (Scheme 5.4). The 1,2- addition step yields these diastereoisomers, which, after nitrogen elimination and ring closure, affords *cis*-**5.11** and *trans*-**5.11**, respectively. Therefore, looking at the ground state energy differences of these two diastereomeric intermediates, could hint to which aziridine would be favoured.

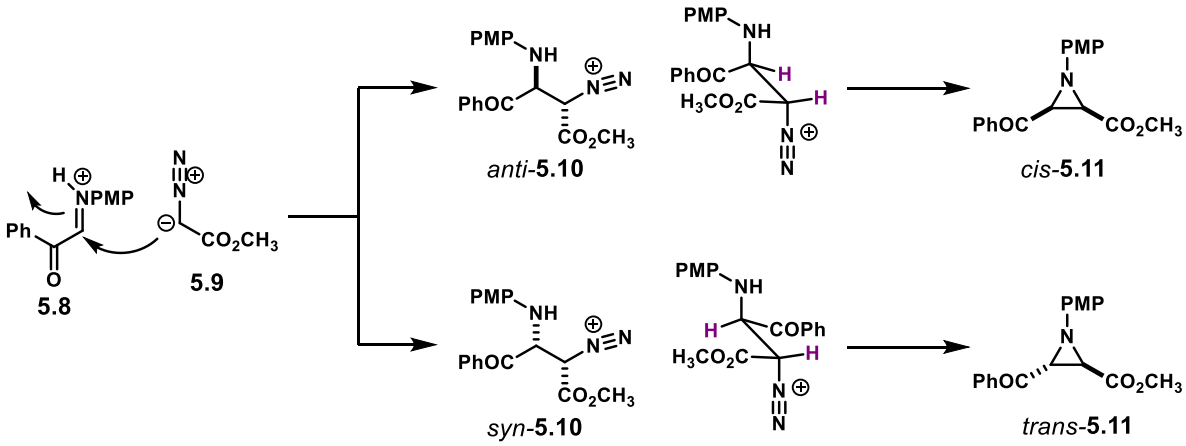

Scheme 5.4: General acid-catalysed aza-Darzens reaction. The 1,2- addition step affords *anti*- and *syn*-**5.10** along with their corresponding enantiomers.

Several conformers were found for each of the two diastereoisomers. The five lowest-energy structures for each are presented in Figure 5.6. A 0.46 kcal mol^{-1} energy difference was calculated for the lowest-energy *syn*- and *anti*- diastereoisomers. *syn*-**5.10** seems to be slightly favoured due to its substituents' arrangement, which sit them as far from each other in a staggered conformation. The phenyl moiety of

the ketone lays in an out-of-plane orientation to avoid steric clash with the rest of the substituents. On the other hand, the PMP group in *anti*-**5.10** clashes with the ester fragment in a gauche conformation—interestingly, the lowest-energy conformations for both diastereoisomers seem to have come from an *(E)*-iminium configuration, which places the aromatic rings as far from each other. Some of the other higher-energy conformers have these substituents positioned in a similar way. *(Z)*-like conformations were also found, neither of which resulted in a global minimum.

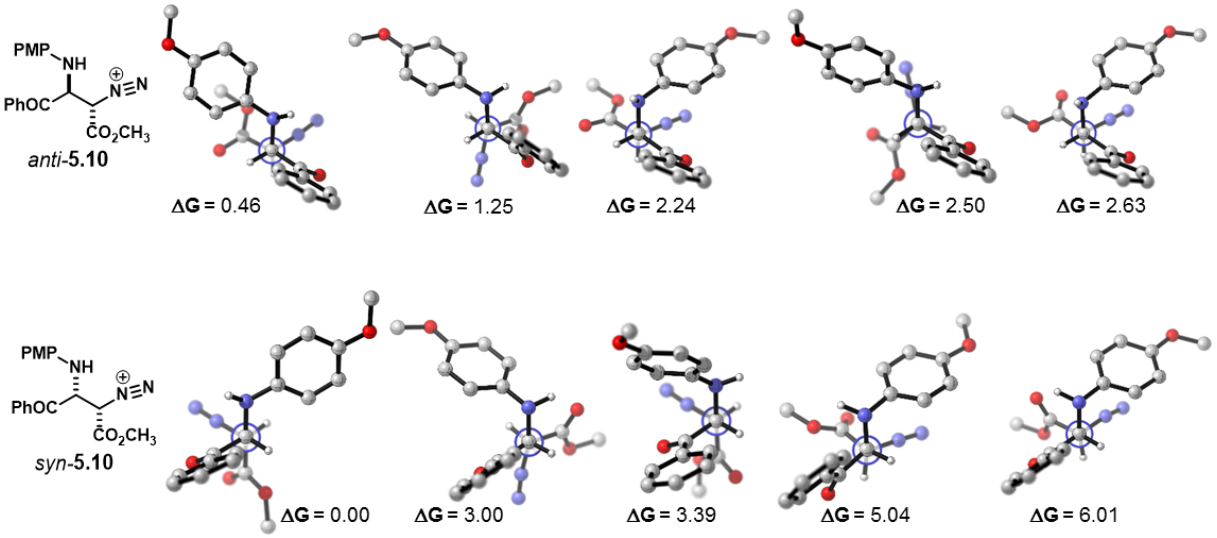

Figure 5.6: Newman projection-like optimised geometries. Top row comprises the five lowest energy conformers of *anti*-**5.10**. Bottom row comprises the five lowest energy conformers of *syn*-**5.10**. Energies were calculated at the ωB97X-D/def2-TZVPP // ωB97X-D/6-31G(*d*) level of theory and are presented in kcal mol^{-1}. Non-critical *H*-atoms are omitted for clarity. *All* energies are relative to *syn*-**5.10**'s lowest-energy conformer (bottom left structure).

The favoured diastereoisomer, *syn*-**5.10**, gives product *trans*-**5.11**. This is contrary to aziridine *cis*-**5.11**, which is the experimentally observed diastereoisomer. It is expected *trans*- aziridines to be favoured over the corresponding *cis*- ones. However, given that the reaction is kinetically controlled, the catalyst might be favouring *anti*-**5.10** in order to get aziridine *cis*-**5.11**. In the case of this reaction, without a chiral catalyst, a 1.7:1[a] *dr* is calculated in favour of diastereoisomer *syn*-**5.10**.

The Newman-like projections along the C3-C2 bond display different 'rotamers' for intermediates **5.10**. According to Hammond's postulate, this rotamers would have a geometry similar to their transition states. Therefore, at least three staggered 'rotameric' transition states for each diastereoisomer can be envisaged when looking the Newman projection of the diazoester approaching the imine (Figure 5.7).

In retrospect, there are three things to consider in the 1,2- addition transition state: the geometry of the iminium ion, the approach of the nucleophile, and the staggered conformations arising from such approach. The latter may enhance secondary interactions to stabilise a particular transition state.

[a] Boltzmann averaged taking into account the conformers shown in Figure 5.6.

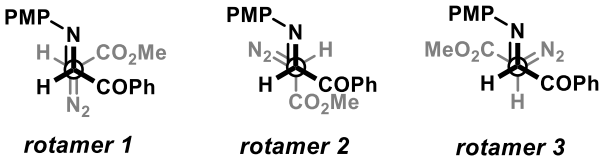

Figure 5.7: At least three staggered rotameric approaches of the diazoester can be participating in the transition state of the 1,2- addition.

In order to study the general acid-catalysed reaction—*i.e.* using iminium **5.8** as the reactive starting material and no model or full catalyst—24 different TSs leading to *anti*-**5.10** were anticipated, which corresponds to the (2*S*,3*S*)-diastereoisomer. These proposed 24 structures arise from taking into account the following features: 1) *E*/*Z* configuration of the iminium ion, 2) *s-cis*/ *s-trans* conformers of the iminium, 3) *s-cis*/ *s-trans* conformers of diazo ester **5.9** and 4) three different staggered rotamers (*cf.* Figure 5.7). The calculated TSs and their energies, relative to the lowest-energy TS are presented in Figure 5.8.

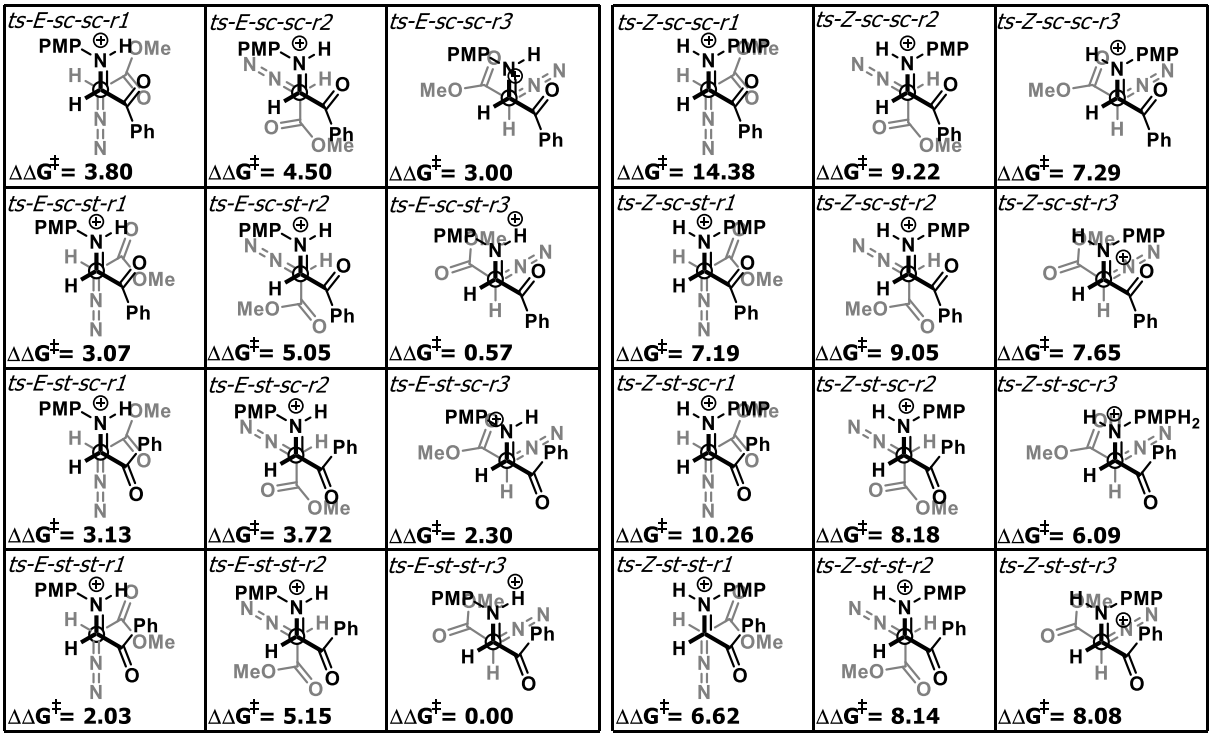

Figure 5.8: Newman projections for 24 transition states yielding (2*S*,3*S*)-*anti*-**5.10** intermediate. Left box shows the *(E)* iminium geometries. Right box shows the *(Z)* iminium geometries. Gas-phase energies were calculated at the ωB97X-D/def2-TZVPP // ωB97X-D/6-31G(*d*) level of theory and are presented in kcal mol^{-1}. Labels correspond to the iminium configuration and conformation,[a] diazoester conformation and orientation relative to the imine. *e.g.* ts-E-sc-sc corresponds to the transition state of the *E s-cis* iminium and the *s-cis* diazoester, the labels r1, r2, r3, correspond to the three possible staggered rotamers.

[a] For the case of the iminium ion with an *(E)*-geometry, all attempts to find TSs with the *s-trans* conformation failed. Those whether did not converged at all or converged to the *s-cis* conformation. This can be tracked back to the iminium ion geometries presented on Figure 5.4. The *s-trans* conformation is disfavoured by 3.46 kcal mol^{-1} over the corresponding *s-cis*. Thus, it is not surprising that *s-trans* conformers prefer to shift to the *s-cis* conformation in the TS. The 'st' label was kept to keep track of the different input geometries.

The predominant trend is that all *(E)*-iminium TS geometries are favoured over the *(Z)* ones. The lowest-energy *(Z)*-iminium TS, ts-Z-st-sc-r3, was found 6.09 kcal mol^{-1} above the lowest of all TSs. This trend agrees with the calculated mean of $\Delta\Delta_{E/Z}G_{imine}$ and $\Delta\Delta_{E/Z}G_{iminium}$ previously discussed. Hence, it is very likely that a TS with an *(E)*-iminium would be the lowest-energy one for the chiral PA-catalysed reaction.

Given that the nitrogen atom is protonated, the *s-cis (E)* configurations of the iminium were highly favoured. Attempts to find TSs with the *s-trans (E)* iminium geometry did not converged or converged to the corresponding *s-cis* conformations. This suggests that the strong hydrogen bond with the adjacent carbonyl group stabilises this particular configuration. Such an intramolecular hydrogen bond is not accessible for the *(Z)* iminium geometries.

The lowest-energy TSs found for the iminium ion with an *(E)* and with a *(Z)* configuration are presented on Figure 5.9. In the case of **TS1-E**, the iminium keeps an *s-cis* conformation due to the strong hydrogen bond that is formed between the N-H moiety and the adjacent carbonyl (2.10 Å). Such interaction locks the reactive *s-cis* conformation. As seen in the N=C-C-O dihedral, -15°, such conformation does not deviates considerably from an ideal 0° dihedral. This means that the geometry of the iminium ion does not suffer a great degree of distortion when going from starting material to TS. However, for **TS1-Z**, this is not the case. The *s-trans* conformation of the iminium deviates considerably from ideality: -92° against 180°. Such arrangement places the π orbitals of the iminium and the carbonyl group orthogonal to each other. Hence, there is little chance that **TS1-Z** might be stabilised by conjugation of these groups, which is possibly be the case for **TS1-E**. Furthermore, the C···C bond-forming distance is shorter in **TS1-E**, 1.99 Å compared with 2.27 Å in **TS1-Z**. The latter, might be larger to avoid steric clash between the reacting species.

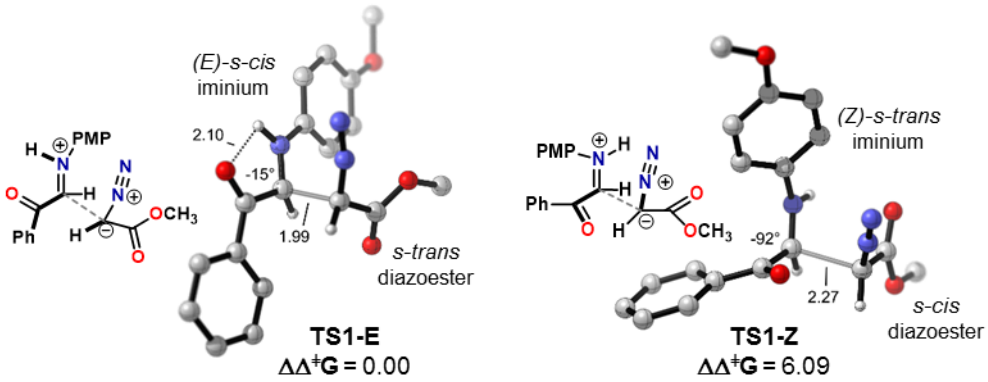

Figure 5.9: Lowest-energy TSs found for the *(E)* and *(Z)* iminium ions. Energies were calculated at the ωB97X-D/def2-TZVPP // ωB97X-D/6-31G(*d*) level of theory and are presented in kcal mol^{-1}. Non-critical H-atoms are omitted for clarity.

In summary, all the factors discussed above seem to be contributing to the 6.09 kcal mol^{-1} energy difference in favour of **TS1-E** over **TS1-Z**. Thus, it can be expected that an *(E)*-iminium geometry would be highly favoured both with a model catalyst and with the full catalytic system.

5.4. Model catalyst approach: Activation modes

Another pattern found in TSs with iminium ions with an *(E)*-geometry is the disposition of the hydrogen atoms attached to the pro-chiral centres and the protonated nitrogen atom. This can lead to different activation modes. The idea is clearer when looking at the Newman projections presented in Figure 5.10. Rotamer 1 has two plausible attachment points in which the catalyst's phosphate group can engage in activation modes: A and C. Rotamer 2 sits the N-H motif next to the hydrogen atom in the pro-chiral centre on the diazo ester. This provides a different attachment position, B, for the catalyst to interact with both substrates in a bifunctional manner. Rotamer 3 has the *H*-atoms in similar dispositions as rotamer 1.

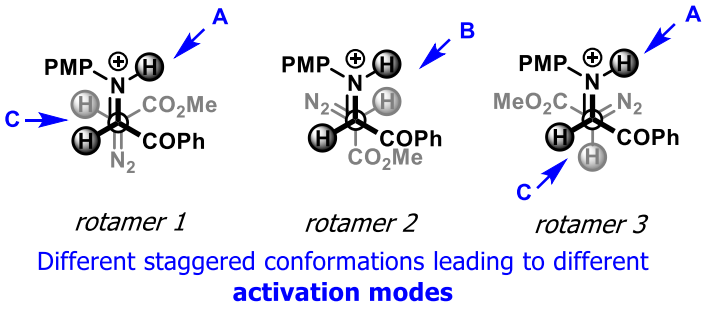

Figure 5.10: Different orientations of relevant hydrogen atoms can serve for the catalyst to anchor the substrates. This suggest that at least three different activation modes are possible for the PA-catalysed reaction.

Within the reaction mechanism, the reactive species will be the iminium ion. Thus, with the aforementioned attachment points, A, B, and C, three different activation modes for the acid-catalysed aza-Darzens reaction are proposed (Figure 5.11). Buta-1,3-diene-1,4-phosphate **5.12** was used as a simplified version of catalyst *(R)-PA*-**5.6** to calculate the TSs involving the proposed activation modes.

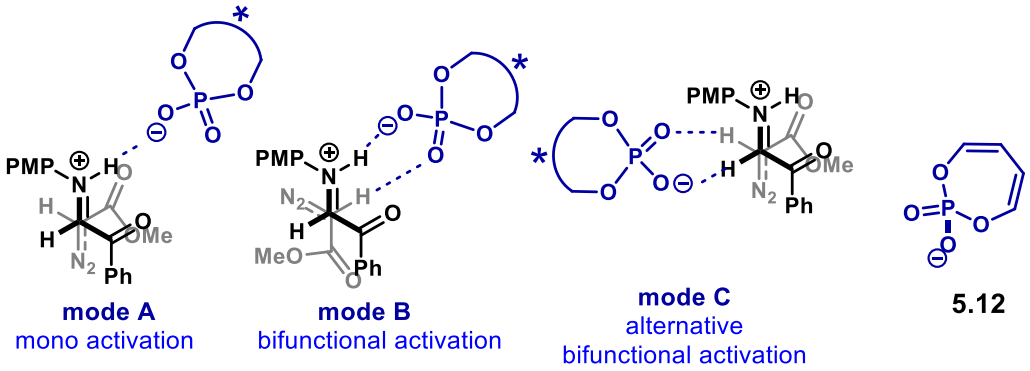

Figure 5.11: Proposed activation modes for the chiral PA-catalysed aza-Darzens reaction.

Activation Mode A. A mono contact interaction is established between the N-H moiety in the iminium ion and the phosphate motif from the catalyst. One of the oxygen atoms from the active site anchors the iminium ion. Given the high conformational flexibility due to a single hydrogen bond, it is not clear how such a TS could achieve high levels of enantiocontrol. However, there is precedent in the literature of single contact activation modes yielding good enantiomeric excesses.[299] In addition, activation mode A

may not be limited only to single contact. Dual coordination of the N-H hydrogen to both oxygen atoms in the phosphate group could also be possible.

Activation Mode B. As proposed, and supported by several computational studies by the group of Jonathan Goodman, a bifunctional activation mode is highly favoured when both reagents are capable of forming hydrogen bonds with the phosphate group. This activation mode has been exhaustively studied for the asymmetric reduction of imines with Hantzsch esters.[143,291,300] Therein, both starting materials form N-H···O-P hydrogen bonds with different oxygen atoms in the phosphate group. Such a rigid TS explains the high enantioinduction levels observed. However, this model applies for heteroatom-H or C-H nucleophiles. For the aza-Darzens reaction under study, there are not 'formal' or common hydrogen bond donors in the diazo ester. Nevertheless, a C-H···O-P interaction with the diazo ester seems feasible. This type of non-classical hydrogen bond has shown to be a stabilising element for bifunctional activation in several asymmetric reactions catalysed by PAs.[301–305] Therefore, a non-classical hydrogen bond between the C-H moiety in the reactive centre of the diazo ester and the catalyst is proposed. This, together with a hydrogen bond form the N-H iminium motif, constitutes activation mode B.

Activation Mode C. In a similar way as mode B, the diazo ester is activated forming a C-H···O-P non-classical hydrogen bond with the catalyst. The iminium ion, however, forms a formyl-like C-H···O-P non-classical hydrogen bond with the catalyst's active site instead of the most common N-H···O-P *H*-bond. The formyl-like hydrogen atom should be electron-deficient enough to engage with the catalyst and direct the iminium ion in an asymmetric fashion. The adjacent carbonyl in **5.8** also contributes to make this hydrogen slightly more electron-deficient. A similar formyl-like interaction has been invoked to account for the high levels of enantiocontrol in a semi-pinacol rearrangement.[305]

In order to assess which activation mode would be the most likely to be operating, the different TSs from Figure 5.8 were evaluated. Each one was calculated with all of the three proposed activation modes, comprising a total of 72 TSs using model catalyst **5.12**. However, most of the initial TS geometries did not converged or converged into another geometry. The successfully optimised TSs are presented on Figure 5.12 in the next page. Twenty different TS using model catalyst **5.12** were found within 16 kcal mol^{-1}. From those TS, eight were found corresponding to activation mode A, five to activation mode B and seven to activation mode C.

For activation mode A, which consists in a mono contact, single hydrogen bond, the three lowest-energy TS were found with a *(Z)*-geometry in the iminium ion. The next five TSs, higher in energy, have an *(E)*-iminium ion and are far higher in energy (Figure 5.12a). For activation mode B, which features bifunctional *H*-bonding from the catalyst to both reacting species, *(E)* and *(Z)* iminium geometries were found. These, not too far in energy from each other (Figure 5.12b). In sharp contrast, activation mode C, through non-classical hydrogen bonding, was found to be the lowest in energy amongst the proposed activation modes. The *(E)*-iminium geometry was highly favoured in this case. The entire activation mode C TSs but one were found with that configuration. For the case of this reaction, with the model catalyst, a bifunctional activation mode through two non-classical hydrogen bonds is suggested as the lowest-energy one. This type of bifunctional activation is very rare and it does not seem to be precedent for it.

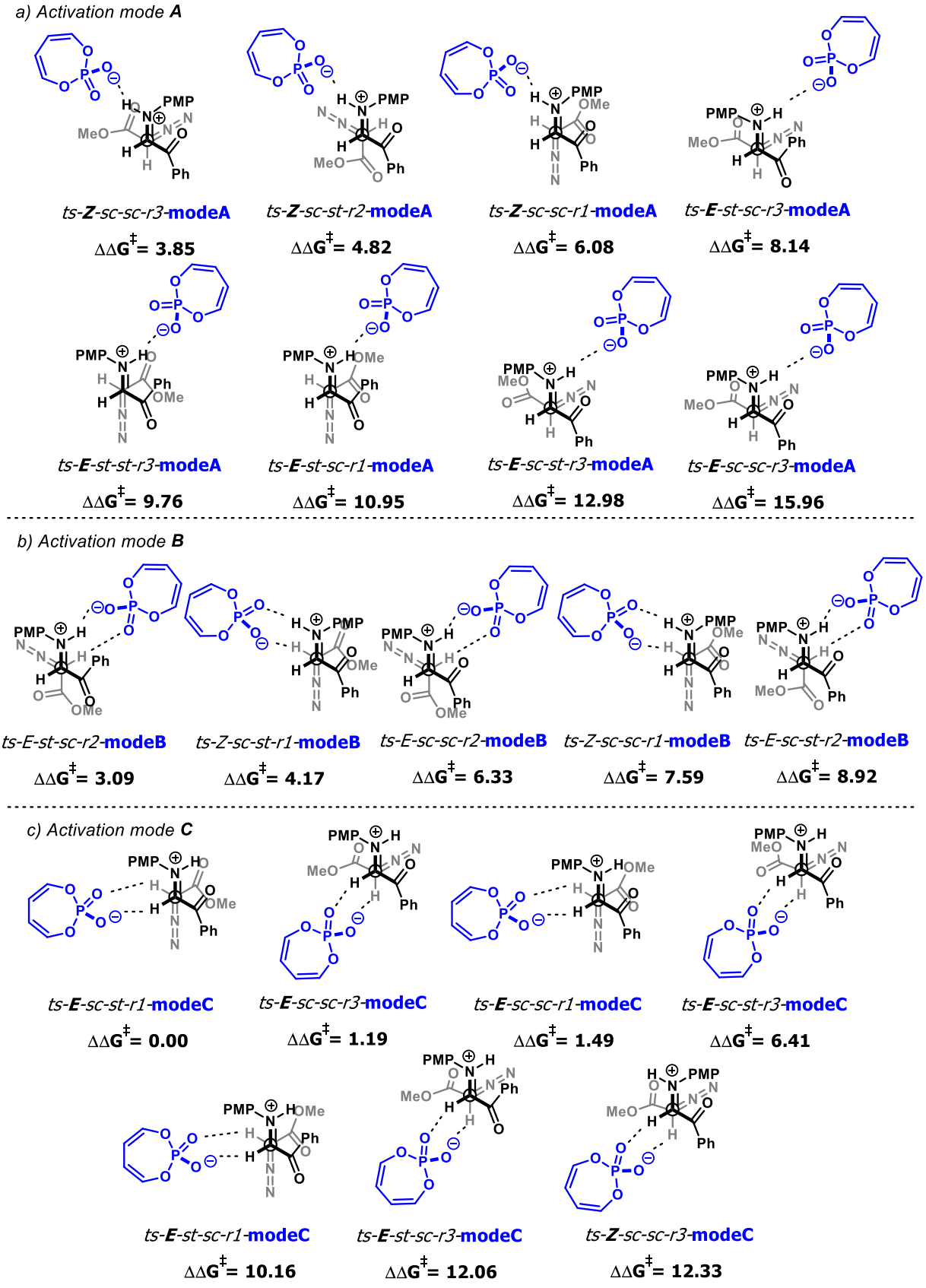

Figure 5.12: TSs found for activation modes A, B and C. Energies were calculated at the ωB97X-D/def2-TZVPP // ωB97X-D/6-31G(*d*) level of theory and are presented in kcal mol^{-1}.

The lowest-energy TSs for each of the three activation modes A, B and C are presented on Figure 5.13. These include those found with an *(E)* and a *(Z)* geometry in the iminium ion.

The lowest-energy TS for a proposed mono activation pathway (mode A) turned to have the iminium in a *Z* configuration, **TS2-Z-modeA**. This contrasts with the fact that the *E* iminium ion is favoured over the corresponding *Z* isomer. Moreover, instead of being a mono activation case, the substrate seems to engage in a dual activation by the phosphate motif. An N-H···O-P hydrogen bond is formed as expected (1.67 Å) which may be the main source of stabilisation. In addition, a formyl-like C-H···O-P interaction is formed with the other oxygen atom in the phosphate (1.99 Å). This interaction seems to be orienting the phenyl rings in the iminium ion as far from each other to avoid steric clash with the model catalyst. However, despite these stabilising interactions, such activation mode was found to be 3.85 kcal^{-1} higher in energy than the most favoured one (later discussed). In sharp contrast, when the iminium has an *E* configuration and is activated through mode A, **TS2-E-modeA**, the energy rises up to 8.14 kcal mol^{-1} respect to the lowest-energy activation mode. In this case, the substrate also engaged in an *H*-bond between the N-H moiety and the phosphate group (1.61 Å). Given that the *E* configuration cannot sit the formyl-type hydrogen on the same side to the N-H moiety, such an extra non-classical H-bond is not present. Thus, this may account for the rise in energy in **TS2-E-modeA**, in comparison with **TS2-Z-modeA**.

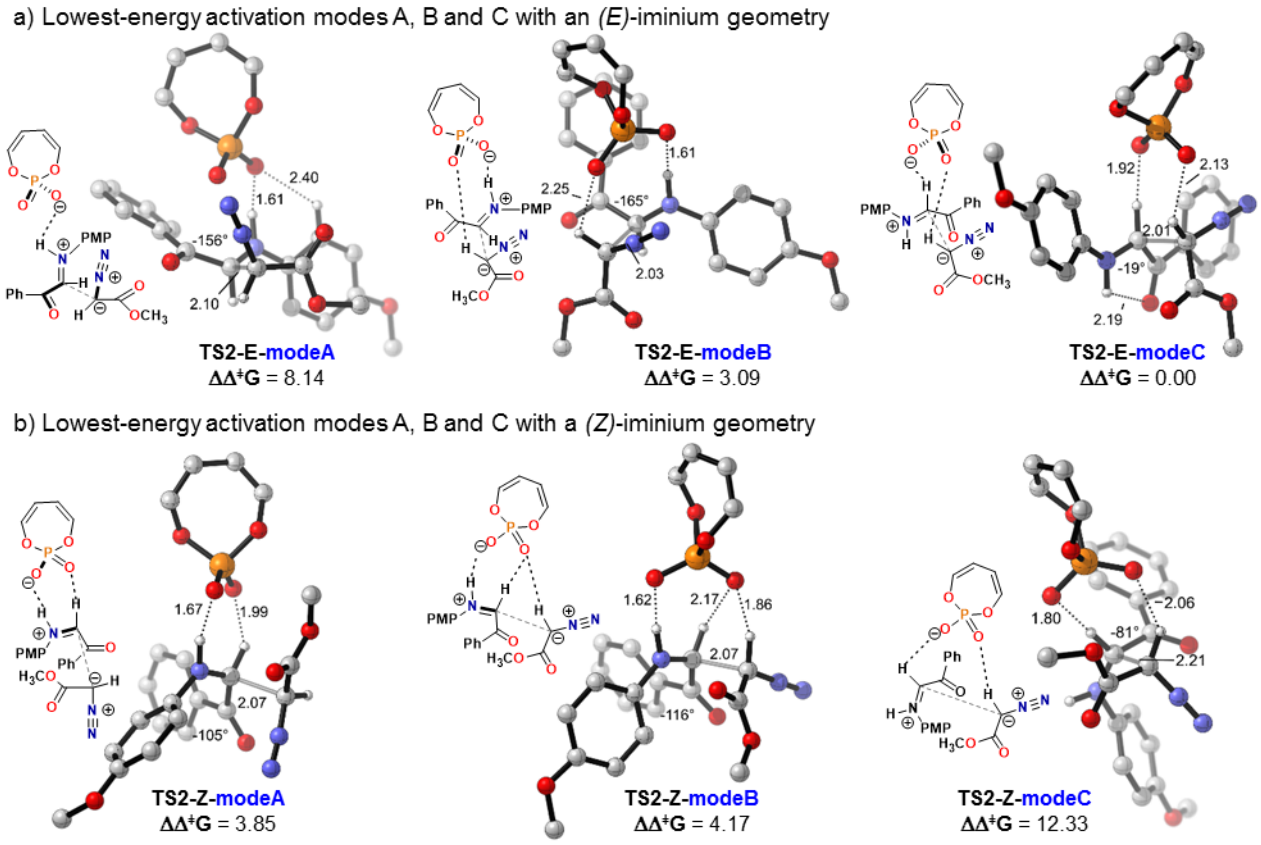

Figure 5.13: Lowest-energy TSs for each of the proposed activation modes A, B and C. Both *(E)* and *(Z)* iminium ion geometries are presented. Energies were calculated at the ωB97X-D/def2-TZVPP // ωB97X-D/6-31G(*d*) level of theory and are presented in kcal mol^{-1}. Distances are given in Å. Non-critical *H*-atoms are omitted for clarity.

Mode B was found to be 3.09 kcal mol^{-1} higher in energy respect to the lowest activation mode. This, for the *(E)* iminium **TS2-E-modeB**. Herein, the iminium ion is activated through an N-H···O-P hydrogen bond (1.61 Å). As predicted for this mechanism, the other oxygen atom in the phosphate group forms a non-classical C-H···O-P hydrogen bond with the diazo ester (2.25 Å). These two interactions account for a bifunctional mode of activation. **TS2-Z-modeB** shows similar interactions. In this case, due to the *(Z)* geometry in the iminium, an additional non-classic hydrogen bond is formed (2.17 Å). The other interactions are also present. The main N-H···O-P H-bond (1.62 Å) and the C-H···O-P non-classical interaction with the diazo ester (1.86 Å). The latter *H*-bond is shorter in **TS2-Z-modeB** than in **TS2-E-modeB**, 1.86 Å against 2.25 Å. Therefore, a shorter distance might push the reactive species and the catalyst closer to each other, possibly, enhancing unfavourable steric clash.

The lowest-energy activation mode was found to be mode C, featuring an *(E)* iminium ion, **TS2-E-modeC**. Because no N-H···O-P bond is formed, this mechanism is likely to be dominated by tight ion pairing. Two short contact interactions are observed between the catalyst's active site and the iminium ion. The non-classical, formyl-like C-H···O-P (1.92 Å) is very likely to be the main source of stabilisation, as well as the *E s-cis* iminium which turned to be the most favoured configuration for the ground state structures. Furthermore, the other non-classical *H*-bond between the CH moiety in the diazo ester and the phosphate (2.13 Å) enables the bifunctional activation.

In the case of **TS2-Z-modeC**, an energy gap of 12.33 kcal mol^{-1} was found relative to **TS2-E-modeC**. This makes the latter TS the highest in energy of those ones presented here. Similarly, no N-H···O-P hydrogen bond can be formed due to the substrates and catalyst's relative location. Nonetheless, a formyl-like C-H interaction from the iminium (1.80 Å) and another one from the diazo ester (2.06 Å) are formed with the phosphate component; these provides a bifunctional activation mode C, yet, highly disfavoured.

Taking everything into account, from the calculations using a model catalyst, bifunctional activation mode C was found to be the most favoured one when the iminium ion has an *(E)*-geometry. This finding was rather surprising as not many PA-catalysed reactions are reported to be activated only through non-classical hydrogen bonds. Nor such an activation mode is generally presented as the lowest-energy one. The second lowest-energy TS, **TS2-E-modeB**, is 3.09 kcal mol^{-1} above **TS2-E-modeC**. Thus, it is very likely that the bifunctional mode C drives the PA-catalysed reaction.

Despite the fact that the model catalyst gave a good initial approach to the reaction mechanism, understanding enantioselectivity needs the calculation of TSs using the full catalyst. In addition, in terms of activation modes, this could give different results due to several reasons. The massive silicon-based scaffolds in the catalyst tighten a side of the chiral pocket (*cf.* Figure 5.1). This leaves less space available for the reacting substrates. Therefore, will limit most of the substrates' conformations, allowing just those structures that fit 'just right' inside the chiral cavity. Furthermore, the tight side of the chiral pocket could leave one of the oxygen atoms from the phosphate motif less available to engage with the substrates. This could be a direct consequence of the different shape of the chiral pocket created by the sp^3 silicon atom.

5.5. Full catalyst approach: Enantioselectivity

In order to save computing time, the ONIOM approach was used to model the reaction with the full catalyst (Figure 5.14).[306] For the TS optimisations, the active site of the catalyst, *i.e.* the phosphate group, and the substrates were included in the ONIOM high layer and calculated using DFT at the ωB97X-D/6-31G(*d*) level of theory. In addition, the substrates were also slightly simplified. The PMP group on the imine was changed for a phenyl group and the ethyl moiety in the diazo ester for a methyl group. The backbone of the catalyst as well as the 3,3' substituents were calculated with molecular mechanics using the universal force field (UFF) in the ONIOM low layer. To account for dispersion effects, as well as to include solvent effects, a single point energy calculation at the ωB97X-D/def2-TZVPP level of theory was done on the ONIOM-optimised structures using the SMD solvation model (toluene). The vibrational analysis from the ONIOM optimisation was used to compute the corrected Gibbs free energies. This approach has been successfully used to study chiral PA-catalysed reactions and explain enantioselectivities. Full computational details are provided in Appendix 1.

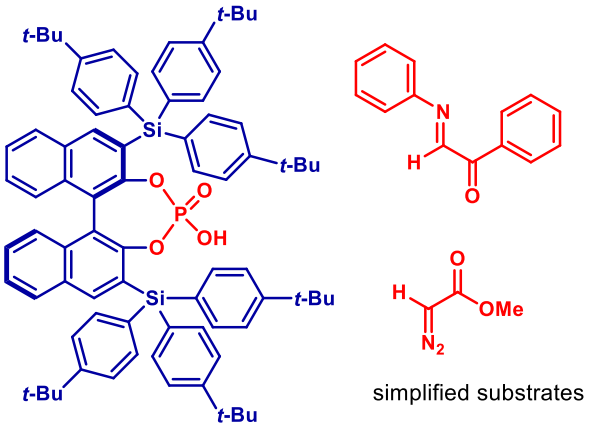

Figure 5.14: ONIOM approach to calculate the TS with the full catalyst. The active site of the catalyst and the simplified substrates, highlighted in red, were treated at the ωB97X-D/6-31G(*d*) level of theory. The catalyst's backbone and 3 3' substituents, highlighted in blue, were treated with the universal force field (UFF). After the ONIOM optimisation, single-point energy calculations at the ωB97X-D/def2-TZVPP/SMD(toluene) level of theory were done in order to report the corrected Gibbs free energies.

Using this ONIOM approach, ten different transition states were found yielding the (2*S*,3*S*) intermediate and another ten yielding the (2*R*,3*R*) one, which in turn undergo the ring closing step to afford the major and minor enantiomers, respectively. The two lowest-energy diastereomeric TSs are presented in Figure 5.15 on the following page. Both the iminium and the diazo ester have the configurations found for their lowest-energy ground state structures: (*E*) *s-cis* for the iminium ion and *s-cis* for the diazo ester (*cf.* Figures 5.4 and 5.5). In addition, both TSs happen through an activation mode C, as found for the TSs using the simplified catalyst. Thus, such activation mode *via* non-classical hydrogen bonding seems to be the favoured one when the full catalyst promotes the reaction.

In **TS1-2S3S**, both starting materials fit inside the largest side of the catalyst's chiral pocket (Figure 5.15a). Whilst the diazo ester allocates itself in most of the empty space of the cavity, the iminium ion tilts in order to occupy the space formed by the silicon-based substituents and the backbone of the BINOL framework (Figure 5.15b). The planar structure of the (*E*) *s-cis* iminium makes this fitting feasible. Little distortion of the iminium ion happens. This can be shown by the C=N-C-C dihedral angle, which only deviates -18.9° from 0°, which corresponds to a fully planar iminium geometry. Due to the encumbered chiral pocket, a bifunctional activation mode for **TS1-2S3S** is not available. Instead, the iminium ion is locked to the catalyst's active site through a non-classic CH···O-P hydrogen bond. Thus, it is possible that the diazo ester is 'pushed to react' by the silicon scaffolds once inside the chiral cavity, given that no CH···O-P was observed in this TS.

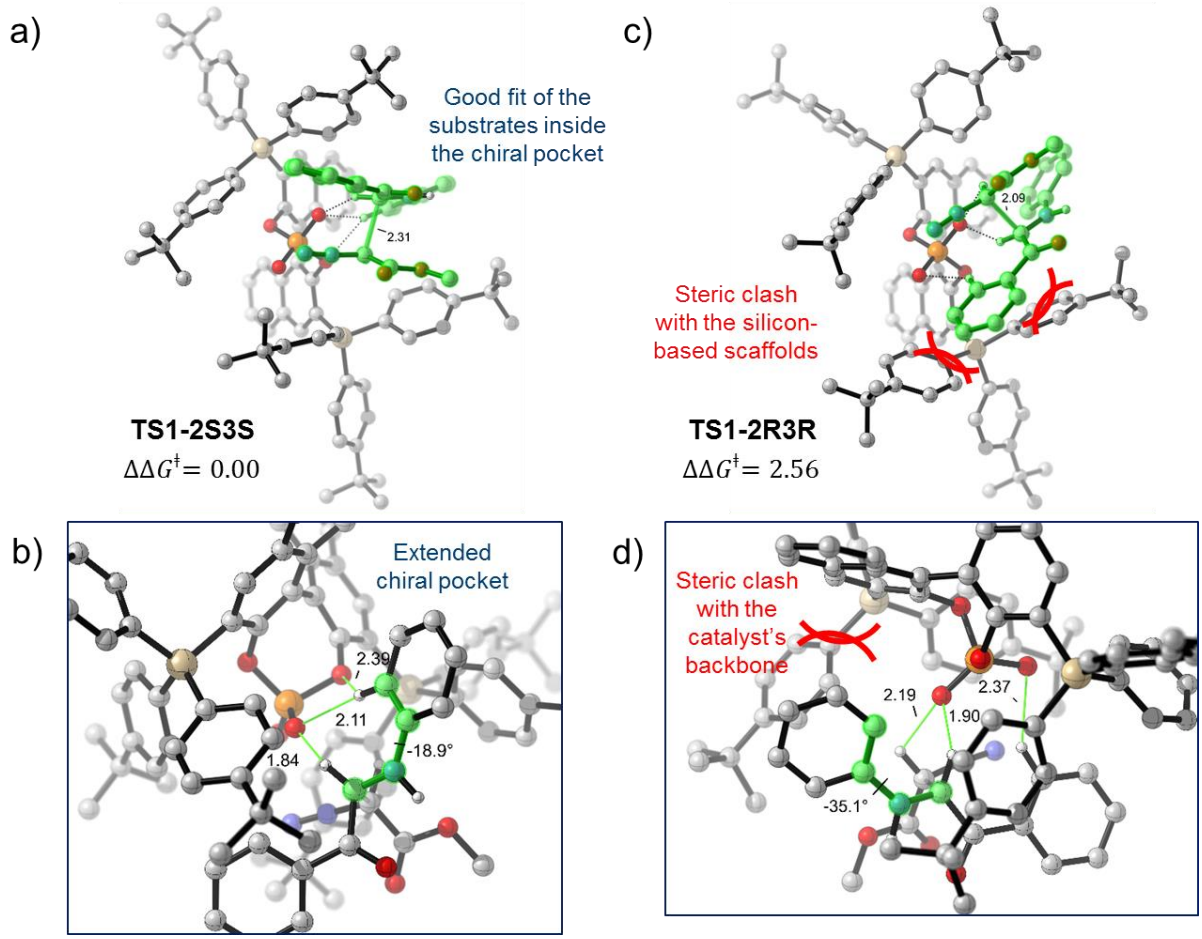

Figure 5.15: a) End-on view of the TS yielding the major enantiomer. Substrates are highlighted in green to emphasise how they fit inside the chiral cavity. b) Close-up to the activation mode C for the major enantiomer. A three-point activation seems to happen with the iminium ion. -18° dihedral angle highlighted in green. c) End-on view of the TS yielding the minor enantiomer. Substrates are highlighted in green. d) Close-up to the activation mode. Dual and bifunctional activation takes place. -35° dihedral angle highlighted in green. Energies are presented in kcal mol^{-1} and distances in Å. Non-critical *H*-atoms are omitted for clarity.

On the other hand, in **TS1-2R3R**, the diazo ester is still occupying the largest side of the chiral pocket. However, the phenyl ring on the ketone side of the (*E*) *s-cis* iminium ion clashes with two of the 4-*tert*-butylphenyl motifs of the silicon-based scaffold (Figure 5.15c). Furthermore, the *N*-phenyl substituent

clashes with the 3,3' scaffolds and with the BINOL framework. This clash makes the *N*-phenyl ring to twist out of its planar shape. This distortion is shown by the C=N-C-C dihedral angles, -18.9° versus -35.1° (Figure 5.15d). In addition, the diazo group from the ester seems to point towards one of the aryl motifs in the other substituent of the catalyst. Because of all these steric repulsions, the TS has to tighten to fit inside the chiral cavity. This is demonstrated by comparing the distances of the C-C bond that is to be formed, 2.31 Å for **TS1-2S3S** versus 2.09 Å for **TS1-2R3R**. In the latter TS, the out-of-fit and distortion of the substrates slightly enlarges the formyl-like hydrogen bond distance with the phosphate group, being 1.84 Å for the major diastereomeric TS and 1.90 Å for the minor one.

In order to quantify how much the iminium ion distorts from its *(E)-s-cis* ground state geometry, a simplified version of the distortion-interaction analysis, developed by the group of Houk, can be applied.[307,308] Taking the SP energy difference between the distorted iminium geometry in the TS and the ground state geometry, can tell what is the energy penalty for the ground state iminium ion to achieve a distorted geometry in a given TS. For the iminium ion in **TS1-2S3S**, such value was found to be 2.89 kcal mol^{-1}, whereas the calculated distortion energy for the iminium in **TS1-2R3R** was 6.67 kcal mol^{-1}. This strongly suggests that the distortion of the iminium ion to fit into the chiral cavity is a main contributor for enantiodiscrimination. Such distortion model has also been applied in other Brønsted acid-catalysed transformations to account for reactivity.[177,309]

An energy difference of 2.56 kcal mol^{-1} is obtained in favour of **TS1-2S3S** over **TS1-2R3R**. This value corresponds to a calculated 98% enantiomeric excess, which is slightly larger than the 90% *ee* observed experimentally. However, the sense of enantioinduction agrees with these calculations.

TSs corresponding to an activation mode A were also found and are presented on Figure 5.16 in the following page. Such TSs are much higher in energy than the corresponding ones with an activation mode C. **TS2-2S3S** was found to be 7.22 kcal mol^{-1} higher in energy than the lowest **TS1-2S3S**. For the minor enantiomer, **TS2-2R3R** turned to be 11.68 kcal mol^{-1} above the global minimum. These large energy gaps might be a consequence of a disfavoured iminium with an *(E) s-trans* geometry, relative to the *s-cis* conformer. The steric clash of the iminium's phenyl motifs in both TSs with the 3,3' substituents in the catalyst could also be increasing their relative energies (Figures 5.16a and 5.16c). In both cases, the diazo ester occupies most of the empty free space in the chiral cavity.

TS2-2S3S engaged in an N-H···O-P hydrogen bond with the catalyst (1.66 Å). This distance is shorter than the formyl-like activation in mode C (1.84 Å). This makes the iminium to be slightly closer to the catalyst's scaffolds and has to be distorted in order to occupy the free space in the chiral pocket (Figures 5.16a and 5.16b). A 12.79 kcal mol^{-1} distortion energy was calculated for the iminium ion in **TS2-2S3S**. Due to the encumbered phosphate group, no interactions with the diazo ester seem to be formed. However, the iminium is triply activated. In addition to the main N-H···O-P hydrogen bond, two extra C-H···O-P interactions are formed: one with the *N*-phenyl group (2.44 Å) and another one with the other phenyl ring (2.04 Å).

On the other hand, the higher energy of **TS2-2R3R** (11.68 kcal mol^{-1}) can be attributed to the numerous steric clashes of the iminium with the massive catalyst's body (Figure 5.16c)—a 12.35 kcal mol^{-1} distortion

energy was calculated for the iminium ion in **TS2-2R3R**. A slightly longer N-H···O-P hydrogen bond is also observed (1.71 Å, Figure 5.16d). A triple contact activation is also present in a similar way as for **TS2-2S3S**. In a similar fashion, the other oxygen atom in the phosphate group is encumbered deep inside the catalyst's chiral pocket, making it unavailable to promote a bifunctional activation with the diazo ester.

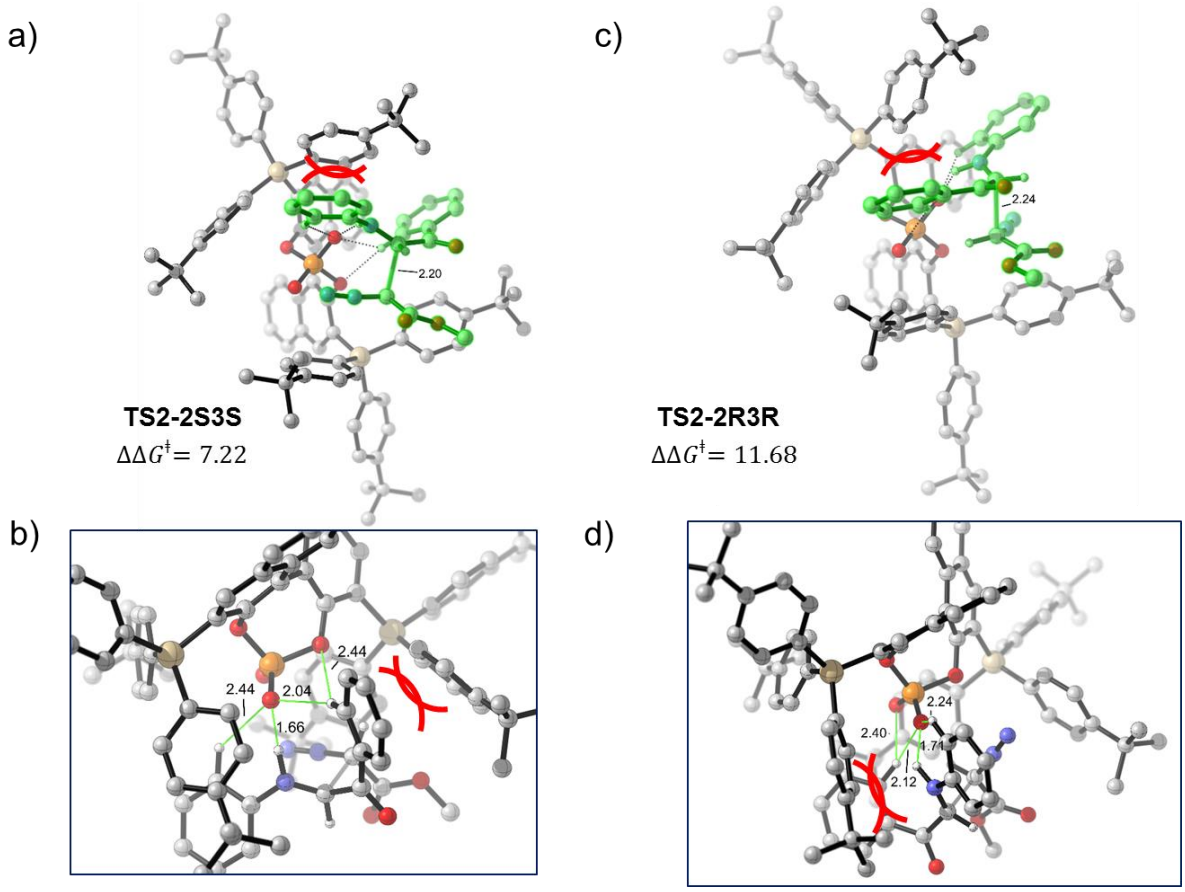

Figure 5.16: a) End-on view of the TS yielding the major enantiomer with an activation mode A. Substrates are highlighted in green. b) Close-up to the activation mode A for the major enantiomer. Both the iminium *E s-trans* geometry and steric clash with the silicon-based scaffolds may be increasing the energy of this activation mode. c) End-on view of the TS yielding the minor enantiomer with an activation mode A. Substrates are highlighted in green. d) Close-up to the activation mode A for the minor enantiomer. Both the iminium *E s-trans* geometry and steric clash of the *N*-phenyl group with the silicon-based scaffolds may be increasing the energy of this activation mode. Energies are presented in kcal mol^{-1} and distances in Å. Non-critical H-atoms are omitted for clarity.

Due to the fact that **TS2-2S3S** and **TS2-2R3R** are much higher in energy than the corresponding **TS1-2S3S** and **TS1-2R3R**, it is very likely that activation mode C is the dominating mechanism taking place in the 1,2- addition step to create both chiral centres. The third-lowest TSs for the major and minor enantiomers were calculated 7.43 and 12.73 kcal mol^{-1} above **TS1-2S3S**, respectively, also activated through an N-H···O-P H-bond. The rest of the calculated TSs are, as expected, much higher in energy.

So far, the ONIOM approach including the full catalyst was able to predict the sense of enantioinduction reported in the publication. In addition, the predicted enantiomeric excess agrees with the experimental values. Thus, the next step was to calculate the TSs leading to the diastereomeric intermediates, which yield the *trans*-aziridines. This, in order to figure out if the catalyst is responsible for controlling

diastereoselectivity as well. Using the same ONIOM methodology, nine TSs were found yielding the *(2S,3R)* intermediate and ten yielding the *(2R,3S)* intermediate. The structures for the three lowest-energy TSs for each diastereoisomer are presented in Figure 5.17.

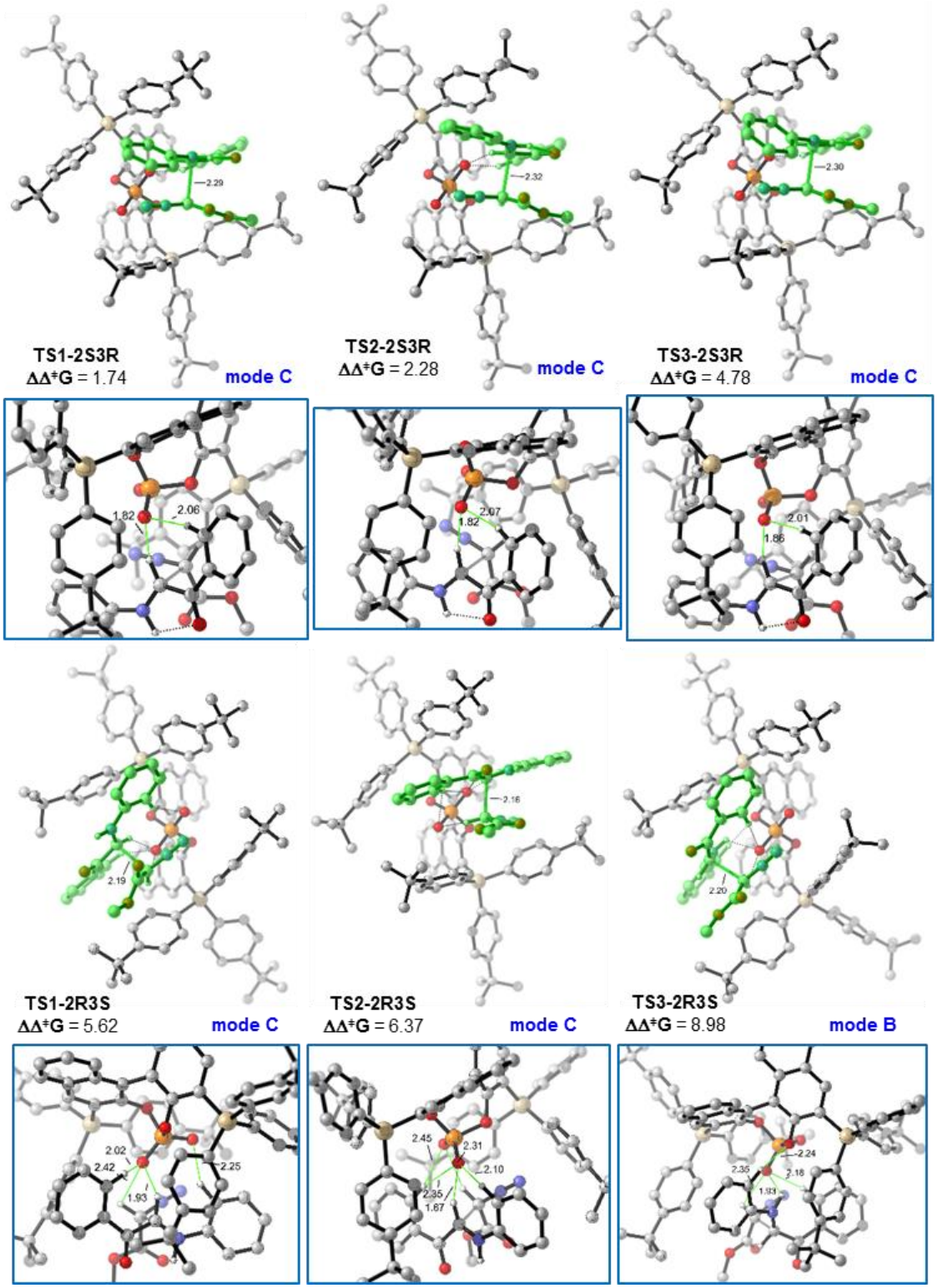

Figure 5.17: Lowest-energy TSs leading to the *syn*-intermediate, which, after ring closing would afford the *trans*-aziridine. Substrates are highlighted in green in the end-on projections for clarity. Energies are relative to **TS1-2S3S** and are presented in kcal mol^{-1} and distances in Å. Non-critical *H*-atoms are omitted for clarity.

The lowest-energy TS leading to the diastereoisomeric product, **TS1-2S3R**, was found 1.74 kcal mol^{-1} above **TS1-2S3S** (*cf.* Figure 5.15a). Therefore, this model also predicts the correct diastereoisomer, albeit with low selectivity. Moreover, the other diastereoisomer, **TS1-2R3S**, is 5.62 kcal mol^{-1} above **TS1-2S3S**, suggesting that the *trans*-aziridine would be disfavoured. In addition, the second and third lowest-energy TSs, **TS2-2S3R** and **TS3-2S3R**, were found at 2.28 and 4.78 kcal mol^{-1}, respectively.

In terms of activation mode, it was found that the TSs yielding the *(2S,3R)* intermediate are predominantly mode C. The iminium ion is anchored to the catalyst's active site *via* a non-classical hydrogen bond from the formyl-like C-H in the iminium. The distance of that C-H···O-P interaction are fairly consistent in **TS1-2S3R**, **TS2-2S3R** and **TS3-2S3R**: 1.82, 1.82 and 1.86 Å, respectively.

For the case of the enantiomer, *(2R,3S)*, their energies, relative to **TS1-2S3S**, were found 5.62, 6.37 and 8.98 kcal mol^{-1}, for **TS1-2R3S**, **TS2-2R3S** and **TS3-2R3S**, respectively. The activation mode of the first two TSs were also found to be mode C, through a non-classical C-H···O-P formyl-like hydrogen bond. However, for **TS3-2R3S**, the activation shifts to mode B. In this latter case, the iminium ion forms a hydrogen bond with the N-H moiety to the phosphate group in the catalyst (1.93 Å). The longer distance, in comparison with the former two mode C TSs, might suggest that a mode B activation has to form a longer N-H H-bond in order to avoid steric clash with the catalyst's scaffolds.

Enantioselectivity—as well as diastereoselectivity—can be explained using the qualitative diagrams presented in Chapter 1 (*cf.* Figure 1.6). To avoid ambiguity, the iminium ion is placed at the front and the diazo ester at the back of the chiral cavity. In addition, two key features are noticed from the TS calculations. In all the cases, the diazo ester, tries to occupy the empty space at the back of the chiral cavity. This avoids steric clash with the catalyst's 3,3' substituents. In addition, in the lowest energy TSs, one of the oxygen atoms in the active site is heavily hindered by the silicon scaffolds, making it unavailable to interact with the iminium ion, thus, the available oxygen is the one anchoring the substrate in order to provide an activation mode C. The diagrams on Schemes 5.5 and 5.6 in the next page account for enantioselectivity and diastereoselectivity in this aza-Darzens reaction, respectively.

In the favoured **TS1-2S3S**, the iminium ion occupies the empty space at the front of the chiral cavity (Scheme 5.5). To avoid steric clash with the front scaffold, it tilts to the right to occupy the empty space. Once the new C-C bond is formed, this gives intermediate **5.13-2S3S**, which places the hydrogen atoms—highlighted in the diagram—in a *syn* relationship to account for the relative stereochemistry in the product. After nitrogen elimination and ring closure **5.14-2R3S** is obtained as the major enantiomer. Therefore, the proposed steric model is in agreement with the absolute configuration of the product.

In **TS1-2R3R**, which leads to the minor enantiomer, however, the oxygen atom on the back anchors the iminium ion. This pushes the substrate towards the front scaffold of the catalyst. Herein, steric clash between the N-Ph motif in the iminium and the front group disfavours this TS by 2.56 kcal mol^{-1}, accounting for enantiocontrol. C-C bond formations gives intermediate **5.13-2R3R** which is also in agreement with the absolute stereochemistry in the minor enantiomeric product **5.14-2S3R**.

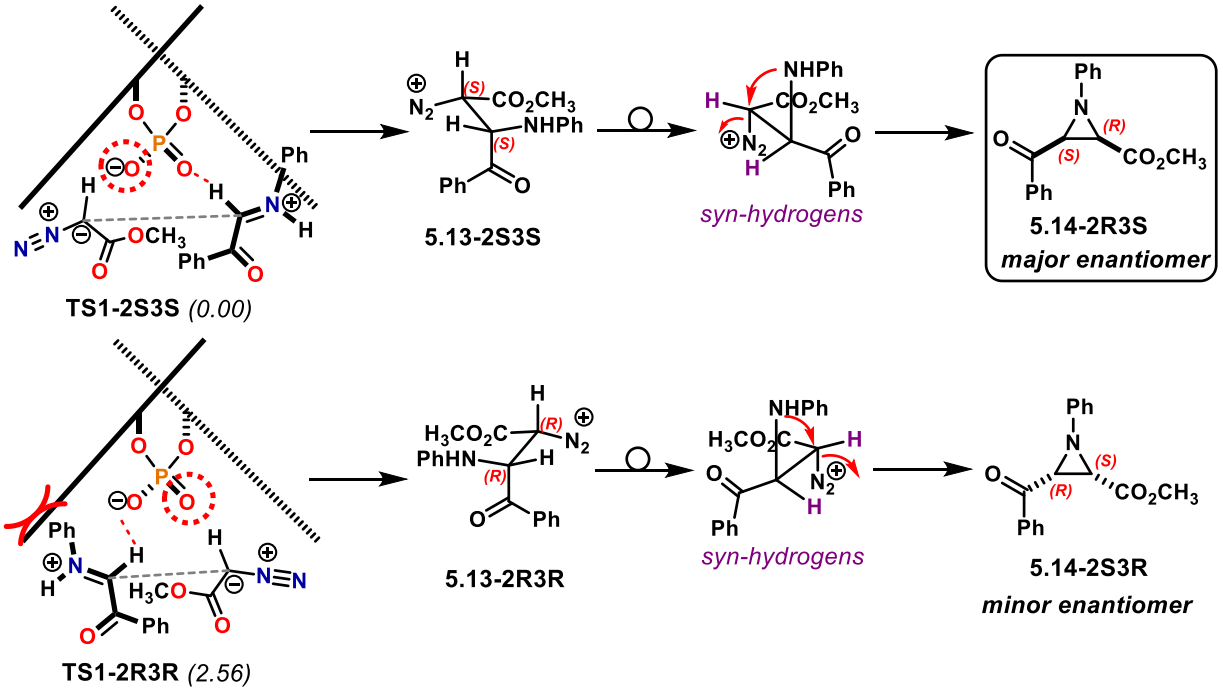

Scheme 5.5: Enantioselectivity model for the aza-Darzens reaction. To avoid ambiguity, the iminium ion is placed on the front and the diazo ester at the back of the chiral cavity. The unavailable oxygen atom in the active site—as discussed in the text—is highlighted in the red circle. The same labels used for the TS are repeated here. Relative energies to the lowest-energy TS are presented in parenthesis and are given in kcal mol^{-1}.

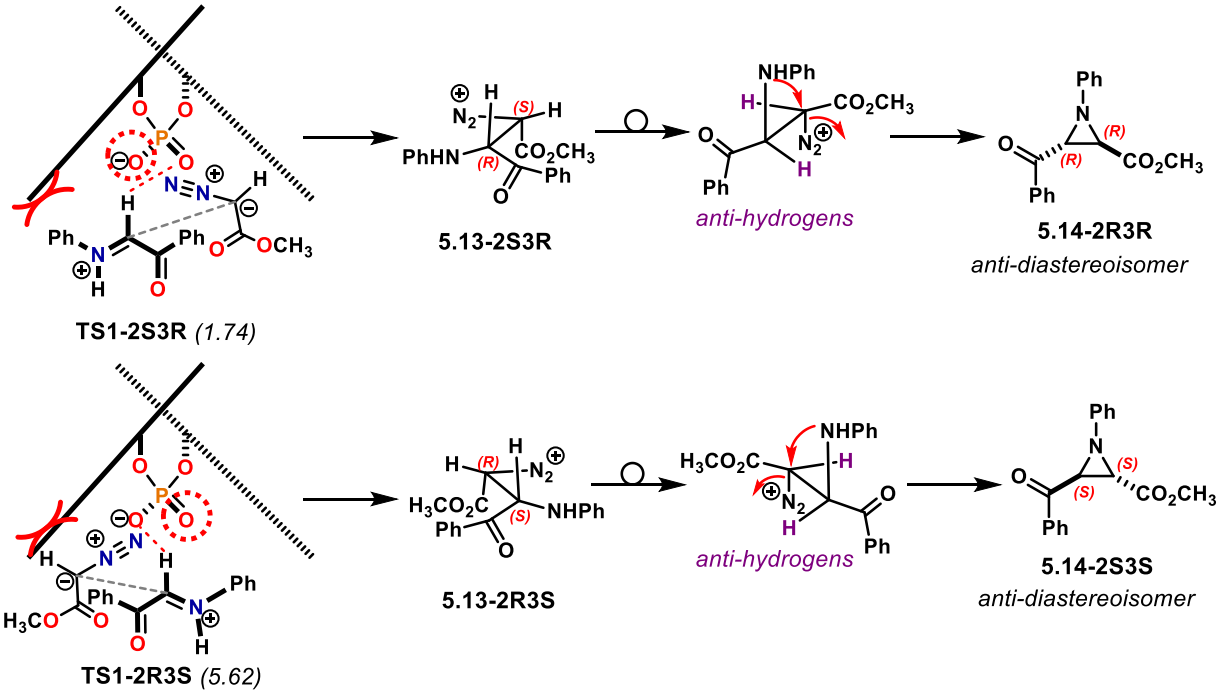

Scheme 5.6: Diastereoselectivity models for the aza-Darzens reaction. To avoid ambiguity, the iminium ion is placed on the front and the diazo ester at the back of the chiral cavity. The unavailable oxygen atom in the active site—as discussed in the text—is highlighted in the red circle. The same labels used for the TS are repeated here. Relative energies to the lowest-energy TS are presented in parenthesis and are given in kcal mol^{-1}.

Diastereoselectivity can also be explained with the qualitative diagrams (Scheme 5.6). In **TS1-2S3R** the iminium ion is anchored to the active site by the oxygen atom in the front—in this case, this oxygen atom is the available one. However, the iminium ion is pushed towards the catalyst's substituent at the front. Herein, the N-Ph motif clashes with such a scaffold. This TS accounts for intermediate **5.13-2S3R**, which sits the highlighted hydrogen atoms in an *anti*-relationship in order to account for the *trans*- diastereomeric product **5.14-2R3R**. The selectivity may not be high but the correct diastereoisomer is predicted by the diagrams as well, *i.e.* **5.14-2R3S** over **5.14-2R3R**.

The same can be argue for the other *anti*- diastereoisomer. In **TS1-2R3S**, the iminium ion is locked to the active site through the oxygen atom at the back. This pushes the substrate to the silicon scaffold on the right. Therefore, the phenyl ring in the substrate clashes with the catalyst, disfavouring such a TS to give **5.13-2R3S** and eventually, the *trans*- diastereomeric product **5.14-2S3S**.

Going back to the enantiomers produced in the reaction, *(2S,3S)* and *(2R,3R)*, it was decided to further explore the potential energy surface (PES) in order to get more insights about the reaction mechanism. This included calculating the complexes formed between the catalyst and the substrates prior to the 1,2-addition step, the intermediate-catalyst complex, the final product-catalyst complex, and the TSs of the ring-closing step, *i.e.* the nitrogen elimination step. Then, plot all of the structures' energies relative to the starting materials and catalyst at an infinite distance. The PES for the reaction yielding the major enantiomer is presented on Figure 5.18 in the following page. Such PESs are constructed considering or assuming that the catalyst is directly involved with every species in the mechanism.

The PES can be divided into two main regions; the 1,2- addition step and the elimination step. The first region, which is highlighted in black and grey, starts with the catalyst, the imine, and the diazo ester at infinite distances, which defines the 0.00 kcal mol^{-1} of the PES. In order to build up the first half of the PES, the three lowest-energy TSs for the 1,2- addition were taken as starting point. These were already calculated and were presented in Figures 5.15a and 5.16b. The intrinsic reaction coordinate (IRC) was calculated in order to get geometries of the complexed substrates prior to the TS and the catalyst-intermediate complex post-TS. Such geometries were reoptimised using the ONIOM approach to get the minima on each side of the minimum energy pathway.

With the optimised geometries, several features arise from the PES. When the catalyst and substrates are at an infinite distance, they start to approach each other to react. During the first step, the catalyst locks the substrates in a geometry similar to what they will be like in the TS, without forming the new C-C bond, of course. Such a reacting complex features similar activation modes as those described previously. For instance, two pre-TSs with an activation mode A were found to be the lowest in energy for the substrate's complexation. These, laying 7.50 and 8.60 kcal mol^{-1} above the separate starting materials. An activation mode C was also found for one of the reacting complex structures. This one, higher in energy (14.32 kcal mol^{-1}). Thus, an energy penalty has to be paid in order to activate the substrates and 'arrange' their geometries in a pre-TS way. Such energy penalty was calculated to be lower for a single contact N-H···O-P H-bond (mode A), in comparison with a formyl-like non-classical C-H···O-P interaction (mode C).

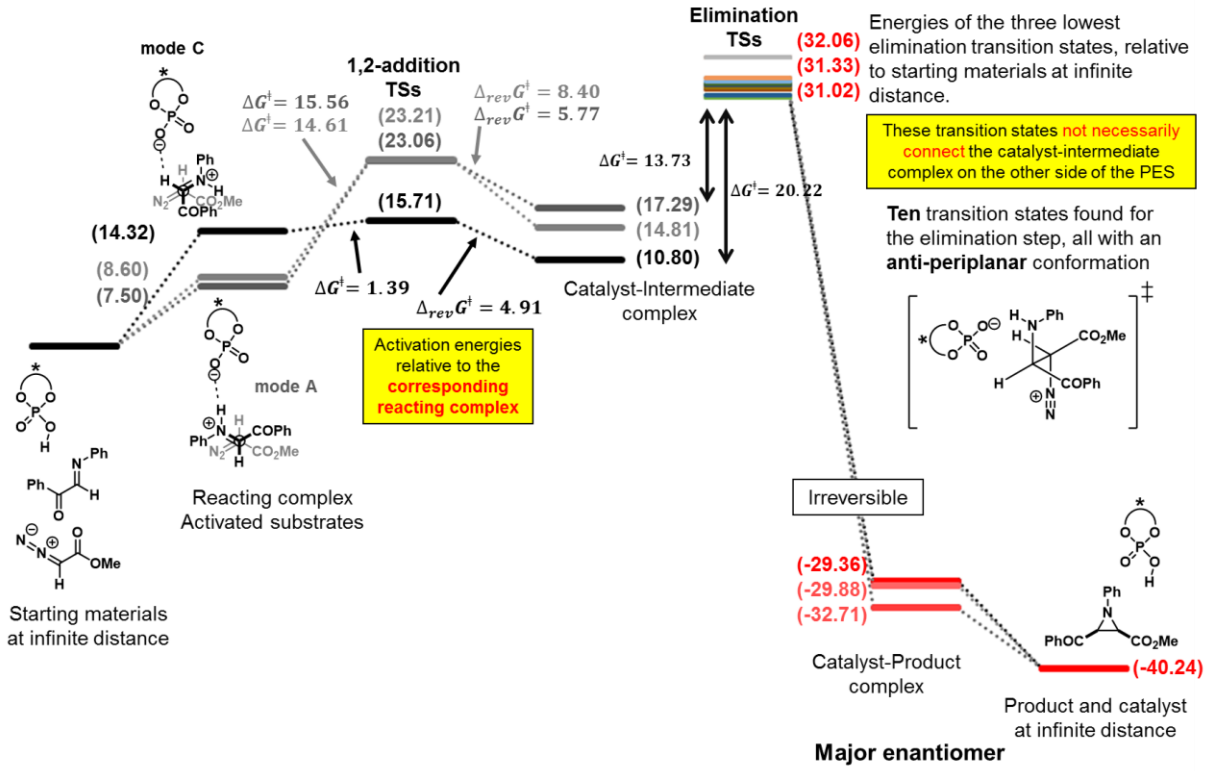

Figure 5.18: PES for the major enantiomer. Numbers in brackets correspond to Gibbs free energies relative to the starting materials and catalyst at an infinite distance (0.00). Energies are presented in kcal mol^{-1}. The full catalyst structure is not shown for clarity.

However, the catalyst-substrates complex is not telling the full story. When the lowest of the activated substrates goes up the PES towards the TS, it turns out that such a TS, with an activation mode A, has a 15.56 kcal mol^{-1} barrier height. On the other hand, for the activated complex *via* mode C, it only takes 1.39 kcal mol^{-1} to reach **TS1-2S3S**, which is activated through the non-classical C-H···O-P hydrogen bond. This yields the lowest-energy pathway as the resting intermediate-catalyst complex lies 10.80 kcal mol^{-1} above the separated starting species defining the PES's zero of energy. The other two intermediate-catalyst complexes were found 14.81 and 17.29 kcal mol^{-1} above this.

In order to construct the second half of the PES, the TSs corresponding to the nitrogen elimination step had to be found and calculated. Ten of such TSs, having the amino group and the leaving nitrogen in an *anti*-periplanar arrangement, were found. Surprisingly, the lowest-energy of these TSs was located at 31.02 kcal mol^{-1} in the PES. This is 20.22 kcal mol^{-1} above the lowest-energy catalyst-intermediate complex coming out of the 1,2- addition step. The remaining elimination TSs were found higher in energy. After the elimination step, the PES enters a thermodynamic sink down to the catalyst-product complex at -32.71 kcal mol^{-1}. Then, the product and catalyst at infinite distance were found at -40.24 kcal mol^{-1}.

A PES was also constructed for the minor enantiomer in a similar fashion (Figure 5.19). The section comprising the 1,2- addition step is in accordance with the enantioselectivity obtained previously (*cf.* Figures 5.15 and 5.16). In this case, the lowest-energy catalyst-intermediate complex was found at 12.77

kcal mol^{-1} relative to the infinitely separated starting materials, higher than the value calculated for the major enantiomer (10.80 kcal mol^{-1}).

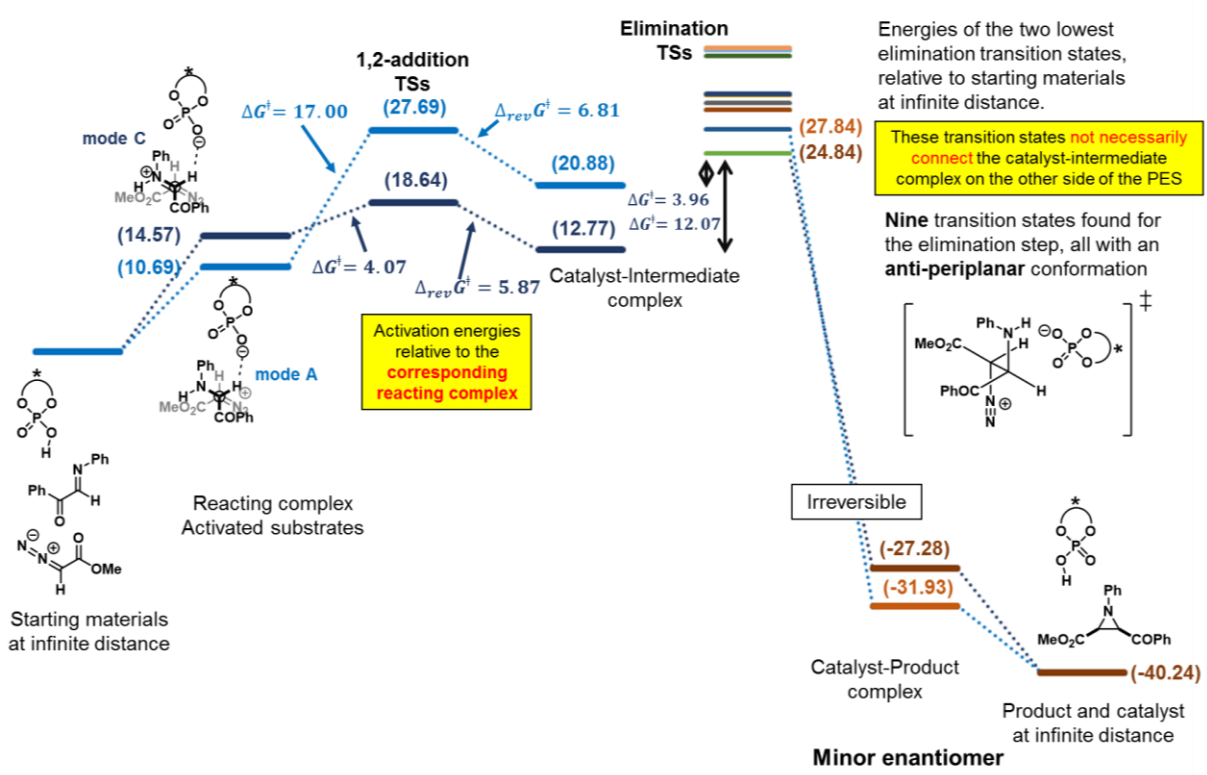

Figure 5.19: PES for the minor enantiomer. Numbers in brackets correspond to Gibbs free energies relative to the starting materials and catalyst at an infinite distance (0.00). Energies are presented in kcal mol^{-1}. The full catalyst structure is not shown for clarity.

For the second part of the PES, nine different TSs, with an *anti*-periplanar arrangement, were found for the elimination step. However, the lowest-energy catalyst-intermediate complex and the lowest-energy elimination TS were found 12.07 kcal mol^{-1} apart from each other. This gap is considerably smaller than the corresponding one for the major enantiomer (20.22 kcal mol^{-1}).

In both cases, for the major and the minor enantiomers, the calculated PESs suggest that the 1,2- addition step, despite being enantiodetermining, might not be rate-determining. If the reaction mechanism followed the PESs presented, a lower enantioselectivity would have been observed. Moreover, had the 1,2-addition step been reversible, the opposite sense of enantioinduction would have been observed. Thus, the second step, the nitrogen elimination, has to happen without assistance of the catalyst. Therefore, for this aza-Darzens reaction, in order to account for the sense and amount of enantioinduction, the enantiodetermining step is controlled by the catalyst, as calculated herein. Then, the catalyst-intermediate would have to dissociate for the elimination step to occur without the catalyst. Given that the two chiral centres are defined in the 1,2- addition step, an uncatalysed nitrogen extrusion seems feasible.

The next part of this computational project comprises the investigation of enantioinduction in the aza-Darzens reaction when catalyst *(R)-PA*-**4** was used. In this case, the authors of the article reported that good enantioselectivity was obtained with such catalyst. However, they observed the opposite sense of

enantioinduction as obtained with the silicon-based catalyst *(R)-PA*-**5.6**. Therefore, using the ONIOM approach, the aza-Darzens reaction with *(R)-PA*-**4** was investigated to find out how the catalyst transfers the chiral information and, how the opposite sense of enantioinduction arises from having different 3,3'-substituents but the same *(R)*-BINOL framework. Thus, the TS leading to the *(2R,3R)* intermediate has to be lower in energy than that for the other enantiomer *(2S,3S)*. This, assuming that the 1,2- addition step is enantiodetermining.

Sixteen TSs were found for the *(2S,3S)* intermediate within 22 kcal mol^{-1} and fifteen for the *(2R,3R)* enantiomer within 16 kcal mol^{-1}. The three lowest-energy TSs for enantiomer *(2S,3S)* and the three lowest-energy ones for enantiomer *(2R,3R)* are presented in Figure 5.20 on the next page. Surprisingly, the lowest-energy TS of them all was calculated for enantiomer *(2S,3S)* which is not in accordance with the sense of enantioinduction observed experimentally. **TS1a-2S3S** features an activation mode C, as found for the reaction with catalyst *(R)-PA*-**5.6**. In this TS, a formyl-like hydrogen bond is formed between the C-H moiety in the *(E)*-iminium and the phosphate motif (1.77 Å). In addition, another C-H···O-P interaction is formed with the diazo ester (2.32 Å). In this case, the iminium ion features an *(E)-s-cis* conformation, as found for the lowest-energy ground state iminium ion. Both of the substrates fit inside the chiral cavity of the catalyst.

On the other hand, the next lowest-energy **TS2a-2S3S** presents an activation mode A and is 3.60 kcal mol^{-1} above **TS1a-2S3S**. Herein, a single mono-contact hydrogen bond is formed with the N-H moiety (1.51 Å). In addition, the iminium ion has an *(E)-s-trans* conformation. This might be due to the fact that the chiral pocket in the catalyst is larger in comparison with the silicon-based scaffolds in the other one. Thus, there is enough space for the substrates to have more conformation flexibility, as suggested by the relatively long distance of the forming C-C bond, 2.82 Å. Such conformational flexibility, however, is limited in *(R)-PA*-**5.6** due to the large size of the catalyst's substituents that create a tighter chiral cavity. **TS3a-2S3S** was found 5.13 kcal mol^{-1} above and displays a bifunctional activation mode B. An N-H···O-P H-bond (1.47 Å) and a non-classical C-H···O-P interaction (2.44 Å) with the diazo ester defines such an activation mode. Herein, the iminium ion has an *(E)-s-trans* conformation as well, presumably also to the unhindered active site of the catalyst.

In sharp contrast, the three lowest-energy TSs leading to the other enantiomer were found featuring a bifunctional activation mode B. This is surprising as the vast majority of the calculated TSs have an activation mode C. In addition, the two-lowest energy TSs have an *(E)-s-trans* iminium ion. Once again, the less restricted chiral pocket in this catalyst allows for more conformational flexibility in the TSs.

TS1a-2R3R was found 2.68 kcal mol^{-1} above **TS1a-2S3S**. This energy difference gives a calculated 98.6% *ee* in favour of the *(2S,3S)* enantiomer. This value is higher than that obtained for the more hindered catalyst *(R)-PA*-**5.6**. In addition, the reported sense of enantioinduction could not be obtained with the ONIOM approach of the full catalyst. There are a number of reasons to explain why this model 'failed' predicting the sense of enantioinduction with catalyst *(R)-PA*-**4**.

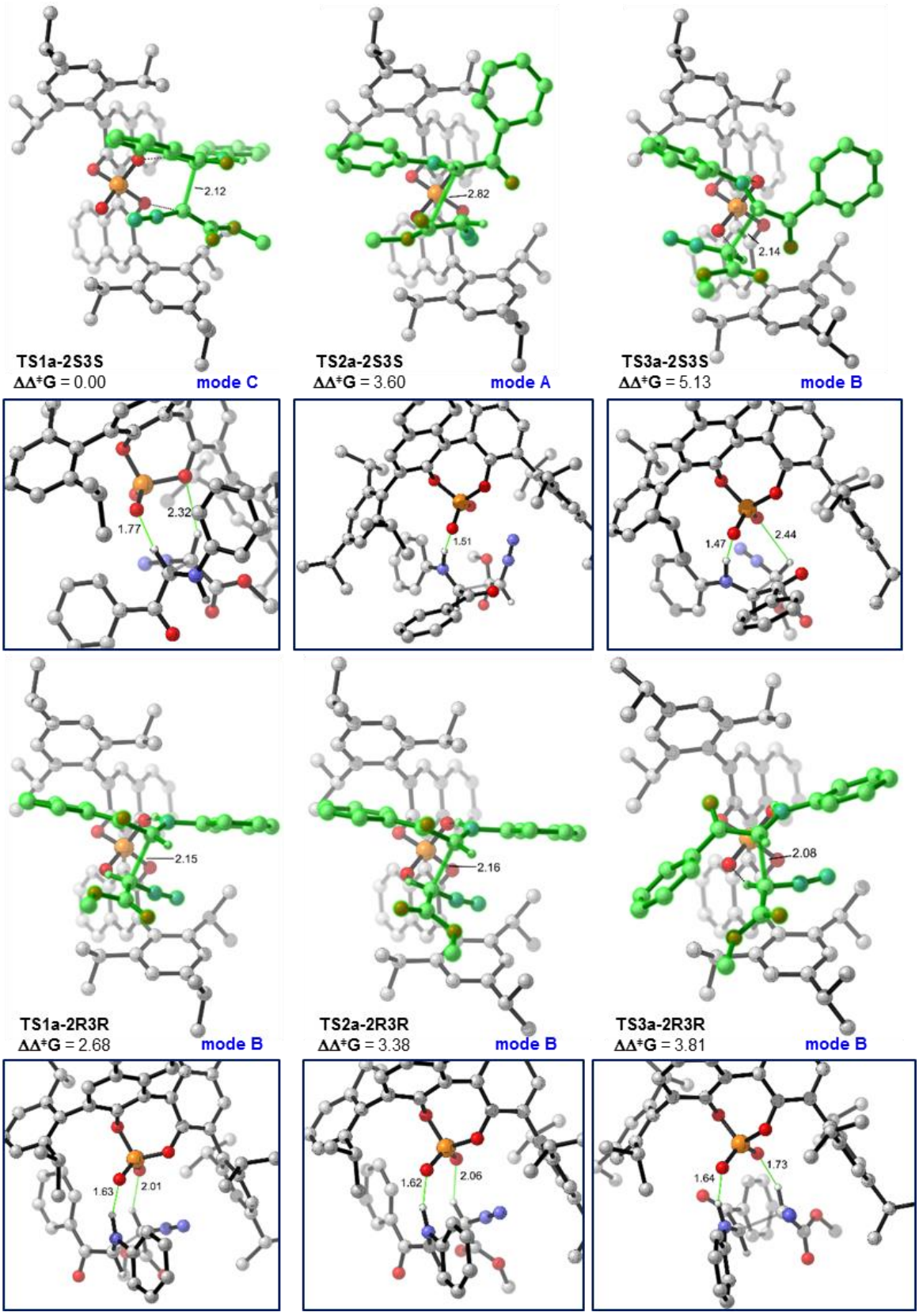

Figure 5.20: End-on projections and close-ups for the three lowest-energy TSs leading to the intermediate major (top two rows) and minor (bottom two rows) enantiomers. Substrates are highlighted in green in the end-on projections for clarity. Energies are presented in kcal mol^{-1} and distances in Å. Non-critical H-atoms are omitted for clarity.

To start with, the active site in catalyst *(R)-PA*-**4** is considerably less hindered than in *(R)-PA*-**5.6**. A more open active site in the former catalyst is likely to allow a much larger number of conformations in the reacting substrates. Therefore, the wrong prediction in the sense of enantioinduction might be attributed to an incomplete conformation search. It can be the case, for the *(2R,3R)* enantiomer that lower energy TS could have been missed in the conformation search. Thus, a more exhaustive conformation search would be one way to address this problem, whether using different conformation search methods or a different force field. Another source of error might be coming from the MM layer in the ONIOM optimisation. However, the UFF has shown good results for modelling 3,3'- aryl scaffolds in PAs.[66,143,310] A more expensive alternative to an ONIOM approach would be modelling the full-catalyst TSs with DFT. Yet, due to the size of the catalyst and the larger number of conformers to be optimised, this might not be the quickest way to study this or similar reactions.

In retrospect, an activation mode C provides the right answer for the sense and amount of enantioinduction observed in the reaction. In such activation mode, the active site of the catalyst locks the iminium ion through a non-classic hydrogen bond established between one of the oxygen atoms in the phosphate motif and a formyl-like C-H moiety in the iminium. The qualitative models described herein—and presented in Figure 5.21—provide a suitable explanation for the stereochemical output. **TS1-2S3S** is favoured over **TS1-2R3R** as it minimises the steric clash of the iminium ion with the catalyst's 3,3' scaffolds. This, however, is not the case for the minor enantiomer. In addition, although the low selectivity, this model also gives the correct diastereoisomer.

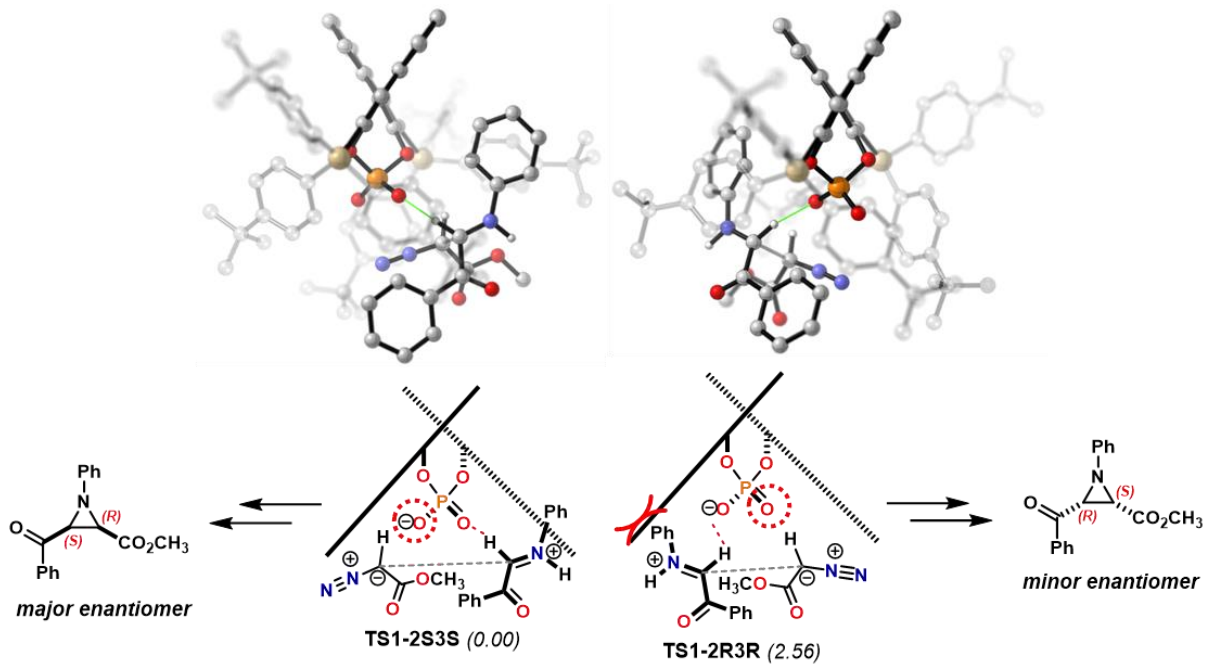

Figure 5.21: Models to account for enantioselectivity. The 3D pictures of the calculated TSs are provided to show the predictive power of the qualitative diagrams. Non-critical hydrogens are omitted for clarity. The aryl groups attached to the silicon atoms are grayed-out for easier visualisation. Energies in parenthesis are given in kcal mol^{-1}.

Retrospect and Conclusions

Enantioselective catalysis is a challenging field. Choosing the right catalyst for a chemical reaction is not always an easy task. Making new molecules and explaining the results of such transformations are part of the skills of an organic chemist.

Throughout the chapters, several conclusions were drawn where appropriate or at the end of each section. However, herein are presented the highlights of the research.

Amongst the huge variety of chiral Brønsted acids, new phosphoric acids were introduced. Methodologies were developed for the synthesis of heavily hindered PAs bearing massive silicon-based scaffolds in the 3,3' positions. In addition, a new type of 3,3' group, based on aryl sulfones, was also developed. Although enantioselectivities were not high for the reactions where these catalysts were tried, it is expected that these molecules would be useful in other asymmetric transformations, whether as chiral Brønsted acids or ligands.

A systematic study was conducted regarding the synthesis of 1,3-oxathiolanes in an enantioselective fashion. Therein, several reaction parameters were varied, including time, temperature, solvent, equivalents of reagents and catalysts. Amongst the screened catalysts, it was found that the synthesis of the compounds under study could be done enantioselectively using PAs or NTPAs. One of the remarkable findings was that the catalyst loading of NTPAs could be lowered to 0.5 mol%. This highlights the superior acidity of NTPAs in comparison with PAs. In addition, such a low catalyst loading was found to be the optimal for a good reactivity-enantioselectivity balance.

Serendipity was also part of this work. The synthesis of a complex chiral polyheterocycle **4.80** was demonstrated to proceed with modest yields and enantioselectivity. One of the remarkable features of this reaction is the impressive level of diastereocontrol, in which the product was obtained as a single diastereoisomer. Furthermore, a suitable reaction mechanism was provided to account for the stereochemical output.

Substantial part of this work comprised the design of ring-closing reactions to afford *N*-heterocycles in an enantioselective fashion. In this context, a Pictet-Spengler reaction was shown to provide access to seven-membered heterocycles. A variety of chiral PAs and NTPAs were evaluated in these transformations, showing that the aforementioned products can be obtained in good yields and in an asymmetric fashion. An iminium ion was proposed to be the reactive intermediate. In addition, it was demonstrated that the use of powdered molecular sieves as water-catching additives in these reactions is detrimental. In this case, the sieves acted as Lewis acids to catalyse the racemic background reaction. Thus, powdered molecular sieves are not recommended in reactions involving iminium ions if the purpose is to achieve enantioselective ring closures.

Finally, an enantioselective aza-Darzens reaction, reported by the group of Akiyama, was studied in a computational perspective. This, in order to account for the stereochemical output. For that purpose, the

ONIOM method was used to calculate the system with the full catalyst. Through these calculations, an alternative mode of activation for the imine substrate was envisaged, different from the usual N-H hydrogen bonding with the catalyst. Therein, the imine is protonated by the acid and the resulting iminium ion interacts with the catalyst through non-classical C-H hydrogen bonds. This activation mode (mode C) was shown to be the lowest in energy. Yet, most importantly, the model developed herein provided the correct amount and sense of enantioinduction as reported by Akiyama and co-workers. In addition, albeit with low diastereoselectivity, the correct diastereoisomer was predicted. Moreover, the findings of these calculations were summarised in sketches that account, in a qualitative way, for the stereochemical output. In most cases, alternative, unconventional or unusual reaction mechanisms can be difficult to prove experimentally. Computational chemistry, whether combined with experiments or on its own, offers useful insights. Such a synergistic experiment-calculation approach is a powerful dyad when understanding chemical transformations, and definitely valuable in the development of asymmetric and catalytic reactions.

Appendix 1

Computational Details—Chapter 5

A1.1. General Remarks

Gas-phase conformation searches were performed using MacroModel interfaced to the Maestro 11 programme.[311] The Monte Carlo Multiple Minimum (MCMM) torsional sampling method was used to generate the initial set of conformers.[312] A maximum of 10000 step was set up to find the most relevant conformers at least 10 times, using an energy window of 15.30 kcal mol^{-1} and a RMSD cut-off of 0.25 Å to eliminate redundant conformers. The OPLS3 force field was used,[118] as implemented on MacroModel, setting a 0.01 threshold converging on gradient. The initial geometries for the conformation searches were generated in the Maestro 11 interface. After the initial set of conformers was acquired, a second redundant conformer elimination was performed using the OPLS3 force field with a RMSD cut-off of 0.25 Å. Such a set was used as initial geometries for the DFT calculations. Further specific details are given in the following relevant sections.

DFT calculations were performed using the Gaussian 16 Rev. A.01 suit of programmes.[313] Specific details, such as the levels of theory employed—*i.e.* DFT functionals, basis sets, solvent models, ONIOM calculations—are given in the following relevant sections. Frequency calculations were conducted on each local minima and transition states, using the same level of theory at which the optimisation was performed, to confirm the nature of the stationary point (freq=noraman). In addition, IRC calculations were done on each TS to verify that it connected the desired local minima on each side of the PES.[314] Ultrafine integration grid was used in all the calculations (integral=grid=ultrafine).

DFT input geometries were prepared and visualised using the GaussView 6 programme.[315] The structures presented in the thesis were generated with the CYLview programme.[316]

Output files for the optimised structures—local minima and TSs—as well as the full list of energies and imaginary frequencies for TSs, are available at the University of Cambridge data repository Apollo (https://doi.org/10.17863/CAM.59358)

A1.2. Starting materials: The uncatalysed reaction

The following computational details and methods account for the results presented on section 5.3.

Input ground state geometries for the starting materials were generated using conformation searches as mentioned in section A1.1. *(E)* and *(Z)* imine and iminium geometries were acquired from the conformation searches regardless the initial input due to the pre-set high energy threshold. The different conformations (E)-s-cis, (E)-s-trans, (Z)-s-cis, (Z)-s-trans, were filtered by visual inspection of the full set

of generated conformers after the second redundant elimination step and were used as input structures for the ground state DFT calculations.

DFT geometry optimisations were done in the gas phase using the ωB97X-D functional[317] and the split valence 6-31G(*d*) basis set.[318] After the optimisations, single-point energies were calculated using the same functional but the def2-TZVPP.[319] Such SP energies were used to correct the calculated Gibbs free energies at the lower level of theory, ωB97X-D/6-31G(*d*). This approach of using two different levels of theory has been shown to be time-efficient in order to calculate accurate energy values, as shown by the group of Goodman.[145] Using this approach, the group of Rzepa benchmarked several DFT functionals and basis sets.[320] Therein, they found that the ωB97X-D functional is one of the best ones to accurately model molecular geometries. In addition, they suggest a triple-ζ basis set in the SP energy step for optimal results. In addition, the group of Jensen also suggest the functional as a suitable one to model chemical processes.[321] Thus, the ωB97X-D/def2-TZVPP // ωB97X-D/6-31G(*d*) level of theory was consistently used throughout the DFT calculations in Chapter 5.

Optimised geometries and energies for intermediates *anti*-**5.10** and *syn*-**5.10** (Figure 5.6) were obtained in the same fashion as mentioned above for the starting materials.

The initial geometries for the TSs presented in Figure 5.8 were generated by hand taking into account the following features: 1) *E*/*Z* configuration of the iminium ion, 2) *s-cis*/ *s-trans* conformers of the iminium, 3) *s-cis*/ *s-trans* conformers of diazo ester **5.9** and 4) three different staggered rotamers (Figure 5.7). This yielded 24 possible combinations. Each input structure was generated individually, optimised at the ωB97X-D/6-31G(*d*) level of theory and SP energy-corrected at the ωB97X-D/def2-TZVPP one. As mentioned in the thesis, not all of these starting structures converged into the desired geometry.

A1.3. Model catalyst approach: Activation modes

The following computational details and methods account for the results presented on section 5.4.

TSs optimisation was conducted in the gas phase at the ωB97X-D/6-31G(*d*) level of theory and the Gibbs free energies were corrected with a SP energy calculation at the ωB97X-D/def2-TZVPP level, also in the gas phase. The opt=(ts, noeigen, cartesian) set of key words in Gaussian provided the most suitable.

Each initial TS structure was constructed individually. For such, each of the TS structures from Figure 5.7 were taken and used to build three input files, each with a different activation mode. As discussed in the thesis, not all of these initial geometries managed to converged after several attempts or converged to similar TSs. The geometrically different TSs for each activation mode are those presented in Figure 5.12.

A1.4. Full catalyst approach: Enantioselectivity

The following computational details and methods account for the results presented on section 5.5.

In order to model the reaction with the full catalyst, the ONIOM method was used.[322,323] This approach has been utilised to model chemical reactions with several atoms.[306,324] For instance, the group of Goodman has shown that the ONIOM method is a suitable one to calculate TSs for chiral PA-catalysed reactions.[143,310]

A schematic standard work flow to model the TSs for the 1,2- addition step is shown in Figure A1, using the *(2S,3S)*-enantiomer as an example.

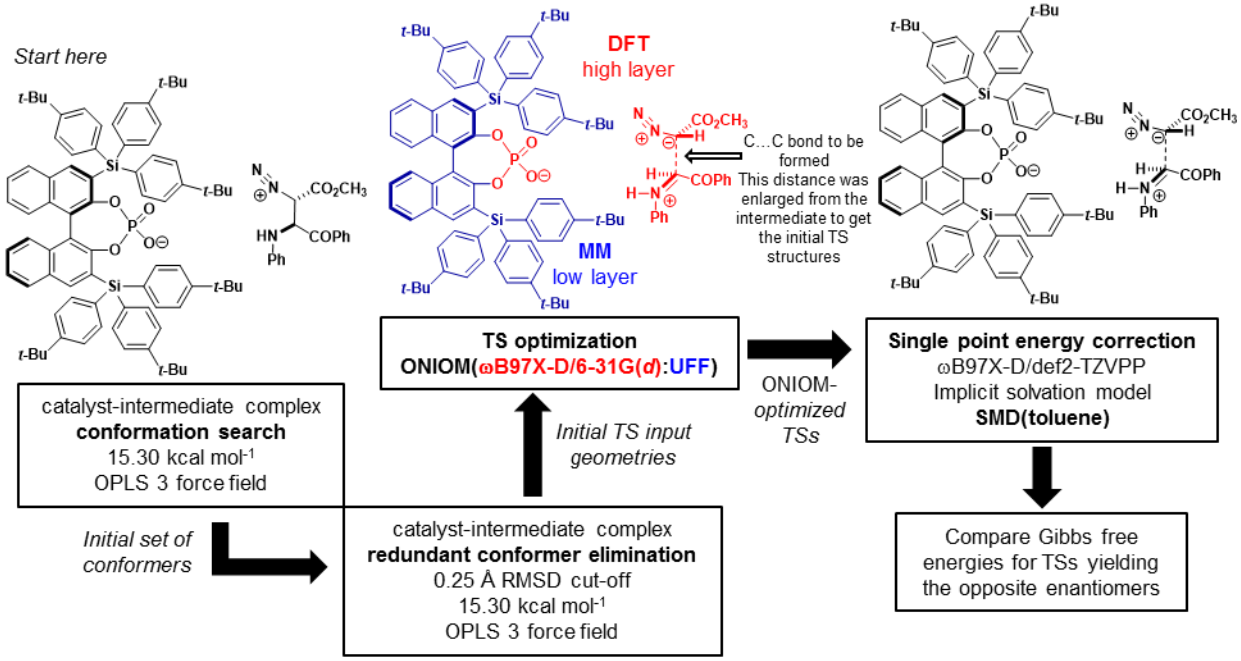

Figure A1: Standard work flow for modelling the reaction with the full catalyst.

As starting point, an initial set of conformers was generated. This one, corresponding to the catalyst-intermediate complex. After the initial conformation search, the obtained conformers underwent a second redundant conformer elimination. The settings for the conformation searches were those outlined in section A1.1. Due to the highly confined active site of the catalyst, unconstrained conformation searches were conducted. In order to build the initial TS geometries, the structures from the conformation searches were taken and the distance of the forming C···C bond was enlarged to resemble that of a TS. This was done manually for each of the conformers.

TS optimisation was done using a two-layer ONIOM method. The high layer was defined by the reacting substrates and the active site of the catalyst—the phosphate group. Such layer was treated with DFT at the ωB97X-D/6-31G(*d*) level of theory. On the other hand, the low layer was defined by the backbone of the catalyst and the 3,3'- substituents. This was modelled with MM using the Universal Force Field (UFF) as implemented in Gaussian.[325] The layer division was chosen taking into account that the actual chemical reaction happens in the active site, thus, the phosphate groups and the reacting substrates are

better described at a quantum chemical lever. However, the catalyst backbone and scaffolds play a steric role, which can be modelled using molecular mechanics. These calculations were conducted in the gas phase.

Taking the ONIOM optimised geometries, SP energy calculations were done on each structure at the ωB97X-D/def2-TZVPP level of theory to correct the Gibbs free energies. Herein, an implicit solvation model was included to account for solvent effects in the reaction. The SMD(toluene) model was chosen for such a purpose.[326]

This workflow was conducted for each of the intermediates of the 1,2- addition step. For the TSs using catalyst *(R)-PA*-**4** the same workflow and levels of theory were used.

Appendix 2

Experimental Details

A2.1. General Remarks and Methods

Solvents for reactions were purified by standard methods. Tetrahydrofuran (THF) and diethyl ether (Et_2O) were pre-dried over sodium wire and distilled from potassium/benzophenone ketyl. Dichloromethane (CH_2Cl_2), acetonitrile (MeCN), propionitrile (EtCN), triethylamine (Et_3N), tetramethylethylenediamine (TMEDA), pyridine (py), benzene and toluene were distilled from CaH_2. Chloroform was dried over activated 4Å molecular sieves. DMF and *m*-xylene were purchased anhydrous in sure-sealed bottles. Molecular sieves were dried by microwave heating followed vacuum heating, then allowed to cool down in vacuum.

Chemicals were used as received unless otherwise specified. Organolithium reagents were titrated using *N*-benzyl benzamide or menthol/bipyridine. Zinc dust was activated by washing with 2% HCl(aq), water, acetone, ether and by heating under vacuum The prepared catalysts (PAs and NTPAs) were stored in a dissecator under argon atmosphere.

Reactions were carried out under an argon atmosphere using oven-dried glassware, unless otherwise specified. Reactions were followed by thin layer chromatography (TLC) using Merck Kieselgel 60 F254 plates. For visualisation, UV light, $KMnO_4$ or phophomolybdic acid/$Ce_2(SO_4)_3$ stains were used. Column chromatography was carried out using Merck Kiesel 60 silica gel (230-400 mesh) under a compressed air positive pressure.

NMR spectra were recorded using one of the following spectrometers: Bruker 400 MHz AVIII HD Smart Probe, Bruker 400 MHz AVIII QNP cryoprobe, Bruker 600 MHz Avance BBI or Bruker 700 MHz AVII+ TBO probe. Spectra were recorded with an internal deuterium lock and are referenced to the residual non-deuterated solvent peak ($CHCl_3$ at 7.26 ppm ^{1}H-NMR, 77.16 ppm ^{13}C-NMR), (C_6H_6 at 7.16 ppm ^{1}H-NMR, 128.06 ppm ^{13}C-NMR), (DMSO at 2.50 ppm ^{1}H-NMR, 39.52 ppm ^{13}C-NMR). ^{1}H-NMR data is reported as follows: chemical shift in ppm, multiplicity (s=singlet, d=doublet, t=triplet, q=quartet, quint=quintet, sext=sextet, sept=septet, multiplet=m), coupling constants *J* in Hz and integration. ^{19}F and ^{31}P NMR spectra were recorded on a Bruker 400 MHz AVIII HD with complete proton decoupling.

High-resolution mass spectra (HRMS) for relevant compounds were recorded by the Department of Chemistry Mass Spectrometry Service (Cambridge, UK) using electrospray (ES+) and electron ionisation (EI) techniques, values are reported to 4 decimal places and are within 5 ppm of the calculated value.

Optical rotations were measured at the sodium D-line (589 nm) in chloroform using a Perkin-Elmer 343 polarimeter; the values are reported in degrees as $[\alpha]_D$ with the concentration, *c*, in g/100 mL and the temperature at which they were recorded.

Melting points were measured on a hot-stage apparatus and are uncorrected.

Enantiomeric ratios were determined by chiral SCF on a Waters ACQUITY UPC2 system with YMC CHIRAL ART SB, SJ or SC columns in a mixed solvent system of supercritical CO_2 and methanol.

A2.2. Molecules from Chapter 2

(R)-2,2'-*bis*(methoxymethoxy)-1,1'-binaphthalene **2.3**

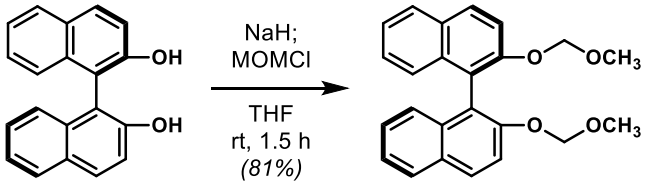

2.2 **2.3**

NaH (1.26 g, 31.5 mmol, 3.0 equiv. 60% dispersion in mineral oil), was washed twice with dry hexane (12 mL) and suspended in dry THF (20 mL). In an ice bath, a solution of *(R)*-BINOL **2.2** (2.99 g, 10.5 mmol, 1.0 equiv.) in dry THF (20 mL) was added *via* cannula. A yellow colouration and H_2 evolution was observed. After addition, the mixture was stirred for 1 h at rt until H_2 evolution ceased. The reaction was cooled in an ice bath and MOMCl (5 mL, 32.9 mmol, 3.1 equiv. 50% solution in MeOAc, freshly prepared) was dropwise added. After addition, the ice bath was removed and the reaction stirred at rt for 1.5 h. An intense yellow colour was observed at the beginning and vanished as the reaction proceeded, observing a white precipitate. The reaction was quenched with the dropwise addition of NH_4Cl (15 mL, saturated solution). The solvent was removed *in vacuo* and the residue partitioned with water (15 mL) and DCM (15 mL). The organic layer was separated and the aqueous phase extracted with DCM (15 mL x3). The combined organic layers were dried over $MgSO_4$ and the solvent partially removed *in vacuo* until *ca.* 1/10 the initial volume. Precipitation with methanol followed by vacuum filtration afforded the desired product (3.20 g, 8.53 mmol, 81%).

Spectral data consistent with the literature[141]

Physical state: white solid

TLC: R_f= 0.34 (25% EtOAc in PE)

mp: 101-103 °C

^{1}H NMR (400 MHz, $CDCl_3$): δ 7.95 (d, *J* = 9.0 Hz, 2H), 7.87 (d, *J* = 8.0 Hz, 2H), 7.61 (d, *J* = 9.0 Hz, 2H), 7.34 (m, 2H), 7.23 (d, *J* = 3.7 Hz, 4H), 5.09 (d, *J* = 6.7 Hz, 2H), 4.98 (d, *J* = 6.6 Hz, 2H), 3.15 (s, 6H)

^{13}C NMR (100 MHz, $CDCl_3$): δ 152.7, 134.1, 129.9, 129.4, 127.9, 126.3, 125.6, 124.1, 121.3, 117.2, 95.1, 55.8

Procedure for MOMCl solution, 50% in MeOAc:[96] A 100 mL three-neck, round bottom flask was fitted with thermometer, condenser and rubber septa and charged with dimethoxymethane (11.5 mL, 130 mmol, 1.0 equiv.) and $ZnBr_2$ (spatula tip, catalytic amount). At rt, acetyl chloride (9.25 mL, 130 mmol, 1.0 equiv.) was dropwise added, slowly. The reaction warms up gently. Temperature was not allowed to go further than 45 °C with a water bath. After 3 h, the MOMCl solution was ready to be used. The solution can be stored for several months under nitrogen in the fridge.

^{1}H NMR (400 MHz, $CDCl_3$): δ 5.46 (s, 2H, MOMCl), 3.66 (s, 3H, MeOAc), 3.51 (s, 3H, MOMCl), 2.05 (s, 3H, MeOAc)

(R)-3,3'-diiodo-2,2'-*bis*(methoxymethoxy)-1,1'-binaphthalene

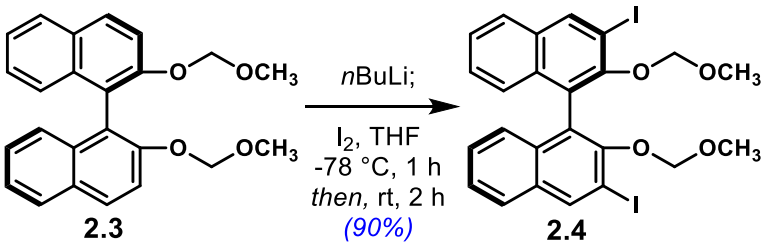

2.3 **2.4**

A round bottom flask was charged with **2.3** (2.03 g, 5.34 mmol, 1.0 equiv.), evacuated, refilled with argon (x3) and dissolved in dry THF (23 mL). At -78 °C (dry ice – acetone bath), *n*BuLi (8.6 mL, 12.8 mmol, 2.4 equiv. 1.5 M solution in hexanes) was dropwise added over 20 min. A yellow solution was observed. After addition, the reaction was stirred for 1 h in an ice bath; after that time, a beige suspension is formed. At -78 °C (dry ice – acetone bath), a solution of iodine (3.79 g, 14.9 mmol, 2.8 equiv.) in dry THF (20 mL, +2 mL rinse) was dropwise added *via* cannula **in the dark**. After addition, the reaction was stirred at -78 °C for 1 h. The dry ice-acetone bath was removed and the reaction stirred for 2 h. The reaction was quenched with $Na_2S_2O_3$ (80 mL, saturated solution) and vigorously stirred for 30 min. The organic layer was separated and the aqueous phase extracted with Et_2O (40 mL x3). The combined organic layers were dried over $MgSO_4$ and the solvent removed *in vacuo*. Column chromatography (5% EtOAc in PE) afforded the pure product (3.02 g, 4.83 mmol, 90%).

Spectral data consistent with the literature[327]

Physical state: light yellow foam

TLC: R_f= 0.48 (20% EtOAc in PE)

^{1}H NMR (400 MHz, $CDCl_3$): δ 8.54 (s, 2H), 7.78 (d, *J* = 8.2 Hz, 2H), 7.43 (m, 2H), 7.30 (m, 2H), 7.17 (d, *J* = 8.5 Hz, 2H), 4.81 (d, *J* = 5.7 Hz, 2H), 4.70 (d, *J* = 5.7 Hz, 2H), 2.60 (s, 6H)

^{13}C NMR (100 MHz, $CDCl_3$): δ 152.3, 140.2, 134.0, 132.4, 127.3, 126.9, 126.7, 126.4, 126.0, 99.6, 92.6, 56.7

(R)-3,3'-diiodo-1,1'-binaphthalene-2,2'-diol

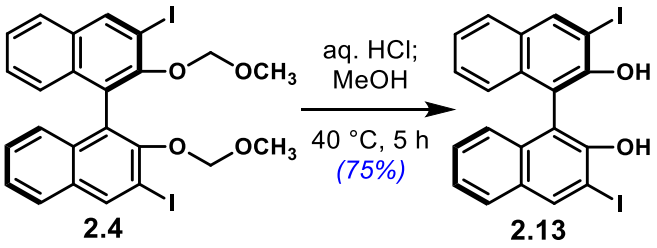

2.4 **2.13**

Note: *There is no need to use dry glassware, dry solvents or argon atmosphere for this reaction.*

MOM-protected BINOL **2.4** (548 mg, 0.875 mmol, 1.0 equiv.) was suspended in methanol (12 mL). At rt, a solution of conc. HCl (0.5 mL) in methanol (6 mL) was added in one portion. After stirring at 40 °C for 4 h, the solvent was removed *in vacuo* and the residue partitioned in Et_2O (16 mL) and water (10 mL). The organic layer was separated and the aqueous phase extracted with Et_2O (10 mL, x3). The combined organic layers were dried over $MgSO_4$ and the solvent removed *in vacuo*. Azeotropic drying with benzene (8 mL, x3) afforded the pure product (354 mg, 0.658 mmol, 75%).

Spectral data consistent with the literature[141]

Physical state: yellowish powder

TLC: R_f= 0.30 (20% EtOAc in hexane)

^{1}H NMR (400 MHz, *d*$_6$-DMSO): δ 8.17 (s, 2H), 7.73 (s, 2H), 7.02 (d, *J*=8.0 Hz, 2H), 6.44 (t, *J*=7.4 Hz, 2H), 6.38 (t, *J*=7.5 Hz, 2H), 5.92 (d, *J*=8.4 Hz, 2H)

^{13}C NMR (100 MHz, *d*$_6$-DMSO): δ 151.7, 139.1, 133.7, 130.0, 126.8, 123.9, 123.4, 114.3, 90.5

(R)-3,3'-dibromo-2,2'-*bis*(methoxymethoxy)-1,1'-binaphthalene **2.25**

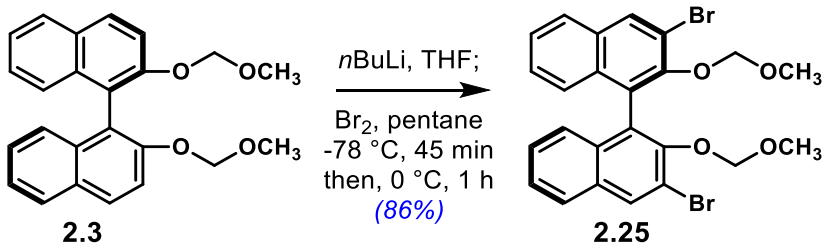

2.3 **2.25**

Important: *Sticking to the following procedure is crucial for the success of this reaction.* ***n-butyl lithium:*** *Titrate solution prior to use, N-benzyl benzamide*[328] *or menthol/bipyridine*[329] *methods yield similar results. If properly stored under argon and in the fridge, the concentration and quality of the solution are well preserved even after several months. Use a new bottle if possible.*

A round bottom flask was charged with **A-2** (3.00 g, 8.0 mmol, 1.0 equiv.), evacuated, refilled with argon (x3) and dissolved in dry THF (24 mL). At -78 °C (dry ice – acetone bath), *n*BuLi (12.8 mL, 19.2 mmol, 2.4 equiv. 1.5 M solution in hexanes) was dropwise added. A yellow solution was obtained. After addition, the reaction was stirred for 1 h in an ice bath; after that time, a beige suspension is formed. Then, at -78 °C (dry ice – acetone bath), a solution of bromine (1.3 mL, 24.0 mmol, 3.0 equiv.) in pentane (6.0 mL, dried over 4A MS) is dropwise added over *ca.* 20 min. After addition, the reaction was stirred at -78 °C for 45 min and for an additional 1 h in an ice bath. The reaction was quenched with $Na_2S_2O_3$ (80 mL, saturated solution) and vigorously stirred for 30 min. Water (40 mL) was added to dissolve the solids. The organic layer was separated and the aqueous phase extracted with EtOAc (25 mL x3). The combined organic layers were washed with brine (50 mL), dried over $MgSO_4$ and the solvent removed *in vacuo*. Column chromatography (5% EtOAc in PE) afforded the pure product (3.65 g, 6.86 mmol, 86%).

Spectral data consistent with the literature[134]

Physical state: white solid or white foam

TLC: R_f= 0.38 (20% EtOAc in PE)

mp: 100-103 °C (recrystallized from hexane)

^{1}H NMR (400 MHz, $CDCl_3$): δ 8.28 (s, 2H), 7.81 (d, *J* = 8.2 Hz, 2H), 7.44 (ddd, *J* = 8.1, 6.9, 1.1 Hz, 2H), 7.31 (ddd, *J* = 8.1, 6.8, 1.2 Hz, 2H), 7.20 (d, *J* = 8.5 Hz, 2H), 4.83 (q, *J* = 5.8 Hz, 4H), 2.58 (s, 6H)

^{13}C NMR (100 MHz, $CDCl_3$): δ 150.2, 133.2, 133.1, 131.6, 127.5, 127.0, 126.7, 126.2, 117.5, 99.3, 56.4

(R)-3,3'-dibromo-1,1'-binaphthalene-2,2'-diol **2.21**

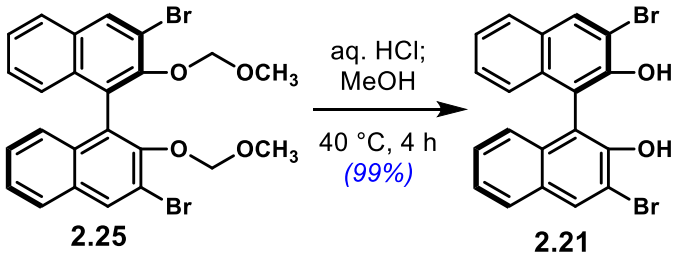

2.25 **2.21**

Note: *There is no need to use dry glassware, dry solvents or argon atmosphere for this reaction.*

MOM-protected BINOL **2.25** (3.52 g, 6.61 mmol, 1.0 equiv.) was suspended in methanol (90 mL). At rt, a solution of conc. HCl (3.8 mL) in methanol (45 mL) was added in one portion. After stirring at 40 °C for 4 h, the solvent was removed *in vacuo* and the residue partitioned in Et_2O (120 mL) and water (40 mL). The organic layer was separated and the aqueous phase extracted with Et_2O (40 mL, x3). The combined organic layers were dried over $MgSO_4$ and the solvent removed *in vacuo*. Azeotropic with benzene (8 mL, x3) afforded the pure product (2.90 g, 6.53 mmol, 99%).

Spectral data consistent with the literature[134]

Physical state: yellowish powder

TLC: R_f= 0.32 (20% EtOAc in hexane)

^{1}H NMR (400 MHz, $CDCl_3$): δ 8.26 (s, 2H), 7.82 (d, *J*=8.1 Hz, 2H), 7.38 (dd, *J*=11.1, 3.9 Hz, 2H), 7.31 (m, 2H), 7.10 (d, *J*=8.4 Hz, 2H), 5.54 (s, 2H)

^{13}C NMR (100 MHz, $CDCl_3$): δ 148.2, 132.9, 129.9, 127.7, 127.6, 125.0, 124.8, 114.8, 112.4

(R)-3,3'-*bis*(2,3,4,5,6-pentafluorophenyl)-1,1'-binaphthalene-2,2'-diol-phosphoric acid *(R)-PA*-**3**

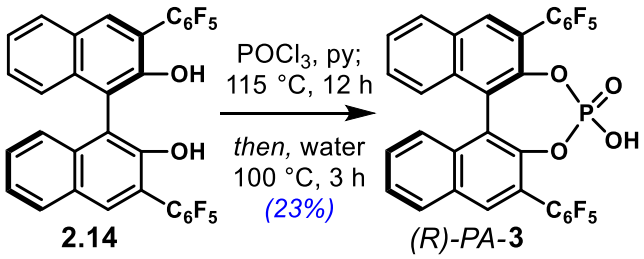

2.14 *(R)-PA*-**3**

A round bottom flask was charged with the BINOL precursor **2.14** (516 mg, 0.83 mmol, 1.0 equiv.) and dried in high vacuum for at least 2 h. Then, the flask was filled with argon the starting material dissolved in dry pyridine (1.7 mL). At rt, phosphorus (V) oxychloride (240 μL, 3.15 mmol, 3.0 equiv.) was added in one portion. A white precipitate is formed after *ca*. 15 min. The mixture was heated to 115 °C and stirred for 12 h. Then, the mixture was cooled down to rt and water (1.7 mL) added dropwise. ***Caution:*** *The reaction is highly exothermic!* A white precipitate is formed. The reaction is then heated to 100 °C and stirred vigorously for 3 h –the precipitate dissolves upon heating. After that, the mixture was cooled down to rt and CH_2Cl_2 was added (5 mL) followed by 1 N HCl (5 mL). The biphasic system was stirred until no solids were observed. The aqueous layer is separated and the organic phase washed with 1 N HCl (5 mL, x2). After the second HCl extraction, the organic phase seems to be pyridine-free –second aqueous wash pH 0. The organic layer was dried over $MgSO_4$ and the solvent removed *in vacuo*. Column chromatography (EtOAc) afforded the clean product as a metals salt. This was dissolved in EtOAc (10 mL) and washed with 6 N HCl (5 mL, x4), the organic layer was then dried over $MgSO_4$ and the solvent removed *in vacuo* to afford the free acid (127 mg, 0.18 mmol, 23%).

Spectral data consistent with the literature[99]

Physical state: light orange powder

TLC: R_f= 0.31 (EtOAc). *Intense bright spot under UV*.

mp: 221-225 °C

$[\alpha]_D$: -154.5° (c=0.81, 25 °C)

^{1}H NMR (700 MHz, $CDCl_3$): δ 8.04 (s, 2H), 8.02 (d, *J*=8.2 Hz, 2H), 7.60 (t, *J*=7.5, 2H), 7.51 (d, *J*=8.5 Hz, 2H), 7.45 (m, 2H)

^{13}C NMR (175 MHz, $CDCl_3$): δ 144.3, 133.8, 133.0, 131.5, 128.9, 128.1, 127.3, 126.9, 122.5, 118.8, 110.8, 110.7

^{31}P NMR (100 MHz, $CDCl_3$): δ 3.94

^{19}F NMR (100 MHz, $CDCl_3$): δ -139.8 (ddd, *J*=872, 22, 7.8 Hz, 5F), -154.4 (t, *J*=21 Hz, 2F), -162.5 (dtd, *J*=357, 22, 7.8 Hz, 5F)

HRMS (m/z): Calc. for $C_{32}H_{12}O_4F_{10}P$: 618.0314. Found: 681.0311

(R)-3,3'-bis(3,5-bis(trifluoromethyl)phenyl)-2,2'-bis(methoxymethoxy)-1,1'-binaphthalene **2.15**

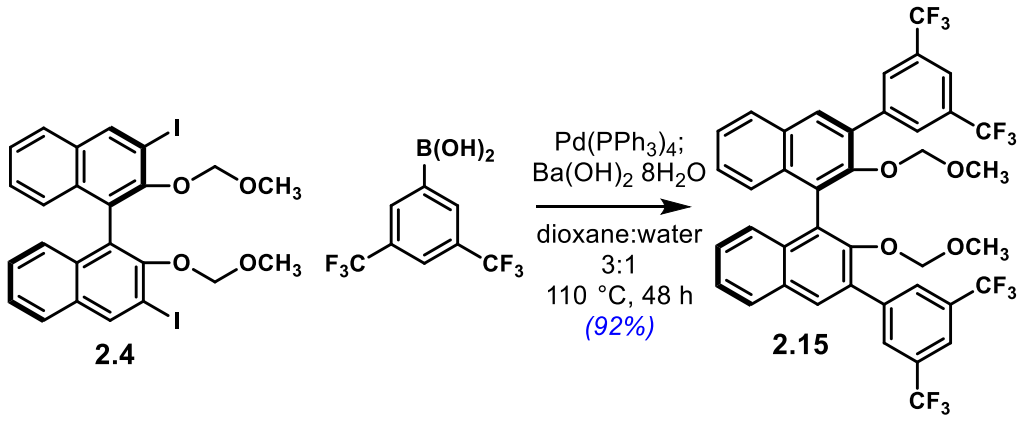

Note: The palladium catalyst was handled inside a glove box under argon atmosphere.

A round bottom flask was charged with **2.4** (313 mg, 0.5 mmol, 1.0 equiv.), 3,5-bis((trifluoromethyl)phenyl) boronic acid (387 mg, 1.5 mmol, 3.0 equiv.), barium hydroxide octahydrate (829 mg, 2.63 mmol, 5.25 equiv.) and $Pd(Ph_3)_4$ (58 mg, 0.05 mmol, 0.1 equiv.). Then, everything was dissolved in dioxane:water (3:1, 17 mL; degassed by bubbling argon trough with sonication for 30 min). The mixture was heated to 110 °C and stirred at that temperature for 48 h. Then, the reaction was cooled down to rt and dioxane removed in vacuo. The residue was partitioned with CH_2Cl_2 (15 mL) and water (10 mL). The organic layer was separated and the aqueous phase extracted with CH_2Cl_2 (10 mL, x3). The combined layers were dried over $MgSO_4$ and the solvent removed in vacuo. Column chromatography (5% EtOAc in hexane) afforded the pure product (370 mg, 0.46 mmol, 93%).

Spectral data consistent with the literature[141]

Physical state: white foam

TLC: R_f= 0.25 (5% EtOAc in hexane).

^{1}H NMR (600 MHz, $CDCl_3$): δ 8.24 (s, 4H), 8.02 (s, 2H), 7.97 (d, *J*=8.1 Hz, 2H), 7.92 (s, 2H), 7.50 (dd, *J*=8.1, 6.8 Hz, 2H), 7.37 (dd, *J*=8.1, 6.8 Hz, 2H), 7.29 (d, *J*=8.5 Hz, 2H), 4.43 (d, *J*=6.0 Hz, 2H), 4.36 (d, *J*=6.0 Hz, 2H), 2.50 (s, 6H)

^{13}C NMR (125 MHz, $CDCl_3$): δ 151.4, 141.3, 134.3, 132.9, 131.9, 131.7, 131.3, 130.8, 130.1, 128.4, 127.6, 126.5, 126.4, 126.1, 124.5, 122.7, 121.2, 99.3, 56.4

^{19}F NMR (100 MHz, $CDCl_3$): δ -62.67

(R)-3,3'- bis(3,5-bis(trifluoromethyl)phenyl)-1,1'-binaphthalene-2,2'-diol **2.16**

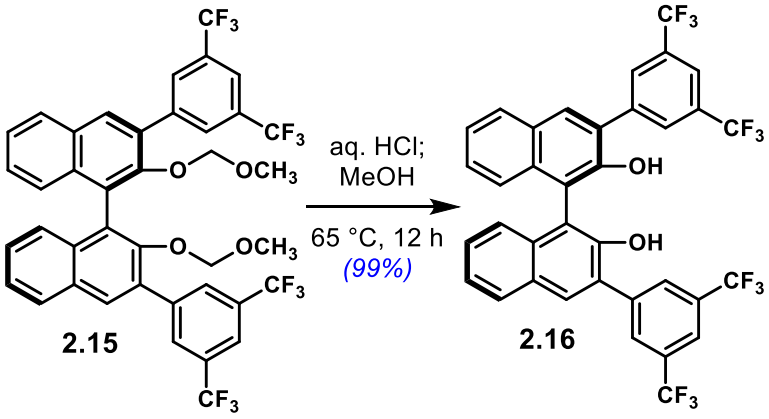

Note: *There is no need to use dry glassware, dry solvents or argon atmosphere for this reaction.*

MOM-protected BINOL **2.15** (337 mg, 0.422 mmol, 1.0 equiv.) was suspended in methanol (60 mL). At rt, a methanolic HCl solution (2.4 mL, 1.25 M) was added in one portion. After stirring at 70 °C for 12 h, the solvent was removed *in vacuo* and the residue partitioned in Et_2O (10 mL) and water (10 mL). The organic layer was separated and the aqueous phase extracted with Et_2O (10 mL, x3). The combined organic layers were dried over $MgSO_4$ and the solvent removed *in vacuo*. Azeotropic drying with benzene (5 mL, x3) afforded the pure product (300 mg, 0.42 mmol, 99%).

Spectral data consistent with the literature[141]

Physical state: white foam

TLC: R_f= 0.52 (10% Et_2O in hexane)

^{1}H NMR (600 MHz, $CDCl_3$): δ 8.24 (s, 4H), 8.13 (s, 2H), 8.01 (d, *J*=8.1 Hz, 2H), 7.92 (s, 2H), 7.49 (m, 2H), 7.43 (m, 2H), 7.24 (d, *J*=8.4 Hz, 2H), 5.37 (s, 2H)

^{13}C NMR (125 MHz, $CDCl_3$): δ 150.0, 139.6, 133.4, 132.5, 131.75, 130.0, 129.6, 129.1, 128.8, 127.9, 125.4, 124.5, 124.1, 122.7, 111.6

^{19}F NMR (100 MHz, $CDCl_3$): δ -62.74

(R)-3,3'-*bis*(3,5-*bis*(trifluoromethyl)phenyl)-1,1'-binaphthalene-2,2'-diol-*N*-triflylphosphoramide *(R)-NTPA*-**3**

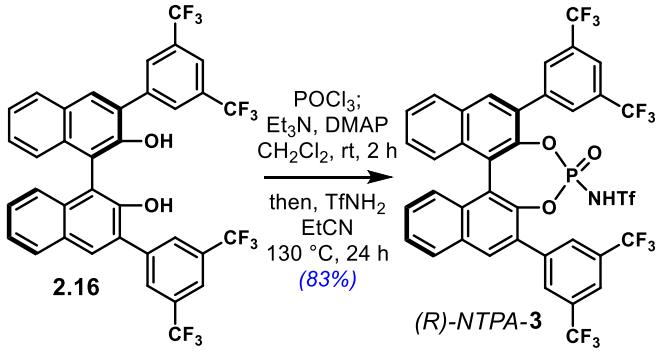

Starting material **2.16** (275 mg, 0.38 mmol, 1.0 equiv.) was dried in high vacuum overnight. Then, DMAP (95 mg, 0.77 mmol, 2.0 equiv.) was added and both regents dissolved in dry CH_2Cl_2 (2 mL). At rt, triethylamine (380 μL, 2.71 mmol, 7.0 equiv.) was added dropwise. Then, in an ice bath, phosphorus (V) oxychloride (54 μL, 0.58 mmol, 1.5 equiv.) was added dropwise. The reaction was stirred for 15 min in the ice bath and then at rt for 2 h. Then, a solution of $TfNH_2$ (115 mg, 0.77 mmol, 2.0 equiv.) in dry EtCN (5.5 mL) was added. The reaction was refluxed at 130 °C for 24 h, then, cooled down to rt, quenched with water (2 mL) and stirred for 1 h. The organic layer was separated and the aqueous phase extracted with EtOAc (5 mL, x3). The combined organic layers were washed with $NaHCO_3$ (5 mL), 6 N HCl (5 mL, x2), dried over $MgSO_4$ and the solvent removed *in vacuo*. Column chromatography (25% EtOAc in hexane) affords the product, presumably as a salt. The product was dissolved in EtOAC (15 mL), washed with 6 N HCl (5 mL, x4) and dried over $MgSO_4$. Removal of solvent *in vacuo* affords the desired product as the free acid (263 mg, 0.29 mmol, 83%).

Spectral data consistent with the literature[84]

Physical state: yellow solid

TLC: R_f= 0.32 (30% hexane in EtOAc). *Intense bright spot under UV*.

mp: 165-170 °C

$[\alpha]_D$: -232.2° (c=0.91, 25 °C)

^{1}H NMR (700 MHz, $CDCl_3$): δ 8.16 (s, 4H), 8.15 (s, 1H), 8.13 (s, 1H), 8.07 (t, *J*=7.6 Hz, 2H), 7.93 (s, 1H), 7.84 (s, 1H), 7.64 (dd, *J*=7.9, 3.8 Hz, 1H), 7.61 (s, 1H), 7.45 (d, *J*=3.4 Hz, 2H), 7.42 (s, 1H), 7.39 (d, *J*=8.4 Hz, 1H)

^{13}C NMR (175 MHz, $CDCl_3$): δ 138.4, 138.1, 132.5, 132.4, 132.2, 132.1, 131.9, 130.4, 130.1, 129.1, 129.0, 128.1, 128.1, 127.4, 127.3, 127.2, 127.1, 124.2, 123.0, 122.7, 122.6, 122.0

^{31}P NMR (100 MHz, $CDCl_3$): δ -3.65

^{19}F NMR (100 MHz, $CDCl_3$): δ -58.00, -74.87

HRMS (m/z): Calc. for $C_{37}H_{17}NO_5F_{15}NaPS$: 926.0223. Found: 926.0222

(R)-3,3'-*bis*(4-methylphenyl)-1,1'-binaphthalene-2,2'-diol-*N*-triflylphosphoramide *(R)-NTPA*-**4**

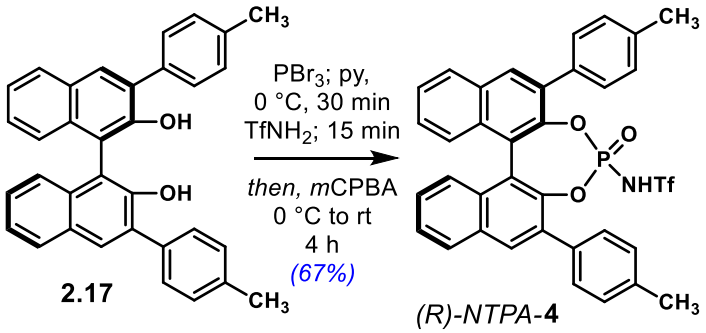

BINOL precursor **2.17** (39 mg, 0.084 mmol, 1.0 equiv.) was dissolved in dry pyridine (1.7 mL). Then, in an ice bath, phosphorus (III) bromide (10 μL, 0.101 mmol, 1.2 equiv.) was added dropwise. The reaction is stirred in the ice bath for 30 min. Then, $TfNH_2$ (25 mg, 0.168 mmol, 2.0 equiv.) was added in one portion and stirred for further 15 min. After that, *m*CPBA (30 mg, 0.168 mmol, 2.0 equiv.) was added in one portion. The reaction was let to reach rt and stirred for 4 h. After that time, was quenched with 1N HCl (4 mL) and partitioned with EtOAc (1 mL). The organic layer was separated and the aqueous phase extracted with EtOAc (2 mL x3). The combined organic layers were washed with 6N HCl (5 mL), dried over $MgSO_4$ and the solvent removed in vacuo. Column chromatography (25% to 40% EtOAc in hexane) afforded the pure product. That product was redissolved in EtOAc (5 mL) and washed with 6N HCl (5 mL x3) to afford the free acid (37 mg, 0.056 mmol, 67%).

Physical state: yellow powder

TLC: R_f= 0.21 (50% hexane in EtOAc). *Intense bright spot under UV*.

mp: 170-174 °C

$[\alpha]_D$: -265.7° (c=0.45, 25 °C)

^{1}H NMR (700 MHz, $CDCl_3$): δ 8.09 (s, 1H), 8.04 (s, 1H), 7.99 (d, *J*=8.3 Hz, 1H), 7.96 (d, *J*=8.2 Hz, 1H), 7.59 (d, *J*=7.9 Hz, 4H), 7.54 (d, *J*=7.7 Hz, 4H), 7.43 (m, 1H), 7.40 (d, *J*=8.8 Hz, 1H), 7.35 (m, 1H), 7.31 (d, *J*=8.5 Hz, 1H), 7.21 (d, *J*=7.9 Hz, 2H), 2.36 (s, 3H), 2.31 (s, 3H)

^{13}C NMR (175 MHz, $CDCl_3$): δ 143.9, 143.8, 143.3, 143.2, 138.2, 138.0, 134.8, 133.9, 133.8, 133.6, 133.3, 133.2, 132.2, 132.1, 131.9, 131.8, 131.7, 131.5, 131.0, 130.4, 130.1, 129.9, 129.4, 129.1, 128.7, 128.6, 128.4, 127.3, 127.1, 127.0, 126.9, 126.7, 126.5, 122.6, 122.5, 21.3, 21.3

^{31}P NMR (100 MHz, $CDCl_3$): δ -5.92

^{19}F NMR (100 MHz, $CDCl_3$): δ -77.36

HRMS (m/z): Calc. for $C_{35}H_{25}NO_5F_3NaPS$: 682.1041. Found: 682.1020

(R)-3,3'-*bis*((2,4,6-tricyclohexyl)-phenyl)-1,1'-binaphthalene-2,2'-diol-*N*-triflylphosphoramide *(R)-NTPA*-**2**

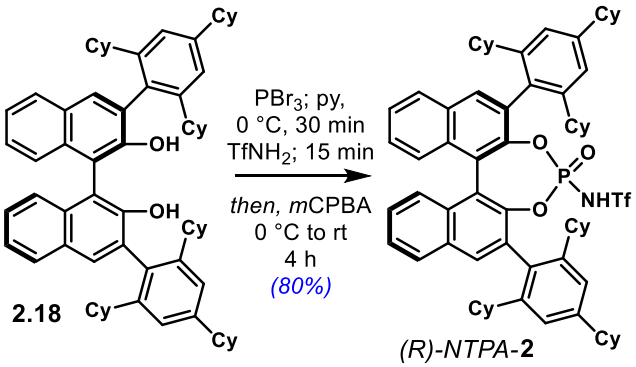

BINOL precursor **2.18** (150 mg, 0.161 mmol, 1.0 equiv.) was dissolved in dry pyridine (3.2 mL). Then, in an ice bath, phosphorus (III) bromide (18 μL, 0.193 mmol, 1.2 equiv.) was added dropwise. The reaction is stirred in the ice bath for 30 min. Then, $TfNH_2$ (48 mg, 0.322 mmol, 2.0 equiv.) was added in one portion and stirred for further 15 min. After that, *m*CPBA (56 mg, 0.322 mmol, 2.0 equiv.) was added in one portion. The reaction was let to reach rt and stirred for 4 h. After that time, was quenched with 1N HCl (8 mL) and partitioned with EtOAc (2 mL). The organic layer was separated and the aqueous phase extracted with EtOAc (4 mL x3). The combined organic layers were washed with 6N HCl (10 mL), dried over $MgSO_4$ and the solvent removed in vacuo. Column chromatography (25% EtOAc in hexane) afforded the pure product. That product was redissolved in EtOAc (10 mL) and washed with 6N HCl (10 mL x3) to afford the free acid (141 mg, 0.125 mmol, 80%).

Spectral data consistent with the literature[330]

Physical state: light orange powder

TLC: R_f= 0.56 (50% hexane in EtOAc). *Intense bright spot under UV*.

mp: 210-215 °C

$[\alpha]_D$: +5.4° (c=0.83, 25 °C)

^{1}H NMR (700 MHz, $CDCl_3$): δ 7.86 (d, *J*=8.2 Hz, 2H), 7.74 (s, 2H), 7.45 (t, *J*=7.3 Hz, 2H), 7.28 (m, 2H), 7.24 (d, *J*=8.1 Hz, 2H), 6.94 (s, 2H), 6.92 (s, 2H), 2.46 (m, 2H), 2.17 (m, 4H), 1.89 (m, 10H), 1.74 (m, 5H), 1.63 (m, 2H), 1.53 (m, 7H), 1.42 (m, 13H), 1.30 (m, 7H), 1.18 (m, 4H), 1.03 (m, 6H), 0.81 (m, 6H)

^{13}C NMR (175 MHz, $CDCl_3$): δ 147.2, 146.7, 146.3, 132.3, 132.1, 131.8, 131.1, 128.2, 126.8, 126.3, 125.6, 122.5, 121.8, 121.7, 44.9, 42.3, 42.0, 37.2, 35.2, 34.8, 34.4, 33.4, 32.8, 29.9, 29.8, 27.5, 27.3, 27.2, 27.1, 26.9, 26.5, 26.4, 26.1

^{31}P NMR (100 MHz, $CDCl_3$): δ 1.58

^{19}F NMR (100 MHz, $CDCl_3$): δ -78.98

HRMS (m/z): Calc. for $C_{69}H_{80}O_5PNSF_3$: 1122.5447 Found: 1122.5452

((3,3'-dibromo-[1,1'-binaphthalene]-2,2'-diyl)bis(oxy))bis(triphenylsilane) **2.26**

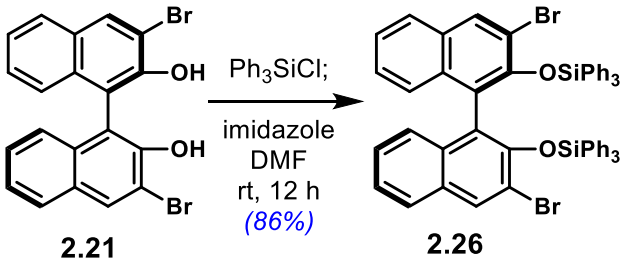

2.21 **2.26**

dibromo-BINOL **2.21** (250 mg, 0.56 mmol, 1.0 equiv.) was dissolved in dry DMF (4.5 mL). Then, imidazole (114 mg, 1.68 mmol, 3.0 equiv.) was added in one portion followed by triphenylsilyl chloride (430 mg, 1.4 mmol, 2.5 equiv.) also in one portion. The reaction was stirred at rt for 12 h. Then, it was poured onto $NaHCO_3$ (30 mL, std. sln.) and partitioned with CH_2Cl_2 (30 mL). The organic layer was separated and the aqueous phase extracted with CH_2Cl_2 (15 mL, x3). The combined organic layers are washed with water (30 mL, x2), dried over $MgSO_4$ and the solvent removed in vacuo. Column chromatography (25% CH_2Cl_2 in PE) afforded the pure product (476 mg, 0.496 mmol, 86%).

Physical state: white powder

TLC: R_f= 0.26 (25% CH_2Cl_2 in PE).

^{1}H NMR (400 MHz, $CDCl_3$): δ 7.68 (s, 2H), 7.42 (d, *J*=8.1 Hz, 2H), 7.28 (m, 18H), 7.17 (dd, *J*=11.2, 3.9 Hz, 2H), 7.13 (t, *J*=7.5 Hz, 12H), 7.06 (m, 2H), 6.85 (d, *J*=8.5 Hz, 2H)

^{13}C NMR (100 MHz, $CDCl_3$): δ 148.4, 135.3, 133.9, 133.4, 132.9, 130.0, 129.6, 127.4, 127.2, 126.3, 126.0, 124.4, 123.6, 117.3

(R)-3,3'- *bis*(triphenylsilyl)-1,1'-binaphthalene-2,2'-diol **2.27**

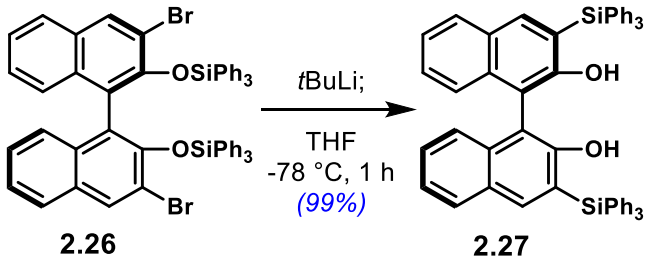

2.26 **2.27**

Important: The starting material is dried in high-vacuum overnight for better results.

Compound **2.26** (334 mg, 0.347 mmol, 1.0 equiv.) was dissolved in dry THF (3.4 mL). Then, at -78 °C, *tert*-butyl lithium (0.85 mL, 1.64 M sln. in pentane, 4.0 equiv.) was added dropwise. After addition, the reaction was stirred at -78 °C for 1 h. The reaction was *quenched at -78 °C* with 1 N HCl (3.4 mL). Then, the reaction was allowed to reach rt. After that, it was diluted with Et_2O (5 mL) and water (5 mL). The organic layer was separated and the aqueous phase extracted with Et_2O (5 mL, x3). The combined organic layers were dried over $MgSO_4$ and the solvent removed in vacuo. Column chromatography (25% CH_2Cl_2 in PE) afforded the pure product (279 mg, 0.34 mmol, 99%).

Spectral data consistent with the literature[125]

Physical state: white solid

TLC: R_f= 0.38 (30% CH_2Cl_2 in PE).

^{1}H NMR (400 MHz, $CDCl_3$): δ 8.01 (s, 2H), 7.78 (d, *J*=7.9 Hz, 2H), 7.73 (m, 12H), 7.50 (t, *J*=7.3 Hz, 12 H), 7.43 (t, *J*=7.2 Hz, 12H), 7.37 (d, *J*=7.8 Hz, 2H), 7.34 (d, *J*=8.1 Hz, 2H), 5.38 (s, 2H)

^{13}C NMR (100 MHz, $CDCl_3$): δ 156.7, 142.2, 136.5, 134.9, 134.4, 129.7, 129.4, 129.2, 128.3, 128.0, 127.9, 124.1, 124.0, 123.8, 110.8

(R)-3,3'-*bis*(triphenylsilyl)-1,1'-binaphthalene-2,2'-diol-phosphoric acid *(R)-PA*-**5**

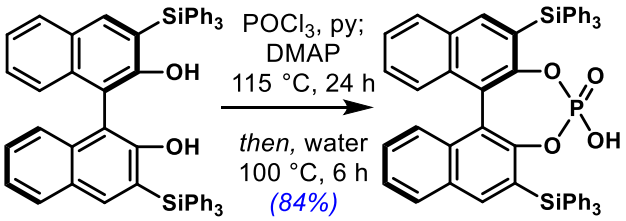

BINOL **2.27** (253mg, 0.32 mmol, 1.0 equiv.) and DMAP (96 mg, 0.79 mmol, 2.5 equiv.) were dissolved in dry pyridine (3.5 mL). At rt, phosphorus (V) oxychloride (180 μL, 1.89 mmol, 6.0 equiv) was added in one portion. The reaction is refluxed at 115 °C for 24 h. Then, quenched with water (7 mL) and further refluxed at 100 °C for 6 h. After that, the reaction is allowed to cool down to rt and diluted with 1N HCl (8 mL) and CH_2Cl_2 (15 mL). The pH of the aqueous phase was taken to pH 2 with 6N HCl. The organic phase was separated and the aqueous layer extracted with CH_2Cl_2 (10 mL, x3). The combined organic layers were washed with 6N HCl (50 mL), dried over $MgSO_4$ and the solvent removed *in vacuo*. Column chromatography (4% MeOH in CH_2Cl_2) afforded the product, presumably as a salt. The product was dissolved in CH_2Cl_2 (40 mL) and thoroughly washed with 6N HCl (50 mL, x2), then, dried over $MgSO_4$ and the solvent removed *in vacuo* to afford the acid in its free form (229 mg, 0.26 mmol, 84%).

Spectral data consistent with the literature[125]

Physical state: free flowing white powder

TLC: R_f= 0.46 (10% MeOH in CH_2Cl_2). *Intense bright spot under UV*.

mp: >300 °C

$[\alpha]_D$: -180.8° (c=0.38, 25 °C)

^{1}H NMR (400 MHz, $CDCl_3$): δ 8.09 (s, 2H), 7.80 (d, *J*=8.1 Hz, 2H), 7.65 (dd, *J*=8.0, 1.4 Hz, 12H), 7.44 (m, 2H), 7.38 (m, 18H), 7.30 (m, 2H), 7.22 (d, *J*=8.5 Hz, 2H)

^{13}C NMR (100 MHz, $CDCl_3$): δ 151.25, 142.1, 136.9, 134.4, 133.9, 131.0, 129.8, 128.9, 128.0, 127.7, 127.0, 126.2, 125.7, 121.5

^{31}P NMR (100 MHz, $CDCl_3$): δ -1.85

HRMS (m/z): Calc. for $C_{56}H_{40}O_4PSi_2$: 863.2203. Found: 863.2237

(R)-3,3'-*bis*(triphenylsilyl)-1,1'-binaphthalene-2,2'-diol-*N*-triflylphosphoramide *(R)-NTPA*-**5**

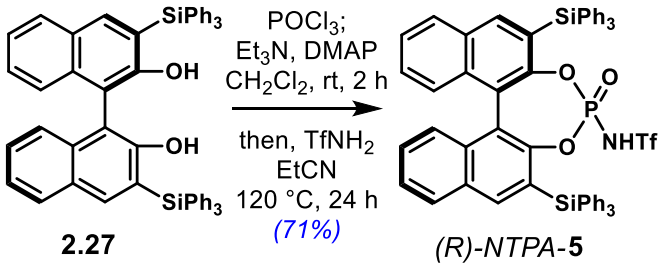

2.27 *(R)-NTPA*-**5**

Starting material **2.27** (278 mg, 0.35 mmol, 1.0 equiv.) was dried in high vacuum overnight. Then, DMAP (85 mg, 0.69 mmol, 2.0 equiv.) was added and both regents dissolved in dry CH_2Cl_2 (1.9 mL). At rt, triethylamine (340 μL, 2.42 mmol, 7.0 equiv.) was added dropwise. Then, in an ice bath, phosphorus (V) oxychloride (39 μL, 0.42 mmol, 1.5 equiv.) was added dropwise. The reaction was stirred for 15 min in the ice bath and then at rt for 2 h. Then, a solution of $TfNH_2$ (109 mg, 0.69 mmol, 2.0 equiv.) in dry EtCN (2 mL) was added. The reaction was refluxed at 120 °C for 24 h, then, cooled down to rt, quenched with water (2 mL) and stirred for 1 h. The organic layer was separated and the aqueous phase extracted with EtOAc (5 mL, x3). The combined organic layers were washed with $NaHCO_3$ (5 mL), 6 N HCl (5 mL, x2), dried over $MgSO_4$ and the solvent removed *in vacuo*. Column chromatography (50% hexane in EtOAc) affords the product, presumably as a salt. The product was dissolved in EtOAC (15 mL), washed with 6 N HCl (5 mL, x4) and dried over $MgSO_4$. Removal of solvent *in vacuo* affords the desired product as the free acid (244 mg, 0.24 mmol, 71%).

Physical state: white solid

TLC: R_f= 0.55 (30% hexane in EtOAc). *Intense bright spot under UV*.

mp: 171-174 °C

$[\alpha]_D$: -113.6° (c=0.51, 25 °C)

^{1}H NMR (400 MHz, $CDCl_3$): δ 8.21 (s, 1H), 7.99 (s, 1H), 7.86 (d, *J*=8.1 Hz, 1H), 7.77 (d, *J*=8.1 Hz, 1H), 7.66 (dd, *J*=8.0, 1.4 Hz, 5H), 7.59 (dd, *J*=8.0, 1.4 Hz, 5H), 7.48 (m, 2H), 7.43 (m, 4H), 7.38 (m, 6H), 7.33 (m, 6H), 7.21 (d, *J*=8.5 Hz, 1H), 7.31 (d, J=8.5 Hz, 1H)

^{13}C NMR (100 MHz, $CDCl_3$): δ 150.3, 150.2, 150.1, 142.9, 142.3, 137.0, 136.7, 136.6, 134.5, 134.4, 133.3, 133.2, 131.3, 131.2, 130.1, 129.7, 129.1, 129.0, 128.4, 128.0, 126.9, 126.2, 126.1, 126.0, 125.1, 121.7, 120.9

^{31}P NMR (100 MHz, $CDCl_3$): δ -8.99

^{19}F NMR (100 MHz, $CDCl_3$): δ -78.65

HRMS (m/z): Calc. for $C_{57}H_{41}NO_5PSSi_2F_3Na$: 1018.1831. Found: 1018.1851

(R)-((3,3'-dibromo-[1,1'-binaphthalene]-2,2'-diyl)bis(oxy))bis(tert-butyldimethylsilane) **2.28**

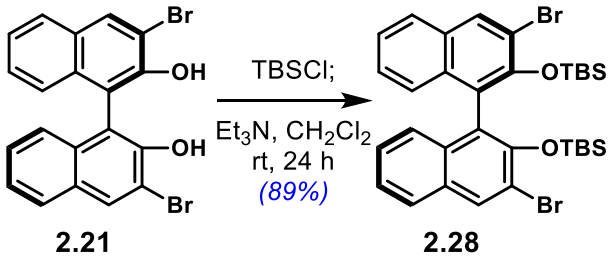

2.21 **2.28**

dibromo-BINOL **2.21** (200 mg, 0.45 mmol, 1.0 equiv.) was dissolved in dry CH_2Cl_2 (4.5 mL). Then, at rt, TBSCl (170 mg, 1.12 mmol, 2.5 equiv.) was added in one portion followed by Et_3N (0.16 mL, 1.12 mmol, 2.5 equiv.), dropwise. The reaction was stirred at rt for 24 h. After that, silica gel was added and the solvent carefully removed in vacuo. The residue was loaded into a silica column and purified with (5% CH_2Cl_2 in PE) to afford the pure product (275 mg, 0.41 mmol, 89%).

Physical state: white foam

TLC: R_f= 0.57 (20% CH_2Cl_2 in PE).

^{1}H NMR (400 MHz, $CDCl_3$): δ 8.21 (s, 2H), 7.75 (m, 2H), 7.33 (ddd, *J*=8.1, 6.8, 1.2 Hz, 2H), 7.21 (ddd, *J*=8.1, 6.8, 1.3 Hz, 2H), 7.11 (m, 2H), 0.83 (s, 18H), 0.00 (s, 6H), -1.08 (s, 6H)

^{13}C NMR (100 MHz, $CDCl_3$): δ 148.9, 134.1, 132.9, 130.2, 127.1, 126.7, 126.5, 124.6, 123.6, 117.7, 26.1, 18.7, -2.8, -3.9

(R)-3,3'-*bis*(*tert*-butyldimethylsilyl)-1,1'-binaphthalene-2,2'-diol **2.29**

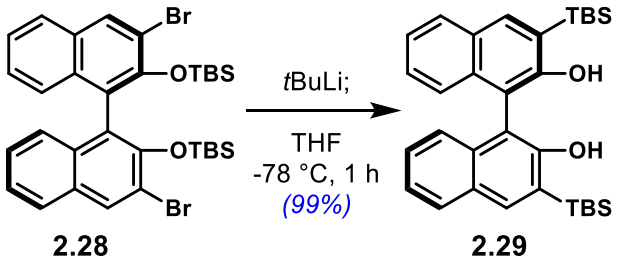

2.28 **2.29**

Important: The starting material is dried in high-vacuum overnight for better results.

Compound **2.28** (275 mg, 0.41 mmol, 1.0 equiv.) was dissolved in dry THF (4 mL). Then, at -78 °C, *tert*-butyl lithium (1.0 mL, 1.64 M sln. in pentane, 4.0 equiv.) was added dropwise. After addition, the reaction was stirred at -78 °C for 1 h. The reaction was *quenched at -78 °C* with 1 N HCl (2.3 mL). Then, the reaction was allowed to reach rt. After that, it was diluted with Et_2O (4 mL) and water (4 mL). The organic layer was separated and the aqueous phase extracted with Et_2O (4 mL, x3). The combined organic layers were dried over $MgSO_4$ and the solvent removed in vacuo. Column chromatography (3% CH_2Cl_2 in hexane) afforded the pure product (210 mg, 0.41 mmol, 99%).

Spectral data consistent with the literature[331]

Physical state: thick clear oil

TLC: R_f= 0.36 (10% CH_2Cl_2 in hexane).

^{1}H NMR (400 MHz, $CDCl_3$): δ 8.12 (s, 2H), 7.91 (d, *J*=7.9 Hz, 2H), 7.36 (dd, *J*=10.9, 4.0 Hz, 2H), 7.31 (m, 2H), 7.12 (d, *J*=8.3 Hz, 2H), 5.26 (s, 2H), 0.98 (s, 18H), 0.47 (s, 6H), 0.46 (s, 6H)

^{13}C NMR (100 MHz, $CDCl_3$): δ 157.3, 139.6, 134.4, 129.2, 128.8, 127.8, 126.8, 124.0, 123.8, 109.8, 31.8, 27.3, 22.8, 17.8, 14.3, -4.3, -4.4

(R)-3,3'-*bis*(*tert*-butyldimethylsilyl)-1,1'-binaphthalene-2,2'-diol-phosphoric acid *(R)-PA*-**6**

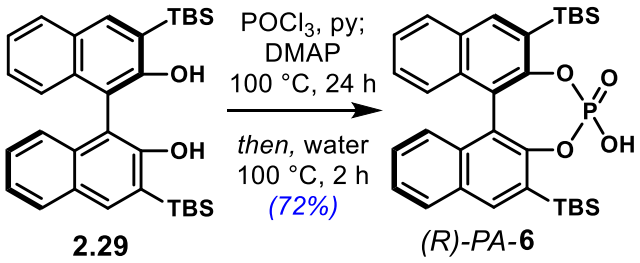

2.29 *(R)-PA*-**6**

BINOL **2.29** (64 mg, 0.12 mmol, 1.0 equiv.) and DMAP (17 mg, 0.14 mmol, 1.1 equiv.) were dissolved in dry pyridine (0.5 mL). At rt, phosphorus (V) oxychloride (34 μL, 0.37 mmol, 3.0 equiv) was added in one portion. The reaction is refluxed at 100 °C for 24 h. Then, quenched with water (1 mL) and further refluxed at 100 °C for 2 h. After that, the reaction is allowed to cool down to rt and diluted with 6N HCl (0.5 mL) and CH_2Cl_2 (5 mL). The pH of the aqueous phase was taken to pH 2 with 6N HCl. The organic phase was separated and the aqueous layer extracted with CH_2Cl_2 5 mL, x3). The combined organic layers were washed with 6N HCl (12 mL), dried over $MgSO_4$ and the solvent removed *in vacuo*. Column chromatography (2% to 10% MeOH in CH_2Cl_2) afforded the product, presumably as a salt. The product was dissolved in CH_2Cl_2 (10 mL) and thoroughly washed with 6N HCl (12 mL, x2), then, dried over $MgSO_4$ and the solvent removed *in vacuo* to afford the acid in its free form (51 mg, 0.089 mmol, 72%).

Physical state: white foam

TLC: R_f= 0.5 (10% MeOH in CH_2Cl_2). *Intense bright spot under UV*.

mp: 222-225 °C

^{1}H NMR (400 MHz, $CDCl_3$): δ 8.13 (s, 2H), 7.94 (d, *J*=8.2 Hz, 2H), 7.45 (t, *J*=7.5 Hz, 2H), 7.25 (t, *J*=7.5 Hz, 2H), 7.09 (d, *J*=8.5 Hz, 2H), 0.92 (s, 18H), 0.67 (s, 6H), 0.50 (s, 6H)

^{13}C NMR (100 MHz, $CDCl_3$): δ 150.55, 139.2, 133.7, 131.1, 128.8, 128.6, 127.2, 126.7, 125.6, 121.0, 27.0, 17.9, -2.8, -4.6

^{31}P NMR (100 MHz, $CDCl_3$): δ 2.75

HRMS (m/z): Calc. for $C_{32}H_{42}O_4PSi_2$: 577.2359. Found: 577.2380

(R)-3,3'-*bis*(*tert*-butyldimethylsilyl)-1,1'-binaphthalene-2,2'-diol-*N*-triflylphosphoramide *(R)-NTPA*-**6**

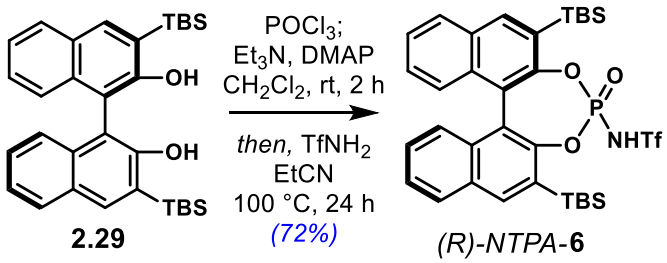

Starting material **2.29** (210 mg, 0.41 mmol, 1.0 equiv.) was dried in high vacuum overnight. Then, DMAP (100 mg, 0.82 mmol, 2.0 equiv.) was added and both regents dissolved in dry CH_2Cl_2 (2 mL). At rt, triethylamine (400 μL, 2.86 mmol, 7.0 equiv.) was added dropwise. Then, in an ice bath, phosphorus (V) oxychloride (58 μL, 0.61 mmol, 1.5 equiv.) was added dropwise. The reaction was stirred for 15 min in the ice bath and then at rt for 2 h. Then, a solution of $TfNH_2$ (128 mg, 0.82 mmol, 2.0 equiv.) in dry EtCN (5.8 mL) was added. The reaction was refluxed at 100 °C for 24 h, then, cooled down to rt, quenched with water (2 mL) and stirred for 1 h. The organic layer was separated and the aqueous phase extracted with EtOAc (5 mL, x3). The combined organic layers were washed with $NaHCO_3$ (6 mL), 6 N HCl (6 mL, x2), dried over $MgSO_4$ and the solvent removed *in vacuo*. Column chromatography (50% hexane in EtOAc) affords the product, presumably as a salt. The product was dissolved in EtOAC (6 mL), washed with 6 N HCl (6 mL, x4) and dried over $MgSO_4$. Removal of solvent *in vacuo* affords the desired product as the free acid (208 mg, 0.29 mmol, 72%).

Physical state: white foam

TLC: R_f= 0.22 (40% EtOAc in hexane). *Intense bright spot under UV*.

mp: 143-145 °C

$[\alpha]_D$: -234.7° (c=1.0, 25 °C)

^{1}H NMR (400 MHz, $CDCl_3$): δ 8.14 (d, *J*=1.9 Hz, 2H), 7.95 (d, *J*=8.2 Hz, 2H), 7.47 (dd, *J*=15.4, 7.8 Hz, 2H), 7.25 (m, 2H), 7.07 (d, *J*=8.5 Hz, 1H), 6.99 (d, *J*=8.5 Hz, 1H), 0.87 (d, *J*=18 Hz, 14H), 0.70 (s, 2H), 0.62 (s, 2H), 0.51 (d, *J*=6.5 Hz, 4H)

^{13}C NMR (100 MHz, $CDCl_3$): δ 150.7, 149.4, 139.4, 133.7, 131.2, 128.7, 128.6, 128.0, 127.5, 126.8, 126.1, 121.1, 120.5, 120.2, 17.8, 15.4, -2.8, -3.8, -4.6, -5.1

^{31}P NMR (100 MHz, $CDCl_3$): δ -6.83

^{19}F NMR (100 MHz, $CDCl_3$): δ -76.41

HRMS (m/z): Calc. for $C_{33}H_{41}NO_5F_3NaSi_2PS$: 730.1831. Found: 730.1815

(R)-((3,3'-dibromo-[1,1'-binaphthalene]-2,2'-diyl)bis(oxy))bis(tris-(3,5-dimethylphenyl)silane) **2.41**

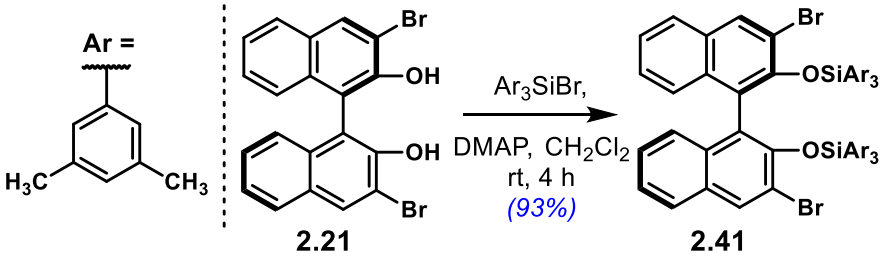

dibromo-BINOL **2.21** (69 mg, 0.16 mmol, 1.0 equiv.) and DMAP (58 mg, 0.47 mmol, 3.0 equiv.) were dissolved in dry CH_2Cl_2 (1.8 mL). Then, at rt, a solution of crude bromo tris-(3,5-dimethylphenyl)silane (*ca.* 160 mg, 0.38 mmol, 2.4 equiv.) in dry CH_2Cl_2 (0.8 mL) was added dropwise. The reaction was stirred for 4 h at rt—after that time, full consumption of the starting material was observed. The reaction was quenched by adding silica gel and carefully removing the solvent under reduced pressure. Column chromatography (5% to 20% CH_2Cl_2 in PE) afforded the pure product (155 mg, 0.14 mmol, 93%).

Physical state: white foam

TLC: R_f= 0.40 (30% CH_2Cl_2 in PE).

^{1}H NMR (400 MHz, $CDCl_3$): δ 7.58 (s, 2H), 7.47 (d, *J*=7.9 Hz, 2H), 7.24 (t, *J*=7.4 Hz, 2H), 7.18 (dd, *J*=8.0, 7.1 Hz, 2H), 7.03 (d, *J*=8.4 Hz, 2H), 6.99 (s, 12H), 6.93 (s, 6H), 2.14 (s, 36H)

^{13}C NMR (100 MHz, $CDCl_3$): δ 148.5, 136.7, 136.4, 134.2, 133.1, 132.8, 132.5, 131.3, 129.8, 127.2, 126.0, 125.9, 123.9, 117.2, 21.6

(R)-3,3'-*bis*(*tris*-(3,5-dimethylphenyl)silyl)-1,1'-binaphthalene-2,2'-diol **2.44**

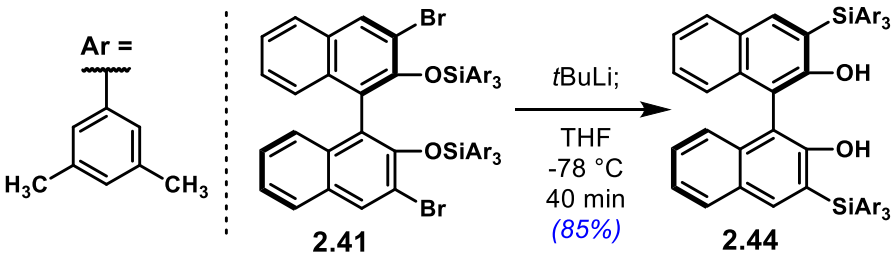

Important: The starting material is dried in high-vacuum overnight for better results.

Compound **2.41** (154 mg, 0.14 mmol, 1.0 equiv.) was dissolved in dry THF (1.5 mL). Then, at -78 °C, *tert*-butyl lithium (0.32 mL, 1.7 M sln. in pentane, 4.0 equiv.) was added dropwise. After addition, the reaction was stirred at -78 °C for 40 min. The reaction was *quenched at -78 °C* with 1 N HCl (2 mL). Then, the reaction was allowed to reach rt. After that, it was diluted with Et_2O (2 mL) and water (2 mL). The organic layer was separated and the aqueous phase extracted with Et_2O (2 mL, x3). The combined organic layers were dried over $MgSO_4$ and the solvent removed in vacuo. Column chromatography (20% CH_2Cl_2 in hexane) afforded the pure product (112 mg, 0.12 mmol, 85%).

Physical state: white solid

TLC: R_f= 0.33 (30% CH_2Cl_2 in hexane).

^{1}H NMR (400 MHz, $CDCl_3$): δ 7.96 (s, 2H), 7.79 (d, *J*=8.2 Hz, 2H), 7.38 (m, 6H), 7.31 (s, 12H), 7.09 (s, 6H), 5.32 (s, 2H), 2.30 (s, 36H)

^{13}C NMR (100 MHz, $CDCl_3$): δ 156.8, 142.0, 137.0, 135.0, 134.2, 134.1, 131.4, 129.3, 129.2, 128.0, 124.5, 124.1, 123.7, 111.2, 21.6

(R)-3,3'-*bis*(*tris*-(3,5-dimethylphenyl)silyl)-1,1'-binaphthalene-2,2'-diol-phosphoric acid *(R)-PA*-**7**

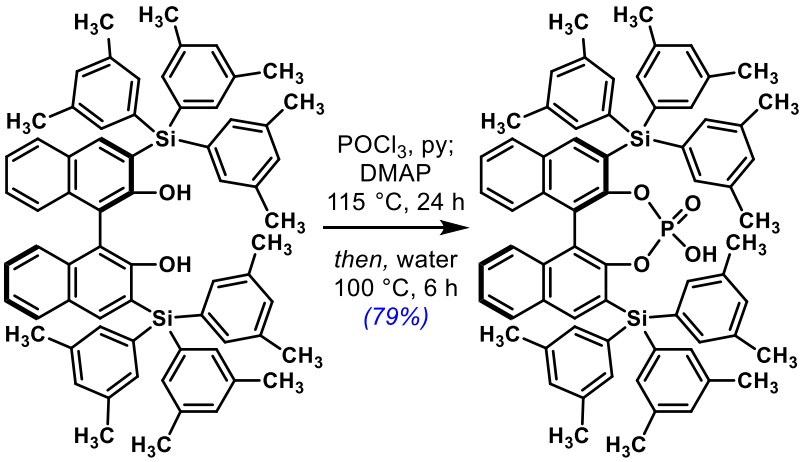

BINOL **2.44** (112 mg, 0.12 mmol, 1.0 equiv.) and DMAP (35 mg, 0.29 mmol, 2.5 equiv.) were dissolved in dry pyridine (1.3 mL). At rt, phosphorus (V) oxychloride (65 μL, 0.69 mmol, 6.0 equiv) was added in one portion. The reaction is refluxed at 115 °C for 24 h. Then, quenched with water (2.6 mL) and further refluxed at 100 °C for 6 h. After that, the reaction is allowed to cool down to rt and diluted with 1N HCl (3 mL) and CH_2Cl_2 (6 mL). The pH of the aqueous phase was taken to pH 2 with 6N HCl. The organic phase was separated and the aqueous layer extracted with CH_2Cl_2 (5 mL, x3). The combined organic layers were washed with 6N HCl (25 mL), dried over $MgSO_4$ and the solvent removed *in vacuo*. Column chromatography (10% acetone in CH_2Cl_2) afforded the product, presumably as a salt. The product was dissolved in CH_2Cl_2 (15 mL) and thoroughly washed with 6N HCl (30 mL, x2), then, dried over $MgSO_4$ and the solvent removed *in vacuo* to afford the acid in its free form (94 mg, 0.09 mmol, 79%).

Physical state: white solid

TLC: R_f= 0.23 (10% acetone in CH_2Cl_2). *Intense bright spot under UV*.

mp: 173-177 °C

$[\alpha]_D$: -93.0° (c=0.23, 25 °C)

^{1}H NMR (400 MHz, $CDCl_3$): δ 8.10 (s, 2H), 7.81 (d, *J*=8.1 Hz, 2H), 7.41 (dd, *J*=11.1, 4.0 Hz, 2H), 7.29 (m, 2H), 7.25 (m, 12H), 7.20 (d, *J*=8.4 Hz, 2H), 7.03 (s, 6H), 2.24 (s, 36H)

^{13}C NMR (100 MHz, $CDCl_3$): δ 151.3, 141.7, 137.2, 134.7, 134.3, 133.9, 131.5, 131.0, 128.9, 127.4, 127.0, 126.8, 125.5, 121.4, 21.6

^{31}P NMR (100 MHz, $CDCl_3$): δ -2.04

HRMS (m/z): Calc. for $C_{68}H_{64}O_4PSi_2$: 1031.4081. Found: 1031.4120

(R)-((3,3'-dibromo-[1,1'-binaphthalene]-2,2'-diyl)bis(oxy))bis(tris-(4-iso-propylphenyl)silane) **2.45**

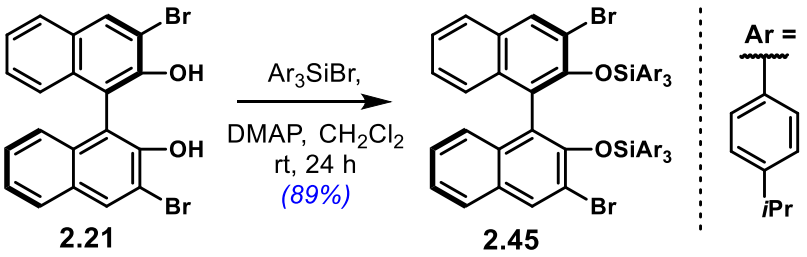

dibromo-BINOL **2.21** (38 mg, 0.085 mmol, 1.0 equiv.) and DMAP (32 mg, 0.255 mmol, 3.0 equiv.) were dissolved in dry CH_2Cl_2 (0.5 mL). Then, at rt, a solution of crude bromo tris-(4-iso-propylphenyl)silane (*ca.* 95 mg, 0.204 mmol, 2.4 equiv.) in dry CH_2Cl_2 (0.5 mL) was added dropwise. The reaction was stirred for 24 h at rt. The reaction was quenched by adding silica gel and carefully removing the solvent under reduced pressure. Column chromatography (10% CH_2Cl_2 in PE) afforded the pure product (92 mg, 0.075 mmol, 89%).

Physical state: white solid

TLC: R_f= 0.37 (20% CH_2Cl_2 in PE).

^{1}H NMR (400 MHz, $CDCl_3$): δ 7.70 (s, 2H), 7.46 (d, *J*=8.1 Hz, 2H), 7.27 (d, *J*=7.9 Hz, 12H), 7.20 (t, *J*=7.4 Hz, 2H), 7.09 (t, *J*=7.5 Hz, 2H), 7.01 (d, *J*=7.9 Hz, 12H), 6.91 (d, *J*=8.5 Hz, 2H), 2.86 (hept, *J*=6.8 Hz, 6H), 1.27 (dd, *J*=6.9, 1.1 Hz, 36H)

^{13}C NMR (100 MHz, $CDCl_3$): δ 149.7, 148.8, 135.5, 133.1, 132.9, 131.5, 129.9, 126.9, 126.2, 126.0, 125.5, 124.2, 123.7, 117.5, 34.1, 24.0, 23.9

(R)-3,3'-*bis*(*tris*-(4-*iso*propylphenyl)silyl)-1,1'-binaphthalene-2,2'-diol **2.46**

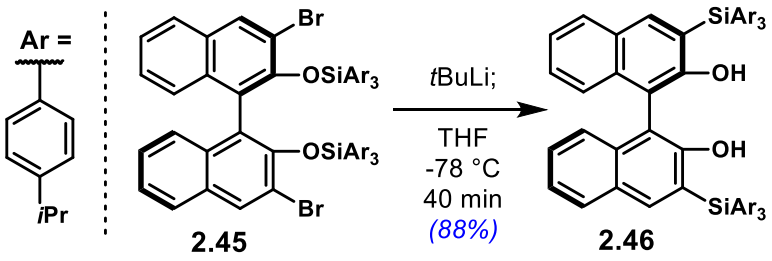

Important: The starting material is dried in high-vacuum overnight for better results.

Compound **2.45** (95 mg, 0.078 mmol, 1.0 equiv.) was dissolved in dry THF (0.8 mL). Then, at -78 °C, *tert*-butyl lithium (0.18 mL, 1.7 M sln. in pentane, 4.0 equiv.) was added dropwise. After addition, the reaction was stirred at -78 °C for 40 min. The reaction was *quenched at -78 °C* with 1 N HCl (0.7 mL). Then, the reaction was allowed to reach rt. After that, it was diluted with Et_2O (6 mL). The organic layer was separated, dried over $MgSO_4$ and the solvent removed in vacuo. Column chromatography (20% CH_2Cl_2 in hexane) afforded the pure product (72 mg, 0.068 mmol, 88%).

Physical state: white solid

TLC: R_f= 0.29 (20% CH_2Cl_2 in hexane).

^{1}H NMR (400 MHz, $CDCl_3$): δ 8.00 (s, 2H), 7.76 (d, *J*=7.7 Hz, 2H), 7.65 (d, *J*=6.5 Hz, 12H), 7.36 (m, 6H), 7.28 (d, *J*=7.9 Hz, 12H), 5.39 (s, 2H), 2.97 (m, 6H), 1.32 (d, *J*=6.6 Hz, 36H)

^{13}C NMR (100 MHz, $CDCl_3$): δ 156.8, 150.1, 142.1, 136.6, 134.8, 131.6, 129.3, 129.2, 128.0, 126.1, 124.4, 124.2, 123.7, 111.0, 34.2, 24.0, 24.0

(R)-3,3'-*bis*(*tris*-(4-*iso*propylphenyl)silyl)-1,1'-binaphthalene-2,2'-diol-phosphoric acid *(R)-PA*-**8**

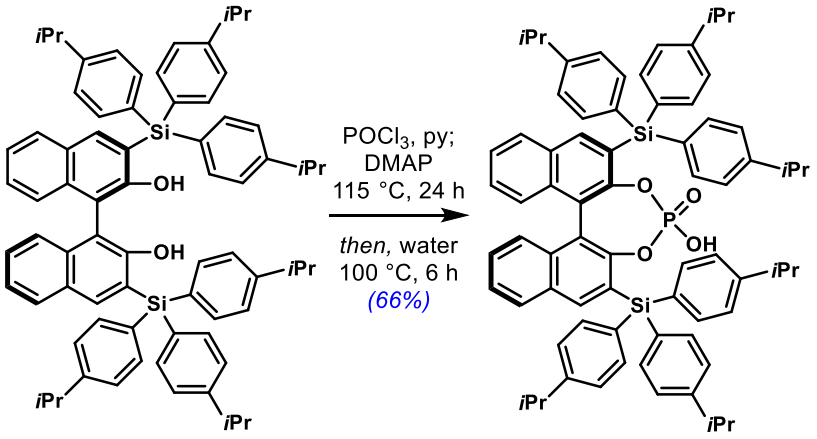

BINOL **2.46** (259 mg, 0.25 mmol, 1.0 equiv.) and DMAP (84 mg, 0.66 mmol, 2.7 equiv.) were dissolved in dry pyridine (3 mL). At rt, phosphorus (V) oxychloride (150 μL, 1.59 mmol, 6.5 equiv) was added in one portion. The reaction is refluxed at 115 °C for 24 h. Then, quenched with water (6 mL) and further refluxed at 100 °C for 6 h. After that, the reaction is allowed to cool down to rt and diluted with 1N HCl (6 mL) and CH_2Cl_2 (20 mL). The pH of the aqueous phase was taken to pH 2 with 6N HCl. The organic phase was separated and the aqueous layer extracted with CH_2Cl_2 (10 mL, x3). The combined organic layers were washed with 6N HCl (50 mL), dried over $MgSO_4$ and the solvent removed *in vacuo*. Column chromatography (3% acetone in CH_2Cl_2) afforded the product, presumably as a salt. The product was dissolved in CH_2Cl_2 (20 mL) and thoroughly washed with 6N HCl (40 mL, x2), then, dried over $MgSO_4$ and the solvent removed *in vacuo* to afford the acid in its free form (180 mg, 0.16 mmol, 66%).

Physical state: slightly yellow solid

TLC: R_f= 0.61 (10% acetone in CH_2Cl_2). *Intense bright spot under UV*.

mp: 193-196 °C

$[\alpha]_D$: -138.4° (c=0.27, 25 °C)

^{1}H NMR (400 MHz, $CDCl_3$): δ 8.14 (s, 2H), 7.81 (d, *J*=8.1 Hz, 2H), 7.59 (d, *J*=7.9 Hz, 12H), 7.42 (t, *J*=7.2 Hz, 2H), 7.29 (m, 2H), 7.22 (d, *J*=7.9 Hz, 12H), 2.89 (hept, *J*=6.9 Hz, 6H), 1.25 (d, *J*=6.9 Hz, 36H)

^{13}C NMR (100 MHz, $CDCl_3$): δ 151.25, 150.3, 141.8, 137.0, 134.3, 131.3, 131.0, 128.9, 127.5, 127.1, 126.9, 126.2, 125.5, 121.5, 34.2, 24.0

^{31}P NMR (100 MHz, $CDCl_3$): δ -1.82

HRMS (m/z): Calc. for $C_{74}H_{76}O_4PSi_2$: 1115.5020. Found: 1115.5040

(R)-((3,3'-dibromo-[1,1'-binaphthalene]-2,2'-diyl)bis(oxy))bis(methyldiphenylsilane) **2.30**

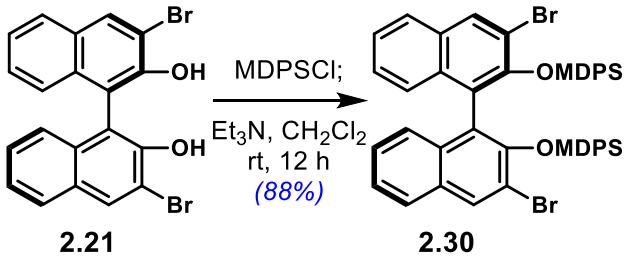

2.21 **2.30**

dibromo-BINOL **2.21** (444 mg, 1.0 mmol, 1.0 equiv.) was dissolved in dry CH_2Cl_2 (10 mL). Then, at rt, MDPSCl (0.53 mL, 2.5 mmol, 2.5 equiv.) was added dropwise followed by Et_3N (0.35 mL, 2.5 mmol, 2.5 equiv.), dropwise. The reaction was stirred at rt for 12 h. After that, the reaction was quenched with water (10 mL). Then, the organic layer was separated and the aqueous layer extracted with CH_2Cl_2 (10 mL, x3). The combined organic layers were dried over $MgSO_4$ and the solvent removed in vacuo. Column chromatography (5% EtOAc in hexane) afforded the pure product (737 mg, 0.88 mmol, 88%).

Physical state: white foam

TLC: R_f= 0.29 (10% EtOAc in hexane).

^{1}H NMR (600 MHz, $CDCl_3$): δ 7.82 (s, 2H), 7.53 (d, *J*=8.2 Hz, 2H), 7.33 (d, *J*=6.9 Hz, 4H), 7.29 (t, *J*=7.5 Hz, 2H), 7.26 (m, 2H), 7.22 (m, 2H), 7.18 (t, *J*=7.5 Hz, 4H), 7.15 (d, *J*=6.7 Hz, 4H), 7.10 (t, *J*=7.4 Hz, 4H), 7.06 (dd, *J*=11.3, 3.9 Hz, 2H), 6.76 (d, *J*=8.5 Hz, 2H), 0.29 (s, 6H)

^{13}C NMR (125 MHz, $CDCl_3$): δ 148.8, 136.1, 135.8, 134.3, 133.7, 133.2, 133.0, 130.1, 129.5, 129.3, 127.5, 127.3, 127.1, 126.4, 126.0, 124.6, 123.7, 117.4, -2.8

(R)-3,3'-*bis*(methyldiphenylsilyl)-1,1'-binaphthalene-2,2'-diol **2.31**

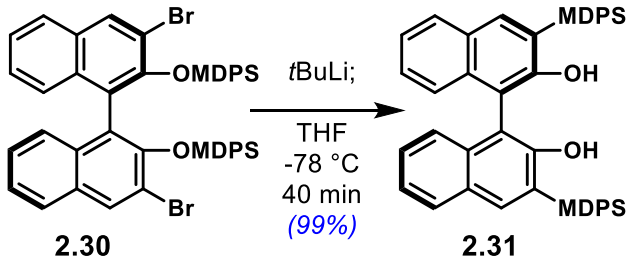

Important: The starting material is dried in high-vacuum overnight for better results.

Compound **2.30** (716 mg, 0.85 mmol, 1.0 equiv.) was dissolved in dry THF (8.6 mL). Then, at -78 °C, *tert*-butyl lithium (2.0 mL, 1.7 M sln. in pentane, 4.0 equiv.) was added dropwise. After addition, the reaction was stirred at -78 °C for 40 min. The reaction was *quenched at -78 °C* with 1 N HCl (4.3 mL). Then, the reaction was allowed to reach rt. After that, it was diluted with Et_2O (7.8 mL). The organic layer was separated and the aqueous phase extracted with Et_2O (8 mL, x3). The combined organic layers were dried over $MgSO_4$ and the solvent removed in vacuo. Column chromatography (8% EtOAc in hexane) afforded the pure product (579 mg, 0.85 mmol, 99%).

Spectral data consistent with the literature[332]

Physical state: white foam

TLC: R_f= 0.35 (10% EtOAc in hexane).

^{1}H NMR (600 MHz, $CDCl_3$): δ 7.89 (s, 2H), 7.76 (dd, *J*=5.8, 3.4 Hz, 2H), 7.61 (t, *J*=6.6 Hz, 8H), 7.41 (m, 12H), 7.32 (m, 4H), 7.19 (m, 2H), 5.24 (s, 2H), 0.99 (s, 6H)

^{13}C NMR (125 MHz, $CDCl_3$): δ 157.0, 140.9, 136.4, 135.3, 135.3, 134.7, 129.5, 129.5, 129.3, 129.0, 128.1, 128.0, 127.9, 125.3, 124.8, 123.9, 110.2, -2.9

(R)-3,3'-*bis*(methyldiphenylsilyl)-1,1'-binaphthalene-2,2'-diol-*N*-triflylphosphoramide *(R)-NTPA*-**7**

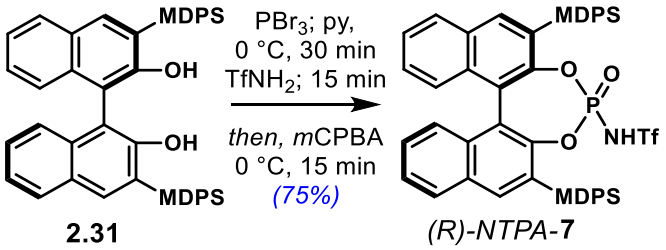

2.31 *(R)-NTPA*-**7**

BINOL precursor **2.31** (150 mg, 0.22 mmol, 1.0 equiv.) was dissolved in dry pyridine (4.4 mL). Then, in an ice bath, phosphorus (III) bromide (25 μL, 0.26 mmol, 1.2 equiv.) was added dropwise. The reaction is stirred in the ice bath for 30 min. Then, $TfNH_2$ (66 mg, 0.44 mmol, 2.0 equiv.) was added in one portion and stirred for further 15 min. After that, *m*CPBA (76 mg, 0.44 mmol, 2.0 equiv.) was added in one portion. The reaction was let to reach rt and stirred for 15 min. After that time, was quenched with 1N HCl (20 mL) and partitioned with EtOAc (10 mL). The organic layer was separated and the aqueous phase extracted with EtOAc (10 mL x3). The combined organic layers were washed with 6N HCl (10 mL), dried over $MgSO_4$ and the solvent removed in vacuo. Column chromatography (25% to 50% EtOAc in hexane) afforded the pure product. That product was redissolved in EtOAc (10 mL) and washed with 6N HCl (10 mL x3) to afford the free acid (144 mg, 0.16 mmol, 75%).

Physical state: yellowish foam

TLC: R_f= 0.25 (50% EtOAc in hexane). *Intense bright spot under UV*.

mp: >280 °C

$[\alpha]_D$: -174.4° (c=0.86, 25 °C)

^{1}H NMR (700 MHz, $CDCl_3$): δ 8.11 (s, 1H), 7.87 (d, *J*=8.2 Hz, 1H), 7.84 (s, 1H), 7.74 (d, *J*=8.2 Hz, 1H), 7.65 (t, *J*=8.3 Hz, 4H), 7.58 (d, *J*=6.8 Hz, 2H), 7.47 (m, 1H), 7.42 (m, 12H), 7.32 (m, 2H), 7.28 (d, *J*=7.6 Hz, 2H), 7.18 (d, *J*=8.5 Hz, 1H), 7.08 (d, *J*=8.5 Hz, 1H), 1.10 (s, 3H), 1.09 (s,3H)

^{13}C NMR (175 MHz, $CDCl_3$): δ 150.1, 150.0, 142.0, 140.9, 136.0, 135.8, 135.7, 135.5, 135.4, 135.1, 134.8, 134.2, 134.0, 131.4, 131.3, 130.2, 130.1, 129.7, 129.5, 128.9, 128.7, 128.6, 128.5, 128.1, 128.0, 127.9, 127.8, 127.1, 126.9, 126.8, 126.3, 126.1, 121.4, 120.7, -2.3, -2.6

^{31}P NMR (100 MHz, $CDCl_3$): δ -7.07

^{19}F NMR (100 MHz, $CDCl_3$): δ -77.29

HRMS (m/z): Calc. for $C_{47}H_{37}NO_5F_3NaSi_2PS$: 894.1518. Found: 894.1539

Phenyl sulfenyl bromide

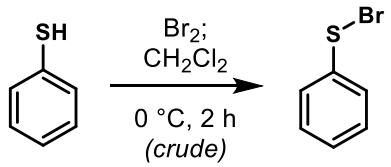

Caution: *The reaction was conducted under argon atmosphere using a balloon to avoid HBr(g) going to the Schlenk line. Work inside an efficient fume cupboard.*

Thiophenol (1.08 mL, 10.6 mmol, 4.3 equiv.) was dissolved in dry CH_2Cl_2 (100 mL). In an ice bath and **in the dark**, bromine (0.56 mL, 11.0 mmol, 4.5 equiv.) is dropwise added. The reaction was stirred in the ice bath and **in the dark** for 2 h. After that, the reaction was thoroughly flushed with argon several times to remove most of the HBr(g). The solvent is removed *in vacuo* and the resulting deep orange-red solid dried under high vacuum **in the dark** for 2 h. The crude product is used immediately in the next reaction without further purification.

Spectral data consistent with the literature.[333]

Physical state: deep orange-red solid

^{1}H NMR (400 MHz, $CDCl_3$): δ 7.50 (d, *J* = 7.7 Hz, 2H), 7.31 (t, *J* = 7.5 Hz, 2H), 7.23 (t, *J* = 7.3 Hz, 1H)

^{13}C NMR (100 MHz, $CDCl_3$): δ 137.2, 129.2, 127.7, 127.3

(R)-3,3'-*bis*(phenylsulfenyl)-2,2'-*bis*(methoxymethoxy)-1,1'-binaphthalene **2.57**

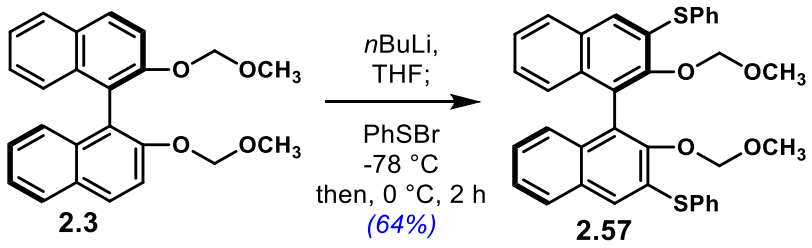

Caution: *Thiophenol may be released during the work-up stage. Work inside an efficient fume cupboard.*

A round bottom flask was charged with **2.3** (914 mg, 2.44 mmol, 1.0 equiv.), evacuated, refilled with argon (x3) and dissolved in dry THF (12 mL). At -78 °C (dry ice – acetone bath), *n*BuLi (3.9 mL, 5.86 mmol, 2.4 equiv. 1.5 M solution in hexanes) was dropwise added. A yellow solution was observed. After addition, the reaction was stirred for 1 h in an ice bath; after that time, a beige suspension is formed. At -78 °C (dry ice – acetone bath), a solution of freshly prepared crude phenylsulfenyl bromide (*ca.* 10.5 mmol, 4.3 equiv.) in dry THF (12 mL, +2 mL rinse) was dropwise added via cannula *–a dense fume may appear*. After addition, the reaction was stirred in an ice bath for 2 h. The reaction was quenched with buffer solution (24 mL, pH 7), then, diluted with water (15 mL) and Et_2O (20 mL). The organic layer was separated and the aqueous phase extracted with Et_2O (20 mL x3). The combined organic layers were dried over $MgSO_4$ and the solvent removed *in vacuo*. Column chromatography (5% EtOAc in PE) afforded the pure product (921 mg, 1.56 mmol, 64%).

Physical state: white foam

TLC: R_f= 0.36 (20% EtOAc in PE)

^{1}H NMR (400 MHz, $CDCl_3$): δ 7.63 (d, *J* = 8.2 Hz, 2H), 7.57 (m, 4H), 7.55 (s, 2H), 7.42 (m, 6H), 7.35 (ddd, *J* = 8.1, 5.1, 3.0 Hz, 2H), 7.22 (d, *J* = 3.4 Hz, 4H), 4.81 (q, *J* = 5.6 Hz, 4H), 2.79 (s, 6H)

^{13}C NMR (100 MHz, $CDCl_3$): δ 151.2, 133.5, 133.4, 132.9, 132.3, 131.2, 129.7, 129.4, 128.3, 127.2, 126.5, 126.3, 126.0, 125.6, 99.0, 56.7

(R)-3,3'-*bis*(phenylsulfonyl)-2,2'-*bis*(methoxymethoxy)-1,1'-binaphthalene **2.58**

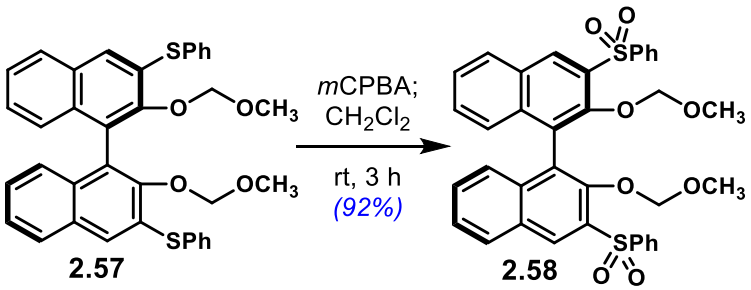

Note: *No need to use anhydrous conditions for this reaction. It can also be done in an open flask.*

Compound **2.57** (153 mg, 0.26 mmol, 1.0 equiv.) was dissolved in CH_2Cl_2 (5 mL). Then, *m*CPBA (315 mg, 1.27 mmol, 5.1 equiv. *ca.* 70%) was added in one portion. The reaction warms up gently. The mixture is stirred at rt for 3 h. After that time, the reaction was quenched with $NaHCO_3$ (5 mL) and $Na_2S_2O_3$ (5 mL). The organic layer was separated and the aqueous phase extracted with CH_2Cl_2 (5 mL, x3). The combined organic layers were dried over $MgSO_4$ and the solvent removed *in vacuo*. This procedure, without further purification, affords the desired product (157 mg, 0.24 mmol, 92%).

Physical state: white solid

TLC: R_f= 0.29 (40% EtOAc in PE)

mp: 248-250 °C

^{1}H NMR (400 MHz, $CDCl_3$): δ 8.90 (s, 2H), 8.05 (d, *J*=8.2 Hz, 2H), 7.99 (m, 4H), 7.60 (t, *J*=7.5 Hz, 2H), 7.48 (m, 6H), 7.31 (m, 2H), 6.97 (d, *J*=8.5 Hz, 2H), 4.79 (d, *J*=5.1 Hz, 2H), 4.35 (d, *J*=5.1 Hz, 2H), 2.10 (s, 6H)

^{13}C NMR (100 MHz, $CDCl_3$): δ 149.7, 141.5, 136.5, 134.7, 133.3, 132.7, 129.9, 129.7, 129.4, 1298.7, 128.5, 127.2, 126.7, 126.0, 100.4, 55.7

(R)-3,3'-*bis*(phenylsulfonyl)-1,1'-binaphthalene-2,2'-diol **2.59**

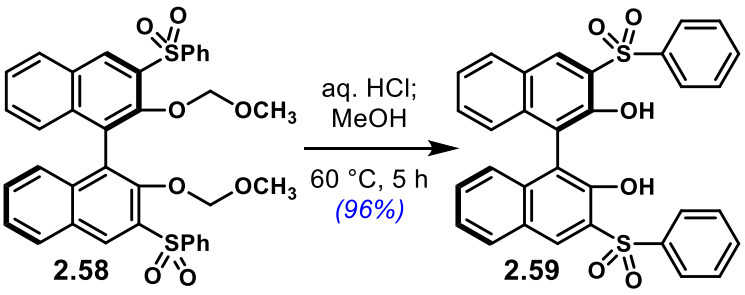

Note: *No need to use anhydrous conditions or argon atmosphere for this reaction.*

Starting material **2.58** (132 mg, 0.2 mmol, 1.0 equiv.) was suspended in methanol (5 mL). Then, at rt, aq. HCl (0.2 mL, *conc.*) was added dropwise. The reaction was stirred at 60 °C for 5 h. Then, cooled down to rt and the volatiles removed *in vacuo*. The residue was partitioned in CH_2Cl_2 (10 mL) and water (10 mL). The organic layer was separated and the aqueous phase extracted with CH_2Cl_2 (5 mL, x3). The combined organic layers were dried over $MgSO_4$ and the solvent removed *in vacuo*. This procedure, without further purification, affords the desired product. Alternatively, column chromatography (20% EtOAc in PE) can be used (110mg, 0.19 mmol, 96%).

Spectral data consistent with the literatre.[157]

Physical state: slightly yellow solid

TLC: R_f= 0.21 (40% EtOAc in PE)

mp: 226-228 °C

$[\alpha]_D$: +153.3° (c=0.36, 25° C)

^{1}H NMR (400 MHz, $CDCl_3$): δ 8.60 (s, 4H), 8.03 (m, 4H), 7.94 (d, *J*=8.0 Hz, 2H), 7.61 (m, 2H), 7.53 (dd, *J*=10.5, 4.7 Hz, 4H), 7.40 (m, 2H), 7.34 (ddd, *J*=8.2, 6.9, 1.3 Hz, 2H), 7.03 (d, *J*=8.4 Hz, 2H)

^{13}C NMR (100 MHz, $CDCl_3$): δ 148.7, 141.5, 136.8, 134.0, 132.5, 130.3, 129.9, 129.6, 127.7, 127.2, 126.5, 125.3, 124.8, 118.1

HRMS (m/z): Calc. for $C_{32}H_{23}O_6S_2$: 567.0936. Found: 567.0960

(R)-3,3'-*bis*(phenylsulfonyl)-1,1'-binaphthalene-2,2'-diol-phosphoric acid *(R)-PA*-**9**

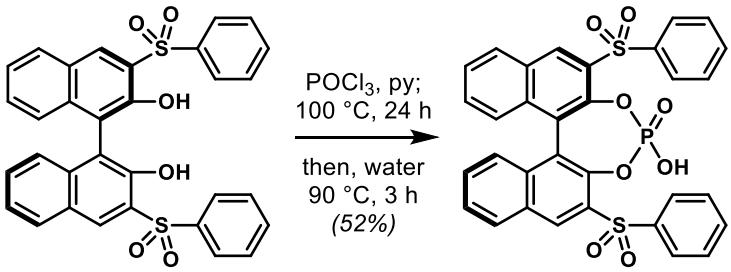

A round bottom flask was charged with **2.59** (96 mg, 0.170 mmol, 1.0 equiv.) and dried in high vacuum for at least 2 h. Then, the flask was filled with argon the starting material dissolved in dry pyridine (0.5 mL). A yellow solution is obtained. At rt, phosphorus (V) oxychloride (48 μL, 0.51 mmol, 3.0 equiv.) was added in one portion. A white precipitate is formed after *ca*. 15 min. The mixture was heated to 100 °C and stirred for 24 h –the precipitate dissolves at 60 °C. Then, the mixture was cooled down to rt and water (0.5 mL) added dropwise. ***Caution:*** *The reaction is highly exothermic!* A white precipitate is formed. The reaction is then heated to 90 °C and stirred vigorously for 3 h –the precipitate dissolves upon heating. After that, the mixture was cooled down to rt and CH_2Cl_2 was added (3 mL) followed by 1 N HCl (2 mL). The biphasic system was stirred until no solids were observed. The aqueous layer is separated and the organic phase washed with 1 N HCl (3 mL, x2). After the second HCl extraction, the organic phase seems to be pyridine-free –second aqueous wash pH 0. The organic layer was dried over $MgSO_4$ and the solvent removed *in vacuo*. Column chromatography (6% to 10% MeOH in CH_2Cl_2) afforded the clean product as a metals salt. This was dissolved in chloroform (7 mL) and washed with 6 N HCl (5 mL, x4), the organic layer was then dried over $MgSO_4$ and the solvent removed *in vacuo* to afford the free acid (55 mg, 0.087 mmol, 52%).

Physical state: light yellow powder

TLC: R_f= 0.18 (10% MeOH in CH_2Cl_2). *Intense bright spot under UV*.

mp: 167-170 °C

$[\alpha]_D$: +190.3° (c=1.1, 25 °C)

^{1}H NMR (400 MHz, $CDCl_3$): δ 8.96 (s, 2H), 8.10 (m, 2H), 8.04 (m, 4H), 7.96 (d, *J*=8.3 Hz, 2H), 7.57 (m, 4H), 7.40 (m, 4H), 7.04 (dd, *J*=8.0, 0.6 Hz, 2H)

^{13}C NMR (100 MHz, $CDCl_3$): δ 149.2, 148.5, 141.4, 140.0, 136.7, 134.7, 130.1, 129.8, 129.8, 128.7, 128.2, 127.6, 127.1, 126.3, 118.0

^{31}P NMR (100 MHz, $CDCl_3$): δ -4.26

HRMS (m/z): Calc. for $C_{32}H_{22}O_8S_2P$: 629.0494. Found: 629.0511

(R)-3,3'-*bis*(phenylsulfonyl)-1,1'-binaphthalene-2,2'-diol-*N*-triflylphosphoramide *(R)-NTPA*-**8**

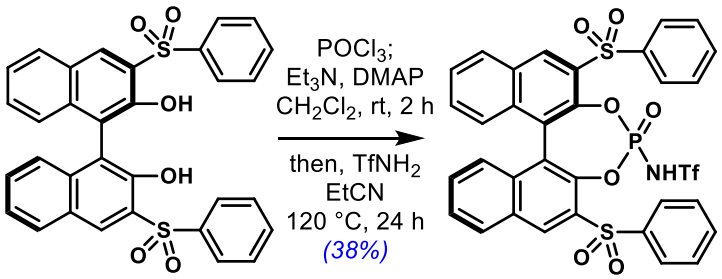

Starting material **2.59** (80.1 mg, 0.14 mmol, 1.0 equiv.) was dried in high vacuum overnight. Then, DMAP (35 mg, 0.28 mmol, 2.0 equiv.) was added and both regents dissolved in dry CH_2Cl_2 (0.8 mL). At rt, triethylamine (138 μL, 0.99 mmol, 7.0 equiv.) was added dropwise. Then, in an ice bath, phosphorus (V) oxychloride (20 μL, 0.21 mmol, 1.5 equiv.) was added dropwise. The reaction was stirred for 15 min in the ice bath and then at rt for 2 h. Then, a solution of $TfNH_2$ (43 mg, 0.28 mmol, 2.0 equiv.) in dry EtCN (2 mL) was added. The reaction was refluxed at 120 °C for 24 h, then, cooled down to rt, quenched with water (1 mL) and stirred for 1 h. The organic layer was separated and the aqueous phase extracted with EtOAc (2 mL, x3). The combined organic layers were washed with $NaHCO_3$ (3 mL), 6 N HCl (3 mL, x2), dried over $MgSO_4$ and the solvent removed *in vacuo*. Column chromatography (25% hexane in EtOAc) affords the product, presumably as a salt. The product was dissolved in EtOAC (15 mL), washed with 6 N HCl (5 mL, x4) and dried over $MgSO_4$. Removal of solvent *in vacuo* affords the desired product as the free acid (40 mg, 0.05 mmol, 38%).

Physical state: white-off solid

TLC: R_f= 0.36 (20% hexane in EtOAc). *Intense bright spot under UV*.

mp: 196-200 °C

$[\alpha]_D$: -84.4 °C (c=1.16, 25 °C)

^{1}H NMR (400 MHz, $CDCl_3$): δ 9.10 (s, 1H), 9.03 (s, 1H), 8.16 (dd, *J*=8.3, 2.9 Hz, 4H), 8.03 (d, *J*=8.0 Hz, 2H), 7.70 (d, *J*=7.7 Hz, 1H), 7.57 (m, 8H), 7.39 (dd, *J*=11.9, 4.5 Hz, 1H), 7.06 (d, *J*=8.7 Hz, 1H), 6.99 (d, *J*=8.6 Hz, 1H), 5.71 (s, br, 1H)

^{13}C NMR (100 MHz, $CDCl_3$): δ 176.4, 171.5, 141.4.141.3, 140.3, 139.0, 135.6, 134.9, 134.7, 134.5, 134.4, 133.9, 132.4, 130.9, 130.5, 130.3, 130.3, 129.7, 129.3, 128.8, 128.6, 128.4, 128.2, 127.3, 126.9. 123.2, 123.1

^{31}P NMR (100 MHz, $CDCl_3$): δ -6.8

^{19}F NMR (100 MHz, $CDCl_3$): δ -76.5

HRMS (m/z): Calc. for $C_{33}H_{22}NO_9S_3F_3P$: 760.0146. Found: 760.0144

(R)-3,3'-*bis*(benzylsulfenyl)-2,2'-*bis*(methoxymethoxy)-1,1'-binaphthalene **2.61**

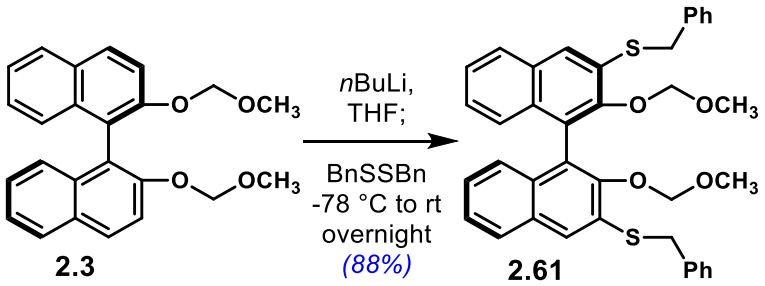

Caution: *Benzyl thiol is released during the work-up stage. Work inside an efficient fume cupboard.*

A round bottom flask was charged with **2.3** (1.01 g, 2.67 mmol, 1.0 equiv.), evacuated, refilled with argon (x3) and dissolved in dry THF (13 mL). At -78 °C (dry ice – acetone bath), *n*BuLi (4.0 mL, 6.41 mmol, 2.4 equiv. 1.6 M solution in hexanes) was dropwise added. A yellow solution was observed. After addition, the reaction was stirred for 1 h in an ice bath; after that time, a beige suspension is formed. At -78 °C (dry ice – acetone bath), a solution of dibenzyl disulfide (1.85 g, 7.48 mmol, 2.8 equiv. Dried overnight in high vacuum) in dry THF (10 mL, +2 mL rinse) was dropwise added via cannula. After addition, the reaction was stirred overnight with the cooling bath on to allow the temperature to increase slowly. The reaction was quenched with NH_4Cl (30 mL), then, diluted with water (10 mL) and Et_2O (10 mL). The organic layer was separated and the aqueous phase extracted with Et_2O (15 mL x3). The combined organic layers were dried over $MgSO_4$ and the solvent removed *in vacuo*. Column chromatography (10% EtOAc in hexane) afforded the pure product (1.46 g, 2.36 mmol, 88%).

Physical state: white foam

TLC: R_f= 0.33 (20% EtOAc in hexane)

mp: 42-44 °C

^{1}H NMR (600 MHz, $CDCl_3$): δ 7.81 (s, 2H), 7.75 (d, *J*=8.2 Hz, 2H), 7.47 (d, *J*=7.4 Hz, 4H), 7.39 (m, 2H), 7.34 (t, *J*=7.6 Hz, 4H), 7.28 (m, 2H), 7.23 (m, 2H), 7.17 (d, *J*=8.5 Hz, 2H), 4.79 (d, *J*=5.5 Hz, 2H), 4.74 (d, *J*=5.5 Hz, 2H), 4.32 (d, *J*=4.0 Hz, 4H), 2.69 (s, 6H)

^{13}C NMR (150 MHz, $CDCl_3$): δ 151.3, 136.9, 132.5, 131.7, 131.1, 129.2, 128.7, 127.7, 127.5, 127.0, 126.5, 126.0, 125.8, 125.6, 98.7, 56.6, 37.3

(R)-3,3'-*bis*(benzylsulfonyl)-2,2'-*bis*(methoxymethoxy)-1,1'-binaphthalene **2.62**

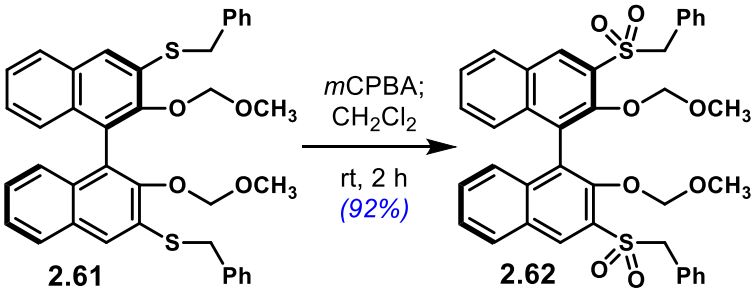

Note: *No need to use anhydrous conditions for this reaction. It can also be done in an open flask.*

Compound **2.61** (258 mg, 0.42 mmol, 1.0 equiv.) was dissolved in CH_2Cl_2 (8 mL). Then, *m*CPBA (508 mg, 2.06 mmol, 5.1 equiv. *ca.* 70%) was added in one portion. The reaction warms up gently. The mixture is stirred at rt for 2 h. After that time, the reaction was quenched with $NaHCO_3$ (8.5 mL) and $Na_2S_2O_3$ (1.7 mL). The organic layer was separated and the aqueous phase extracted with CH_2Cl_2 (8 mL, x3). The combined organic layers were dried over $MgSO_4$ and the solvent removed *in vacuo*. Column chromatography (20% to 30% EtOAc in hexane) affords the pure product (262 mg, 0.38 mmol, 92%).

Physical state: white foam

TLC: R_f= 0.32 (40% EtOAc in hexane)

mp: 83-86 °C

^{1}H NMR (600 MHz, $CDCl_3$): δ 8.58 (s, 2H), 7.98 (d, *J*=8.1 Hz, 2H), 7.55 (t, *J*=7.3 Hz, 2H), 7.50 (t, *J*=7.6 Hz, 2H), 7.41 (m, 4H), 7.32 (d, *J*=6.7 Hz, 6H), 7.21 (d, *J*=8.5 Hz, 2H), 5.11 (d, *J*=5.4Hz, 2H), 4.86 (d, *J*=13.8 Hz, 2H), 4.83 (d, *J*=5.4 Hz, 2H), 4.69 (d, *J*=13.8 Hz, 2H), 2.66 (s, 6H)

^{13}C NMR (150 MHz, $CDCl_3$): δ 150.2, 136.6, 134.0, 132.2, 131.1, 130.0, 129.8, 129.4, 129.0, 128.8, 128.0, 127.5, 126.8, 126.1, 101.2, 61.5, 56.7

(R)-3,3'-*bis*(benzylsulfonyl)-1,1'-binaphthalene-2,2'-diol **2.63**

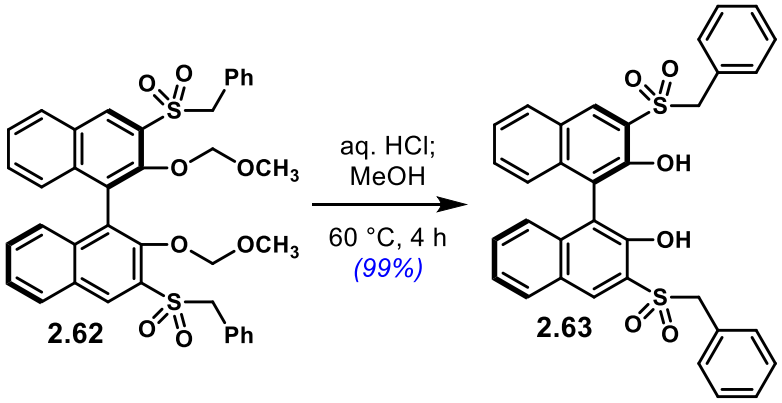

Note: *No need to use anhydrous conditions or argon atmosphere for this reaction.*

Starting material **2.62** (220 mg, 0.32 mmol, 1.0 equiv.) was suspended in methanol (8 mL). Then, at rt, aq. HCl (0.2 mL, *conc.*) was added dropwise. The reaction was stirred at 60 °C for 4 h. Then, cooled down to rt and the volatiles removed *in vacuo*. The residue was partitioned in CH_2Cl_2 (10 mL) and water (10 mL). The organic layer was separated and the aqueous phase extracted with CH_2Cl_2 (5 mL, x3). The combined organic layers were dried over $MgSO_4$ and the solvent removed *in vacuo*. This procedure, without further purification, affords the clean desired product. (190 mg, 0.32 mmol, 99%).

Physical state: white foam

TLC: R_f= 0.32 (50% EtOAc in hexane)

mp: 95-100 °C

$[\alpha]_D$: +90.4° (c=2.07, 25 °C)

^{1}H NMR (600 MHz, $CDCl_3$): δ 8.22 (s, 2H), 8.00 (s, 2H), 7.83 (m, 2H), 7.40 (m, 4H), 7.30 (t, *J*=7.4 Hz, 2H), 7.24 (t, *J*=7.5 Hz, 4H), 7.16 (d, *J*=7.3 Hz, 4H), 7.00 (m, 2H), 4.55 (d, *J*=4.3 Hz, 4H)

^{13}C NMR (150 MHz, $CDCl_3$): δ 149.1, 137.1, 133.4, 131.0, 130.3, 129.9, 129.3, 129.0, 127.4, 125.3, 124.9, 122.9, 117.4, 63.3

HRMS (m/z): Calc. for $C_{34}H_{27}O_6S_2$: 595.1249. Found: 595.1250

(R)-3,3'-bis(benzylsulfonyl)-1,1'-binaphthalene-2,2'-diol-phosphoric acid *(R)-PA*-**10**

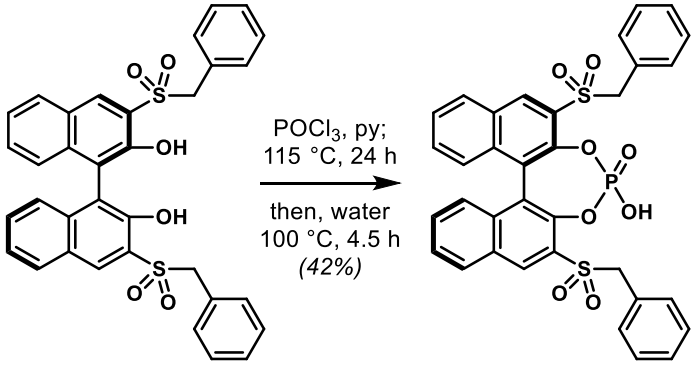

A round bottom flask was charged with **2.63** (158 mg, 0.25 mmol, 1.0 equiv.) and DMAP (77 mg, 0.63 mmol, 2.4 equiv.) and dried in high vacuum for at least 2 h. Then, the flask was filled with argon the starting materials dissolved in dry pyridine (1.2 mL). A bright yellow solution is obtained. At rt, phosphorus (V) oxychloride (143 μL, 1.52 mmol, 6.0 equiv.) was added in one portion. A white precipitate is formed after *ca*. 15 min. The mixture was heated to 115 °C and stirred for 24 h –the precipitate dissolves after 3 h. Then, the mixture was cooled down to rt and water (1.2 mL) added dropwise. ***Caution:*** *The reaction is highly exothermic!* A white precipitate is formed. The reaction is then heated to 100 °C and stirred vigorously for 4.5 h –the precipitate dissolves upon heating. After that, the mixture was cooled down to rt and CH_2Cl_2 was added (5 mL) followed by 1 N HCl (5 mL). The biphasic system was stirred until no solids were observed. The aqueous layer is separated (pH 4) and the organic phase washed with 1 N HCl (5 mL, x2). After the second HCl extraction, the organic phase seems to be pyridine-free –second aqueous wash pH 0. The organic layer was dried over $MgSO_4$ and the solvent removed *in vacuo*. Column chromatography (6% MeOH in CH_2Cl_2) afforded the clean product as a metal salt. This was dissolved in CH_2Cl_2 (7 mL) and washed with 6 N HCl (5 mL, x4), the organic layer was then dried over $MgSO_4$ and the solvent removed *in vacuo* to afford the free acid (74 mg, 0.11 mmol, 42%).

Physical state: light yellow powder

TLC: R_f= 0.20 (10% MeOH in CH_2Cl_2). *Intense bright spot under UV*.

mp: 147-152 °C

^{1}H NMR (700 MHz, $CDCl_3$): δ 8.22 (s, 2H), 7.99 (s, 2H), 7.83 (dd, *J*=6.5, 2.9 Hz, 2H), 7.41 (m, 4H), 7.30 (t, *J*=7.4 Hz, 2H), 7.24 (t, *J*=7.6 Hz, 4H), 7.15 (d, *J*=7.4 Hz, 4H), 7.01 (m, 2H), 4.55 (m, 4H)

^{13}C NMR (175 MHz, $CDCl_3$): δ 149.1, 137.1, 133.4, 131.0, 130.4, 129.9, 129.3, 129.0, 127.4, 125.3, 124.9, 122.9, 117.5, 63.3

^{31}P NMR (100 MHz, $CDCl_3$): δ 25.0

HRMS (m/z): Calc. for $C_{34}H_{26}O_8S_2P$: 657.0807. Found: 657.0810

(R)-3,3'-*bis*(phenylsulfenyl)-1,1'-binaphthalene-2,2'-diol **2.60**

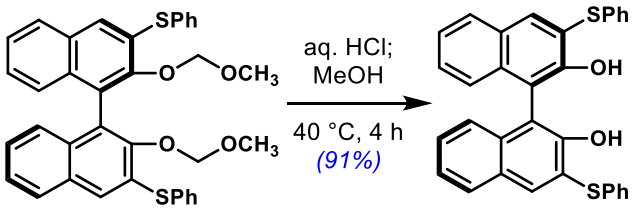

Note: *No need to use anhydrous conditions or argon atmosphere for this reaction.*

Starting material **2.57** (350 mg, 0.59 mmol, 1.0 equiv.) was suspended in methanol (12 mL). Then, at rt, aq. HCl (0.2 mL, *conc.*) was added dropwise. The reaction was stirred at 40 °C for 4 h. Then, cooled down to rt and the volatiles removed *in vacuo*. The residue was partitioned in CH_2Cl_2 (10 mL) and water (10 mL). The organic layer was separated and the aqueous phase extracted with CH_2Cl_2 (5 mL, x3). The combined organic layers were dried over $MgSO_4$ and the solvent removed *in vacuo*. Column chromatography (50% CH_2Cl_2 in PE) afforded the desired product (274mg, 0.55 mmol, 91%).

Spectral data consistent with the literature.[155]

Physical state: white foam

TLC: R_f= 0.25 (50% CH_2Cl_2 in PE)

mp: 69-73 °C

$[\alpha]_D$: +97.7° (c=0.53, 25 °C)

^{1}H NMR (400 MHz, $CDCl_3$): δ 8.17 (s, 2H), 7.82 (d, *J*=7.8 Hz, 2H), 7.37 (d, *J*=6.8 Hz, 2H), 7.34 (dd, *J*= 4.1, 1.3 Hz, 2H), 7.30 (d, *J*=4.3 Hz, 8H), 7.22 (m, 4H), 6.34 (s, 2H)

^{13}C NMR (100 MHz, $CDCl_3$): δ 151.0, 136.2, 135.1, 134.6, 129.5, 129.3, 128.7, 128.3, 127.9, 127.0, 124.9, 124.4, 121.3, 114.9

2,4,6-tri*iso*propylbenzenesunfonyl fluoride **2.67**

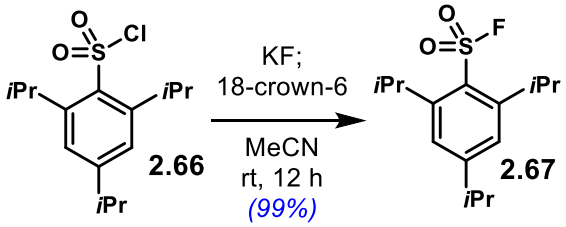

Sulfonyl chloride **2.66** (5.62 g, 18.0 mmol. 1.0 equiv.) was suspended in dry acetonitrile (60 mL). Then, potassium fluoride (5.23g, 90.0 mmol, 5.0 equiv.) was added in one portion followed by 18-crown-6 (240 mg, 0.90 mmol, 0.05 equiv.). The reaction was stirred at rt for 12 h. After that, the solvent was removed *in vacuo*. The residue was dissolved in EtOAc (150 mL), washed with water (60 mL, x3) and brine (60 mL). Then, dried over $MgSO_4$ and the solvent removed *in vacuo*. This procedure affords the clean product without further purification. Otherwise, column chromatography (hexane to 5% EtOAc in hexane) to purify (5.2 g, 18.0 mmol, 99%).

Spectral data consistent with the literatre.[159]

Physical state: white solid

^{1}H NMR (600 MHz, $CDCl_3$): δ 7.23 (s, 2H), 3.95 (dhept, *J*=6.7, 2.2 Hz, 2H), 2.94 (hept, *J*=6.9 Hz, 1H), 1.29 (d, *J*=6.7 Hz, 12H), 1.27 (d, *J*=6.9 Hz, 6H)

^{13}C NMR (150 MHz, $CDCl_3$): δ 155.5, 150.9, 124.1(d, *J*=1.3 Hz), 34.6, 30.3(d, *J*=2.4 Hz), 24.7, 23.6

^{19}F NMR (100 MHz, $CDCl_3$): δ 73.4

(R)-3,3'-*bis*((2,4,6-tri*iso*propylphenyl)sulfonyl)-1,1'-binaphthalene-2,2'-diol **2.69**

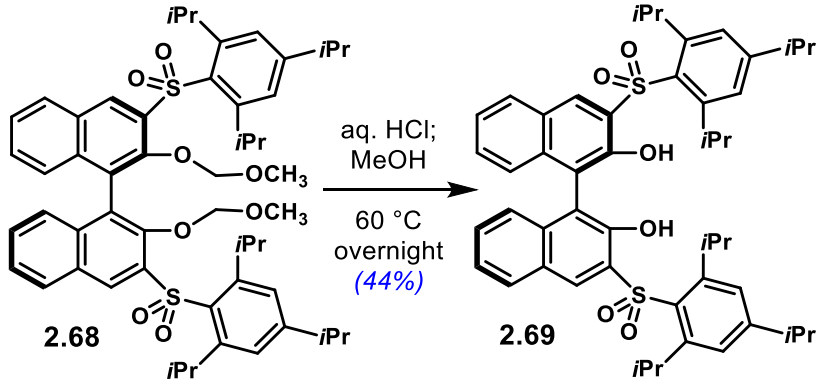

Note: *No need to use anhydrous conditions or argon atmosphere for this reaction.*

Starting material **2.68** (572 mg, 0.63 mmol, 1.0 equiv.) was suspended in methanol (12.5 mL). Then, at rt, aq. HCl (0.4 mL, *conc.*) was added dropwise. The reaction was stirred at 60 °C for 12 h. Then, cooled down to rt and the volatiles removed *in vacuo*. The residue was partitioned in CH_2Cl_2 (10 mL) and water (10 mL). The organic layer was separated and the aqueous phase extracted with CH_2Cl_2 (5 mL, x3). The combined organic layers were dried over $MgSO_4$ and the solvent removed *in vacuo*. Column chromatography (20% EtOAc in hexane) affords the desired product (230 mg, 0.28 mmol, 44%).

Physical state: white solid

TLC: R_f= 0.43 (25% EtOAc in hexane)

mp: 270-272 °C

$[\alpha]_D$: +97.0° (c=0.55, 25° C)

^{1}H NMR (600 MHz, $CDCl_3$): δ 8.64 (s, 2H), 8.13 (s, 2H), 8.82 (dd, *J*=6.5, 2.9 Hz, 2H), 7.36 (m, 4H), 7.23 (s, 4H), 7.13 (dd, *J*=6.9, 2.5 Hz, 2H), 4.26 (hept, *J*=6.7 Hz, 4H), 2.95 (hept, *J*=6.9 Hz, 2H), 1.29 (d, *J*=6.9 Hz, 12H), 1.24 (d, *J*=6.7 Hz, 12H), 1.18 (d, *J*=6.7 Hz, 12H)

^{13}C NMR (150 MHz, $CDCl_3$): δ 154.6, 151.4, 149.0, 136.1, 133.4, 130.6, 130.1, 129.6, 129.4, 127.3, 124.9, 124.9, 124.3, 117.7, 34.4, 29.6, 24.9, 24.7, 23.7, 23.7

HRMS (m/z): Calc. for $C_{50}H_{58}O_6S_2$: 818.3675. Found: 818.3670

(R)-3,3'-bis((2,4,6-triisopropylphenyl)sulfonyl)-1,1'-binaphthalene-2,2'-diol-phosphoric acid *(R)-PA*-**11**

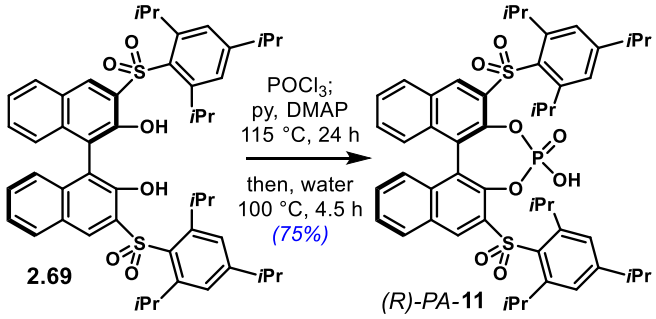

A round bottom flask was charged with **2.69** (230 mg, 0.28 mmol, 1.0 equiv.) and DMAP (86 mg, 0.70 mmol, 2.5 equiv.) and dried in high vacuum for at least 2 h. Then, the flask was filled with argon the starting materials dissolved in dry pyridine (1.5 mL). A bright yellow solution is obtained. At rt, phosphorus (V) oxychloride (157 μL, 1.68 mmol, 6.0 equiv.) was added in one portion. The mixture was heated to 115 °C and stirred for 24 h. Then, the mixture was cooled down to rt and water (1.5 mL) added dropwise. ***Caution:*** *The reaction is highly exothermic!* A white precipitate is formed. The reaction is then heated to 100 °C and stirred vigorously for 4.5 h –the precipitate dissolves upon heating. After that, the mixture was cooled down to rt and CH_2Cl_2 was added (8 mL) followed by 1 N HCl (8 mL). The biphasic system was stirred until no solids were observed. The aqueous layer is separated (pH 4) and the organic phase washed with 1 N HCl (10 mL, x2). After the second HCl extraction, the organic phase seems to be pyridine-free –second aqueous wash pH 0. The organic layer was dried over $MgSO_4$ and the solvent removed *in vacuo*. Column chromatography (5% hexane in EtOAc) afforded the clean product as a metal salt. This was dissolved in CH_2Cl_2 (15 mL) and washed with 1 N HCl (10 mL, x3), the organic layer was then dried over $MgSO_4$ and the solvent removed *in vacuo* to afford the free acid (183 mg, 0.21 mmol, 75%).

Physical state: light yellow powder

TLC: R_f= 0.35 (EtOAc). *Intense bright spot under UV*.

mp: 294-296 °C

$[\alpha]_D$: -129.9° (c=0.66, 28.4 °C)

^{1}H NMR (400 MHz, $CDCl_3$): δ 8.79 (s, 2H), 8.09 (d, *J*=8.2 Hz, 2H), 7.60 (t, *J*=7.5 Hz, 2H), 7.40 (m, 2H), 7.15 (s, 4H), 7.03 (d, *J*=8.6 Hz, 2H), 4.25 (m, 4H), 2.86 (m, 2H), 1.29 (d, *J*=6.7 Hz, 12H), 1.21 (dd, *J*=6.9, 3.3 Hz, 12H), 0.98 (d, *J*=6.7 Hz, 12H)

^{13}C NMR (100 MHz, $CDCl_3$): δ 154.4, 151.2, 143.0, 142.9, 135.6, 135.6, 134.3, 132.2, 131.6, 131.6, 130.2, 130.0, 127.4, 126.6, 126.5, 124.4, 124.3, 123.3, 123.3, 34.3, 34.2, 29.6, 29.4, 25.4, 25.4, 24.3, 24.2, 23.6, 23.6, 23.5

^{31}P NMR (100 MHz, $CDCl_3$): δ -0.90

HRMS (m/z): Calc. for $C_{50}H_{58}O_8PS_2$: 881.3311. Found: 881.3331

A2.3. Molecules from Chapter 3

Compound **3.46**

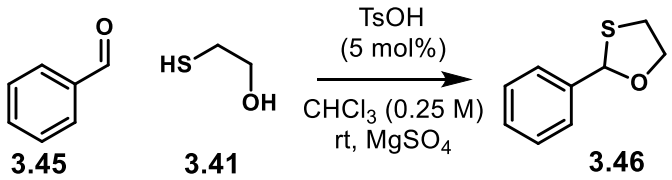

3.45 **3.41** **3.46**

Reactions to obtained compound **3.46**, both in a racemic fashion and enantioselectively were conducted in a 0.15 mmol scale. To simplify the screenings, stock solutions of benzaldehyde **3.45** and 2-mercapto ethanol **3.41** were prepared in the appropriate solvents as indicated in the text. Herein, a representative example is provided using chloroform and TsOH as catalyst.

Stock solution of benzaldehyde **3.45**: 180 μL in 3.4 mL of dry chloroform. This solution delivers 0.15 mmol, 1.0 equiv. in 0.3 mL. *Stock solution of 2-mercapto ethanol* **3.41**: 148 μL in 3.4 mL of dry chloroform. This solution delivers 0.18 mmol, 1.2 equiv. in 0.3 mL. When 0.3 mL of each solution are combined, it sums up 0.6 mL and provides **3.45** in a 0.25 M concentration.

In a 1 dram vial, tosic acid (1.46 mg, 0.0075 mmol, 0.05 equiv.) (or the corresponding catalyst) and $MgSO_4$ (50 mg) were weighed. The vial was evacuated and refilled with argon (x3). Then, at rt, 0.3 mL of **3.45** stock solution was added, followed by 0.3 mL of **3.41** stock solution. The reaction was stirred at rt for 24 h. After that time, the reaction is directly loaded into a silica column and the desired product purified (50% CH_2Cl_2 in hexane).

Spectral data consistent with the literature[334]

Physical state: clear thick oil

TLC: R_f= 0.30 (50% CH_2Cl_2 in hexane).

^{1}H NMR (400 MHz, $CDCl_3$): δ 7.49 (m, 2H), 7.36 (m, 3H), 6.08 (s, 1H), 4.54 (ddd, *J*=9.2, 6.4, 3.1 Hz, 1H), 3.97 (td, *J*=9.0, 6.1 Hz, 1H), 3.29 (ddd, *J*=9.8, 8.8, 6.4 Hz, 1H), 3.20 (m, 1H)

^{13}C NMR (100 MHz, $CDCl_3$): δ 129.1, 128.7, 128.5, 126.7, 87.1, 72.0, 34.1

SFC settings: λ_{max}=250 nm, column SB, flow rate = 2.5 mL min^{-1}, 3% MeOH in CO_2, tr1=3.10 min, tr2=3.71 min

Compound **3.49**

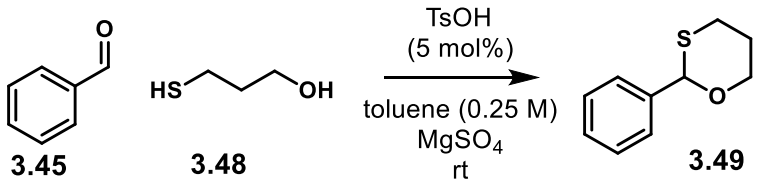

3.45 **3.48** **3.49**

Reactions to obtained compound **3.49**, both in a racemic fashion and enantioselectively were conducted in a 0.15 mmol scale. To simplify the screenings, stock solutions of benzaldehyde **3.45** and 3-mercapto propanol **3.41** were prepared in the appropriate solvents as indicated in the text. Herein, a representative example is provided using toluene and TsOH as catalyst.

Stock solution of benzaldehyde **3.45**: 180 μL in 3.4 mL of dry toluene. This solution delivers 0.15 mmol, 1.0 equiv. in 0.3 mL. *Stock solution of 3-mercapto propanol* **3.48**: 182 μL in 3.4 mL of dry toluene. This solution delivers 0.18 mmol, 1.2 equiv. in 0.3 mL. When 0.3 mL of each solution are combined, it sums up 0.6 mL and provides **3.45** in a 0.25 M concentration.

In a 1 dram vial, tosic acid (1.46 mg, 0.0075 mmol, 0.05 equiv.) (or the corresponding catalyst) and $MgSO_4$ (50 mg) were weighed. The vial was evacuated and refilled with argon (x3). Then, at rt, 0.3 mL of **3.45** stock solution was added, followed by 0.3 mL of **3.48** stock solution. The reaction was stirred at rt for 24 h. After that time, the reaction is directly loaded into a silica column and the desired product purified (50% CH_2Cl_2 in hexane).

Spectral data consistent with the literature[334]

Physical state: clear oil

TLC: R_f= 0.30 (50% CH_2Cl_2 in hexane).

^{1}H NMR (400 MHz, $CDCl_3$): δ 7.47 (m, 2H), 7.33 (m, 3H), 5.79 (s, 1H), 4.34 (ddt, *J*=12.0, 4.0, 1.9 Hz, 1H), 3.80 (td, *J*=12.3, 2.1 Hz, 1H), 3.23 (td, *J*=13.0, 2.8 Hz, 1H), 2.84 (m, 1H), 2.12 (m, 1H), 1.77 (m, 1H)

^{13}C NMR (100 MHz, $CDCl_3$): δ 139.6, 128.6, 128.5, 126.3, 84.7, 70.8, 29.4, 25.8

SFC settings: λ_{max}=257 nm, column SB, flow rate = 2.5 mL min^{-1}, 5% MeOH in CO_2, tr1=3.21 min, tr2=4.81 min

A2.4. Molecules from Chapter 4

Ethyl (E)-hepta-4,6-dienoate **4.52**

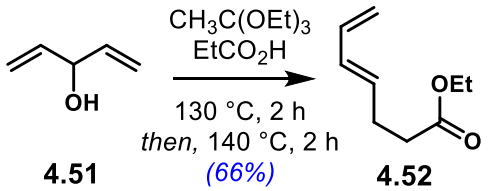

4.51 **4.52**

Divinyl carbinol **4.51** (8 mL, 80.6 mmol, 1.0 equiv.) was dissolved in triethylorthoacetate (100 mL, 548 mmol, 6.8 equiv.). Then, propionic acid was added (0.3 mL, 4.1 mmol, 0.05 equiv.). The reaction was refluxed at 130 °C for 1 h. After that, the reflux condenser was changed for a simple distillation apparatus. Heating was continued for 1 h to distil ethanol out of the reaction. Then, the condenser was put back and the mixture refluxed for further 2 h. After that time, the product was isolated by vacuum distillation (98-100 °C at 25 mmHg). (8.2 g, 53 mmol, 66%).

Spectral data consistent with the literature[335]

Physical state: clear liquid

TLC: R_f= 0.43 (10% Et_2O in PE).

^{1}H NMR (400 MHz, $CDCl_3$): δ 6.28 (dt, *J*=17.0, 10.2 Hz, 1H), 6.08 (dd, *J*=15.2, 10.4 Hz, 1H), 5.68 (ddd, *J*=13.6, 7.8, 4.0 Hz, 1H), 5.10 (d, *J*=17.0 Hz, 1H), 4.98 (d, *J*=10.1 Hz, 1H), 4.12 (q, *J*=7.1 Hz, 2H), 2.39 (d, *J*=3.0 Hz, 4H), 1.24 (t, *J*=7.1 Hz, 3H)

^{13}C NMR (100 MHz, $CDCl_3$): δ 173.1, 137.0, 132.8, 132.1, 115.8, 60.5, 34.0, 27.9, 14.4

(E)-hepta-4,6-dienamide **4.53**

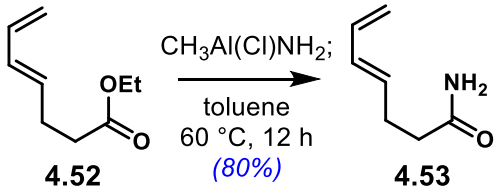

Preparation of $CH_3Al(Cl)NH_2$ solution

Ammonium chloride (4.2 g, 77.8 mmol, 3.0 equiv.) was suspended in dry toluene (40 mL). Then, in an ice bath, a solution of trimethyl aluminium (40 mL, 2.0 M sln. in toluene, 77.8 mmol, 3.0 equiv.) was added dropwise over 30 min. Then, the ice bath is removed and the mixture stirred for 2 h at rt. This procedure yields a 1.0 M solution of $CH_3Al(Cl)NH_2$ in toluene.

Ester **4.52** (4 g, 25.9 mmol, 1.0 equiv.) was dissolved in dry toluene (30 mL) and transferred via cannula to the fresh solution of the aluminium complex. Then, the reaction is stirred at 60 °C for 12 h. After that time, the reaction is cooled in an ice bath and quenched with 2 N HCl (120 mL), added dropwise. EtOAc (40 mL) is added after quenching. The organic layer was separated and the aqueous phase extracted with EtOAc (100 mL, x3). The combined organic layers were washed with brine (100 mL), dried over $MgSO_4$ and the solvent removed in vacuo. Column chromatography (EtOAc) afforded the pure product (2.61 g, 20.8 mmol, 80%).

Spectral data consistent with the literature[336]

Physical state: white solid

TLC: R_f= 0.26 (EtOAc).

^{1}H NMR (400 MHz, $CDCl_3$): δ 6.28 (dt, *J*=16.9, 10.2 Hz, 1H), 6.09 (dd, *J*=15.2, 10.4 Hz, 1H), 5.69 (m, 1H), 5.10 (d, *J*=16.8 Hz, 1H), 4.99 (d, *J*=10.2 Hz, 1H), 2.41 (dd, *J*=14.5, 7.0 Hz, 2H), 2.30 (m, 2H)

^{13}C NMR (100 MHz, $CDCl_3$): δ 175.0, 136.9, 132.8, 132.2, 116.0, 35.4, 28.3

(E)-hepta-4,6-dien-1-amine **4.47**

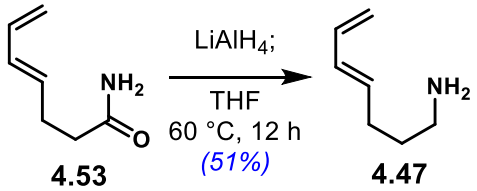

4.53 **4.47**

Amide **4.53** (0.68 g, 4.45 mmol, 1.0 equiv.) was dissolved in dry THF (45 mL). In an ice bath, $LiAlH_4$ (1.7 g, 44.5 mmol, 10 equiv.) was added portion wise. Then, the reaction was stirred at 60 °C for 12 h. After that time, the reaction was cooled in an ice bath and quenched by the sequential addition of water (1.8 mL), 15% NaOH (1.8 mL) and water (5.4 mL). Then, $MgSO_4$ was added and the mixture stirred for 1 h. The precipitate was filtered and the solvent removed in vacuo. Column chromatography (10% MeOH in CH_2Cl_2 with 5% Et_3N) afforded the pure product (227 mg, 2.04 mmol, 51%).

Spectral data consistent with the literature[337]

Physical state: yellow oil

TLC: R_f= 0.27 (10% MeOH in CH_2Cl_2 with 5% Et_3N).

^{1}H NMR (400 MHz, C_6D_6): δ 6.30 (dt, *J*=17.0, 10.3 Hz, 1H), 6.05 (dd, *J*=15.1, 10.4 Hz, 1H), 5.55 (m, 1H), 5.07 (d, *J*=16.9 Hz, 1H), 4.93 (d, *J*=10.1 Hz, 1H), 3.47 (s, 2H), 2.56 (t, *J*=7.1 Hz, 2H), 1.99 (q, *J*=7.2 Hz, 2H), 1.46 (m, 2H)

^{13}C NMR (100 MHz, C_6D_6): δ 137.7, 134.8, 131.9, 115.0, 41.3, 32.1, 30.1

2,3,4,5,6,8a-hexahydro-1H-indolizin-4-ium trifluoroacetate **4.50**

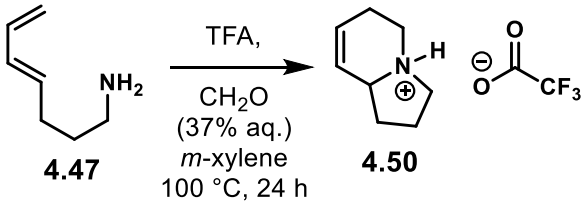

4.47 **4.50**

Amine **4.47** (22 mg, 0.19 mmol, 1.0 equiv.) was dissolved in dry *m*-xylene (0.4 mL). Then, at rt, TFA (16 μL, 0.19 mmol, 1.0 equiv.) was added. Then, formaldehyde (30 μL, 37% aq. sln. 0.39 mmol, 2.0 equiv.) was added. The reaction was stirred at 100 °C for 24 h. After that time, the reaction was cooled to rt and $MgSO_4$ added. The mixture was loaded into a short pad of silica gel, eluted with pentane (3 mL), then CH_2Cl_2 (3 mL) and finally with methanol (3 mL). Each elution was collected separately. The solvent in the last fraction was removed under a stream of nitrogen.

Physical state: white solid

TLC: R_f= 0.32 (30% IPA in CH_2Cl_2).

^{1}H NMR (400 MHz, $CDCl_3$): δ 12.85 (s, 1H), 5.97 (dtd, *J*=10.3, 4.0, 2.3 Hz, 1H), 5.66 (ddd, *J*=10.5, 4.4, 2.1 Hz, 1H), 4.36 (ddt, *J*=10.1, 5.1, 2.5 Hz, 1H), 3.75 (m, 2H), 3.44 (m, 1H), 3.18 (m, 1H), 3.05 (m, 1H), 2.39 (m, 2H), 2.10 (m, 2H), 1.83 (dt, *J*= 14.2, 6.4 Hz, 1H)

^{13}C NMR (100 MHz, $CDCl_3$): δ 124.9, 124.8, 58.7, 51.1, 44.7, 29.8, 22.2, 19.8

LCMS ES+ TIC(m/z): calc. 124.11, found: 124.32

LCMS ES- TIC(m/z): calc. 112.99, found: 112.96

(E)-N-((E)-hepta-4,6-diene-1-yl)-1-phenylmethanimine **4.57**

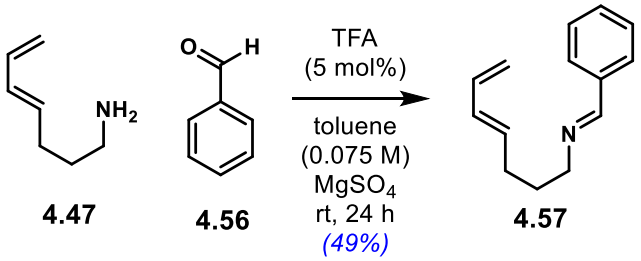

4.47 **4.56** **4.57**

In a 3.5 mL vial, $MgSO_4$ (25 mg) was weighted. Then, amine **4.47** (20 mg, 0.18 mmol, 1.2 equiv.) was dissolved in dry toluene (2 mL). Then, benzaldehyde (15 μL, 0.15 mmol, 1.0 equiv.) was added, followed by TFA. The reaction was vigorously stirred for 24 h. After that time, the reaction was quenched by adding a few drops of Et_3N. Then, the mixture was loaded into a short silica column and eluted with 10% Et_3N in hexane to afford imine **4.57** (12.6 mg, 0.063 mmol, 49%).

This procedures applies for the reactions presented on Table 4.3

Physical state: clear oil

TLC: R_f= 0.66 (20% IPA in hexane with 10% Et_3N).

^{1}H NMR (400 MHz, $CDCl_3$): δ 8.28 (s, 1H), 7.73 (dd, *J*=6.6, 2.9 Hz, 2H), 7.41 (m, 3H), 6.32 (dt, *J*=17.0, 10.2 Hz, 1H), 6.08 (dd, *J*=15.2, 10.4 Hz, 1H), 5.74 (m, 1H), 5.09 (d, *J*=16.9 Hz, 1H), 4.97 (d, *J*=10.1 Hz, 1H), 3.63 (t, *J*=6.8 Hz, 2H), 2.18 (q, *J*=7.2 Hz, 2H), 1.82 (quint, *J*=7.1 Hz, 2H)

^{13}C NMR (100 MHz, $CDCl_3$): δ 161.3, 137.4, 136.4, 134.8, 131.6, 130.7, 128.7, 128.2, 115.1, 61.1, 30.4, 30.3

(E)-5-bromopenta-1,3-diene **4.69**

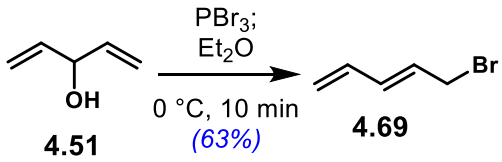

Phosphorus (III) bromide (194 μL, 2.06 mmol, 0.4 equiv.) was dissolved in dry Et_2O (2.6 mL). The solution was chilled in an ice bath. Then, divinyl carbinol **4.51** (0.5 mL, 5.14 mmol, 1.0 equiv.) was added dropwise. The reaction was stirred in the ice bath for 10 min. Then, it was quenched with brine (1 mL) and diluted with Et_2O (2 mL). The aqueous layer was separated and the organic phase was washed with $NaHCO_3$ (std. sln. 1 mL, x3) and brine (1 mL). Column chromatography (5% Et_2O in 30-40 PE) afforded the pure product (474 mg, 3.22 mmol, 63%).

Spectral data consistent with the literature[338]

Physical state: yellowish liquid

TLC: R_f= 0.56 (10% Et_2O in PE).

^{1}H NMR (400 MHz, $CDCl_3$): δ 6.31 (m, 2H), 5.89 (m, 1H), 5.28 (d, *J*=15.3 Hz, 1H), 5.17 (d, *J*=9.3 Hz, 1H), 4.03 (d, *J*=7.8 Hz, 2H)

^{13}C NMR (100 MHz, $CDCl_3$): δ 135.7, 135.4, 129.3, 119.6, 33.0

(E)-1-nitro-2-(penta-2,4-dien-1-yl)benzene **4.71**

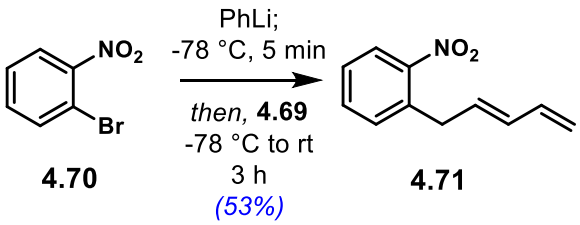

4.70 **4.71**

Phenyl lithium (2 mL, 1.9 M sln, in Bu_2O, 3.74 mmol, 2.2 equiv.) was diluted in dry THF (32 mL). Then, at -78 °C, a solution of 2-bromonitrobenzene (687 mg, 3.40 mmol, 1.0 equiv.) in dry THF (4 mL) was added dropwise. The reaction is stirred at -78 °C for 5 min. Then, bromide **4.69** (0.25 mL, 1.70 mmol, 1.0 equiv.) was added quickly in one portion. The reaction was stirred for 3 h allowing the temperature to reach rt. After that time, the reaction was quenched with NH_4Cl (20 mL, std. sln.) and water (5 mL). The organic layer was separated and the aqueous phase extracted with Et_2O (20 mL, x2). The combined organic layers were dried over $MgSO_4$ and the solvent removed in vacuo. Column chromatography (5% EtOAc in hexane) afforded the pure product (168 mg, 0.88 mmol, 53%).

Spectral data consistent with the literature[339]

Physical state: orange oil

TLC: R_f= 0.38 (10% EtOAc in hexane).

^{1}H NMR (400 MHz, $CDCl_3$): δ 7.93 (m, 1H), 7.54 (m, 1H), 7.37 (m, 2H), 6.32 (dt, *J*=16.9, 10.3 Hz, 1H), 6.12 (dd, *J*=15.2, 10.4 Hz, 1H), 5.84 (m, 1H), 5.15 (d, *J*=16.8 Hz, 1H), 5.04 (d, *J*=10.2 Hz, 1H), 3.72 (d, *J*=6.8 Hz, 2H)

^{13}C NMR (100 MHz, $CDCl_3$): δ 136.6, 135.2, 135.2, 133.4, 133.2, 132.0, 130.9, 127.5, 124.9, 116.8, 35.9

(E)-2-(penta-2,4-dien-1-yl)aniline **4.68**

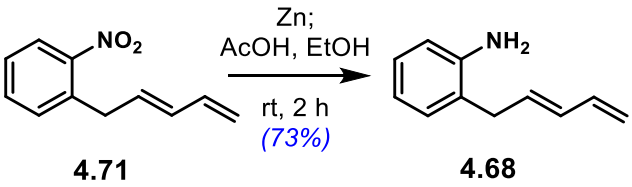

Nitro compound **4.71** (65 mg, 0.34 mmol, 1.0 equiv.) was dissolved in absolute ethanol (1.3 mL). Then, zinc dust (113 mg, 1.72 mmol, 5.0 equiv.) was added in one portion. At rt, acetic acid (0.1 mL, 1.72 mmol, 5.0 equiv.) was added dropwise. The reaction was stirred vigorously for 2 h. After that time, the reaction is filtered through celite. The flask and the celite are thoroughly washed with EtOAc. The solvent was removed in vacuo and the residue trated with $NaHCO_3$ (5 mL, std. sln.) and water (2 mL). The aqueous solution was partitioned with EtOAc (5 mL). The organic layer was separated and the aqueous phase extracted with EtOAc (5 mL, x3). The combined organic layers were washed with brine and the solvent removed in vacuo. Column chromatography (10% EtOAc in hexane) afforded the pure aniline (39.2 mg, 0.25 mmol, 73%).

Spectral data consistent with the literature[340]

Physical state: yellowish oil-liquid

TLC: R_f= 0.19 (10% EtOAc in hexane).

^{1}H NMR (400 MHz, $CDCl_3$): δ 7.07 (dd, *J*=15.9, 7.8 Hz, 2H), 6.76 (t, *J*=7.4 Hz, 1H), 6.69 (d, *J*=7.9 Hz, 1H), 6.35 (dt, *J*=17.0, 10.3 Hz, 1H), 6.12 (dd, *J*=15.2, 10.4 Hz, 1H), 5.84 (dt, *J*=15.2, 6.4 Hz, 1H), 5.13 (d, *J*=17.0 Hz, 1H), 5.02 (d, *J*=10.1 Hz, 1H), 3.64 (s, 2H), 3.35 (d, *J*=6.3 Hz, 2H)

^{13}C NMR (100 MHz, $CDCl_3$): δ 144.8, 136.8, 132.3, 132.0, 130.3, 127.7, 124.2, 119.0, 116.2, 116.0, 35.3

Compound **4.80**. As presented on Table 4.6

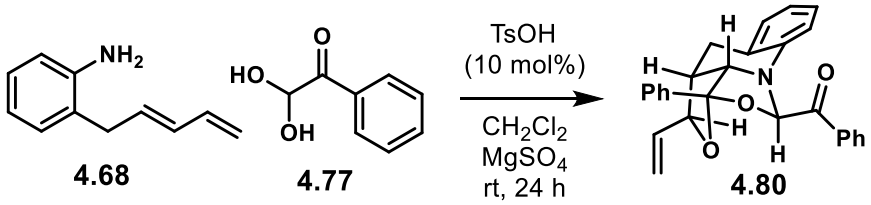

4.68 4.77 4.80

The following procedure corresponds to the racemic reaction. For the enantioselective reactions presented on Table 4.7, the same procedure applies using the chiral catalysts mentioned in the text.

Aniline **4.68** (16 mg, 0.1 mmol, 1.0 equiv.) was dissolved in dry CH_2Cl_2 (1 mL). Then, $MgSO_4$ (70 mg) was added, followed by phenyl glyoxal (37 mg, 0.25 mmol, 2.5 equiv.). Then, at rt, tosic acid (1.86 mg, 0.01 mmol, 0.1 equiv.) was added in one portion. The reaction was stirred at rt for 24 h. After that time, the reaction is loaded into a silica column and eluted with 5% EtOAc in hexane to afford the pure product (11.7 mg, 0.029 mmol, 29%).

Physical state: white solid

mp: 152-153 °C

TLC: R_f= 0.19 (10% EtOAc in hexane).

^{1}H NMR (600 MHz, $CDCl_3$): δ 8.25 (dd, *J*=8.3, 1.1 Hz, 2H), 7.64 (t, *J*=7.4 Hz, 1H), 7.51 (m, 4H), 7.31 (m, 3H), 7.06 (dd, *J*=14.4, 7.6 Hz, 2H), 6.79 (td, *J*=7.4, 0.6 Hz, 1H), 6.29 (s, 1H), 6.23 (d, *J*=8.0 Hz, 1H), 6.01 (ddd, *J*=17.3, 10.3, 7.2 Hz, 1H), 5.33 (t, *J*=13.4, 2H), 4.42 (dd, *J*=10.2, 7.3 Hz, 1H), 4.26 (d, *J*=4.4 Hz, 1H), 3.14 (dd, *J*=17.2, 5.5 Hz, 1H), 2.74 (dd, *J*=17.1, 1.2 Hz, 1H), 2.56 (ddd, *J*=10.1, 5.9, 1.81 Hz, 1H)

^{13}C NMR (150 MHz, $CDCl_3$): δ 193.9, 141.2, 138.6, 135.6, 134.4, 134.1, 129.8, 129.6, 129.0, 129.0, 128.4, 127.9, 126.8, 119. 5, 118.9, 118.4, 115.7, 113.7, 94.1, 83.6, 69.0, 40.8, 24.3

LCMS ES+ TIC(m/z): calc. 410.49(+H), 276.14. Found: 410.41, 276.29

HRMS (m/z): Calc. for $C_{27}H_{24}NO_3$: 410.1756. Found: 410.1764

SFC settings: λ_{max}=246 nm, column SB, flow rate = 2.5 mL min^{-1}, 10% MeOH in CO_2, tr1=5.77 min, tr2=7.14 min

1,3-dimethoxy-5-(2-nitrobenzyl)benzene **4.117**

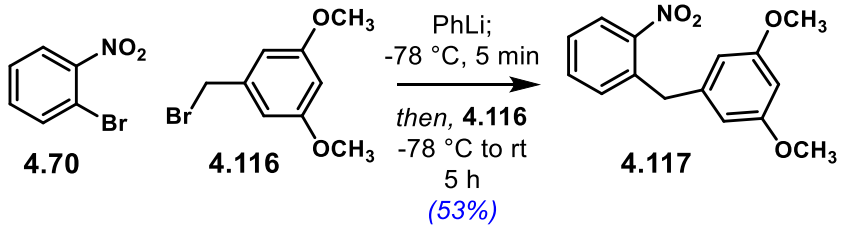

Phenyl lithium (0.95 mL, 1.9 M sln, in Bu_2O, 1.8 mmol, 1.2 equiv.) was diluted in dry THF (14 mL). Then, at -78 °C, a solution of 2-bromonitrobenzene (303 mg, 1.5 mmol, 1.0 equiv.) in dry THF (2 mL) was added dropwise. The reaction is stirred at -78 °C for 5 min. Then, a solution of bromide **4.116** (0.52 g, 2.25 mmol, 1.5 equiv.) in dry THF (2 mL) was added dropwise. The reaction was stirred for 5 h allowing the temperature to reach rt. After that time, the reaction was quenched with NH_4Cl (10 mL, std. sln.) and water (2 mL). The organic layer was separated and the aqueous phase extracted with EtOAc (10 mL, x3). The combined organic layers were washed with brine (20 mL), dried over $MgSO_4$ and the solvent removed in vacuo. Column chromatography (10% EtOAc in hexane) afforded the pure product (216 mg, 0.79 mmol, 53%).

Physical state: orange oil

TLC: R_f= 0.35 (20% EtOAc in hexane).

^{1}H NMR (600 MHz, $CDCl_3$): δ 7.93 (dd, *J*=8.2, 1.3 Hz, 1H), 7.51 (td, *J*=7.6, 1.4 Hz, 1H), 7.37 (td *J*=8.2, 1.4 Hz, 1H), 7.28 (dd, *J*=7.7, 1.0 Hz, 1H), 6.34 (t, *J*=2.3 Hz, 1H), 6.31 (d, *J*=2.3 Hz, 2H), 4.24 (s, 2H), 3.75 (s, 6H)

^{13}C NMR (150 MHz, $CDCl_3$): δ 161.1, 149.4, 141.1, 135.5, 133.1, 132.5, 127.6, 124.9, 107.4, 98.5, 55.4, 38.6

2-(3,5-dimethoxybenzyl)aniline **4.91**

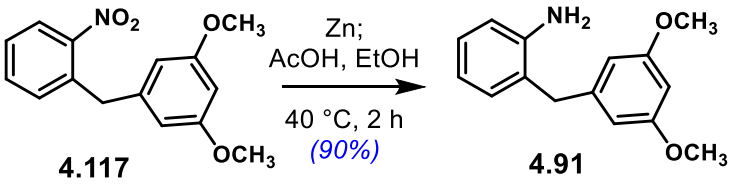

4.117 **4.91**

Nitro compound **4.117** (112 mg, 0.41 mmol, 1.0 equiv.) was dissolved in absolute ethanol (2 mL). Then, zinc dust (134 mg, 2.05 mmol, 5.0 equiv.) was added in one portion. At rt, acetic acid (0.12 mL, 2.05 mmol, 5.0 equiv.) was added dropwise. The reaction was stirred vigorously for 2 h at 40 °C. After that time, the reaction is filtered through celite. The flask and the celite are thoroughly washed with EtOAc. The solvent was removed in vacuo and the residue trated with $NaHCO_3$ (6 mL, std. sln.) and water (3 mL). The aqueous solution was partitioned with EtOAc (6 mL). The organic layer was separated and the aqueous phase extracted with EtOAc (6 mL, x3). The combined organic layers were washed with brine and the solvent removed in vacuo. Column chromatography (10% EtOAc in hexane) afforded the pure aniline (89 mg, 0.37 mmol, 90%).

Physical state: yellow solid

TLC: R_f= 0.17 (20% EtOAc in hexane).

^{1}H NMR (600 MHz, $CDCl_3$): δ 7.09 (td, *J*=7.7, 1.5 Hz, 1H), 7.07 (d, *J*=7.5 Hz, 1H), 6.77 (td, *J*=7.4, 1.1 Hz, 1H), 6.67 (dd, *J*=7.9, 1.0 Hz, 1H), 6.36 (d, *J*=2.2 Hz, 2H), 6.33 (t, *J*=2.2 Hz, 1H), 3.85 (s, 2H), 3.75 (s, 6H), 3.53 (s, 2H)

^{13}C NMR (150 MHz, $CDCl_3$): δ 161.2, 144.9, 142.1, 131.0, 127.8, 124.9, 118.9, 116.0, 106.8, 98.3, 55.4, 38.5

Compound **4.90**

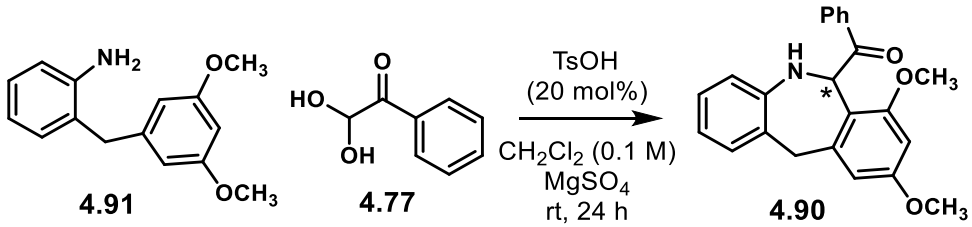

The following procedure corresponds to the racemic reaction. For the enantioselective reactions presented on Table 4.9 and 4.10, the same procedure applies using the chiral catalysts mentioned in the text.

Aniline **4.91** (27 mg, 0.11 mmol, 1.0 equiv.) was dissolved in dry CH_2Cl_2 (1.1 mL). Then, $MgSO_4$ (40 mg) was added, followed by phenyl glyoxal (18 mg, 0.12 mmol, 1.1 equiv.). Then, at rt, tosic acid (4.18 mg, 0.022 mmol, 0.2 equiv.) was added in one portion. The reaction is stirred at rt for 24 h. After that time, the mixture is loaded into a silica column and eluted with 20% EtOAc in hexane in order to afford the pure product (20.1 mg, 0.056 mmol, 51%).

Physical state: white solid

TLC: R_f= 0.18 (20% EtOAc in hexane).

^{1}H NMR (600 MHz, $CDCl_3$): δ 7.89 (dd, *J*=8.3, 1.2 Hz, 2H), 7.49 (m, 1H), 7.37 (dd, *J*=10.9, 4.8 Hz, 2H), 6.99 (d, *J*=7.5 Hz, 2H), 6.60 (ddd, *J*=12.6, 9.5, 4.5 Hz, 2H), 6.45 (d, *J*=2.4 Hz, 1H), 6.40 (s, 1H), 6.24 (d, *J*=2.4 Hz, 1H), 5.23 (s, 1H), 4.66 (d, *J*=15.3 Hz, 1H), 3.76 (s, 3H), 3.67 (d, *J*=15.4 Hz, 1H), 3.41 (s, 3H)

^{13}C NMR (150 MHz, $CDCl_3$): δ 196.9, 160.6, 156.0, 144.7, 141.9, 135.8, 132.8, 130.7, 128.4, 128.0, 127.5, 121.3, 118.1, 117.9, 117.4, 105.6, 97.9, 57.0, 55.4, 55.4, 40.7

LCMS ES+ TIC(m/z): calc. 360.16(+H). Found: 359.99

HRMS (m/z): Calc. for $C_{23}H_{22}NO_3$: 360.1600. Found: 360.1603

SFC settings: λ_{max}=240 nm, column SC, flow rate = 2.5 mL min^{-1}, 20% MeOH in CO_2, tr1=7.81 min, tr2=8.54 min

Compound **4.121**

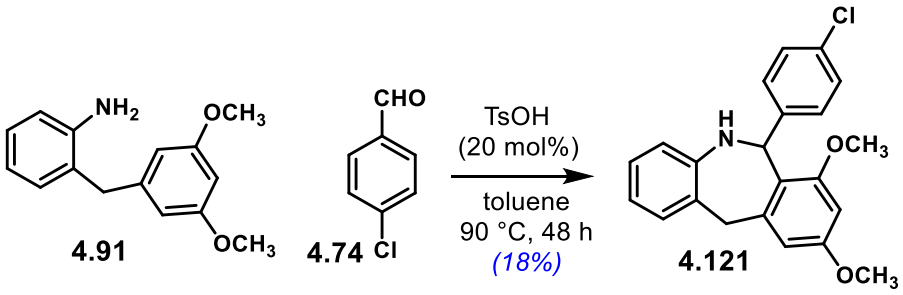

Aniline **4.91** (27 mg, 0.11 mmol, 1.0 equiv.) was dissolved in dry toluene (1.1 mL). Then, $MgSO_4$ (40 mg) and 4-chlorobenzaldehyde (16.8 mg, 0.12 mmol, 1.1 equiv.) were added. At rt, tosic acid (4.18 mg, 0.022 mmol, 0.2 equiv.) was added in one portion. The reaction is stirred at 90 °C for 48 h. After that time, the mixture is cooled down to rt and loaded into a silica column. Elution with 10% EtOAc in hexane afforded the pure product (7.3 mg, 0.019 mmol, 18%).

Physical state: white solid

TLC: R_f= 0.30 (20% EtOAc in hexane).

^{1}H NMR (600 MHz, $CDCl_3$): δ 7.24 (m, 4H), 6.99 (t, *J*=7.6 Hz, 1H), 6.92 (d, *J*=7.4 Hz, 1H), 6.61 (t, *J*=7.3 Hz, 1H), 6.57 (d, *J*=8.0 Hz, 1H), 6.41 (d, *J*=2.3 Hz, 1H), 6.32 (d, *J*=2.2 Hz, 1H), 6.08 (s, 1H), 4.59 (s, 1H), 3.99 (d, *J*=14.7 Hz, 1H), 3.83 (s, 3H), 3.79 (s, 3H), 3.10 (d, *J*=14.7 Hz, 1H)

^{13}C NMR (150 MHz, $CDCl_3$): δ 160.1, 157.2, 144.8, 144.8, 141.7, 132.0, 130.2, 128.4, 127.7, 127.6, 123.0, 119.9, 118.1, 117.1, 105.5, 96.7, 55.9, 55.4, 51.6, 39.9

1,3-dimethoxy-5-(2-nitrophenoxy)benzene **4.130**

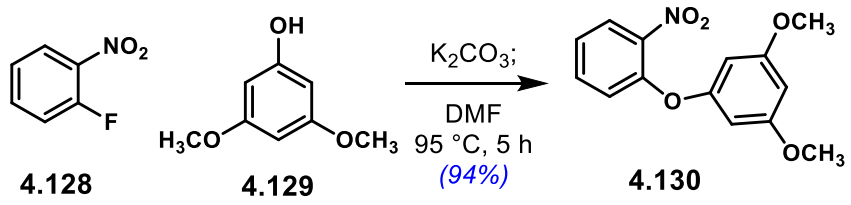

4.128 **4.129** **4.130**

3,5-dimethoxy phenol (1.54 g, 10 mmol, 1.0 equiv.) was dissolved in dry DMF (42 mL). Then, potassium carbonate (1.52 g, 11 mmol, 1.1 equiv.) was added, followed by 2-fluoronitrobenzene (1.05 mL, 10 mmol, 1.0 equiv.). The reaction was stirred at 95 °C for 5 h. After that time, DMF was removed in vacuo. The residue was partitioned with water (50 mL) and EtOAc (25 mL). The organic layer was separated and the aqueous phase extracted with EtOAc (25 mL, x3). The combined organic layers were washed with brine (50 mL), dried over $MgSO_4$ and the solvent removed in vacuo. Column chromatography (15% EtOAc in PE) afforded the pure product (2.58 g, 9.37 mmol, 94%).

Spectral data consistent with the literature[341]

Physical state: yellow oil

TLC: R_f= 0.26 (20% EtOAc in PE).

^{1}H NMR (600 MHz, $CDCl_3$): δ 7.93 (m, 1H), 7.51 (ddd, *J*=8.5, 7.4, 1.7 Hz, 1H), 7.20 (m, 1H), 7.08 (dd, *J*=8.4, 1.2 Hz, 1H), 6.27 (t, *J*=2.2 Hz, 1H), 6.19 (d, *J*=2.2 Hz, 2H), 3.75 (s, 6H)

^{13}C NMR (150 MHz, $CDCl_3$): δ 161.9, 157.7, 150.3, 141.4, 134.3, 125.7, 123.5, 121.0, 97.7, 96.7, 55.6

2-(3,5-dimethoxyphenoxy)aniline **4.131**

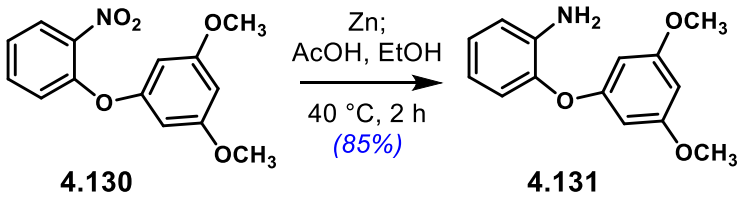

4.130 **4.131**

Nitro compound **4.130** (2.58 g, 9.37 mmol, 1.0 equiv.) was dissolved in absolute ethanol (50 mL). Then, zinc dust (3.24 g, 49.6 mmol, 5.0 equiv.) was added in one portion. At rt, acetic acid (2.8 mL, 49.6 mmol, 5.0 equiv.) was added dropwise. The reaction was stirred vigorously for 2 h at 40 °C. After that time, the reaction is filtered through celite. The flask and the celite are thoroughly washed with EtOAc. The solvent was removed in vacuo and the residue trated with $NaHCO_3$ (100 mL, std. sln.) and water (100 mL). The aqueous solution was partitioned with EtOAc (50 mL). The organic layer was separated and the aqueous phase extracted with EtOAc (50 mL, x3). The combined organic layers were washed with brine and the solvent removed in vacuo. Column chromatography (20% EtOAc in hexane) afforded the pure aniline (2.03 g, 8.25 mmol, 85%).

Spectral data consistent with the literature[341]

Physical state: yellow oil

TLC: R_f= 0.25 (20% EtOAc in hexane).

^{1}H NMR (600 MHz, $CDCl_3$): δ 6.99 (m, 1H), 6.92 (dd, *J*=8.0, 1.4 Hz, 1H), 6.81 (dd, *J*=7.9, 1.5 Hz, 1H), 6.72 (ddd, *J*=8.0, 7.5, 1.6 Hz, 1H), 6.19 (t, *J*=2.1, 1H), 6.15 (m, 1H), 3.78 (s, 2H), 3.74 (s, 6H)

^{13}C NMR (150 MHz, $CDCl_3$): δ 161.7, 159.6, 142.6, 138.9, 125.3, 120.8, 118.9, 116.6, 95.7, 94.9, 55.5

Compound **4.136**

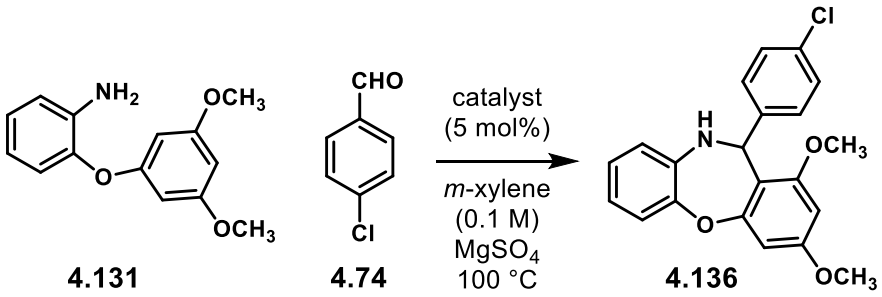

The following procedure corresponds to the racemic reaction. For the enantioselective reactions presented on Tables 4.16 and 4.17, the same procedure applies using the chiral catalysts mentioned in the text.

In a 1 dram vial, $MgSO_4$ (60 mg), 4-chlorobenzaldehyde (15.5 mg, 0.11 mmol, 1.1 equiv.) and the corresponding catalyst (5 mol%) were weighted. Then, aniline **4.131** (24.5 mg, 0.1 mmol, 1.0 equiv.) was added in one portion as a solution in m-xylene (1 mL). The reaction was then stirred at 100 °C and followed by TLC. The reaction was loaded into a silica column and eluted with 15% EtOAc in hexane to obtain the pure product.

Physical state: white solid

TLC: R_f= 0.27 (20% EtOAc in hexane).

^{1}H NMR (600 MHz, $CDCl_3$): δ 7.21 (m, 4H), 7.01 (dd, *J*=7.9, 1.3 Hz, 1H), 6.90 (td, *J*=7.7, 1.4 Hz, 1H), 6.65 (m, 2H), 6.33 (m, 2H), 5.88 (s, 1H), 4.52 (s, 1H), 3.85 (s, 3H), 3.78 (s, 3H)

^{13}C NMR (150 MHz, $CDCl_3$): δ 160.8, 158.7, 157.1, 144.2, 143.3, 137.8, 132.2, 128.3, 127.3, 125.2, 122.1, 118.9, 118.2, 115.5, 98.5, 95.2, 56.1, 55.6, 51.5

HRMS (m/z): Calc. for $C_{21}H_{19}NO_3Cl$: 368.1053. Found: 368.1053

SFC settings: λ_{max}=205 nm, column SC, flow rate = 2.5 mL min^{-1}, 10% MeOH in CO_2, tr1=10.48 min, tr2=11.03 min

Appendix 3

NMR spectra

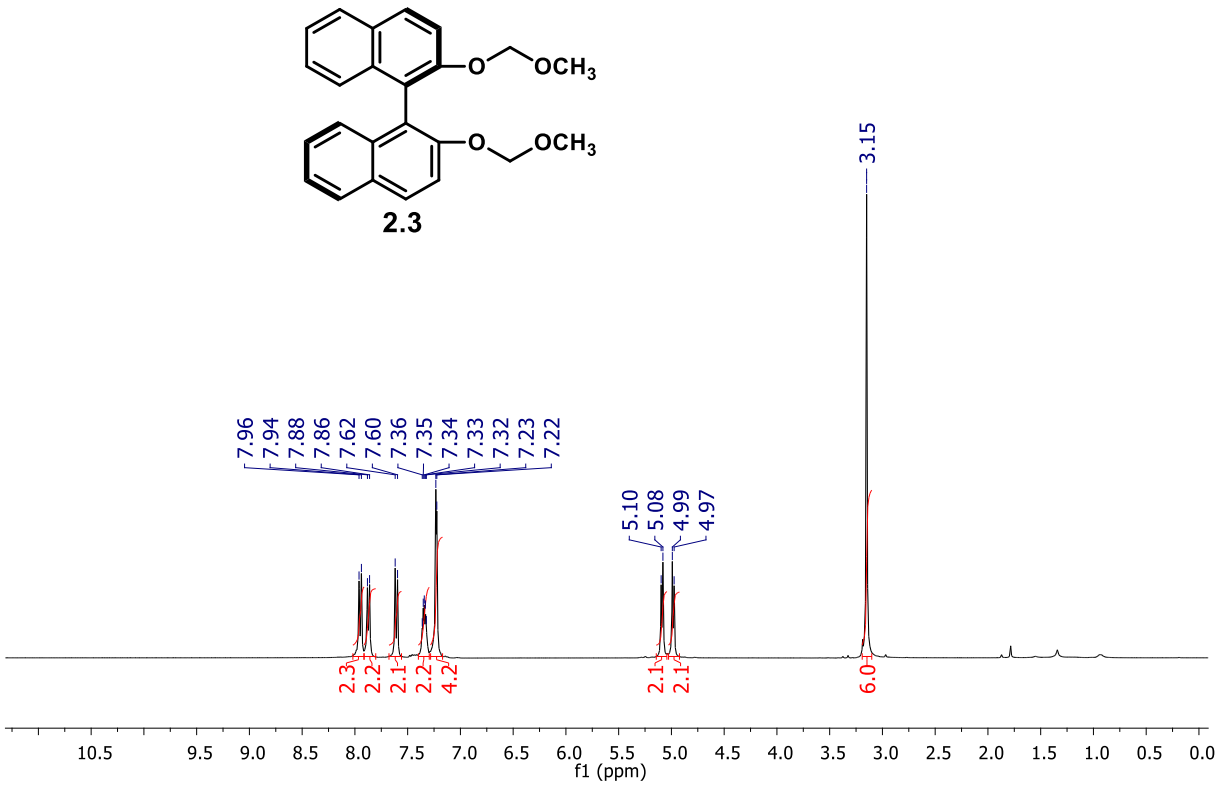
O
OCH3
O
OCH3
2.3
7.96
7.94
7.88
7.86
7.62
7.60
7.36
7.35
7.34
7.33
7.32
7.23
7.22
5.10
5.08
4.99
4.97
3.15
2.3
2.2
2.1
2.2
4.2
2.1
2.1
6.0
10.5
9.5
9.0
8.5
8.0
7.5
7.0
6.5
6.0
5.5
5.0
4.5
4.0
3.5
3.0
2.5
2.0
1.5
1.0
0.5
0.0
f1 (ppm)

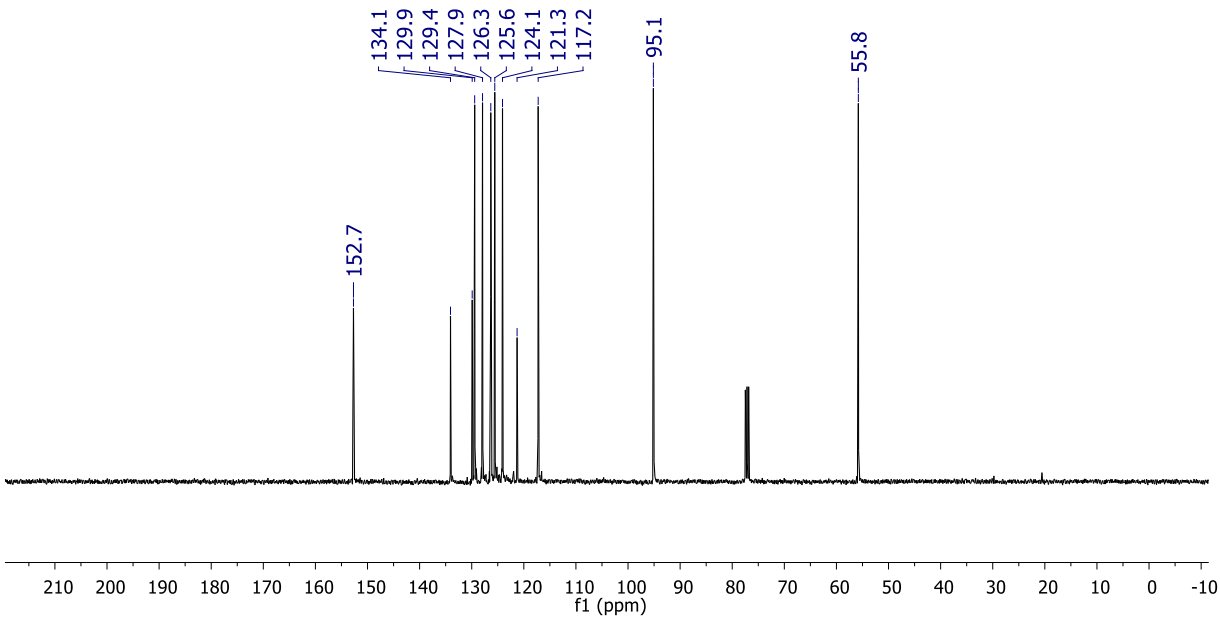
134.1
129.9
129.4
127.9
126.3
125.6
124.1
121.3
117.2
152.7
95.1
55.8
210
200
190
180
170
160
150
140
130
120
110
100
90
80
70
60
50
40
30
20
10
0
-10
f1 (ppm)

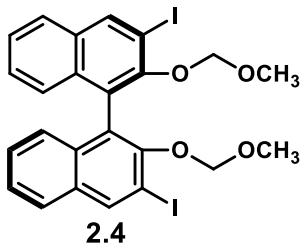
I
O
OCH3
O
OCH3
I

2.4

2.60
8.54
7.79
7.77
7.45
7.44
7.43
7.41
7.41
7.32
7.32
7.30
7.30
7.28
7.28
7.18
7.16
4.82
4.80
4.70
4.69
2.0
2.0
2.0
2.0
2.0
2.1
2.1
6.2
10.5 10.0 9.5 9.0 8.5 8.0 7.5 7.0 6.5 6.0 5.5 5.0 4.5 4.0 3.5 3.0 2.5 2.0 1.5 1.0 0.5 0.0
f1 (ppm)

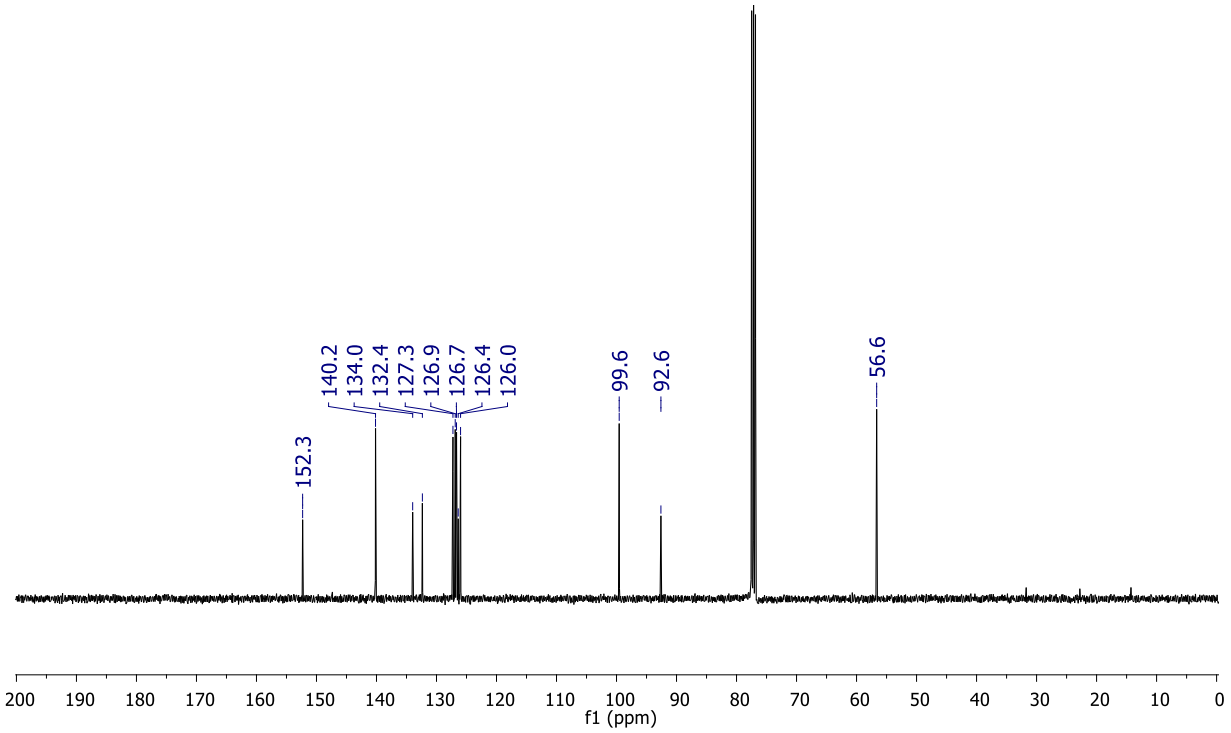
152.3
140.2
134.0
132.4
127.3
126.9
126.7
126.4
126.0
99.6
92.6
56.6
200 190 180 170 160 150 140 130 120 110 100 90 80 70 60 50 40 30 20 10 0
f1 (ppm)

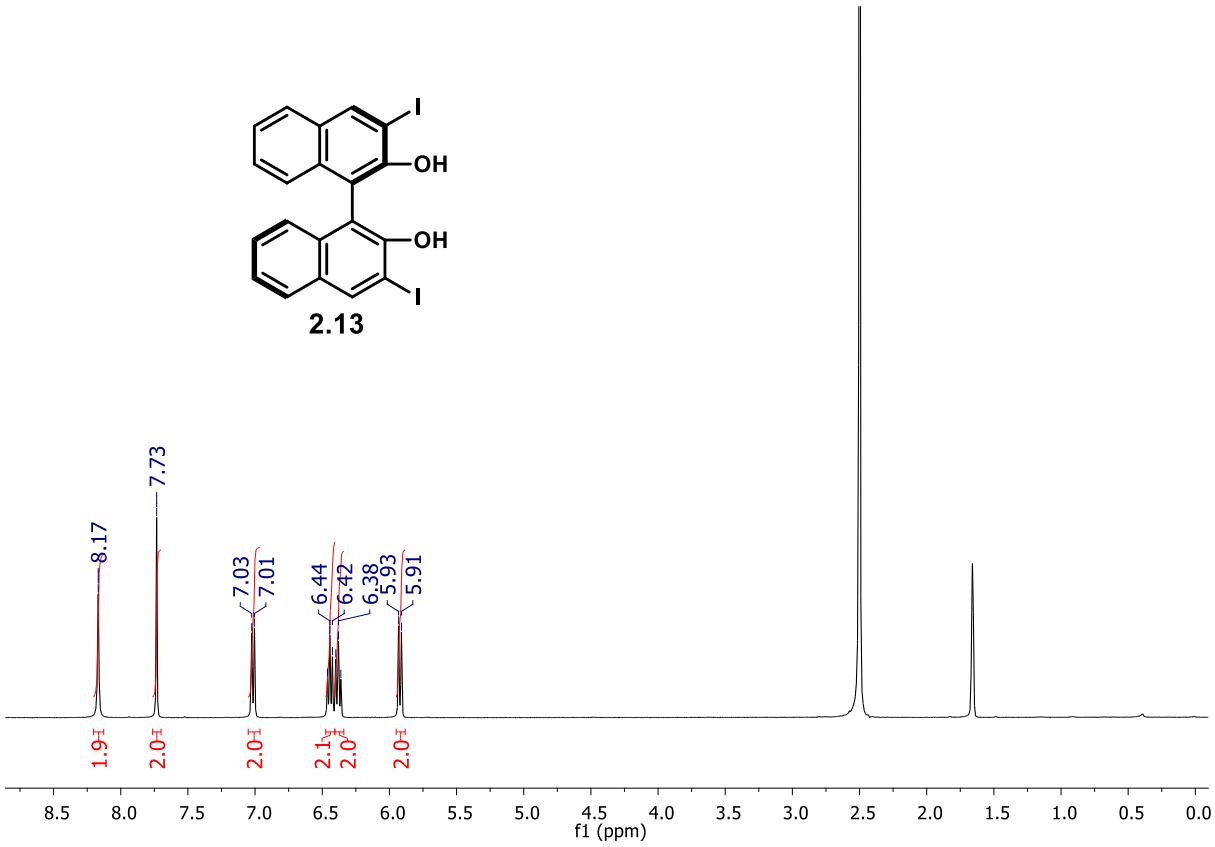
I
OH
OH
I
8.17
7.73
7.03
7.01
6.44
6.42
6.38
5.93
5.91
1.9
2.0
2.0
2.1
2.0
2.0
8.5 8.0 7.5 7.0 6.5 6.0 5.5 5.0 4.5 4.0 3.5 3.0 2.5 2.0 1.5 1.0 0.5 0.0
f1 (ppm)

2.13

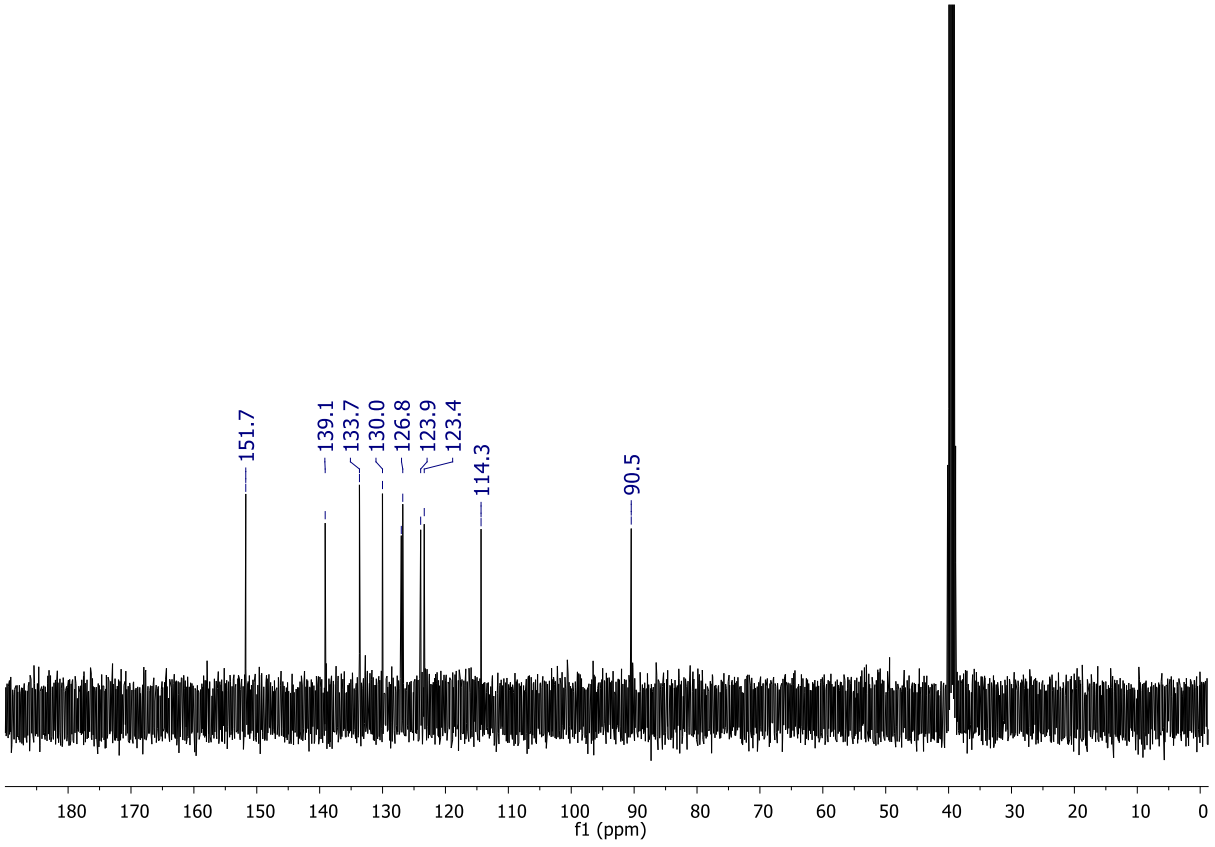
151.7
139.1
133.7
130.0
126.8
123.9
123.4
114.3
90.5
180 170 160 150 140 130 120 110 100 90 80 70 60 50 40 30 20 10 0
f1 (ppm)

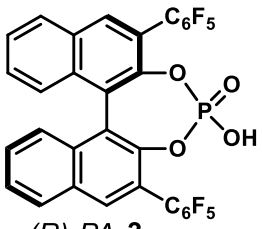
C6F5
O
O
P
OH
O
C6F5

*(R)-PA-***3**

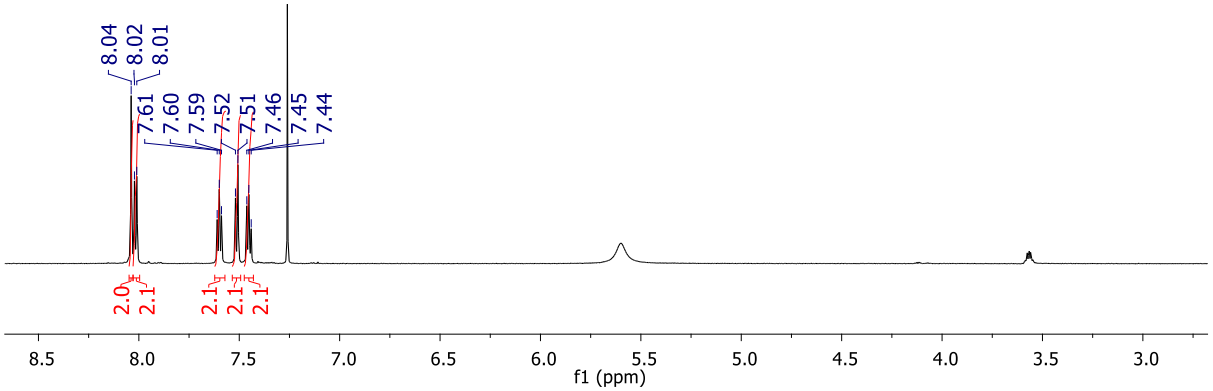
8.04
8.02
8.01
7.61
7.60
7.59
7.52
7.51
7.46
7.45
7.44
2.0
2.1
2.1
2.1
2.1
8.5
8.0
7.5
7.0
6.5
6.0
5.5
5.0
4.5
4.0
3.5
3.0
f1 (ppm)

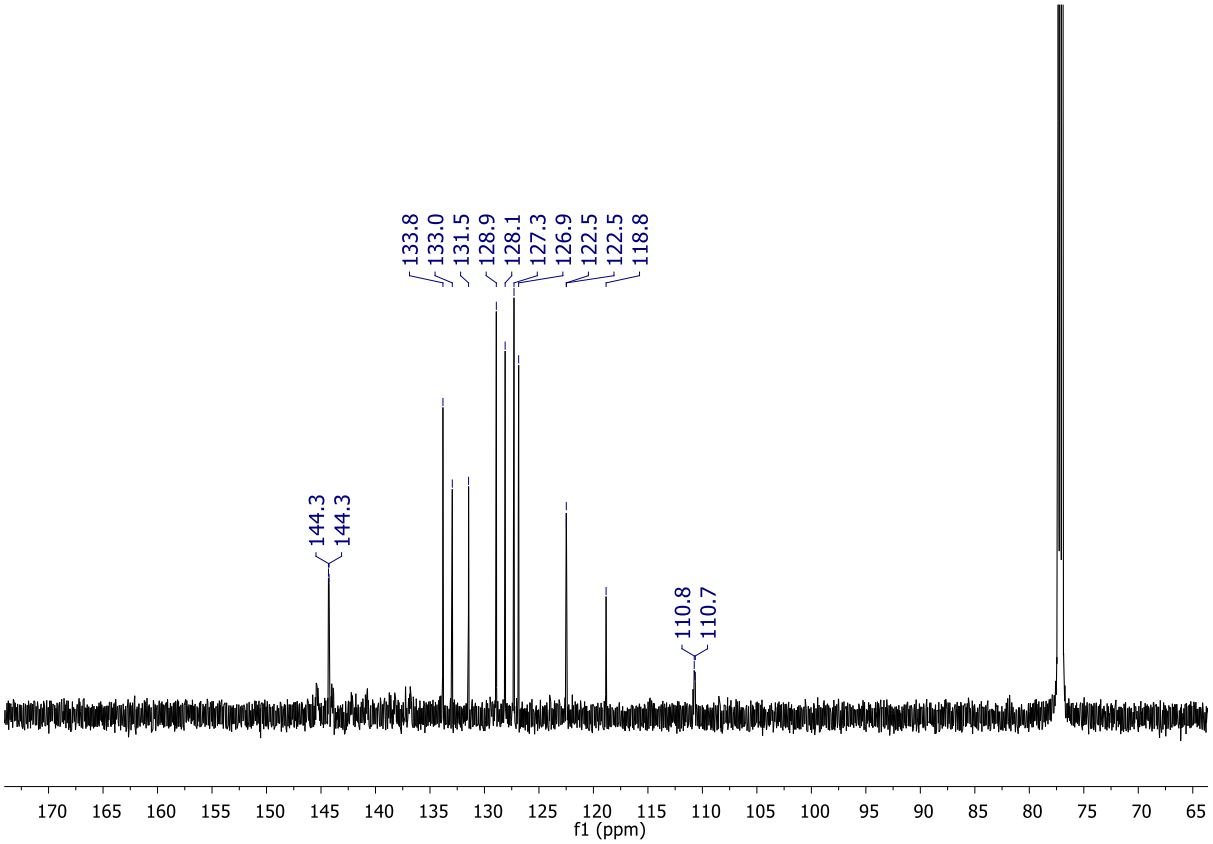
133.8
133.0
131.5
128.9
128.1
127.3
126.9
122.5
122.5
118.8
144.3
144.3
110.8
110.7
170
165
160
155
150
145
140
135
130
125
120
115
110
105
100
95
90
85
80
75
70
65
f1 (ppm)

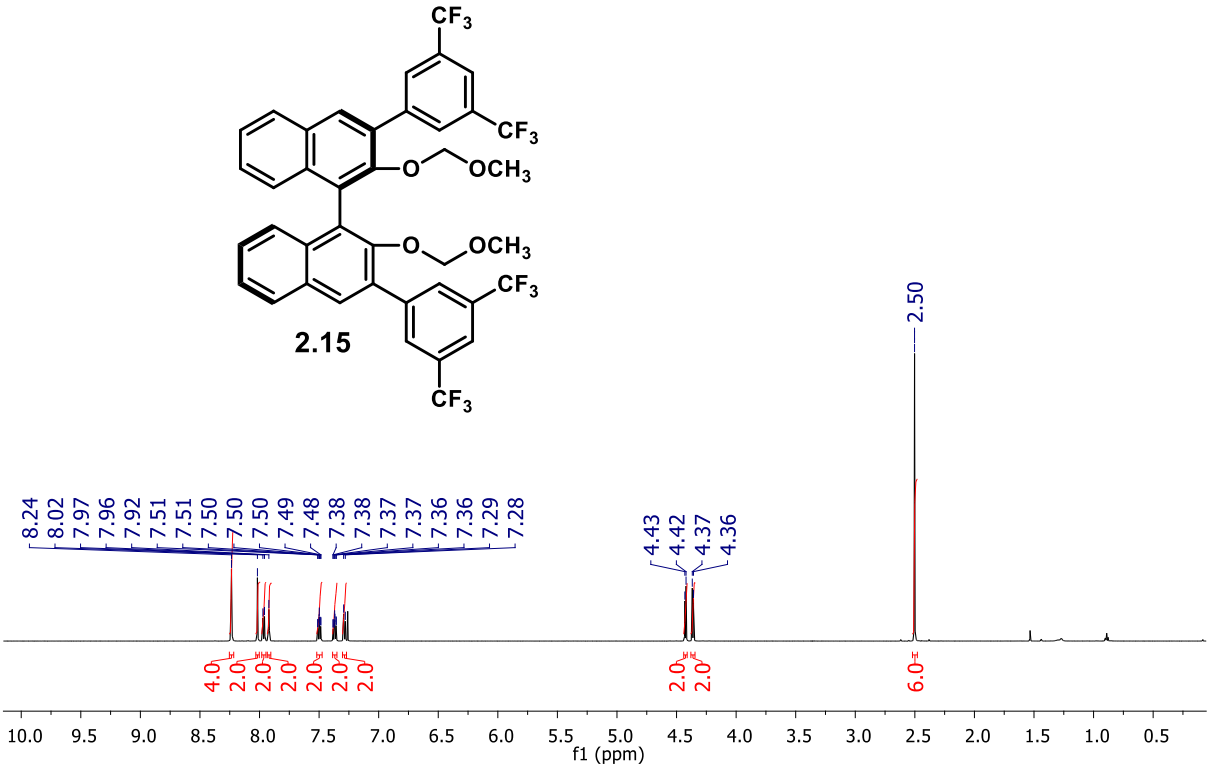
CF3
CF3
O
OCH3
O
OCH3
CF3
CF3
2.15
8.24
8.02
7.97
7.96
7.92
7.51
7.51
7.50
7.50
7.50
7.49
7.48
7.38
7.38
7.37
7.37
7.36
7.36
7.29
7.28
4.43
4.42
4.37
4.36
2.50
4.0
2.0
2.0
2.0
2.0
2.0
2.0
2.0
2.0
6.0
10.0 9.5 9.0 8.5 8.0 7.5 7.0 6.5 6.0 5.5 5.0 4.5 4.0 3.5 3.0 2.5 2.0 1.5 1.0 0.5
f1 (ppm)

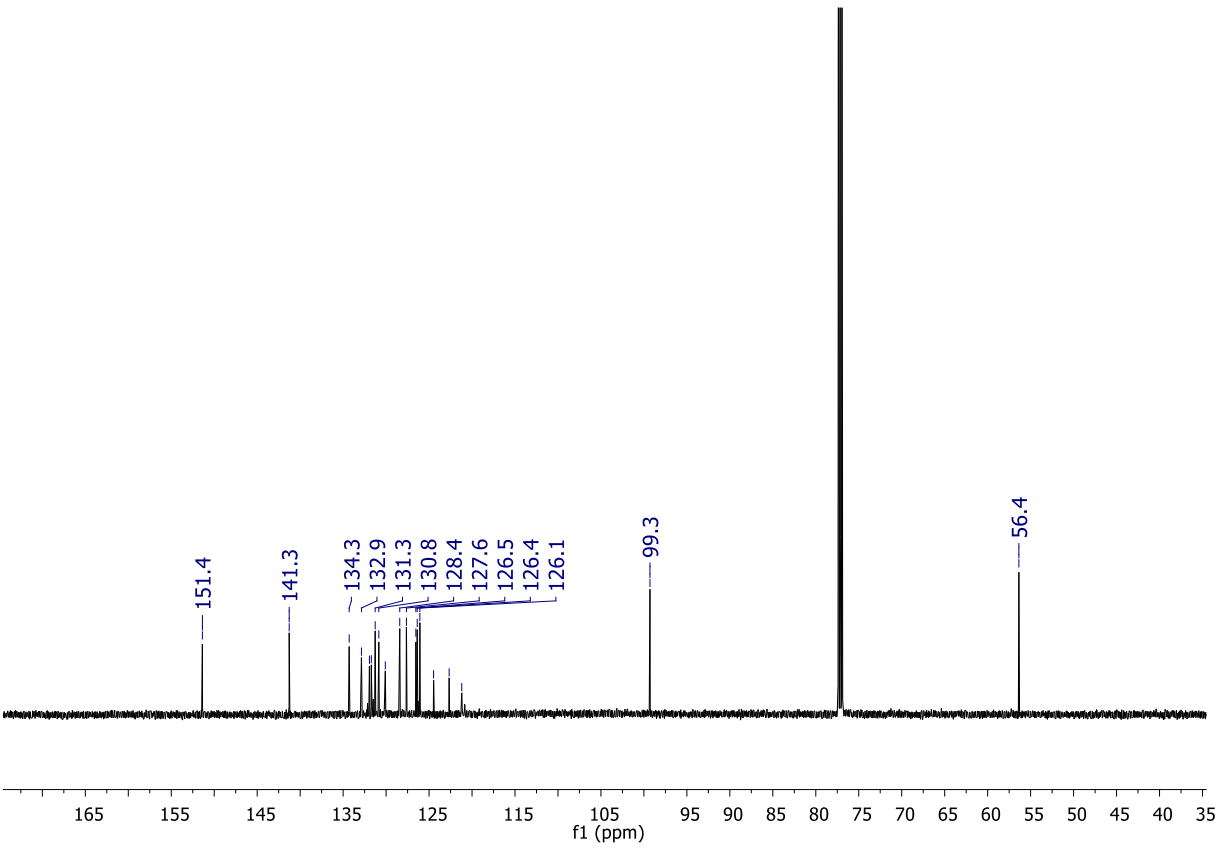
151.4
141.3
134.3
132.9
131.3
130.8
128.4
127.6
126.5
126.4
126.1
99.3
56.4
165 155 145 135 125 115 105 95 90 85 80 75 70 65 60 55 50 45 40 35
f1 (ppm)

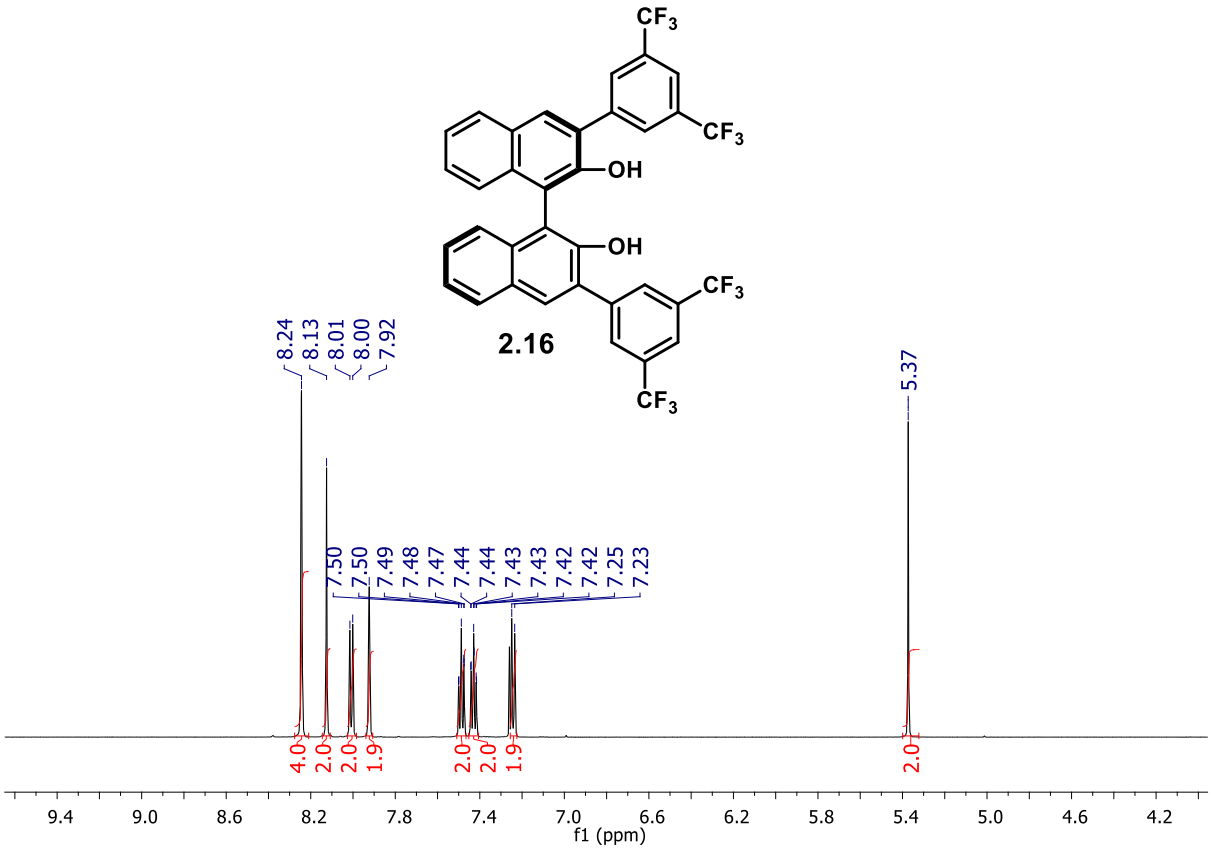
CF3
CF3
OH
OH
CF3
CF3
2.16
8.24
8.13
8.01
8.00
7.92
7.50
7.50
7.49
7.48
7.47
7.44
7.44
7.43
7.43
7.42
7.42
7.25
7.23
5.37
4.0
2.0
2.0
1.9
2.0
2.0
1.9
2.0
9.4
9.0
8.6
8.2
7.8
7.4
7.0
6.6
6.2
5.8
5.4
5.0
4.6
4.2
f1 (ppm)

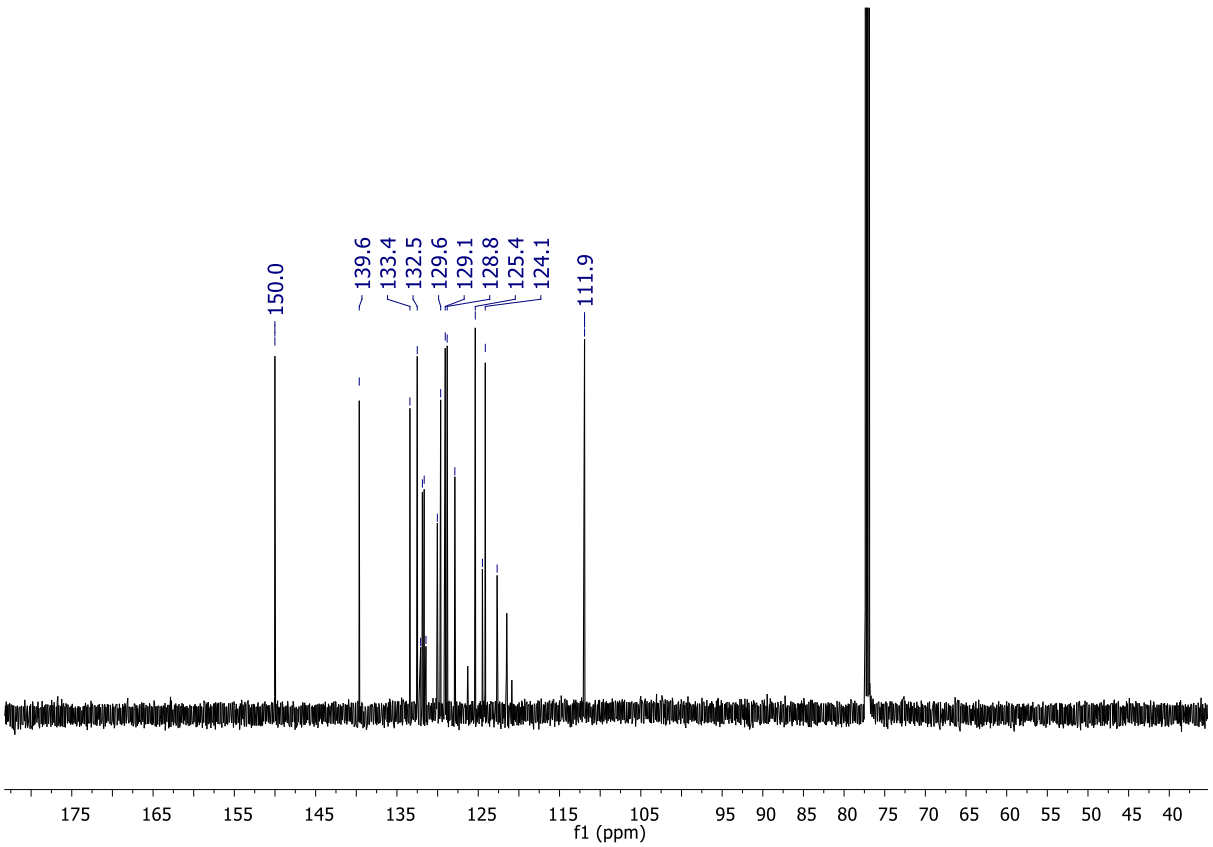
150.0
139.6
133.4
132.5
129.6
129.1
128.8
125.4
124.1
111.9
175
165
155
145
135
125
115
105
95
90
85
80
75
70
65
60
55
50
45
40
f1 (ppm)

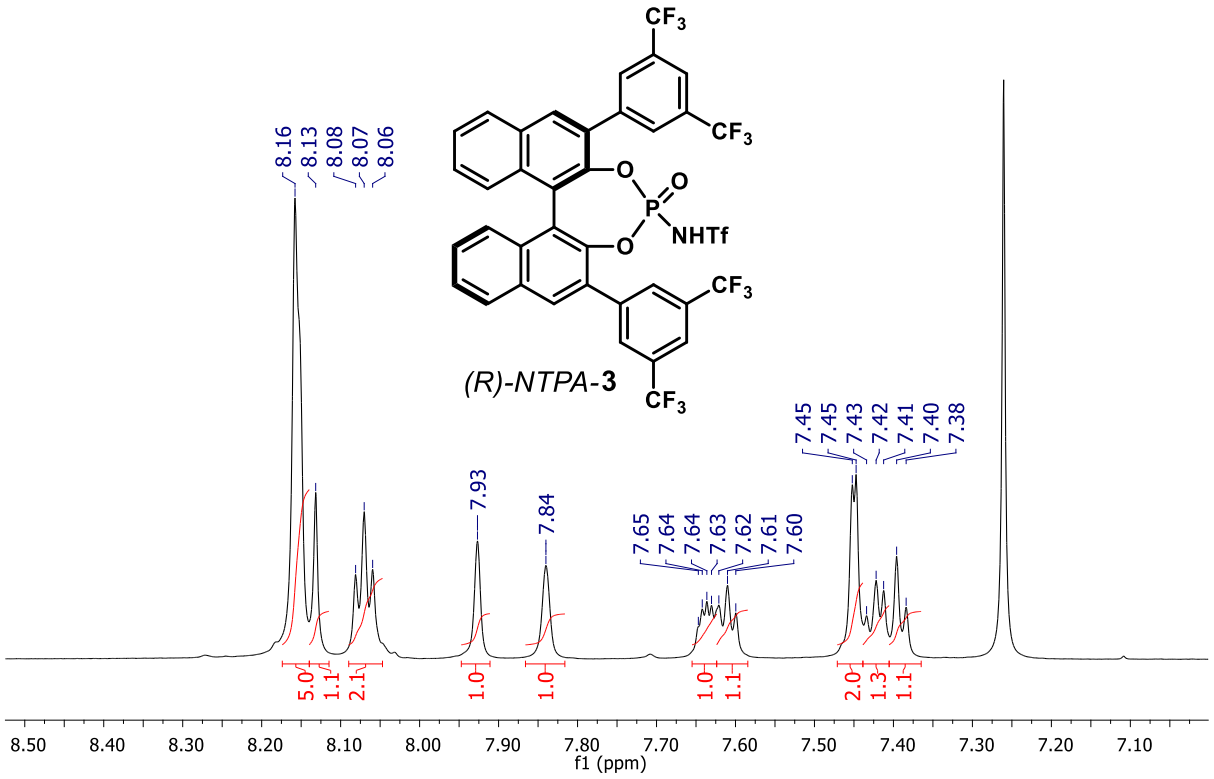
CF3
CF3
O
O
P
O
NHTf
O
CF3
CF3
(R)-NTPA-3
8.16
8.13
8.08
8.07
8.06
7.93
7.84
7.65
7.64
7.64
7.63
7.62
7.61
7.60
7.45
7.45
7.43
7.42
7.41
7.40
7.38
5.0
1.1
2.1
1.0
1.0
1.0
1.1
2.0
1.3
1.1
8.50 8.40 8.30 8.20 8.10 8.00 7.90 7.80 7.70 7.60 7.50 7.40 7.30 7.20 7.10
f1 (ppm)

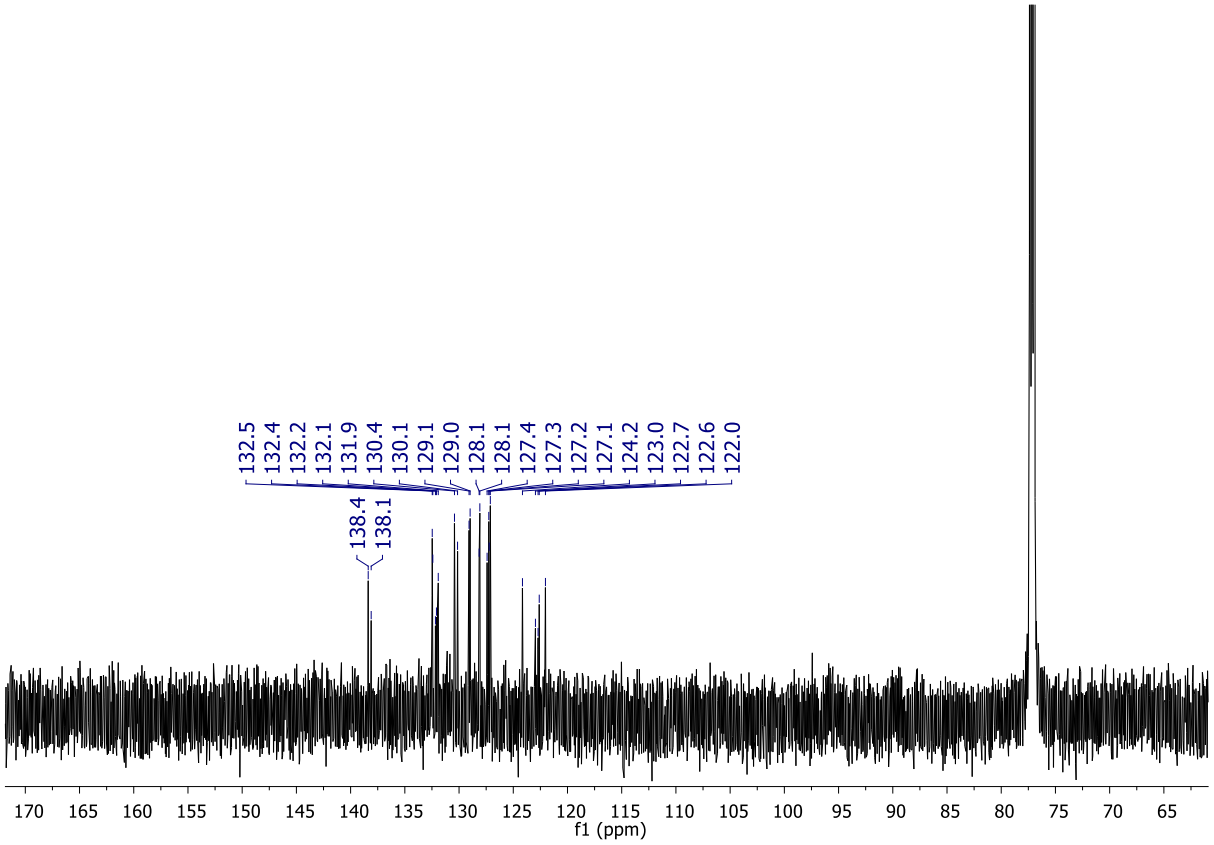
132.5
132.4
132.2
132.1
131.9
130.4
130.1
129.1
129.0
128.1
128.1
127.4
127.3
127.2
127.1
124.2
123.0
122.7
122.6
122.0
138.4
138.1
170 165 160 155 150 145 140 135 130 125 120 115 110 105 100 95 90 85 80 75 70 65
f1 (ppm)

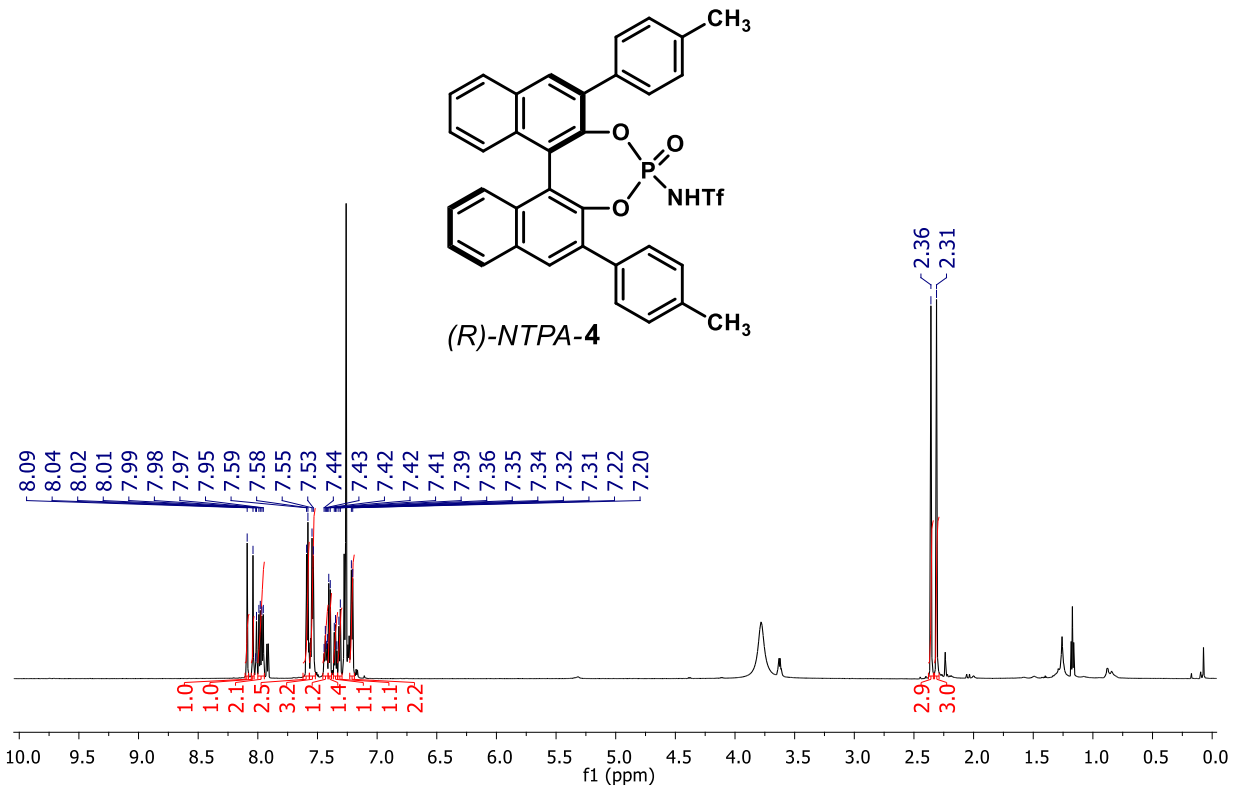
CH3
O
O
P
O
NHTf
O
CH3
(R)-NTPA-4
8.09
8.04
8.02
8.01
7.99
7.98
7.97
7.95
7.59
7.58
7.55
7.53
7.44
7.43
7.42
7.42
7.41
7.39
7.36
7.35
7.34
7.32
7.31
7.22
7.20
2.36
2.31
1.0
1.0
2.1
2.5
3.2
1.2
1.4
1.1
1.1
2.2
2.9
3.0
10.0 9.5 9.0 8.5 8.0 7.5 7.0 6.5 6.0 5.5 5.0 4.5 4.0 3.5 3.0 2.5 2.0 1.5 1.0 0.5 0.0
f1 (ppm)

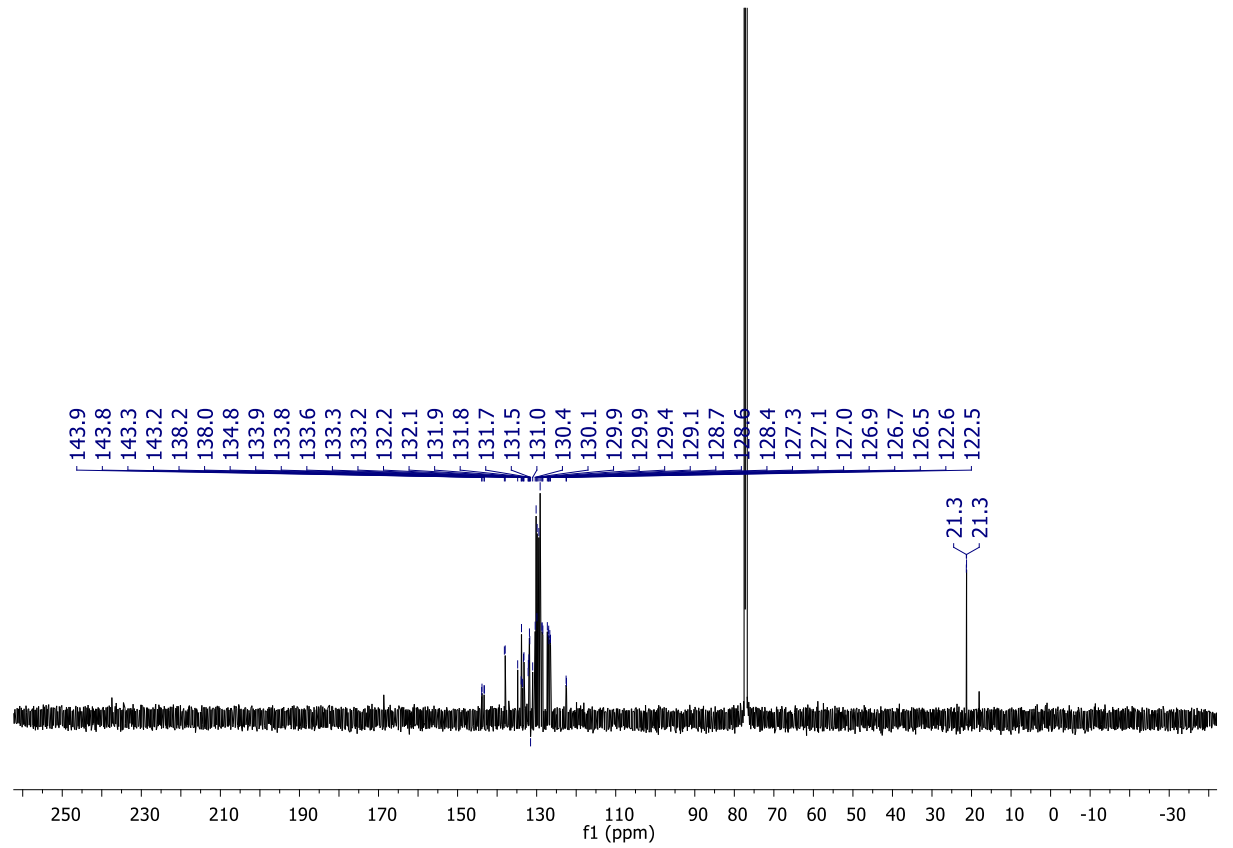
143.9
143.8
143.3
143.2
138.2
138.0
134.8
133.9
133.8
133.6
133.3
133.2
132.2
132.1
131.9
131.8
131.7
131.5
131.0
130.4
130.1
129.9
129.9
129.4
129.1
128.7
128.6
128.4
127.3
127.1
127.0
126.9
126.7
126.5
122.6
122.5
21.3
21.3
250 230 210 190 170 150 130 110 90 80 70 60 50 40 30 20 10 0 -10 -30
f1 (ppm)

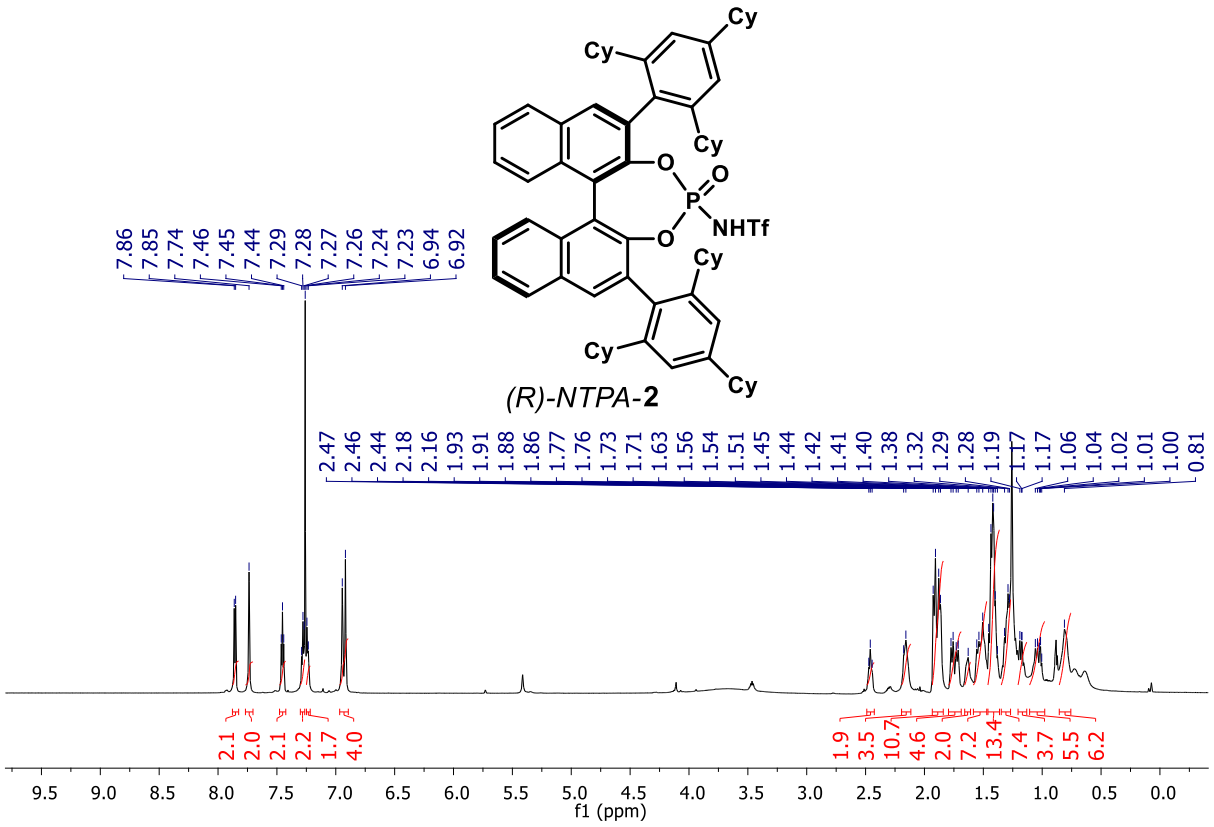
Cy
Cy
Cy
O
O
P
O
NHTf
Cy
Cy
Cy
(R)-NTPA-2
7.86
7.85
7.74
7.46
7.45
7.44
7.29
7.28
7.27
7.26
7.24
7.23
6.94
6.92
2.47
2.46
2.44
2.18
2.16
1.93
1.91
1.88
1.86
1.77
1.76
1.73
1.71
1.63
1.56
1.54
1.51
1.45
1.44
1.42
1.41
1.40
1.38
1.32
1.29
1.28
1.19
1.17
1.17
1.06
1.04
1.02
1.01
1.00
0.81
2.1
2.0
2.1
2.2
1.7
4.0
1.9
3.5
10.7
4.6
2.0
7.2
13.4
7.4
3.7
5.5
6.2
f1 (ppm)

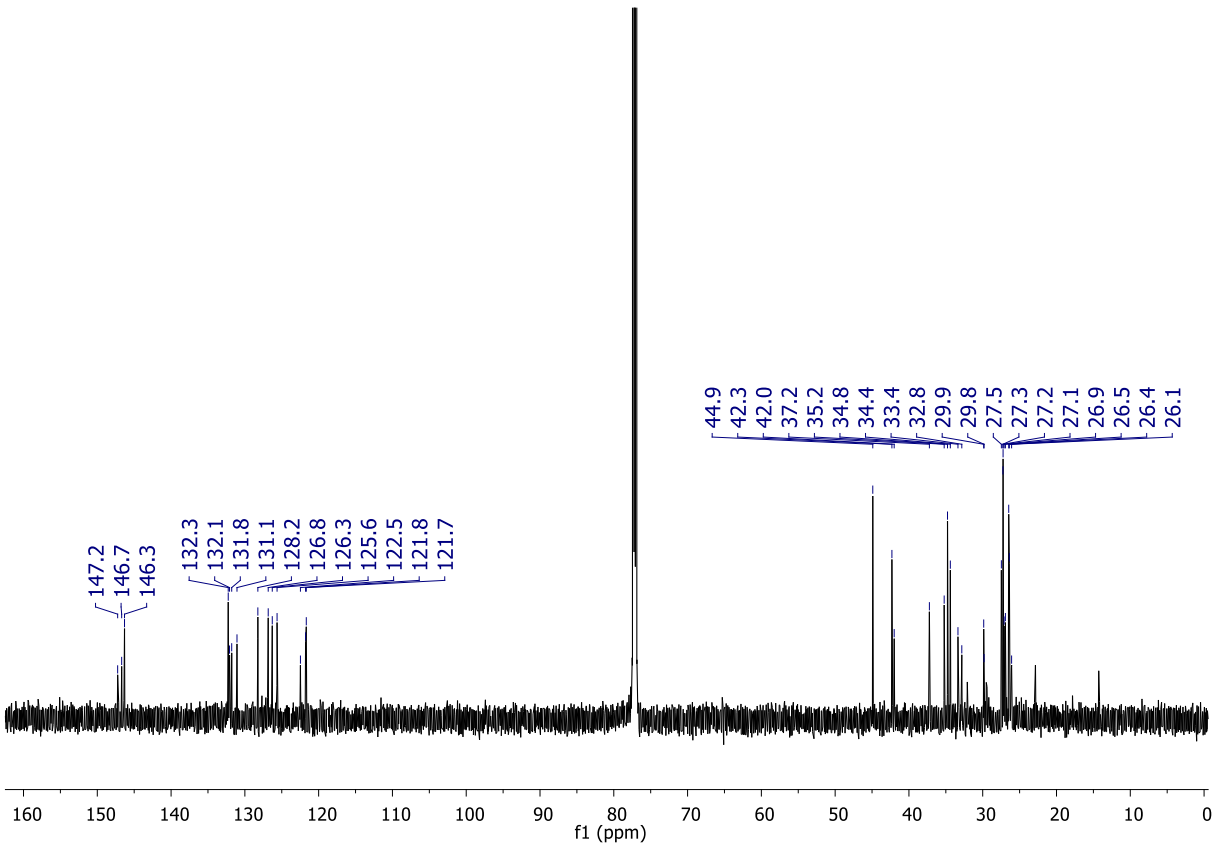
147.2
146.7
146.3
132.3
132.1
131.8
131.1
128.2
126.8
126.3
125.6
122.5
121.8
121.7
44.9
42.3
42.0
37.2
35.2
34.8
34.4
33.4
32.8
29.9
29.8
27.5
27.3
27.2
27.1
26.9
26.5
26.4
26.1
f1 (ppm)

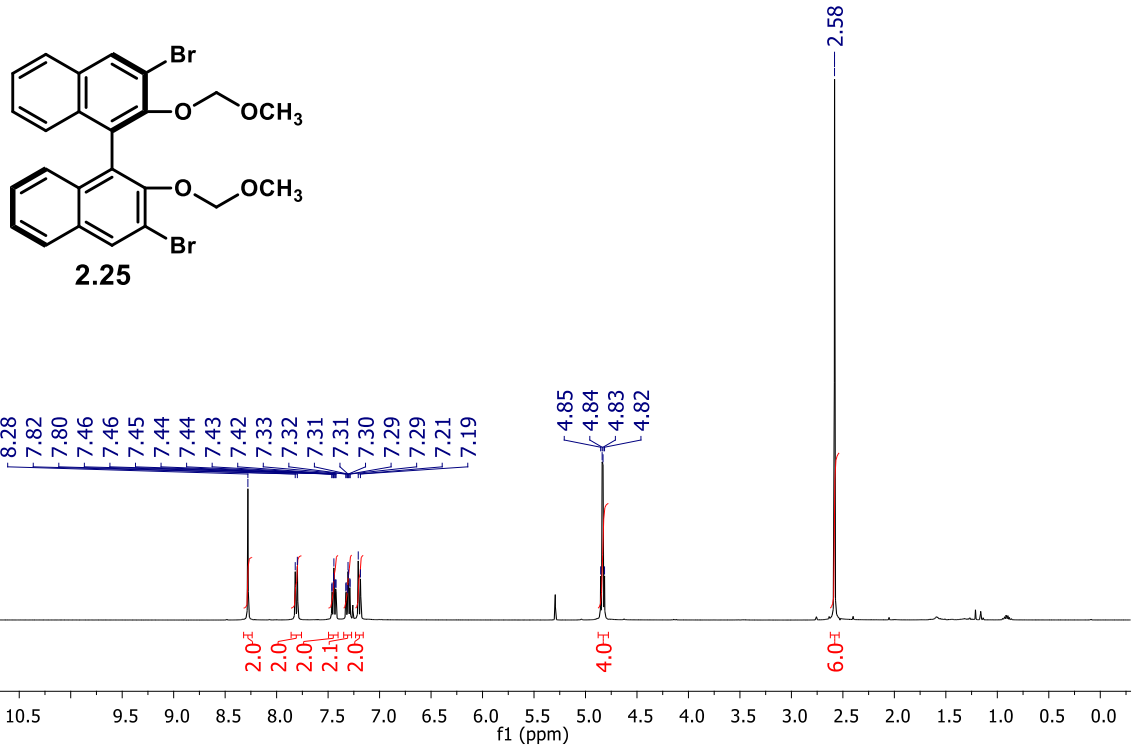
Br
O
OCH3
O
OCH3
Br
2.25
2.58
8.28
7.82
7.80
7.46
7.46
7.45
7.44
7.44
7.43
7.42
7.33
7.32
7.31
7.31
7.30
7.29
7.29
7.21
7.19
4.85
4.84
4.83
4.82
2.0
2.0
2.0
2.1
2.0
4.0
6.0
f1 (ppm)

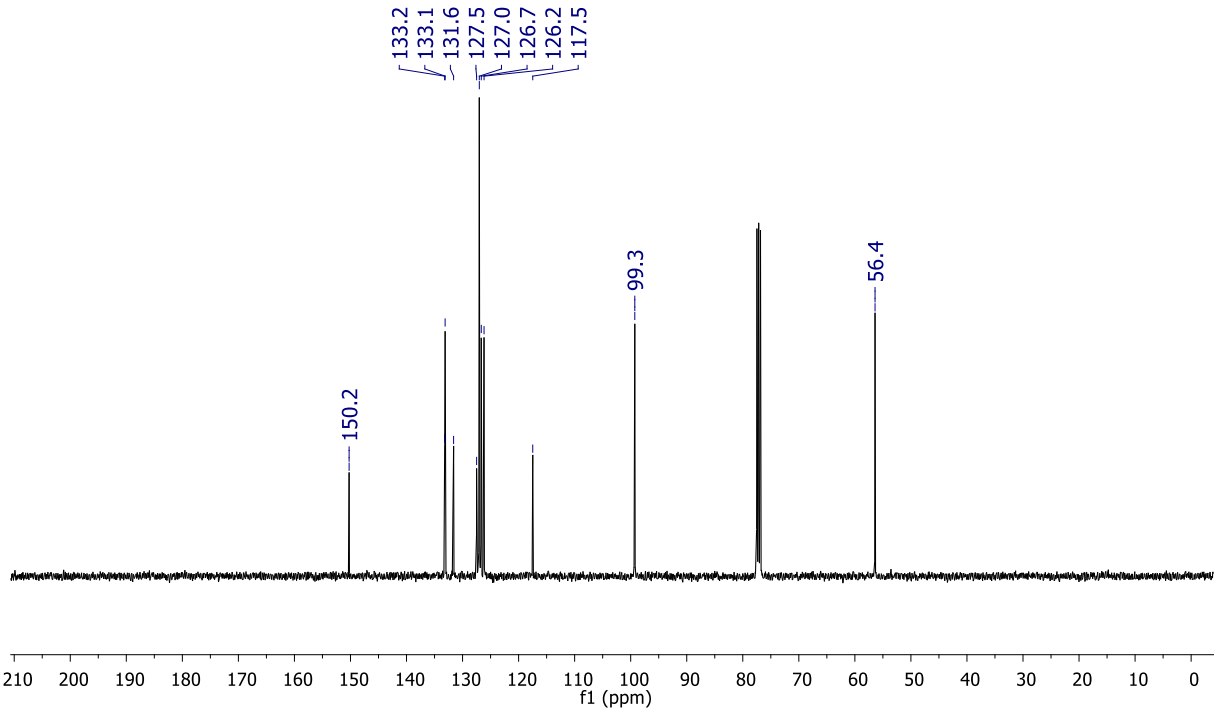
133.2
133.1
131.6
127.5
127.0
126.7
126.2
117.5
150.2
99.3
56.4
f1 (ppm)

gc2-132

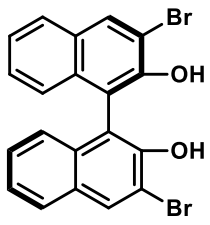

2.21

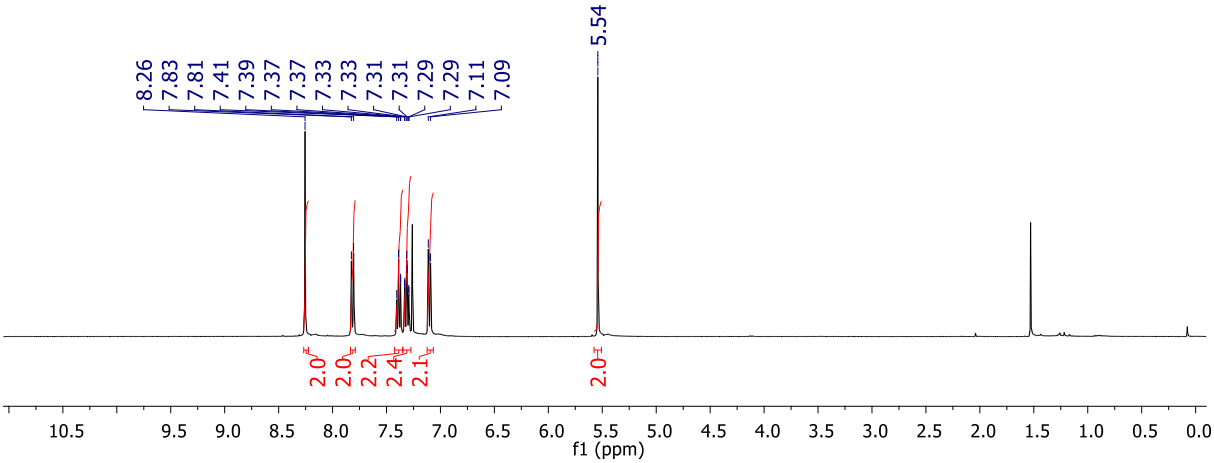

gc2-132
Standard 13C 400MHz BBFO "Smart" probe

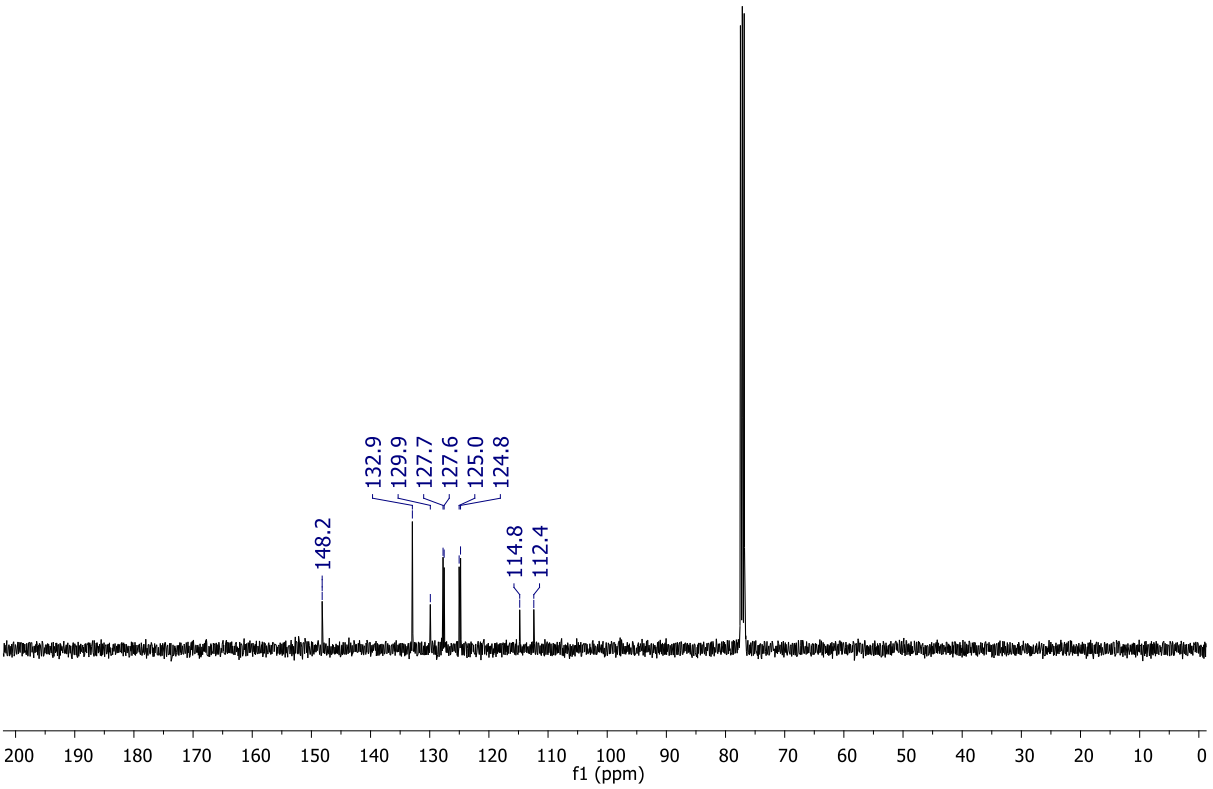

gc2-30_r

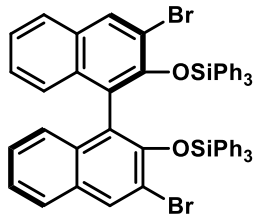

2.26

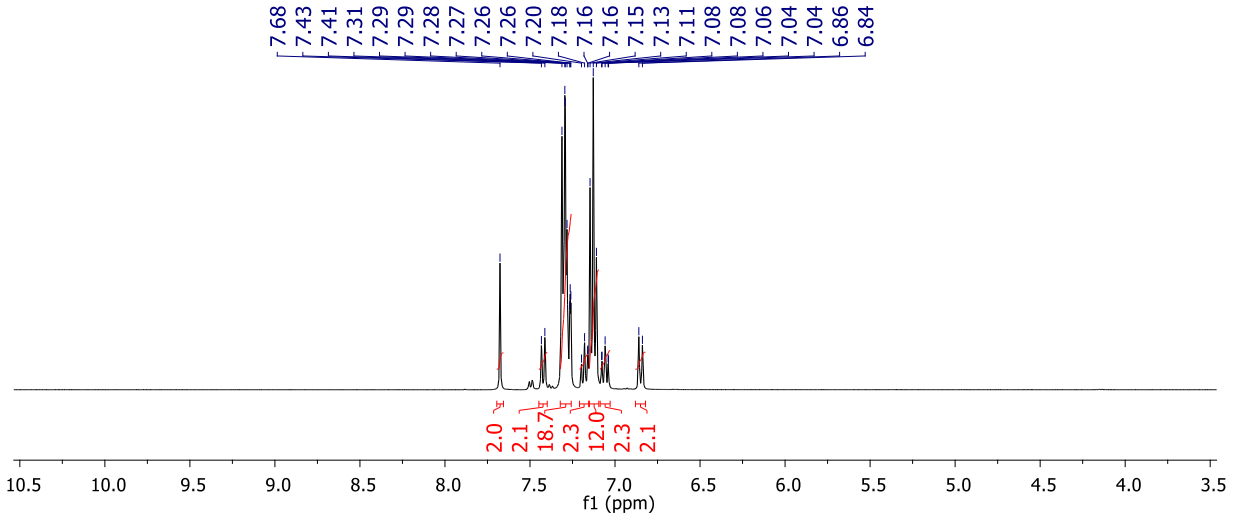

gc2-30_r
Standard 13C 400MHz BBFO "Smart" probe

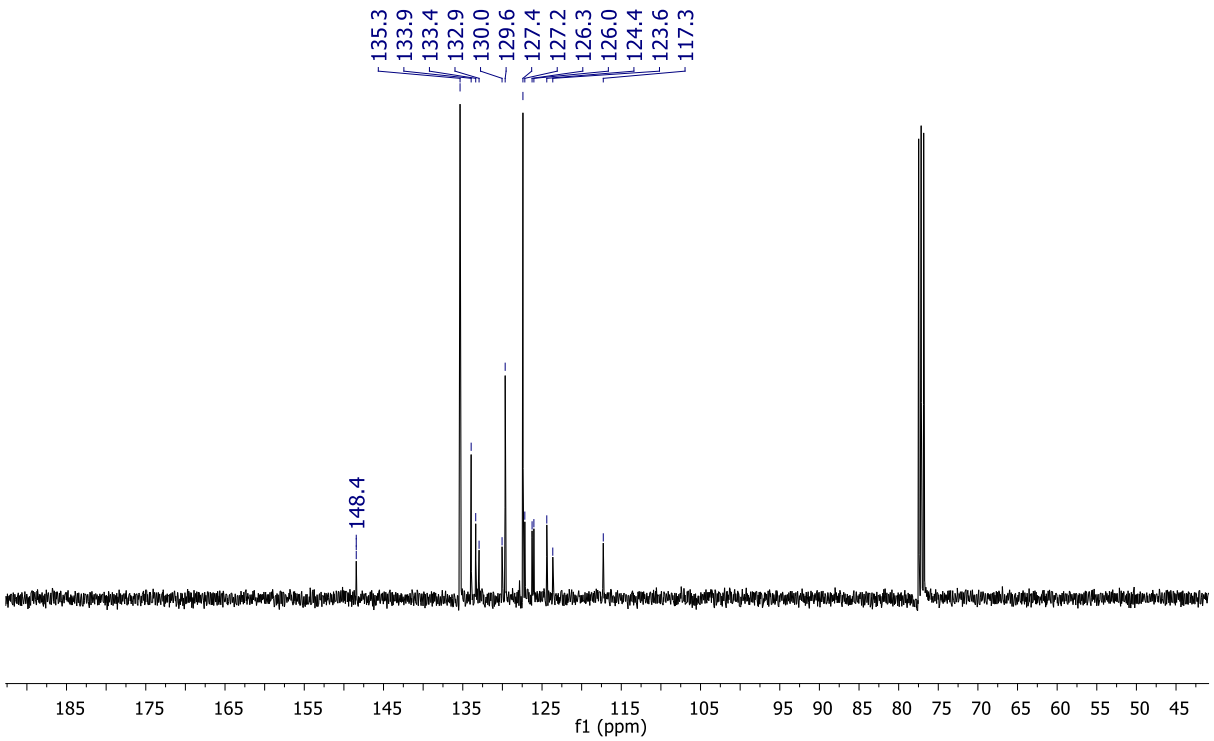

gc2-140

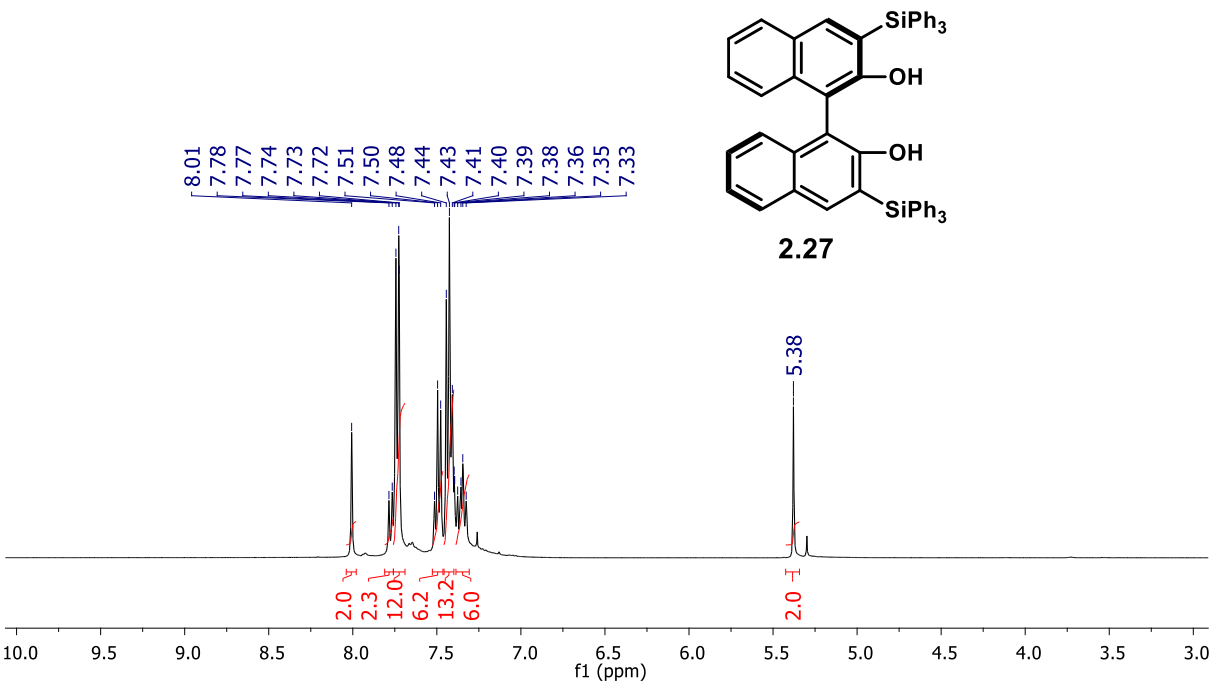

gc2-140
Standard 13C 400MHz BBFO "Smart" probe

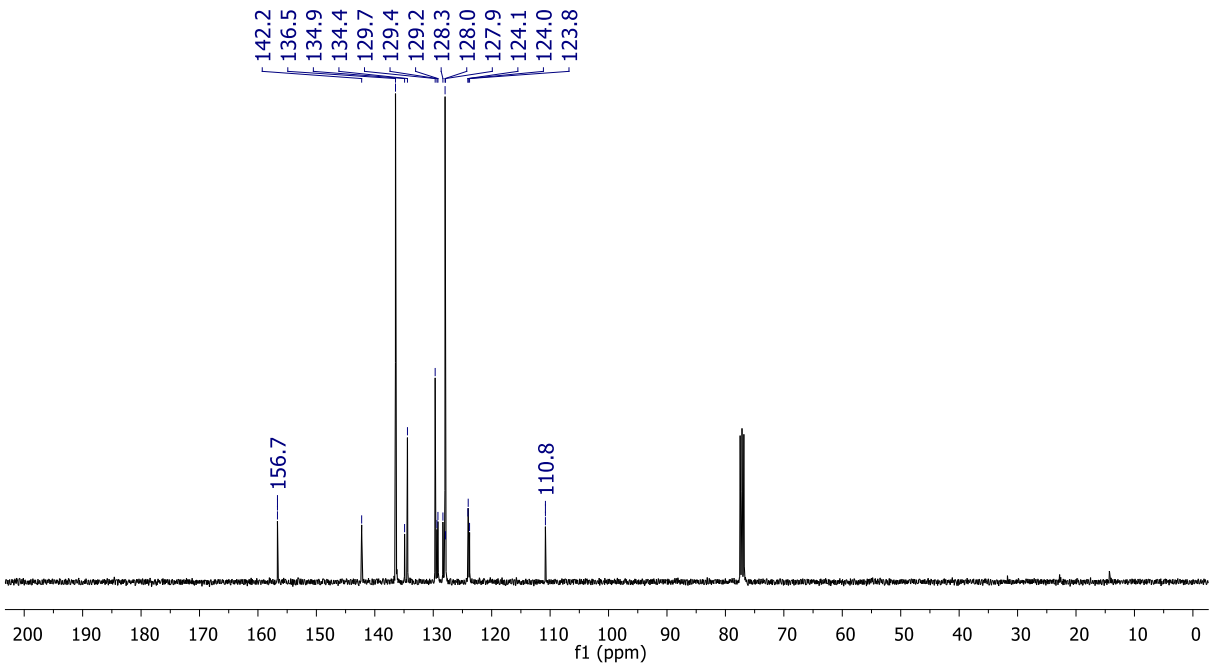

gc2-184

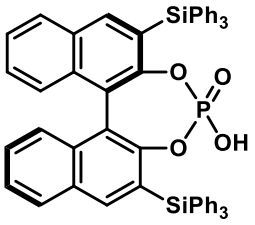

*(R)-PA-***5**

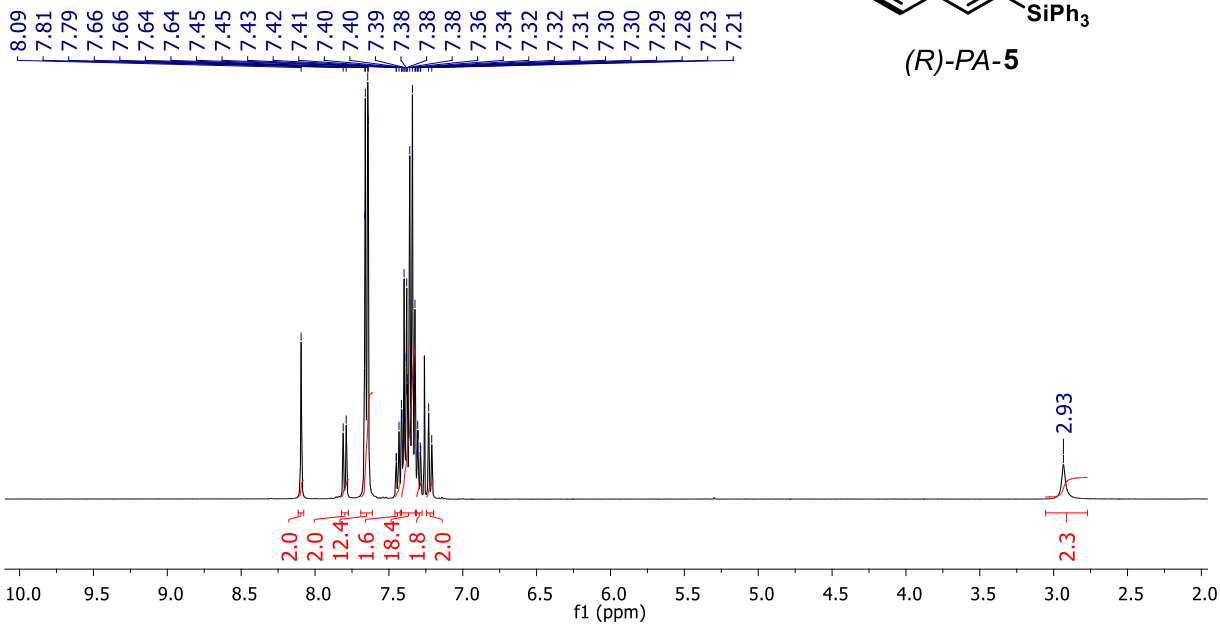

gc2-184
Standard 13C 400MHz BBFO "Smart" probe

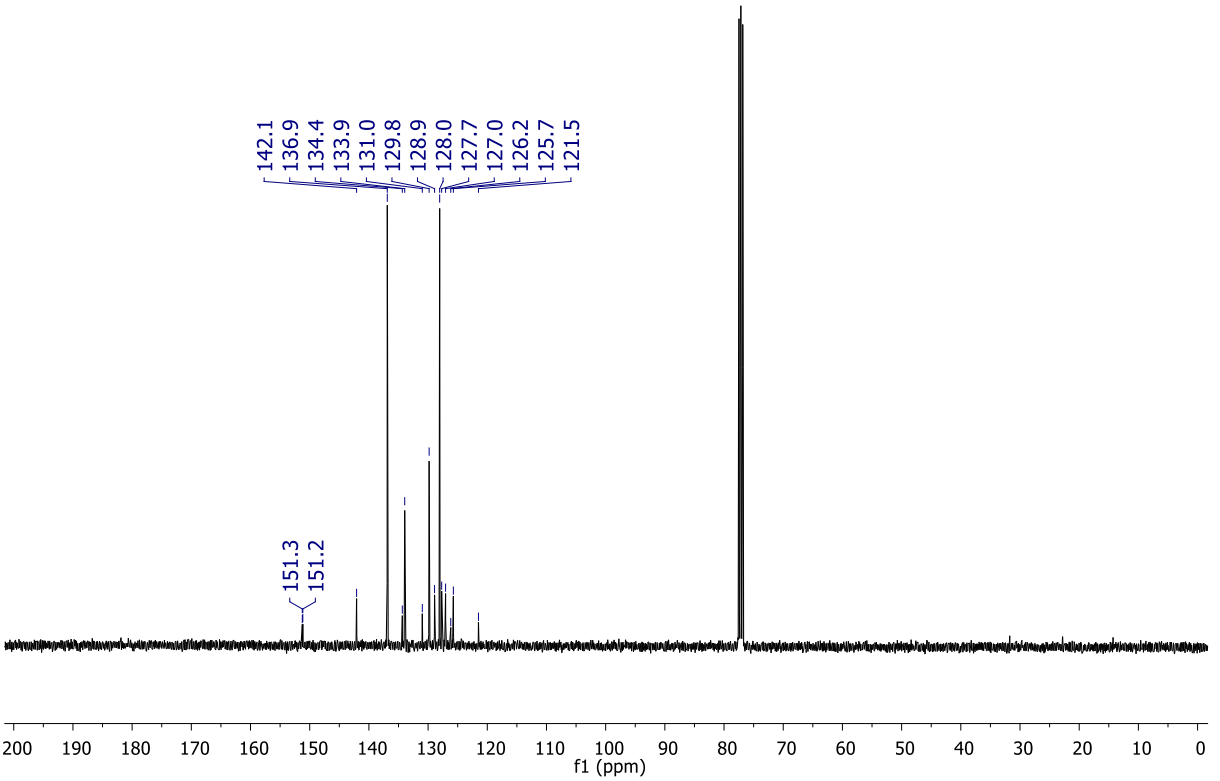

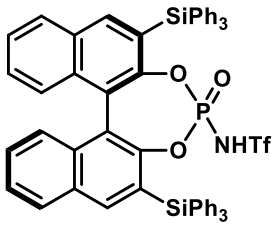
SiPh3
O
O
P
O
NHTf
SiPh3

*(R)-NTPA-***5**

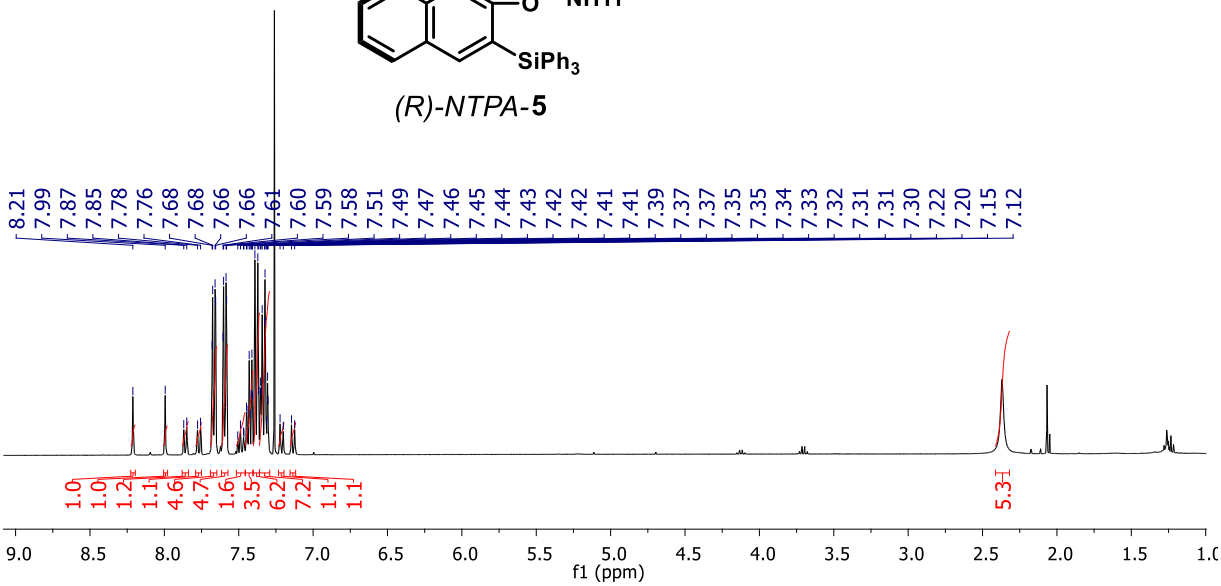
8.21 7.99 7.87 7.85 7.78 7.76 7.68 7.68 7.66 7.66 7.61 7.60 7.59 7.58 7.51 7.49 7.47 7.46 7.45 7.44 7.43 7.42 7.42 7.41 7.41 7.39 7.37 7.37 7.35 7.35 7.34 7.33 7.32 7.31 7.31 7.30 7.22 7.20 7.15 7.12
1.0 1.0 1.2 1.1 4.6 4.7 1.6 3.5 6.2 7.2 1.1 1.1
5.3
9.0 8.5 8.0 7.5 7.0 6.5 6.0 5.5 5.0 4.5 4.0 3.5 3.0 2.5 2.0 1.5
f1 (ppm)

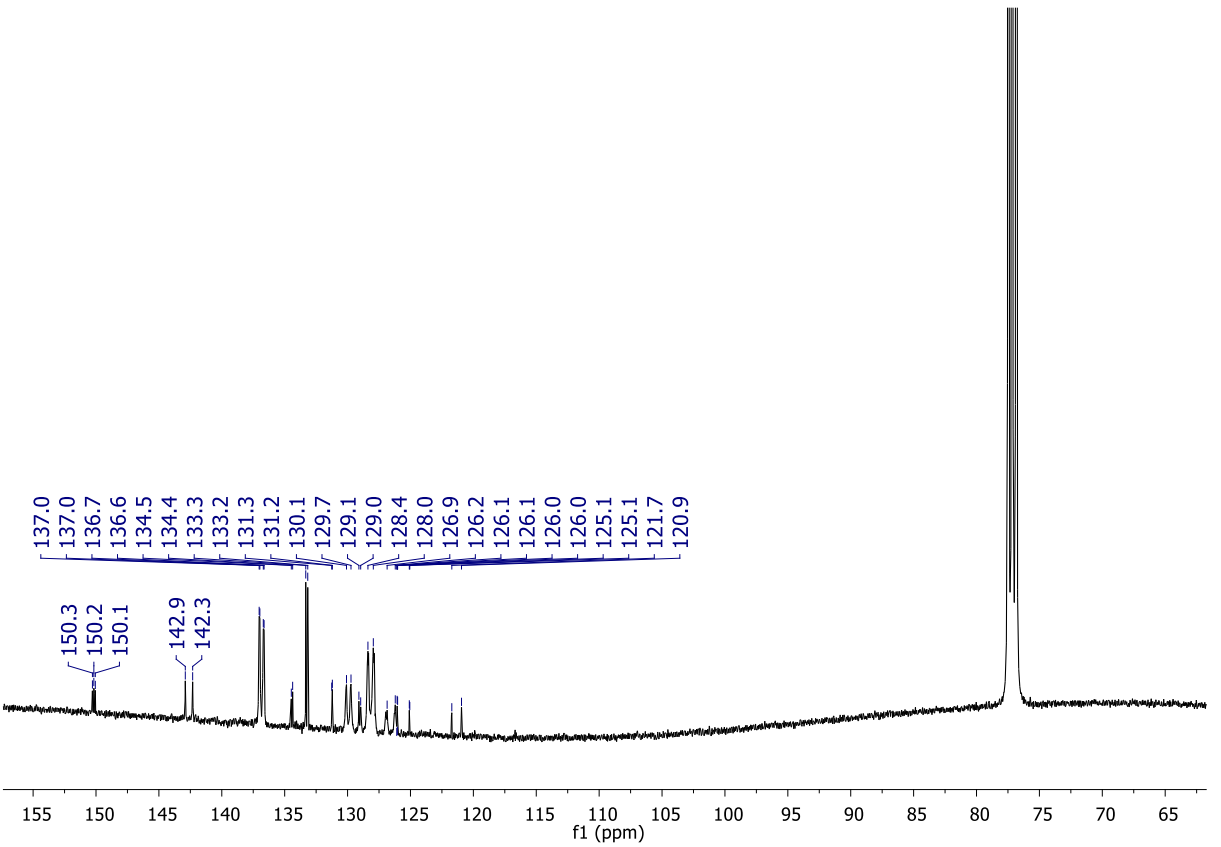
137.0 137.0 136.7 136.6 134.5 134.4 133.3 133.2 131.3 131.2 130.1 129.7 129.1 129.0 128.4 128.0 126.9 126.2 126.1 126.1 126.0 126.0 125.1 125.1 121.7 120.9
150.3 150.2 150.1 142.9 142.3
155 150 145 140 135 130 125 120 115 110 105 100 95 90 85 80 75 70 65
f1 (ppm)

gc2-78

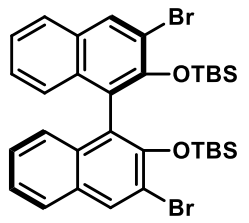

2.28

gc2-78
Standard 13C 400MHz BBFO "Smart" probe

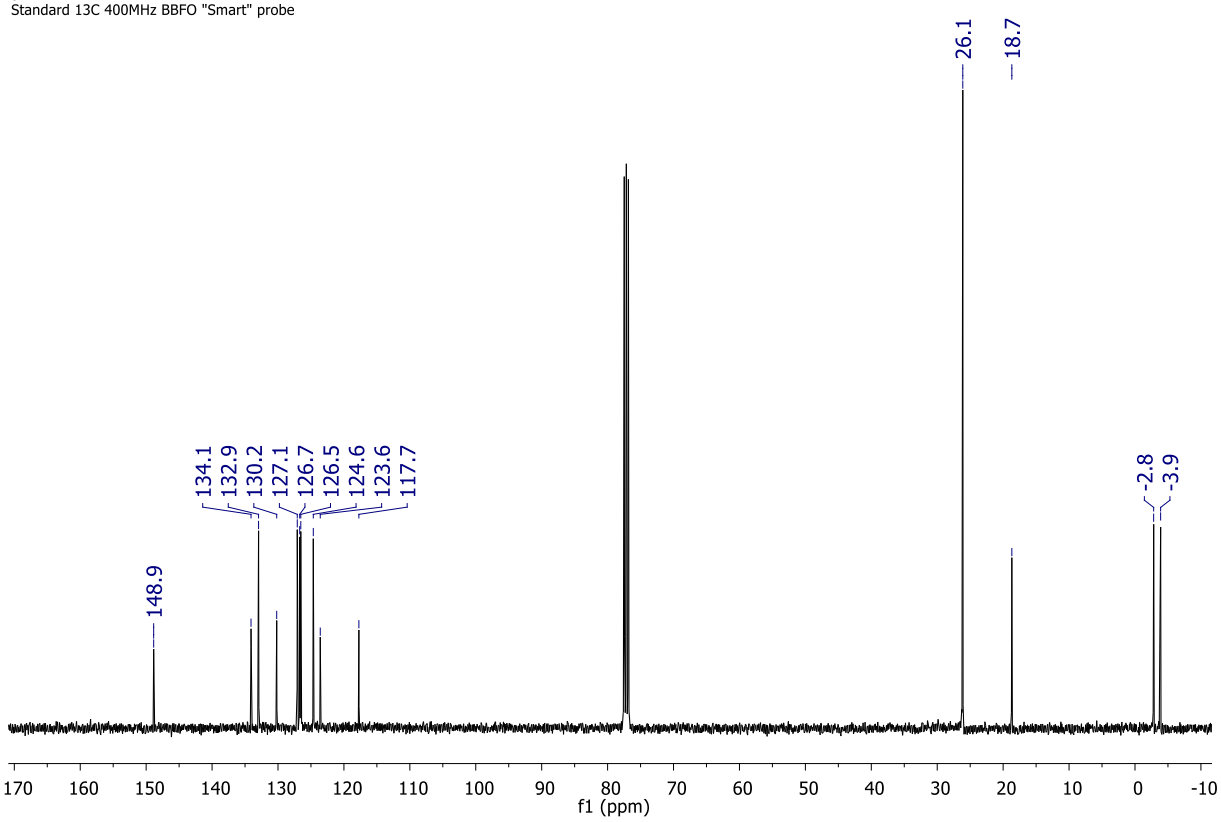

gc2-138

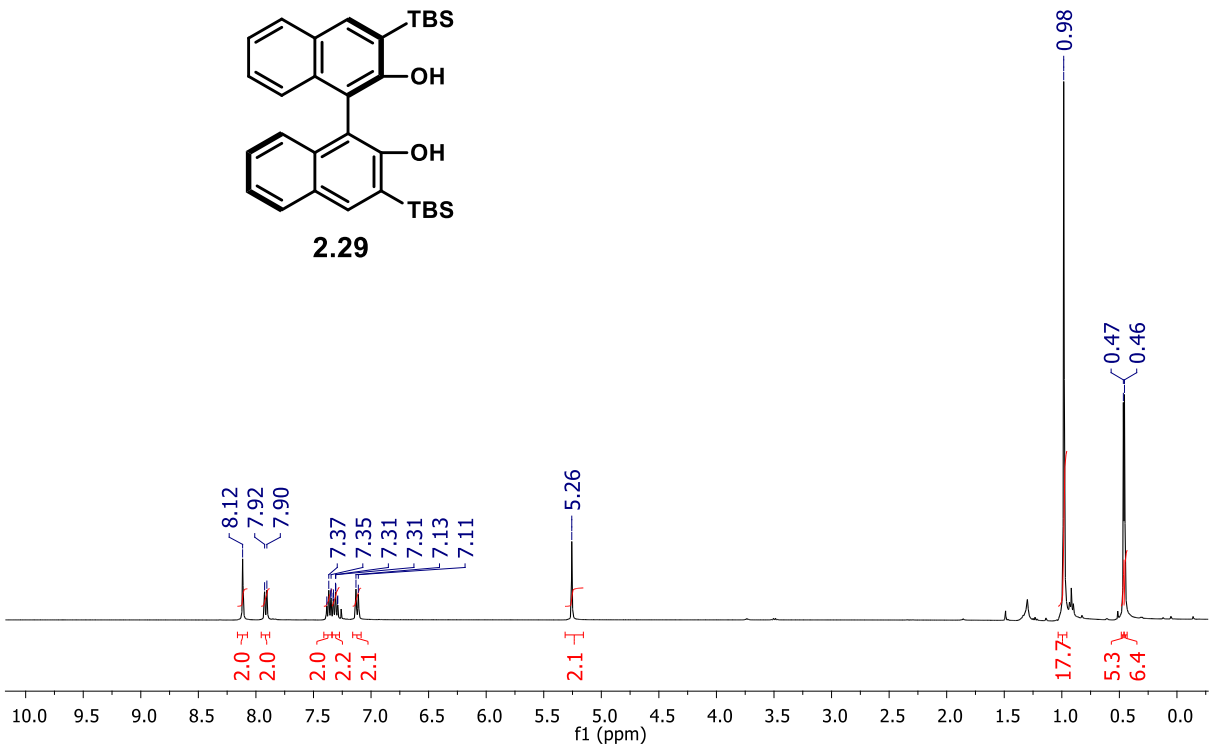

gc2-138
Standard 13C 400MHz BBFO "Smart" probe

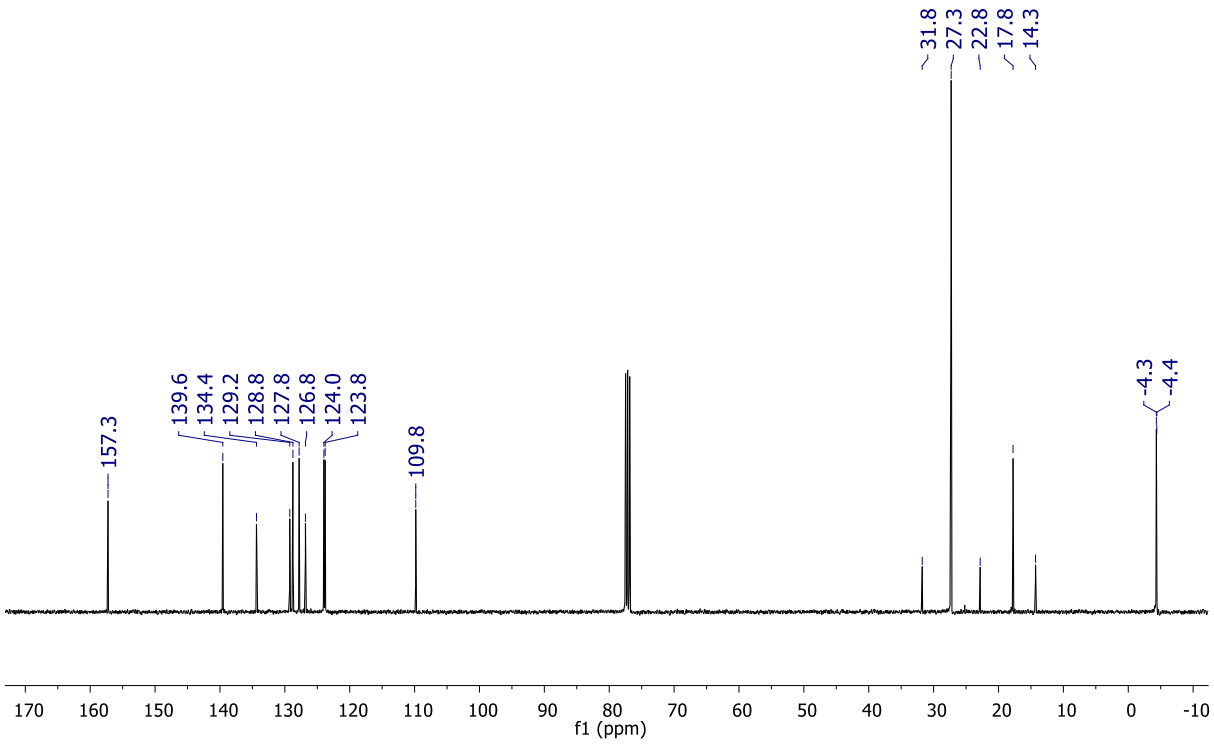

gc2-172

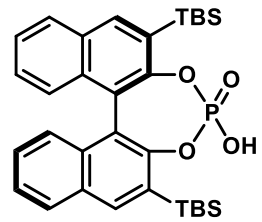

*(R)-PA-***6**

gc2-172
Standard 13C 400MHz BBFO "Smart" probe

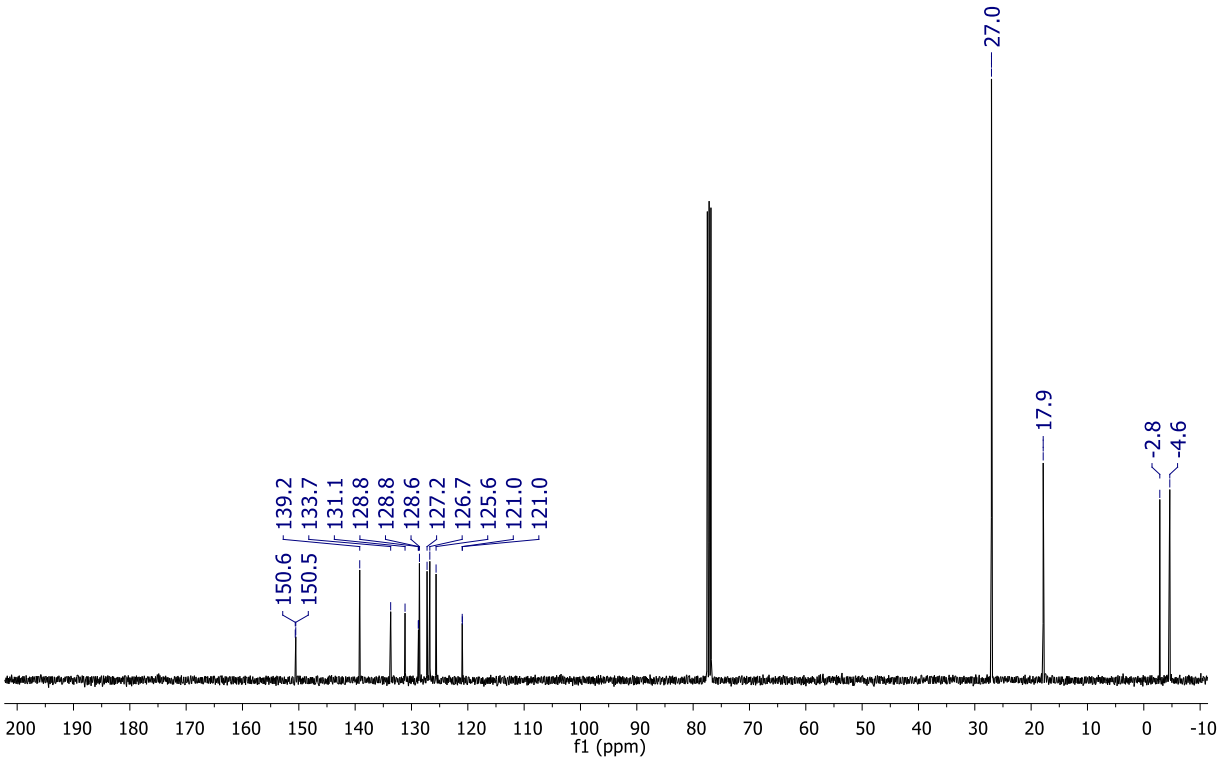

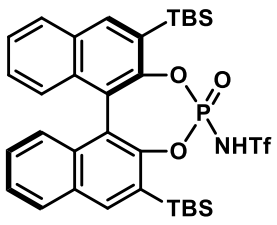
TBS
O
O
P
O
NHTf
TBS

*(R)-NTPA-***6**

0.90
0.85
0.70
0.62
0.51
0.50
8.14
8.13
7.96
7.94
7.50
7.48
7.46
7.44
7.08
7.06
7.01
6.98
1.9
1.9
2.0
3.7
1.0
1.1
13.6
2.2
2.2
4.5
9.5 9.0 8.5 8.0 7.5 7.0 6.5 6.0 5.5 5.0 4.5 4.0 3.5 3.0 2.5 2.0 1.5 1.0 0.5 0.0 -0.5
f1 (ppm)

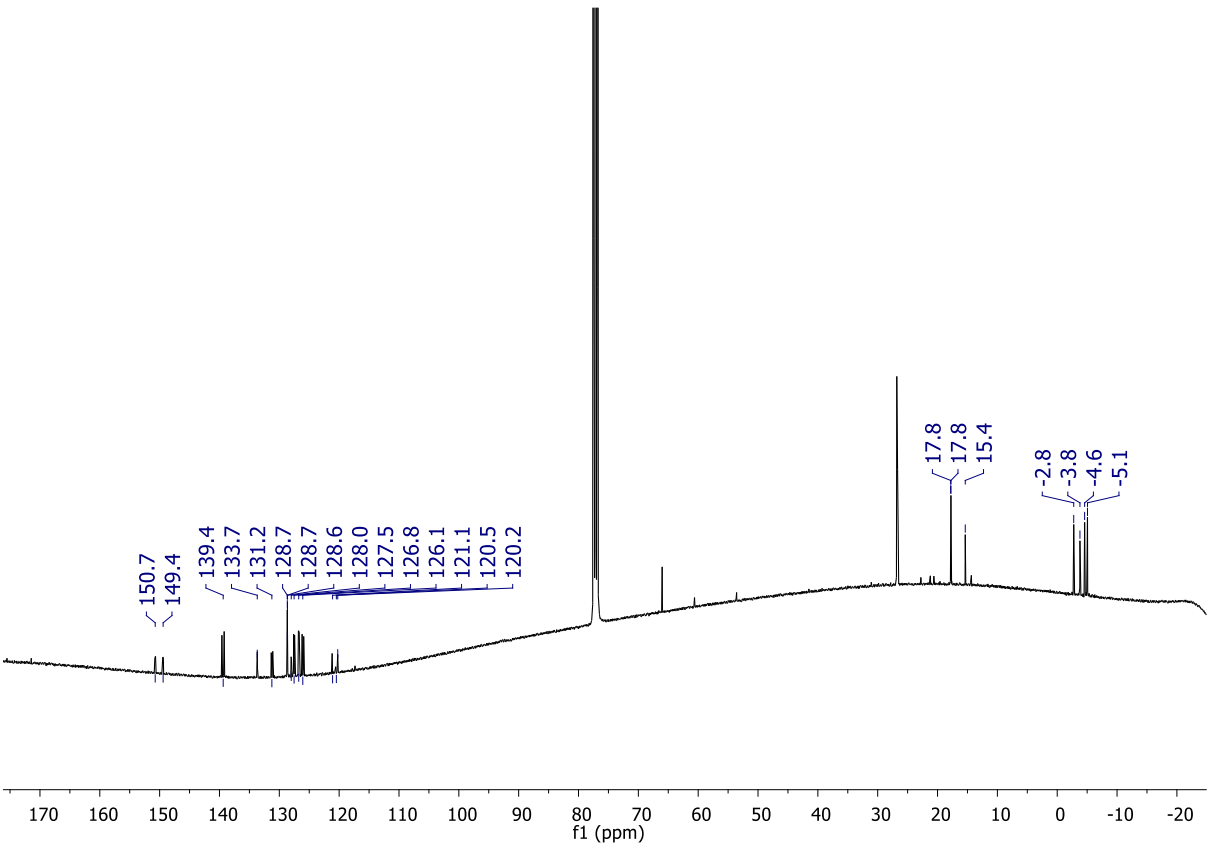
150.7
149.4
139.4
133.7
131.2
128.7
128.7
128.6
128.0
127.5
126.8
126.1
121.1
120.5
120.2
17.8
17.8
15.4
-2.8
-3.8
-4.6
-5.1
170 160 150 140 130 120 110 100 90 80 70 60 50 40 30 20 10 0 -10 -20
f1 (ppm)

gc2-122_pure

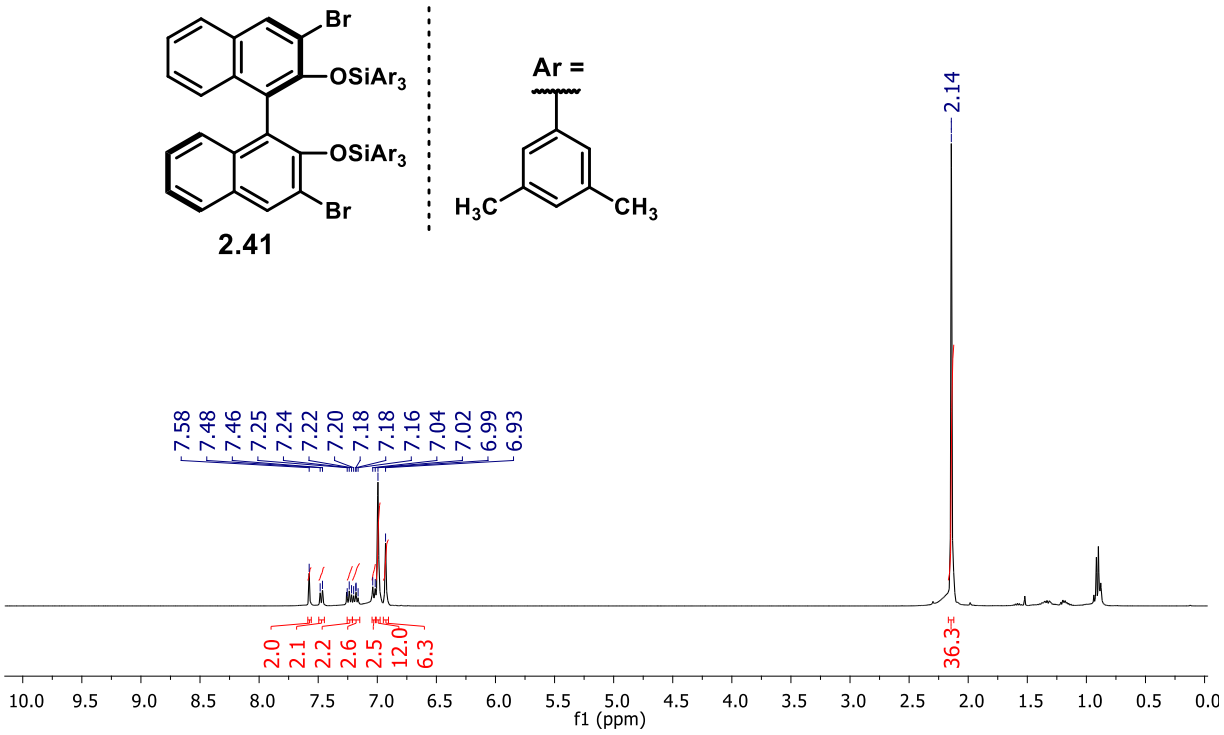

gc2-122
Standard 13C 400MHz BBFO "Smart" probe

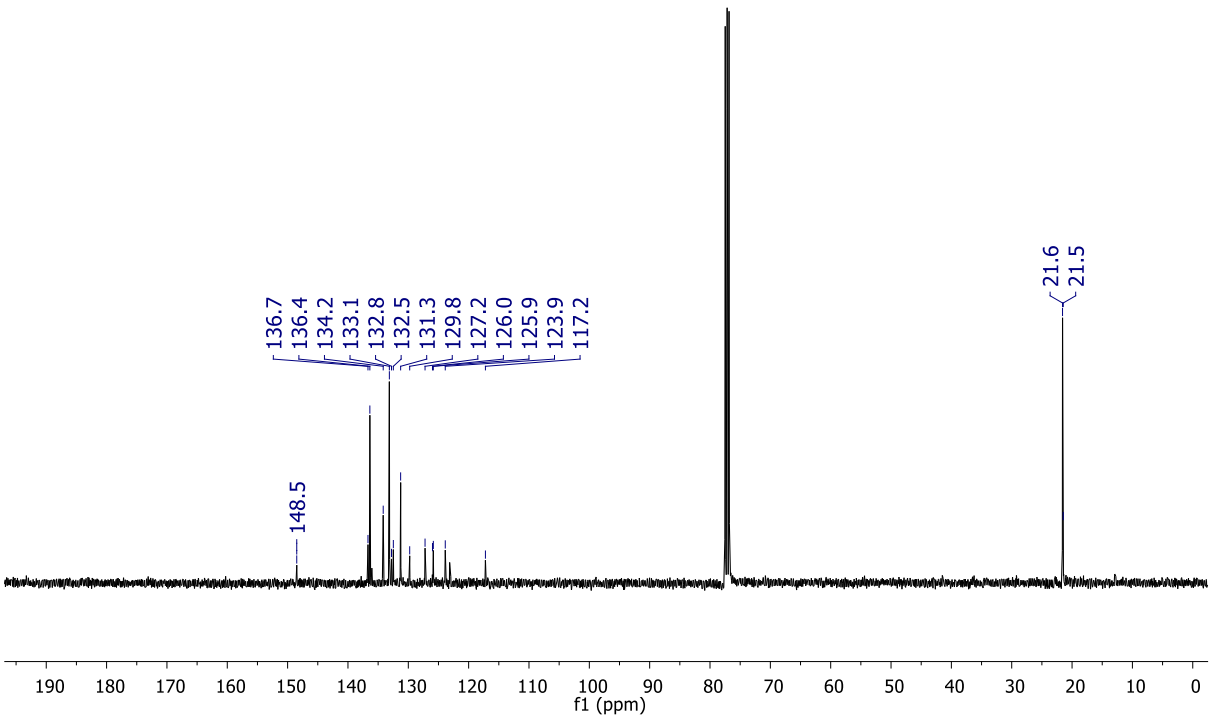

gc2-142

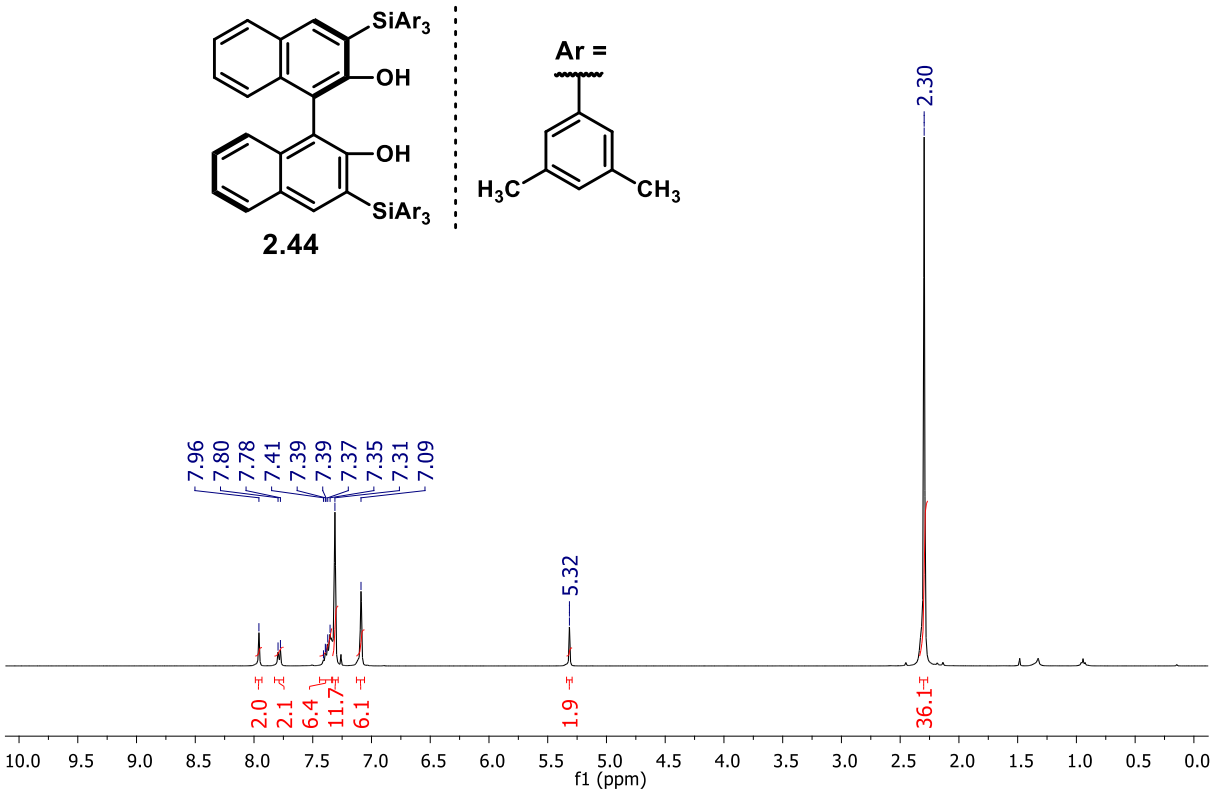

gc2-142
Standard 13C 400MHz BBFO "Smart" probe

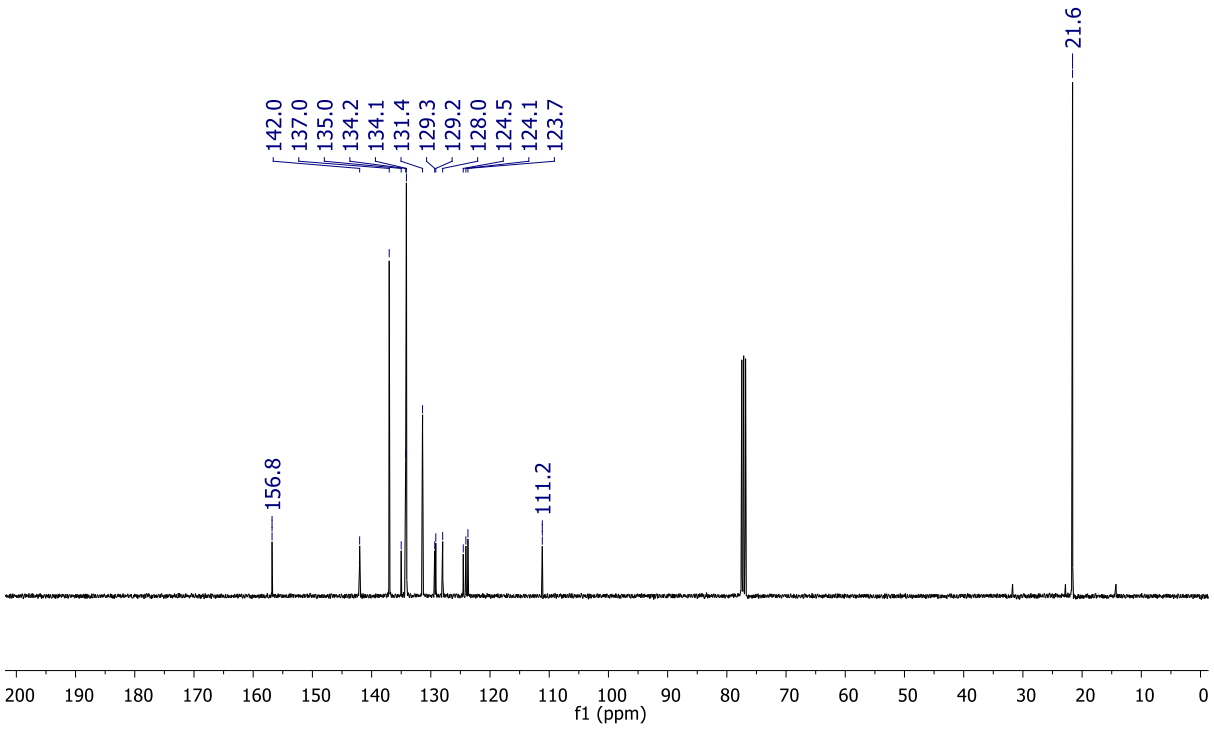

gc2-186

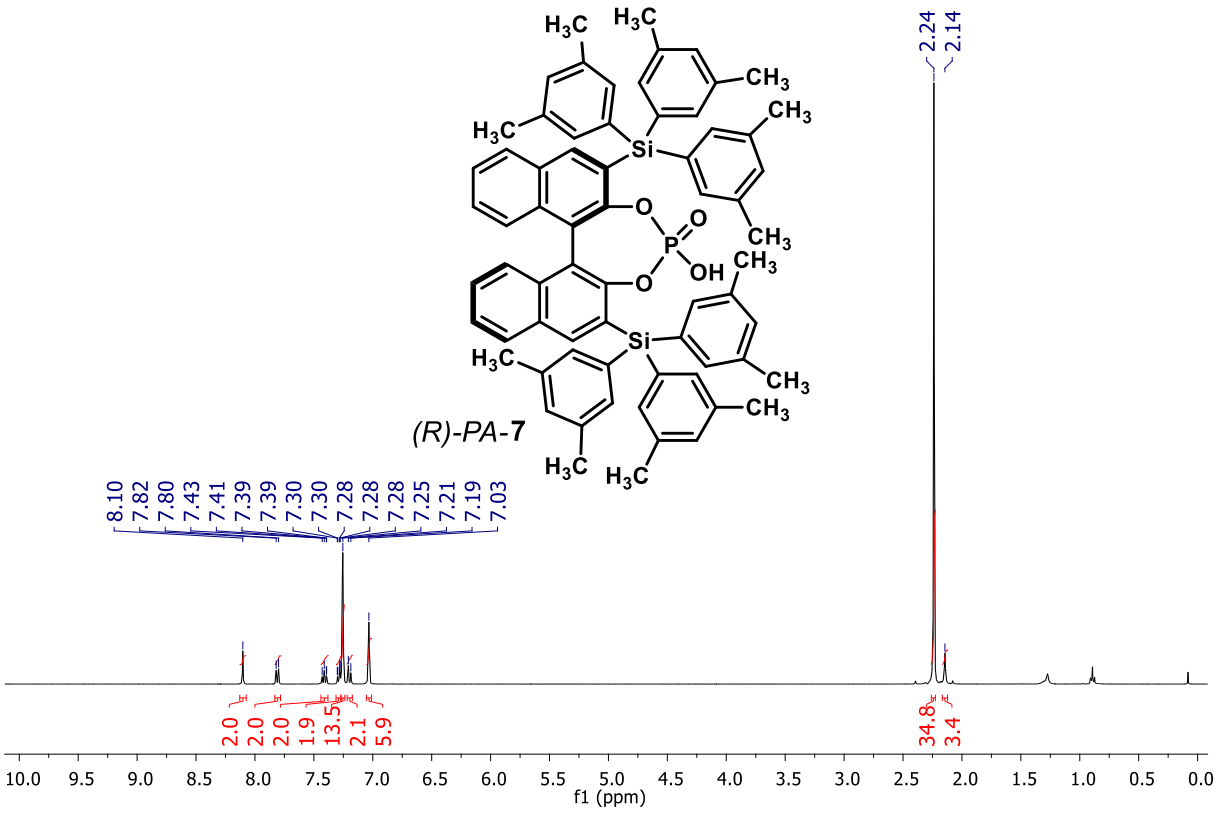

gc2-186
Standard 13C 400MHz BBFO "Smart" probe

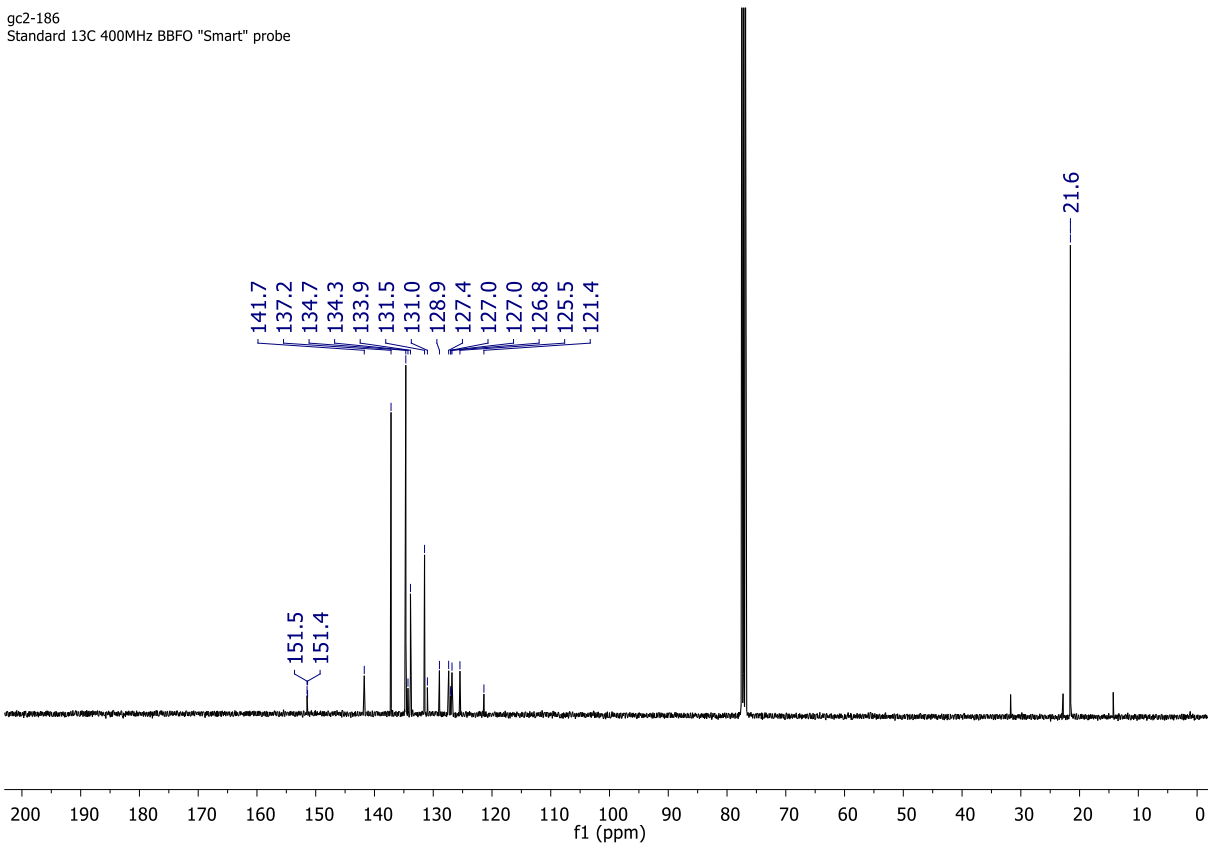

gc2-162

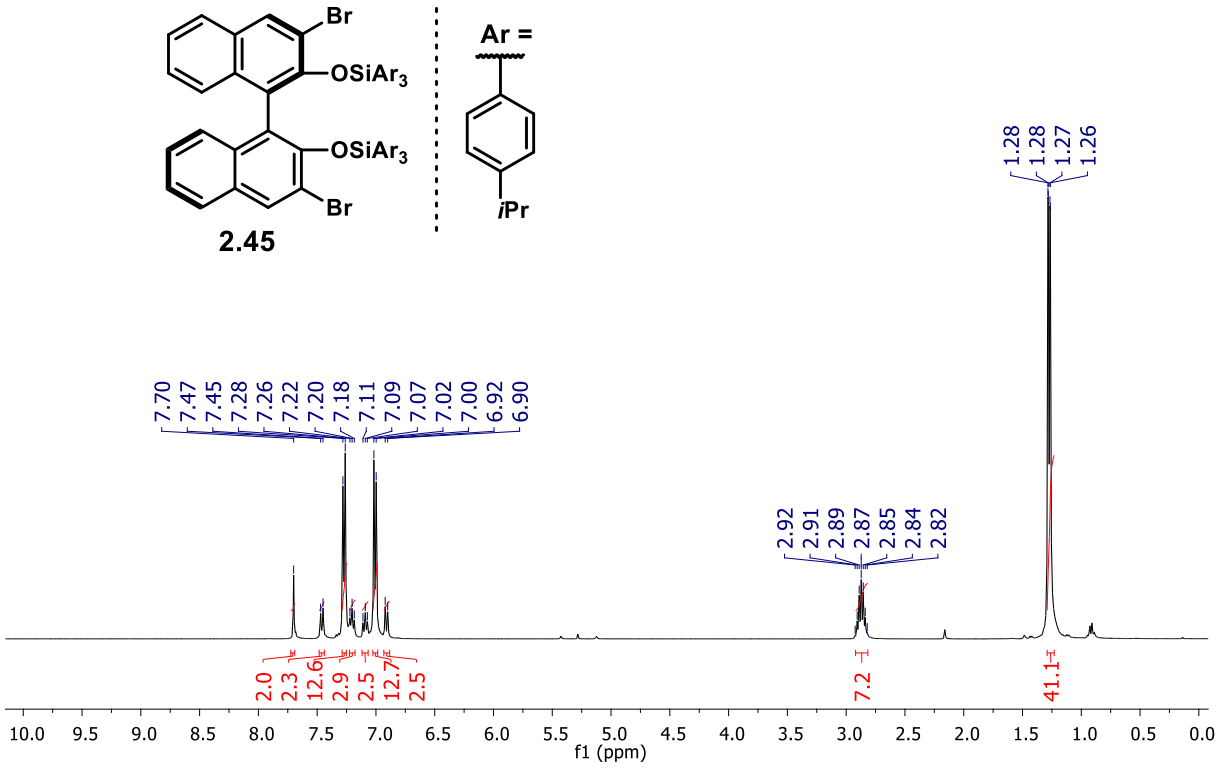

gc2-162
Standard 13C 400MHz BBFO "Smart" probe

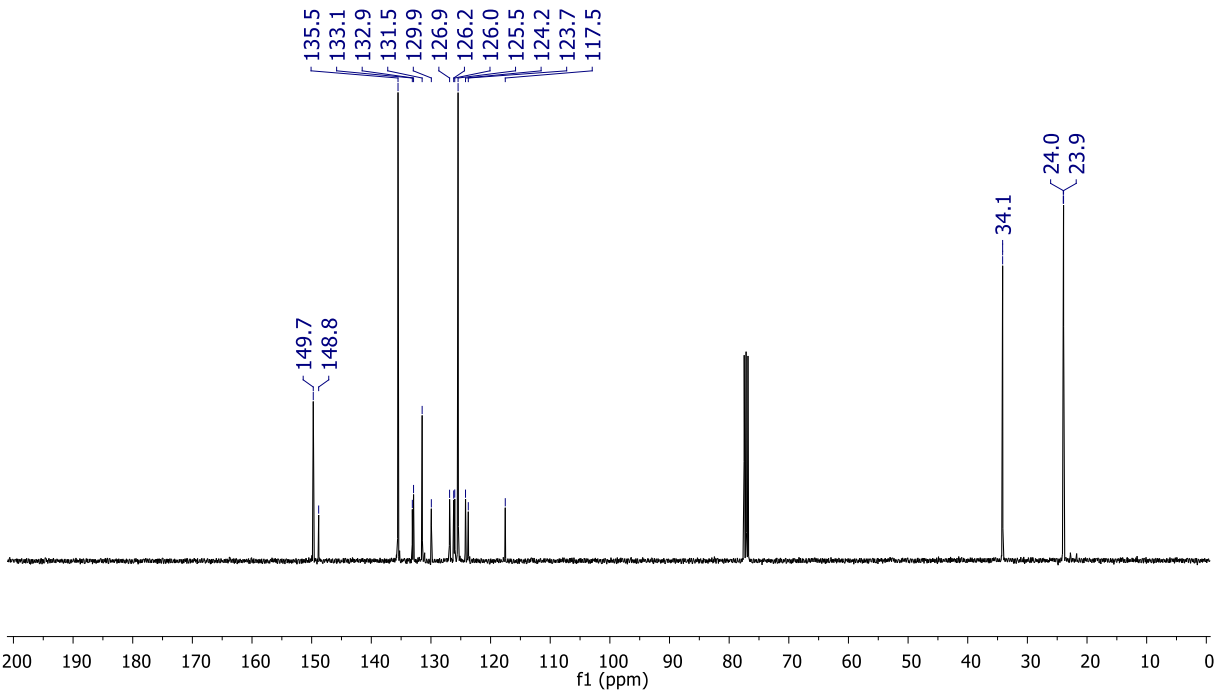

gc2-164

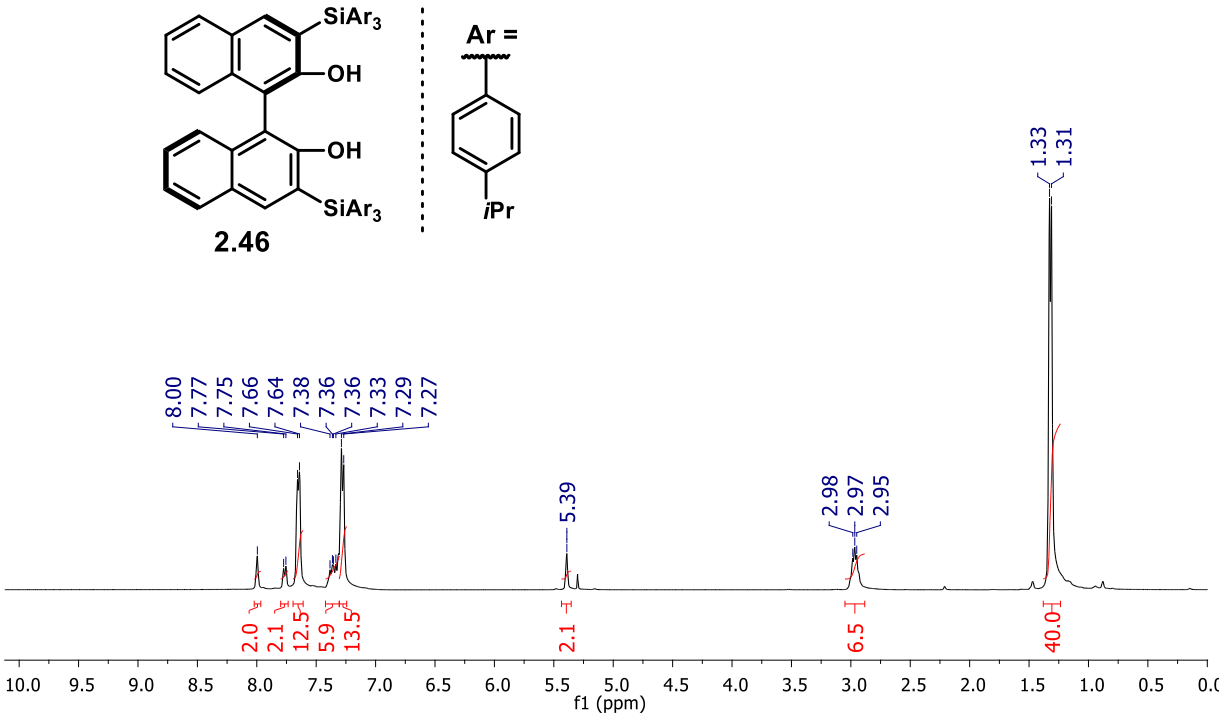

gc2-164
Standard 13C 400MHz BBFO "Smart" probe

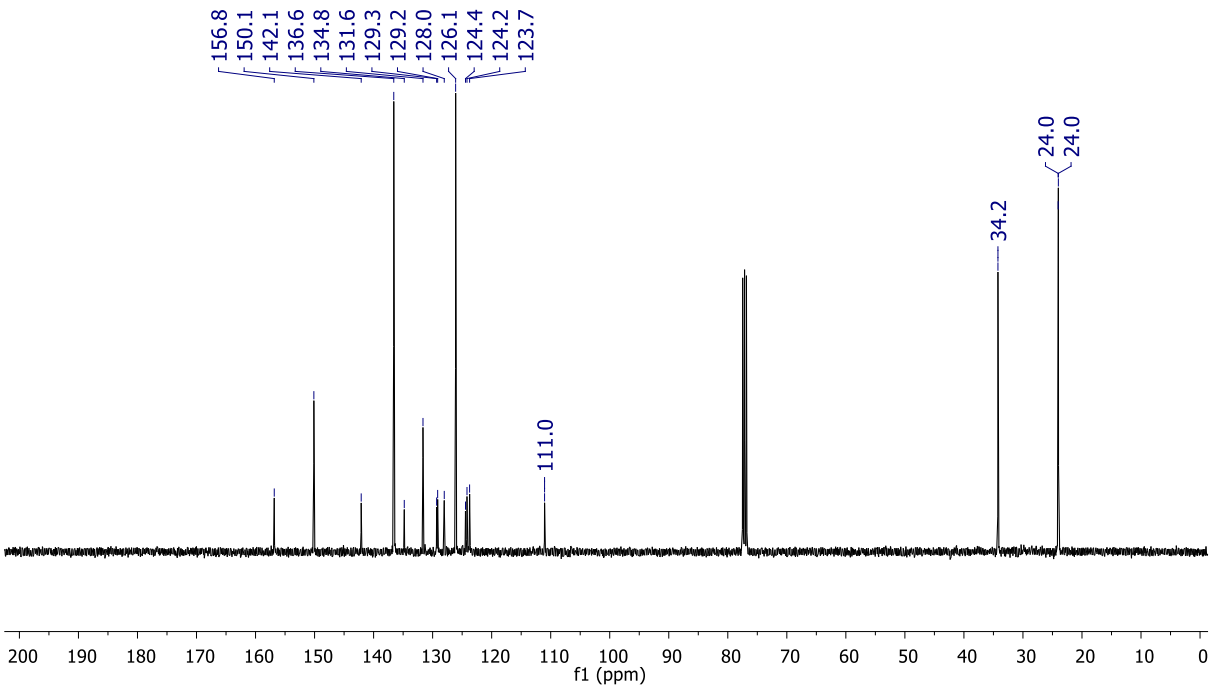

gc2-194

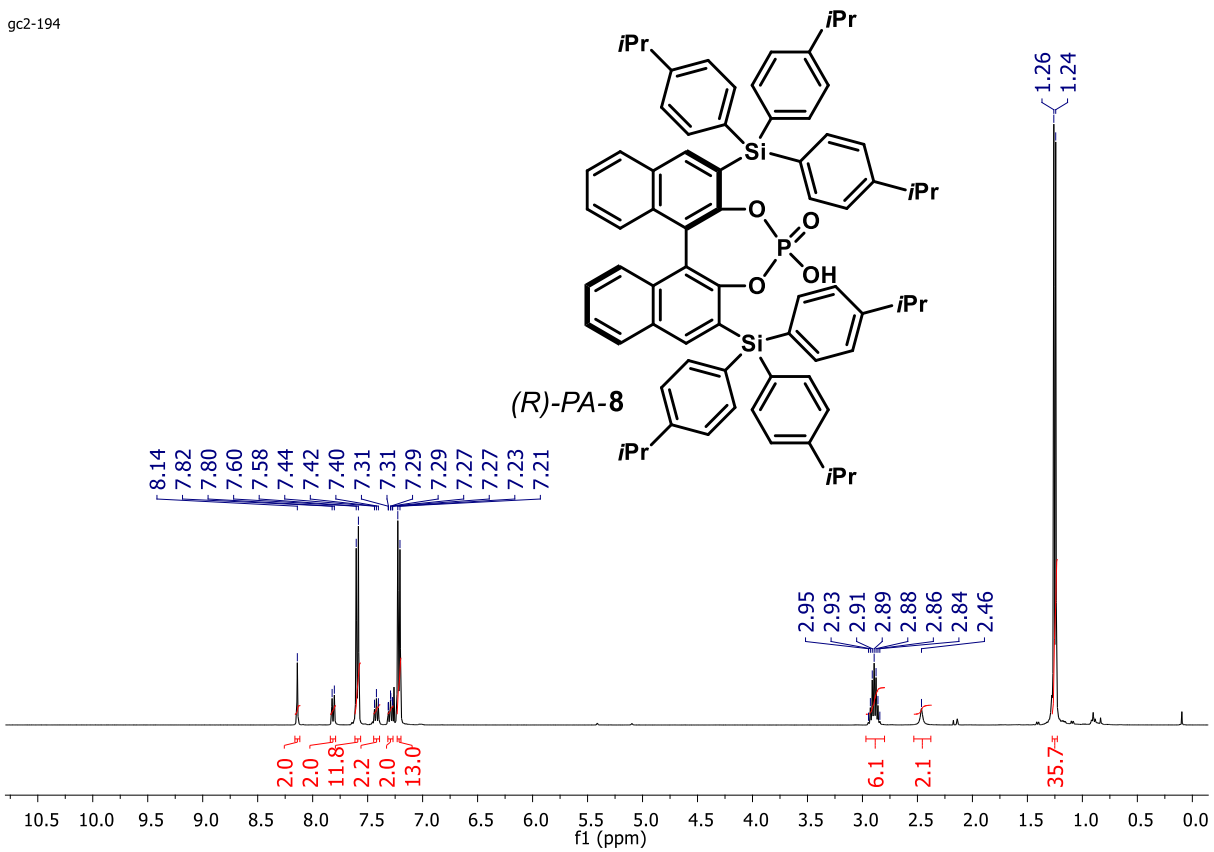

gc2-194
Standard 13C 400MHz BBFO "Smart" probe

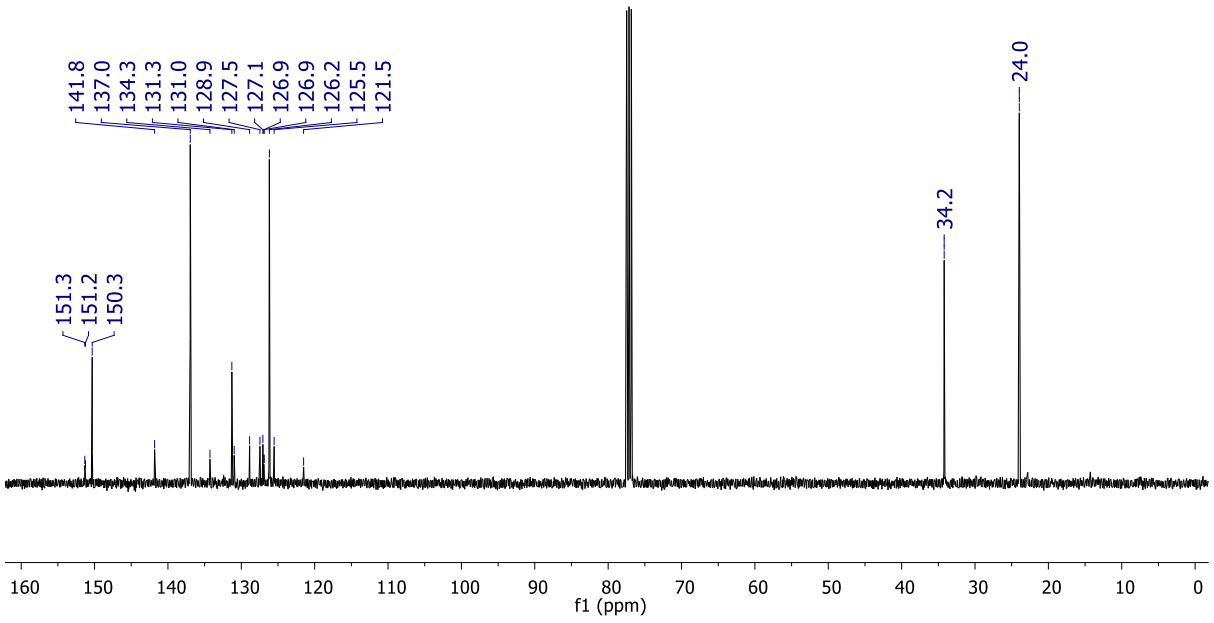

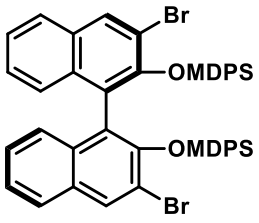
Br
OMDPS
OMDPS
Br

2.30

7.82
7.54
7.53
7.34
7.33
7.30
7.29
7.28
7.26
7.26
7.25
7.24
7.23
7.22
7.21
7.19
7.18
7.17
7.16
7.14
7.11
7.10
7.09
7.07
7.07
7.06
7.05
6.77
6.76
0.29
2.0
2.2
4.2
2.3
2.1
2.7
4.3
4.0
4.2
2.1
2.0
6.2
10.0 9.5 9.0 8.5 8.0 7.5 7.0 6.5 6.0 5.5 5.0 4.5 4.0 3.5 3.0 2.5 2.0 1.5 1.0 0.5 0.0 -0.5
f1 (ppm)

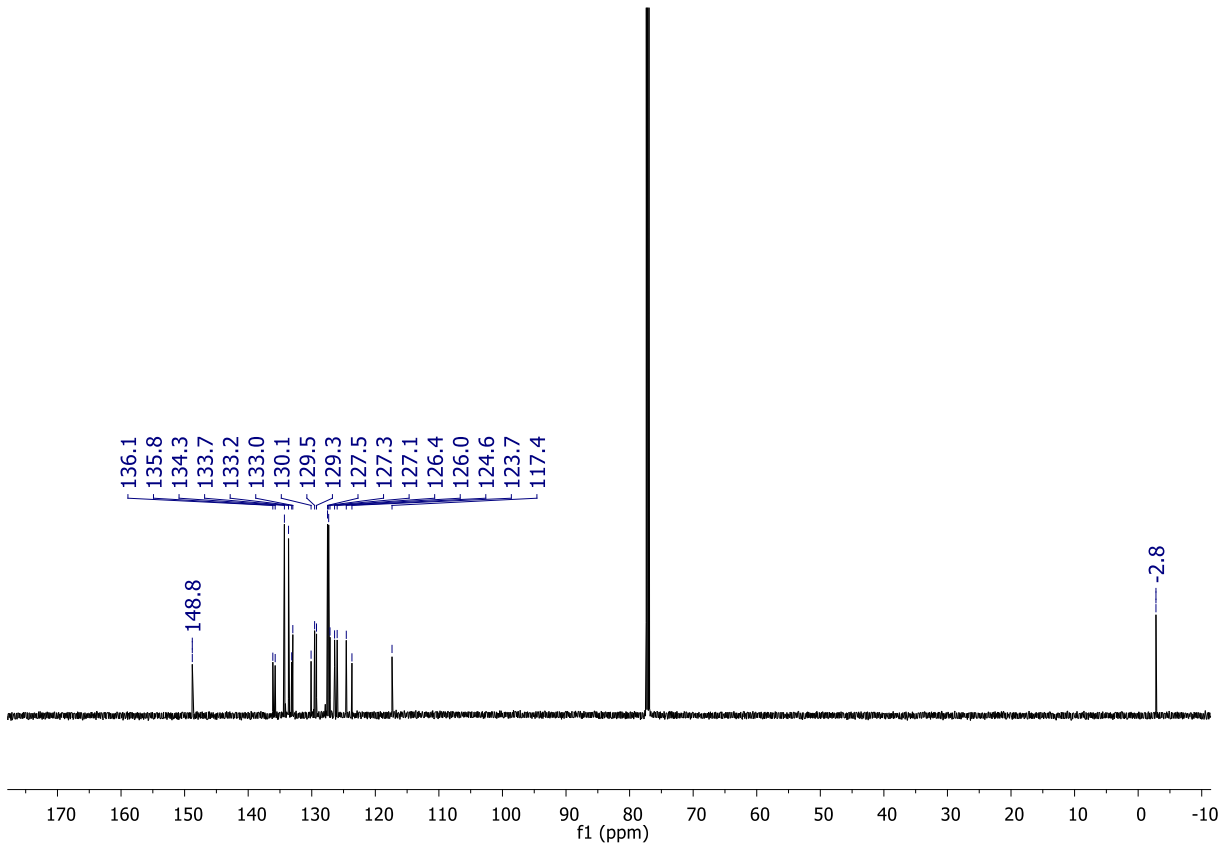
136.1
135.8
134.3
133.7
133.2
133.0
130.1
129.5
129.3
127.5
127.3
127.1
126.4
126.0
124.6
123.7
117.4
148.8
-2.8
170 160 150 140 130 120 110 100 90 80 70 60 50 40 30 20 10 0 -10
f1 (ppm)

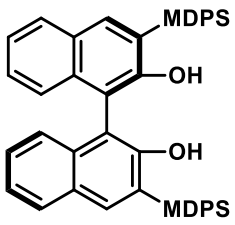
MDPS
OH
OH
MDPS

2.31

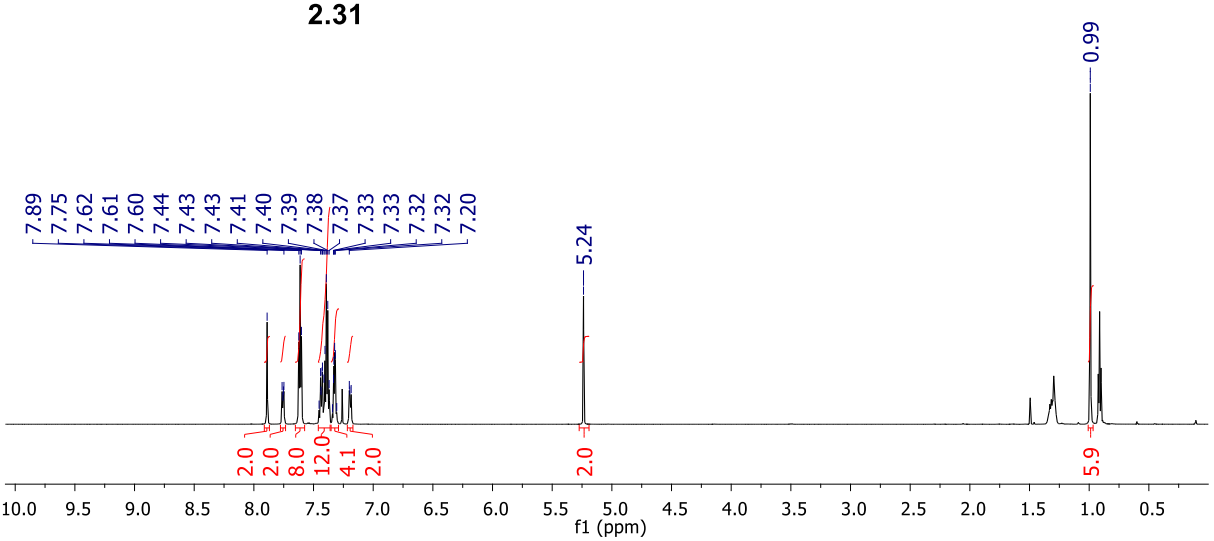
7.89
7.75
7.62
7.61
7.60
7.44
7.43
7.43
7.41
7.40
7.39
7.38
7.37
7.33
7.33
7.32
7.32
7.20
5.24
0.99
2.0
2.0
8.0
12.0
4.1
2.0
2.0
5.9
f1 (ppm)

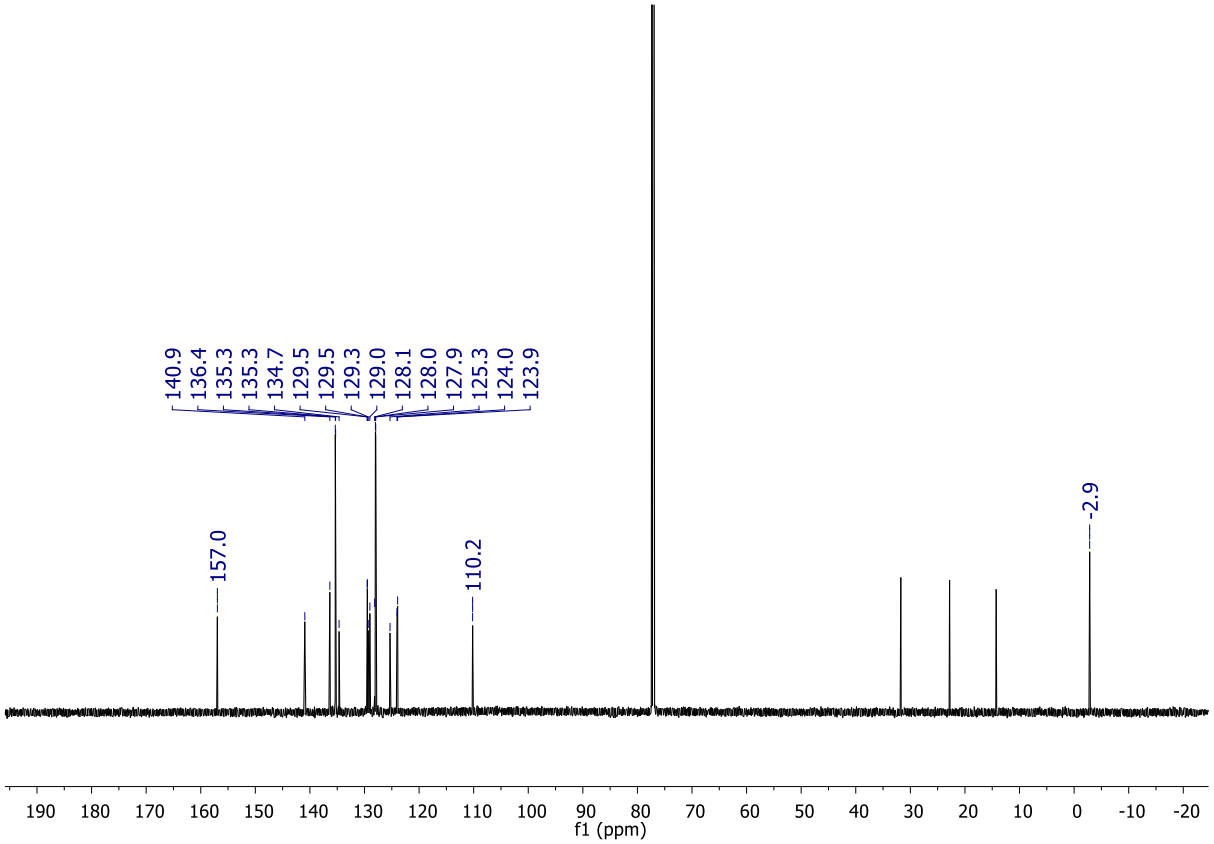
140.9
136.4
135.3
135.3
134.7
129.5
129.5
129.3
129.0
128.1
128.0
127.9
125.3
124.0
123.9
157.0
110.2
-2.9
f1 (ppm)

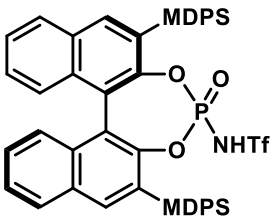
MDPS
O
O
P
O
NHTf
MDPS

*(R)-NTPA-***7**

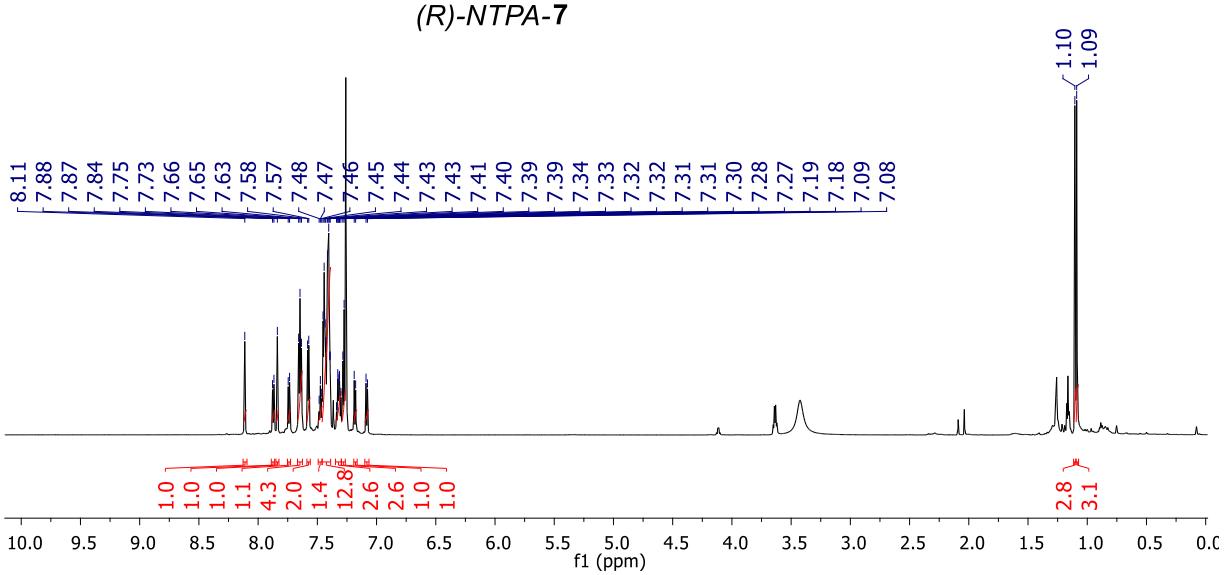
8.11
7.88
7.87
7.84
7.75
7.73
7.66
7.65
7.63
7.58
7.57
7.48
7.47
7.46
7.45
7.44
7.43
7.43
7.41
7.40
7.39
7.39
7.34
7.33
7.32
7.32
7.31
7.31
7.30
7.28
7.27
7.19
7.18
7.09
7.08
1.10
1.09
1.0
1.0
1.0
1.1
4.3
2.0
1.4
12.8
2.6
2.6
1.0
1.0
2.8
3.1
10.0
9.5
9.0
8.5
8.0
7.5
7.0
6.5
6.0
5.5
5.0
4.5
4.0
3.5
3.0
2.5
2.0
1.5
1.0
0.5
0.0
f1 (ppm)

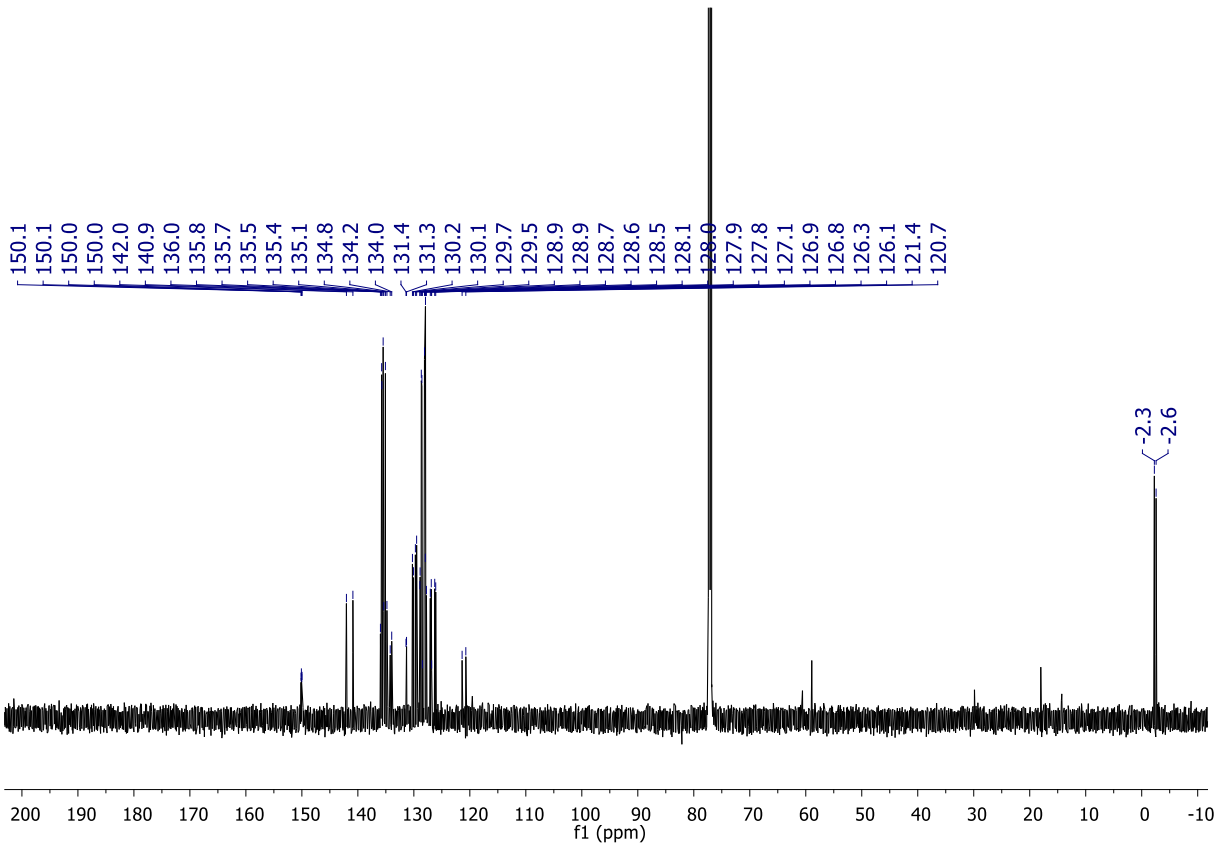
150.1
150.1
150.0
150.0
142.0
140.9
136.0
135.8
135.7
135.5
135.4
135.1
134.8
134.2
134.0
131.4
131.3
130.2
130.1
129.7
129.5
128.9
128.9
128.7
128.6
128.5
128.1
128.0
127.9
127.8
127.1
126.9
126.8
126.3
126.1
121.4
120.7
-2.3
-2.6
200
190
180
170
160
150
140
130
120
110
100
90
80
70
60
50
40
30
20
10
0
-10
f1 (ppm)

gc3-30

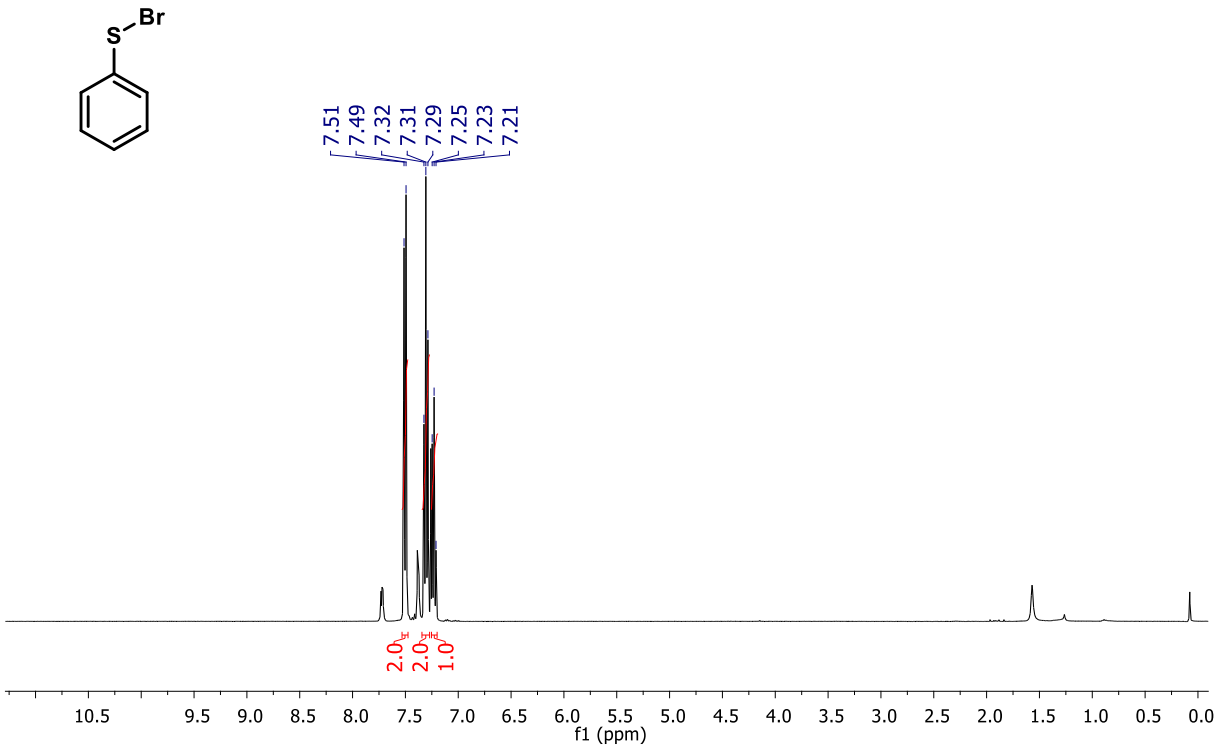

gc3-30
Standard 13C 400MHz BBFO "Smart" probe

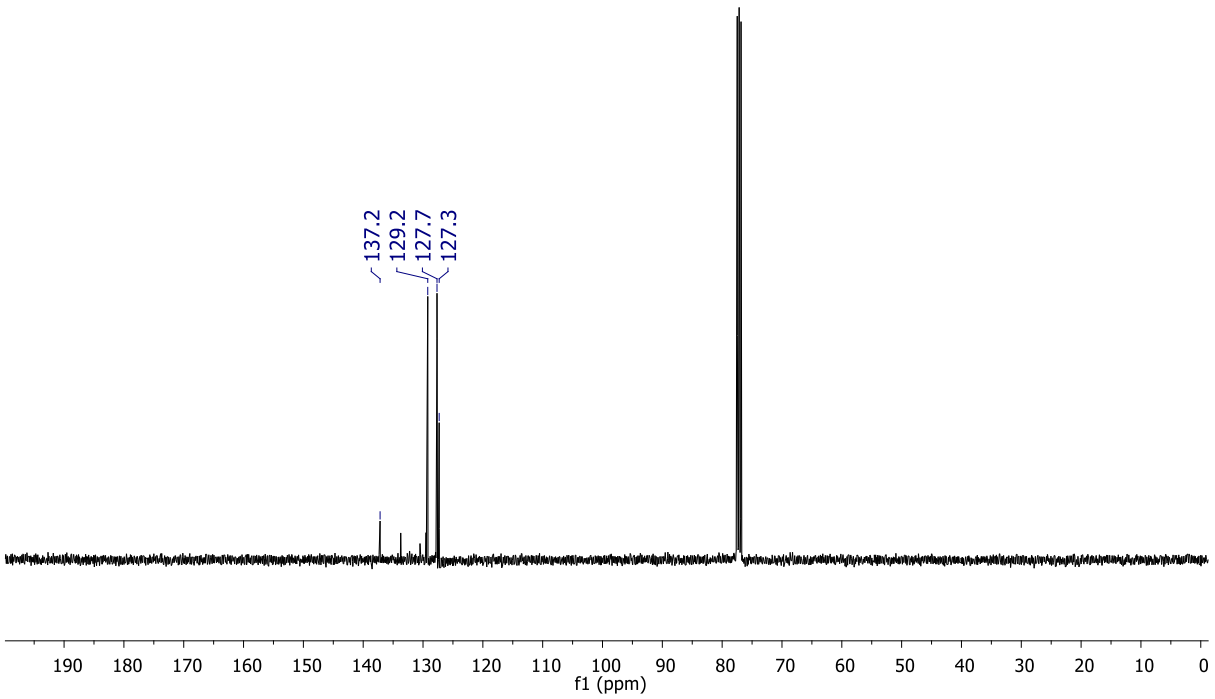

gc3-32

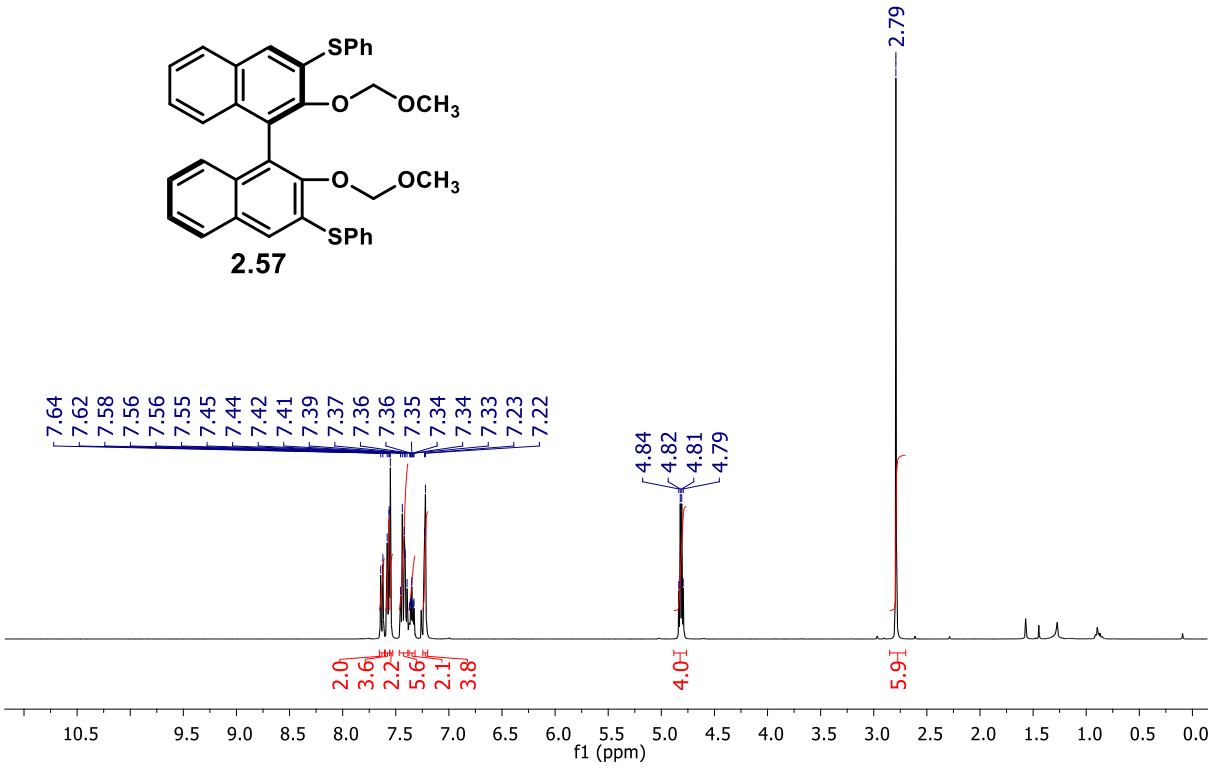

gc3-32
Standard 13C 400MHz BBFO "Smart" probe

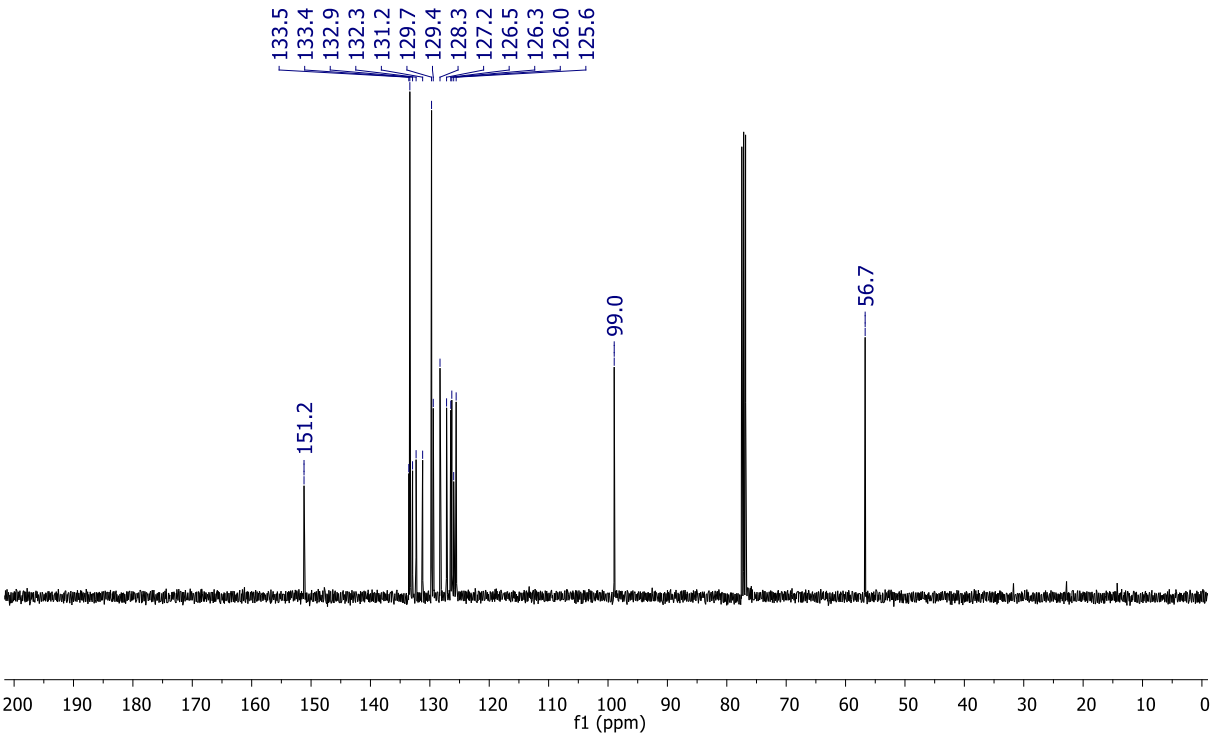

gc3-86crude
Standard 1H 400MHz BBFO "Smart" probe

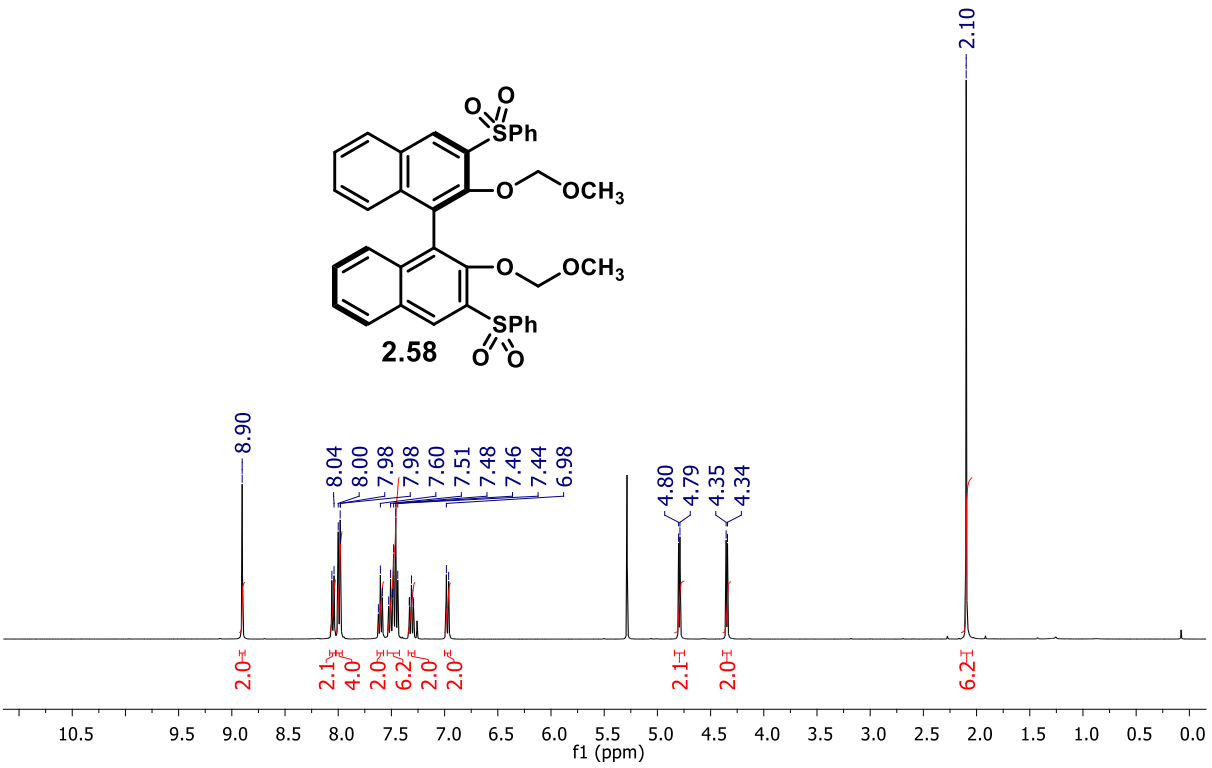

gc3-86crude
Standard 13C 400MHz BBFO "Smart" probe

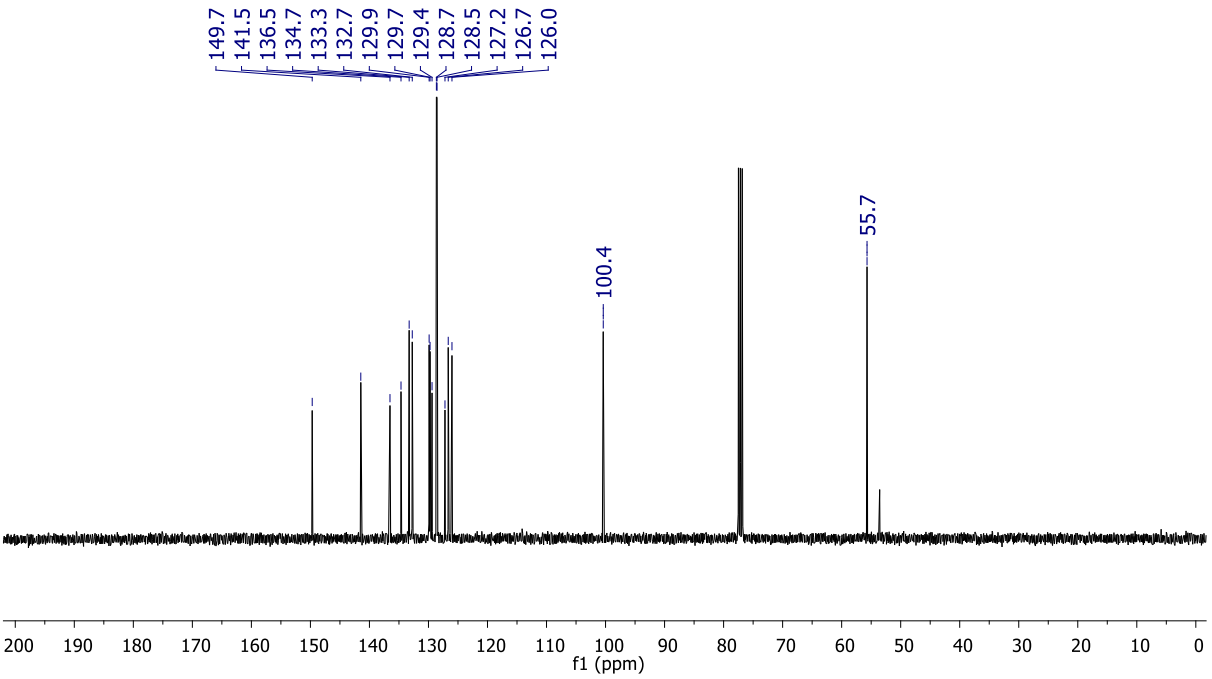

gc3-200
Standard 1H 400MHz BBFO "Smart" probe

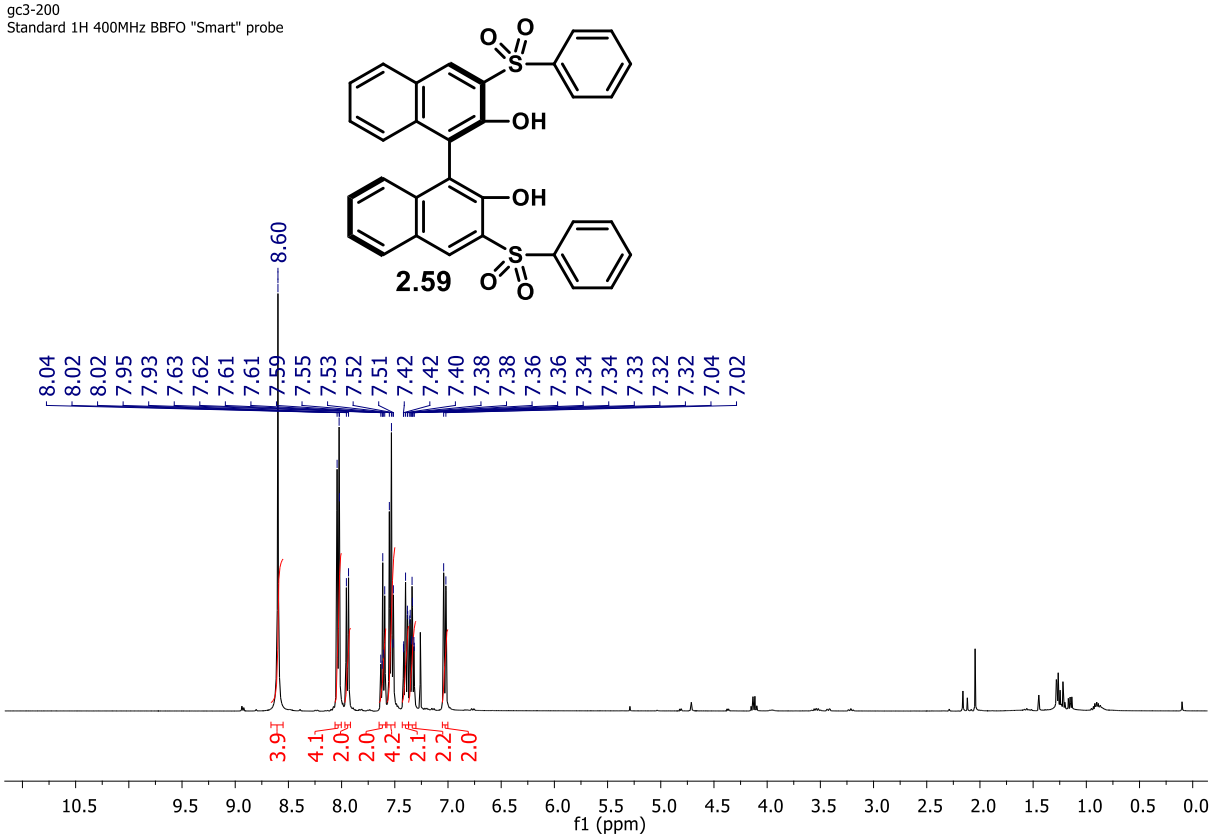

gc3-200
Standard 13C 400MHz BBFO "Smart" probe

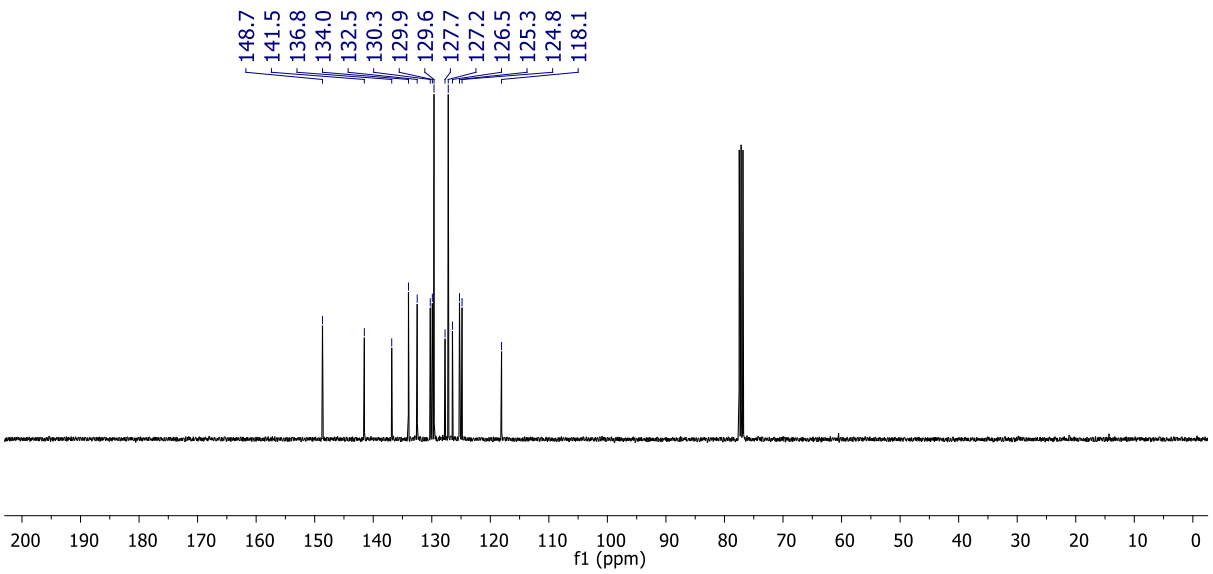

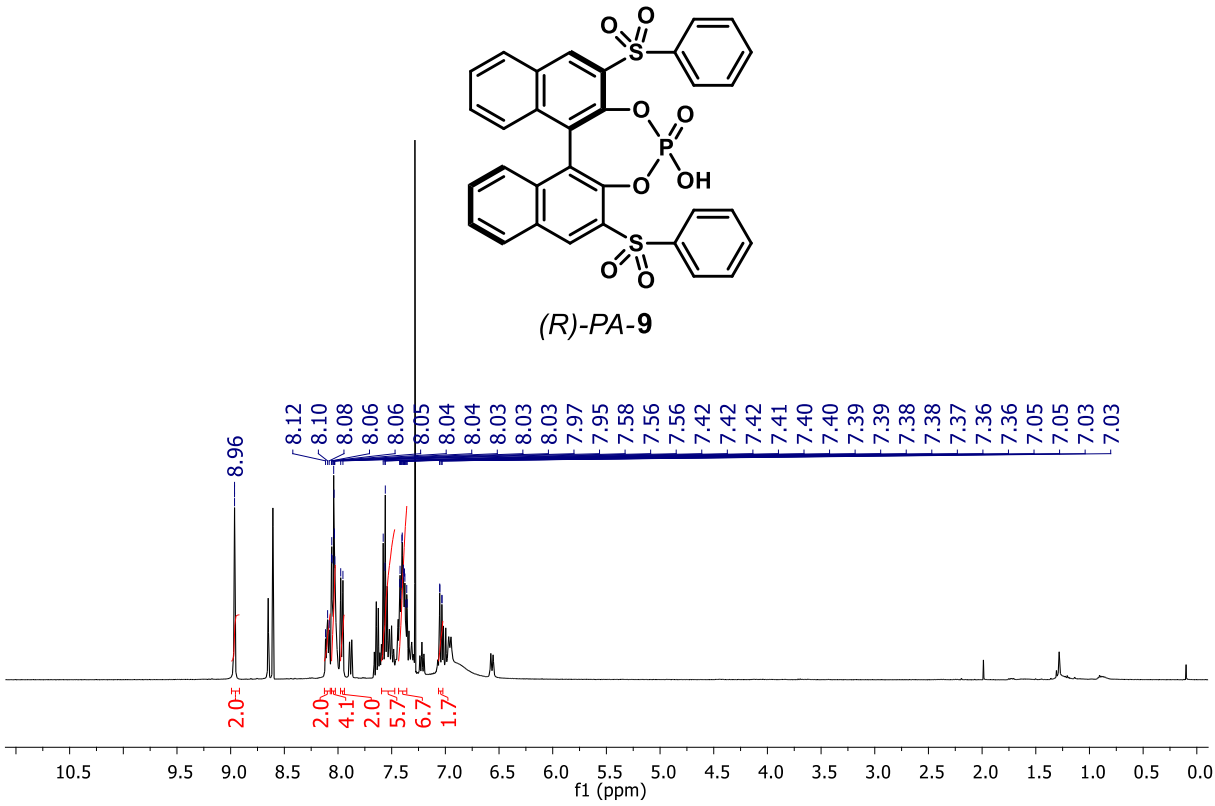
(R)-PA-9
8.96
8.12
8.10
8.08
8.06
8.06
8.05
8.04
8.04
8.03
8.03
8.03
7.97
7.95
7.58
7.56
7.56
7.42
7.42
7.42
7.41
7.40
7.40
7.39
7.39
7.38
7.38
7.37
7.36
7.36
7.05
7.05
7.03
7.03
2.0
2.0
4.1
2.0
5.7
6.7
1.7
f1 (ppm)

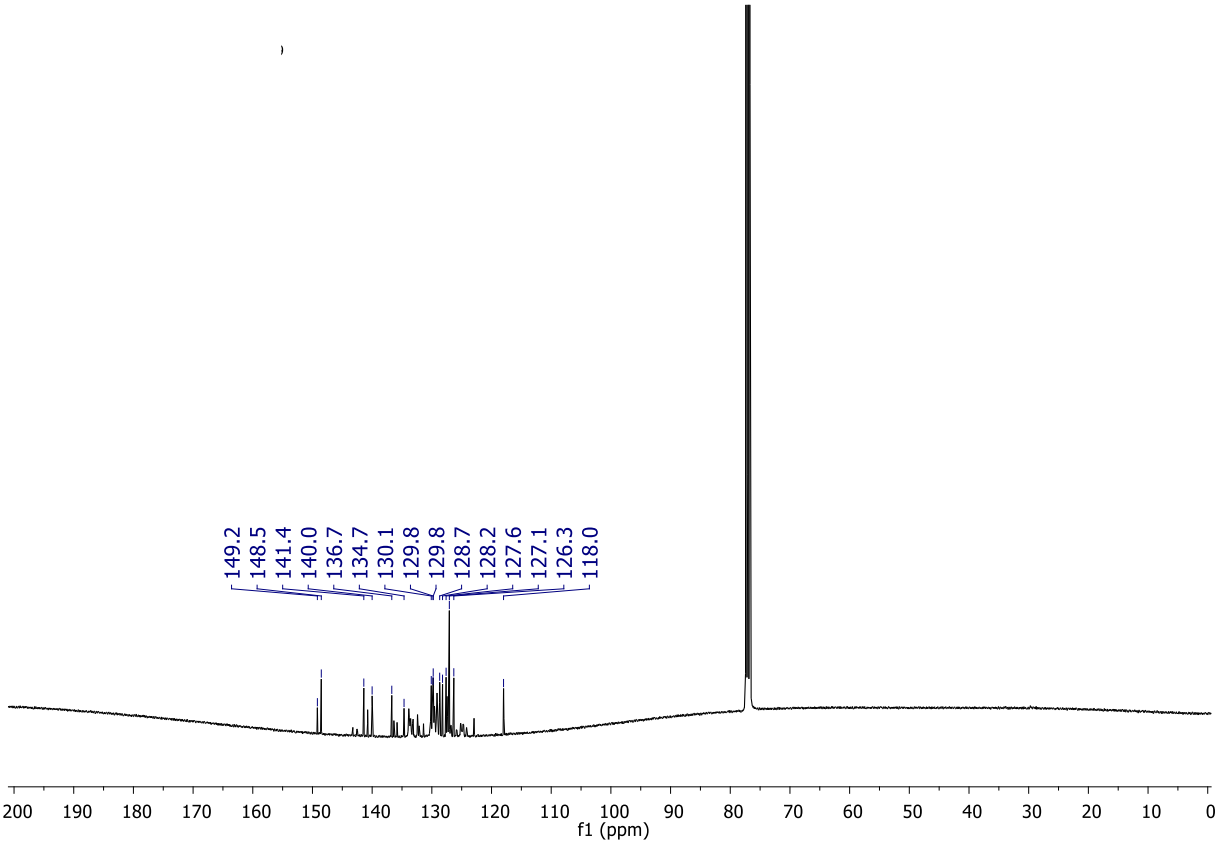
149.2
148.5
141.4
140.0
136.7
134.7
130.1
129.8
129.8
128.7
128.2
127.6
127.1
126.3
118.0
f1 (ppm)

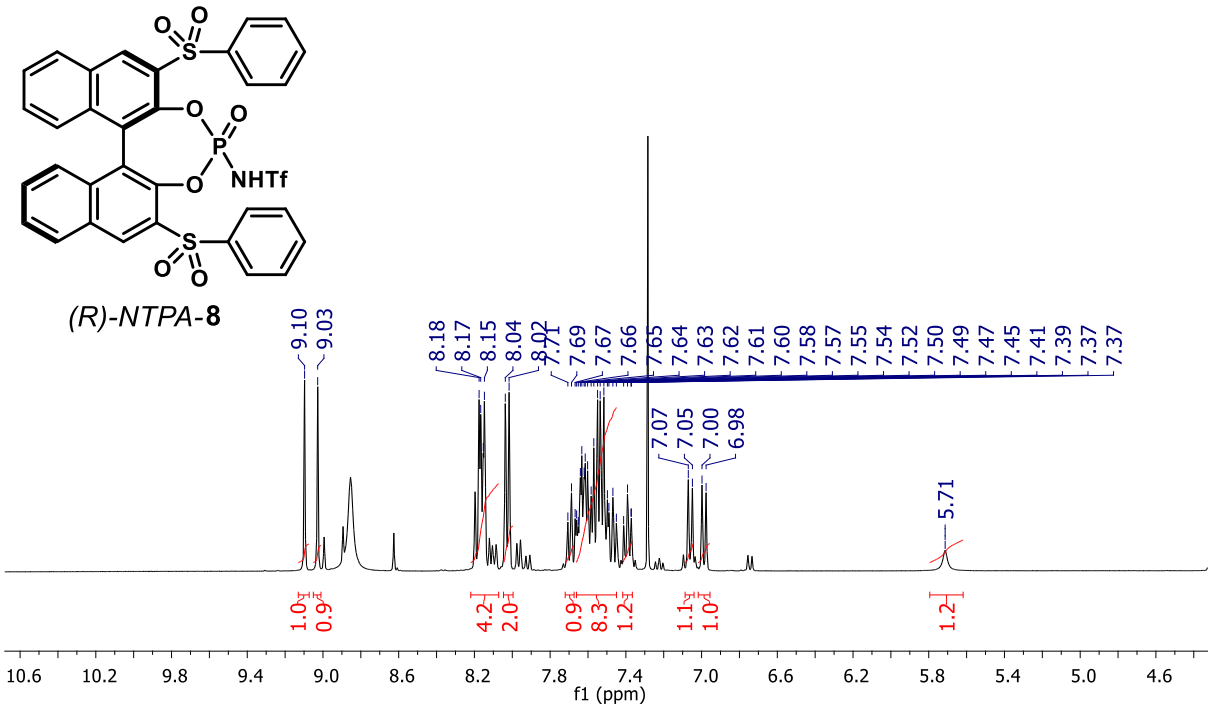
NHTf
(R)-NTPA-8
9.10
9.03
8.18
8.17
8.15
8.04
8.02
7.71
7.69
7.67
7.66
7.65
7.64
7.63
7.62
7.61
7.60
7.58
7.57
7.55
7.54
7.52
7.50
7.49
7.47
7.45
7.41
7.39
7.37
7.37
7.07
7.05
7.00
6.98
5.71
1.0
0.9
4.2
2.0
0.9
8.3
1.2
1.1
1.0
1.2
10.6
10.2
9.8
9.4
9.0
8.6
8.2
7.8
7.4
7.0
6.6
6.2
5.8
5.4
5.0
4.6
f1 (ppm)

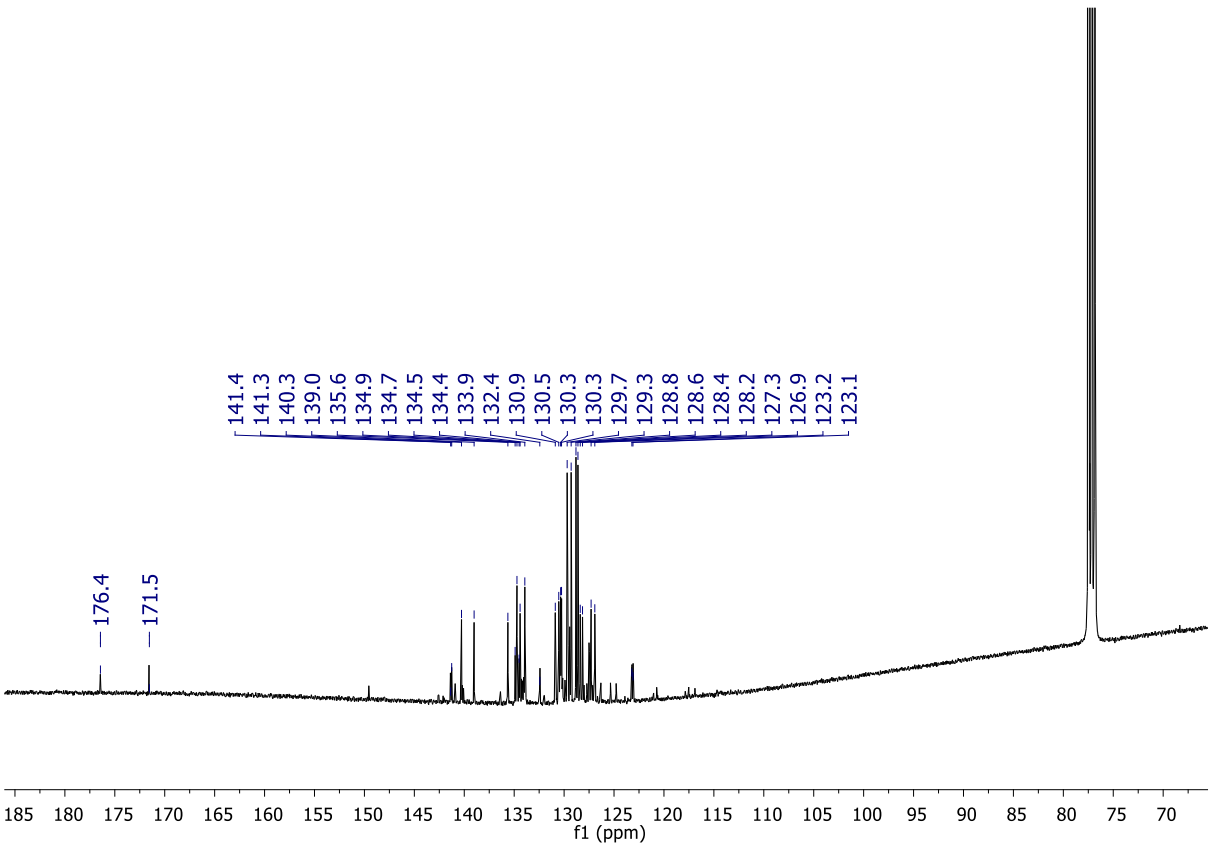
141.4
141.3
140.3
139.0
135.6
134.9
134.7
134.5
134.4
133.9
132.4
130.9
130.5
130.3
130.3
129.7
129.3
128.8
128.6
128.4
128.2
127.3
126.9
123.2
123.1
176.4
171.5
185
180
175
170
165
160
155
150
145
140
135
130
125
120
115
110
105
100
95
90
85
80
75
70
f1 (ppm)

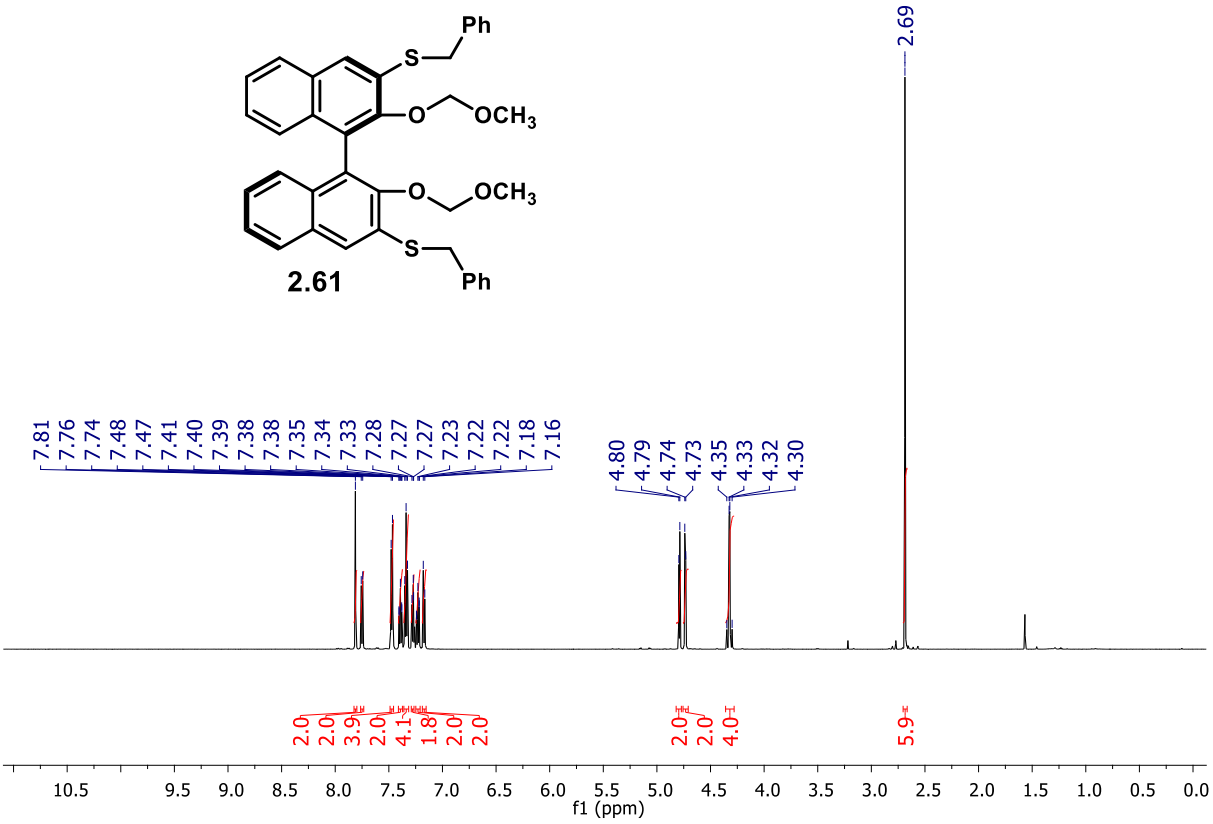
Ph
S
O
OCH3
O
OCH3
S
Ph
2.61
2.69
7.81
7.76
7.74
7.48
7.47
7.41
7.40
7.39
7.38
7.38
7.35
7.34
7.33
7.28
7.27
7.27
7.23
7.22
7.22
7.18
7.16
4.80
4.79
4.74
4.73
4.35
4.33
4.32
4.30
2.0
2.0
3.9
2.0
4.1
1.8
2.0
2.0
2.0
2.0
4.0
5.9
10.5
9.5
9.0
8.5
8.0
7.5
7.0
6.5
6.0
5.5
5.0
4.5
4.0
3.5
3.0
2.5
2.0
1.5
1.0
0.5
0.0
f1 (ppm)

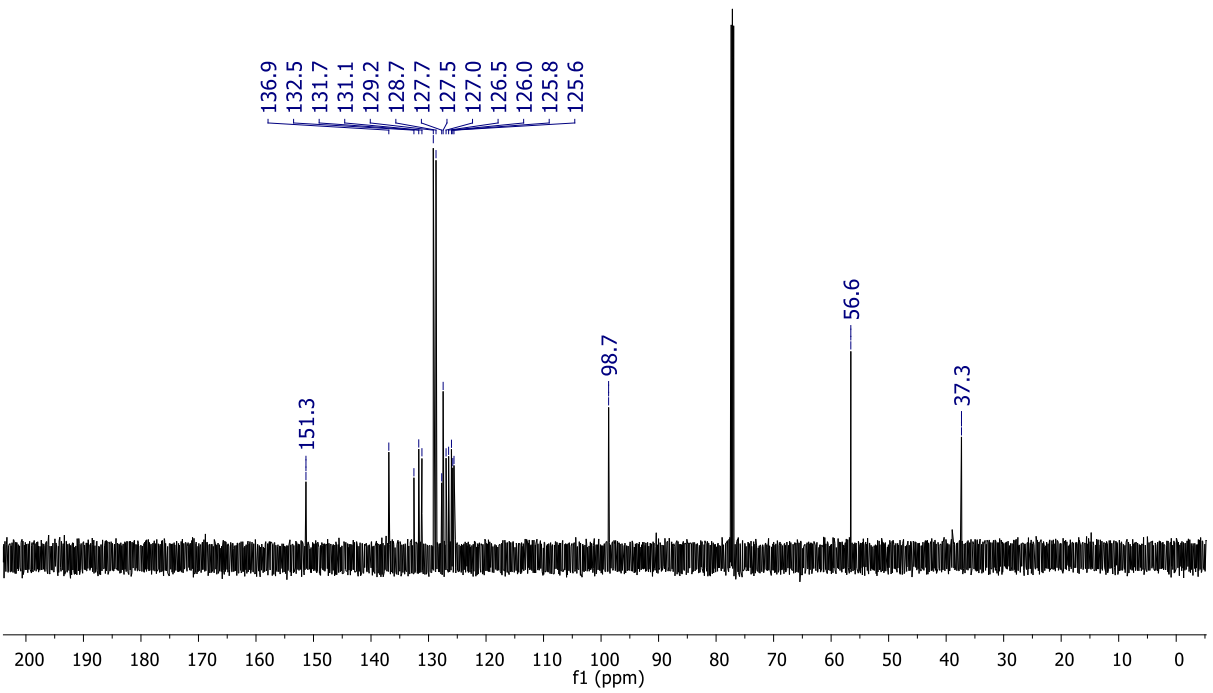
136.9
132.5
131.7
131.1
129.2
128.7
127.7
127.5
127.0
126.5
126.0
125.8
125.6
151.3
98.7
56.6
37.3
200
190
180
170
160
150
140
130
120
110
100
90
80
70
60
50
40
30
20
10
0
f1 (ppm)

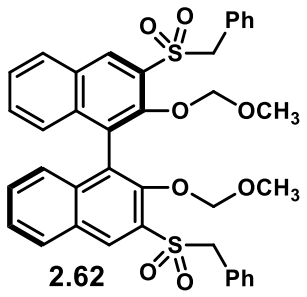
O
O
Ph
S
O
OCH3
O
OCH3
S
O
O
Ph

2.62

8.58
7.98
7.97
7.56
7.55
7.54
7.51
7.50
7.49
7.42
7.42
7.41
7.33
7.32
7.21
7.20
5.11
5.10
4.88
4.85
4.83
4.82
4.70
4.67
2.66
2.0
2.0
2.1
2.0
4.0
6.0
2.0
2.0
2.0
2.0
2.0
6.1
9.5
9.0
8.5
8.0
7.5
7.0
6.5
6.0
5.5
5.0
4.5
4.0
3.5
3.0
2.5
2.0
1.5
1.0
0.5
f1 (ppm)

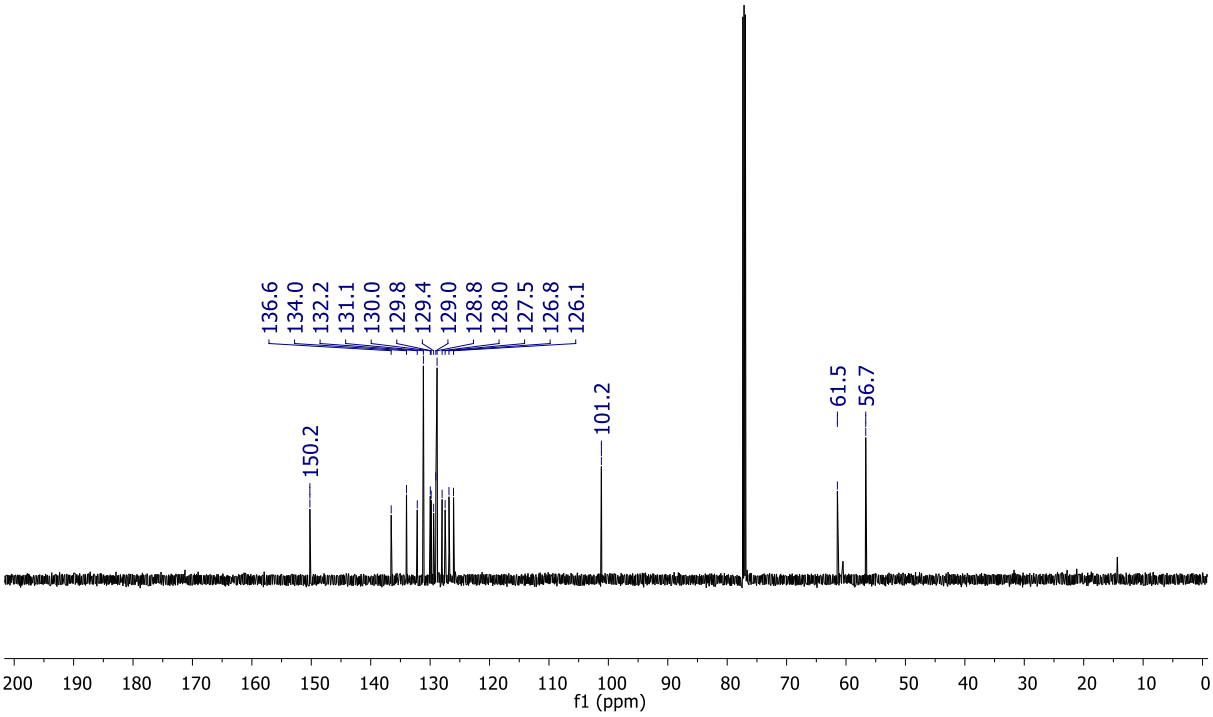
136.6
134.0
132.2
131.1
130.0
129.8
129.4
129.0
128.8
128.0
127.5
126.8
126.1
150.2
101.2
61.5
56.7
200
190
180
170
160
150
140
130
120
110
100
90
80
70
60
50
40
30
20
10
0
f1 (ppm)

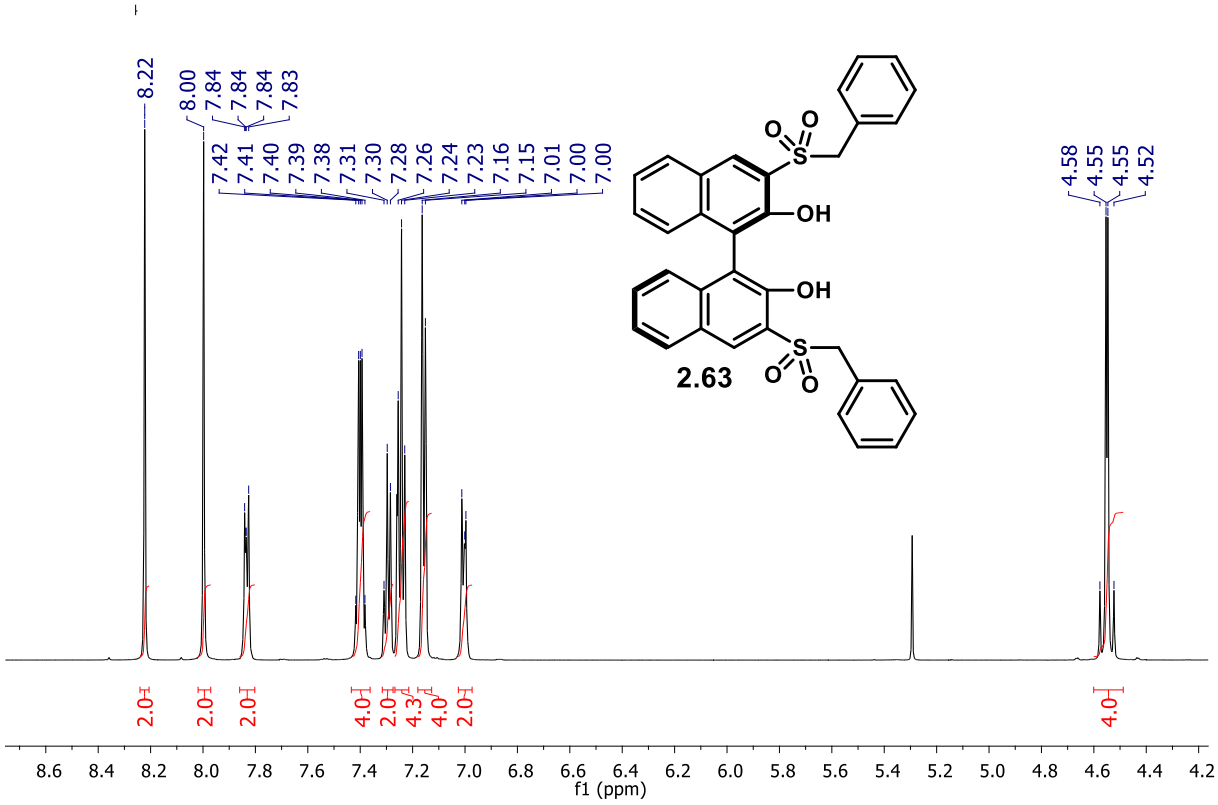
8.22
8.00
7.84
7.84
7.84
7.83
7.42
7.41
7.40
7.39
7.38
7.31
7.30
7.28
7.26
7.24
7.23
7.16
7.15
7.01
7.00
7.00
4.58
4.55
4.55
4.52
OH
OH
2.63
2.0
2.0
2.0
4.0
2.0
4.3
4.0
2.0
4.0
f1 (ppm)

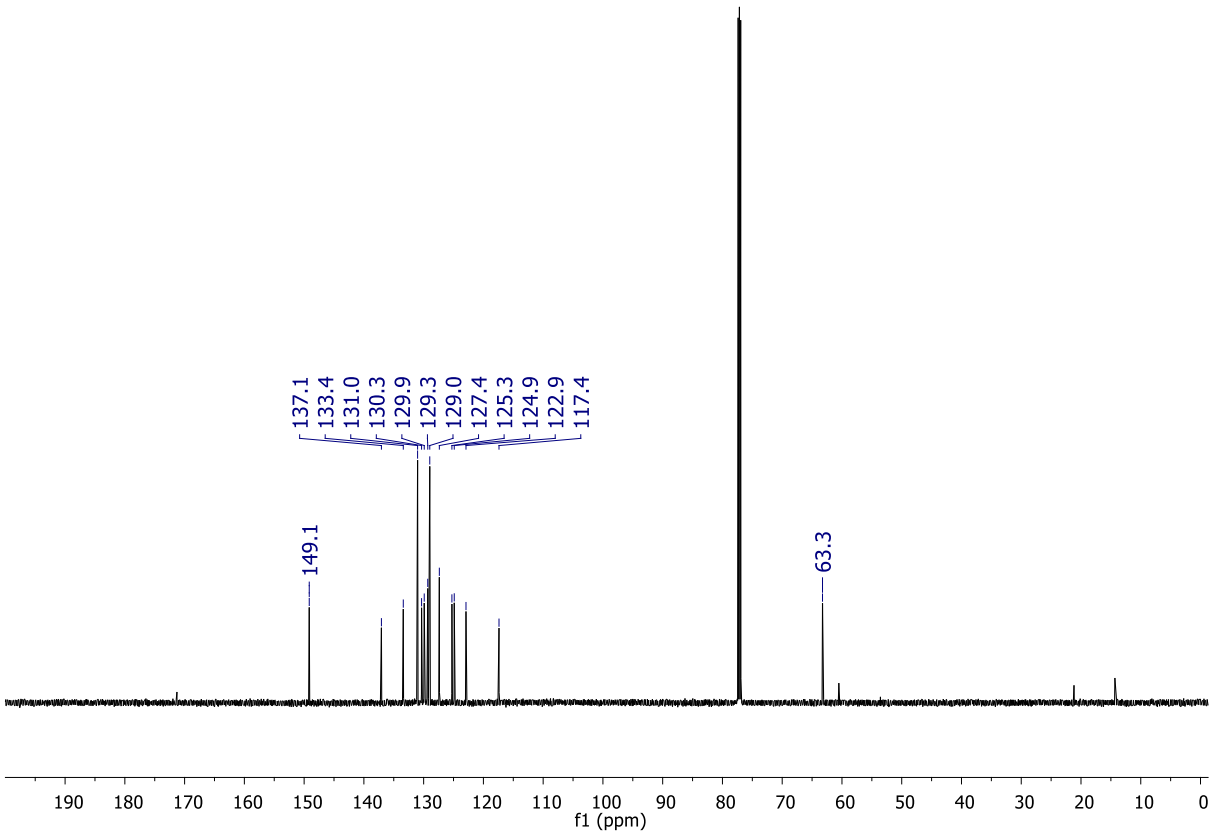
137.1
133.4
131.0
130.3
129.9
129.3
129.0
127.4
125.3
124.9
122.9
117.4
149.1
63.3
f1 (ppm)

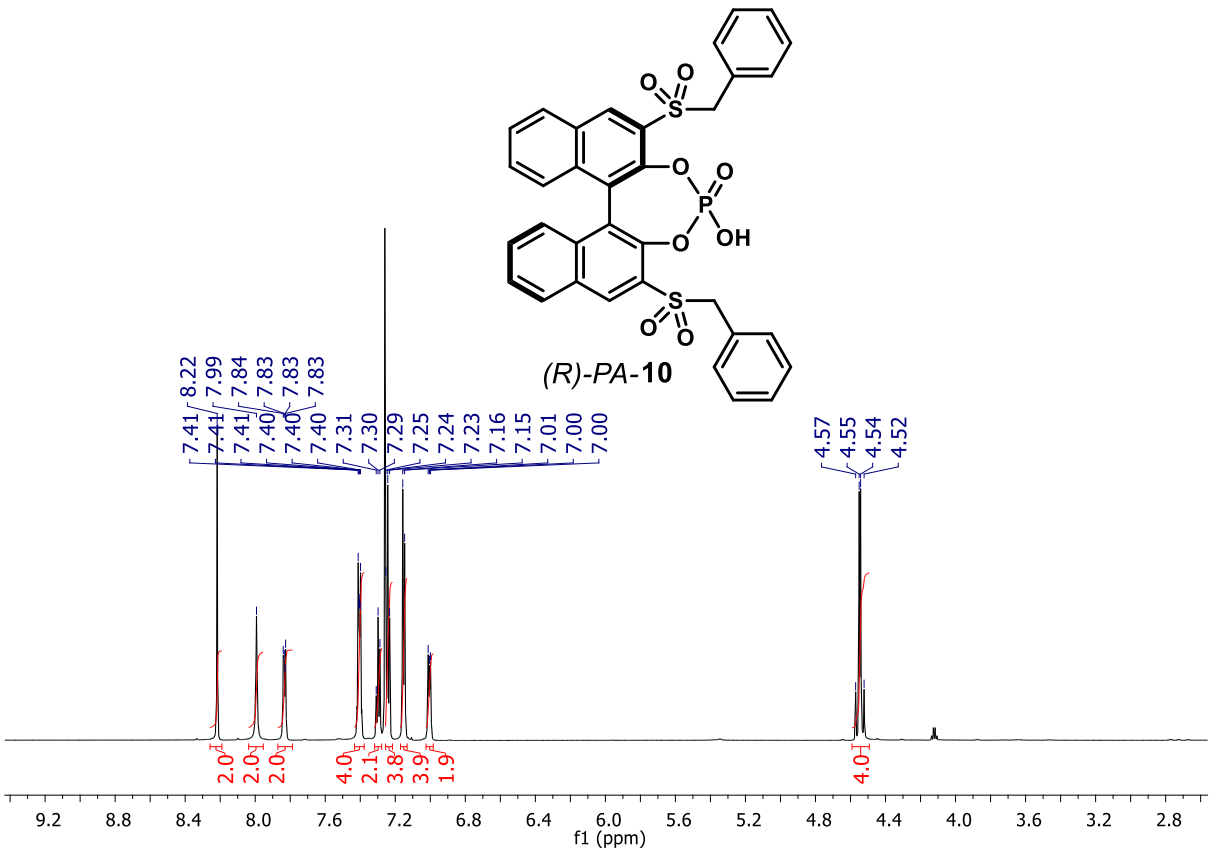
(R)-PA-10
8.22
7.99
7.84
7.83
7.83
7.83
7.41
7.41
7.41
7.40
7.40
7.40
7.31
7.30
7.29
7.25
7.24
7.23
7.16
7.15
7.01
7.00
7.00
4.57
4.55
4.54
4.52
2.0
2.0
2.0
4.0
2.1
3.8
3.9
1.9
4.0
f1 (ppm)

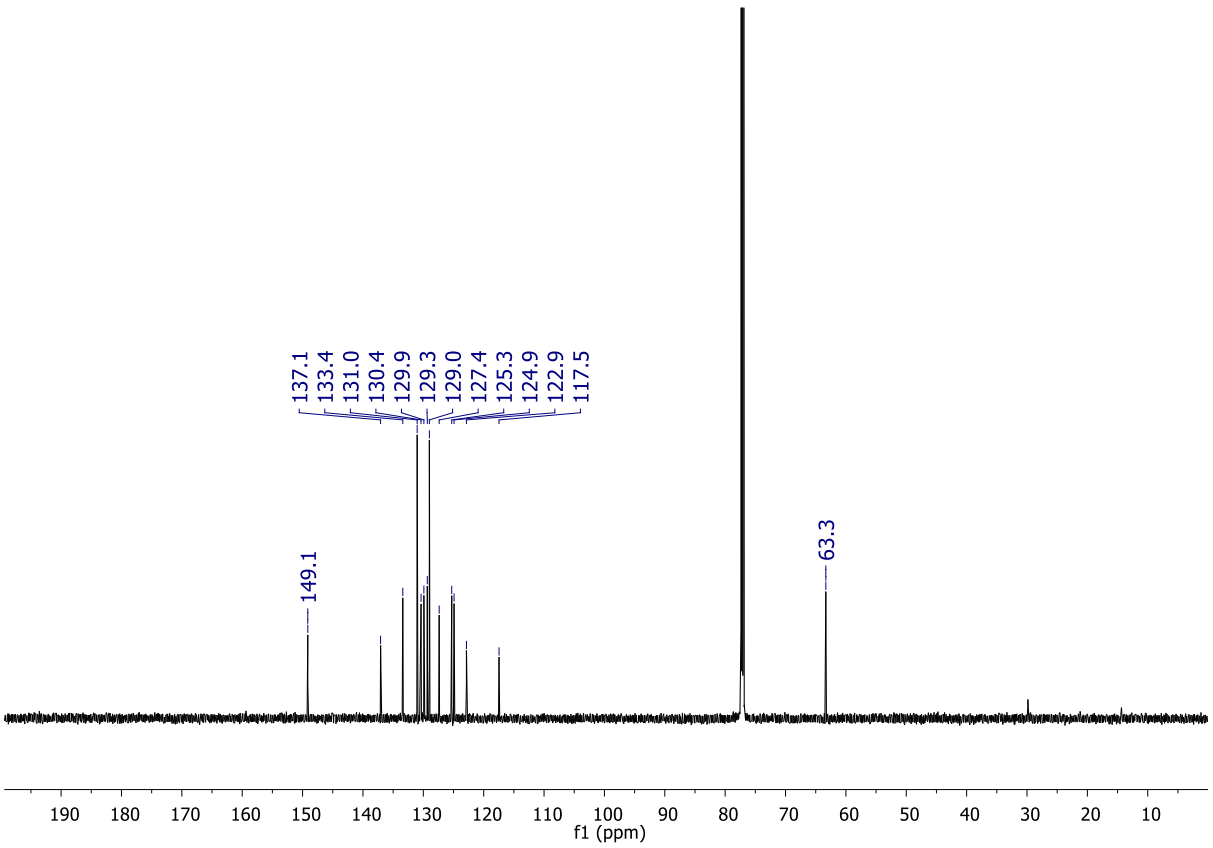
137.1
133.4
131.0
130.4
129.9
129.3
129.0
127.4
125.3
124.9
122.9
117.5
149.1
63.3
f1 (ppm)

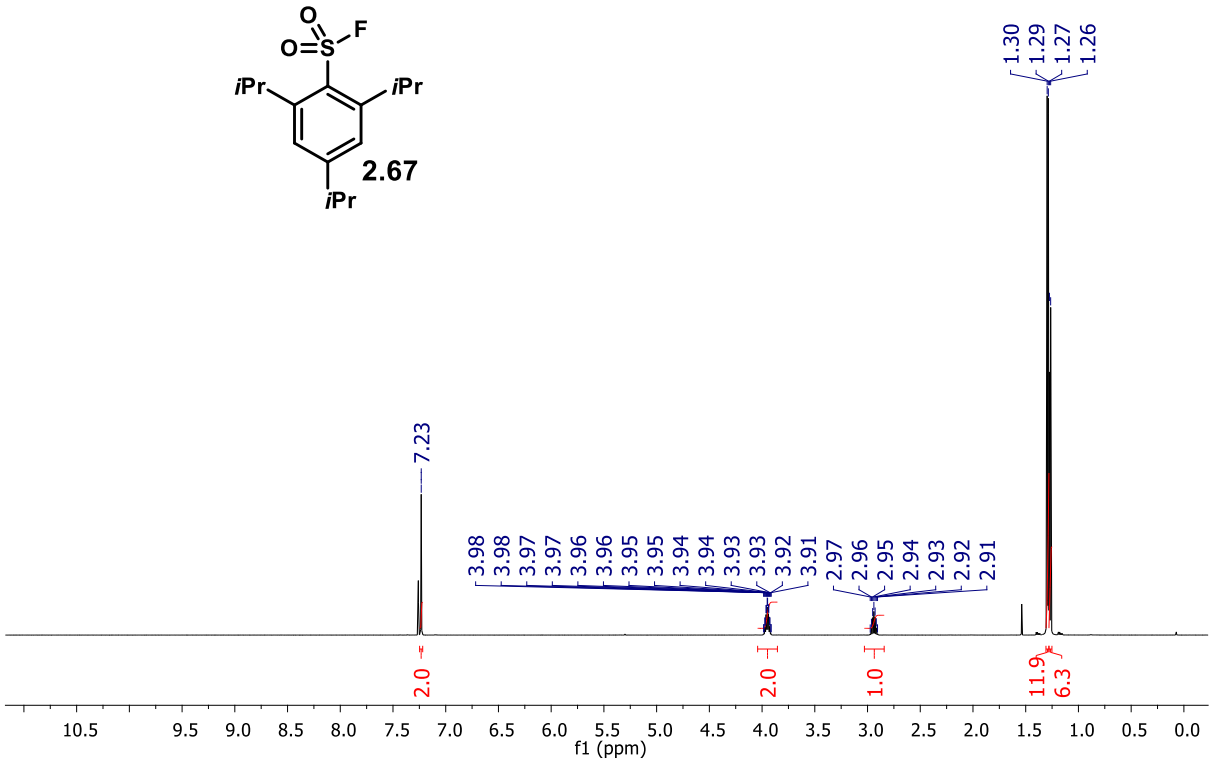
O
O=S
F
iPr
iPr
iPr
2.67
1.30
1.29
1.27
1.26
7.23
3.98
3.98
3.97
3.97
3.96
3.96
3.95
3.95
3.94
3.94
3.93
3.93
3.92
3.91
2.97
2.96
2.95
2.94
2.93
2.92
2.91
2.0
2.0
1.0
11.9
6.3
10.5
9.5
9.0
8.5
8.0
7.5
7.0
6.5
6.0
5.5
5.0
4.5
4.0
3.5
3.0
2.5
2.0
1.5
1.0
0.5
0.0
f1 (ppm)

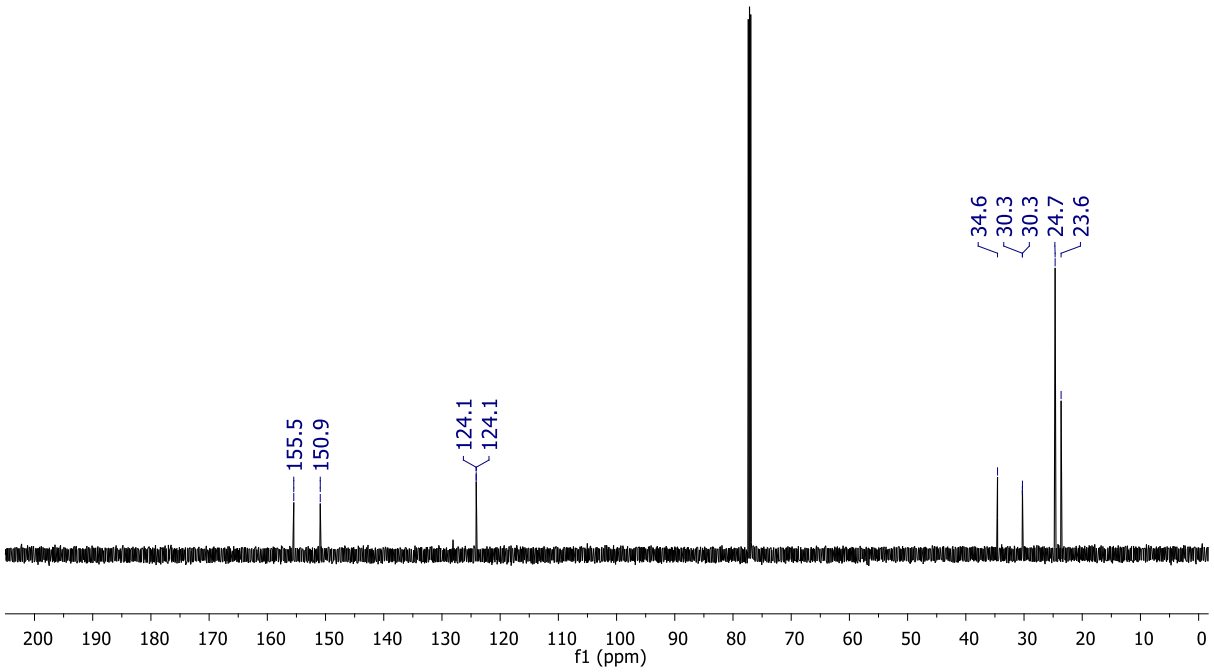
34.6
30.3
30.3
24.7
23.6
155.5
150.9
124.1
124.1
200
190
180
170
160
150
140
130
120
110
100
90
80
70
60
50
40
30
20
10
0
f1 (ppm)

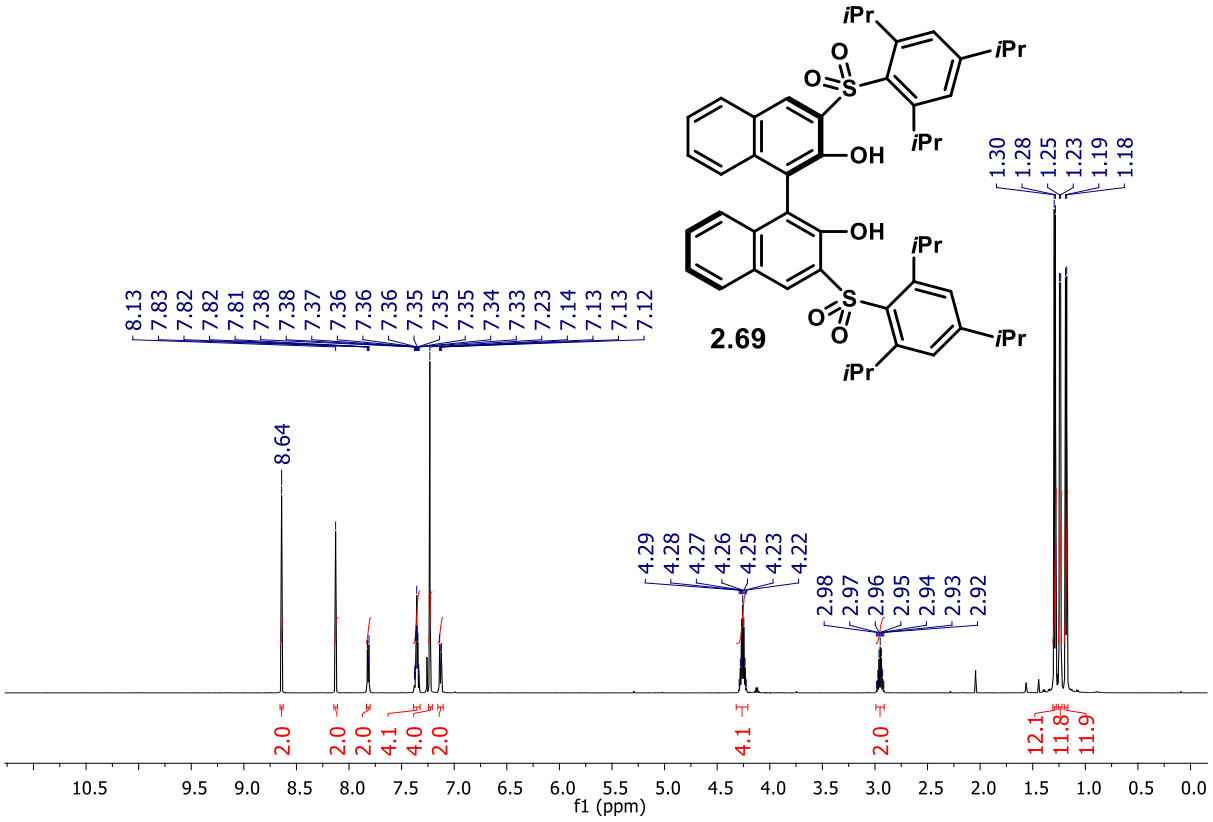
iPr
iPr
iPr
O
O
S
OH
OH
iPr
iPr
S
O
O
iPr
iPr
2.69
8.13
7.83
7.82
7.82
7.81
7.38
7.38
7.37
7.36
7.36
7.36
7.35
7.35
7.35
7.34
7.33
7.23
7.14
7.13
7.13
7.12
8.64
4.29
4.28
4.27
4.26
4.25
4.23
4.22
2.98
2.97
2.96
2.95
2.94
2.93
2.92
1.30
1.28
1.25
1.23
1.19
1.18
2.0
2.0
2.0
4.1
4.0
2.0
4.1
2.0
12.1
11.8
11.9
10.5
9.5
9.0
8.5
8.0
7.5
7.0
6.5
6.0
5.5
5.0
4.5
4.0
3.5
3.0
2.5
2.0
1.5
1.0
0.5
0.0
f1 (ppm)

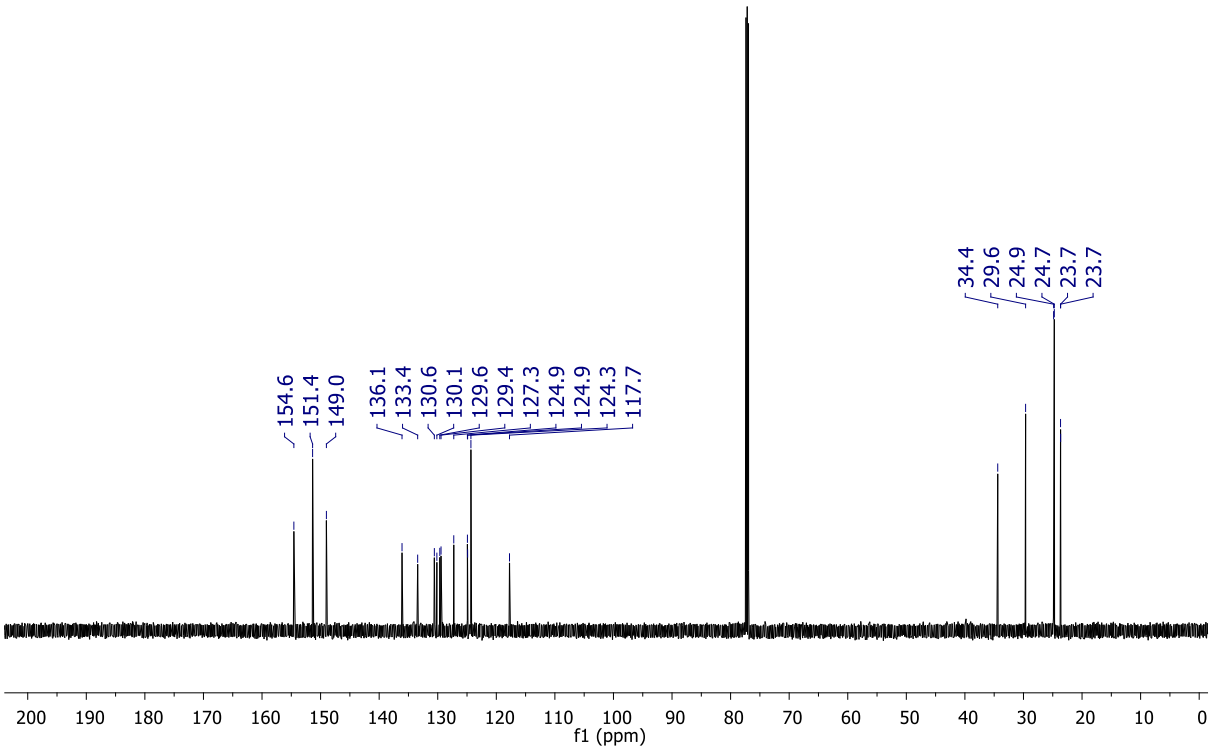
154.6
151.4
149.0
136.1
133.4
130.6
130.1
129.6
129.4
127.3
124.9
124.9
124.3
117.7
34.4
29.6
24.9
24.7
23.7
23.7
200
190
180
170
160
150
140
130
120
110
100
90
80
70
60
50
40
30
20
10
0
f1 (ppm)

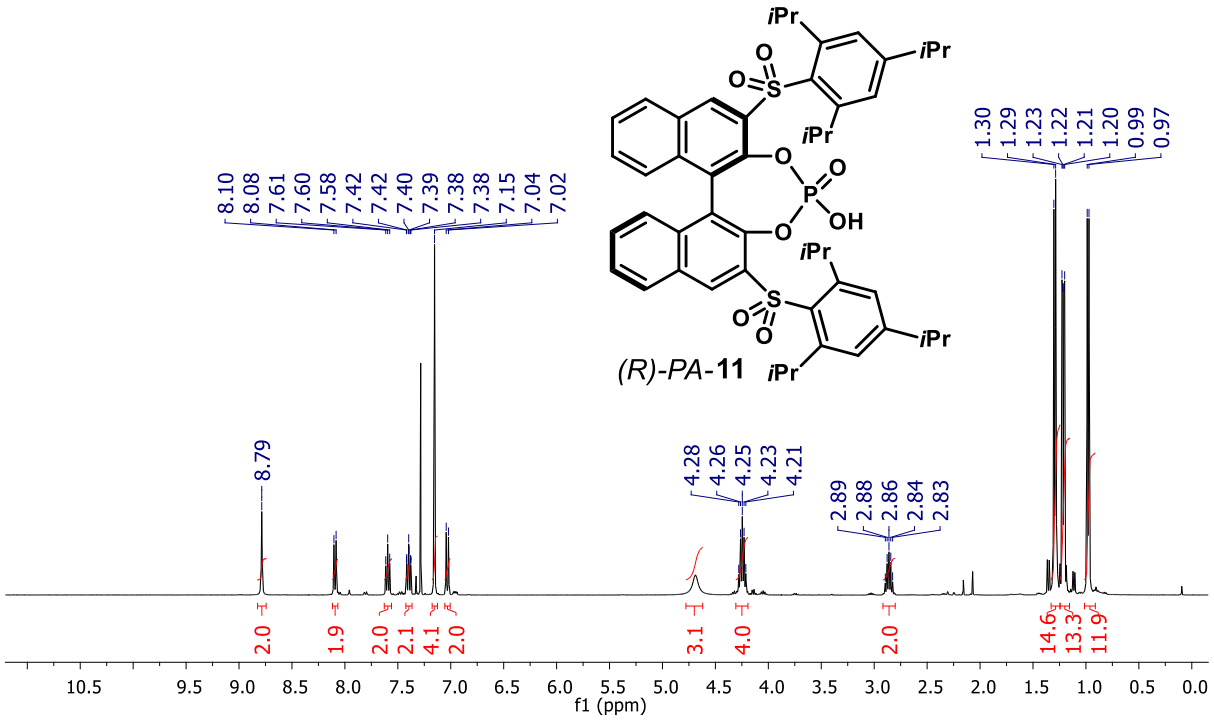
iPr
iPr
iPr
iPr
iPr
iPr
O
O
S
O
P
OH
O
O
S
O
O
(R)-PA-11
8.10
8.08
7.61
7.60
7.58
7.42
7.42
7.40
7.39
7.38
7.38
7.15
7.04
7.02
8.79
4.28
4.26
4.25
4.23
4.21
2.89
2.88
2.86
2.84
2.83
1.30
1.29
1.23
1.22
1.21
1.20
0.99
0.97
2.0
1.9
2.0
2.1
4.1
2.0
3.1
4.0
2.0
14.6
13.3
11.9
10.5
9.5
9.0
8.5
8.0
7.5
7.0
6.5
6.0
5.5
5.0
4.5
4.0
3.5
3.0
2.5
2.0
1.5
1.0
0.5
0.0
f1 (ppm)

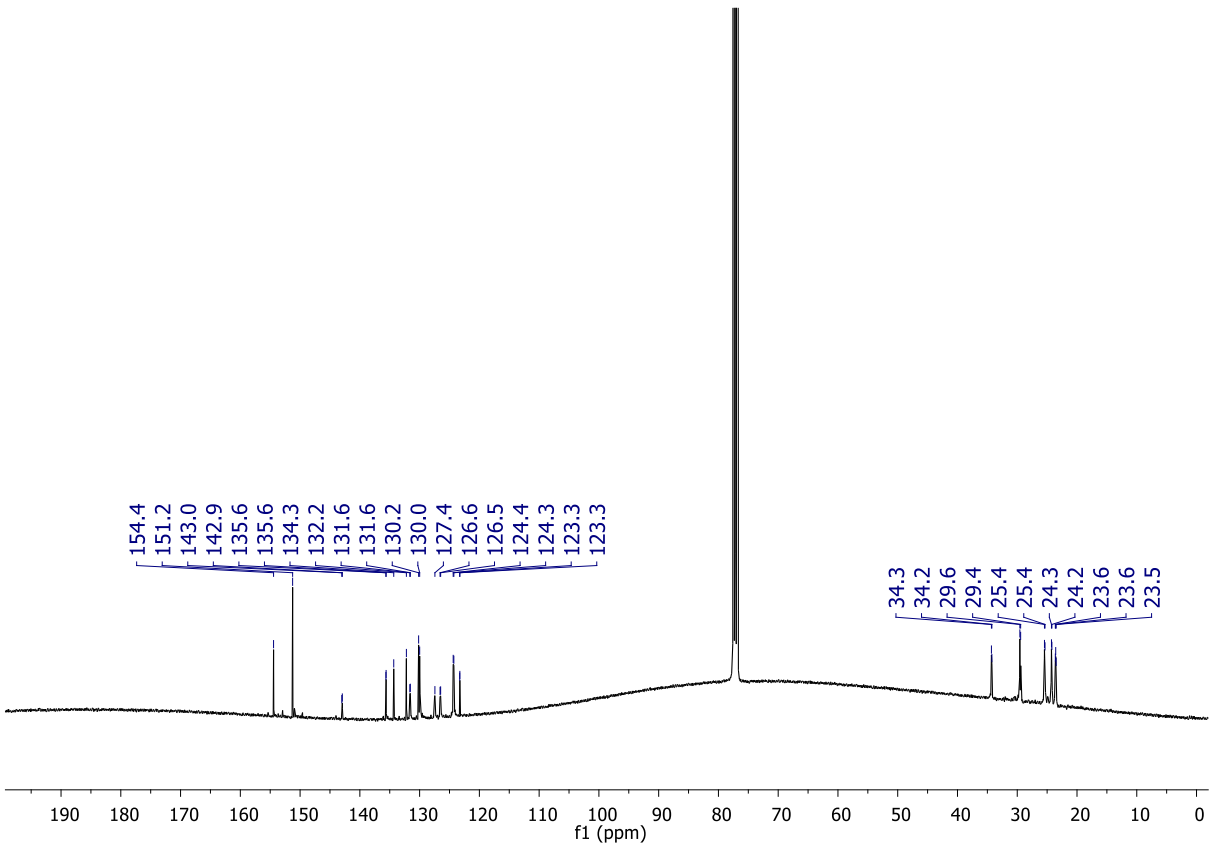
154.4
151.2
143.0
142.9
135.6
135.6
134.3
132.2
131.6
131.6
130.2
130.0
127.4
126.6
126.5
124.4
124.3
123.3
123.3
34.3
34.2
29.6
29.4
25.4
25.4
24.3
24.2
23.6
23.6
23.5
190
180
170
160
150
140
130
120
110
100
90
80
70
60
50
40
30
20
10
0
f1 (ppm)

gc3-84
Standard 1H 400MHz BBFO "Smart" probe

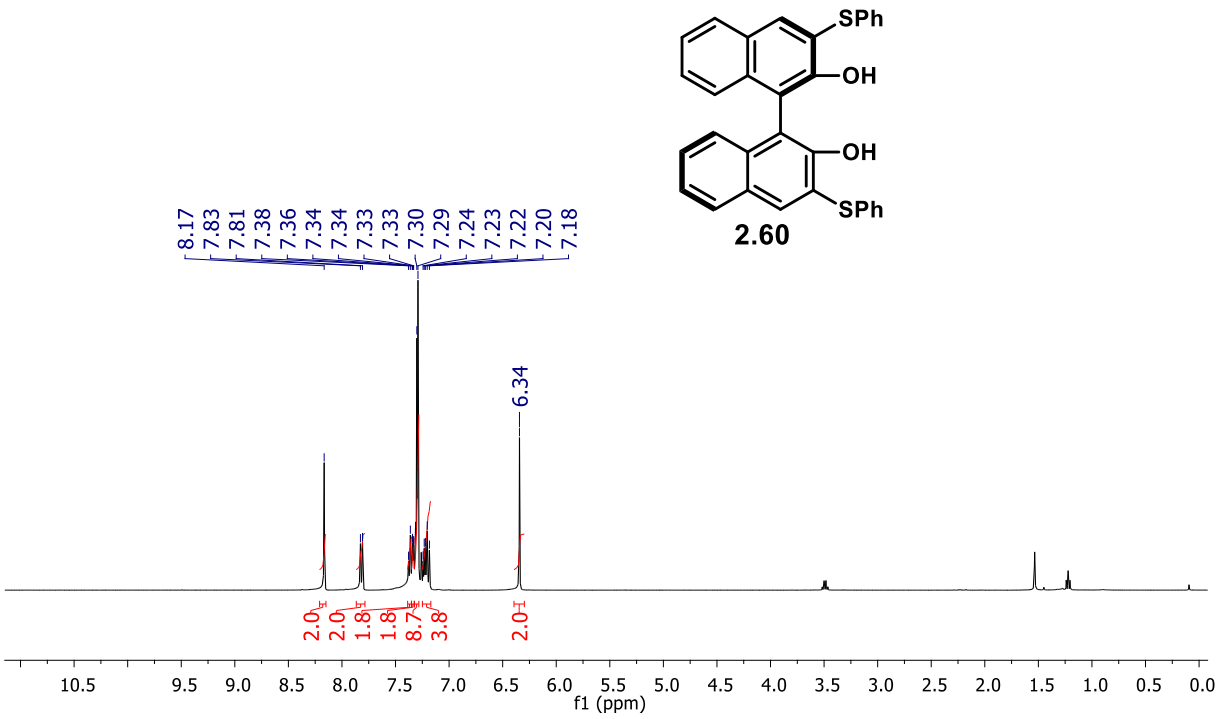

gc3-84

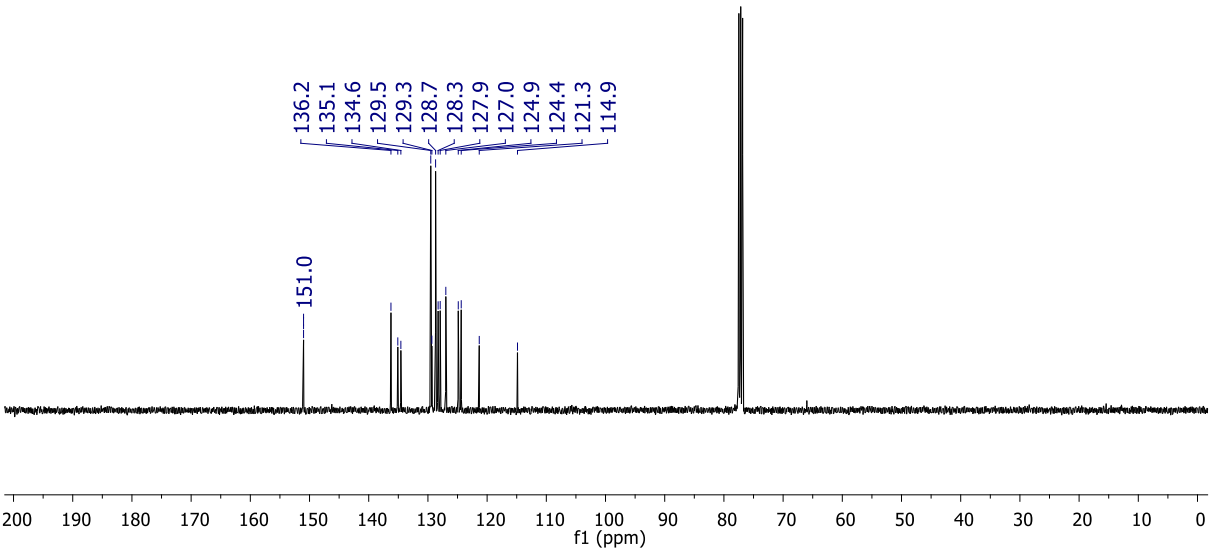

141-gc1-54
Standard 1H 400MHz BBFO "Smart" probe

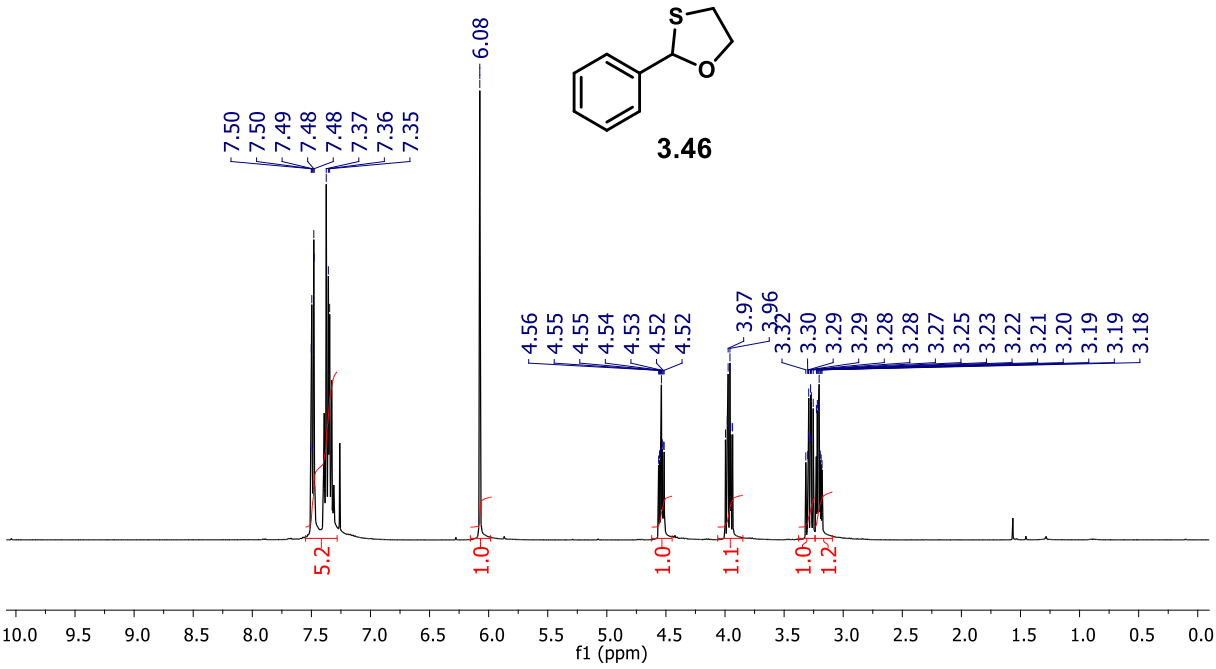

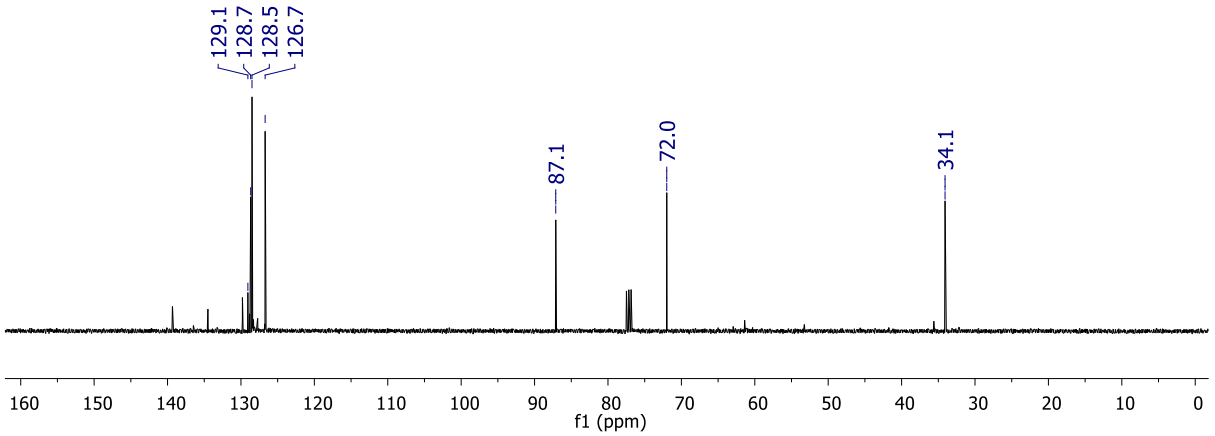

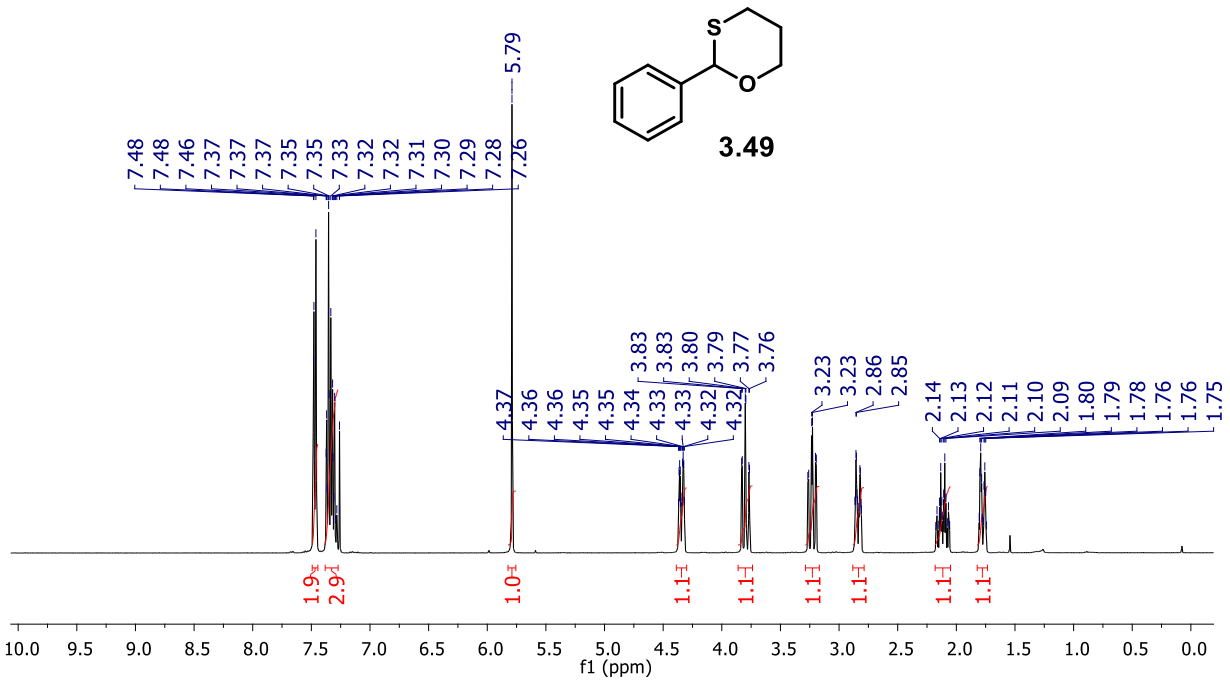
S
O
3.49
7.48 7.48 7.46 7.37 7.37 7.37 7.35 7.35 7.33 7.32 7.32 7.31 7.30 7.29 7.28 7.26
5.79
4.37 4.36 4.36 4.35 4.35 4.34 4.33 4.33 4.32 4.32
3.83 3.83 3.80 3.79 3.77 3.76
3.23 3.23 2.86 2.85
2.14 2.13 2.12 2.11 2.10 2.09 1.80 1.79 1.78 1.76 1.76 1.75
1.9 2.9 1.0 1.1 1.1 1.1 1.1 1.1 1.1
10.0 9.5 9.0 8.5 8.0 7.5 7.0 6.5 6.0 5.5 5.0 4.5 4.0 3.5 3.0 2.5 2.0 1.5 1.0 0.5 0.0
f1 (ppm)

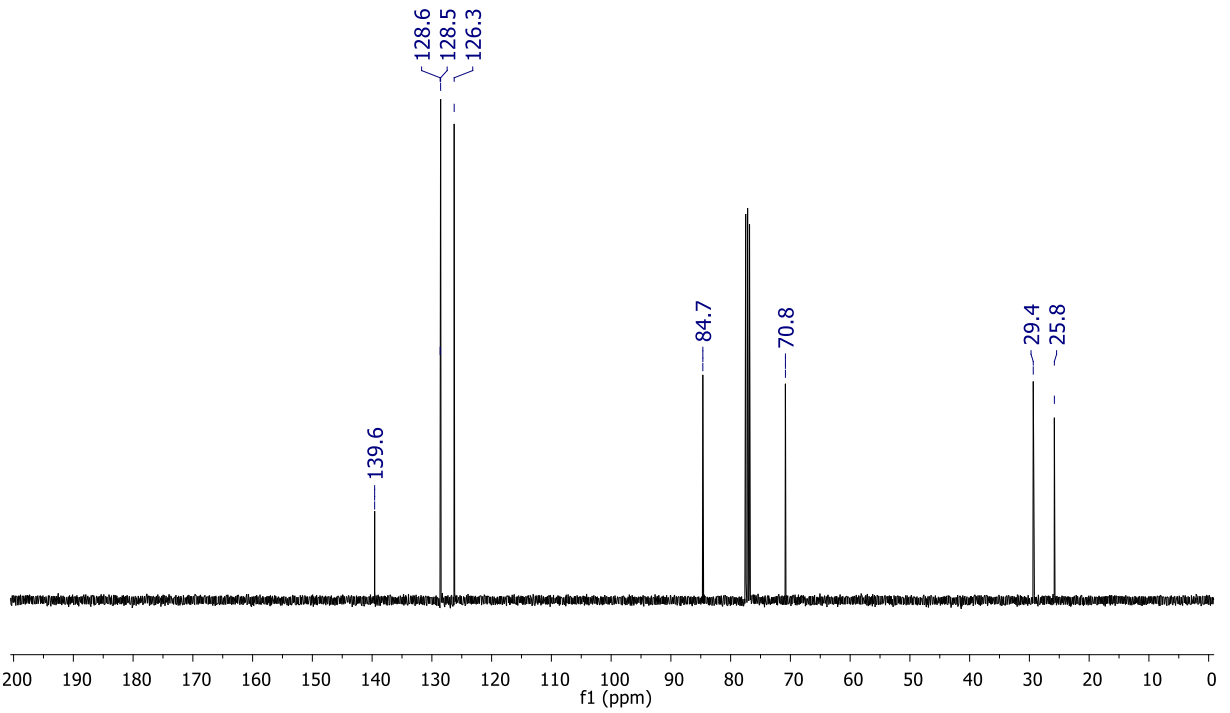
128.6
128.5
126.3
139.6
84.7
70.8
29.4
25.8
200 190 180 170 160 150 140 130 120 110 100 90 80 70 60 50 40 30 20 10 0
f1 (ppm)

gc3-162
Standard 1H 400MHz BBFO "Smart" probe

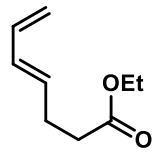

4.52

gc3-162
Standard 13C 400MHz BBFO "Smart" probe

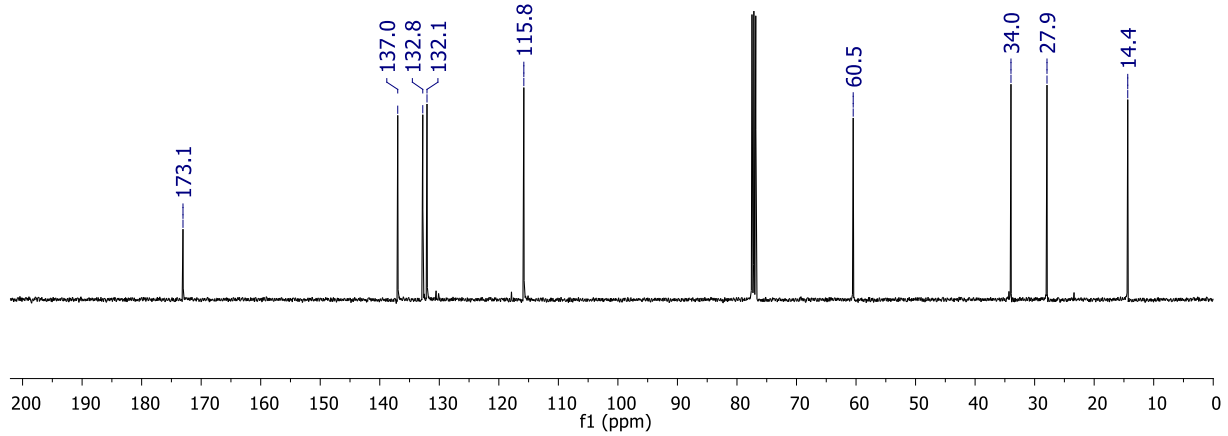

gc3-56

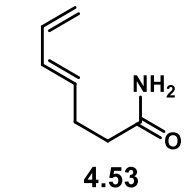

4.53

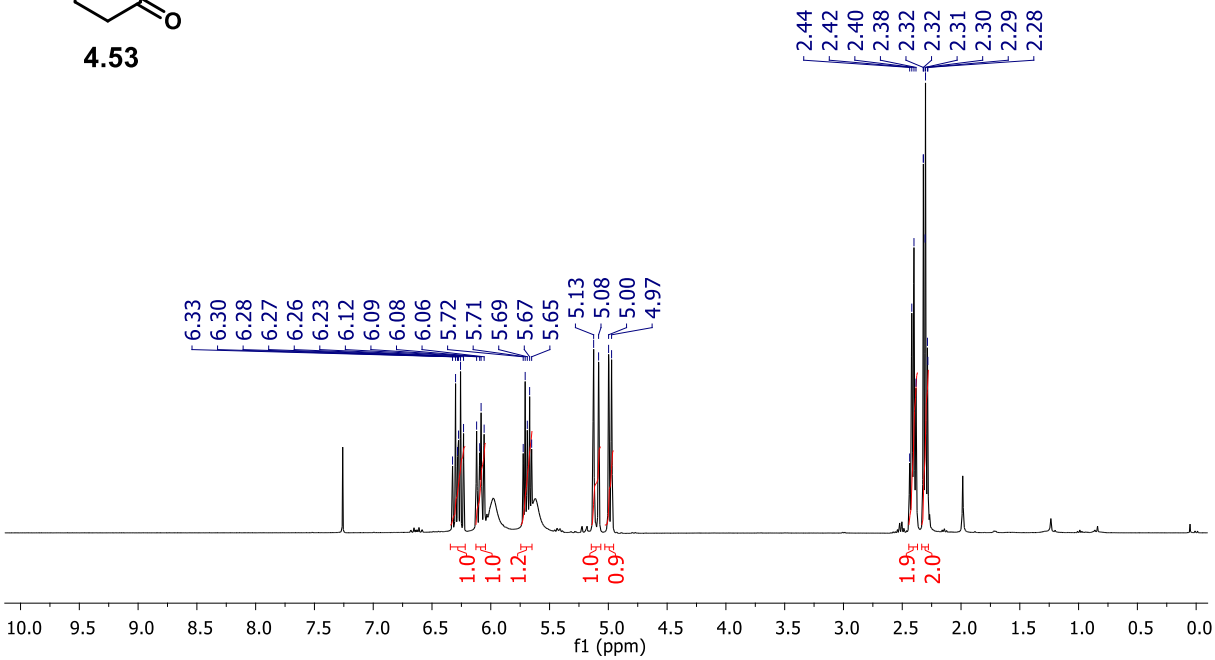

gc3-56
Standard 13C 400MHz BBFO "Smart" probe

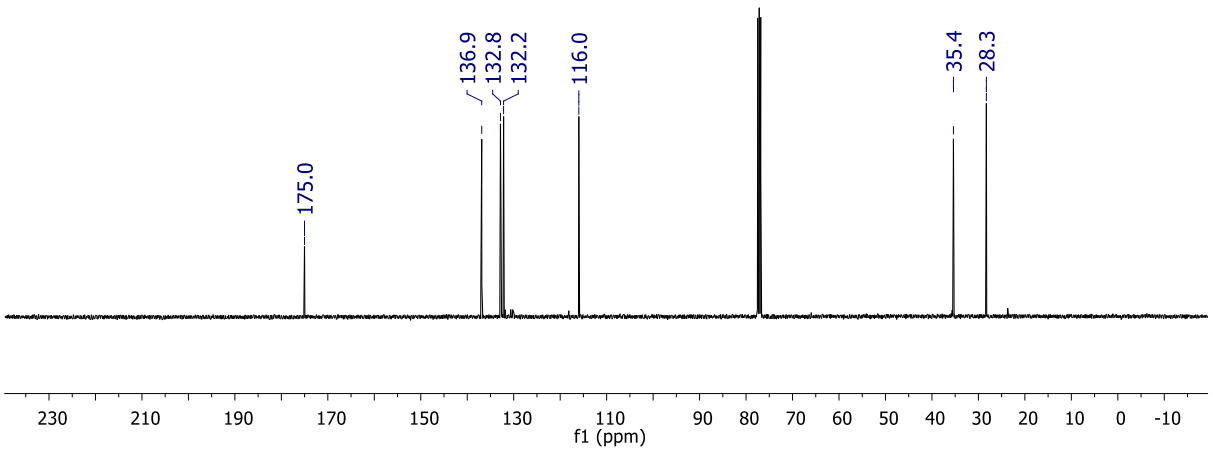

gc3-100
Standard 1H 400MHz BBFO "Smart" probe

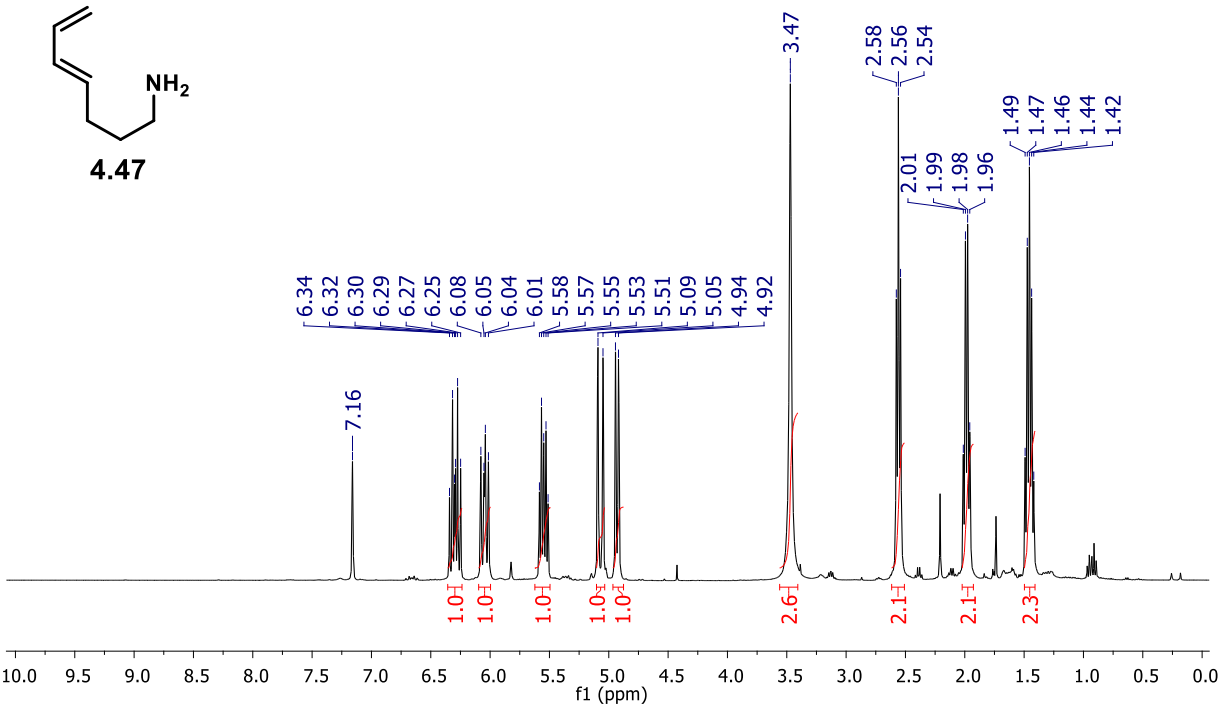

gc3-100
Standard 13C 400MHz BBFO "Smart" probe

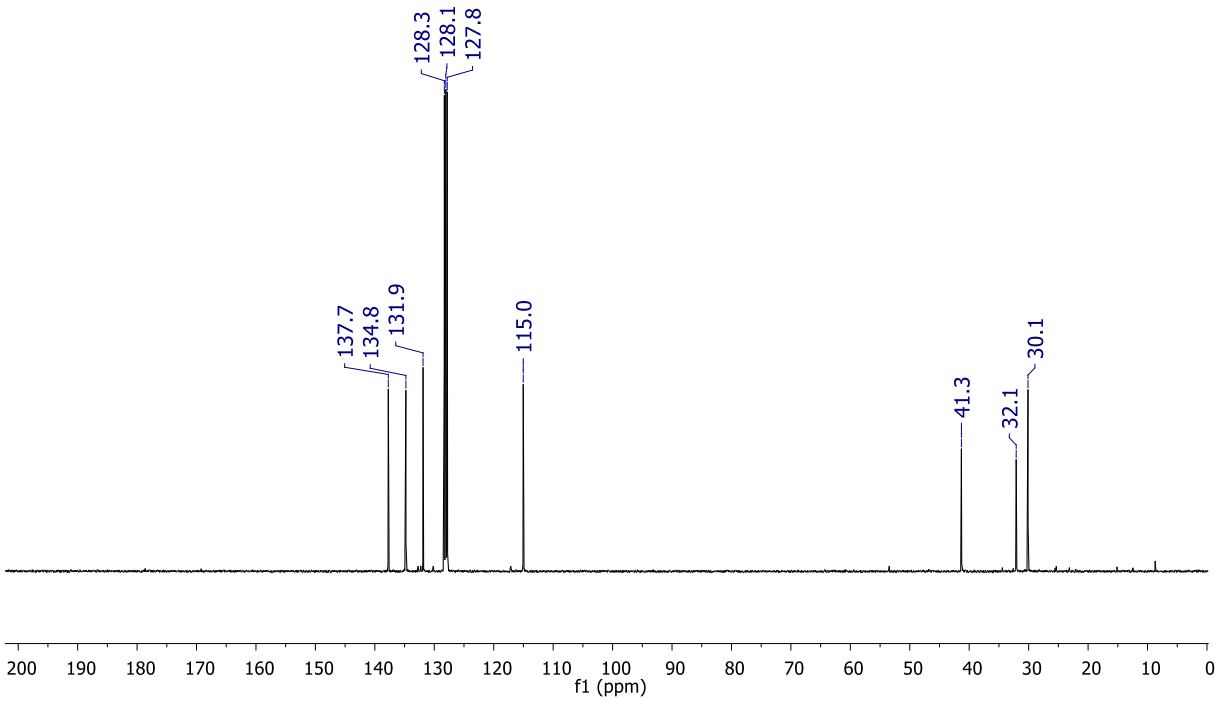

gc3-186_flush
Standard 1H 400MHz BBFO "Smart" probe

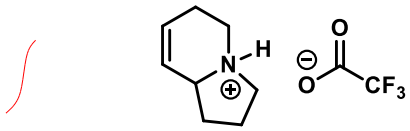

4.50

gc3-184_flush-longrun
Standard 13C 400MHz BBFO "Smart" probe

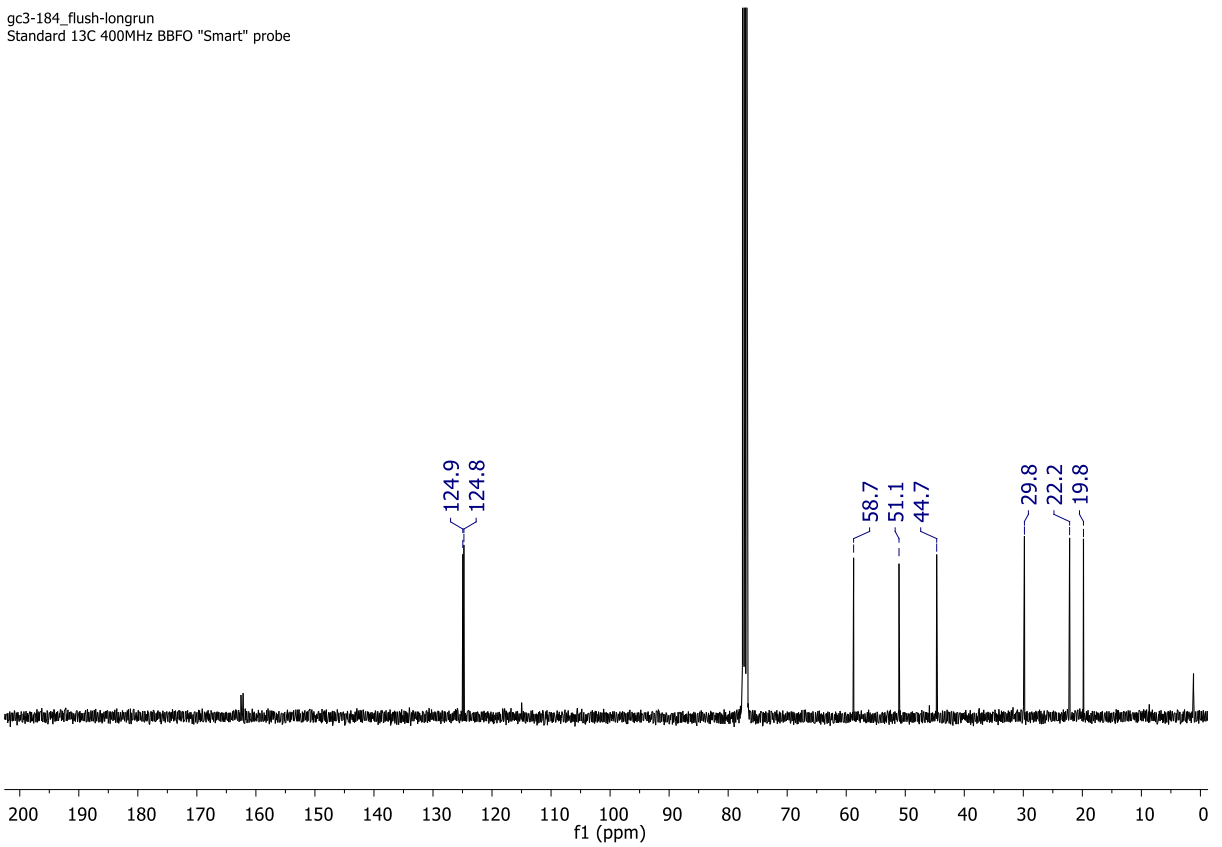

gc3-104_3
Standard 1H 400MHz BBFO "Smart" probe

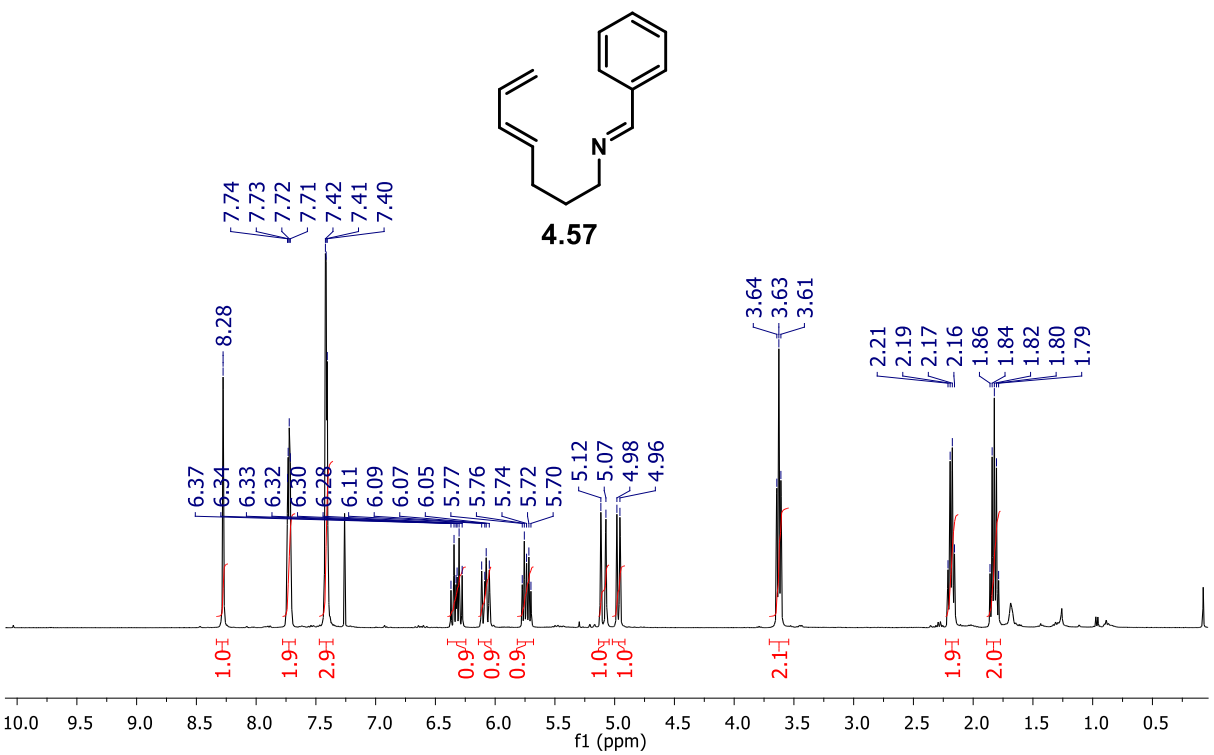

gc3-104_3
Standard 13C 400MHz BBFO "Smart" probe

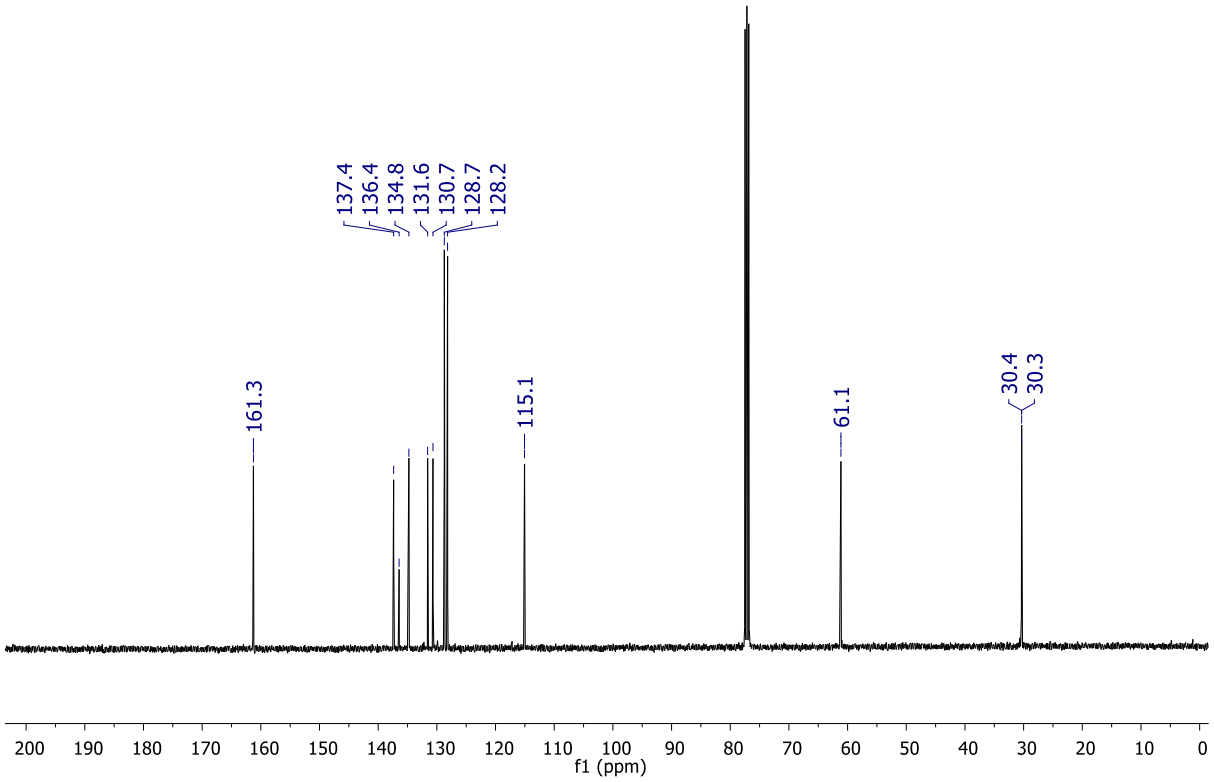

gc4-108
Standard 1H 400MHz BBFO "Smart" probe

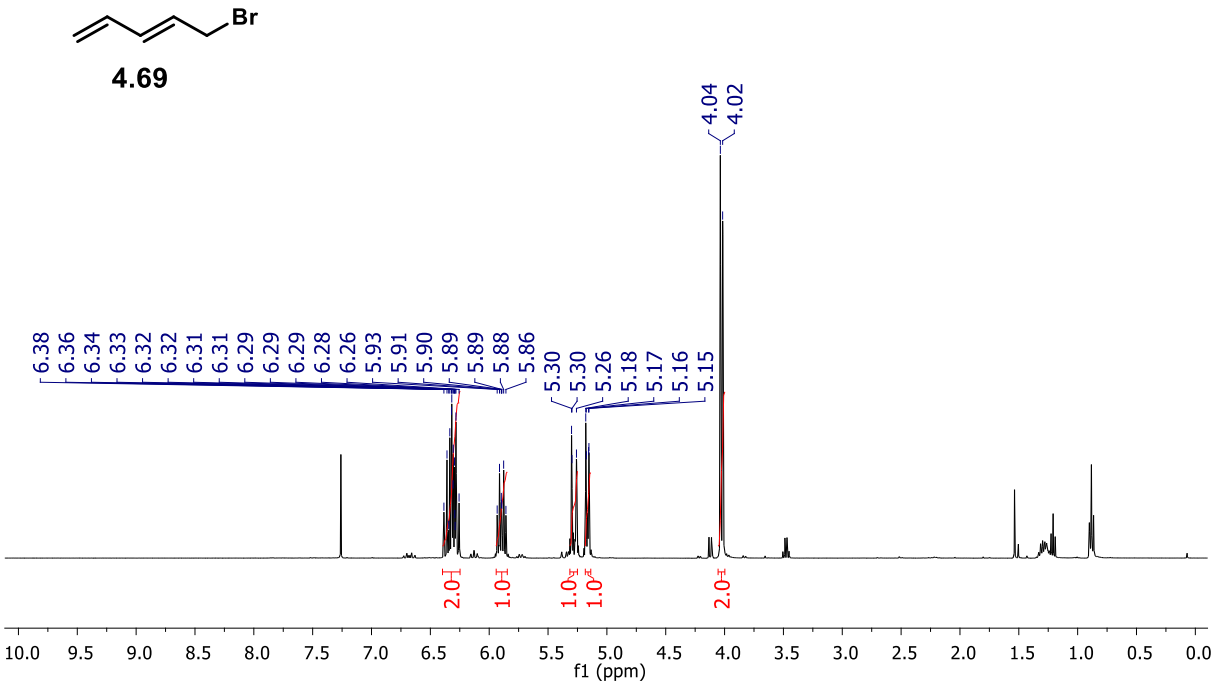

gc4-108
Standard 13C 400MHz BBFO "Smart" probe

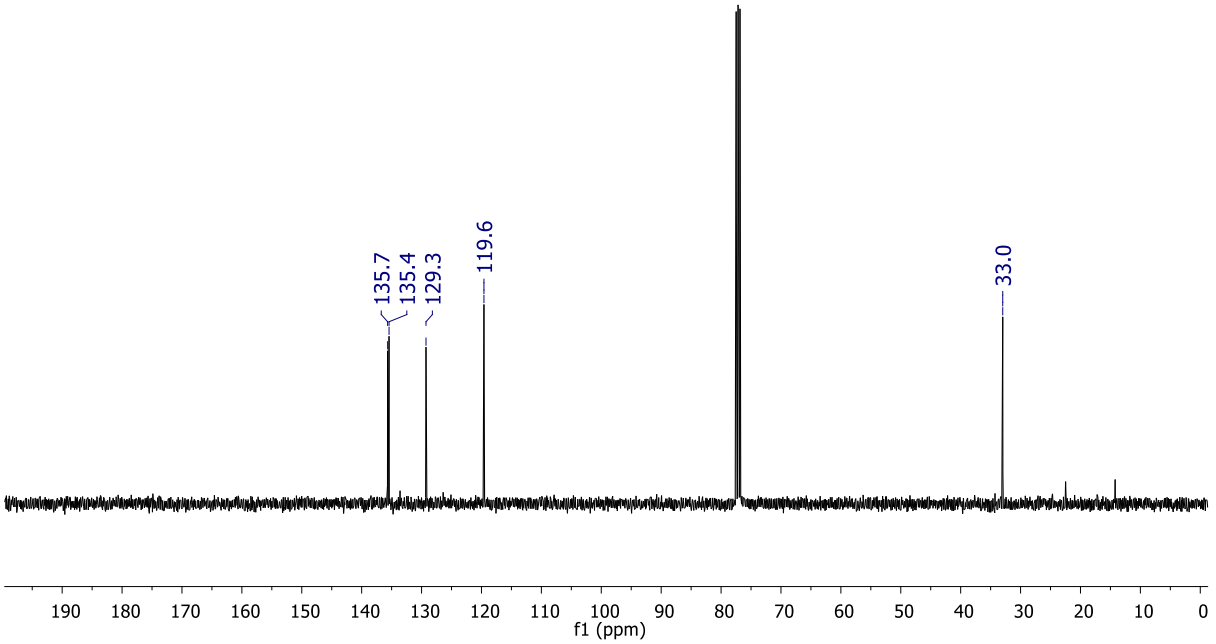

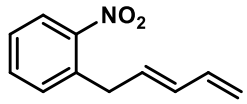
NO2

4.71

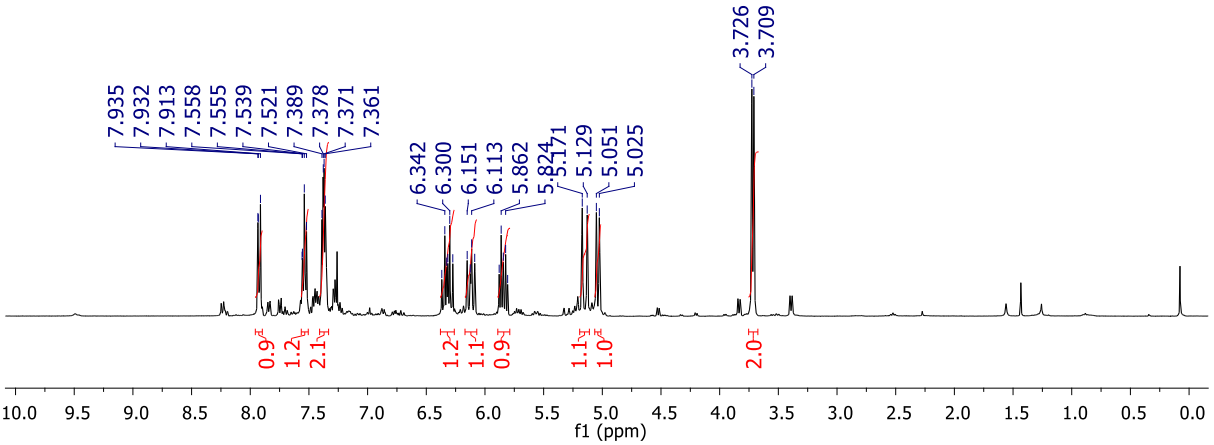
7.935
7.932
7.913
7.558
7.555
7.539
7.521
7.389
7.378
7.371
7.361
6.342
6.300
6.151
6.113
5.862
5.824
5.171
5.129
5.051
5.025
3.726
3.709
0.9
1.2
2.1
1.2
1.1
0.9
1.1
1.0
2.0
10.0 9.5 9.0 8.5 8.0 7.5 7.0 6.5 6.0 5.5 5.0 4.5 4.0 3.5 3.0 2.5 2.0 1.5 1.0 0.5 0.0
f1 (ppm)

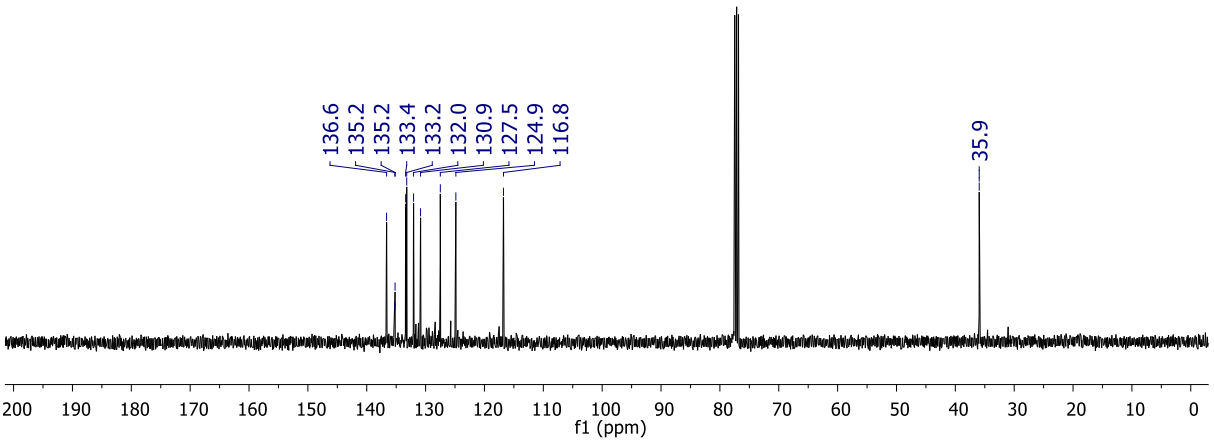
136.6
135.2
135.2
133.4
133.2
132.0
130.9
127.5
124.9
116.8
35.9
200 190 180 170 160 150 140 130 120 110 100 90 80 70 60 50 40 30 20 10 0
f1 (ppm)

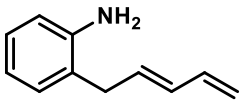
NH2

4.68

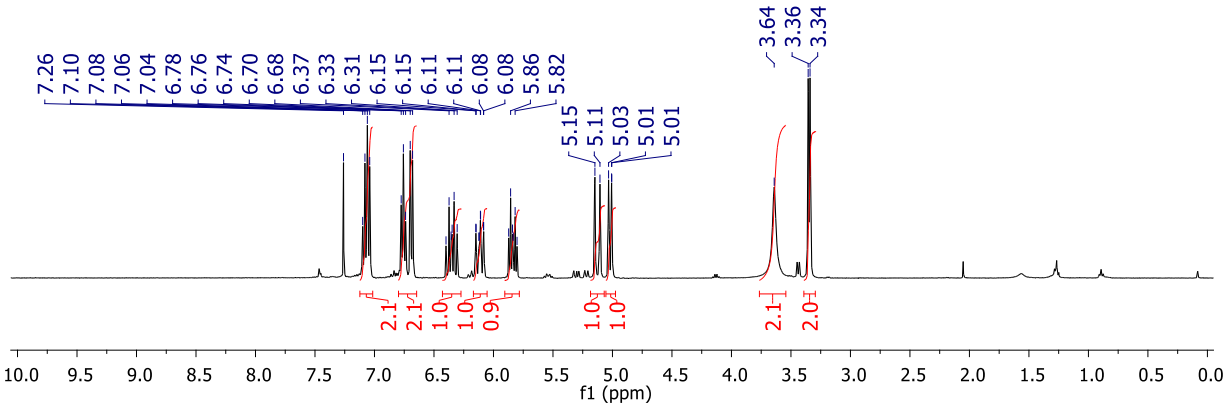
7.26
7.10
7.08
7.06
7.04
6.78
6.76
6.74
6.70
6.68
6.37
6.33
6.31
6.15
6.15
6.11
6.11
6.08
6.08
5.86
5.82
5.15
5.11
5.03
5.01
5.01
3.64
3.36
3.34
2.1
2.1
1.0
1.0
0.9
1.0
1.0
2.1
2.0
10.0 9.5 9.0 8.5 8.0 7.5 7.0 6.5 6.0 5.5 5.0 4.5 4.0 3.5 3.0 2.5 2.0 1.5 1.0 0.5 0.0
f1 (ppm)

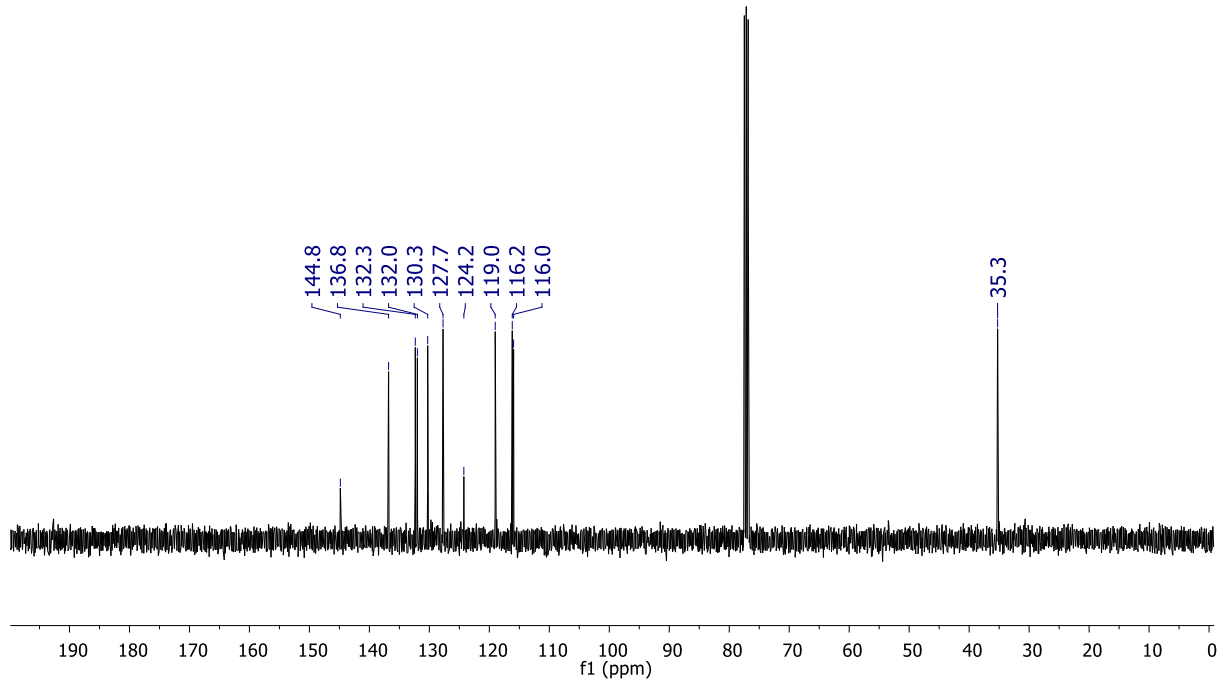
144.8
136.8
132.3
132.0
130.3
127.7
124.2
119.0
116.2
116.0
35.3
190 180 170 160 150 140 130 120 110 100 90 80 70 60 50 40 30 20 10 0
f1 (ppm)

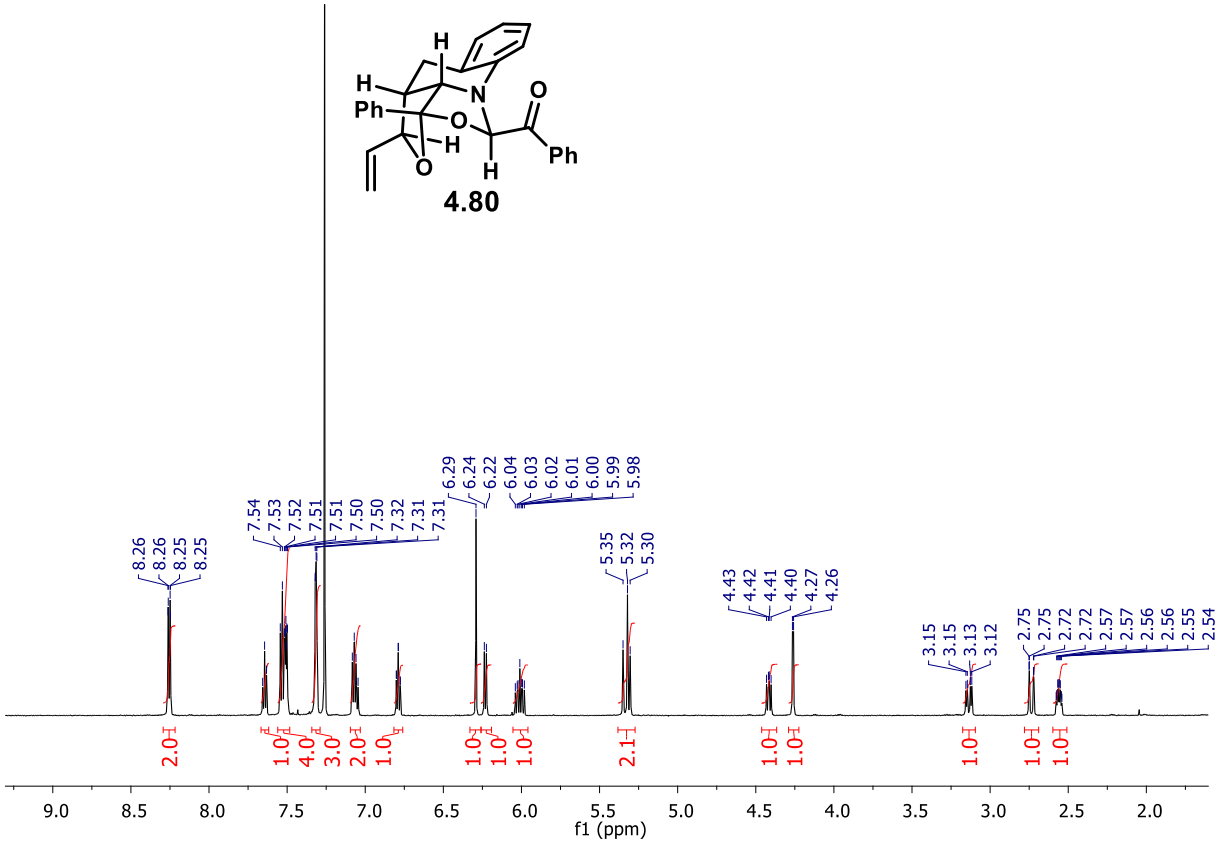
H
H
Ph
N
O
O
H
O
H
Ph
4.80
8.26
8.26
8.25
8.25
7.54
7.53
7.52
7.51
7.51
7.50
7.50
7.32
7.31
7.31
6.29
6.24
6.22
6.04
6.03
6.02
6.01
6.00
5.99
5.98
5.35
5.32
5.30
4.43
4.42
4.41
4.40
4.27
4.26
3.15
3.15
3.13
3.12
2.75
2.75
2.72
2.72
2.57
2.57
2.56
2.56
2.55
2.54
2.0
1.0
4.0
3.0
2.0
1.0
1.0
1.0
1.0
2.1
1.0
1.0
1.0
1.0
1.0
9.0
8.5
8.0
7.5
7.0
6.5
6.0
5.5
5.0
4.5
4.0
3.5
3.0
2.5
2.0
f1 (ppm)

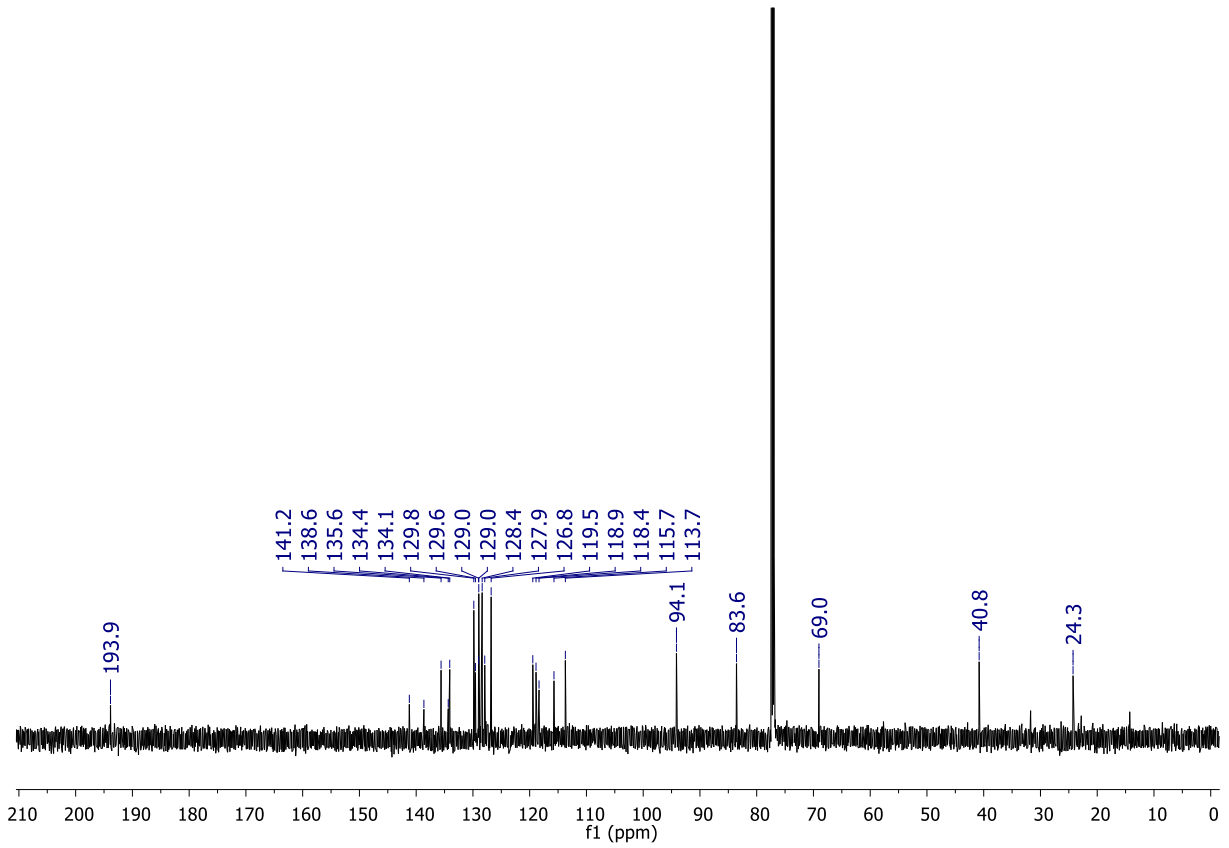
141.2
138.6
135.6
134.4
134.1
129.8
129.6
129.0
129.0
128.4
127.9
126.8
119.5
118.9
118.4
115.7
113.7
193.9
94.1
83.6
69.0
40.8
24.3
210
200
190
180
170
160
150
140
130
120
110
100
90
80
70
60
50
40
30
20
10
0
f1 (ppm)

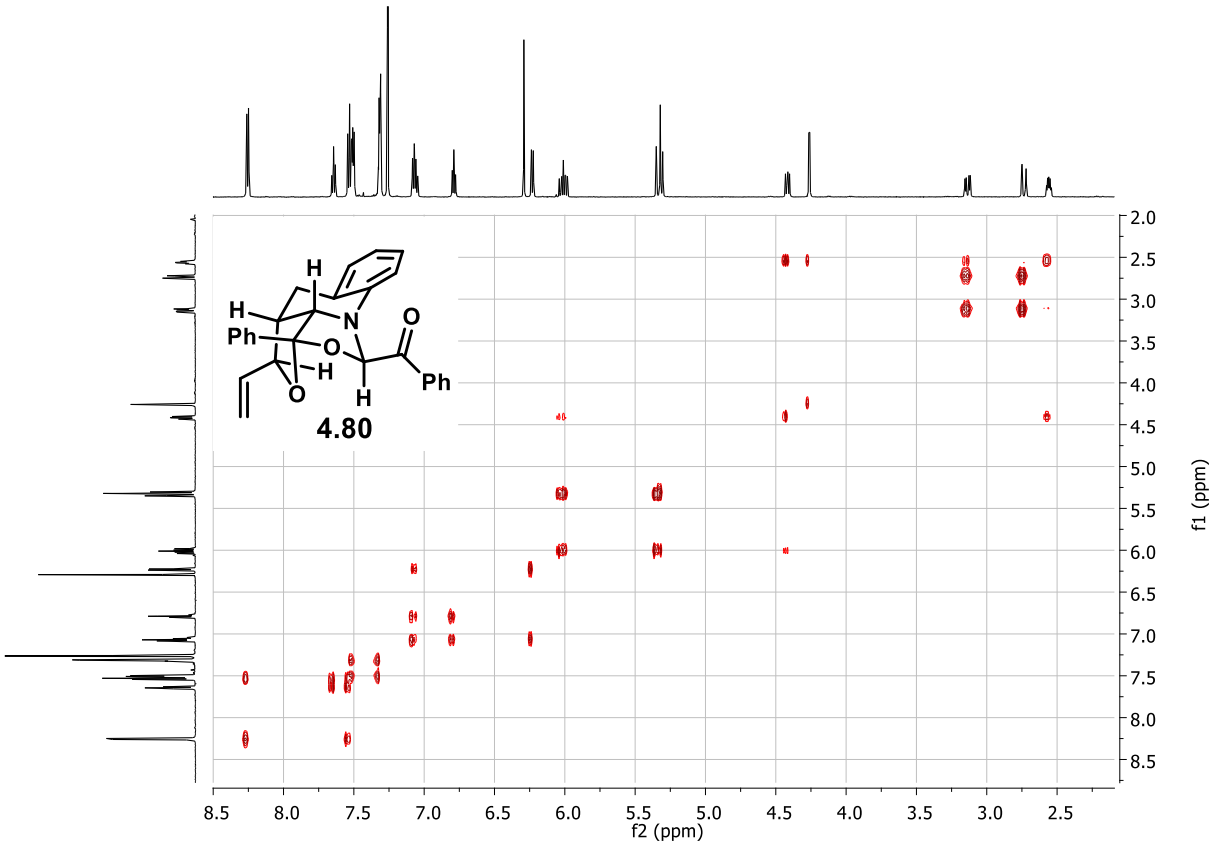
H
H
Ph
N
O
O
H
O
H
Ph
4.80
f2 (ppm)
f1 (ppm)

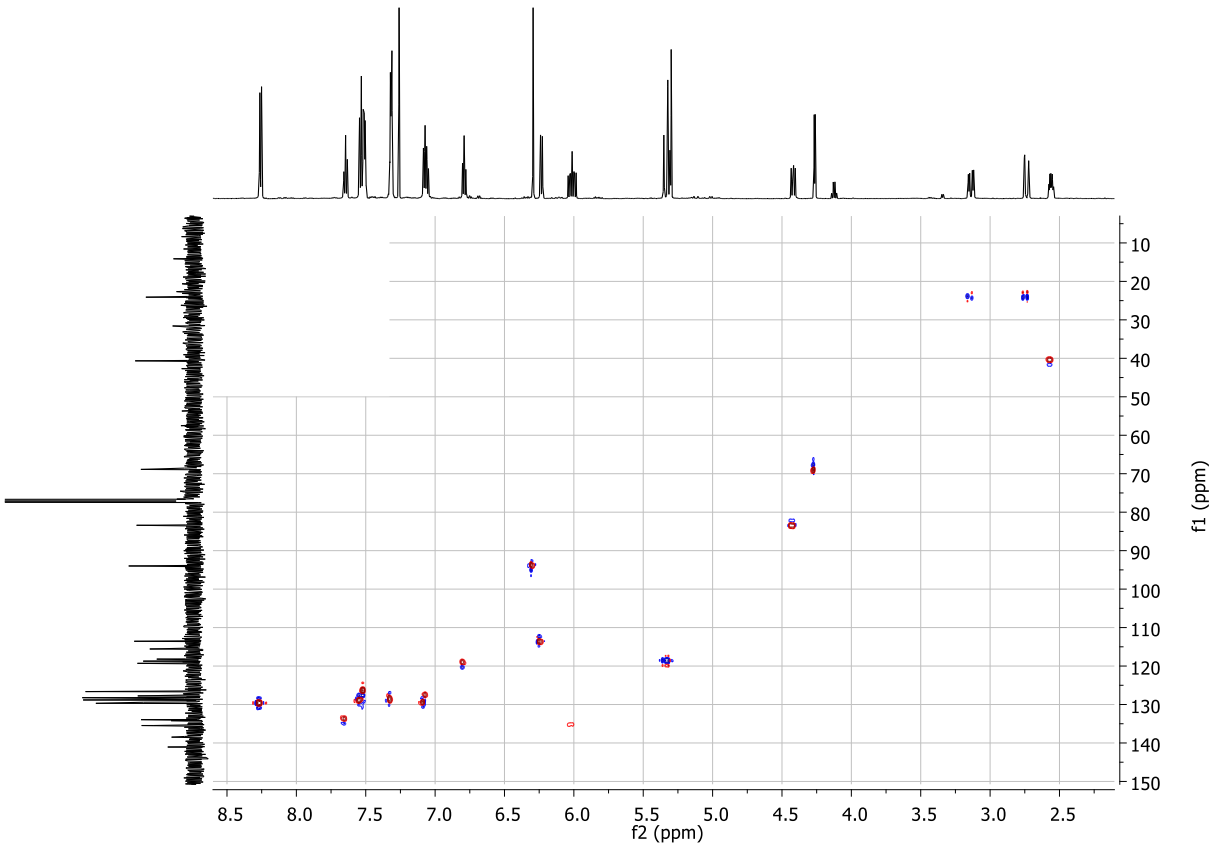
f2 (ppm)
f1 (ppm)

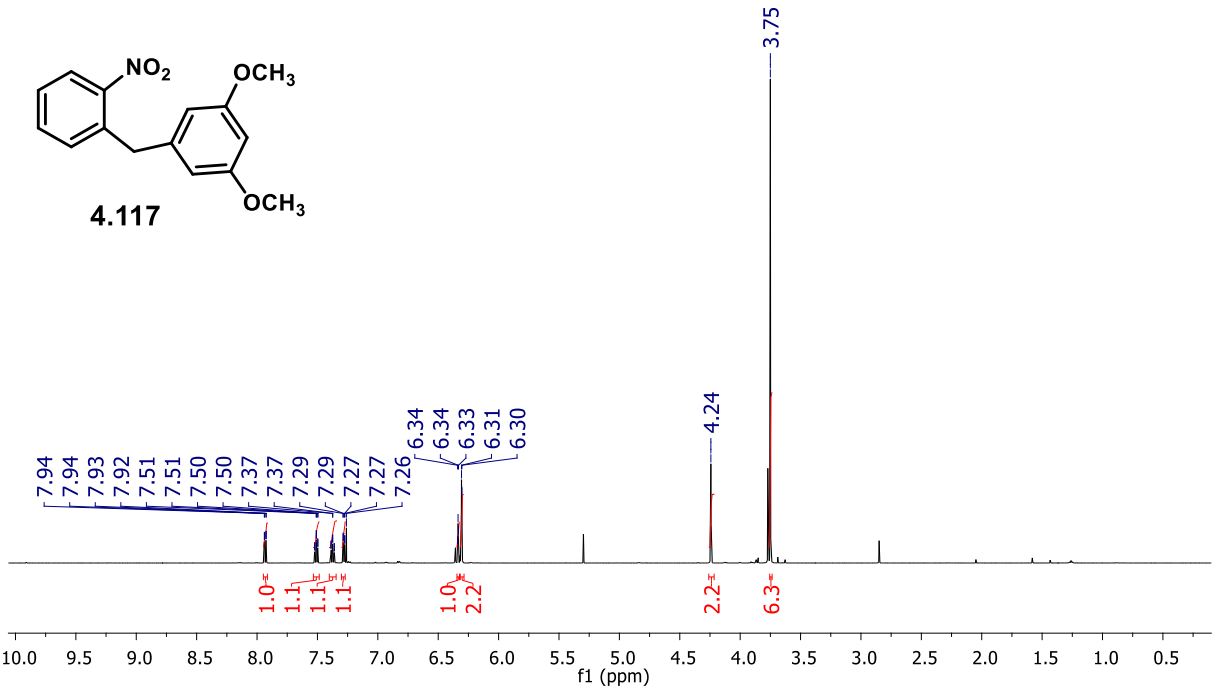
NO2
OCH3
OCH3
4.117
3.75
4.24
7.94
7.94
7.93
7.92
7.51
7.51
7.50
7.50
7.37
7.37
7.29
7.29
7.27
7.27
7.26
6.34
6.34
6.33
6.31
6.30
1.0
1.1
1.1
1.1
1.0
2.2
2.2
6.3
10.0 9.5 9.0 8.5 8.0 7.5 7.0 6.5 6.0 5.5 5.0 4.5 4.0 3.5 3.0 2.5 2.0 1.5 1.0 0.5
f1 (ppm)

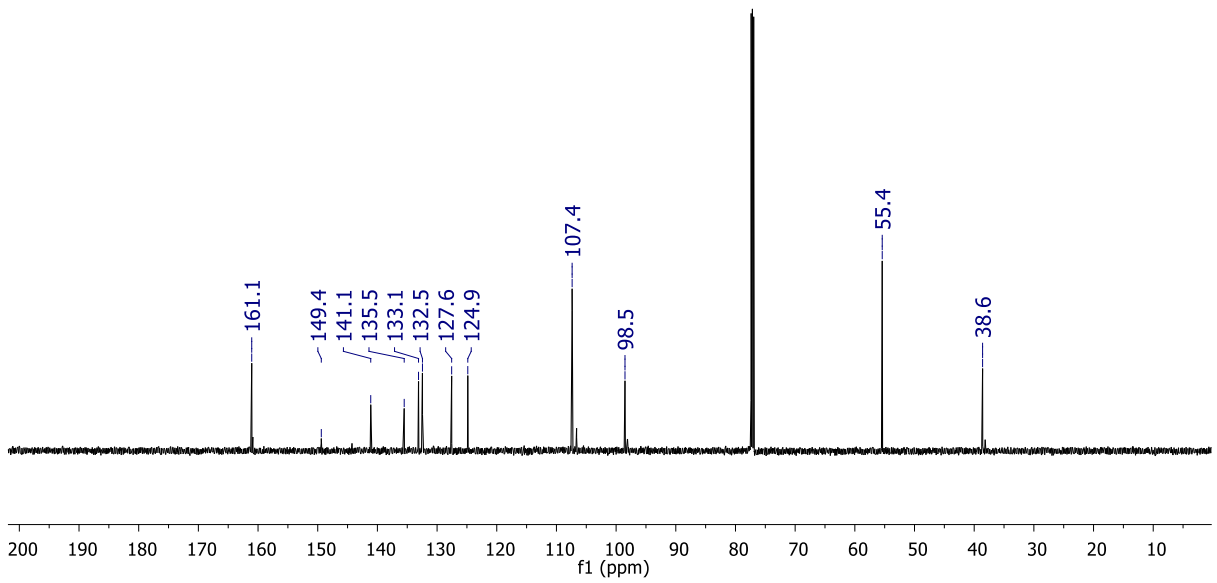
161.1
149.4
141.1
135.5
133.1
132.5
127.6
124.9
107.4
98.5
55.4
38.6
200 190 180 170 160 150 140 130 120 110 100 90 80 70 60 50 40 30 20 10
f1 (ppm)

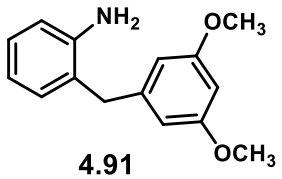
NH2
OCH3
OCH3

4.91

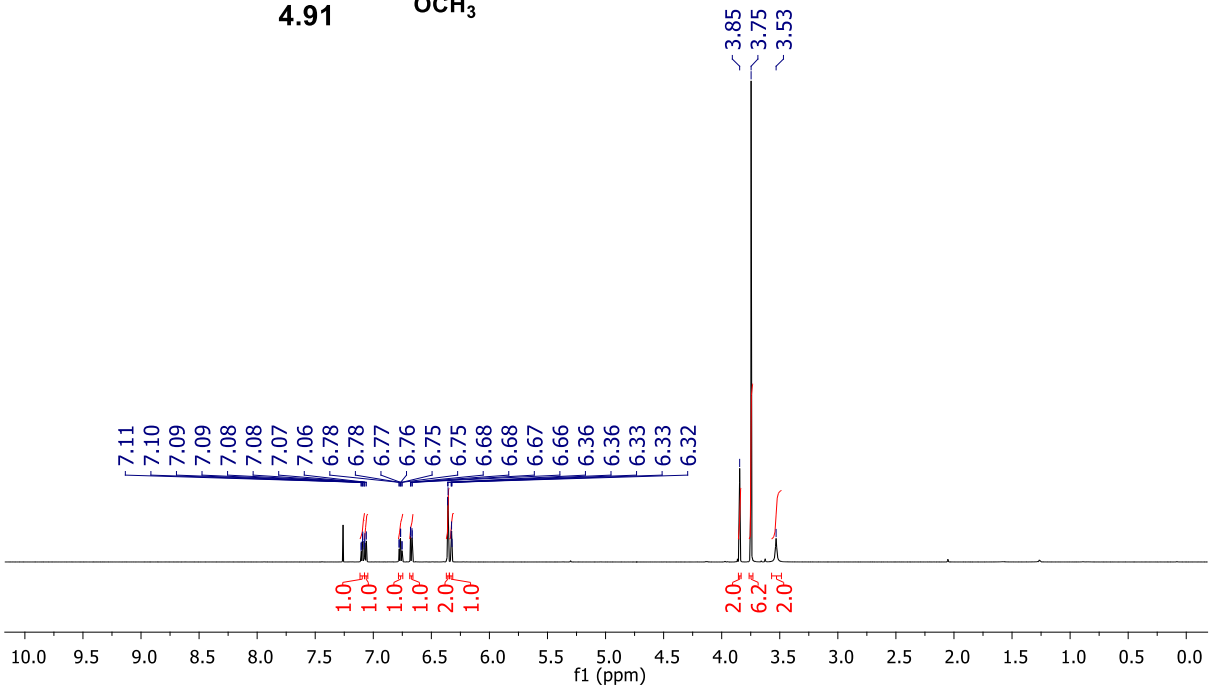
3.85
3.75
3.53
7.11
7.10
7.09
7.09
7.08
7.08
7.07
7.06
6.78
6.78
6.77
6.76
6.75
6.75
6.68
6.68
6.67
6.66
6.36
6.36
6.33
6.33
6.32
1.0
1.0
1.0
1.0
2.0
1.0
2.0
6.2
2.0
10.0 9.5 9.0 8.5 8.0 7.5 7.0 6.5 6.0 5.5 5.0 4.5 4.0 3.5 3.0 2.5 2.0 1.5 1.0 0.5 0.0
f1 (ppm)

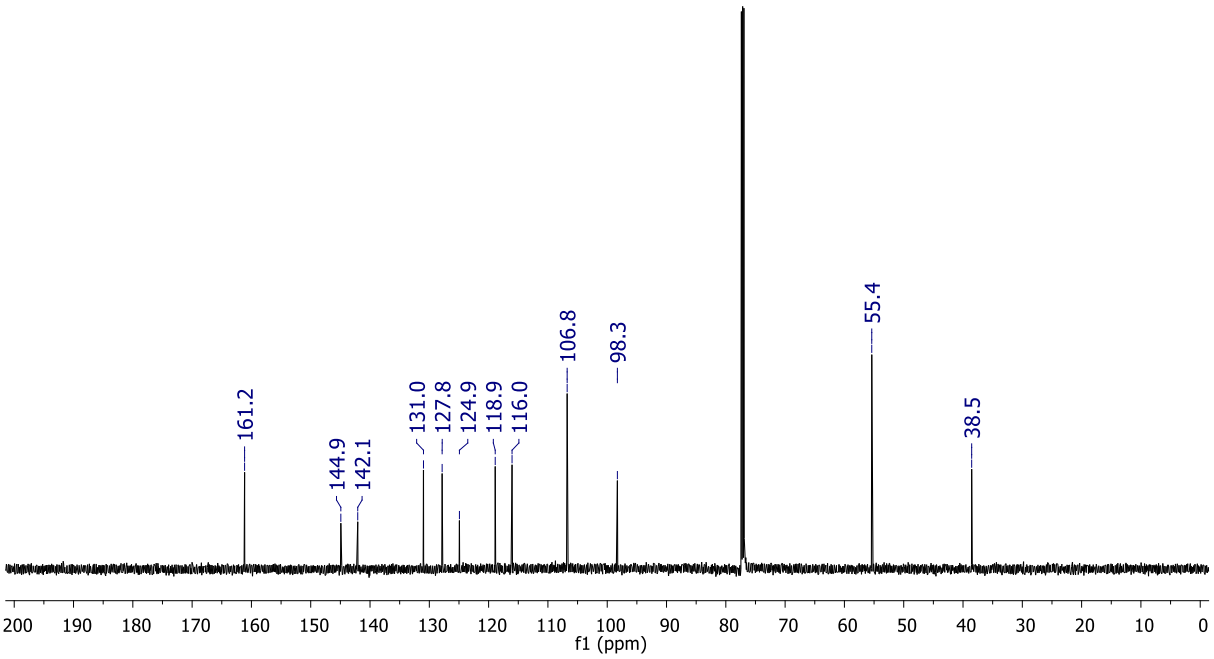
161.2
144.9
142.1
131.0
127.8
124.9
118.9
116.0
106.8
98.3
55.4
38.5
200 190 180 170 160 150 140 130 120 110 100 90 80 70 60 50 40 30 20 10 0
f1 (ppm)

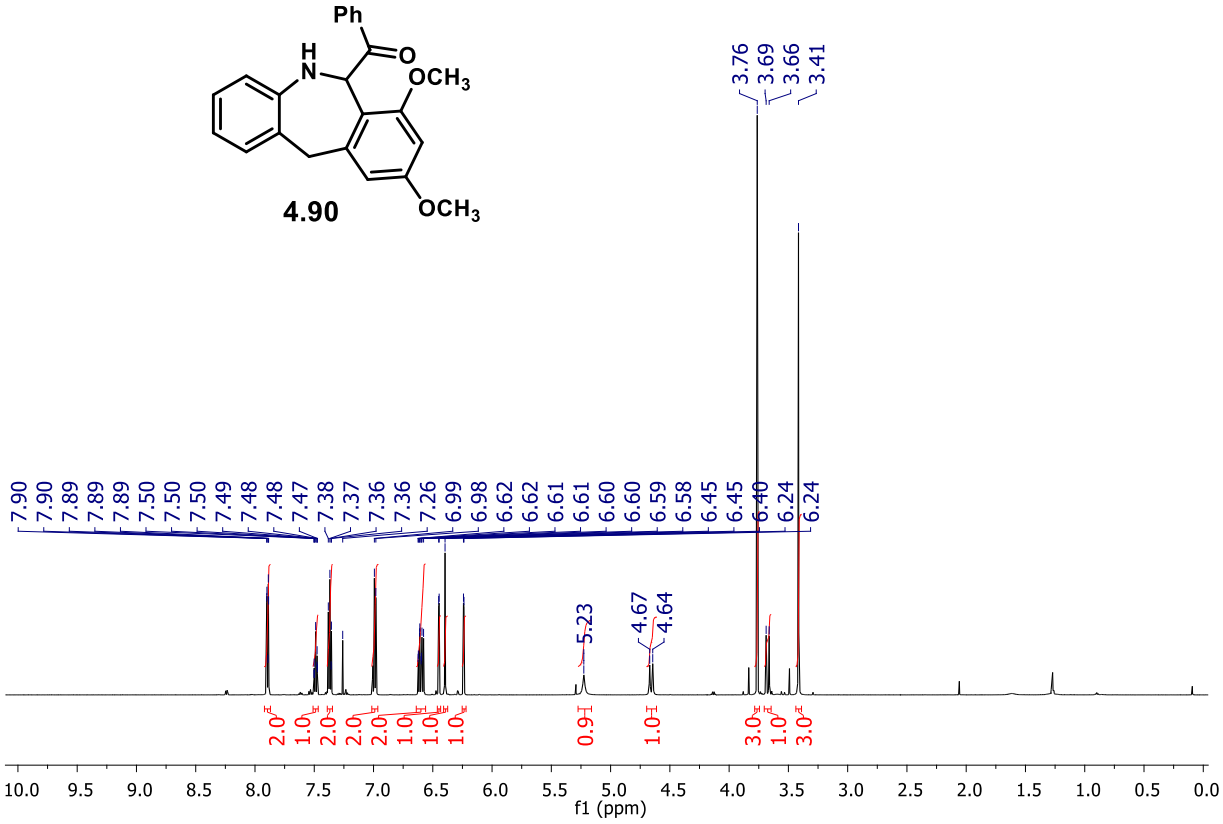
Ph
H
N
O
OCH3
OCH3
4.90
3.76
3.69
3.66
3.41
7.90
7.90
7.89
7.89
7.89
7.50
7.50
7.50
7.49
7.48
7.48
7.47
7.38
7.37
7.36
7.36
7.26
6.99
6.98
6.62
6.62
6.61
6.61
6.60
6.60
6.59
6.58
6.45
6.45
6.40
6.24
6.24
5.23
4.67
4.64
2.0
1.0
2.0
2.0
2.0
1.0
1.0
1.0
0.9
1.0
3.0
1.0
3.0
10.0 9.5 9.0 8.5 8.0 7.5 7.0 6.5 6.0 5.5 5.0 4.5 4.0 3.5 3.0 2.5 2.0 1.5 1.0 0.5 0.0
f1 (ppm)

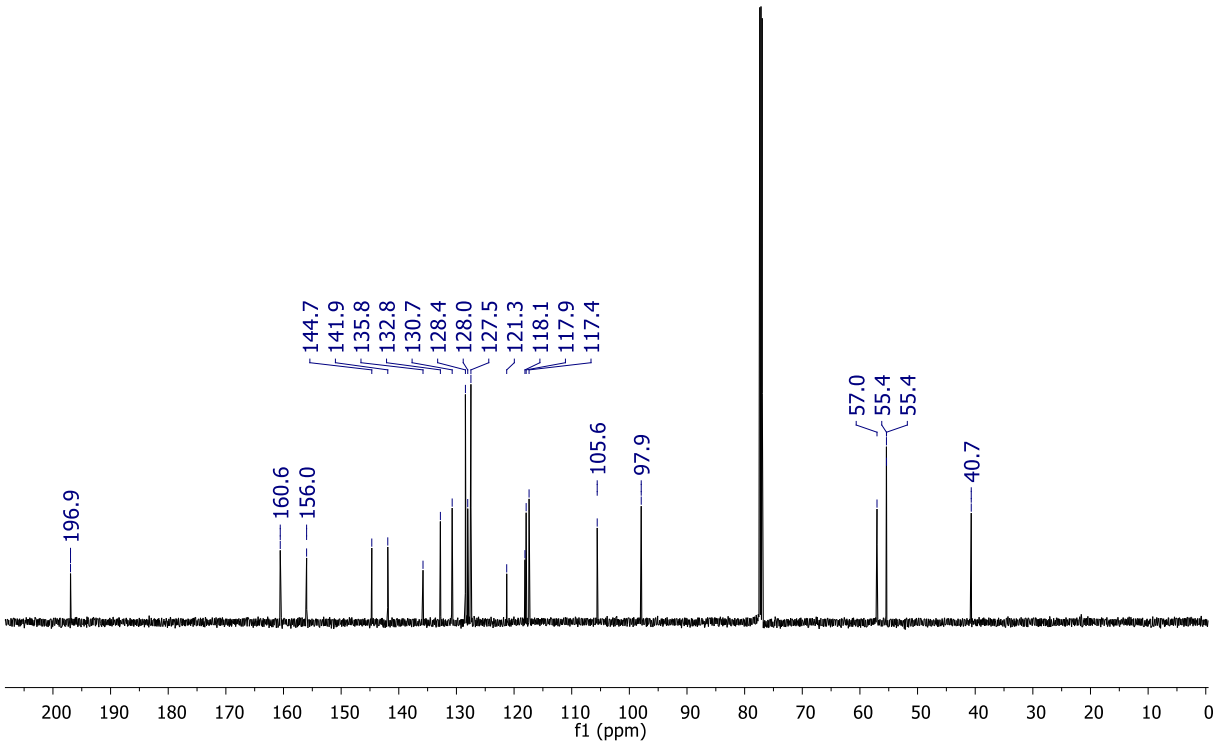
196.9
160.6
156.0
144.7
141.9
135.8
132.8
130.7
128.4
128.0
127.5
121.3
118.1
117.9
117.4
105.6
97.9
57.0
55.4
55.4
40.7
200 190 180 170 160 150 140 130 120 110 100 90 80 70 60 50 40 30 20 10 0
f1 (ppm)

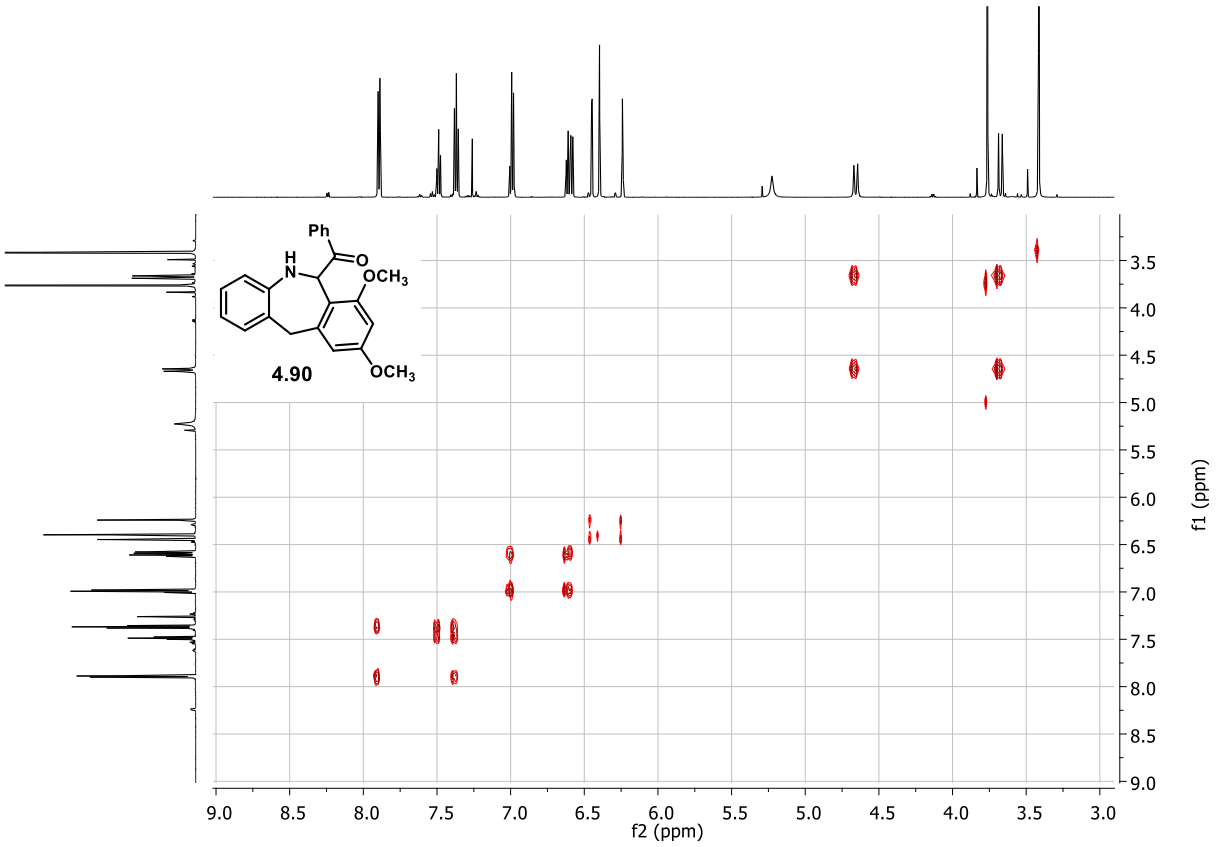
Ph
O
H
N
OCH3
OCH3
4.90
f2 (ppm)
f1 (ppm)

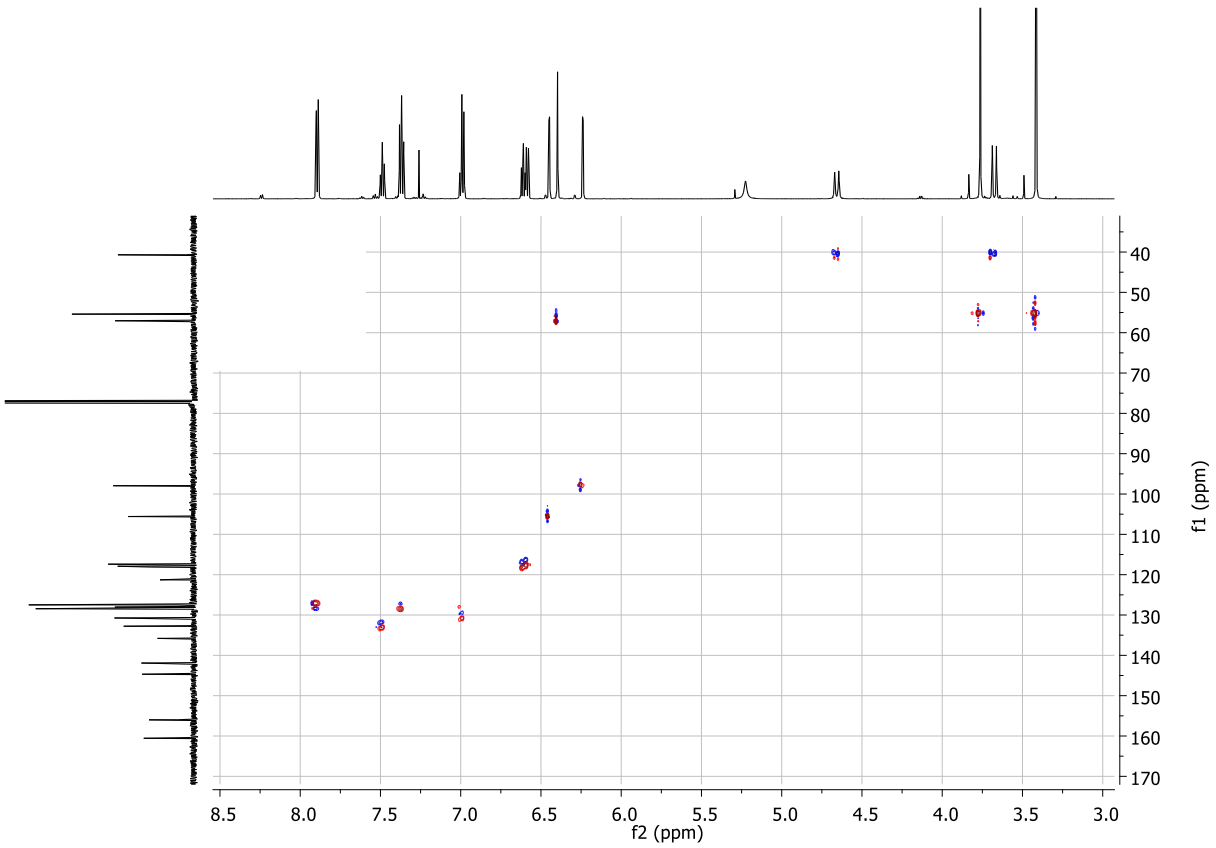
f2 (ppm)
f1 (ppm)

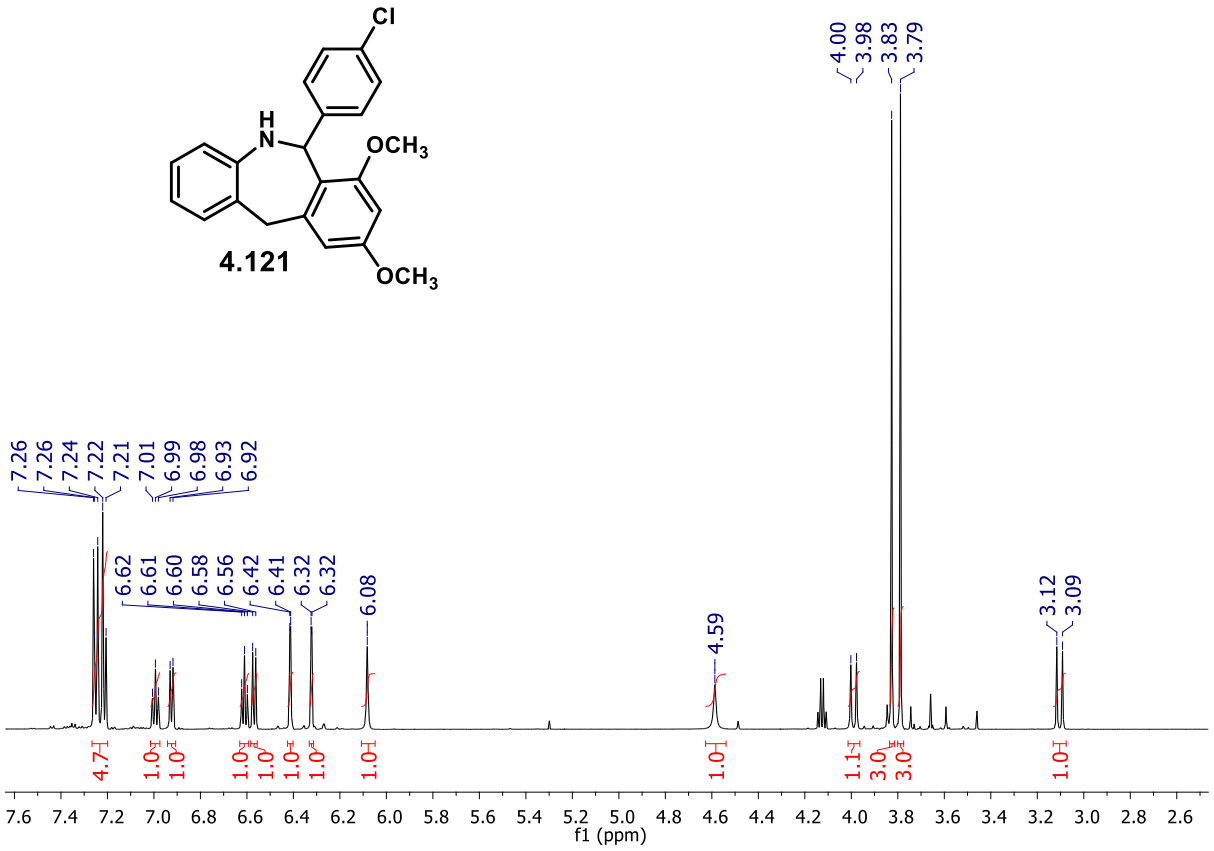
Cl
H
N
OCH3
OCH3
4.121
7.26
7.26
7.24
7.22
7.21
7.01
6.99
6.98
6.93
6.92
6.62
6.61
6.60
6.58
6.56
6.42
6.41
6.32
6.32
6.08
4.59
4.00
3.98
3.83
3.79
3.12
3.09
4.7
1.0
1.0
1.0
1.0
1.0
1.0
1.0
1.1
3.0
3.0
1.0
7.6 7.4 7.2 7.0 6.8 6.6 6.4 6.2 6.0 5.8 5.6 5.4 5.2 5.0 4.8 4.6 4.4 4.2 4.0 3.8 3.6 3.4 3.2 3.0 2.8 2.6
f1 (ppm)

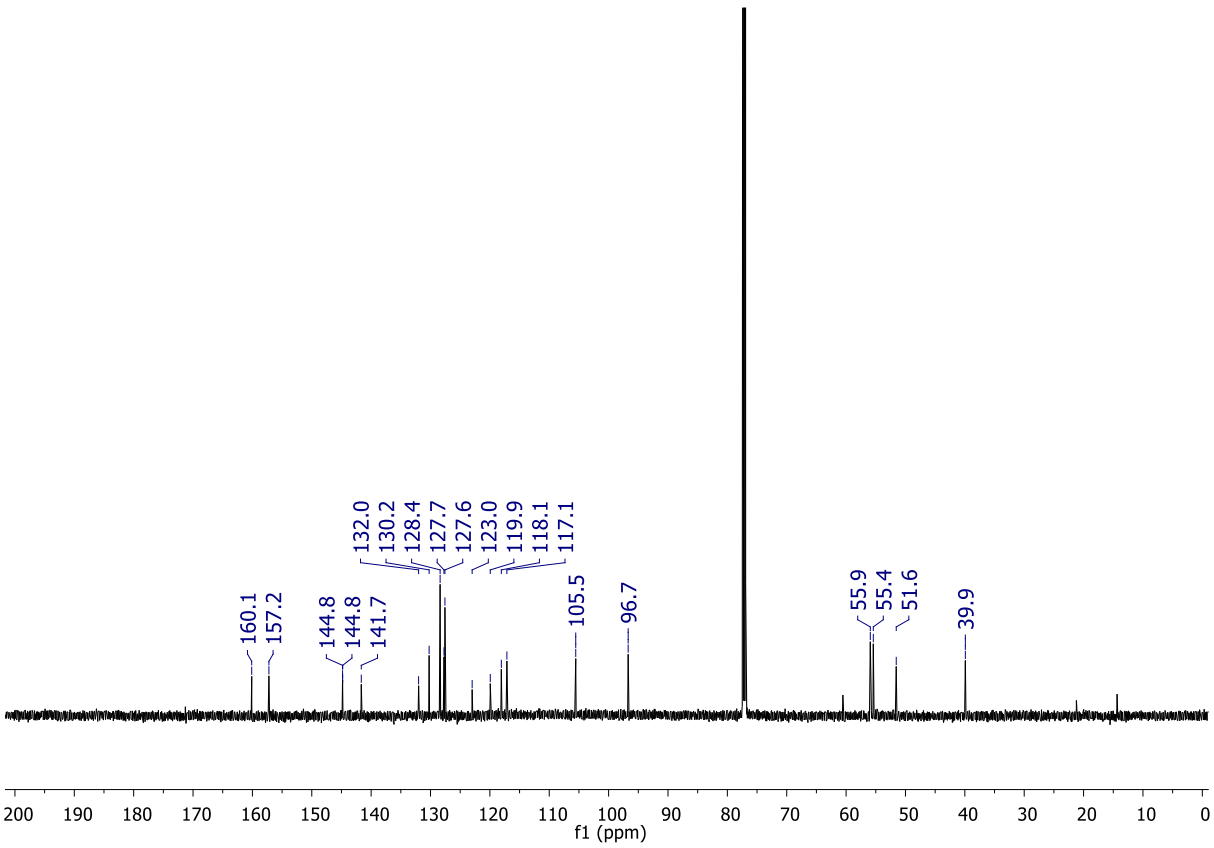
160.1
157.2
144.8
144.8
141.7
132.0
130.2
128.4
127.7
127.6
123.0
119.9
118.1
117.1
105.5
96.7
55.9
55.4
51.6
39.9
200 190 180 170 160 150 140 130 120 110 100 90 80 70 60 50 40 30 20 10 0
f1 (ppm)

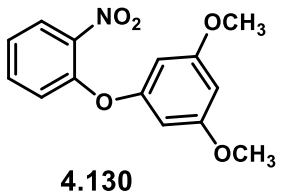
NO2
OCH3
O
OCH3

4.130

3.75
6.28
6.27
6.27
6.19
6.19
7.94
7.94
7.94
7.93
7.92
7.92
7.52
7.52
7.51
7.51
7.51
7.50
7.49
7.49
7.21
7.21
7.20
7.18
7.18
7.09
7.09
7.08
7.08
1.0
1.0
1.0
1.0
1.0
2.0
6.1
10.0 9.5 9.0 8.5 8.0 7.5 7.0 6.5 6.0 5.5 5.0 4.5 4.0 3.5 3.0 2.5 2.0 1.5 1.0 0.5
f1 (ppm)

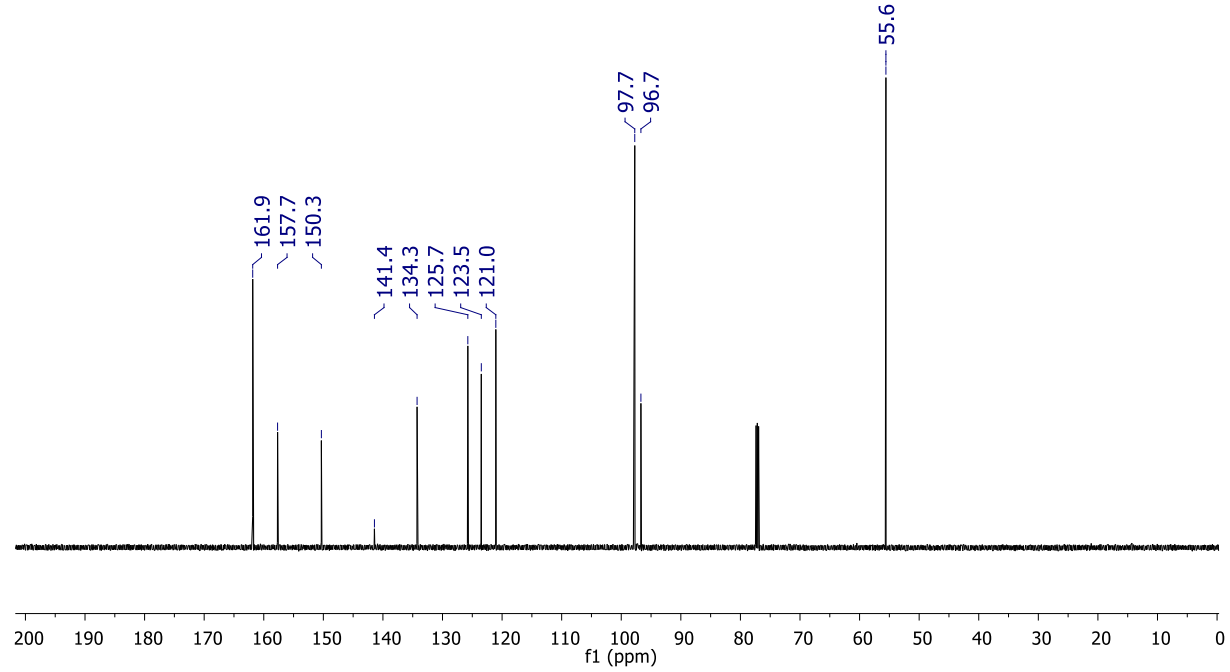
55.6
97.7
96.7
161.9
157.7
150.3
141.4
134.3
125.7
123.5
121.0
200 190 180 170 160 150 140 130 120 110 100 90 80 70 60 50 40 30 20 10 0
f1 (ppm)

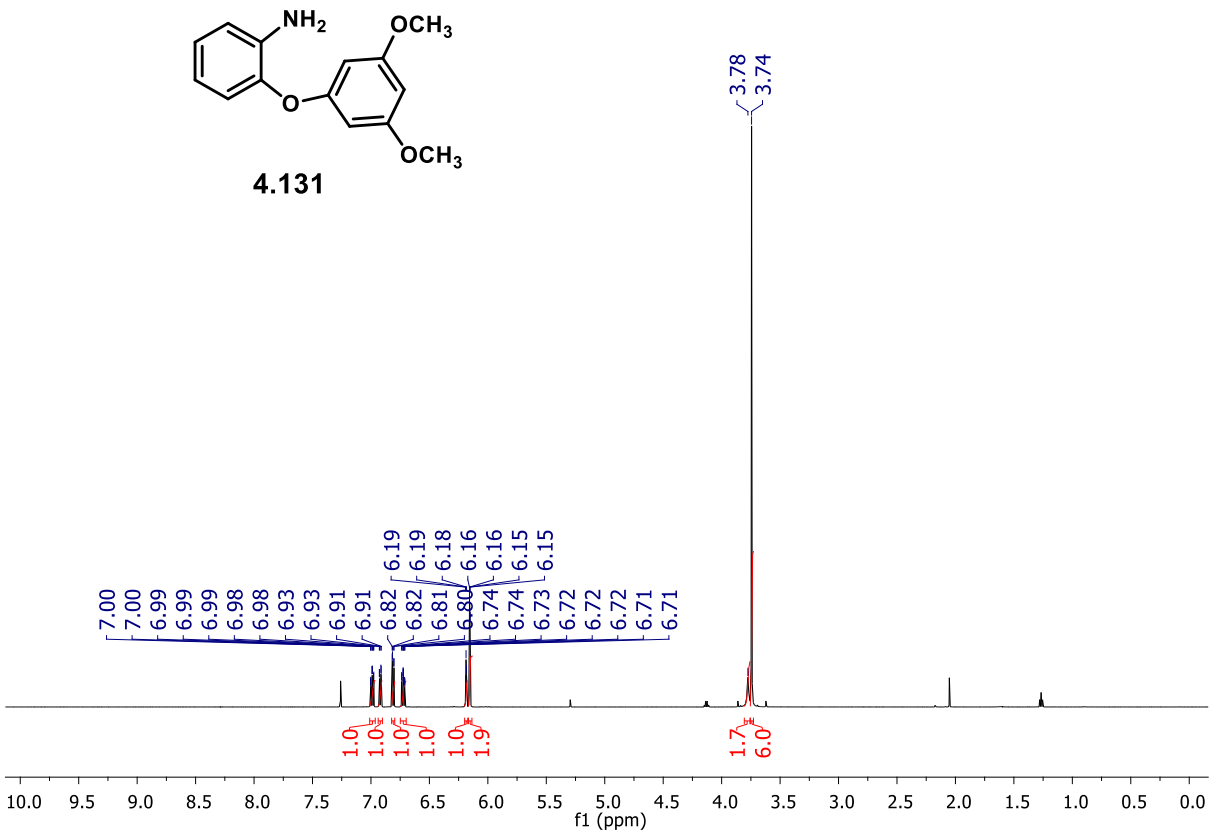
NH2
OCH3
O
OCH3
4.131
3.78
3.74
7.00
7.00
6.99
6.99
6.99
6.98
6.98
6.93
6.93
6.91
6.91
6.82
6.82
6.81
6.80
6.74
6.74
6.73
6.72
6.72
6.71
6.71
6.19
6.19
6.18
6.16
6.16
6.15
6.15
1.0
1.0
1.0
1.0
1.0
1.9
1.7
6.0
10.0 9.5 9.0 8.5 8.0 7.5 7.0 6.5 6.0 5.5 5.0 4.5 4.0 3.5 3.0 2.5 2.0 1.5 1.0 0.5 0.0
f1 (ppm)

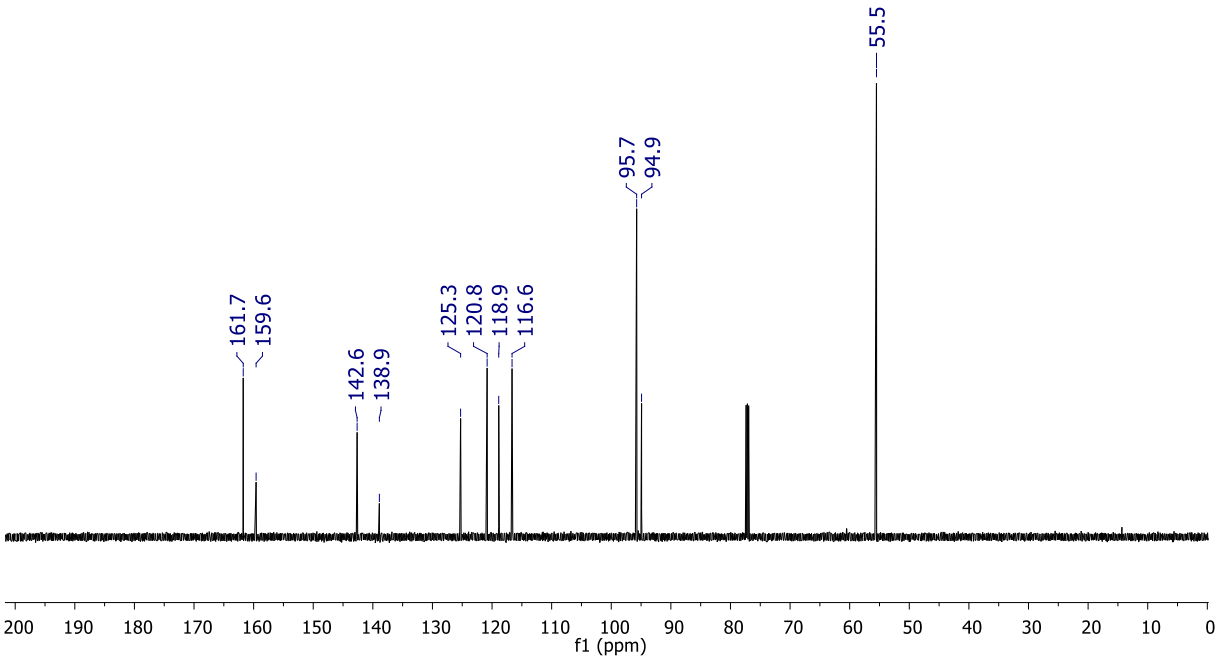
55.5
95.7
94.9
161.7
159.6
142.6
138.9
125.3
120.8
118.9
116.6
200 190 180 170 160 150 140 130 120 110 100 90 80 70 60 50 40 30 20 10 0
f1 (ppm)

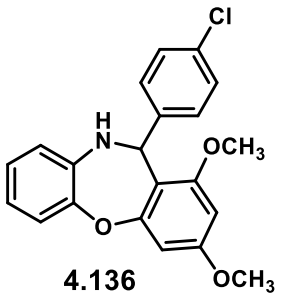
Cl
H
N
OCH3
O
OCH3

4.136

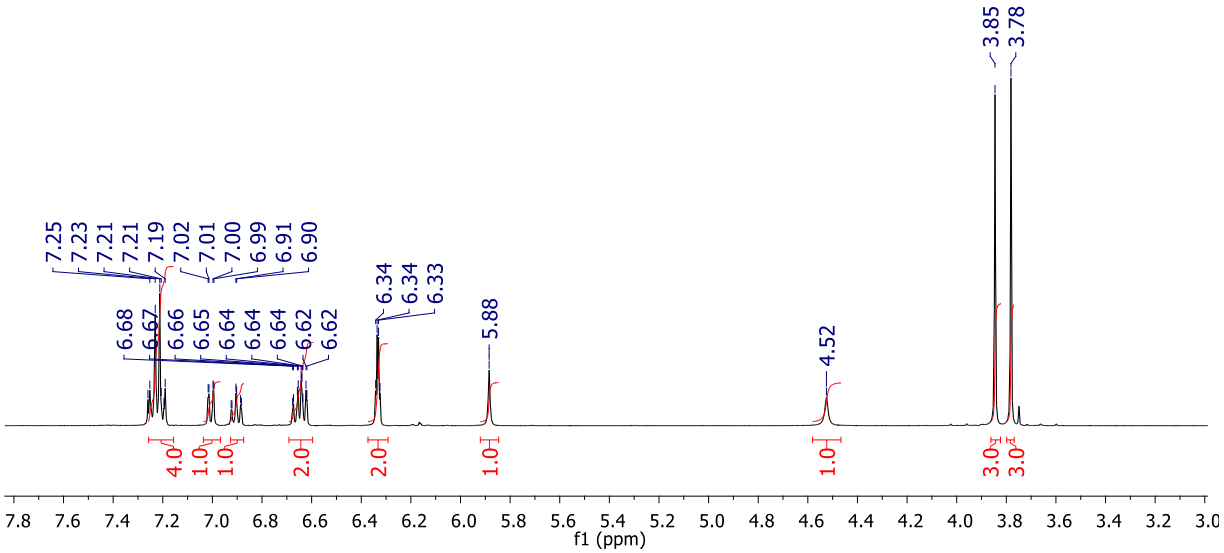
7.25
7.23
7.21
7.21
7.19
7.02
7.01
7.00
6.99
6.91
6.90
6.68
6.67
6.66
6.65
6.64
6.64
6.64
6.62
6.62
6.34
6.34
6.33
5.88
4.52
3.85
3.78
4.0
1.0
1.0
2.0
2.0
1.0
1.0
3.0
3.0
f1 (ppm)

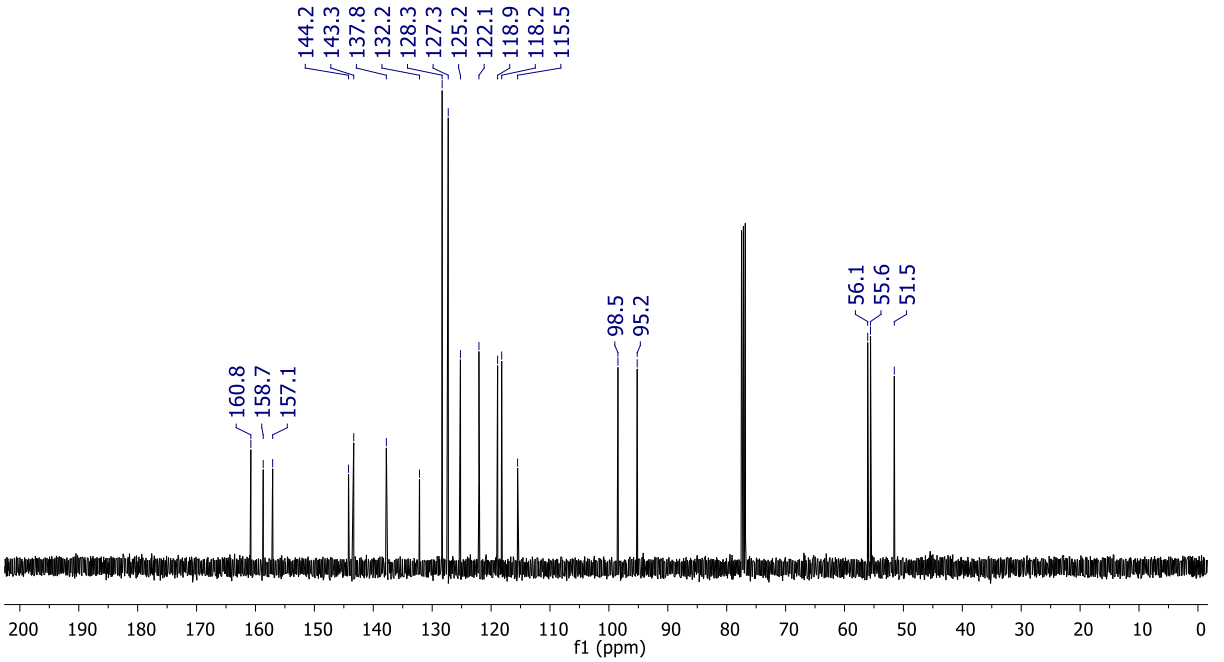
144.2
143.3
137.8
132.2
128.3
127.3
125.2
122.1
118.9
118.2
115.5
160.8
158.7
157.1
98.5
95.2
56.1
55.6
51.5
f1 (ppm)

References

1 L. Bernardi, M. Fochi, M. C. Franchini and A. Ricci, *Org. Biomol. Chem.*, 2012, **10**, 2911–2922.

2 J. Saeyad and B. List, *Org. Biomol. Chem.*, 2005, **3**, 719–724.

3 T. Akiyama, *Chem. Rev.*, 2007, **107**, 5744–5758.

4 M. Mahlau and B. List, *Angew. Chemie - Int. Ed.*, 2013, **52**, 518–533.

5 G. Zhan, W. Du and Y. C. Chen, *Chem. Soc. Rev.*, 2017, **46**, 1675–1692.

6 I. Agranat, H. Caner and J. Caldwell, *Nat. Rev. Drug Discov.*, 2002, 1, 753–768.

7 H. Caner, E. Groner, L. Levy and I. Agranat, *Drug Discov. Today*, 2004, 9, 105–110.

8 J. Alemán and S. Cabrera, *Chem. Soc. Rev.*, 2013, **42**, 774–793.

9 D. M. Walden, O. M. Ogba, R. C. Johnston and P. H. Y. Cheong, *Acc. Chem. Res.*, 2016, **49**, 1279–1291.

10 A. G. Doyle and E. N. Jacobsen, *Chem. Rev.*, 2007, **107**, 5713–5743.

11 M. S. Taylor and E. N. Jacobsen, *Angew. Chemie Int. Ed.*, 2006, **45**, 1520–1543.

12 T. Akiyama, J. Itoh, K. Yokota and K. Fuchibe, *Angew. Chemie - Int. Ed.*, 2004, **43**, 1566–1568.

13 D. Uraguchi and M. Terada, *J. Am. Chem. Soc.*, 2004, **126**, 5356–5357.

14 M. Yamanaka, J. Itoh, K. Fuchibe and T. Akiyama, *J. Am. Chem. Soc.*, 2007, **129**, 6756–6764.

15 I. D. Gridnev, M. Kouchi, K. Sorimachi and M. Terada, *Tetrahedron Lett.*, 2007, **48**, 497–500.

16 D. Parmar, E. Sugiono, S. Raja and M. Rueping, *Chem. Rev.*, 2014, **114**, 9047–9153.

17 M. Terada, *Chem. Commun.*, 2008, 4097.

18 A. Zamfir, S. Schenker, M. Freund and S. B. Tsogoeva, *Org. Biomol. Chem.*, 2010, **8**, 5262–5276.

19 J. M. M. Verkade, L. J. C. Van Hemert, P. J. L. M. Quaedflieg and F. P. J. T. Rutjes, *Chem. Soc. Rev.*, 2008, **37**, 29–41.

20 J. Shen and C. H. Tan, *Org. Biomol. Chem.*, 2008, **6**, 3229–3236.

21 F. E. Held, D. Grau and S. B. Tsogoeva, *Molecules*, 2015, **20**, 16103–16126.

22 J. Yu, F. Shi and L.-Z. Gong, *Acc. Chem. Res.*, 2011, **44**, 1156–1171.

23 M. Rueping, A. Kuenkel and I. Atodiresei, *Chem. Soc. Rev.*, 2011, **40**, 4539–4549.

24 S. J. Connon, *Angew. Chemie - Int. Ed.*, 2006, **45**, 3909–3912.

25 P. Renzi, J. Hioe and R. M. Gschwind, *Acc. Chem. Res.*, 2017, **50**, 2936–2948.

26 R. B. Sunoj, *Acc. Chem. Res.*, 2016, **49**, 1019–1028.

27 R. Maji, S. C. Mallojjala and S. E. Wheeler, *Chem. Soc. Rev.*, 2018, **47**, 1142–1158.

28 J. M. Brunel, *Chem. Rev.*, 2005, **105**, 857–897.

29 N. T. McDougal and S. E. Schaus, *J. Am. Chem. Soc.*, 2003, **125**, 12094–12095.

30 F. Xu, D. Huang, C. Han, W. Shen, X. Lin and Y. Wang, *J. Org. Chem.*, 2010, **75**, 8677–8680.

31 A. Rahman and X. Lin, *Org. Biomol. Chem.*, 2018, **16**, 4753–4777.

32 X. H. Chen, W. Q. Zhang and L. Z. Gong, *J. Am. Chem. Soc.*, 2008, **130**, 5652–5653.

33 L. He, X. H. Chen, D. N. Wang, S. W. Luo, W. Q. Zhang, J. Yu, L. Ren and L. Z. Gong, *J. Am. Chem. Soc.*, 2011, **133**, 13504–13518.

34 T. Akiyama, Y. Saitoh, H. Morita and K. Fuchibe, *Adv. Synth. Catal.*, 2005, **347**, 1523–1526.

35 Y. Huang, A. K. Unni, A. N. Thadani and V. H. Rawal, *Nature*, 2003, **424**, 146.

36 Z. Hassan, E. Spuling, D. M. Knoll, J. Lahann and S. Bräse, *Chem. Soc. Rev.*, 2018, **47**, 6947–6963.

37 E. Xie, S. Huang and X. Lin, *Org. Lett.*, 2019, **21**, 3682–3686.

38 V. B. Birman, A. L. Rheingold and K. C. Lam, *Tetrahedron Asymmetry*, 1999, **10**, 125–131.

39 Z. Zheng, Y. Cao, Q. Chong, Z. Han, J. Ding, C. Luo, Z. Wang, D. Zhu, Q. L. Zhou and K. Ding, *J. Am. Chem. Soc.*, 2018, **140**, 10374–10381.

40 G. Q. Chen, B. J. Lin, J. M. Huang, L. Y. Zhao, Q. S. Chen, S. P. Jia, Q. Yin and X. Zhang, *J. Am. Chem. Soc.*, 2018, **140**, 8064–8068.

41 W. Guo, Q. Liu, J. Jiang and J. Wang, *Org. Lett.*, 2020, **22**, 3110–3113.

42 K. Kaupmees, N. Tolstoluzhsky, S. Raja, M. Rueping and I. Leito, *Angew. Chemie - Int. Ed.*, 2013, **52**, 11569–11572.

43 D. Nakashima and H. Yamamoto, *J. Am. Chem. Soc.*, 2006, **128**, 9626–9627.

44 C. H. Cheon and H. Yamamoto, *Chem. Commun.*, 2011, **47**, 3043–3056.

45 T. Akiyama and K. Mori, *Chem. Rev.*, 2015, **115**, 9277–9306.

46 M. Rueping, B. J. Nachtsheim, W. Ieawsuwan and I. Atodiresei, *Angew. Chemie - Int. Ed.*, 2011, **50**, 6706–6720.

47 L. Ratjen, M. Van Gemmeren, F. Pesciaioli and B. List, *Angew. Chemie - Int. Ed.*, 2014, **53**, 8765–8769.

48 V. N. Wakchaure, P. S. J. Kaib, M. Leutzsch and B. List, *Angew. Chemie - Int. Ed.*, 2015, **54**, 11852–11856.

49 T. James, M. Van Gemmeren and B. List, *Chem. Rev.*, 2015, **115**, 9388–9409.

50 P. Christ, A. G. Lindsay, S. S. Vormittag, J. M. Neudörfl, A. Berkessel and A. C. O'Donoghue, *Chem. - A Eur. J.*, 2011, **17**, 8524–8528.

51 K. M. Diemoz and A. K. Franz, *J. Org. Chem.*, 2019, **84**, 1126–1138.

52 K. Rothermel, M. Melikian, J. Hioe, J. Greindl, J. Gramüller, M. Žabka, N. Sorgenfrei, T. Hausler, F. Morana

and R. M. Gschwind, *Chem. Sci.*, 2019, **10**, 10025–10034.

53 C. Yang, X. S. Xue, J. L. Jin, X. Li and J. P. Cheng, *J. Org. Chem.*, 2013, **78**, 7076–7085.

54 C. Yang, X. S. Xue, X. Li and J. P. Cheng, *J. Org. Chem.*, 2014, **79**, 4340–4351.

55 G. Caballero-García, G. Mondragón-Solórzano, R. Torres-Cadena, M. Díaz-García, J. Sandoval-Lira and J. Barroso-Flores, *Molecules*, 2018, **24**, 79.

56 J. Sandoval-Lira, G. Mondragón-Solórzano, L. I. Lugo-Fuentes and J. Barroso-Flores, *J. Chem. Inf. Model.*, 2020, **60**, 1445–1452.

57 R. S. Paton, J. M. Goodman and S. C. Pellegrinet, *Org. Lett.*, 2009, **11**, 37–40.

58 L. Simón and J. M. Goodman, *J. Am. Chem. Soc.*, 2009, **131**, 4070–4077.

59 L. Simón and J. M. Goodman, *J. Org. Chem.*, 2011, **76**, 1775–1788.

60 L. Simón and J. M. Goodman, *J. Org. Chem.*, 2010, **75**, 589–597.

61 M. N. Grayson, S. C. Pellegrinet and J. M. Goodman, *J. Am. Chem. Soc.*, 2012, **134**, 2716–2722.

62 M. N. Grayson and J. M. Goodman, *J. Am. Chem. Soc.*, 2013, **135**, 6142–6148.

63 M. N. Grayson and J. M. Goodman, *J. Org. Chem.*, 2013, **78**, 8796–8801.

64 M. N. Grayson and J. M. Goodman, *J. Org. Chem.*, 2015, **80**, 2056–2061.

65 L. M. Overvoorde, M. N. Grayson, Y. Luo and J. M. Goodman, *J. Org. Chem.*, 2015, **80**, 2634–2640.

66 J. P. Reid and J. M. Goodman, *J. Am. Chem. Soc.*, 2016, **138**, 7910–7917.

67 B. N. Falcone, M. N. Grayson and J. B. Rodriguez, *J. Org. Chem.*, 2018, **83**, 14683–14687.

68 T. Hashimoto, H. Nakatsu, K. Yamamoto and K. Maruoka, *J. Am. Chem. Soc.*, 2011, **133**, 9730–9733.

69 S. P. Bew, J. Liddle, D. L. Hughes, P. Pesce and S. M. Thurston, *Angew. Chemie - Int. Ed.*, 2017, **56**, 5322–5326.

70 D. Enders, A. Rembiak and M. Seppelt, *Tetrahedron Lett.*, 2013, **54**, 470–473.

71 J. F. Bai, H. Sasagawa, T. Yurino, T. Kano and K. Maruoka, *Chem. Commun.*, 2017, **53**, 8203–8206.

72 F. Zhou and H. Yamamoto, *Angew. Chemie - Int. Ed.*, 2016, **55**, 8970–8974.

73 Z. Wei, J. Zhang, H. Yang and G. Jiang, *Org. Lett.*, 2019, **21**, 2790–2794.

74 P. C. Knipe and M. D. Smith, *Org. Biomol. Chem.*, 2014, **12**, 5094–5097.

75 M. Klussmann, L. Ratjen, S. Hoffmann, V. Wakchaure, R. Goddard and B. List, *Synlett*, 2010, **2010**, 2189–2192.

76 M. Hatano, K. Moriyama, T. Maki and K. Ishihara, *Angew. Chemie Int. Ed.*, 2010, **49**, 3823–3826.

77 M. Terada and K. Kanomata, *Synlett*, 2011, **2011**, 1255–1258.

78 K. Mori, A. Miyake and T. Akiyama, *Chem. Lett.*, 2014, **43**, 137–139.

79 L. Simón and R. S. Paton, *J. Am. Chem. Soc.*, 2018, **140**, 5412–5420.

80 M. Rueping, B. J. Nachtsheim, R. M. Koenigs and W. Ieawsuwan, *Chem. - A Eur. J.*, 2010, **16**, 13116–13126.

81 A. Jolit, C. F. Dickinson, K. Kitamura, P. M. Walleser, G. P. A. Yap and M. A. Tius, *European J. Org. Chem.*, 2017, **2017**, 6067–6076.

82 Y. Hatanaka, S. Nantaku, Y. Nishimura, T. Otsuka and T. Sekikaw, *Chem. Commun.*, 2017, **53**, 8996–8999.

83 L. Villar, U. Uria, J. I. Martínez, L. Prieto, E. Reyes, L. Carrillo and J. L. Vicario, *Angew. Chemie - Int. Ed.*, 2017, **56**, 10535–10538.

84 S. Lee, P. S. J. Kaib and B. List, *Synlett*, 2017, **28**, 1478–1480.

85 P. S. J. Kaib, L. Schreyer, S. Lee, R. Properzi and B. List, *Angew. Chemie - Int. Ed.*, 2016, **55**, 13200–13203.

86 L. Liu, H. Kim, Y. Xie, C. Fares, P. S. J. Kaib, R. Goddard and B. List, *J. Am. Chem. Soc.*, 2017, **139**, 13656–13659.

87 L. L. Tolstikova, A. V. Bel'skikh and B. A. Shainyan, *Russ. J. Gen. Chem.*, 2010, **80**, 1258–1262.

88 L. L. Tolstikova, A. V. Bel'skikh and B. A. Shainyan, *Russ. J. Gen. Chem.*, 2009, **79**, 1752–1754.

89 E. Kasprzycka, V. A. Trush, V. M. Amirkhanov, L. Jerzykiewicz, O. L. Malta, J. Legendziewicz and P. Gawryszewska, *Chem. - A Eur. J.*, 2017, **23**, 1318–1330.

90 M. Shimizu, J. Kikuchi, A. Kondoh and M. Terada, *Chem. Sci.*, 2018, **9**, 5747–5757.

91 J. Kikuchi and M. Terada, *Angew. Chemie - Int. Ed.*, 2019, **58**, 8458–8462.

92 J. Kikuchi, Y. Aizawa and M. Terada, *Org. Chem. Front.*, 2020, 1383–1387.

93 A. Gade and N. Patil, *Synlett*, 2017, **28**, 1096–1100.

94 A. Borovika and P. Nagorny, *Tetrahedron*, 2013, **69**, 5719–5725.

95 J. Jacques and C. Fouquey, *Org. Synth.*, 1989, **67**, 1.

96 M. A. Berliner and K. Belecki, *J. Org. Chem.*, 2005, **70**, 9618–9621.

97 T. Gatzenmeier, P. S. J. Kaib, J. B. Lingnau, R. Goddard and B. List, *Angew. Chemie Int. Ed.*, 2018, **57**, 2464–2468.

98 S. Brenet, C. Minozzi, B. Clarens, L. Amiri and F. Berthiol, *Synthesis (Stuttg).*, 2015, **47**, 3859–3873.

99 N. Momiyama, H. Nishimoto and M. Terada, *Org. Lett.*, 2011, **13**, 2126–2129.

100 P. Q. Le, T. S. Nguyen and J. A. May, *Org. Lett.*, 2012, **14**, 6104–6107.

101 A. Jolit, C. F. Dickinson, K. Kitamura, P. M. Walleser, G. P. A. Yap and M. A. Tius, *European J. Org. Chem.*, 2017, **2017**, 6067–6076.

102 I. Čorić and B. List, *Nature*, 2012, **483**, 315–319.

103 L. Schreyer, R. Properzi and B. List, *Angew. Chemie - Int. Ed.*, 2019, **58**, 12761–12777.

104 S. Liao, I. Čorić, Q. Wang and B. List, *J. Am. Chem. Soc.*, 2012, **134**, 10765–10768.

105 J. H. Kim, I. Čorić, S. Vellalath and B. List, *Angew. Chemie Int. Ed.*, 2013, **52**, 4474–4477.

106 L. Liu, M. Leutzsch, Y. Zheng, M. W. Alachraf, W. Thiel and B. List, *J. Am. Chem. Soc.*, 2015, **137**, 13268–13271.

107 Y. Xie, G.-J. Cheng, S. Lee, P. S. J. Kaib, W. Thiel and B. List, *J. Am. Chem. Soc.*, 2016, **138**, 14538–14541.

108 S. Lee, P. S. J. Kaib and B. List, *J. Am. Chem. Soc.*, 2017, **139**, 2156–2159.

109 J. Kim, A. Tap, L. Liu and B. List, *Synlett*, 2016, **28**, 333–336.

110 L. Simón and R. S. Paton, *Org. Biomol. Chem.*, 2016, **14**, 3031–3039.

111 G. Jindal and R. B. Sunoj, *Angew. Chemie Int. Ed.*, 2014, **53**, 4432–4436.

112 D. M. Walden, O. M. Ogba, R. C. Johnston and P. H. Y. Cheong, *Acc. Chem. Res.*, 2016, **49**, 1279–1291.

113 R. B. Sunoj, *Acc. Chem. Res.*, 2016, **49**, 1019–1028.

114 L. M. Overvoorde, M. N. Grayson, Y. Luo and J. M. Goodman, *J. Org. Chem.*, 2015, **80**, 2634–2640.

115 J. P. Reid, L. Simón and J. M. Goodman, *Acc. Chem. Res.*, 2016, **49**, 1029–1041.

116 M. N. Grayson, S. C. Pellegrinet and J. M. Goodman, *J. Am. Chem. Soc.*, 2012, **134**, 2716–2722.

117 T. A. Halgren, *J. Comput. Chem.*, 1996, **17**, 490–519.

118 E. Harder, W. Damm, J. Maple, C. Wu, M. Reboul, J. Y. Xiang, L. Wang, D. Lupyan, M. K. Dahlgren, J. L. Knight, J. W. Kaus, D. S. Cerutti, G. Krilov, W. L. Jorgensen, R. Abel and R. A. Friesner, *J. Chem. Theory Comput.*, 2016, **12**, 281–296.

119 A. D. Becke, *J. Chem. Phys.*, 1993, **98**, 5648–5652.

120 C. Lee, W. Yang and R. G. Parr, *Phys. Rev. B*, 1988, **37**, 785–789.

121 Y. Zhao and D. G. Truhlar, *Theor. Chem. Acc.*, 2008, **120**, 215–241.

122 G. B. Rowland, E. B. Rowland, Y. Liang, J. A. Perman and J. C. Antilla, *Org. Lett.*, 2007, **9**, 2609–2611.

123 J. Itoh, K. Fuchibe and T. Akiyama, *Angew. Chemie Int. Ed.*, 2008, **47**, 4016–4018.

124 K. Mori, M. Wakazawa and T. Akiyama, *Chem. Sci.*, 2014, **5**, 1799–1803.

125 R. I. Storer, D. E. Carrera, Y. Ni and D. W. C. MacMillan, *J. Am. Chem. Soc.*, 2006, **128**, 84–86.

126 I. A. Khan and A. K. Saxena, *J. Org. Chem.*, 2013, **78**, 11656–11669.

127 B. Westermann, *Angew. Chemie Int. Ed.*, 2003, **42**, 151–153.

128 T. Akiyama, T. Suzuki and K. Mori, *Org. Lett.*, 2009, **11**, 2445–2447.

129 N. Li, X.-H. Chen, J. Song, S.-W. Luo, W. Fan and L.-Z. Gong, *J. Am. Chem. Soc.*, 2009, **131**, 15301–

15310.

130 K. Maruoka, T. Itoh, Y. Araki, T. Shirasaka and H. Yamamoto, *Bull. Chem. Soc. Jpn.*, 1988, **61**, 2975–2976.

131 N. Momiyama, Y. Yamamoto and H. Yamamoto, *J. Am. Chem. Soc.*, 2007, **129**, 1190–1195.

132 H. N. Nguyen, H. Lee, S. Audörsch, A. L. Reznichenko, A. J. Nawara-Hultzsch, B. Schmidt and K. C. Hultzsch, *Organometallics*, 2018, **37**, 4358–4379.

133 L.-Z. Gong and L. Pu, *Tetrahedron Lett.*, 2000, **41**, 2327–2331.

134 Y. (Andy) Xu, G. C. Clarkson, G. Docherty, C. L. North, G. Woodward and M. Wills, *J. Org. Chem.*, 2005, **70**, 8079–8087.

135 S. Munusamy and S. Kulathu Iyer, *Tetrahedron: Asymmetry*, 2016, **27**, 492–497.

136 N. Momiyama, H. Tabuse, H. Noda, M. Yamanaka, T. Fujinami, K. Yamanishi, A. Izumiseki, K. Funayama, F. Egawa, S. Okada, H. Adachi and M. Terada, *J. Am. Chem. Soc.*, 2016, **138**, 11353–11359.

137 W. Hu, J. Zhou, X. Xu, W. Liu and L. Gong, *Org. Synth.*, 2011, **88**, 406–417.

138 A. L. Reznichenko and K. C. Hultzsch, *Organometallics*, 2013, **32**, 1394–1408.

139 R. K. Akhani, M. I. Moore, J. G. Pribyl and S. L. Wiskur, *J. Org. Chem.*, 2014, **79**, 2384–2396.

140 A. Bartoszewicz, M. Kalek, J. Nilsson, R. Hiresova and J. Stawinski, *Synlett*, 2008, **2008**, 37–40.

141 T. R. Wu, L. Shen and J. M. Chong, *Org. Lett.*, 2004, **6**, 2701–2704.

142 E. J. Corey, H. Cho, C. Rücker and D. H. Hua, *Tetrahedron Lett.*, 1981, **22**, 3455–3458.

143 L. Simón and J. M. Goodman, *J. Am. Chem. Soc.*, 2008, **130**, 8741–8747.

144 N. Chéron, D. Jacquemin and P. Fleurat-Lessard, *Phys. Chem. Chem. Phys.*, 2012, **14**, 7170–7175.

145 L. Simón and J. M. Goodman, *Org. Biomol. Chem.*, 2011, **9**, 689–700.

146 R. Kargbo, Y. Takahashi, S. Bhor, G. R. Cook, G. C. Lloyd-Jones and I. R. Shepperson, *J. Am. Chem. Soc.*, 2007, **129**, 3846–3847.

147 G. Huang, Z. Yin and X. Zhang, *Chem. - A Eur. J.*, 2013, **19**, 11992–11998.

148 C. Börner, M. R. Dennis, E. Sinn and S. Woodward, *European J. Org. Chem.*, 2001, **2001**, 2435–2446.

149 M. Á. Fernández-Ibáñez, B. Maciá, M. G. Pizzuti, A. J. Minnaard and B. L. Feringa, *Angew. Chemie Int. Ed.*, 2009, **48**, 9339–9341.

150 J. Aydin, K. S. Kumar, M. J. Sayah, O. A. Wallner and K. J. Szabó, *J. Org. Chem.*, 2007, **72**, 4689–4697.

151 S. Lou and S. E. Schaus, *J. Am. Chem. Soc.*, 2008, **130**, 6922–6923.

152 J. Long, J. Hu, X. Shen, J. Baoming and K. Ding, *J. Am. Chem. Soc.*, 2002, **124**, 10–11.

153 J. P. H. Charmant, A. M. Dyke and G. C. Lloyd-Jones, *Chem. Commun.*, 2003, 380–381.

154 A. Kamimura, T. Nokubi, R. Watanabe, M. Ishikawa, K. Nasu, H. Uno and M. Sumimoto, *J. Org. Chem.*,

2014, **79**, 1068–1083.

155 C. Börner, M. R. Dennis, E. Sinn and S. Woodward, *European J. Org. Chem.*, 2001, **2001**, 2435–2446.

156 F. Beaulieu and V. Snieckus, *J. Org. Chem.*, 1994, **59**, 6508–6509.

157 X. Li, J. B. Hewgley, C. A. Mulrooney, J. Yang and M. C. Kozlowski, *J. Org. Chem.*, 2003, **68**, 5500–5511.

158 Y.-L. Hsu, C.-C. Yang, T.-C. Chou, C.-H. Tai, L.-Y. Chen, S.-L. Fu, J.-J. Lin and L.-C. Lo, *Tetrahedron*, 2016, **72**, 58–68.

159 L. Matesic, N. A. Wyatt, B. H. Fraser, M. P. Roberts, T. Q. Pham and I. Greguric, *J. Org. Chem.*, 2013, **78**, 11262–11270.

160 H. Liu and X. Jiang, *Chem. - An Asian J.*, 2013, **8**, 2546–2563.

161 C. Christophersen and U. Anthoni, *Sulfur reports*, 1986, **4**, 365–442.

162 C.-S. Jiang, W. E. G. Müller, H. C. Schröder and Y.-W. Guo, *Chem. Rev.*, 2012, **112**, 2179–2207.

163 N. Wang, P. Saidhareddy and X. Jiang, *Nat. Prod. Rep.*, 2020, **37**, 246–275.

164 M. Feng, B. Tang, S. H. Liang and X. Jiang, *Curr. Top. Med. Chem.*, 2016, **16**, 1200–16.

165 M. A. Abdalla and K. H. Mühling, *J. Appl. Bot. Food Qual.*, 2019, **92**, 204–215.

166 S. Brigg, N. Pribut, A. E. Basson, M. Avgenikos, R. Venter, M. A. Blackie, W. A. L. van Otterlo and S. C. Pelly, *Bioorg. Med. Chem. Lett.*, 2016, **26**, 1580–1584.

167 Y. Su, J.-B. Ling, S. Zhang and P.-F. Xu, *J. Org. Chem.*, 2013, **78**, 11053–11058.

168 A. Bertamino, M. Soprano, S. Musella, M. R. Rusciano, M. Sala, E. Vernieri, V. Di Sarno, A. Limatola, A. Carotenuto, S. Cosconati, P. Grieco, E. Novellino, M. Illario, P. Campiglia and I. Gomez-Monterrey, *J. Med. Chem.*, 2013, **56**, 5407–5421.

169 K. Arya, P. Tomar and J. Singh, *RSC Adv.*, 2014, **4**, 3060–3064.

170 V. V. Vintonyak, K. Warburg, H. Kruse, S. Grimme, K. Hübel, D. Rauh and H. Waldmann, *Angew. Chemie Int. Ed.*, 2010, **49**, 5902–5905.

171 J.-S. Yu, H.-M. Huang, P.-G. Ding, X.-S. Hu, F. Zhou and J. Zhou, *ACS Catal.*, 2016, **6**, 5319–5344.

172 R. Rios, H. Sundén, I. Ibrahem, G.-L. Zhao and A. Córdova, *Tetrahedron Lett.*, 2006, **47**, 8679–8682.

173 X. Tian, Y. Liu and P. Melchiorre, *Angew. Chemie Int. Ed.*, 2012, **51**, 6439–6442.

174 S. E. Denmark, S. Rossi, M. P. Webster and H. Wang, *J. Am. Chem. Soc.*, 2014, **136**, 13016–13028.

175 K. Liao, F. Zhou, J.-S. Yu, W.-M. Gao and J. Zhou, *Chem. Commun.*, 2015, **51**, 16255–16258.

176 M. Ding, F. Zhou, Y.-L. Liu, C.-H. Wang, X.-L. Zhao and J. Zhou, *Chem. Sci.*, 2011, **2**, 2035.

177 X. Hong, H. B. Küçük, M. S. Maji, Y. F. Yang, M. Rueping and K. N. Houk, *J. Am. Chem. Soc.*, 2014, **136**, 13769–13780.

178 C. Beceño, P. Chauhan, A. Rembiak, A. Wang and D. Enders, *Adv. Synth. Catal.*, 2015, **357**, 672–676.

179 D. Qian, L. Wu, Z. Lin and J. Sun, *Nat. Commun.*, 2017, **8**, 1–9.

180 L. Zhang, Y. Han, A. Huang, P. Zhang, P. Li and W. Li, *Org. Lett.*, 2019, **21**, 7415–7419.

181 L. A. McAllister, S. Brand, R. de Gentile and D. J. Procter, *Chem. Commun.*, 2003, 2380–2381.

182 L. A. McAllister, R. A. McCormick, S. Brand and D. J. Procter, *Angew. Chemie Int. Ed.*, 2005, **44**, 452–455.

183 L. A. McAllister, R. A. McCormick, K. M. James, S. Brand, N. Willetts and D. J. Procter, *Chem. - A Eur. J.*, 2007, **13**, 1032–1046.

184 M. Miller, W. Tsang, A. Merritt and D. J. Procter, *Chem. Commun.*, 2007, 498–500.

185 M. Miller, J. C. Vogel, W. Tsang, A. Merrit and D. J. Procter, *Org. Biomol. Chem.*, 2009, **7**, 589–597.

186 L. H. S. Smith, T. T. Nguyen, H. F. Sneddon and D. J. Procter, *Chem. Commun.*, 2011, **47**, 10821–10823.

187 L. H. S. Smith, S. C. Coote, H. F. Sneddon and D. J. Procter, *Angew. Chemie Int. Ed.*, 2010, **49**, 5832–5844.

188 J. H. Kim, A. Tap, L. Liu and B. List, *Synlett*, 2017, **28**, 333–336.

189 G. N. Sakhabutdinova, G. Z. Raskil'dina, I. P. Baikova, S. S. Zlotskii and R. M. Sultanova, *Chem. Heterocycl. Compd.*, 2019, **55**, 1222–1227.

190 K. K. Rana, C. Guin, S. Jana and S. C. Roy, *Tetrahedron Lett.*, 2003, **44**, 8597–8599.

191 R. Ballini, G. Bosica, R. Maggi, A. Mazzacani, P. Righi and G. Sartori, *Synthesis (Stuttg).*, 2001, **2001**, 1826–1829.

192 A. Kumar, N. Jain, S. Rana and S. Chauhan, *Synlett*, 2004, **2004**, 2785–2787.

193 H. Firouzabadi, N. Iranpoor, A. A. Jafari and M. R. Jafari, *J. Mol. Catal. A Chem.*, 2006, **247**, 14–18.

194 H. Alinezhad and S. Fallahi, *Chinese Chem. Lett.*, 2012, **23**, 927–929.

195 V. T. Kamble, B. P. Bandgar, D. B. Muley and N. S. Joshi, *J. Mol. Catal. A Chem.*, 2007, **268**, 70–75.

196 F. Shirini, P. Sadeghzadeh and M. Abedini, *Chinese Chem. Lett.*, 2009, **20**, 1457–1460.

197 B. Karimi and L. Ma'mani, *Synthesis (Stuttg).*, 2003, **2003**, 2503–2506.

198 F. Shirini, S. K. Mirhashemi, A. Pourvali and M. Abedini, *Chinese Chem. Lett.*, 2011, **22**, 421–423.

199 M. Shamma and W. A. Slusarchyk, *Chem. Rev.*, 1964, **64**, 59–79.

200 J. Kim and M. Movassaghi, *Chem. Soc. Rev.*, 2009, **38**, 3035–3050.

201 S. QIU, H. SUN, A.-H. ZHANG, H.-Y. XU, G.-L. YAN, Y. HAN and X.-J. WANG, *Chin. J. Nat. Med.*, 2014, **12**, 401–406.

202 J. A. Joule, *Adv. Heterocycl. Chem.*, 2016, **119**, 81–106.

203 N. Kerru, L. Gummidi, S. Maddila, K. K. Gangu and S. B. Jonnalagadda, *Molecules*, 2020, **25**, 1909.

204 Y. Shen, W.-J. Liang, Y.-N. Shi, E. J. Kennelly and D.-K. Zhao, *Nat. Prod. Rep.*, 2020, **37**, 763–796.

205 D. C. Blakemore, L. Castro, I. Churcher, D. C. Rees, A. W. Thomas, D. M. Wilson and A. Wood, *Nat. Chem.*, 2018, **10**, 383–394.

206 H. Waldmann, in *Organic Synthesis Highlights II*, Wiley-VCH Verlag GmbH, Weinheim, Germany, 1995, pp. 37–47.

207 M.-H. Cao, N. J. Green and S.-Z. Xu, *Org. Biomol. Chem.*, 2017, **15**, 3105–3129.

208 S. Yao, S. Saaby, R. G. Hazell and K. A. Jørgensen, *Chem. - A Eur. J.*, 2000, **6**, 2435–2448.

209 P. D. Bailey, P. D. Smith, F. Pederson, W. Clegg, G. M. Rosair and S. J. Teat, *Tetrahedron Lett.*, 2002, **43**, 1067–1070.

210 H. Sundén, I. Ibrahem, L. Eriksson and A. Córdova, *Angew. Chemie Int. Ed.*, 2005, **44**, 4877–4880.

211 V. Eschenbrenner-Lux, P. Küchler, S. Ziegler, K. Kumar and H. Waldmann, *Angew. Chemie Int. Ed.*, 2014, **53**, 2134–2137.

212 Y. Deng, S. Kumar, K. Wheeler and H. Wang, *Chem. - A Eur. J.*, 2015, **21**, 7874–7880.

213 Y. Li, C. Barløse, J. Jørgensen, B. D. Carlsen and K. A. Jørgensen, *Chem. - A Eur. J.*, 2017, **23**, 38–41.

214 J. Yu, F. Shi and L.-Z. Gong, *Acc. Chem. Res.*, 2011, **44**, 1156–1171.

215 T. Akiyama, Y. Tamura, J. Itoh, H. Morita and K. Fuchibe, *Synlett*, 2006, **2006**, 0141–0143.

216 J. Itoh, K. Fuchibe and T. Akiyama, *Angew. Chemie Int. Ed.*, 2006, **45**, 4796–4798.

217 C. Beceño, T. Krappitz, G. Raabe and D. Enders, *Synthesis (Stuttg).*, 2015, **47**, 3813–3821.

218 T. Akiyama, H. Morita and K. Fuchibe, *J. Am. Chem. Soc.*, 2006, **128**, 13070–13071.

219 L. He, M. Bekkaye, P. Retailleau and G. Masson, *Org. Lett.*, 2012, **14**, 3158–3161.

220 L. He, G. Laurent, P. Retailleau, B. Folléas, J.-L. Brayer and G. Masson, *Angew. Chemie Int. Ed.*, 2013, **52**, 11088–11091.

221 Z. Chen, B. Wang, Z. Wang, G. Zhu and J. Sun, *Angew. Chemie Int. Ed.*, 2013, **52**, 2027–2031.

222 L. Z. Li, C. S. Wang, W. F. Guo, G. J. Mei and F. Shi, *J. Org. Chem.*, 2018, **83**, 614–623.

223 F. Bartoccini, M. Mari, M. Retini, S. Bartolucci and G. Piersanti, *J. Org. Chem.*, 2018, **83**, 12275–12283.

224 H. H. Liao, C. C. Hsiao, I. Atodiresei and M. Rueping, *Chem. - A Eur. J.*, 2018, **24**, 7718–7723.

225 M. Kretzschmar, F. Hofmann, D. Moock and C. Schneider, *Angew. Chemie - Int. Ed.*, 2018, **57**, 4774–4778.

226 P. Buonora, J.-C. Olsen and T. Oh, *Tetrahedron*, 2001, **57**, 6099–6138.

227 K. A. Jørgensen, *Angew. Chemie Int. Ed.*, 2000, **39**, 3558–3588.

228 P. A. Grieco and M. D. Kaufman, *J. Org. Chem.*, 1999, **64**, 7586–7593.

229 P. A. Grieco and M. D. Kaufman, *J. Org. Chem.*, 1999, **64**, 6041–6048.

230 N. T. Tam, E.-J. Jung and C.-G. Cho, *Org. Lett.*, 2010, **12**, 2012–2014.

231 S. D. Larsen and P. A. Grieco, *J. Am. Chem. Soc.*, 1985, **107**, 1768–1769.

232 M. G. Memeo and P. Quadrelli, *Chem. - A Eur. J.*, 2012, **18**, 12554–12582.

233 M. A. McCarrick, Y. D. Wu and K. N. Houk, *J. Org. Chem.*, 1993, **58**, 3330–3343.

234 Y. Sook Park, B.-S. Lee and I. Lee, *New J. Chem.*, 1999, **23**, 707–715.

235 A. Whiting and C. M. Windsor, *Tetrahedron*, 1998, **54**, 6035–6050.

236 R. G. Iafe and K. N. Houk, *J. Org. Chem.*, 2008, **73**, 2679–2686.

237 A. G. Ross, X. Li and S. J. Danishefsky, *J. Am. Chem. Soc.*, 2012, **134**, 16080–16084.

238 L. I. Willems, M. Verdoes, B. I. Florea, G. A. van der Marel and H. S. Overkleeft, *ChemBioChem*, 2010, **11**, 1769–1781.

239 J. I. Levin, E. Turos and S. M. Weinreb, *Synth. Commun.*, 1982, **12**, 989–993.

240 S. Hong and T. J. Marks, *J. Am. Chem. Soc.*, 2002, **124**, 7886–7887.

241 S. Hong, A. M. Kawaoka and T. J. Marks, *J. Am. Chem. Soc.*, 2003, **125**, 15878–15892.

242 P. D. Bailey, P. D. Smith, F. Pederson, W. Clegg, G. M. Rosair and S. J. Teat, *Tetrahedron Lett.*, 2002, **43**, 1067–1070.

243 R. W. Layer, *Chem. Rev.*, 1963, **63**, 489–510.

244 C. Godoy-Alcántar, A. K. Yatsimirsky and J.-M. Lehn, *J. Phys. Org. Chem.*, 2005, **18**, 979–985.

245 I. Bosque, E. Bagdatli, F. Foubelo and J. C. Gonzalez-Gomez, *J. Org. Chem.*, 2014, **79**, 1796–1804.

246 L. J. Peterson and J. P. Wolfe, *Adv. Synth. Catal.*, 2015, **357**, 2339–2344.

247 M. C. Pirrung, M. Wedel and Y. Zhao, *Synlett*, 2002, **2002**, 0143–0145.

248 M. C. Pirrung, Y. R. Lee, K. Park and J. B. Springer, *J. Org. Chem.*, 1999, **64**, 5042–5047.

249 A. Howarth, K. Ermanis and J. M. Goodman, *Chem. Sci.*, 2020, **11**, 4351–4359.

250 S. G. Smith and J. M. Goodman, *J. Am. Chem. Soc.*, 2010, **132**, 12946–12959.

251 K. Ermanis, K. E. B. Parkes, T. Agback and J. M. Goodman, *Org. Biomol. Chem.*, 2016, **14**, 3943–3949.

252 K. Ermanis, K. E. B. Parkes, T. Agback and J. M. Goodman, *Org. Biomol. Chem.*, 2017, **15**, 8998–9007.

253 K. Ermanis, K. E. B. Parkes, T. Agback and J. M. Goodman, *Org. Biomol. Chem.*, 2019, **17**, 5886–5890.

254 A. Pictet and T. Spengler, *Berichte der Dtsch. Chem. Gesellschaft*, 1911, **44**, 2030–2036.

255 J. Stöckigt, A. P. Antonchick, F. Wu and H. Waldmann, *Angew. Chemie Int. Ed.*, 2011, **50**, 8538–8564.

256 M. M Heravi, V. Zadsirjan and M. Malmir, *Molecules*, 2018, **23**, 943.

257 A. Calcaterra, L. Mangiardi, G. Delle Monache, D. Quaglio, S. Balducci, S. Berardozzi, A. Iazzetti, R. Franzini, B. Botta and F. Ghirga, *Molecules*, 2020, **25**, 414.

258 M. S. Taylor and E. N. Jacobsen, *J. Am. Chem. Soc.*, 2004, **126**, 10558–10559.

259 I. T. Raheem, P. S. Thiara, E. A. Peterson and E. N. Jacobsen, *J. Am. Chem. Soc.*, 2007, **129**, 13404–13405.

260 R. S. Klausen and E. N. Jacobsen, *Org. Lett.*, 2009, **11**, 887–890.

261 Y. Lee, R. S. Klausen and E. N. Jacobsen, *Org. Lett.*, 2011, **13**, 5564–5567.

262 R. S. Klausen, C. R. Kennedy, A. M. Hyde and E. N. Jacobsen, *J. Am. Chem. Soc.*, 2017, **139**, 12299–12309.

263 J. Seayad, A. M. Seayad and B. List, *J. Am. Chem. Soc.*, 2006, **128**, 1086–1087.

264 N. V. Sewgobind, M. J. Wanner, S. Ingemann, R. de Gelder, J. H. van Maarseveen and H. Hiemstra, *J. Org. Chem.*, 2008, **73**, 6405–6408.

265 M. E. Muratore, C. A. Holloway, A. W. Pilling, R. I. Storer, G. Trevitt and D. J. Dixon, *J. Am. Chem. Soc.*, 2009, **131**, 10796–10797.

266 A. S. K. Hashmi and C. Hubbert, *Angew. Chemie Int. Ed.*, 2010, **49**, 1010–1012.

267 Z. Chen and D. L. J. Clive, *J. Org. Chem.*, 2010, **75**, 7014–7017.

268 N. Kaur, *Synth. Commun.*, 2019, **49**, 617–661.

269 E. K. Davison and J. Sperry, *J. Nat. Prod.*, 2017, **80**, 3060–3079.

270 S. K. Sharma, S. Sharma, P. K. Agarwal and B. Kundu, *European J. Org. Chem.*, 2009, **2009**, 1309–1312.

271 X. Li, D. Chen, H. Gu and X. Lin, *Chem. Commun.*, 2014, **50**, 7538–7541.

272 A. Rahman, E. Xie and X. Lin, *Org. Biomol. Chem.*, 2018, **16**, 1367–1374.

273 S. G. Wang, L. Han, M. Zeng, F. L. Sun, W. Zhang and S. L. You, *Org. Biomol. Chem.*, 2012, **10**, 3202–3209.

274 E. Aranzamendi, N. Sotomayor and E. Lete, *ACS Omega*, 2017, **2**, 2706–2718.

275 C. A. Merlic, C. C. Aldrich, J. Albaneze-Walker, A. Saghatelian and J. Mammen, *J. Org. Chem.*, 2001, **66**, 1297–1309.

276 S. Combes and J.-P. Finet, *Synth. Commun.*, 1997, **27**, 3769–3778.

277 M. Al-Sanea, M. Ali Khan, A. Abdelazem, S. Lee, P. Mok, M. Gamal, M. Shaker, M. Afzal, B. Youssif and N. Omar, *Molecules*, 2018, **23**, 297.

278 J. Lv and S. Luo, *Chem. Commun.*, 2013, **49**, 847–858.

279 A. Sinibaldi, V. Nori, A. Baschieri, F. Fini, A. Arcadi and A. Carlone, *Catalysts*, 2019, **9**, 928.

280 L. Simón and R. S. Paton, *J. Am. Chem. Soc.*, 2018, **140**, 5412–5420.

281 A. Parra, S. Reboredo, A. M. Martín Castro and J. Alemán, *Org. Biomol. Chem.*, 2012, **10**, 5001.

282 J. Lv, L. Zhang, S. Hu, J.-P. Cheng and S. Luo, *Chem. - A Eur. J.*, 2012, **18**, 799–803.

283 S. Li, J. Lv and S. Luo, *Org. Chem. Front.*, 2018, **5**, 1787–1791.

284 J. B. Sweeney, in *Aziridines and Epoxides in Organic Synthesis*, Wiley-VCH Verlag GmbH & Co. KGaA, Weinheim, FRG, 2006, pp. 117–144.

285 L. Degennaro, P. Trinchera and R. Luisi, *Chem. Rev.*, 2014, 114, 7881–7929.

286 H. Pellissier, *Adv. Synth. Catal.*, 2014, 356, 1899–1935.

287 J. M. de los Santos, A. M. Ochoa de Retana, E. Martínez de Marigorta, J. Vicario and F. Palacios, *ChemCatChem*, 2018, **10**, 5092–5114.

288 T. Akiyama, T. Suzuki and K. Mori, *Org. Lett.*, 2009, **11**, 2445–2447.

289 X. Zeng, X. Zeng, Z. Xu, M. Lu and G. Zhong, *Org. Lett.*, 2009, **11**, 3036–3039.

290 T. Hashimoto, H. Nakatsu, K. Yamamoto and K. Maruoka, *J. Am. Chem. Soc.*, 2011, **133**, 9730–9733.

291 L. Simón and J. M. Goodman, *J. Org. Chem.*, 2011, **76**, 1775–1788.

292 J. P. Reid and J. M. Goodman, *Chem. - A Eur. J.*, 2017, **23**, 14248–14260.

293 J. P. Reid, K. Ermanis and J. M. Goodman, *Chem. Commun.*, 2019, **55**, 1778–1781.

294 T. L. Troyer, H. Muchalski, K. B. Hong and J. N. Johnston, *Org. Lett.*, 2011, **13**, 1790–1792.

295 J. E. Johnson, N. M. Morales, A. M. Gorczyca, D. D. Dolliver and M. A. McAllister, *J. Org. Chem.*, 2001, **66**, 7979–7985.

296 M. E. Belowich and J. F. Stoddart, *Chem. Soc. Rev.*, 2012, **41**, 2003–2024.

297 J. Bjørgo, D. R. Boyd, C. G. Watson, W. B. Jennings and D. M. Jerina, *J. Chem. Soc. Perkin Trans. 2*, 1974, 1081–1084.

298 G. A. Jeffrey, *Crystallogr. Rev.*, 2003, **9**, 135–176.

299 J. P. Reid and J. M. Goodman, *Org. Biomol. Chem.*, 2017, **15**, 6943–6947.

300 L. Simón and J. M. Goodman, *J. Org. Chem.*, 2010, **75**, 1831–1840.

301 M. N. Grayson, S. C. Pellegrinet and J. M. Goodman, *J. Am. Chem. Soc.*, 2012, **134**, 2716–2722.

302 M. N. Grayson and J. M. Goodman, *J. Am. Chem. Soc.*, 2013, **135**, 6142–6148.

303 M. N. Grayson, M. J. Krische and K. N. Houk, *J. Am. Chem. Soc.*, 2015, **137**, 8838–8850.

304 M. N. Grayson, Z. Yang and K. N. Houk, *J. Am. Chem. Soc.*, 2017, **139**, 7717–7720.

305 B. N. Falcone, M. N. Grayson and J. B. Rodriguez, *J. Org. Chem.*, 2018, **83**, 14683–14687.

306 L. W. Chung, W. M. C. Sameera, R. Ramozzi, A. J. Page, M. Hatanaka, G. P. Petrova, T. V. Harris, X. Li, Z. Ke, F. Liu, H. B. Li, L. Ding and K. Morokuma, *Chem. Rev.*, 2015, 115, 5678–5796.

307 F. M. Bickelhaupt and K. N. Houk, *Angew. Chemie - Int. Ed.*, 2017, 56, 10070–10086.

308 P. Yu, Z. Yang, Y. Liang, X. Hong, Y. Li and K. N. Houk, *J. Am. Chem. Soc.*, 2016, **138**, 8247–8252.

309 J. P. Lovie-Toon, C. M. Tram, B. L. Flynn and E. H. Krenske, *ACS Catal.*, 2017, **7**, 3466–3476.

310 L. Simón and J. M. Goodman, *J. Am. Chem. Soc.*, 2009, **131**, 4070–4077.

311 F. Mohamadi, N. G. J. Richards, W. C. Guida, R. Liskamp, M. Lipton, C. Caufield, G. Chang, T. Hendrickson and W. C. Still, *J. Comput. Chem.*, 1990, **11**, 440–467.

312 G. Chang, W. C. Guida and W. C. Still, *J. Am. Chem. Soc.*, 1989, **111**, 4379–4386.

313 M. J. Frisch, G. W. Trucks, H. B. Schlegel, G. E. Scuseria, M. a. Robb, J. R. Cheeseman, G. Scalmani, V. Barone, G. a. Petersson, H. Nakatsuji, X. Li, M. Caricato, a. V. Marenich, J. Bloino, B. G. Janesko, R. Gomperts, B. Mennucci, H. P. Hratchian, J. V. Ortiz, a. F. Izmaylov, J. L. Sonnenberg, Williams, F. Ding, F. Lipparini, F. Egidi, J. Goings, B. Peng, A. Petrone, T. Henderson, D. Ranasinghe, V. G. Zakrzewski, J. Gao, N. Rega, G. Zheng, W. Liang, M. Hada, M. Ehara, K. Toyota, R. Fukuda, J. Hasegawa, M. Ishida, T. Nakajima, Y. Honda, O. Kitao, H. Nakai, T. Vreven, K. Throssell, J. a. Montgomery Jr., J. E. Peralta, F. Ogliaro, M. J. Bearpark, J. J. Heyd, E. N. Brothers, K. N. Kudin, V. N. Staroverov, T. a. Keith, R. Kobayashi, J. Normand, K. Raghavachari, a. P. Rendell, J. C. Burant, S. S. Iyengar, J. Tomasi, M. Cossi, J. M. Millam, M. Klene, C. Adamo, R. Cammi, J. W. Ochterski, R. L. Martin, K. Morokuma, O. Farkas, J. B. Foresman and D. J. Fox, 2016, Gaussian 16, Revision A.01, Gaussian, Inc., Wallin.

314 K. Fukui, *Acc. Chem. Res.*, 1981, **14**, 363–368.

315 R. Dennington, T. A. Keith and J. M. Millam, 2016, GaussView, Version 6, Semichem Inc. Shawnee Missio.

316 C. Y. Legault, 2009, CYLview, 1.0b.

317 J. Da Chai and M. Head-Gordon, *Phys. Chem. Chem. Phys.*, 2008, **10**, 6615–6620.

318 R. Ditchfield, W. J. Hehre and J. A. Pople, *J. Chem. Phys.*, 1971, **54**, 720–723.

319 F. Weigend and R. Ahlrichs, *Phys. Chem. Chem. Phys.*, 2005, **7**, 3297–3305.

320 A. Armstrong, R. A. Boto, P. Dingwall, J. Contreras-García, M. J. Harvey, N. J. Mason and H. S. Rzepa, *Chem. Sci.*, 2014, **5**, 2057–2071.

321 Y. Minenkov, Å. Singstad, G. Occhipinti and V. R. Jensen, *Dalt. Trans.*, 2012, **41**, 5526–5541.

322 S. Dapprich, I. Komáromi, K. S. Byun, K. Morokuma and M. J. Frisch, *J. Mol. Struct. THEOCHEM*, 1999, **461**–**462**, 1–21.

323 T. Vreven, K. Morokuma, Ö. Farkas, H. B. Schlegel and M. J. Frisch, *J. Comput. Chem.*, 2003, **24**, 760–769.

324 L. W. Chung, H. Hirao, X. Li and K. Morokuma, *Wiley Interdiscip. Rev. Comput. Mol. Sci.*, 2012, 2, 327–350.

325 A. K. Rappé, C. J. Casewit, K. S. Colwell, W. A. Goddard and W. M. Skiff, *J. Am. Chem. Soc.*, 1992, **114**, 10024–10035.

326 A. V Marenich, C. J. Cramer and D. G. Truhlar, *J. Phys. Chem. B*, 2009, **113**, 6378–96.

327 T. Ooi, M. Kameda and K. Maruoka, *J. Am. Chem. Soc.*, 2003, **125**, 5139–5151.

328 A. F. Burchat, J. M. Chong and N. Nielsen, *J. Organomet. Chem.*, 1997, **542**, 281–283.

329 H.-S. Lin and L. A. Paquette, *Synth. Commun.*, 1994, **24**, 2503–2506.

330 M. Zhuang and H. Du, *Org. Biomol. Chem.*, 2014, **12**, 4590–4593.

331 K. Maruoka, T. Itoh, Y. Araki, T. Shirasaka and H. Yamamoto, *Bull. Chem. Soc. Jpn.*, 1988, **61**, 2975–2976.

332 A. L. Reznichenko, T. J. Emge, S. Audörsch, E. G. Klauber, K. C. Hultzsch and B. Schmidt, *Organometallics*, 2011, **30**, 921–924.

333 J. Wallbaum, L. K. B. Garve, P. G. Jones and D. B. Werz, *Org. Lett.*, 2017, **19**, 98–101.

334 Y.-C. Liu, D. M. Reddy, X.-A. Chen, Y.-C. Shieh and C.-F. Lee, *European J. Org. Chem.*, 2020, **2020**, 2542–2552.

335 A. K. Ghosh and G. Gong, *J. Org. Chem.*, 2006, **71**, 1085–1093.

336 N. A. Khatri, H. F. Schmitthenner, J. Shringarpure and S. M. Weinreb, *J. Am. Chem. Soc.*, 1981, **103**, 6387–6393.

337 P. A. Grieco, P. Galatsis and R. F. Spohn, *Tetrahedron*, 1986, **42**, 2847–2853.

338 J. Linder, A. J. Blake and C. J. Moody, *Org. Biomol. Chem.*, 2008, **6**, 3908–3916.

339 H. Lebel, M. Davi, S. Díez-González and S. P. Nolan, *J. Org. Chem.*, 2007, **72**, 144–149.

340 L. S. Hegedus, P. M. Winton and S. Varaprath, *J. Org. Chem.*, 1981, **46**, 2215–2221.

341 L. De Munck, V. Sukowski, C. Vila, M. C. Muñoz and J. R. Pedro, *Org. Chem. Front.*, 2017, **4**, 1624–1628.